EVALUATION OF CONCRETE PATCH REPAIRS

by

Konstantinos Grigoriadis

BEng (Honours), MSc

Dissertation submitted in fulfilment of the requirement for the award of

PhD

in

Civil Engineering

School of Engineering and Mathematical Sciences

City University

London

January 2005

TABLE OF CONTENTS

LIST OF TABLES

LIST OF FIGURES

ACKNOWLEDGEMENTS

Professor D. Chamberlain	City University	For his supervision, patience, continuous support and valuable advice throughout the period required for the completion of this dissertation
Mr M. Dymock Mr A. Edwards	MC-Building Chemicals	For the donation of repair materials
Mr Paul Bravery	SIKA	For the donation of repair materials
Professor B. T. Meggitt Dr W. Boyle	City University	For providing fringe-based laser interferometry equipment
Mr J. Couper	Fibre Measurements	For measuring the roughness of concrete substrate surfaces using fringe-based laser interferometry equipment
Dr P. Liatsis Dr E. Milonidis	City University	For assisting with MATLAB programming
Mr P. Beckworth Mr J. Hooker Mr J. Rose	City University	For their technical assistance
My parents and my brother		For their continuous encouragement and support all these years of my studies in the United Kingdom

DECLARATION

I grant powers of discretion to the University Librarian to allow this dissertation to be copied in whole or in part without further reference to me. This permission covers only single copies made for study purposes, subject to normal conditions of acknowledgements.

SYNOPSIS

Experiments were carried out to study: a) the parameters which influence the efficiency and quality of remote robotic hydroerosion for removing defective concrete, b) the flexural behaviour of 6 different types of generic repair materials, c) the water permeability of the above 6 types of generic repair materials, and d) the parameters which influence the adhesive strength of patch repairs. In order to evaluate the efficiency and quality of remote robotic hydroerosion, 4 sets of parameters (concrete, pressure, generating unit, demolishing unit and nozzle parameters) were investigated using 7 series of tests. The flexural behaviour of 6 different types of generic repair materials was investigated by performing 160 flexural tests on solid, unrepaired and repaired beam specimens. The water permeability of the above 6 different types of repair materials was investigated by using ISAT and absorption by immersion tests on 100x100x100 mm cubes. Finally, 4 parameters (type of substrate surface, strength of substrate, type of repair material and use of bonding/agent primer), which influence the mode of failure and value of the adhesive strength of patch repairs were investigated by performing 300 pull-off tests. In the experimental study, fringe-based laser interferometry was used to measure and characterise the roughness of concrete substrates prior to repair. Results obtained using the above method proved the ability of remote robotic hydroerosion to produce surfaces with higher roughness values which in turn promote the adhesive strength between concrete substrates and repair materials.

SYMBOLS

A	Carbonation coefficient
A	Wetted area
A	Cross-sectional area of flow
A	area
A_f	Area of the fractured surface
C	Concentration
D	Depth of carbonation
D	Diffusion coefficient
D	Diameter of core
Da	Average double amplitude
d	Diameter of the circular area
F	Mass flux
F_r	Ratio of failure load
F_T	Tensile (pull-off) force
I	Hydraulic gradient
L	Distance between the transmitting and the receiving transducers
Lo	Actual profile length
Lr	Profile length ratio
m	Mass of flowing substance
N	Represents which of the 5 sampling lengths the parameter is related
n	Parameter suffix
Q	Flow rate
R	Mean peak-to valley height
RΔa	Centre line average slope
RΔq	Root mean square slope
Ssc	Mean summit curvature
Sdr	Developed interfacial area ratio
SΔq	Root mean square slope
S_{PO}	Pull-off strength
s	sorptivity
T	Time taken by the pulse to travel the distance
T	Scale of the parameter
t	Time of exposure
t	time
t	Coefficient of permeability
v	Pulse velocity
v	Volume of fluid absorbed
v	Volume of dry quartz sand
x	distance
y	Depth of the core
α	Inclination angle of the core
2α	Double amplitude
Δ	Distance between corresponding measuring points
λ	Wavelength

ABBREVIATIONS

AAR	Alkali Aggregate Reaction
ACI	American Concrete Institute
ANSI	American National Standards Institute
ASTM	American Society for Testing and Materials
BRE	Building Research Establishment
BS	British Standard
BS EN	British Standard European Norm
CEM	Cement Marked
EPI	Electrochemical Potential Imbalance
ESA	European Space Agency
FFT	Fast Fourier Transform
GGBS	Ground Granulated Blastfurnace Slag
GPR	Ground Penetrating Radar
HEROIC	Hydro-Erosion for Repair Of In-situ Concrete
ICRI	International Concrete Research Institute
ISAT	Initial Surface Absorption Test
ISO	International Organization for Standardisation
IT	Infrared Thermography
MEK	Methyl/ethyl/ketone
NDT	Non Destructive Testing
OPC	Ordinary Portland Cement
OPCC	Ordinary Portland Cement Concrete
OPCM	Ordinary Portland Cement Mortar
P	Pocket Concrete Slab Specimen
PFA	Pulverised Fuel Ash
PL	Plain Concrete Slab Specimen
pr BS EN	pre-British Standard European Norm
RC	Reinforced Concrete Pocket Slab Specimen
RHCC	Rapid Hardening Cement Concrete
RMS	Root Mean Square
SASW	Spectral Analysis of Surface Waves
SBR	Latex
SEM	Scanning Electron Microscope
SRI	Surface Roughness Index
ST	Stepped Concrete Slab Specimen
TSP	Trisodium Phosphate
VSI	Vertical Scanning Interferometer

CHAPTER 1

INTRODUCTION

1.1 INTRODUCTION

The aim of this chapter is to describe the effect that various concrete disintegration mechanisms, abnormal loading and poor workmanship have on concrete durability. In addition, the various stages of a typical patch repair scheme are presented. Next, the scope of this research is presented followed by a description of the structure of the thesis.

1.2 CONCRETE DECAY

In many countries around the world, large numbers of concrete structures such as buildings, bridges, tunnels, dams, and nuclear power stations are approaching or have approached a state where repair is necessary due to various concrete disintegration mechanisms, abnormal loading or poor workmanship.

1.3 CONCRETE DISINTEGRATION MECHANISMS

The main concrete disintegration mechanisms include:

- Acid attack
- Carbonation
- Alkali aggregate reaction
- Freeze-thaw cycles
- Chloride penetration
- Cast-in chlorides
- Sulphate attack

1.3.1 Acid attack

In the presence of moisture gases such as SO_2 and CO_2 which are present in the atmosphere, acids are formed which attack concrete. The acids react with the $Ca(OH)_2$ of the hydrated cement paste resulting in the decomposition of the hydrated cement paste. Acid attack occurs at pH values below 6.5. The severity of the attack increases as acidity increases. At pH values of 5.5 severe attack takes place whereas, at pH values of 4.5 the attack is very severe. Another factor influencing the rate of acid attack is the ability of hydrogen ions to diffuse through the cement gel produced after $Ca(OH)_2$ has been dissolved and leached out. Finally, the rate of acid attack is reduced when aggregates become exposed because the vulnerable surface is smaller and acid has to travel around the aggregates.

1.3.2 Carbonation

Carbonation of concrete is a special case of acid attack and is caused by the reaction between acidic gases in the atmosphere such as CO_2 and the products of cement hydration. Normal air contains CO_2 in relatively low concentrations of approximately 0.03%. In large industrial cities the level of CO_2 in the atmosphere is 0.3% and exceptionally, up to 1%. CO_2 penetrates into the pores of concrete by diffusion and reacts with the $Ca(OH)_2$ dissolved in the pore water as shown below:

$$CO_2 + Ca(OH)_2 \rightarrow CaCO_3 + H_2O \qquad (1.1)$$

Carbonation proceeds progressively from the external surface of concrete exposed to CO_2 towards the inner concrete. As the carbonated layer increases and becomes thicker, the distance that the CO_2 must diffuse through to meet $Ca(OH)_2$ is increased and the carbonated zone itself gives more resistance to gas flow. Studies on the rate of

carbonation both in the laboratory and in structures indicate that the depth of carbonation increases with time as shown below:

$$D = At^{1/2} \quad (1.2)$$

where:

D is the depth of carbonation (mm)

A is the carbonation coefficient (mm/year$^{1/2}$)

t is the time of exposure (years)

The above expression is not valid when the exposure conditions are not steady. The rate of carbonation depends on the moisture content of the concrete, which varies with the distance from its surface. Very dry concrete carbonates at a slower rate than damp concrete. This is because dry $Ca(OH)_2$ reacts very slowly with CO_2, whereas, the reaction is much faster and more complete when a surface film of water, saturated with the solid, is present on the grains of the $Ca(OH)_2$. On the other hand, if the pores in hydrated cement paste are filled with water the rate of carbonation will be very slow since the diffusion of CO_2 in water is four orders of magnitude slower than in air. Carbonation can proceed at a rate of up to 1 mm per year. However, in good quality concrete the rate of carbonation is very slow.

As the carbonation front proceeds the free $Ca(OH)_2$ is depleted. The effect of this reaction is that the pH of the pore water in hardened Portland cement paste is reduced from 13.5 to a value of about 9. When all $Ca(OH)_2$ has become carbonated the value of pH is reduced to about 8.5. By reducing the pH the passivity of the oxide film formed on the surface of steel reinforcement embedded in concrete is destroyed. When steel is depassivated and the environment is acidic or mildly alkaline, corrosion can take place,

provided moisture and oxygen necessary for the reactions of corrosion can gain access into concrete.

1.3.3 Alkali Aggregate Reaction (AAR)

Alkali aggregate reaction (AAR) can lead to expansion and severe cracking of concrete structures. Although the mechanisms that cause alkali aggregate reaction are not fully understood, it is widely accepted that in the presence of moisture alkali hydroxides from the cement react with certain aggregates such as reactive forms of silica. The result of this deleterious reaction is the formation of a gel around the reacting aggregates. The alkali-silicate gel around the aggregates attracts water by absorption or by osmosis and thus increases in volume. This expansion creates forces that cause tension cracks to form, around the aggregates. When tension cracks form more moisture penetrates the concrete, accelerating the alkali aggregate reaction. The main factor influencing the rate of the alkali aggregate reaction is the size of the siliceous particles. Fine particles 20-30 μm lead to expansion within one to two months, whereas larger particles lead to expansion after some years. Other factors influencing the speed of the alkali aggregate reaction are the porosity of the aggregate, the quantity of the alkalis in the cement, the availability of water in the cement paste and the permeability of the cement paste.

1.3.4 Freeze-thaw cycles

When the temperature of saturated concrete is lowered to 0 ^{0}C the water held in the capillary pores in the hardened cement paste freezes in a manner similar to the freezing in the pores of a rock. The freezing water expands as it is converted into ice leading to an increase in volume of approximately 9%. The expansion of the volume of water causes localised tension forces that fracture the surrounding concrete mix. The

fracturing occurs in small pieces, working from the outer surfaces inward. If subsequent thawing is followed by re-freezing, further expansion takes place. Hence, repeated cycles of freezing and thawing have a cumulative effect. For freeze-thaw cycles to have a deterioration effect the concrete should be more than 92% saturated. If the concrete is not saturated more than 92% then there is enough space to accommodate the expansion of water. Deterioration due to freeze-thaw cycles generally takes place on horizontal surfaces that are exposed to water, or on vertical surfaces that are at the water line in submerged portions of structures. The main factors influencing the rate of freeze-thaw deterioration are the porosity of concrete, the number of freeze-thaw cycles, the amount of entrained air, the use of aggregates with small capillary structure and high absorption, and the existence of horizontal surfaces in the structure that trap standing water.

1.3.5 Chloride penetration

Chlorides can be introduced into concrete by coming into direct contact with environments containing chlorides, such as de-icing salts or sea water. Chloride penetration from an external source is to some extent analogous to carbonation. If water with high levels of chloride ions is in contact with concrete saturated with chloride-free water diffusion of chloride ions into the concrete will take place in an attempt to produce a uniform chloride ion concentration in the water of the capillary pores. Penetration of chlorides starts at the surface and moves towards the inner concrete. The factors influencing the rate of chloride penetration are the amount of chlorides coming into contact with the concrete, the permeability of the concrete, and the amount of moisture present. Eventually the concentration of chloride ions in contact with the steel reinforcement destroys the passivity of the oxide film formed on the surface of steel reinforcement embedded in concrete. When steel is depassivated corrosion of the steel

reinforcement will take place in the presence of moisture and oxygen in accordance with the following reactions:

$$Fe^{++} + 2Cl^{-} \rightarrow FeCl_2 \quad (1.3)$$

$$FeCl_2 + 2H_2O \rightarrow Fe(OH)_2 + 2HCl \quad (1.4)$$

Since the volume of the products of corrosion is considerably greater compared to the volume of the original steel tensile forces are generated causing the concrete to crack and delaminate. When cracks and delaminations occur the rate of corrosion is accelerated because of the easy access of chloride ions, moisture and oxygen into the concrete.

1.3.6 Cast-in chlorides

Chlorides can be present in reinforced concrete even before the structure is in service. Chlorides can be introduced deliberately during construction in the form of accelerating admixtures such as $CaCl_2$, or through the use of inadequately washed sea dredged aggregates containing NaCl. Historically the use of $CaCl_2$ as an accelerating admixture in the UK was banned in 1978. However, it is still present in older concrete structures. Chlorides occur in either water soluble or acid soluble form. Chlorides used as accelerating admixtures are water soluble, whereas, those found on sea dredged aggregates may be only acid soluble. Water soluble chlorides are the most dangerous, since they readily become free to attack the surrounding steel reinforcement. BS 8110: Part 1[1] and BS EN 206: Part 1[2] set limits for acceptable chloride levels in structural concrete. For reinforced concrete made with OPC the limit of chloride ion content is 0.40% by mass of cement. The approach adopted by ACI 318[3] is to consider water soluble chloride ions only. On that basis, the chloride ion content of reinforced concrete

is limited to 0.15% by mass of cement. The two values are not substantially different from each other since the water soluble chlorides are only a part of the total chloride content.

1.3.7 Sulphate attack

Soluble sulphates such as $NaSO_4$, $CaSO_4$ and $MgSO_4$ present in soils and groundwater react with calcium aluminate hydrates of hydrated cement paste such as hydrated C_3A and $Ca(OH)_2$. Na_2SO_4 and $CaSO_4$ are more common whereas, $MgSO_4$ is less common but more destructive. The result of the reaction is the formation of gypsum and ettringite with volume greater than the products entering the reaction. Gypsum and ettringite expand, pressurise and disrupt the hydrated cement paste leading to cracking and disintegration of the cement matrix. The damage usually starts at the edges and corners and is followed by progressive cracking, spalling and mass deterioration. Sulphate attack occurs only when the concentration of soluble sulphate ions exceeds a certain threshold. Above that, the rate of sulphate attack increases with an increase in the strength of the solution, but beyond a concentration of about 0.5% of $MgSO_4$ or 1% of $NaSO_4$ the rate of increase in the intensity of the attack becomes smaller. BS 8110: Part 1[1] set limits for acceptable sulphate levels in structural concrete. For reinforced concrete made with OPC the limit of sulphate ion content expressed as SO_3 is 4% by mass of cement. Other factors influencing the rate of sulphate attack are the presence of water, the composition of cement, and the permeability of concrete.

In late 1990's a number of cases involving the thaumasite form of sulphate attack (TSA) were reported to ten bridge foundations in Gloucestershire, UK. TSA is different from the conventional form of sulphate attack because it is the calcium silicate hydrates C_2S and C_3S of hydrated cement paste which are targeted for reaction and not the

calcium aluminate hydrates. The result of the reaction is the formation of the rare mineral thaumasite. The formation of thaumasite is accompanied by a reduction in the binding ability of the affected cement paste in the hardened concrete, resulting in a loss of strength and transformation into a soft, incohesive mass. TSA is depended upon large quantities of water and the rate of deterioration is significantly increased at cold temperatures below 15 ^{0}C.

1.4 ABNORMAL LOADING

The main types of abnormal loading include:

- Fire loading
- Earthquake loading

1.4.1 Fire loading

When the concrete is exposed to fire the free water evaporates, and above approximately 150 ^{0}C the water chemically bound in the hydrated C_2S and C_3S is released. In some cases the surface layer of the concrete is not able to resist the pressure of water steam, and a spalling occurs. If the concrete has low permeability, the moisture content is high or the heating rate is fast the spalling can become a steam explosion comprising large parts. When the concrete does not spall the release of water causes shrinkage of the hydrated cement paste, while the aggregate and the steel reinforcement are subjected to a thermal expansion. Subsequently, stresses will develop in the composite steel/concrete material, and from approximately 300 ^{0}C microcraks will pierce through the matrix. The microcracks will cause a reduction of the strength and the modulus of elasticity. Above approximately 400 ^{0}C the crystals of $Ca(OH)_2$ will

begin decomposing into calcium oxide and water in accordance with the following reaction:

$$Ca(OH)_2 \rightarrow CaO + H_2O \uparrow \quad (1.5)$$

The above process reduces the strength of the concrete and reaches its highest intensity at about 535 ^{0}C. During the cooling phase which has a period of 1 week after the fire exposure, the strength of the concrete is reduced even further. This is due to the tendency of CaO to absorb water from the ambient air, giving rise to an expansion which opens the cracks already formed. Hence, the reduction in the strength of concrete depends on the temperature level, the applied load, the type of the aggregate used and the amount of $Ca(OH)_2$ crystals in the matrix. Typically, the reduction in the strength of concrete during the cooling phase is approximately 20%.

Pozzolans are able to react chemically with the $Ca(OH)_2$ of the Portland cement, and if the pozzolana used has a sufficient content of Al_2O_3, the resulting crystals may become heat resistant. Using proper pozzolanas and aggregates of a modest heat expansion a fire resistant concrete can be made from Portland cement.

1.4.2 Earthquake loading

Earthquakes, even moderate ones, can severely damage concrete structures leading to partial or full collapse. All types of structural elements can be affected by the action of seismic loading.

Slabs can be damaged in the form of cracks usually parallel to the steel reinforcement caused by a variety of reasons such as:

- Differential grouts of elements in the frame
- Hyper compression from the impact of the vertical component of the earthquake

- Bad estimation of the loads
- Poor workmanship in the arrangement of steel reinforcement, in construction joints, and in the maintenance of concrete after spreading.

Beams can be damaged in one of the following modes:

- Cracks orthogonal to the axis of the beam along the tension zone of the span
- Shear failure near the supports
- Flexural cracks on the lower or upper face of the beams at the supports
- Shear or flexural failure at the points where secondary beam or cut of columns are supported by the beam under consideration
- X-shaped shear cracks in short beams which connect shear walls

Although beam damage does not jeopardise the safety of the structure, is the most common type of damage in buildings.

Columns can be damaged in one of the following two ways:

- Damage due to cyclic flexure and low shear under strong axial compression
- Damage due to cyclic shear and low flexure under strong axial compression

In the first case, damage occurs in the form of failure at the top and bottom of columns with moderate to high slenderness ratio. The high value of the bending moment at these points together with the axial force, results to the crushing of the compression zone of concrete, successively on both faces of the column. The smaller the number of links in these areas, the higher their susceptibility to this type of damage. The crushing of the compression zone takes place first by spalling of the concrete cover followed by the expansion and crushing of the concrete core. This phenomenon is usually followed by

buckling of steel bars in compression and by link fracture. The fracture of the links and the disintegration of concrete lead to shortening of the column under the action of the axial force. Hence, this type of damage is very serious because the column not only loses its stiffness, it also loses its ability to carry vertical loads.

In the second case, damage occurs in the form of X-shapped cracks in the weakest zone of columns with moderate to small slenderness ratios. The worst form of this type of damage is the explosive cleavage failure of short columns, which usually leads to a spectacular collapse of the building. The main reason for this type of failure is that the flexural capacity of columns with moderate to small slenderness ratio is higher than their shear capacity, and as a result shear failure prevails. The frequency of this type of damage is lower compared to the failure at the top and bottom of the column. It usually occurs in columns of the ground floor, where, due to the large dimensions of the cross-section of the columns, the slenderness ratio is low. It also occurs in short columns, which have either been designed as short, or have been reduced to short because of adjacent masonry construction, which was not accounted for in the design.

Shear walls can be damaged in one of the following ways:

- Cracks in positions of badly built connections such as conjunction joints and fixing scale-positions
- Flexural cracks at the basis of tall walls that behave as ground cantilevers
- Slant cracks from shear lateral forces

The last two cases are more common and occur due to the fact that the shear walls were not properly tested and not efficiently reinforced.

Finally, damage of beam-column joints is very important since it can lead to collapse. In most cases damage in the form of cracks and displacements is due to poor workmanship or poor steel reinforcement arrangement.

1.5 POOR WORKMANSHIP

Poor workmanship during the construction of concrete structures can lead to serious structural defects. The most common structural defects include:

- Improper placement of steel reinforcement
- Inadequate depth cover to steel reinforcement
- Premature removal of formworks
- Improper column form placement
- Segregation
- Construction tolerances
- Plastic settlement
- Plastic shrinkage
- Honeycomb and rock pockets

Steel reinforcement is placed in concrete structures to carry the tensile loads. If the steel reinforcement is misplaced, the concrete memebr may not be able to carry the tensile loads. In reinforced concrete structures beams and columns are usually heavily reinforced members. Lap splices require overlaps of bars and may result in a mat of steel that concrete can not pass through during placement and consolidation. This may result in either a visible, or worse, a hidden void around the steel reinforcement. In prestressed concrete elements such as beams correct placement of post-tensioned cable

is critical to achieve the designed structural load carrying capacity. Improper placement may result in tension stresses, causing the concrete to crack.

Concrete cover acts as a physical barrier, protecting the steel reinforcement from O_2 and H_2O. In addition, the high alkalinity of concrete is a natural inhibitor. If the concrete cover is inadequate, it will not provide the necessary long-term protection. Shifted steel reinforcement bar cages may also cause the steel reinforcement to lose proper cover.

Premature removal of formwork before the concrete reached adequate strength may result in compressive and tensile stresses, causing cracking, deflection, and possible collapse.

Improper column formwork placement may lead to potential punching shear failure. Columns are usually cast prior to the placement of the slab/beam formwork. The exact elevation of the slab/beam bottom may not be precisely determined when the columns are cast. If the column is cast too tall and penetrates the slab/beam concrete, critical shear stresses may occur because of inadequate shear capacity area between the column and the slab/beam.

Segregation of concrete results in nonuniform distribution of its constituents. Differences in particle and specific gravity of the constituents of concrete create a tendency for the longer and more dense materials to settle and the finer and lighter materials to rise. Improper handling, excessive vibration and lack of cohesion are the causes of this problem. Segregation causes upper surfaces to have excessive paste, fines, and water/cement ratio. The resultant concrete may not have acceptable durability.

Structural members such as columns that are cast out of tolerance pose aesthetic and structural problems. Members cast out of tolerance may have improper cross section and concrete cover leading to eccentric loading.

Plastic settlement cracking is caused by the settlement of plastic concrete around fixed reinforcement, leaving a plastic tear above the bar and a possible void beneath the bar. Plastic concrete settlement is caused by low sand content and high water content, large size bars, poor thermal insulation, low humidity, insufficient vibration, and movement of formwork.

Plastic shrinkage occurs primarily as a result of rapid evaporation of free water while the concrete is in its plastic state and in the early stages of initial set. Since evaporation is the main source of water loss plastic shrinkage is most common in construction of slabs. Shrinkage results in cracking when it produces tension stresses greater than the stress capacity of newly placed concrete. Plastic shrinkage cracking rarely fractures aggregate, but separates around the aggregate. In many cases plastic shrinkage cracks can lead to points of thermal and dry shrinkage movement, intensifying the cracking.

Honeycomb is a void created in concrete due to failure of the mortar to effectively fill the spaces among coarse aggregate particles. Rock pockets are generally severe conditions of honeycomb in which an excessive volume of aggregate is formed. Honeycomb is caused by highly congested reinforcement, leaking at the joints, severe grout loss, reinforcement too close to the forms, high temperature, low workability, use of very large coarse size aggregate, and insufficient placement and consolidation.

1.6 REPAIR STRATEGY

The objective of any repair scheme should be the production of a durable long-lasting repair at a relatively low cost. A typical patch repair scheme of a reinforced concrete structure is shown in Figure 1.1.

Evaluation of concrete structures using either destructive or non-destructive testing methods	Chapter 1 Appendix 1
↓	
Definition of the characteristics of repair (crack sealing, patch repair or strengthening/stabilisation)	Chapter 1
↓	
Removal of deteriorated concrete using acceptable removal methods	Chapter 2 and 4
↓	
Cleaning, repair and protection of steel reinforcement that has been corroded	Chapter 3
↓	
Preparation and evaluation of concrete substrate surface	Chapter 3, 5 and 6
↓	
Selection of appropriate repair materials with suitable mechanical properties	Chapter 7
↓	
Installation and curing of the repair material	Chapter 11
↓	
Evaluation of the repair	Chapter 8, 9, 10 and 11

Figure 1.1 General patch repair scheme of a reinforced concrete structure

1.6.1 Concrete evaluation

The evaluation of concrete structures is carried out using either destructive or non-destructive testing (NDT) methods. The most common destructive method is core sampling. BS 1881: Part 120[4], BS EN 12504 Part 1[5] and ASTM C 42[6] give recommendations and procedures for taking, examining and testing drilled cores. NDT methods can be divided into the following groups:

- Visual Inspection
- Strength estimation methods (Schmidt hammer, penetration resistance, pull-out, break-off and pull-off tests)
- Stress-wave propagation methods (ultrasonic pulse velocity, pulse-echo, impact-echo and SASW methods)
- Nuclear methods (radiometry and radiography)
- Penetrability methods (water-absorption, water-permeability and air-permeability tests)
- Magnetic and electrical methods (covermeter, half-cell potential and linear polarisation methods)
- Infrared thermography (IT)
- Ground penetrating radar (GPR)

ACI 228.1R[7] reviews the various strength estimation methods used for estimating the in-situ strength of new and existing concrete structures, whereas, ACI 228.2R[8] provides a review of the rest NDT methods used for evaluating the condition of concrete and steel reinforcement in structures.

NDT methods are increasingly used for the evaluation of concrete structures. This increase is due to a number of factors such as:

- Technological improvements in hardware and software for data acquisition and analysis
- Ability to perform rapid, comprehensive assessments of existing large structures
- Economic advantages in assessing large volumes of concrete compared with core sampling

A review of all NDT methods is given in **Appendix 1**

1.6.2 Types of concrete repairs

Based on the results of the evaluation a decision on the type and characteristics of the required repair can be made. Concrete repairs can be generally identified as belonging to one of the following three main types:

- Crack sealing
- Patch repair
- Strengthening/stabilisation

Patch repair is perhaps the most common type of concrete repair. It can be defined as the repair of relatively small areas in mainly large surface elements of the structure such as bridge and car park decks, bridge piers, and building shear walls. The anatomy of a typical patch repair is shown in Figure 1.2 adopted from Emmons[9].

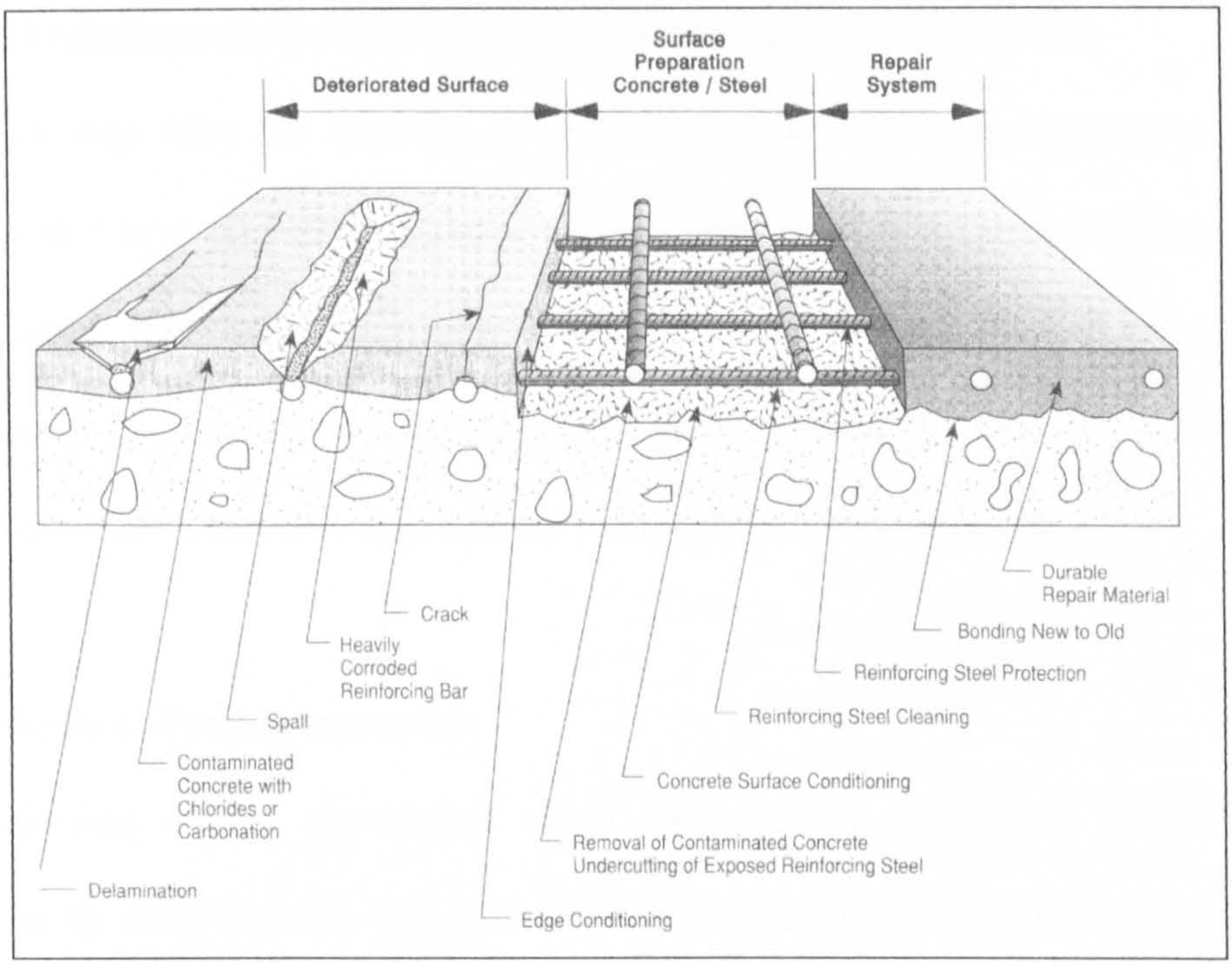

Figure 1.2 Anatomy of a typical patch repair adopted from Emmons[9]

1.6.3 Removal of defective concrete

A number of different methods can be used for the removal of defective concrete. These include:

- Machine-mounted demolishing attachments
- Mechanical or chemical splitting
- Sawing and cutting methods
- Pneumatic chipping hammers
- Thermal demolition methods
- Hydrodemolition

From the above removal methods hydrodemolition/hydroerosion is a relatively new technique that is increasingly used in the construction industry especially in the repair of bridge and car park decks.

1.6.4 Steel reinforcement and concrete substrate surface preparation

The next step after the removal of defective concrete is the preparation of steel reinforcement and concrete substrate surface. Preparation of steel reinforcement is accomplished by cleaning, repairing and protecting steel bars from corrosion. Preparation of concrete substrate surface is accomplished by removing contaminants and surface defects that can significantly reduce the adhesive strength.

1.6.5 Selection of repair materials

The selection of the appropriate repair materials is a complex process and is influenced by many factors. The selected materials should satisfy the requirements for strength. In addition, they should be compatible with the concrete substrate. The most common repair materials used in the construction industry include:

- Ordinary Portland Cement (OPC) mortar
- Ordinary Portland Cement (OPC) concrete
- Rapid Hardening Cement (RHC) concrete
- High strength concrete
- Polymer-modified concrete
- Polymer concrete
- Preplaced-aggregate concrete
- Shotcrete
- Fibre-reinforced concretes and shotcretes

1.6.6 Evaluation of patch repairs

Evaluation of patch repairs is usually based on assessing the adhesive strength between the concrete substrate and the repair material. For this purpose a number of different test methods have been developed which include:

- Tensile bond tests
- Shear bond tests
- Slant shear tests
- Patch repair tests

1.7 OBJECTIVES

The top level objective of this research is to investigate patch repair technology.

Sub-objectives are identified as follows:

- To review the effect of disintegration mechanisms, abnormal loading and poor workmanship on the long-term durability of concrete structures
- To review the various methods used for the removal of defective concrete and highlight the advantages of hydrodemolition/hydroerosion over traditional methods of concrete removal
- To investigate the significant influence of adequate preparation of steel reinforcement and concrete substrate surface on the long-term success of a repair
- To carry out remote robotic hydroerosion experiments and investigate the parameters that influence the efficiency and quality of the operation
- To investigate the importance of substrate surface roughness on the adhesive strength of the repair and methods for measuring and characterising the roughness of substrate concrete surfaces prior to repair

- To measure and characterise the roughness of concrete substrate surfaces prior to repair
- To compare the roughness of concrete substrate surfaces obtained using different methods of concrete removal (hydroerosion and pneumatic chipping hammers) and demonstrate the ability of hydroerosion to produce rougher surfaces
- To investigate and critically assess the factors that affect the selection of repair materials
- To review and select for experimentation the various test methods used for evaluating the quality of patch repairs
- To measure and compare the flexural strength behaviour of different types of generic repair materials by performing flexural strength tests on repaired unreinforced concrete beam specimens and thus give a basis for selection
- To determine the permeability properties between different types of generic repair materials by performing absorption by immersion and initial surface absorption tests on cubes
- To repair the above two different types of concrete substrate surface slab specimens using three different types of generic repair materials (OPC mortar, OPC concrete and Polymer-modified concrete)
- To measure the adhesive strength of the patch repaired slab specimens using the pull-off test
- To investigate the effect of different types of substrate surface roughness produced by different methods of concrete removal on the adhesive strength of patch repairs
- To investigate the effect of substrate compressive strength on the adhesive strength of patch repairs

- To investigate the effect of different types of generic repair materials on the adhesive strength of patch repairs
- To investigate the effect of cement based slurry bonding agents/primers on the adhesive strength of patch repairs

1.8 SCOPE OF RESEARCH

The success of every patch repair scheme is influenced by many factors. The main scope of this research is to investigate the various stages of a typical patch repair scheme. For this reason the main disintegration mechanisms of concrete and their effects on the long-term durability of concrete are described. Next, a review of the various methods used for removing defective concrete with particular reference to remote robotic hydroerosion is made. Aspects of steel reinforcement and concrete substrate surface preparation are then described. Next, a review of the various methods used for measuring and characterising concrete substrate surfaces prior to repair is made. The results of measuring and characterising the surface roughness of concrete substrate specimens obtained using 2 different methods of concrete removal (electric chipping hammer and remote robotic hydroerosion) are then presented and discussed. A review of the main types of repair materials used in the construction industry is then made, followed by a review of the various test methods used for evaluating the quality of patch repairs with particular reference to pull-off test as being the only method available for assessing the adhesive strength of patch repairs in-situ. Next, an experimental evaluation of the flexural behaviour of various types of generic repair materials is performed, followed by an experimental evaluation of their water permeability properties. Finally, the concrete substrate specimens produced for measuring and characterising concrete substrate surfaces are repaired using 3 different

types of generic repair materials. After curing of the repair material, the repaired slabs are subjected to pull-off tests in order to investigate the various parameters which influence adhesive strength.

1.9 STRUCTURE OF THESIS

The work in this thesis is divided into 12 main chapters:

Chapter 2: This chapter lists and describes the various methods used for removal of defective concrete. The methods discussed include machine mounted demolishing attachments, mechanical and chemical splitters, sawing and cutting methods, pneumatic chipping hammers, thermal demolition methods and hydrodemolition. Applications, advantages and limitations of each method are briefly discussed. Finally, particular reference to hydrodemolition/hydroerosion is made as being the most effective method for removal of defective concrete and preparation of concrete surfaces prior to installation of repair materials.

Chapter 3: This chapter describes the various methods used for steel reinforcement cleaning, repair and protection. It also describes the various contaminants and surface defects commonly found in concrete structures. Finally, methods used for removing contaminants and surface anomalies from concrete substrate surfaces prior to the application of repair materials are described.

Chapter 4: This chapter deals with the experimental research which was conducted by the author as an extension of the HEROIC[10] project. This investigates the factors that influence the efficiency and quality of remote robotic hydroderosion. The experimental equipment, manufacture of slab specimens, and the various tests performed using remote robotic hydroerosion are described. Finally, analysis and interpretation of results obtained from the various tests is also made.

Chapter 5: This chapter investigates methods for measuring and characterising surface topography in various fields of science and engineering. In addition, a review of the relatively small number of methods developed in the past for measuring and characterising the surface of concrete substrates prior to repair is also made.

Chapter 6: This chapter presents the experimental results of two different methods (sand area method and 3D fringe-based laser interferometry method) for measuring and characterising the surface roughness of concrete. For this, substrate specimens were obtained using two different methods of concrete removal (pneumatic chipping hammers and remote robotic hydroerosion).

Chapter 7: This chapter describes the various properties that repair materials must have to satisfy all requirements for a durable long-lasting repair. It also lists and describes the main types of generic repair materials used in construction industry. Applications, advantages and limitations of each type of generic repair material are briefly described. Finally, reference to bonding agents/primers that are used to protect steel reinforcement and improve adhesive strength between the concrete substrate and the repair material is also made.

Chapter 8: This chapter investigates the various test methods used for evaluating the quality of patch repairs by mainly assessing the adhesive strength between the concrete substrate and the repair material. The test methods discussed include tensile bond, shear bond, slant shear, and patch repair tests.

Chapter 9: This chapter deals with the experimental evaluation of various types of generic repair materials when subjected to flexure. In order to study the flexural behaviour of repair materials in a more realistic way and not by testing the flexural strength of specimens made entirely from the repair material itself, a parametric study on composite repaired unreinforced beams is performed.

Chapter 10: This chapter deals with the experimental evaluation of the water permeability properties of the generic repair materials selected in Chapter 9. In order to study the water permeability of repair materials the absorption by immersion test and the initial surface absorption test (ISAT) were employed.

Chapter 11: This chapter deals with the results of a parametric study performed to study the effect of different factors on the adhesive strength of patch repairs. The factors investigated include: 2 different types of concrete substrate surfaces, 4 different types of concrete substrates with w/c ratios ranging from 0.4 to 0.55, 3 different types of generic repair materials, and the effect of a cement-based slurry bonding agent/primer.

Chapter 12: This chapter gives conclusions against each of the objectives stated in Chapter 1. Each objective is stated prefacing the corresponding conclusions. In addition, suggestions for future work concentrated on the field of assessing concrete patch repairs are presented.

Finally, it should be noted that this thesis does not follow the standard way of presenting a literature review of the subject under investigation in one chapter (usually chapter 2) specially devoted for this purpose. Instead, various aspects of concrete patch repair technology are reviewed throughout the thesis.

CHAPTER 2

METHODS FOR REMOVING DEFECTIVE CONCRETE

2.1 INTRODUCTION

The next step after the evaluation of a concrete structure and the identification of defective areas is the removal of defective concrete using acceptable removal methods. Selection of the appropriate removal method should be based on the nature and extent of the deterioration as well as knowledge of the advantages and disadvantages of each removal method. The objective of this chapter is to review the various methods used for removal of defective concrete. The methods discussed include: machine mounted demolishing attachments, mechanical and chemical splitters, sawing and cutting methods, pneumatic chipping hammers, thermal demolition methods and hydrodemolition/hydroerosion. Applications, advantages and limitations of each method are briefly discussed. In this research, conventional hammer preparation has been experimentally compared with hydro-erosion preparation, the latter proving to be the more effective method for removal of defective concrete and preparation of concrete substrate surfaces prior to installation of repair materials.

2.2 CONCRETE REMOVAL METHODS

2.2.1 General

Removal of defective concrete is usually concerned with deteriorated or contaminated concrete. Removal methods should not damage the surrounding sound concrete. However, some sound concrete should also be removed to allow for adequate repair geometry and to prepare embedded steel reinforcement. Hence, the removal method should be able to achieve uniform depth excavation over defective and adjacent sound

concrete areas. In general, deteriorated concrete surfaces are not uniform. Areas that require repair should be modified to provide for simple layouts. The layouts should be based on reducing boundary edge length and eliminate acute angles as shown by the solid lines in Figure 2.1 adopted from Chamberlain et al[11]. Excessive or complex edge conditions such as those shown by the shaded lines in Figure 2.1 are usually produced by trying to closely follow the shape of the defective concrete. Such edge conditions often result in shrinkage stress concentrations and cracking and should be avoided. The effectiveness of different removal methods varies for defective and sound concrete. The removal methods selected for each project should minimise damage to sound concrete and steel reinforcement and should be safe and economical.

Finally, the ability of different removal methods to produce clean and rough substrate surfaces varies considerably. Rough surfaces seem to improve the mechanical interlocking and consequently the adhesive strength between the concrete substrate and the repair material. If the substrate surface on the other hand is smooth, the adhesive strength is often but not always very low.

Abudayyeh et al[12] and EM 1110-2-2002[13] provide an analytical description of the various concrete removal methods, their advantages and their limitations.

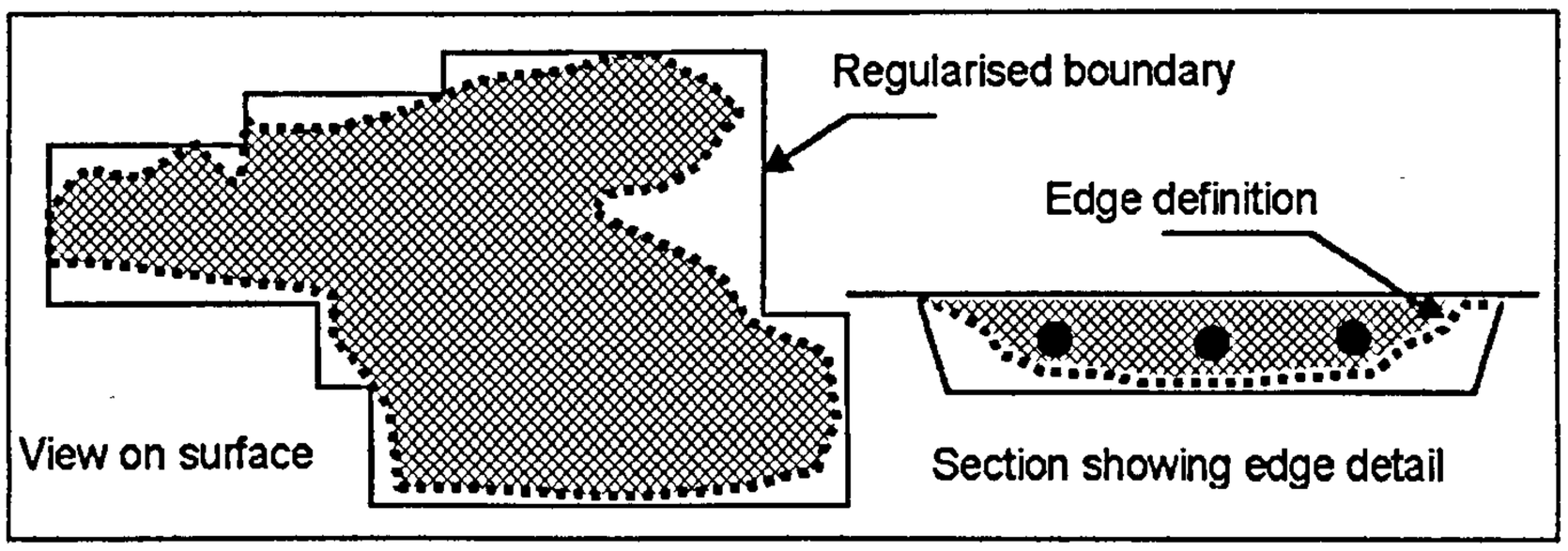

Figure 2.1 Concrete removal layout adopted from Chamberlain et al [11]

2.2.2 Machine-mounted demolition attachments

Machine-mounted demolition attachments include hydraulic hammers, whiphammers and crushers. Hydraulic hammers can be used for demolition of bridge decks, piers, slabs, and pavements. They have high removal rates varying from 1 to 95 m^3/h, increased mobility including under water use and remote control operation, and can be used under harsh weather conditions. Another advantage of hydraulic hammers is the reduced physical stress on operating staff in comparison with conventional hand-held hammers. However, they generate large amounts of noise, dust, and vibrations. Whiphammers can be used for bridge deck removal. They have high removal rates varying from 6 to 17 m^3/h. However, they require high energy input. Crushers can be used for partial or full bridge removal. They can achieve removal rates of up to 2 m^3/h. Their main advantage over hydraulic hammers is that they do not generate large amounts of noise, dust, and vibrations. In addition, they can be used under harsh weather conditions. Another advantage of crushers is their ability to cut rapidly and safely steel reinforcement. However, like whiphammers they require high energy input.

2.2.3 Splitting methods

Splitting methods can be divided into two categories: mechanical and chemical. Both mechanical and chemical splitters can be used for partial or full removal. The rate of removal for both methods depends on the hardness of concrete and orientation of steel reinforcement. Mechanical splitters are hand-held splitting tools that apply hydraulic pressure to concrete causing it to fragment. They are inexpensive and do not cause vibration. In addition, they produce small amounts of dust and leave the remaining concrete undamaged. Another advantage of mechanical splitters is that they can be used underwater. However, they are time consuming and require the use of breakers to

expose steel reinforcement. Chemical splitters are expansive agents that undergo a large increase in volume when properly mixed. These agents are placed in holes drilled in concrete at pre-specified points. When the agents expand in the holes, the concrete splits. Chemical splitters are safe and do not cause vibration, noise or dust. However, they are more expensive and time consuming when compared to mechanical splitters.

2.2.4 Pneumatic chipping hammers

Pneumatic chipping hammers are hand-held percussion tools used for partial removal of deteriorated concrete and are powered by air compressors, electricity or petrol engines. The rate of removal depends on the quality of concrete, the skill of the operator and ease of access. For an average pneumatic chipping hammer the rate of removal varies from 0.03 to 0.5 m^3/h. Pneumatic chipping hammers are easy to operate but they generate large amounts of noise, dust and vibration. In addition, the removal rate is low. However, the most important disadvantage of pneumatic chipping hammers is that the remaining concrete may be extensively microcracked and the steel reinforcement damaged. According to Hindo[14] the concrete remaining after partial removal using pneumatic chipping hammers contains microcracks in approximately the upper 9 mm of the exposed surface as shown in Figure 2.2 adopted from Conjet[15]. Depending on their sizes and densities, these cracks can significantly reduce adhesive strength and are very likely to contribute to the premature delamination of patch repairs as shown by Silfwerbrand[16] and Ingversson and Eriksson[17].

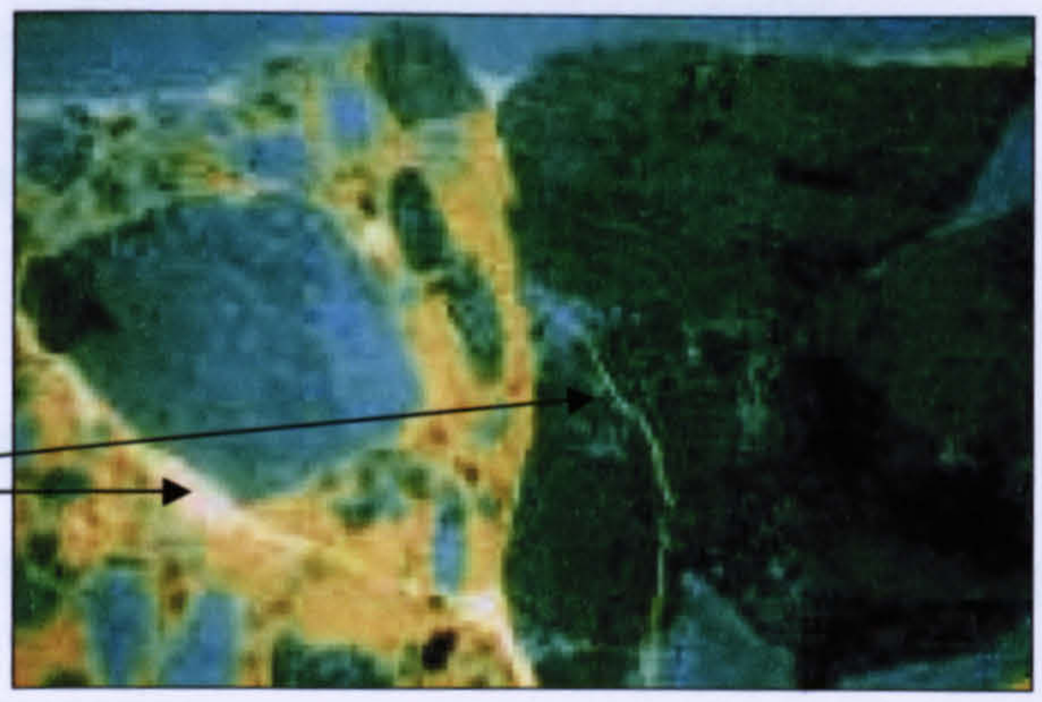

Figure 2.2 Photograph taken from a microscope showing the existence of microcracks after the use of pneumatic chipping hammers adopted from Conjet[15]

2.2.5 Sawing and cutting methods

Sawing and cutting methods include diamond blade saws and diamond wire cutting systems. Both can be used for partial removal of defective concrete. The rate of removal varies from 0.07 to 0.6 m^3/h. Blade saws are generally used to cut concrete structural members such as bridge decks into large pieces, which can then be easily removed using an overhead crane. Wet cutting diamond saw blades are the most common type of diamond saw blades used to cut concrete. Dry cutting diamond saw blades are also available, but should be used on low power saws. The most common type of diamond cutting wire consists of industrial diamonds electroplated to a steel bead that is strung onto a wire rope. The beads are separated by partially compressed steel springs. Another diamond wire system consists of impregnated beads. These beads have higher concentrations of smaller diamonds throughout the thickness of the bead. This allows for effective cutting of concrete with high concentrations of reinforcement. Concrete sawing and cutting methods produce clean edges and do not generate dust and vibrations. However, diamond blade saws can produce a limited depth of cut when compared to diamond wire cutting systems. In addition, difficulties can arise using

diamond blade saws when the blade comes in contact with reinforcement running parallel to the cut. Finally, some diamond cutting wire systems are expensive.

2.2.6 Thermal demolition methods

Thermal demolition techniques can be used for partial removal of concrete and are classified into three categories:

- Thermal boring and cutting
- Cracking and peeling
- Breaking and peeling

Thermal boring and heating technique can be used for the partial removal of defective concrete and is based on using high temperature to heat and melt the concrete. The heat is generated using flame, plasma, or laser beam. The cutting speed varies from 20 to 40 cm/min and depends on the quality of concrete, type of coarse aggregates, amount of steel reinforcement, smoothness of discharge of molten slag, and skill of the operator. The technique does not cause vibration, produces low levels of noise, and it can be used in places that are not easily accessible. However, it is quite expensive when compared to mechanical methods. In addition, it generates large amounts of fumes and there is an increased fire risk. Cracking and peeling technique is based on removing the concrete cover by electrically heating the steel reinforcement. Breaking and peeling technique is based on braking the concrete by directly heating it using electric energy.

2.2.7 Hydrodemolition/hydroerosion

Hydrodemolition is also known as hydroblasting, hydrojetting or waterjetting and is a relatively new method for the removal of defective concrete. It can be used on horizontal or vertical surfaces such as bridge and car park decks, shear walls in

buildings, and bridge piers. The method was first used in Italy in 1979 in order to remove concrete on the Viadotto del Lago. In 1984 it was introduced in Sweden and Canada as part of major bridge repair programs. During the last decade it was extensively used in repair projects all over the world as shown in Figures 2.3 and 2.4.

Hydroerosion on the other hand is a precise form of hydrodemolition using sensor feedback to control better the quality and quantity of concrete removal.

Figure 2.3 Removal of defective concrete from Liberty bridge in USA

Figure 2.4 Hydrodemolition of a bridge pier in Sweden

Hydrodemolition/hydroerosion is based on the use of high-pressure water jet to break up the concrete by disintegrating the cement matrix between aggregates. The disintegration is achieved by the following three mechanisms, which occur simultaneously:

- Cavitation, in which the rapidly changing pressures in flowing water produce shock waves with magnitudes sufficient to break up the cement matrix
- Pressurization of cracks and pores, which breaks the concrete in tension
- Direct impact of the water jet, which removes loosened fragments

During the above processes the aggregates themselves are not fractured.

A typical hydrodemolition system is shown in Figure 2.5 adopted from Momber[18] and is composed of two distinct parts: A pressure generating unit and a demolishing unit. The pressure generating unit is an ultra-high pressure plunger pump capable of generating water pressures up to 2500 bar. The demolishing unit is either a hand-held gun or a mobile housing unit onto which one or more nozzles are mounted. In a mobile housing unit the mounted nozzle is mechanically controlled and capable of moving across the concrete surface. Although, hand-held guns are relatively easy to use, hydrodemolition of large plane areas such as bridge and car park decks is usually carried out using a mobile housing unit. In the case of hydroerosion the demolishing unit is a mobile robot housing unit onto which a nozzle is mounted. The robot has an electronic brain and uses sensor feedback to control the quality and efficiency of concrete removal.

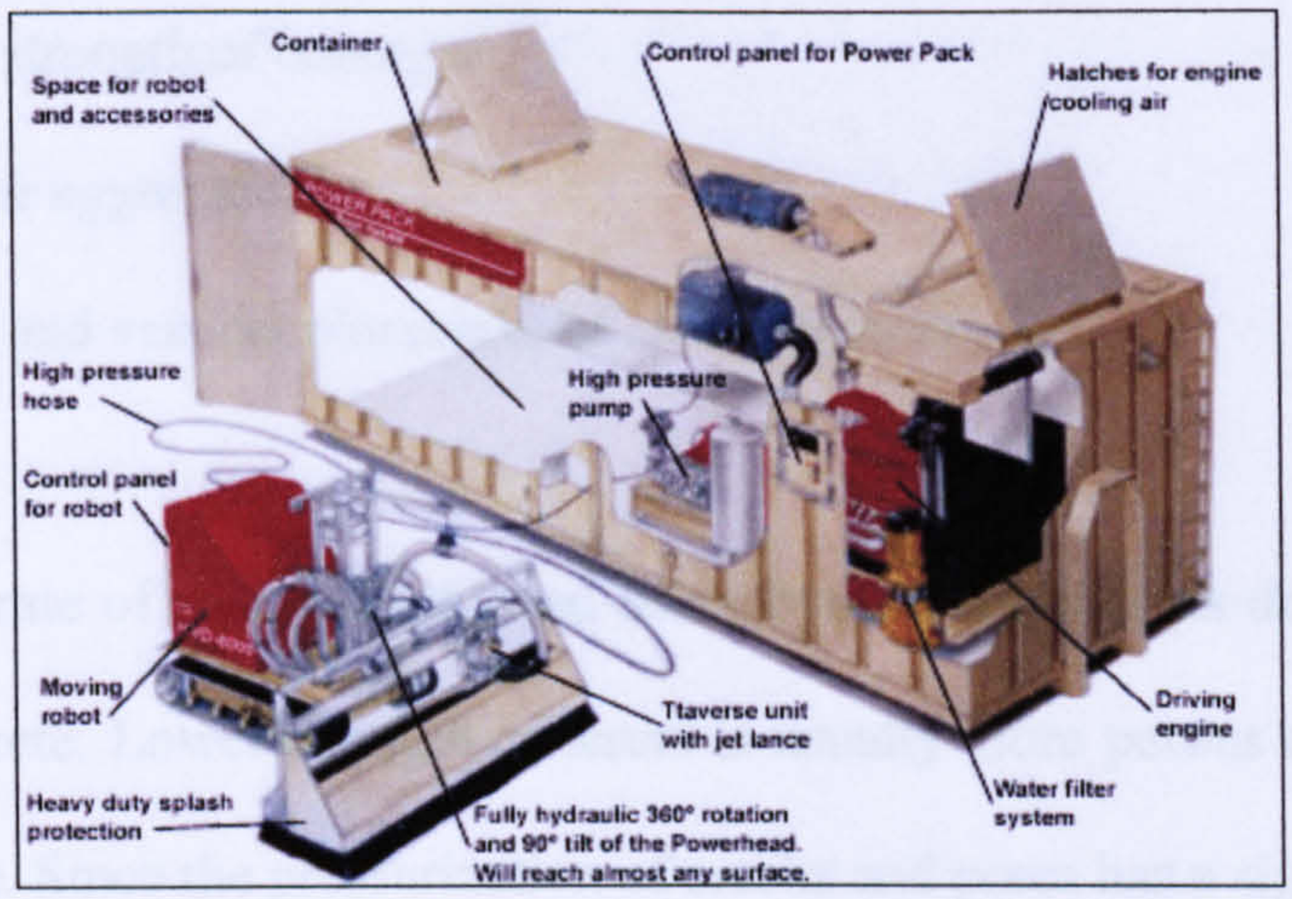

Figure 2.5 Typical remote hydrodemolition system adopted from Momber[18]

The water jet nozzle is an extremely important component of any hydrodemolition system. In the nozzle, the potential energy of the incoming pressurized water is converted into the kinetic energy of the exiting high-speed water jet. Based on their design nozzles can be classified into two groups: continuous nozzles and discontinuous nozzles. For operational water pressures up to 1000 bar continuous nozzles are most frequently used. They have a conical shape design and made from hardened steel. Discontinuous nozzles are becoming more increasingly used for ultra-high water pressures and are distinguished by a sapphire-made insert.

Four sets of parameters influence the depth and hence the rate of removal. These are:

- Concrete parameters
- Pressure generating unit parameters
- Demolishing unit parameters
- Nozzle parameters

Concrete parameters that influence the mean depth and hence the rate of removal include:

- Compressive strength of concrete
- Maximum size aggregate
- Size, spacing and vertical placement of steel reinforcement

The depth and rate of removal achieved using hydrodemolition is depended upon the porosity of concrete. Lower strength concrete is usually more porous compared to high strength concrete. Since the pressurization of cracks and pores has a significant effect on the disintegration of the cement matrix between aggregates, the depth and consequently the rate of removal is directly related to the volume of pore space, and thus the compressive strength of concrete. According to Warner[19] the required water pressure for demolishing good quality concrete should be at a range of 3-3.5 times the compressive strength of concrete. The maximum size of aggregate in the concrete and hence, the ratio of large aggregate volume to cement matrix volume influence the mean depth and rate of removal. Since the water jet disintegrates only the cement matrix of the concrete, the aggregates remain essentially intact. According to Lohrey[20] more time and energy may be required to demolish concrete mixes that have more large aggregate by volume, indicating a lower volume of cement matrix. This condition is valid provided that the volume of cement matrix is not so low and the overall compressive strength of concrete is lower than a normal level. Finally, the size, spacing and vertical placement of steel reinforcement affect the removal operation. The most critical variable regarding steel reinforcement is its cover depth. In many cases, the amount of cover varies considerably over the area of bridge and car park decks. Hence, when hydrodemolition is performed over such areas the quality and efficiency of the excavation may be reduced.

The parameters of the pressure generating unit which influence the depth and hence the rate of removal are:

- Water pressure
- Flow rate

Typical water pressures used in hydrodemolition projects are generally in the range of 550 to 3500 bar, with flow rates varying from 19 to 300 l/min. The amount of concrete removed depends on the hydrodemolition energy, which is the product of the water pressure and the flow rate. Low flow rates require relatively high water pressures, whereas the same amount of removal can be accomplished by using higher flow rates combined with lower water pressures. Based on the above, two different approaches regarding optimal water pressure and flow rate have been developed in the United States during the last decade. The first approach is based on the use of hydrodemolition equipment operating at water pressure of 1170 bar and flow rate ranging from 190 to 300 l/min. The second approach is based on the use of hydrodemolition equipment operating at ultra-high water pressure of 2300 bar and flow rate of approximately 120 l/min. Although, both sets of water pressure/flow rate parameters can equally well demolish concrete, the second set of parameters involving ultra-high water pressure and lower flow rate tends to have a more gentle effect on the concrete. According to Warner[19] hydrodemolition of open structures such as bridge decks can be carried out using lower water pressure/higher flow rate parameters, whereas hydrodemolition of car park structures and other enclosed areas can be accomplished using ultra-high water pressure/lower flow rate set of parameters.

The parameters of the demolishing unit which influence the depth and hence the rate of removal are:

- Distance of the nozzle from the surface of the concrete (stand off distance)
- Traverse speed of the nozzle
- Spacing between two successive crossings of the nozzle

When the distance of the nozzle from the surface of the concrete increases, the stream of water jet diverges and hence the effective diameter of the water jet decreases. As a result, the intensity cutting power of the water jet is reduced. Variations in traverse speed of the nozzle affect the amount of hydrodemolition energy delivered by the system per unit area of concrete traversed. The longer a fixed-energy water jet stays in one place the deeper the depth of excavation. Hence, the slower the nozzle traverses the concrete surface the more hydrodemolition energy will be delivered per unit area. Variations in strength or a non-uniform distribution of internal defects will result to different removal depths across the surface of the concrete. By periodically adjusting the traverse speed of the nozzle a uniform depth of removal can be achieved over a concrete surface of non-uniform strength. Traverse spacing has a significant effect on the topography of the eroded surface and the overall removal rate. If the spacing is too large, then there is a possibility of cement matrix disintegration without aggregates actually being knocked out. This can lead to an unsuitable surface preparation since repair materials can not easily fill deep voids.

Finally, the parameters of the nozzle that influence the depth and hence, the rate of removal are:

- Diameter of the nozzle
- Force of the nozzle

If the nozzle diameter is small then there is a possibility of cement matrix disintegration without aggregates actually being knocked out. This can lead to an unsuitable surface

preparation since repair materials can not easily fill deep voids. By using nozzles with diameters of approximately 1 mm this effect can be avoided. The force of the nozzle influences the penetrating ability of the nozzle and is depended upon the water pressure and flow rate of the pressure generating unit.

The main advantages of hydrodemolition against traditional methods of concrete removal mentioned above include:

- Selective removal of defective concrete without damaging or removing excessive amounts of good quality concrete
- High efficiency resulting in faster project completion
- Rough and clean surface profile leading to a good mechanical bond between the old concrete and the repair material
- No introduction of microcracks on the remaining concrete compared to traditional methods of concrete removal as shown in Figure 2.6 adopted from Conjet[15]
- No damage of existing steel reinforcement
- Cleaning and removal of rust from existing steel reinforcement
- Significant reduction in noise, dust, and vibration levels

Figure 2.6 Photograph taken from a microscope showing the absence of microcracks after the use of hydrodemolition adopted from Conjet[15]

The main disadvantage of hydrodemolition is the need for large quantities of water that must be obtained, handled and disposed. The water must be directed to appropriate areas for collection and controlled so that it does not flow into areas of the structure that must remain dry. Water that has been used in hydrodemolition projects is usually very alkaline and contains a large amount of suspended solids that require neutralization and separation before it can enter sanitary or storm sewers.

2.3 CONCLUSION

In this chapter a review of concrete removal methods was carried out. The advantages and disadvantages of machine mounted demolishing attachments, mechanical and chemical splitters, sawing and cutting methods, pneumatic chipping hammers, thermal demolition methods and hydrodemolition/hydroerosion were covered. Based on the advantages and disadvantages of the above concrete removal methods, the hydroerosion form of hydrodemolition is considered to be the best option for removing concrete especially in large areas such as bridge and car park decks. In general, more experimental research regarding the parameters influencing the efficiency and quality of hydroerosion needs to be carried out. In chapter 6, surfaces prepared by pneumatic hammering and hydroerosion are measured. They are compared for their effect on the quality of repairs on chapter 11. In the next chapter, preparation of steel reinforcement and substrate concrete surface is studied.

CHAPTER 3

STEEL REINFORCEMENT AND SUBSTRATE CONCRETE SURFACE PREPARATION

3.1 INTRODUCTION

The next step after removal of defective concrete is the preparation of steel reinforcement and substrate concrete surface. Preparation of both steel reinforcement and substrate concrete surface is of great importance regarding the success and long-term durability of patch repairs. Inadequate preparation of steel reinforcement can lead to reduced load carrying capacity, whereas inadequate preparation of substrate surface can lead to corrosion of steel reinforcement, problems regarding curing of the repair material and reduction in the adhesive strength between concrete substrates and repair materials. The main objectives of this chapter are: (a) to review the various methods used for steel reinforcement cleaning, repair and protection (b) to review the various methods used for removing contaminants, loose particles and surface anomalies from concrete substrate surfaces.

3.2 STEEL REINFORCEMENT CLEANING REPAIR AND PROTECTION

3.2.1 General

Corrosion of steel reinforcement is usually present in conjunction with concrete deterioration. Heavy layers of rust that build up on steel reinforcement bars during the corrosion process are the main cause of concrete delamination and spalling. Complete removal of rust is essential to the long-term success of patch repairs. According to Emmons[9] many patch repairs have failed within a few years of completion due to insufficient cleaning of the corroded steel reinforcement. For this purpose, removal of

concrete around the full circumference of the steel bars is necessary. Failure to remove concrete around the full circumference of the steel bars has a number of highly negative consequences that are highlighted by Vaysburd et al[21]. Contaminated concrete may be present around the full circumference of the steel bars and will promote corrosion immediately after the installation of the repair material. In addition, existing layers of rust in the steel bars will not be completely removed. However, the most important consequence is that the tensile stresses generated by the corrosion of the steel bars will be applied at the interface of the concrete substrate and the repair material. If the adhesive strength between the concrete substrate and the repair material is equal to the tensile strength of the concrete substrate or repair material the repair will last for a relatively long period of time. However, site experience suggests that even under the best conditions, the adhesive strength is usually lower than the tensile strength of the concrete substrate or repair material. Hence, in this case the repair will not last for a long period of time. On the other hand removal around the full circumference of the steel bars will allow the repair material to encapsulate the bars, providing a relatively uniform electrochemical environment, and to anchor the repair material to the substrate. During removal care should be taken to ensure that further damage to the steel reinforcement is avoided. Pneumatic chipping hammers can damage the steel reinforcement if they are used without regard to the location of the reinforcement. ICRI[22] provides guidelines for concrete repairs involving steel reinforcement.

3.2.2 Methods of removing rust from steel reinforcement

The next step after removal of concrete around the full circumference of steel bars is the removal of all heavy rust and scale to promote maximum bond with repair materials. A tightly bonded light oxide build-up may develop after cleaning. This usually does not

influence the bond. The most commonly used steel reinforcement cleaning methods include:

- Needle scalers
- Sand blasting
- Power wire cleaning
- Hydroblasting

Needle scalers are pneumatic tools utilising a group of small diameter steel rods powered by an internal piston. The steel rods hit the intended surface, causing removal of rust. Needle scalers are effective for removal of heave oxide layers, as well as for surface cleaning of small areas of concrete.

Sand blasting is an effective method for removing heavy oxide layers from steel reinforcement. However, high levels of dust can be a problem when using this method. Injection of water at the nozzle can be used to reduce dust levels.

Power wire brush is an effective tool for removing oxide layers from steel reinforcement. However, wire brushing can be a very slow and ineffective operation when steel bars have to be cleaned on the back side.

Hydroblasting (207 to 690 bar) is a very effective method for removing heavy oxide layers from steel reinforcement without causing any dust.

3.2.3 Methods of repair and protection of steel reinforcement

In many cases corrosion results in considerable or even complete loss in cross section that significantly reduces the ultimate load carrying capacity of the member. According to Emmons[9], if a steel bar has lost 25% or more of its cross section or if two or more adjacent steel bars have lost 20% of their cross section then repair is required. Repair of steel reinforcement bars can be carried out either by providing supplemental bar over

affected length or by complete bar replacement. Protection of repaired steel reinforcement can be accomplished using one of the following systems:

- Encapsulation
- Cathodic protection/sacrificial anode
- Cathodic protection/impressed current
- Alkaline slurry coating

Encapsulation is based on insulating the steel bars from electrical currents in the surrounding concrete by covering them with epoxy. The method is very effective when all bars in the member are protected. However, when bars are partially covered, either within the repair zone or adjacent to the repair, electrical currents can become concentrated in the unprotected bars, and accelerated corrosion can take place.

Cathodic protection/sacrificial anode method can be accomplished by coating the bars with a sacrificial metal such as zinc. However, since this method is sacrificial, the duration of protection is depended upon the severity of the environment that promotes corrosion. In addition, this method is used only on an experimental basis.

Cathodic protection/impressed current method is based on reversing the flow of electric current that causes corrosion. Anodes are installed on or near the surface of the concrete member and are electrically connected to the reinforcing bars. Electrical current is transmitted into the circuit, protecting the reinforcing bars. However, the impressed current should be balanced in accordance with the environment on a regular basis in order to provide protection. Hence, continuous monitoring and necessary adjustments are needed.

Alkali slurry coating can be used to protect the steel bars. In some cases non-passivating epoxies are used as a binder for the passivating alkaline fillers.

3.3 PREPARATION OF CONCRETE SUBSTRATE SURFACE

3.3.1 General

The overall success and performance of patch repair materials applied to concrete substrates is largely dependent upon the preparation of bond surface after removal of defective concrete. The objective of surface preparation and cleaning is to provide a sound, dry, even and level bond surface free of contaminants and defects. Holl and O'Connor[23] describe the various surface contaminants and defects commonly found in concrete substrates prior to repair.

3.3.2 Types of surface contaminants

Surface contaminants can be described as liquid or solid materials that have the potential to cause adhesion, curing and/or problems related with the application of repair materials to concrete. Surface contaminants must be properly and completely removed before any application of repair materials can take place. Examples of surface contaminants commonly encountered during patch repairs include:

- Curing compounds
- Dust
- Efflorescence
- Laitance
- Form release agents
- Oil, grease, tar, and gum

Curing compounds are liquid solutions that are commonly applied to newly cast concrete surfaces to promote hydration curing by retarding water loss due to

evaporation. Some curing compounds may be compatible with repair materials but it is always best to completely remove them.

Dust may be present either due to industrial pollution or from work being performed in the immediate area. Dust should be removed either by vacuum cleaning or using oil-free compressed air. Failure to remove dust will result in poor adhesion between the substrate and the repair material, leading to premature failure of the repair.

Efflorescence is a powdery white and in some cases crystalline deposit of water soluble salts that migrate to the concrete surface with water. The salts are left on the concrete surface when the water evaporates. Movement of water and dissolved salts will be from the hot to the cold side of a concrete member. Efflorescence must be removed from the concrete surface to prevent loss of adhesion between the concrete substrate and the repair material.

Laitance is a thin weak layer of partially hydrated cement paste 1.6 mm up to 3.2 mm thick at the top of the concrete caused by extended open time during finishing in cooler temperatures and/or overworking the finish and transporting cement fines to the surface. Laitance must be completely removed from the surface of the concrete to prevent loss of adhesion between the concrete substrate and the repair material.

Form release agents are used to facilitate the removal of forms from cured concrete and are strong bond breakers that can cause adhesion problems if they are transferred to bond surface.

Oil, grease, tar, and gum can be introduced to concrete from vehicular traffic or machinery and can penetrate deeply into concrete making effective removal difficult. They can cause adhesion problems if not completely removed. They can also bleed through the repair material to cause staining.

3.3.3 Types of surface defects

Surface defects can significantly influence the performance of repair materials. Examples of surface defects commonly encountered during patch repairs include:

- Ridges
- Eggshell
- Tie holes
- Sacking or rubbing

Ridges are high points that have a relatively sharp surface. Repair materials applied over ridges will be uneven and low in film thickness due to surface tension pull-back of the repair material at the edges of the ridge. Ridges should be removed by grinding or stoning to a flat plane surface followed by a light wire brushing to remove dust and laitance, followed in turn by a vacuum or air blast cleaning.

Eggshell is a very thin, and in some cases transparent film of laitance and bleed water residues that forms over air pockets in the concrete surface. This thin film can be very easily broken open exposing the hole beneath. Eggshells should be located, broken open, cleaned out and patched flush with the surrounding surface.

Tie holes are small holes that remain in the concrete after the concrete form tie bars have been removed. Tie holes should be cleaned out and patched flush with the surrounding surface.

Sacking or rubbing is the hand application of sand/cement mortar over new concrete. Sacking can cover minor surface defects and fill small voids. However, it is a very weak layer having very low adhesive strength. If present, sacking must be removed prior to the application of any repair materials.

3.3.4 Surface cleaning methods

Surface cleaning methods should produce a clean sound surface free of loose particles and contaminants that will promote mechanical interlocking between the repair material and the concrete substrate. The most commonly used surface cleaning methods include:

- Chemical cleaning
- Hydrocarbon solvents
- Steam cleaning
- Chemical stripping
- Steel shot blasting
- Sand blasting
- Vacuum cleaning/air blast cleaning
- Etching acid
- Hydroblasting

Chemical cleaning should follow the requirements and recommendations of standards such as ASTM D 4258[24] and ASTM D 4261[25]. It is generally based on utilising hot water solutions of trisodium phosphate (TSP) or commercial products such as detergents, cleaners, and emulsifiers to dissolve and remove contaminants from the surface. Thorough rinsing and flushing with clean water is necessary to remove any chemical cleaning residues on the surface of substrate concrete.

The most common hydrocarbon solvents include mineral spirits, methyl/ethyl/ketone (MEK), and Xylene. These solvents should only be used for selective cleaning applications and not for general cleaning purposes as they may dissolve the contaminants and spread them over a large surface area as well as drive them deeper into the concrete. Selective usage should strictly follow the manufacturer instructions.

Steam cleaning should follow the requirements and recommendations of standards such as ASTM D 4258[24] and ASTM D 4261[25]. Steam cleaning machines are used to produce quantities of wet or dry steam that is directed at the surface in a high concentration and at a velocity sufficient to soften and remove contaminants. Detergents, degreasers, and other chemicals are quite often added to the water to significantly increase the effectiveness of the method. Steam cleaning generally provides an efficient and effective method for removing many forms of water soluble contaminants that may be present on the surface. However, steam cleaning will only remove surface contaminants and not those in the pores of the concrete.

Chemical stripping is a wet method of surface cleaning and is based on utilising methylene chloride and hydroxide based alkaline chemicals to soften or dissolve cured coatings for subsequent mechanical removal. The method requires additional cleaning and surface preparation prior to the application of repair materials. It should never be used as the only cleaning method as contaminants in the form of removed materials and the high pH chemical stripping itself are always left behind. Tests based on ASTM D 4262[26] should be performed to verify that the alkaline chemicals have been neutralised. Chemical stripping is usually confined to small areas that can not prepared more effectively.

Steel shot blasting should follow the requirements and recommendations of standards such as ASTM D 4258[24] and ASTM D 4259[27]. The method is based on impacting the surface with high velocity steel shot abrasive. The shot blasting media is available in a range of shapes and sizes and is thrown against the concrete from an enclosed high velocity rotating paddle wheel. If only laitance is to be removed the steel shot abrasive should be of fine grade. The abrasive, dust, and contaminants are then removed by a separate dust collector. The cleaned steel shot is then recycled to the blast wheel where

the cycle is repeated. Use of shot blasting usually results in surface removal of up to 3mm per pass. Shot blasting is a clean, dust-free and very effective method for removing hardened films of contamination and texturing horizontal concrete surfaces without the use of water or chemicals. However, steel shot blasting is not very effective for the removal of rubbery elastomeric materials.

Sand blasting should follow the requirements and recommendations of standards such as ASTM D 4258[24], ASTM D 4259[27] and ASTM D 4285[28]. The method is based on impacting the surface with a high velocity stream of fine mineral aggregate abrasives propelled by clean compressed air. The blasting medium usually consists of hard angular mineral aggregates with a value of at least 6.5 on the Mohs' mineral hardness scale. In general, larger abrasive sizes are used for cleaning concrete surfaces whereas, smaller abrasive sizes are used for cleaning steel surfaces. If only laitance is to be removed the sand abrasives should have a diameter of 350-840 microns. Wet sand blasting cleaning can be used when low dust levels are required. Sand blasting is a very effective method for removing hardened films of contamination and texturing concrete surfaces without the use of water or chemicals. However, like shot blasting is not very effective on the removal of rubbery elastomeric materials.

Vacuum cleaning/air blast cleaning should follow the requirements and recommendations of standards such as ASTM D 4258[24] and ASTM D 4261[25]. Vacuum cleaning or air blast cleaning using oil-free compressed air is the final step to remove dirt and dust on a prepared surface immediately prior to application of repair materials. Vacuum cleaning is usually preferable to air blast cleaning when dust levels should be limited.

Acid etching should follow the requirements and recommendations of standards such as ASTM D 4258[24] and ASTM D 4260[29]. The method is usually accomplished with

10% solution of muriatic (hydrochloric) acid in clean water. Although, acid etching roughness the surface it does not remove laitance or other loose materials. Hence, prior to application the surface should be pre-wet and all oil, grease, paint, sealers, gum, tar and any other foreign materials should be removed to ensure uniform etching of the surface. In many cases it is advisable to use a pressure wash/rinse with a minimum pressure of 140 bar. Pressure washing removes the fines out of the pores in the surface and ensures removal of acid-weakened and etched surface layer of the concrete. Removal of such material significantly reduces the possibility of adhesive bond failure between the repair material and the concrete substrate. Prior to the application of repair materials the surface should be checked in accordance with ASTM D 4262[26] to ensure that it has been neutralised. Acid etching should only be used when no other method is possible.

Hydroblasting (207 to 690 bar) is a very effective method for cleaning concrete substrate surfaces by removing the most common types of surface contaminants and unsound particles.

3.4 CONCLUSION

In this chapter a review of the various methods used for steel reinforcement and concrete substrate preparation was carried out. From the various methods described only hydroblasting can be used for cleaning steel reinforcement by removing heavy oxide layers as well as cleaning concrete substrate surfaces by removing contaminants and unsound particles. In addition, it does not create any dust or vibrations and the noise levels are very low. Based on the above hydroblasting is considered to be the best option for steel reinforcement and concrete substrate preparation prior to the application of repair materials.

Figure 3.1 adopted from Eammons[9] summarises the sequence of steps involved in steel reinforcement and substrate concrete surface preparation prior to repair.

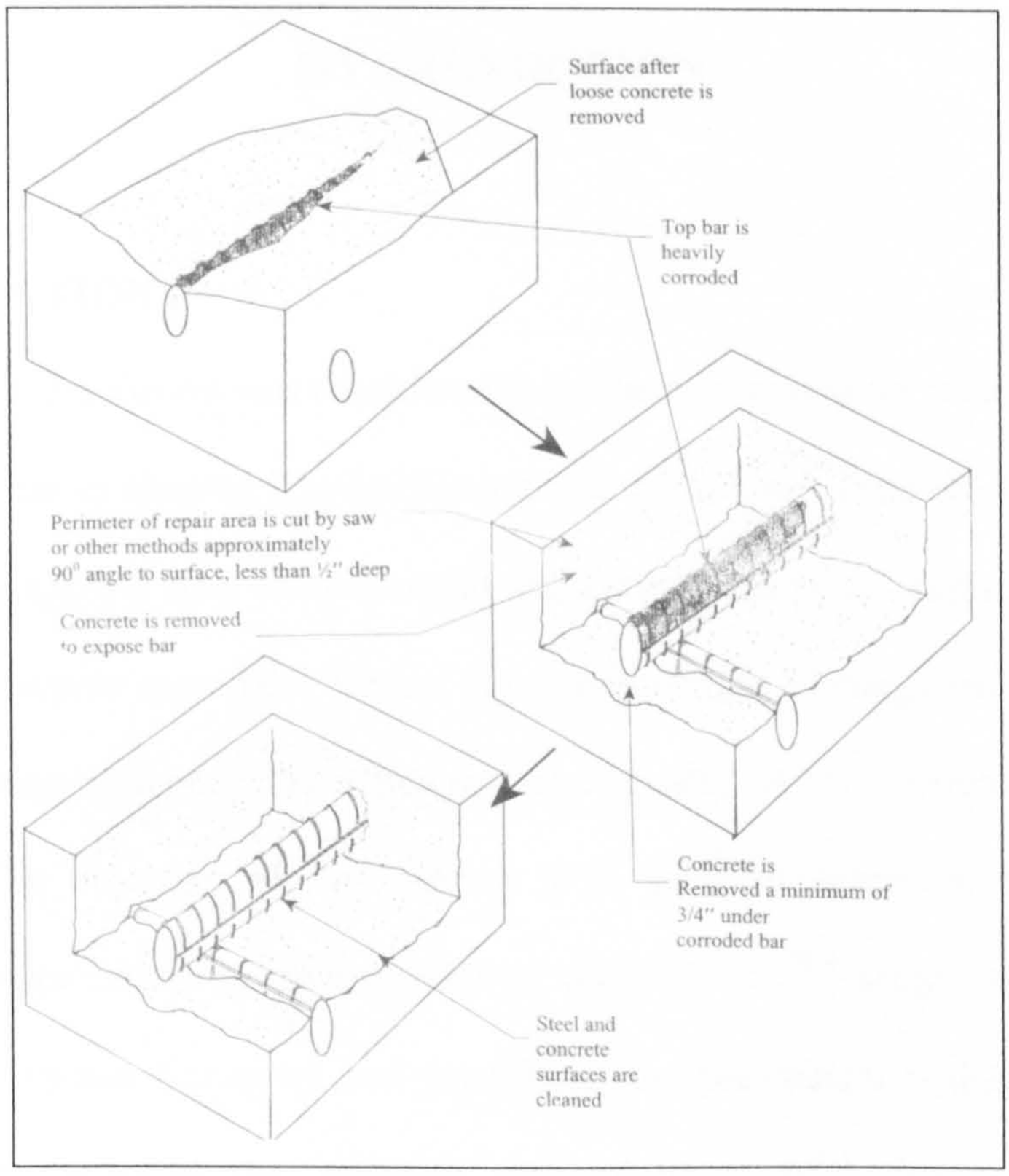

Figure 3.1 Summary of the sequence of steps involved in steel reinforcement and substrate concrete surface preparation prior to repair adopted from Eammons[9]

CHAPTER 4

EXPERIMENTAL EVALUATION OF REMOTE ROBOTIC HYDROEROSION

4.1 INTRODUCTION

In chapter 2, hydroerosion was considered to be the best option for removing defective concrete, whereas in chapter 3 hydroblasting was considered to be the best option for cleaning and preparing steel reinforcement and concrete substrate surfaces prior to the application of repair materials. Hence, an experimental investigation regarding the parameters which influence the efficiency and quality of the operation is of great importance. The objective of this chapter is to perform extensive remote robotic hydroerosion experiments as an extension of the HEROIC[10] project (Hydro-Erosion for Repair Of In-situ Concrete) and investigate the parameters which influence the efficiency and quality of the operation. The efficiency of hydroerosion is mainly governed by the rate of concrete removal, whereas the quality is largely depended upon the topography of the eroded surface. The experimental equipment, manufacture of slab specimens, and the various tests performed are described. Finally, analysis and interpretation of results obtained from the various tests is also made.

4.2 HYDROEROSION RESEARCH PROGRAM

4.2.1 Remote robotic hydroerosion equipment

As discussed in chapter 2 the demolishing unit of a hydrodemolition system is either a hand-held gun or mobile housing unit onto which one or more nozzles are mounted. However, the power that can be delivered using a manually operated demolishing unit is limited by health and safety considerations. Hence, it is important to develop

hydroderosion systems that take advantage of robotic technology. Compared with hydrodemolition, remote robotic based hydroerosion systems offer greater tool-handling capacity, precision and productivity. In addition, they offer improved working conditions, reduced fatigue levels and injury risks for the operator. A number of commercial remote hydrodemolition systems are available. However, they are not able to successfully remove concrete on a real-time controlled basis. They operate on a fixed water pressure and nozzle traverse speed over the entire concrete surface. After a typical crossing of the nozzle, there are random craters, corresponding to areas of weak or defective concrete. In practice, excavations at a uniform depth, over both strong and weak concrete and with good edge definition are required prior to repair. In a case of a fixed water pressure, this can be achieved by varying the traverse speed of the nozzle over areas of different compressive strength during the operation. For this reason, a remote robotic hydroerosion system was developed as part of the HEROIC[10] project to investigate the efficiency and quality of remote hydroerosion. The main advantage of the above system is its ability to remove concrete on a real-time controlled basis by adjusting the traverse speed of the nozzle over areas of different compressive strength. The remote hydroerosion system was comprised of a pressure generating unit shown in Figure 4.1 and a demolishing unit shown in Figure 4.2. The pressure generating unit consisted of an URAGA ultra-high pressure plunger pump, whereas, the demolishing unit was a MENASA three-dimensional cartesian robot onto which a continuous nozzle was mounted. The robot was capable of velocity and displacement control on three axis (X, Y, Z) as shown in Figure 4.3. Each axis was made up of an electric motor, a gear box, an encoder, a mechanical screw, a servo amplifier, and a motor controller as shown in Figure 4.4. The maximum reaction force was 80 Kg on the Z axis and 10 Kg on the other two axes. The maximum speed was 96 mm/s on the Y axis and 53 mm/s on the

other two axes with a positional accuracy of ± 0.1 mm on all axes. Shielding was provided by covering the X axis with a rigid cover and flaps for the nozzle to travel between, while the Y axis was protected using a concertina of sufficient fabric strength. Side panels made of high strength plastic were used for additional protection as shown in Figure 4.5. The robot had a working area of 400x400 mm and was controlled using a personal computer housed in an industrial cabinet as shown in Figure 4.6. The operating water pressure, flow rate and nozzle diameter were 1800 bar, 20 l/min and 0.9 mm respectively. Finally, a compact triangulating laser system was mounted on the robot and used to measure the depth of the excavations. Depths were determined by the laser on 10 mm spaced profiles. Non-reflecting data points were digitally filtered prior to plotting. The accuracy in depth measurements was better than 1 mm out of plane (Z axis) and 3 mm in plane (X-Y axes).

Figure 4.1 URAGA ultra-high plunger pump

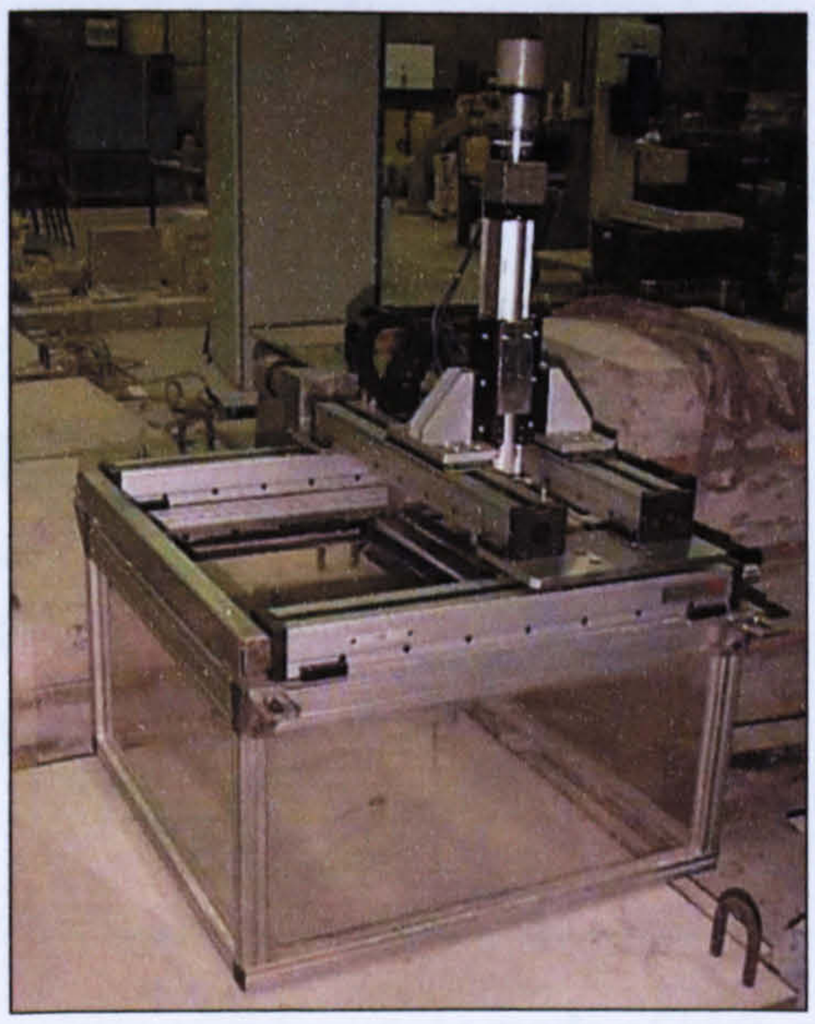

Figure 4.2 MENASA three-dimensional cartesian robot

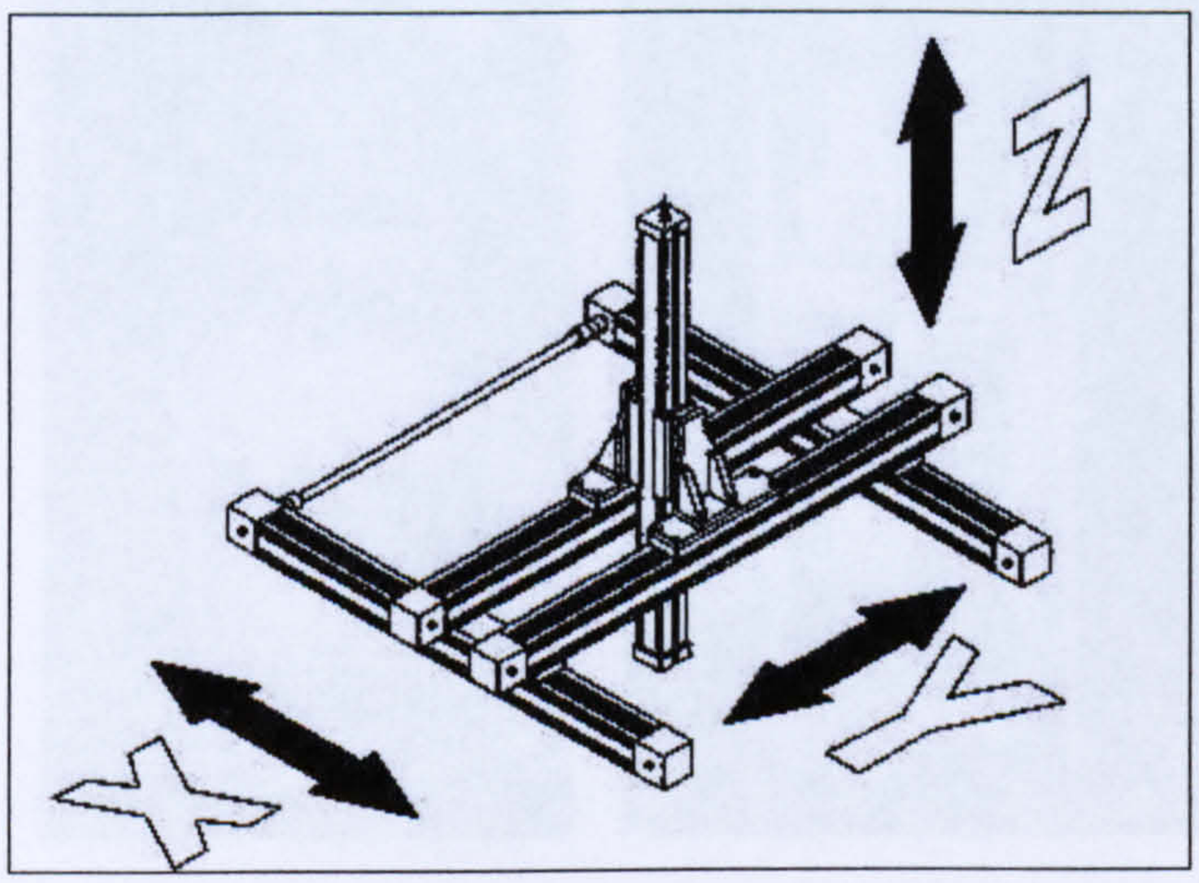

Figure 4.3 Schematic of X, Y and Z axes

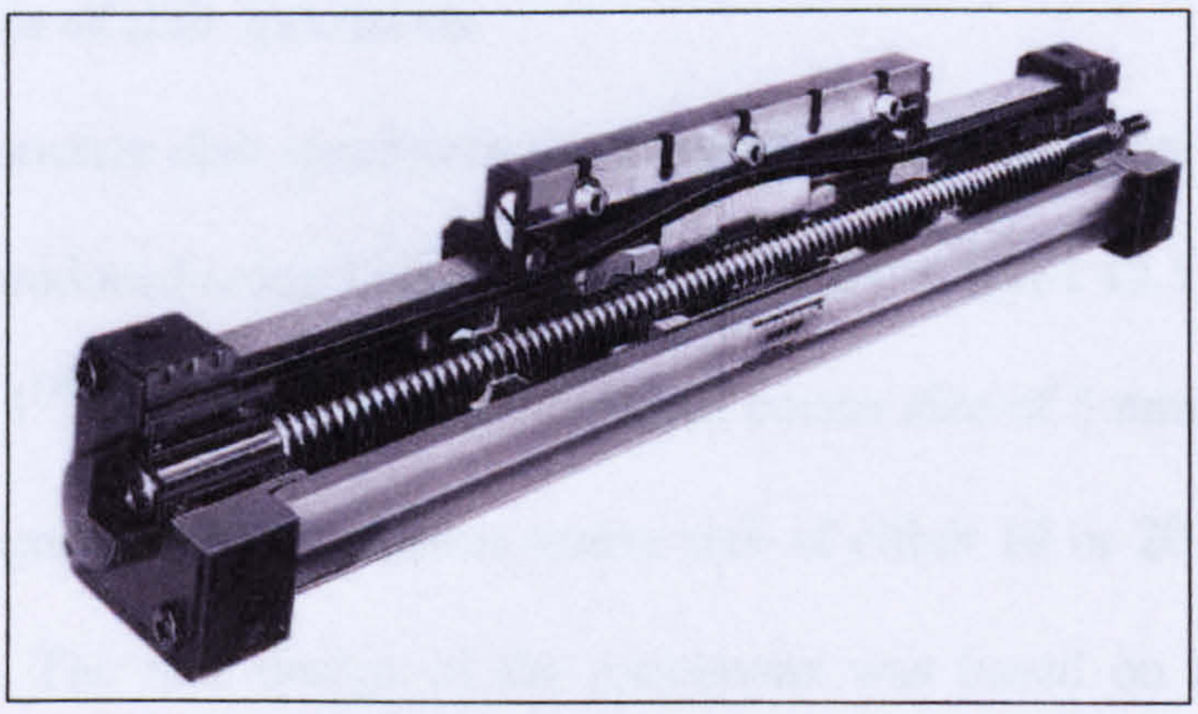

Figure 4.4 Components of axis

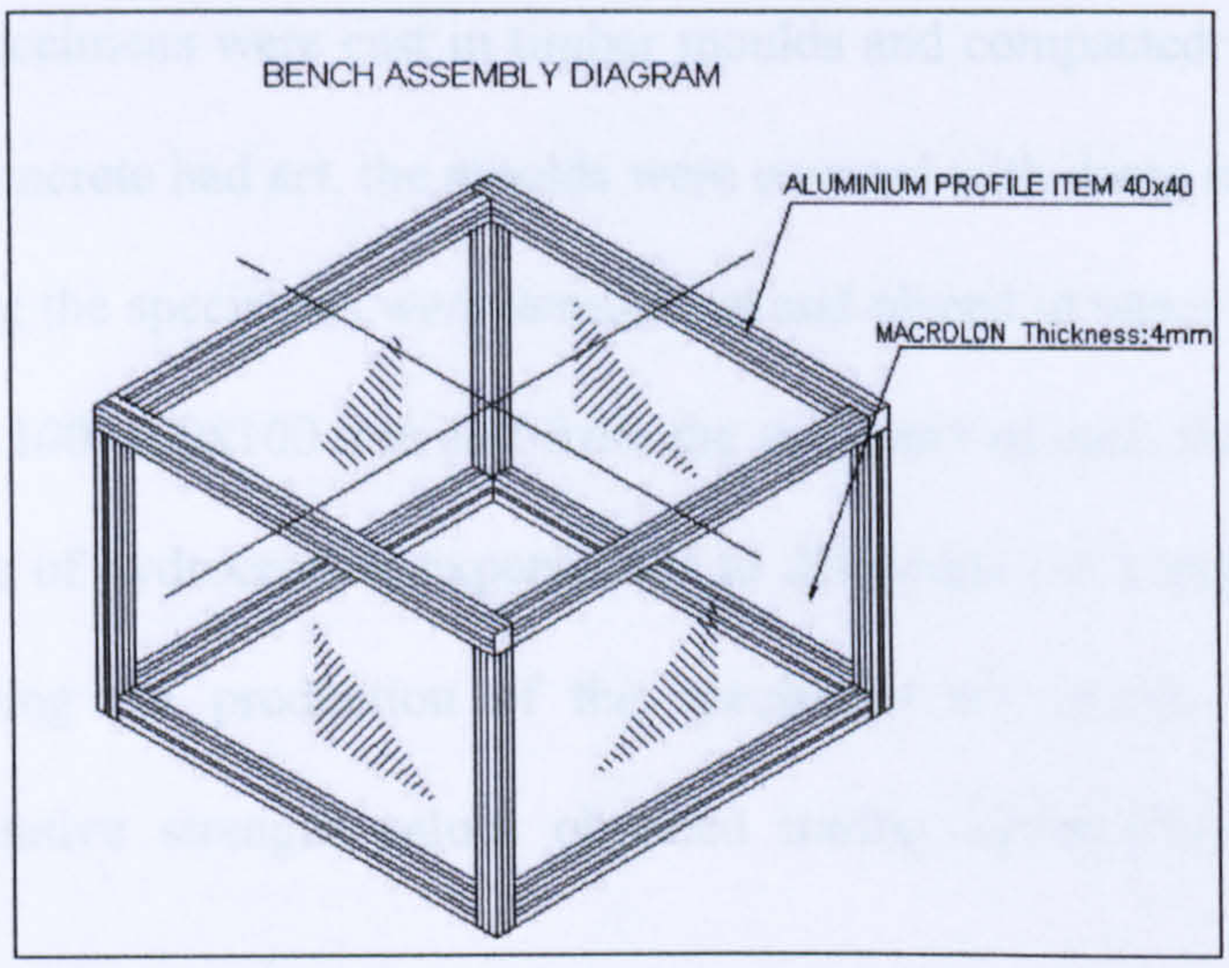

Figure 4.5 Schematic of side panels made of high strength plastic

Figure 4.6 Computer used to control the robot

4.2.2 Manufacture of slab specimens

Four series of concrete slab specimens were produced for hydroerosion purposes. The specimens were produced using Lafarge Blue Circle OPC CEM-I 42.5 N conforming to BS EN 197: Part 1[30]. Sharp sand with maximum coarse size of 5 mm was used as fine aggregate. River gravel with maximum coarse size of either 10 or 20 mm was used as coarse aggregate. The mix design of the specimens was based on the guidelines of BRE[31]. Five different mix types were used. Details of each mix type are shown in

Table 4.1. The specimens were cast in timber moulds and compacted using a vibrating table. After the concrete had set, the moulds were covered with damp rags. Twenty-four hours after casting the specimens were demoulded and placed in water for twenty-seven days. Four cubes 100x100x100 mm cast from the same mix of each slab specimen were tested at the time of hydroerosion experiments to determine the compressive strength. Photographs during the production of the specimens are shown in **Appendix 2,** whereas, compressive strength values obtained during hydroerosion are shown in **Appendix 3.**

Mix Type	Maximum Coarse Size Aggregate (mm)	w/c	Estimated Compressive Strength (N/mm^2)	Cement:Sand:Aggregate
1	10	0.40	60-65	1:1.34:1.85
2	10	0.45	50-55	1:1.55:2.15
3	10	0.55	30-35	1:2.00:2.76
4	20	0.40	60-65	1:1.32:2.56
5	20	0.45	50-55	1:1.52:2.94

Table 4.1 Mix Type characteristics

The first series of specimens consisted of 16 plain concrete slabs with dimensions of 400x400x125 mm as shown in Figure 4.7. Details of series 1 specimens are shown in Table 4.2.

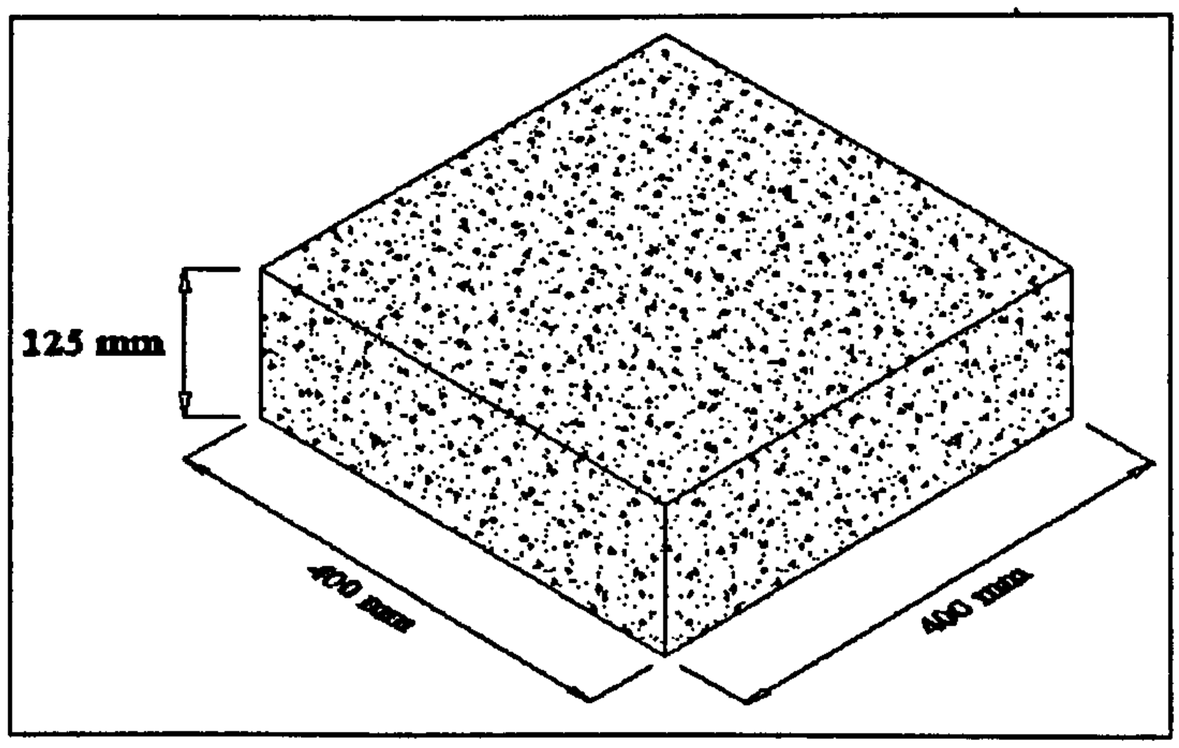

Figure 4.7 Schematic of plain slab

Ref.	Max. aggregate size (mm)	Compressive strength (N/mm^2)
PL 1	10	52.40
PL 2	10	57.35
PL 3	10	47.60
PL 4	10	48.45
PL 5	20	57.87
PL 6	20	57.87
PL 7	20	61.30
PL 8	20	62.80
PL 9	10	56.73
PL 10	10	56.73
PL 11	10	52.27
PL 12	10	50.53
PL 13	10	52.27
PL 14	10	64.20
PL 15	10	32.44
PL 16	10	32.44

Table 4.2 Details of series 1 plain slabs

The second series of specimens consisted of 6 concrete slabs with dimensions of 400x400x125 mm that had a pocket of weak concrete contained within the stronger concrete surround as shown in Figure 4.8. The maximum aggregate size for all slabs was 10 mm. Details of series 2 specimens are shown in Table 4.3.

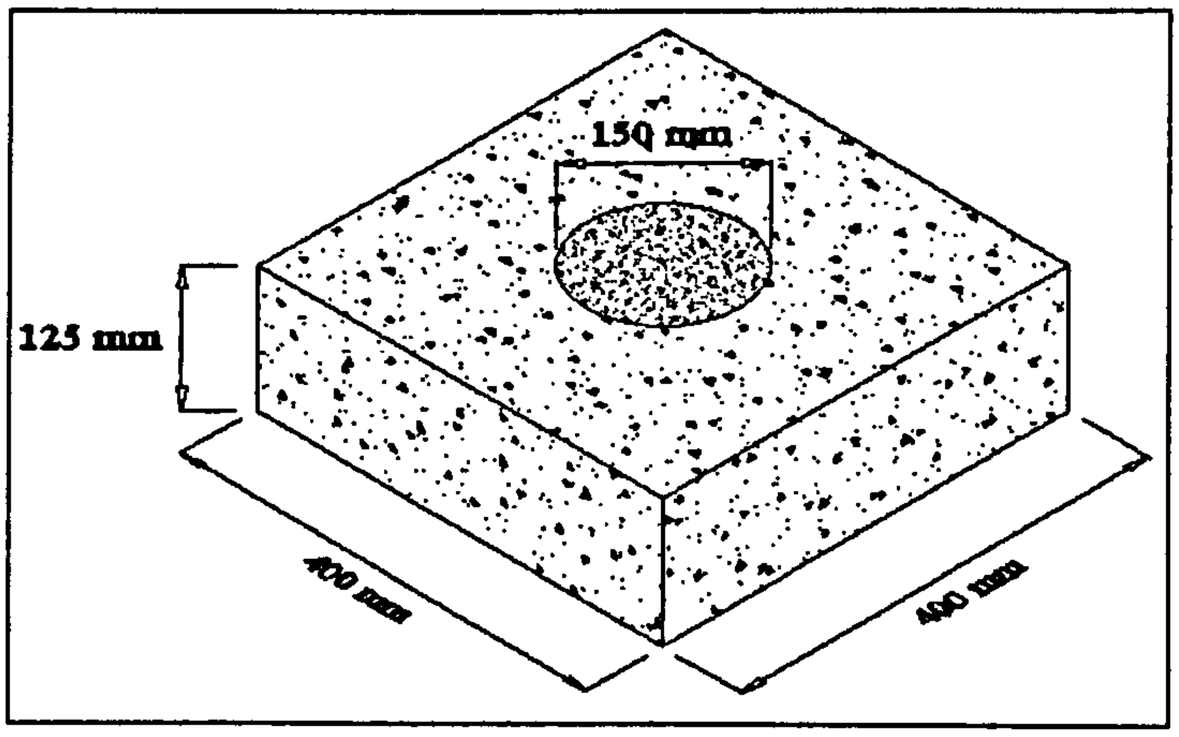

Figure 4.8 Schematic of pocket slab

Ref	Max. aggregate size (mm)	Pocket diameter (mm)	Pocket depth (mm)	Compressive strength (N/mm^2)	
				Strong concrete	Weak concrete
P 1	10	150	40	60.93	33.23
P 2	10	150	40	60.93	33.23
P 3	10	150	40	60.43	33.63
P 4	10	150	40	56.33	27.15
P 5	10	150	40	56.33	27.15
P 6	10	150	40	56.33	27.15

Table 4.3 Details of series 2 pocket slabs

The third series of specimens consisted of 6 reinforced concrete slabs with dimensions of 400x400x125 mm that had a pocket of weak concrete contained within the stronger concrete surround as shown in Figure 4.9. The reinforcement of each slab consisted of 3 deformed steel bars with diameters of either 16 or 20 mm. The bars were placed at a depth of 30 mm from the top surface. The above bar diameters were selected as being representative of bar diameters typically used in the construction industry. The maximum aggregate size for all slabs was 10 mm. Details of series 3 specimens are shown in Table 4.4.

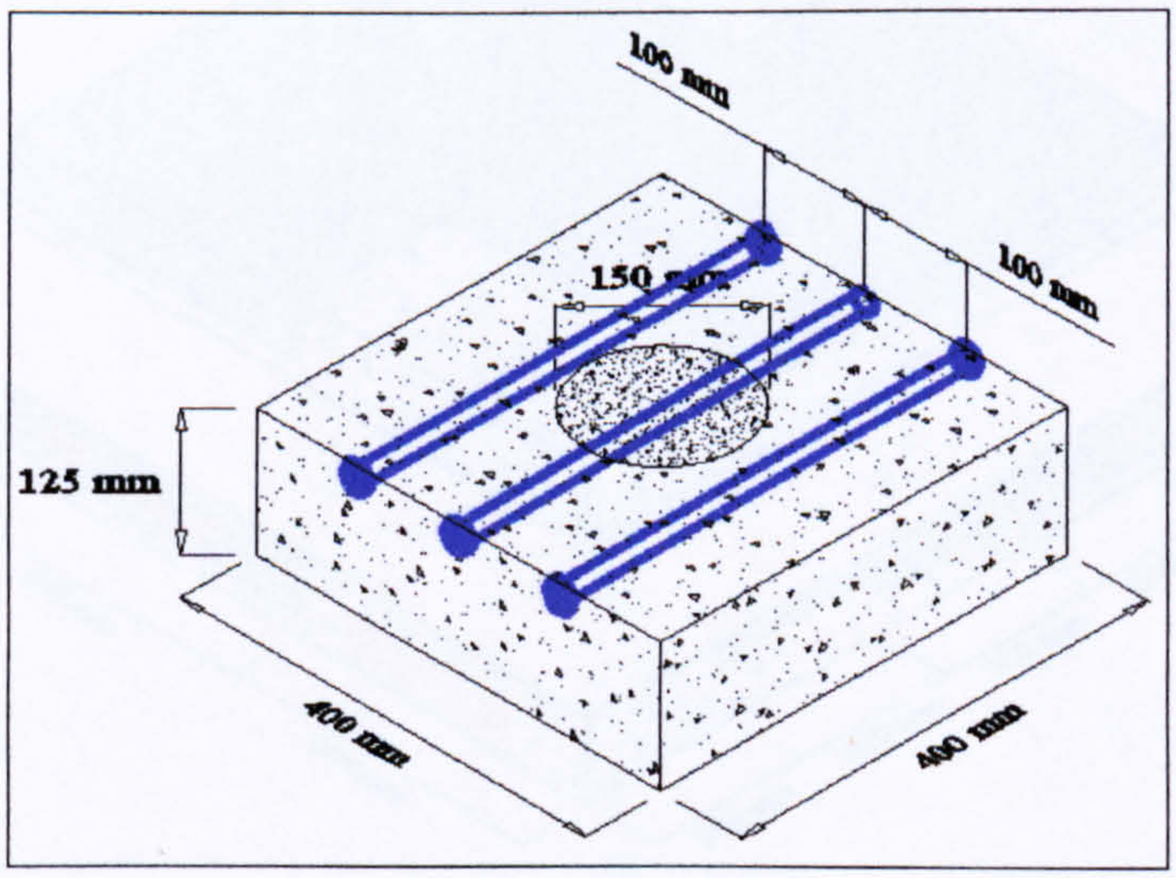

Figure 4.9 Schematic of reinforced pocket slab

Ref	Pocket diameter (mm)	Pocket depth (mm)	Steel bars	Spacing (mm)	Cover (mm)	Compressive strength (N/mm^2)	
						Strong concrete	Weak concrete
RC 1	150	70	3 NOS Φ 16	100	30	57.77	31.64
RC 2	150	70	3 NOS Φ 16	100	30	57.77	31.64
RC 3	150	70	3 NOS Φ 16	100	30	49.80	30.23
RC 4	150	70	3 NOS Φ 20	100	30	50.20	31.28
RC 5	150	70	3 NOS Φ 20	100	30	50.20	31.28
RC 6	150	70	3 NOS Φ 20	100	30	64.17	45.97

Table 4.4 Details of series 3 reinforced concrete pocket slabs

The fourth series of specimens consisted of 2 concrete stepped slabs with dimensions of 1200x1200x150 mm that comprised two areas with significantly different compressive strength values as shown in Figure 4.10. The slabs were formed like two staircases running in opposite directions. The high strength concrete was cast first and laid below the low strength concrete. The maximum size aggregate for both slabs was 10 mm. Details of series 4 slabs are shown in Table 4.5

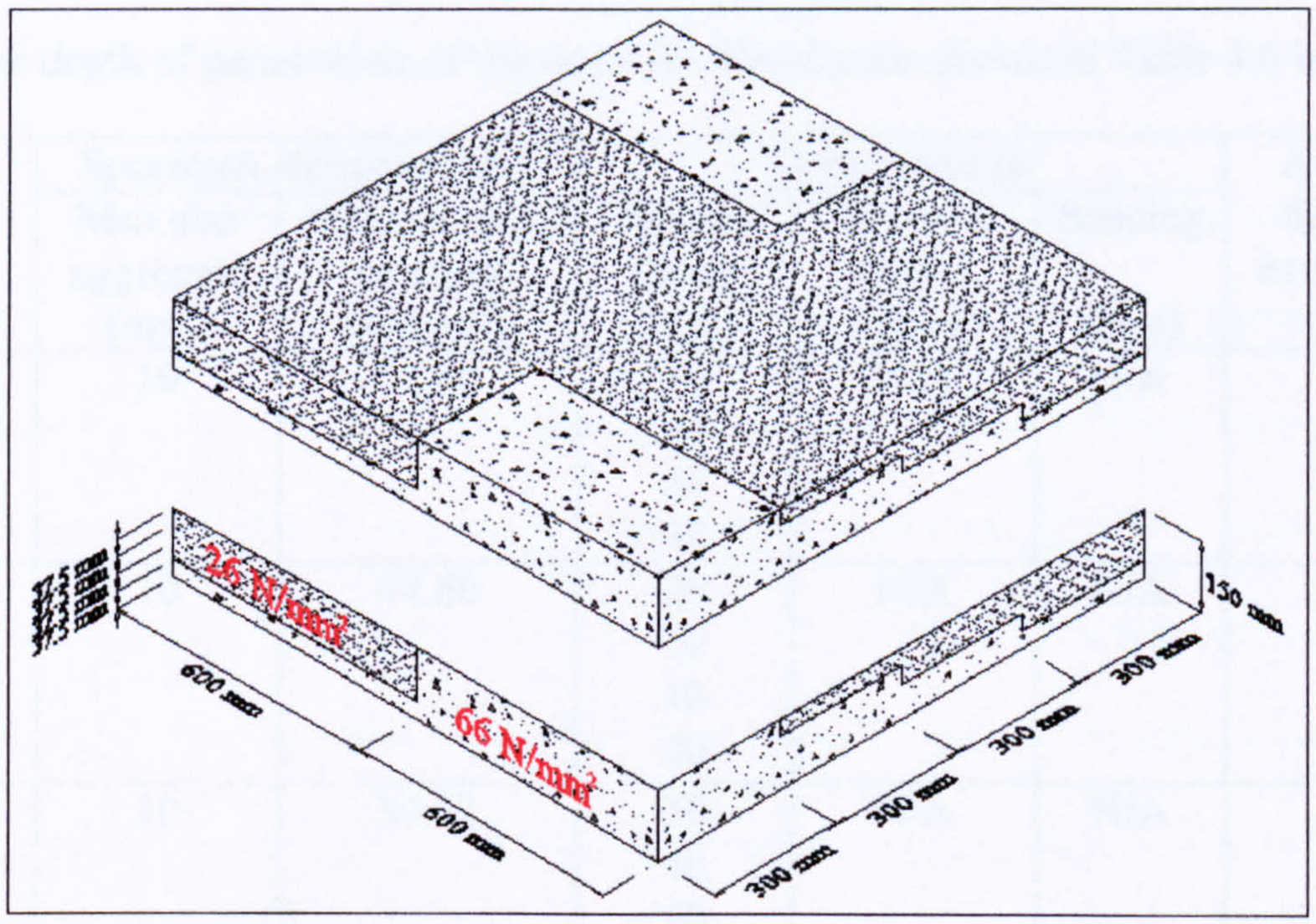

Figure 4.10 Schematic of Stepped slab ST 1

Ref.	Compressive strength (N/mm^2)	
	Strong concrete	Weak concrete
ST 1	66.00	26.40
ST 2	52.00	36.30

Table 4.5 Details of series 4 stepped slabs

In addition, to the above four series of specimens one reinforced concrete slab of uniform compressive strength with dimensions of 1200x1200x150 mm was used to investigate the effect of different operating water pressures on the removal rate of concrete.

4.2.3 Hydroerosion test program

The effects of various parameters influencing the quality and quantity of hydroerosion process were investigated by performing the following types of tests:

1) Nozzle offset test was performed to investigate the effect that stand off distance has on the depth of penetration of the water jet. Results are shown in Table 4.6 below:

Ref.	Specimen characteristics		Robot settings			Average depth of excavation (mm)
	Max size aggregate (mm)	Compressive strength (N/mm^2)	Nozzle Offset (mm)	Traverse Speed (mm/s)	Spacing (mm)	
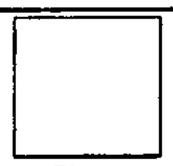 PL 1	10	52.40	10 20 30 40	N/A	N/A	N/A
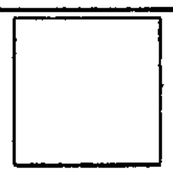 PL 3	10	47.60	20 30 40 50	N/A	N/A	N/A
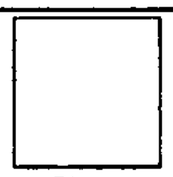 PL 12	10	50.53	30 40 50 60	N/A	N/A	N/A

Table 4.6 Nozzle offset test results

Nozzle offset test indicated that a stand off distance of 20 mm should be used that optimises water jet depth penetration and does not cause significant over break of concrete.

2) Exposure test was performed to investigate the effect that traverse speed has on the amount of concrete removed. Results are shown in Table 4.7 below:

Ref.	Specimen characteristics		Robot settings			Average depth of excavation (mm)
	Max size aggregate (mm)	Compressive strength (N/mm^2)	Nozzle Offset (mm)	Traverse Speed (mm/s)	Spacing (mm)	
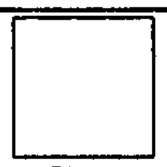 PL 4	10	48.45	20	Zone 1 20 Zone 2 40	20	Zone 1 25 Zone 2 20
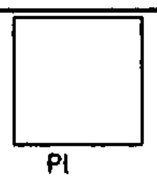 PL 7	20	61.30	20	Zone 1 30 Zone 2 50	20	Zone 1 22 Zone 2 17

Table 4.7 Exposure test results

For the purposes of the exposure test two slabs (PL 4 and PL 7) were tested. Two excavations were performed in each slab to investigate the influence of traverse speed on mean removal depth. A traverse spacing and a nozzle offset of 20 mm were used for all excavations. For slab PL 4 traverse speeds of 20 mm/s and 40 mm/s were used. In the first excavation using a traverse speed of 20 mm/s good edge definition was produced with a mean removal depth of approximately 25 mm. In the second excavation using a traverse speed of 40 mm/s the average removal depth was reduced to approximately 20 mm. Ridges were apparent in both excavations indicating that the traverse spacing of 20 mm was too great. For slab PL 7 traverse speeds of 30 mm/s and 50 mm/s were used. In the first excavation using a traverse speed of 30 mm/s the

average removal depth was approximately 22 mm. In the second excavation using a traverse speed of 50 mm/s the average removal depth was reduced to approximately 17 mm. For both traverse speeds poor edge definition was achieved and the excavation was non-uniform. However, experiments in both slabs confirmed the effect of traverse speed on the amount of concrete removed. Hence, the slower the nozzle traverses the concrete surface the more hydrodemolition energy will be delivered per unit area resulting in greater removal depths.

3) Path test was performed to investigate the optimum traverse spacing for slabs with different maximum size aggregate (10 mm and 20 mm). Experimental results are shown in Table 4.8 below:

Ref.	Specimen characteristics		Robot settings			Average depth of excavation (mm)
	Max size aggregate (mm)	Compressive strength (N/mm^2)	Nozzle Offset (mm)	Traverse Speed (mm/s)	Spacing (mm)	
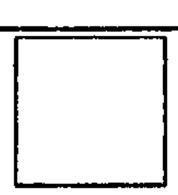 PL 2	10	57.35	20	35	15	25
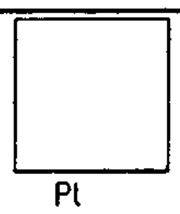 PL 5	20	57.87	20	35	30	15
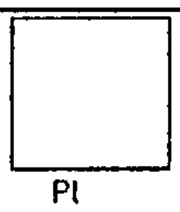 PL 6	20	57.87	20	35	10	25
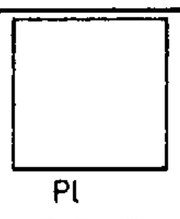 PL 9	10	56.73	20	35	15	22
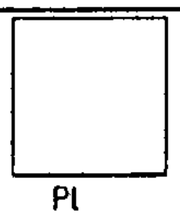 PL 10	10	56.73	20	35	35	14

Table 4.8 Path test results

For the purposes of path test five slabs (PL 2, PL 5, PL 6, PL 9, and PL 10) were used. A single excavation was performed in each slab to investigate the influence of traverse spacing on mean removal depth. Slabs PL 2, PL 9 and PL 10 were produced using 10 mm maximum size aggregate, whereas, slabs PL 5 and PL 6 had maximum size aggregate of 20 mm. All slabs had similar compressive strength of approximately 57 N/mm^2. A traverse speed of 35 mm/s and a nozzle offset of 20 mm were used for all excavations. Slab PL 2 was excavated using a traverse spacing of 15 mm. Good quality excavation was achieved to a mean removal depth of 25 mm. No ridging was apparent in the excavation. Slab PL 9 was excavated using a traverse spacing of 15 mm. Good quality excavation was achieved to a mean removal depth of 22 mm. Slab PL 10 was excavated using a traverse spacing of 35 mm. Although, the edge definition was satisfactory, a shallow, non-uniform excavation was produced with ridges clearly visible. The removal depth varied from 7-10 mm to 18-20 mm. Slab PL 6 was excavated using a traverse spacing of 10 mm. Good quality excavation without ridging was achieved. The mean removal depth was approximately 25 mm. Finally, slab PL 5 was excavated using a traverse spacing of 30 mm. Although, the edge definition was good, a shallow, non-uniform excavation was produced with ridges clearly visible. The mean removal depth was approximately 15 mm. The above results confirmed the influence of traverse spacing on the mean depth of removal and overall quality of the excavation. Hence, for traverse spacing between 10-15 mm good quality uniform excavation without ridging at a mean removal depth of 25 mm can be achieved. However, when the traverse spacing is increased to 30-35 mm the excavation is shallow and non-uniform. In addition, ridging is clearly visible.

4) Rate test was performed to investigate the effect of fixed nozzle offset, traverse speed, and spacing over slabs with different compressive strength values. Experimental results are shown in Table 4.9

Ref.	Specimen characteristics		Robot settings			Average depth of excavation (mm)
	Max size aggregate (mm)	Compressive strength (N/mm^2)	Nozzle Offset (mm)	Traverse Speed (mm/s)	Spacing (mm)	
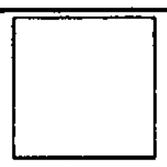 PL 11	10	52.27	20	30	20	20
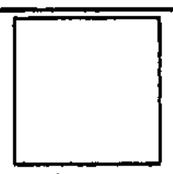 PL 13	10	52.27	20	30	20	22
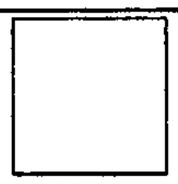 PL 14	10	64.20	20	30	20	22
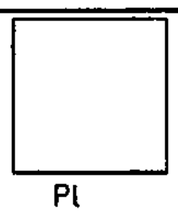 PL 15	10	32.44	20	30	20	10
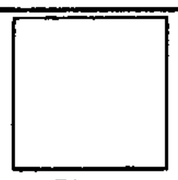 PL 16	10	32.44	20	30	20	10

Table 4.9 Rate test results

For the purposes of rate test five slabs (PL 11, PL 13, PL 14, PL 15, and PL 16) were used. A single excavation was performed in each slab to investigate the influence of compressive strength on the mean removal depth. A nozzle offset of 20 mm, traverse speed of 30 mm/s and spacing of 20 mm were used for all excavations. Selection of the above traverse spacing seems to be in a disagreement with the outcome of path test according to which, a traverse spacing of 10-15 mm should be used to achieve good quality uniform excavation without ridging at a mean removal depth of 25 mm. However, a traverse spacing of 20 mm can theoretically have a more gentle effect on

concrete (especially lower compressive strength slab specimens) without seriously influencing the quality and quantity of the excavation. All slabs were produced using 10 mm maximum size aggregate. The compressive strength of slabs PL 11 and PL 13 was 52.27 N/mm^2, while, the compressive strength of slab PL 14 was 64.20 N/mm^2. Finally, the compressive strength of slabs PL 15 and PL16 was 32.44 N/mm^2. For slab PL 11 a uniform excavation was achieved with slight traces of ridges. However, the edge definition was poor. The mean depth of removal was approximately 20 mm. For slab PL 13 a non-uniform excavation was achieved with traces of ridging clearly visible. Good edge definition was achieved on two sides. The mean removal depth was 22 mm. For slab PL 14 a uniform excavation was achieved with no signs of ridging. However, the edge definition was poor. The mean removal depth was 22 mm. For slab PL 15 a highly non-uniform shallow excavation with deep ridges was achieved. The edge definition was good. The removal depth was varying from a few mm to 25 mm between ridges. Finally, for slab PL 16 a highly non-uniform shallow excavation with deep ridges was achieved. However, as with slab PL 15 the edge definition was good. The removal depth was varying from few mm to 25 mm between ridges.

5) Pocket test was performed to investigate the effect of fixed nozzle offset, traverse speed, and spacing over concrete surfaces of varying compressive strength. Experimental results are shown in Table 4.10

Ref	Specimen characteristics			Robot settings			Average depth of excavation (mm)
	Max size aggregate (mm)	Compressive strength (N/mm^2)		Nozzle offset (mm)	Traverse speed (mm/s)	Spacing (mm)	
		Strong concrete	Weak concrete				
 P 1	10	60.93	33.23	20	30	20	15
 P 2	10	60.93	33.23	20	30	15	18
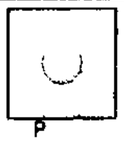 P 4	10	56.33	27.15	20	30	10	22
 RC 1	10	57.77	31.64	20	25	10	17
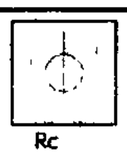 RC 3	10	49.80	30.23	20	25	10	16

Table 4.10 Pocket test results

For the purposes of rate test five slabs (P 1, P 2, P 4, RC 1, and RC 3) were used. A single excavation was performed in each slab to investigate the effect of constant nozzle offset, traverse speed, and spacing over concrete surfaces of varying compressive strength. All slabs were produced using 10 mm maximum size aggregate. Slab P 1 was excavated using a nozzle offset, traverse speed, and spacing of 20 mm, 30 mm/s, and 20 mm respectively. The compressive strength of strong concrete was 60.93 N/mm^2, while the compressive strength of weak concrete was 33.23 N/mm^2. An uneven excavation with traces of ridges was achieved. The edge definition was poor and the mean depth of

removal was approximately 15 mm with no significant increase over the weak area (pocket) of the slab. Slab P 2 was excavated using a nozzle offset, traverse speed, and spacing of 20 mm, 30 mm/s, and 15 mm respectively. The compressive strength of strong concrete was 60.93 N/mm^2, while the compressive strength of weak concrete was 33.23 N/mm^2. An uneven excavation with traces of ridges over the weak area of the slab was achieved. The edge definition was poor and the mean depth of removal was approximately 18 mm with no significant increase over the weak area of the slab. Slab P 4 was excavated using a nozzle offset, traverse speed, and spacing of 20 mm, 30 mm/s, and 10 mm respectively. The compressive strength of strong concrete was 56.33 N/mm^2, while the compressive strength of weak concrete was 27.15 N/mm^2. A uniform excavation without ridging was achieved. Good edge definition was achieved on three sides. The mean depth of removal was approximately 22 mm with no significant increase over the weak area of the slab. Slab RC 1 was excavated using a nozzle offset, traverse speed, and spacing of 20 mm, 25 mm/s, and 10 mm respectively. The compressive strength of strong concrete was 57.77 N/mm^2, while the compressive strength of weak concrete was 31.64 N/mm^2. A non-uniform and shallow excavation over the weak area and uniform over the surrounding stronger concrete without ridging was achieved. The reinforcing bars were partially exposed and good edge definition on three sides was achieved. The mean depth of removal was approximately 27 mm with no significant increase over the weak area of the slab. Slab RC 3 was excavated using the same settings for the nozzle offset, traverse speed and spacing as for slab RC 1. The compressive strength of strong concrete was 49.80 N/mm^2, while the compressive strength of weak concrete was 30.23 N/mm^2. A non-uniform and shallow excavation over the weak area and uniform over the surrounding stronger concrete without ridging was achieved. The reinforcing bars were partially exposed and good edge definition on

three sides was achieved. The mean depth of removal was approximately 16 mm with no significant increase over the weak area of the slab.

6) Varying rate test was performed to investigate the effect of varying traverse speed over concrete surfaces of varying compressive strength, while, nozzle offset and traverse spacing were kept constant. Two sets of tests were performed. The first set of tests was performed on small slabs (400x400x125 mm) while the second set of tests was performed on big slabs (1200x1200x150 mm). Experimental results are shown in Tables 4.11 and 4.12.

Ref	Specimen characteristics			Robot settings			Average depth of excavation (mm)
	Max size aggregate (mm)	Compressive strength (N/mm^2)		Nozzle offset (mm)	Traverse speed (mm/s)	Spacing (mm)	
		Strong concrete	Weak concrete				
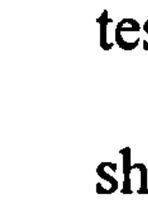 P 3	10	60.43	33.63	20	W area 40 S area 30	10	25
 P 5	10	56.33	27.15	20	W area 30 S area 20	10	23
P 6	10	56.33	27.15	20	W area 30 S area 20	10	20
 RC 2	10	57.77	31.64	20	W area 20 S area 40	10	24
 RC 4	10	50.20	31.28	20	W area 20 S area 40	10	24
 RC 5	10	50.20	31.28	20	W area 20 S area 40	10	22
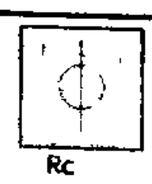 RC 6	10	64.17	45.97	20	W area 5 S area 40	10	N/A

Table 4.11 Varying rate test on small slabs

For the first set of tests seven small slabs (P 3, P 5, P 6, RC 2, RC 4, RC 5, and RC 6) were used. Each slab was excavated to investigate the effect of varying traverse speed over concrete surfaces of varying compressive strength. All slabs were produced using 10 mm maximum size aggregate. Nozzle offset of 20 mm and traverse spacing of 10 mm were used for all excavations. Slab P 3 was excavated using traverse speeds of 40 mm/s for the weak area and 30 mm/s for the strong area. The compressive strength of strong concrete was 60.43 N/mm^2, while, the compressive strength of weak concrete was 33.63 N/mm^2. A non-uniform excavation with no traces of ridges was achieved. The edge definition was good and the mean depth of removal was approximately 25 mm with no significant increase over the weak area of the slab. Slab P 5 was excavated using traverse speeds of 30 mm/s for the weak area and 20 mm/s for the strong area. The compressive strength of strong concrete was 56.33 N/mm^2, while, the compressive strength of weak concrete was 27.15 N/mm^2. A non-uniform excavation with no traces of ridges was achieved. The edge definition was good and the mean depth of removal was approximately 23 mm with no significant increase over the weak area of the slab. Slab P 6 was excavated using traverse speeds of 30 mm/s for the weak area and 20 mm/s for the strong area. The compressive strength of strong concrete was 56.33 N/mm^2, while, the compressive strength of weak concrete was 27.15 N/mm^2. A non-uniform excavation with no traces of ridges was achieved. The edge definition was good and the mean depth of removal was approximately 20 mm with no significant increase over the weak area of the slab. Slab RC 2 was excavated using traverse speeds of 20 mm/s for the weak area and 40 mm/s for the strong area. The compressive strength of strong concrete was 57.77 N/mm^2, while, the compressive strength of weak concrete was 31.64 N/mm^2. A non-uniform shallow excavation over the weak area and uniform over the surrounding stronger concrete without ridging was achieved. Good edge

definition was achieved on two sides and the reinforcing bars were partially exposed. The mean depth of removal was approximately 24 mm. Although, a significantly deeper excavation was expected over the weak area of the slab due to the significant difference in compressive strength and traverse speed this did not occur. Slab RC 4 was excavated using traverse speeds of 20 mm/s for the weak area and 40 mm/s for the strong area. The compressive strength of strong concrete was 50.20 N/mm^2, while, the compressive strength of weak concrete was 31.28 N/mm^2. A non-uniform shallow excavation over the weak area and uniform over the surrounding stronger concrete without ridging was achieved. Poor edge definition was achieved and the reinforcing bars were partially exposed. The mean depth of removal was approximately 24 mm. Although, a significantly deeper excavation was expected over the weak area of the slab due to the significant difference in compressive strength and traverse speed this did not occur. Slab RC 5 was excavated using the same traverse speed settings as for slabs RC 2 and RC 4. The compressive strength of strong concrete was 50.20 N/mm^2, while, the compressive strength of weak concrete was 31.28 N/mm^2. A non-uniform shallow excavation over the weak area and uniform over the surrounding stronger concrete without ridging was achieved. Good edge definition was achieved and the reinforcing bars were partially exposed. The mean depth of removal was approximately 22 mm. Although, a significantly deeper excavation was expected over the weak area of the slab due to the significant difference in compressive strength and traverse speed this did not occur. Finally, slab RC 6 was excavated using traverse speeds of 5 mm/s for the weak area and 40 mm/s for the strong area. The compressive strength of strong concrete was 64.17 N/mm^2, while, the compressive strength of weak concrete was 45.97 N/mm^2. A considerably deeper excavation over the weak area compared to the surrounding

stronger concrete without ridging was achieved. Good edge definition was achieved on three sides and the reinforcing bars were fully exposed.

Ref.	Compressive strength		Robot operating parameters			Average removal depth	
	Strong concrete	Weak concrete	Nozzle offset (mm)	Traverse speed (mm/s)	Spacing (mm)	Strong concrete	Weak concrete
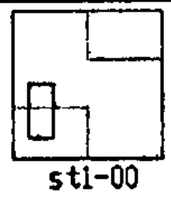 ST 1-00	66.00	26.40	20	W area 5 S area 5	10	29	45
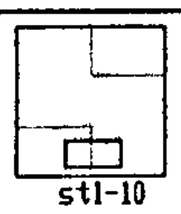 ST 1-10	66.00	26.40	20	W area 5 S area 5	10	21	61
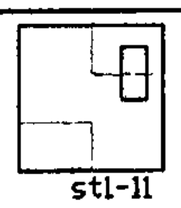 ST 1-11	66.00	26.40	20	W area 10 S area 5	10	18	37
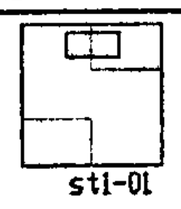 ST 1-01	66.00	26.40	20	W area 10 S area 5	10	27	51
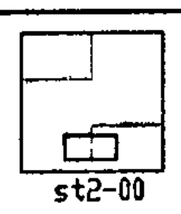 ST 2-00	52.00	36.30	20	W area 15 S area 5	10	18	17
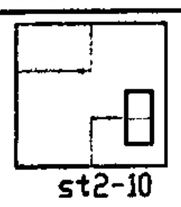 ST 2-10	52.00	36.30	20	W area 15 S area 4	10	23	20
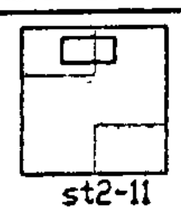 ST 2-11	52.00	36.30	20	W area 10 S area 3	10	25	27
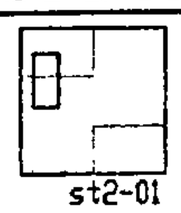 ST 2-01	52.00	36.30	20	W area 7 S area 2	10	37	28

Table 4.12 Varying rate test results on big slabs

For the second set of tests two big slabs (ST 1 and ST 2) were used. Each slab was excavated in four different positions to investigate the effect of varying traverse speed

over concrete surfaces of varying compressive strength. Each test position was comprised of two concrete surfaces with considerable difference in compressive strength. All slabs were produced using 10 mm maximum size aggregate. Nozzle offset of 20 mm and traverse spacing of 10 mm were used for all excavations. Slab ST 1 was excavated in ST 1-00, ST 1-10, ST 1-11, and ST 1-01 positions. The compressive strength of the strong area was 66 N/mm^2 and the compressive strength of the weak area was 26.40 N/mm^2. Position ST 1-00 was excavated using a traverse speed of 5 mm/s for both strong and weak areas. A good quality uniform excavation without ridging over both strong and weak areas was achieved. The edge definition was good on all four sides and the removal depth was considerably higher over the weaker area. Position ST 1-10 was excavated using the same traverse speed settings as for ST 1-00. Same results as for ST 1-00 were achieved. Position ST 1-11 was excavated using a traverse speed of 5 mm/s for the strong area and 10 mm/s for the weak area. A good quality uniform excavation without ridging over both strong and weak areas was achieved. The edge definition was good on all four sides and the removal depth was higher over the weaker area. Position ST 1-01 was excavated using the same traverse speed settings as for ST 1-11. Same results as for ST 1-11 were achieved. Slab ST 2 was excavated in ST 2-00, ST 2-10, ST 2-11, and ST 2-01 positions. The compressive strength of the strong area was 52.00 N/mm^2 and the compressive strength of the weak area was 36.30 N/mm^2. Position ST 2-00 was excavated using a traverse speed of 5 mm/s for the strong area and 15 mm/s for the weak area. A good quality excavation without ridging over both strong and weak areas was achieved. The edge definition was good on all four sides and the removal depth was approximately equal over both strength areas. Position ST 2-10 was excavated using a traverse speed of 4 mm/s for the strong area and 15 mm/s for the weak area. Similar results as for position ST 2-10 were achieved. Position ST 2-11 was

excavated using a traverse speed of 3 mm/s for the strong area and 10 mm/s for the weak area. Similar results as for positions ST 2-00 and ST 2-10 were achieved. Position ST 2-01 was excavated using a traverse speed of 2 mm/s for the strong area and 7 mm/s for the weak area. Similar results as for positions ST 2-00, ST 2-10, and ST 2-11 were achieved.

Based on the above results a traverse speed ratio of 1/2 to 1/3.5 can be used to achieve a uniform depth excavation over strong and weak concrete.

7) Pressure test was performed to investigate the effect of different operating water pressures on the rate of removal. Experimental results are shown in Table 4.13 and Figure 4.11

Pressure (bar)	Volume of excavation (ml)	Time of excavation (s)	Rate of removal (ml/min)
1600	620	256	145
1800	750	289	156
2000	800	283	170

Table 4.13 Pressure test results

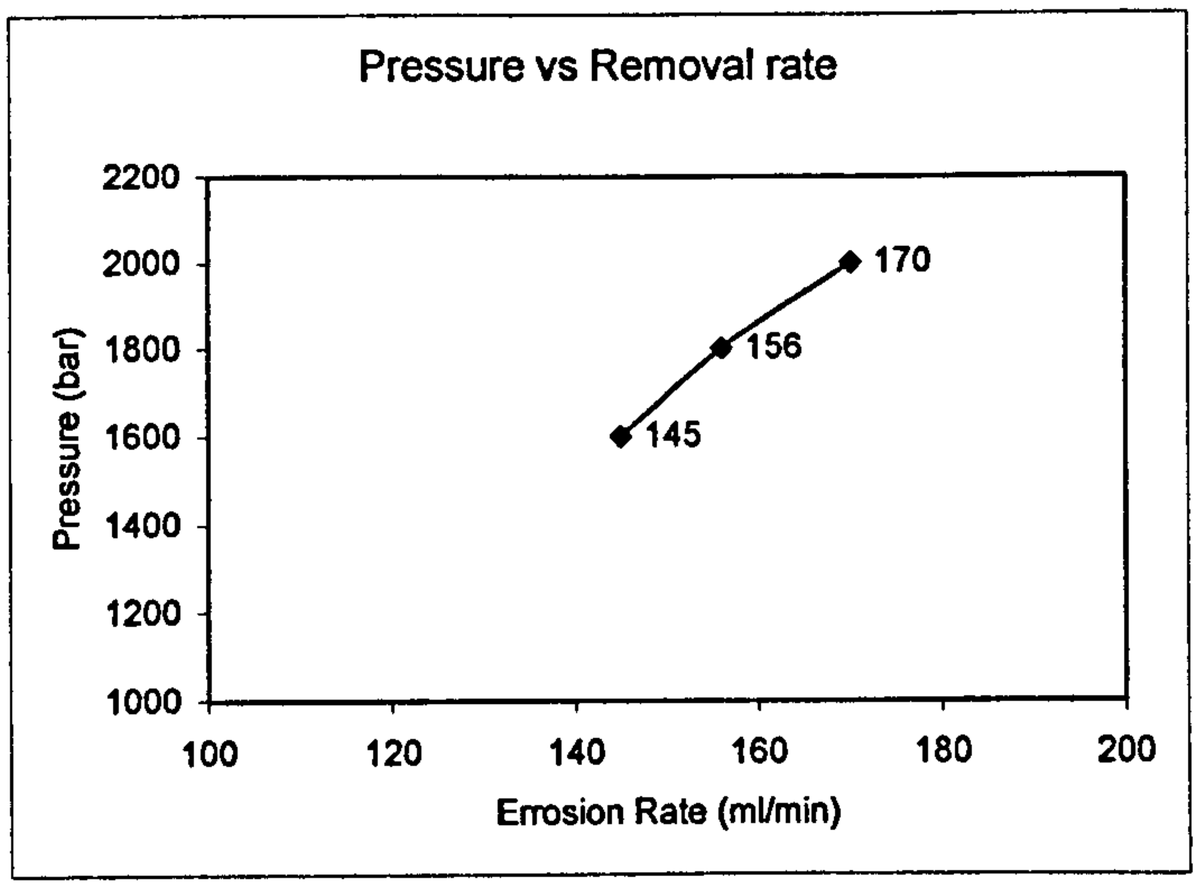

Figure 4.11 Pressure versus removal rate

Three excavations were performed using different operating water pressures. The first excavation was performed using an operational water pressure of 1600 bar. The volume of concrete removed was 620 ml and the time of excavation was 256 s resulting in a removal rate of 145 ml/min. The second excavation was performed using an operational water pressure of 1800 bar. The volume of concrete removed was 750 ml and the time of excavation was 289 s resulting in a removal rate of 156 ml/min. The third excavation was performed using an operational water pressure of 2000 bar. The volume of concrete removed was 800 ml and the time of excavation was 283 s resulting in a removal rate of 170 ml/min. From the above results it is obvious that as the water pressure increases the removal rate increases. However, the selection of the appropriate water pressure should take into account the running costs and load imposed on the pressure generating unit.

Pictures of all excavations performed are shown in **Appendix 4** while, graphs of the topographies of the excavated areas obtained using the laser equipment are shown in **Appendix 5.**

4.3 CONCLUSION

Seven different types of tests (Nozzle offset, exposure, path, rate, pocket, varying rate, and pressure tests) were performed to investigate the various parameters influencing the quality and quantity of remote robotic hydroerosion. Nozzle offset test was performed to investigate the effect that stand off distance has on the depth of penetration of the water jet. Results indicated that a stand off distance of 20 mm should be used that optimises water jet depth penetration and does not cause significant over break of concrete. Exposure test was performed to investigate the effect that traverse speed has on the amount of concrete removed. Results indicated that the optimum traverse speed should be between 20-35 mm/s. Path test was performed to investigate the optimum

traverse spacing for slabs with different maximum size aggregate (10 mm and 20 mm). Results indicated that for traverse spacing between 10-15 mm good quality uniform excavation without ridging at a mean removal depth of 25 mm can be achieved. However, when the traverse spacing is increased to 30-35 mm the excavation is shallow and non-uniform. In addition, ridging is clearly visible. Rate test was performed to investigate the effect of fixed nozzle offset, traverse speed, and spacing over slabs with different compressive strengths. Results indicated a slight increase in removal depth when the compressive strength is decreased. Pocket test was performed to investigate the effect of fixed nozzle offset, traverse speed, and spacing over concrete surfaces of varying compressive strength. Results were inconclusive. They did not produce greater removal depths over weak pocket areas as it was expected. Varying rate test was performed to investigate the effect of varying traverse speed over concrete surfaces of varying compressive strength, while, nozzle offset and traverse spacing were kept constant. Results indicated that is possible to achieve the same removal depth over both strong and weak areas of a concrete surface by using 2 different traverse speeds over strong and weak areas. For this purpose, a traverse speed ratio of 1/2 to 1/3.5 should be used over strong and weak concrete. Finally, pressure test was performed to investigate the effect of different operating water pressures on the rate of removal. Results clearly indicated an increase on the removal rate when the operating pressure is increased. Table 4.14 summarises all the experimental results of remote robotic hydroerosion investigation.

Type of test	Purpose	Outcome
Nozzle offset test	Investigate the effect that stand off distance has on the depth of penetration of the water jet	A stand off distance of 20 mm should be used that optimises water jet depth penetration and does not cause significant over break of concrete
Exposure test	Investigate the effect that traverse speed has on the amount of concrete removed	A traverse speed between 20-35 mm/s should be used which produces a good edge definition and a removal depth between 22-25 mm
Path test	Investigate the optimum traverse spacing for slabs with different maximum size aggregate (10 mm and 20 mm)	A traverse spacing between 10-15 mm should be used which is able to produce good quality uniform excavations without ridging at a mean removal depth of 25 mm
Rate test	Investigate the effect of fixed nozzle offset, traverse speed, and spacing over slabs with different compressive strength values	A slight increase in removal depth can be achieved over areas of weak or defective concrete
Pocket test	Investigate the effect of fixed nozzle offset, traverse speed, and spacing over concrete surfaces of varying compressive strength	Inconclusive
Varying rate test	Investigate the effect of varying traverse speed over concrete surfaces of varying compressive strength, while, nozzle offset and traverse spacing were kept constant	A uniform depth excavation over both strong and weak concrete areas can be achieved by using 2 different traverse speeds over strong and weak areas. The above result can be achieved by using a traverse speed ratio of 1/2 to 1/3.5 over strong and weak concrete
Pressure test	Investigate the effect of different operating water pressures on the rate of removal	A clear increase on the removal rate can be achieved by increasing the water pressure

Table 4.14 Summary of remote robotic hydroerosion experimental results

CHAPTER 5

ASPECTS OF SURFACE ROUGHNESS

5.1 INTRODUCTION

The success and long-term durability of every patch repair scheme is significantly influenced by the adhesive strength developed at the bonding interface between the concrete substrate and the repair material. In turn, the adhesive strength is significantly influenced by the roughness of the concrete substrate surface. In general, the rougher the substrate surface the higher the adhesive strength. However, different concrete removal methods tend to produce substrate surfaces with significantly different roughness values. Hence, the ability of measuring and characterising the roughness of substrate concrete surfaces is of great importance for evaluating different removal methods. The objective of this chapter is to justify and choose the best method for concrete substrate surface characterisation. For this reason, a review of the relatively small number of methods developed in the past for measuring and characterising the surface of concrete substrates prior to repair is made.

5.2 PROPERTIES THAT INFLUENCE SURFACE TOPOGRAPHY

Surface topography has a different meaning to different people. Many disciplines such as: physics, chemistry, tribology, metrology, manufacturing, mechanical and civil engineering are related to or have influence on surface topography. According to Griffiths[32] the topography of a surface is influenced by the following three properties:

- Roughness
- Waviness
- Form

Roughness is directly related to the generating mechanism and describes the irregularities caused by each grit, particle, or spark. Roughness can be divided into two categories: the roughness related to the generating mechanism and the micro-roughness caused by disturbances within each generating mechanism.

Waviness is related to the texture upon which the roughness is superimposed and as such is less related to the generating mechanism itself. Waviness is usually caused by workpiece or machine deflection

Form is related more to the workpiece or machine tool and is concerned with large deviations.

In practice, Roughness, waviness and form are never separate but superimposed on top of each other.

5.3 SURFACE TOPOGRAPHY MEASUREMENT METHODS APPLIED TO VARIOUS DISCIPLINES

According to ANSI[33] the methods for measuring and characterising surface topography can be classified into three types:

- Contacting methods
- Tape sectioning
- Non-contacting or optical methods

A review of contacting methods and tape sectioning is given by Thomas[34], whereas Maerz[35] provides a review of optical methods.

Among the contacting methods, stylus type profilometers provide precise measurements along a linear traverse. In most cases the vertical deflection of the stylus

is recorded as a function of position. Other contacting methods include tactile tests, measurement of static friction, measurement of kinetic friction, use of rolling ball measurements, and measurement of the compliance of a metal sphere with a rough surface.

Taper sectioning is used in metallurgy and is based on cutting across a surface at a low angle α to physically amplify the height of roughness by $\cot\alpha$.

Optical methods include optical reflecting instruments, light microscopy, electron microscopy, speckle metrology, interferometry, and laser profilometry. Light microscopy is based on employing a light microscope that illuminates a rough surface with a thin slit of light at an angle of 45^0. The surface is observed at an angle of 90^0 from the direction of illumination. The projected slit appears as a straight line if the surface is flat and as a progressively more undulating line as the roughness of the surface increases. Electron microscopy is based on employing a scanning electron microscope (SEM) that uses a focused beam of electrons to record the surface. The sample to be measured has to be conducting and placed in a vacuum chamber. Electrons are then counted bouncing back onto a sensor that then translates the count into intensity for that position. The sample is then scanned and the acquired image is displayed by the SEM raster. Although the resolution of the image can be increased it is not possible to measure depths on the surface using electron microscopy. Hence, electron microscopy produces a high-resolution photograph of the surface, which can be used for feature detection. However, depth measurements can be obtained using the stereo pairs technique, where two photo-micrographs are taken of the same area at different angles and compared. Interferometry is based on employing the vertical scanning interferometer (VSI) that makes use of interference fringes produced when monochromatic or laser light is reflected off a rough surface and a flat reference surface.

The fringes are contours of roughness of about one-half the wavelength of the light used. Thus, the method is suitable only to surfaces with small amplitude roughness.

5.4 SURFACE TOPOGRAPHY CHARACTERISATION PARAMETERS APPLIED TO THE FIELD OF CONCRETE REPAIR

Once a satisfactory profile of the surface topography is obtained, it can be analysed and represented using a variety of methods. Unfortunately there is no universal number, parameter or descriptor that can be used to analyse and represent the topography of a surface. A large number of 2D and 3D roughness parameters have been developed to characterise the topography of a surface for various processes and applications. Predev[36] provides a review of the various 2D parameters, whereas Griffiths[32] reviews both 2D and 3D parameters

5.4.1 2D Roughness parameters

The range of 2D parameters calculated from a trace may be represented using the formula:

$$\text{Parameter} = T_{nN} \tag{5.1}$$

where:

T represents the scale of the parameter. When parameters are calculated from an unfiltered trace, the designation P is used instead of T. After filtering, depending upon the sample length chosen, the parameters calculated are given the designation R for roughness or W for waviness.

n represents the parameter suffix, that denotes the type calculated. For example a is average, q is root mean square (RMS), sk is skew etc.

N represents which of the five sample lengths the parameter is related. For example the RMS value of the third sample is Rq3

According to Griffiths[32] the 2D parameters calculated from a trace can be divided into 6 groups that describe various attributes of the topography. These are:

- Amplitude parameters, which are simply related to heights and/or depths of the topography
- Amplitude distribution parameters, which are related to the amplitude distribution function, bearing area curve or cumulative distribution function that describes its shape
- Slope parameters, which are related to the differential heights
- Spatial parameters, which are related to the longitudinal spacing of features
- Other parameters, which for example combine amplitude and spacing
- Motif parameters, which are based on the characteristic shapes

ISO 4287[37], ISO 13565: Part 2[38] and ISO 12085[39] describe 14, 5 and 3 2D parameters, respectively.

In order to study the effect of surface roughness on the adhesive strength, 2D parameters which describe the ability of surfaces to promote mechanical interlocking between concrete substrates and repair materials should be chosen and evaluated. Based on the above criterion, 2D parameters which according to Griffiths[32], Predev[36] and Maertz et al[40] seem to be important for mechanical interlocking are shown in Table 5.1.

2D roughness parameters		
Parameter		Description
RΔq	Root mean square slope ISO 4287[37]	$R\Delta q = \sqrt{\frac{1}{L}\int_0^L \left(\frac{dy(x)}{dx}\right)^2 dx} = \sqrt{\frac{1}{L}\sum_{n=1}^{N}(y_{n+1}-y_n)^2}$ (5.2) Root mean square of the ordinate slopes dy/dx within the sampling length
RΔa	Center line average slope	$R\Delta a = \frac{1}{L}\int_0^L \left\lvert\frac{dy(x)}{dx}\right\rvert dx = \frac{1}{L}\sum_{n=1}^{N}\lvert y_{n+1}-y_n\rvert$ (5.3)
Lo	Actual profile length	$Lo = \int_0^L \sqrt{1+\left[\frac{dy(x)}{dx}\right]^2} dx = \sum_{n=1}^{N}\sqrt{\left(\frac{L}{N}\right)^2+(y_{n+1}-y_n)^2}$ (5.4)
Lr	Profile length ratio	$Lr = \frac{Lo}{L}$ (5.5)

Table 5.1 2D roughness parameters which provide a measure of the ability of a surface to promote mechanical interlocking

Both RΔq and RΔa are important for properties such as mechanical interlocking. A surface with high RΔq and RΔa values can provide better mechanical interlocking compared to a surface with low RΔq and RΔa values. Lo is the actual profile length and is important in properties such as mechanical interlocking. A surface with high peaks and deep valleys would have a higher Lo compared to a surface with low peaks and shallow valleys. Lo is not an ISO parameter. Lr is the profile length ratio and is equal to the actual profile length Lo divided by the horizontal component of the profile L. For most surfaces used in engineering Lr is close to 1 and typically less than 1.01.

5.4.2 3D Roughness parameters

In many cases, the parameters determined from a single 2D trace are not able to define the topography of a surface satisfactory because surfaces interact in three dimensions and not two.

The range of 3D parameters calculated from a trace may be represented using the formula:

Parameter = T_n (5.6)

where:

T T represents the scale of the parameter. Since all 3D parameters are related to area the designation S is used instead of T.

n n represents the parameter suffix, which denotes the type calculated. For example a is average, q is root mean square (RMS), sk is skew etc.

According to Griffiths[32] 3D parameters can be divided into 5 groups that describe various attributes of the topography. These are:

- Area height parameters
- Height distribution parameters
- Spatial parameters
- Hybrid parameters
- Functional parameters

Stout et al[41] and Standsurf et al[42] describe 14 and 3 parameters respectively.

In order to study the effect of surface roughness on the adhesive strength, 3D parameters which describe the ability of surfaces to promote mechanical interlocking between concrete substrates and repair materials should be chosen and evaluated. Based on the above criterion, 3D parameters which according to Griffiths[32] seem to be important for mechanical interlocking are shown in Table 5.2.

3D ROUGHNESS PARAMETERS		
Parameter		Description
SΔq	RMS slope Stout et al[41]	$S\Delta q = \sqrt{\frac{1}{(M-1)(N-1)}\sum_{j=1}^{N}\sum_{i=1}^{M}\rho_{ij}}$ (5.7) where: $\rho_{ij} = \left[\left(\frac{\partial \eta(x,y)}{\partial x}\right)^2 + \left(\frac{\partial \eta(x,y)}{\partial y}\right)^2\right]^{0.5}_{x=xi,y=yj}$ (5.8)
Ssc	Mean summit curvature Stout et al[41]	$Ssc = \frac{1}{2}\frac{1}{n}\sum_{k=1}^{n}\left[\frac{\partial \eta^2(x,y)}{\partial x^2} + \frac{\partial \eta^2(x,y)}{\partial y^2}\right]_{\text{for any summit}}$ (5.9)
Sdr	Developed interfacial area ratio Stout et al[41]	$Sdr = \frac{\sum_{n=1}^{N-1}\sum_{m=1}^{M-1}A_{mn} - (M-1)(N-1)\Delta x\,\Delta y}{(M-1)(N-1)\Delta x\,\Delta y}100\%$ (5.10)

Table 5.2 3D roughness parameters which provide a measure of the ability of a surface to promote mechanical interlocking

SΔq and Sdr are the 3D equivalents of the 2D RΔq and Lr. Both SΔq and Sdr like their 2D equivalent RΔq and Lr are important for properties such as mechanical interlocking. A surface with high SΔq and Sdr can provide better mechanical interlocking compared to a surface with low SΔq and Sdr values.

5.5 MEASUREMENT AND CHARACTERISATION OF SURFACE TOPOGRAPHY IN THE FIELD OF CONCRETE REPAIR

In the field of concrete repair, the term surface roughness can be used to describe the topography of the concrete substrate surface prior to repair. The overall success and long-term durability of a concrete patch repair is highly depended upon the interface bond between the concrete substrate and the repair material. Interface bond consists of mechanical interlocking and adhesion. The effect of mechanical interlocking is determined by the surface roughness of the concrete substrate, whereas, adhesion is produced by the development of chemical bonds between the paste of the repair

material and the cured concrete substrate. Hence, adhesion is influenced by the variables that normally influence paste-aggregate bond. Although, adhesion develops as the repair material cures, the contribution of mechanical interlocking stays the same. However, improved surface roughness results in improved mechanical interlocking which in turn increases the interface bond. Hence, in a case of a rougher surface, more area is available for the paste to adhere and mechanical interlocking significantly increases the capacity of the bond interface as can be seen in Figure 5.1 adopted from Delatte et al[43].

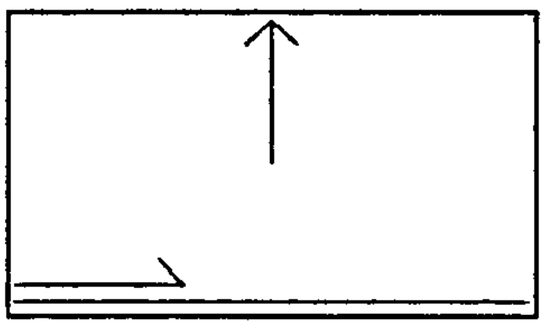

a) Shear and tensile stresses

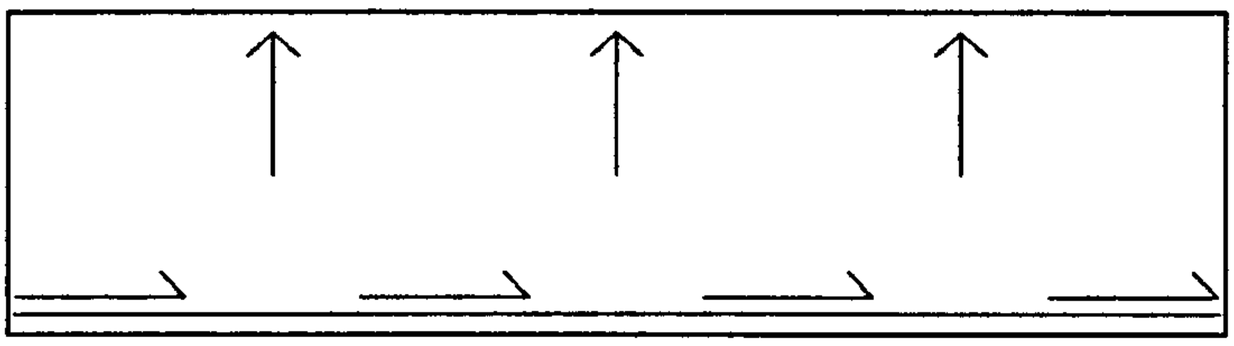

b) Smooth surface

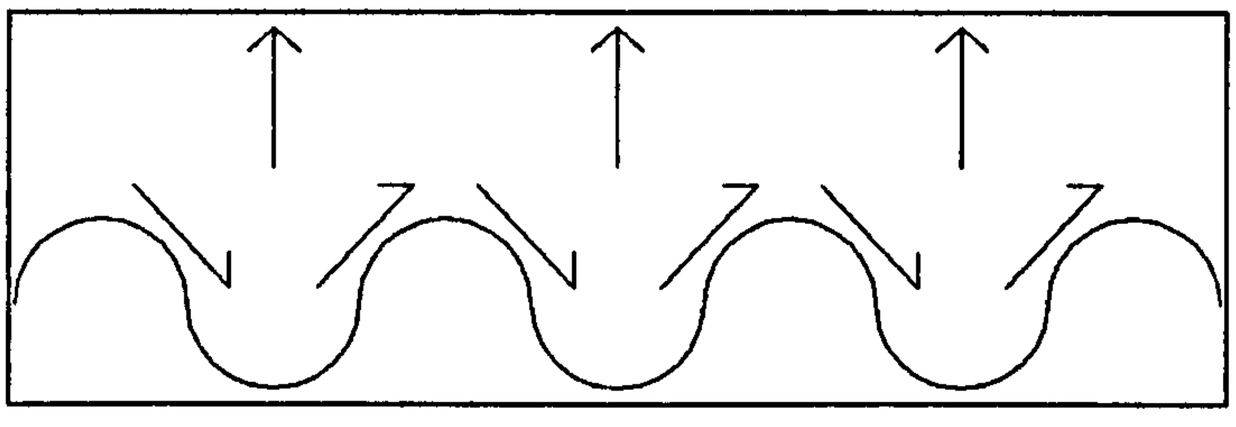

c) Rough surface

Figure 5.1 Effect of surface roughness on bond adopted from Dellate et al[43]

In order to study the influence of surface roughness on the bond between concrete substrate and the repair material, the surface roughness needs to be measured and characterised. However, in the field of concrete repair, with the exception of the sand area method proposed in prBS EN 1504: Part 10[44] no standard method for measuring

and characterising the roughness of concrete substrates prior to repair has been adopted. A schematic of sand area method is shown in Figure 5.2. The method is based on measuring the mean peak-to-valley height R expressed in mm of a horizontal surface. For this purpose 50 cm^3 of dry quartz sand with a grain size of 0.2-0.5 mm are distributed in a circular configuration on the test surface, in such a way that the indentations are just filled. Next, the mean of three measured diameters taken in different positions across the circular area covered by the sand is obtained. The mean diameter d is also known as Surface Roughness Index (SRI). The lower the SRI the higher the roughness of the surface. Finally, the mean peak-to-valley height R is defined as the height of an imaginary cylinder with diameter d and sand volume V and is obtained from the following formula:

$$R = \frac{4V}{\pi d^2} \text{ (mm)} \qquad (5.11)$$

where:

V is the volume of the dry quartz sand equal to 50 cm^3 or 5000 mm^3

d is the mean diameter of the circular area in mm

The higher the mean peak-to-valley height R the higher the roughness of the surface.

Sand area method is quick and very simple to perform on site. However, it is a very crude method. In addition, it can only be used on horizontal surfaces.

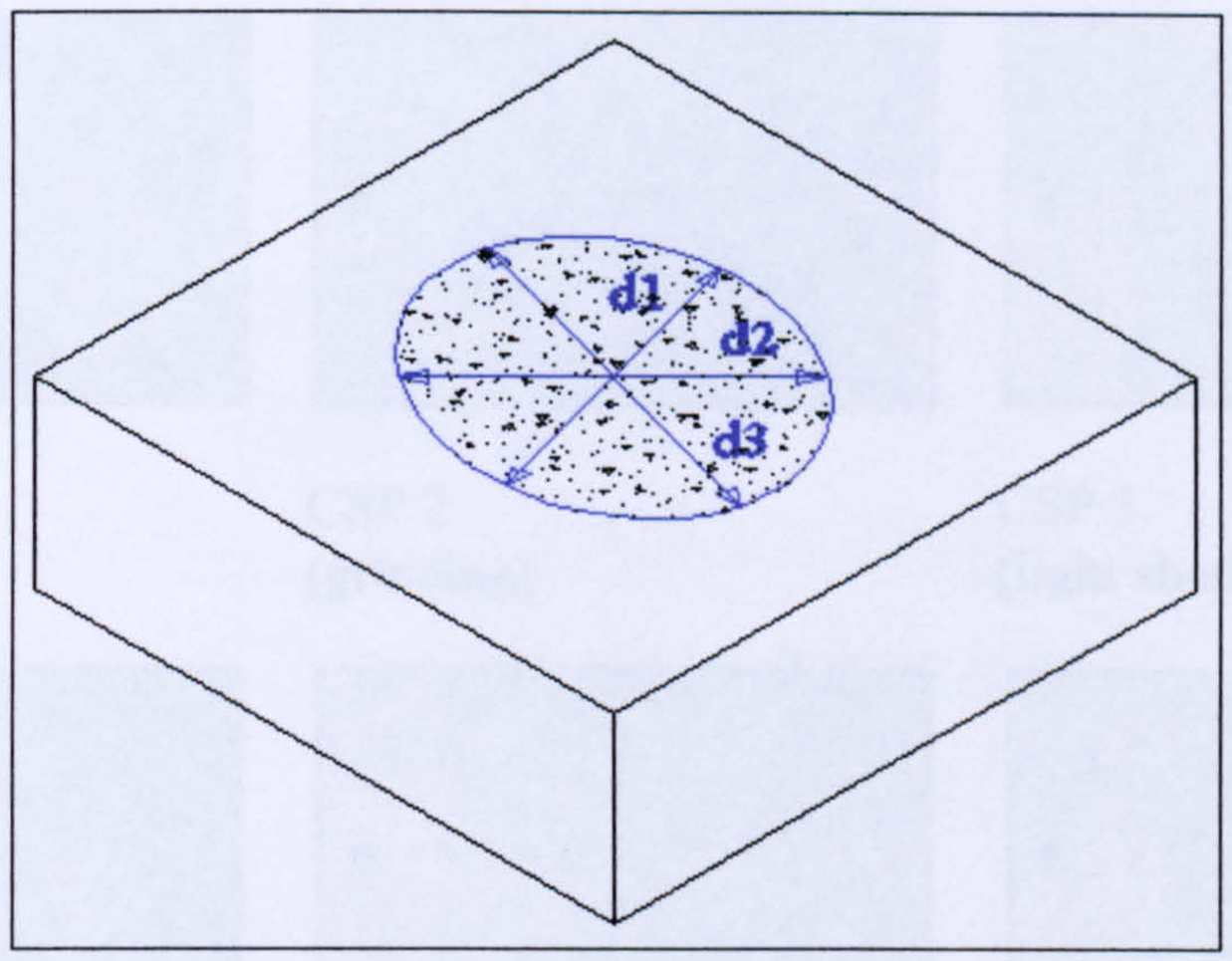

Figure 5.2 Schematic of sand area method

The surface roughness of concrete substrates can be characterised by comparing them to Concrete Surface Profiles (CSP) in the form of 9 plastic model surfaces produced by ICRI[45]. These profiles replicate different levels of surface roughness obtained using different methods of concrete removal. Each profile carries a CSP number ranging from a base line of CSP 1 (nearly flat) through CSP 9 (very rough). CSP models are shown in Figure 5.3, while, a guide for selecting repair materials based on the type of surface roughness of the concrete substrate is shown in Table 5.3 adopted from ICRI[45]

CSP 1
(acid etched)

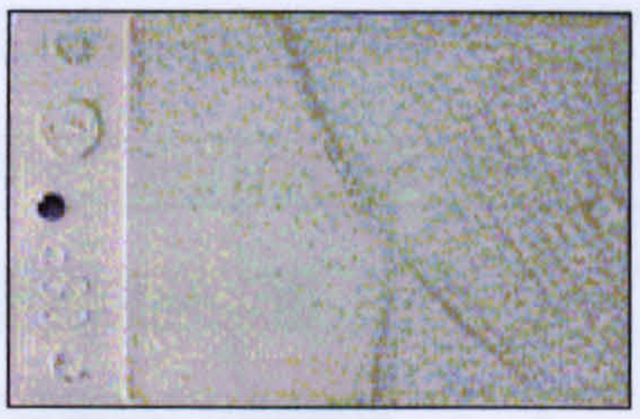

CSP 2
(grinding)

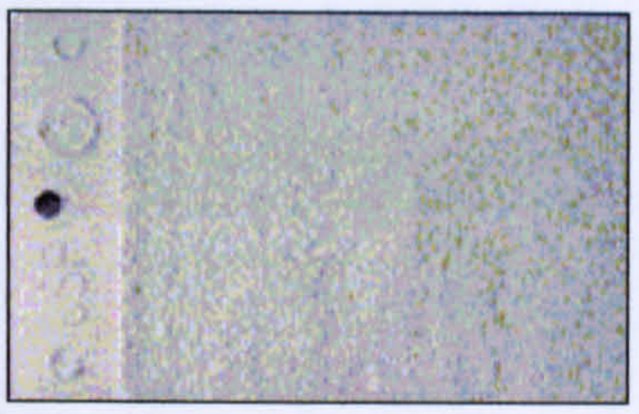

CSP 3
(light shotblast)

CSP 4
(light scarification)

CSP 5
(medium shotblast)

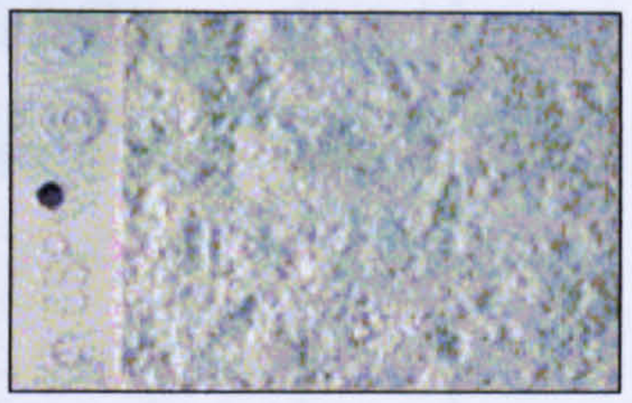

CSP 6
(medium scarification)

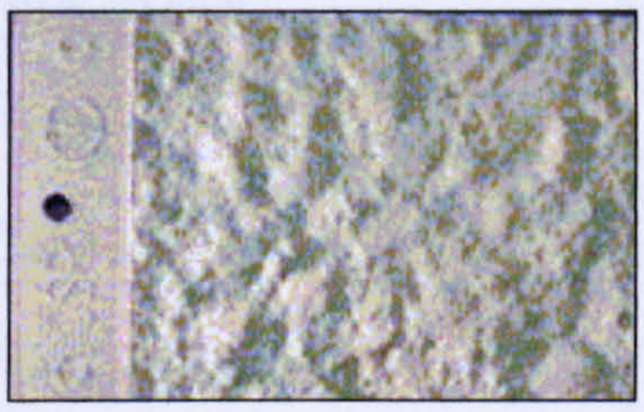

CSP 7
(heavy abrasive blast)

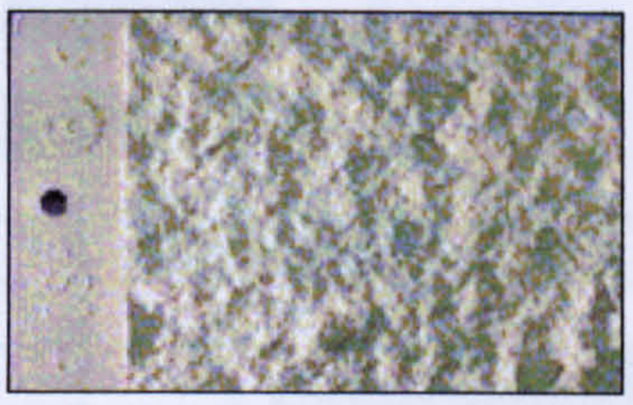

CSP 8
(scabbled)

CSP 9
(heavy scarification)

Figure 5.3 Concrete surface profiles adopted from ICRI[45]

	Concrete surface profile								
Coating to be applied	CSP 1	CSP 2	CSP 3	CSP 4	CSP 5	CSP 6	CSP 7	CSP 8	CSP 9
Sealers 0-75 μm	■	■							
Thin-Film 0.1-0.25 mm	■	■	■						
High-Build 0.25-1 mm			■	■	■				
Self-Levelling 1.25-3 mm				■	■	■			
Polymer Overlay 3-6 mm					■	■	■	■	■
Preparation methods	CSP 1	CSP 2	CSP 3	CSP 4	CSP 5	CSP 6	CSP 7	CSP 8	CSP 9
Detergent scrubbing	■								
Low-pressure water cleaning	■								
Acid etching		■	■						
Grinding		■	■						
Sand blasting			■	■	■				
Steel shotblasting			■	■	■	■	■	■	
Scarifying				■	■	■	■	■	
Needle scaling					■	■	■		
High-pressure water jetting						■	■	■	■
Scabbling							■	■	■
Flame blasting								■	■
Milling/rotomilling									■

Table 5.3 Guide for characterising concrete substrates produced using different removal methods and selecting appropriate types of repair materials adopted from ICRI[45]

A number of methods are available for measuring and characterising the surface texture of concrete pavements in the field of highway engineering, but no method is accepted as standard. Holt and Musgrove[46] provide a review of these methods.

Fiebrich[47] tried to characterise surface roughness by the ratio between the surface occupied by aggregate and the cement paste, while, Vaneevelt[48] by the maximum depth. Silfwerbrand[49] proposed a different method for measuring and characterising surface roughness in his study of strength and behaviour of concrete bridge decks. For this purpose automatic laser profilometry equipment was developed. The method is based on transforming the measured surface profile to a saw-toothed curve as shown in Figure 5.4.

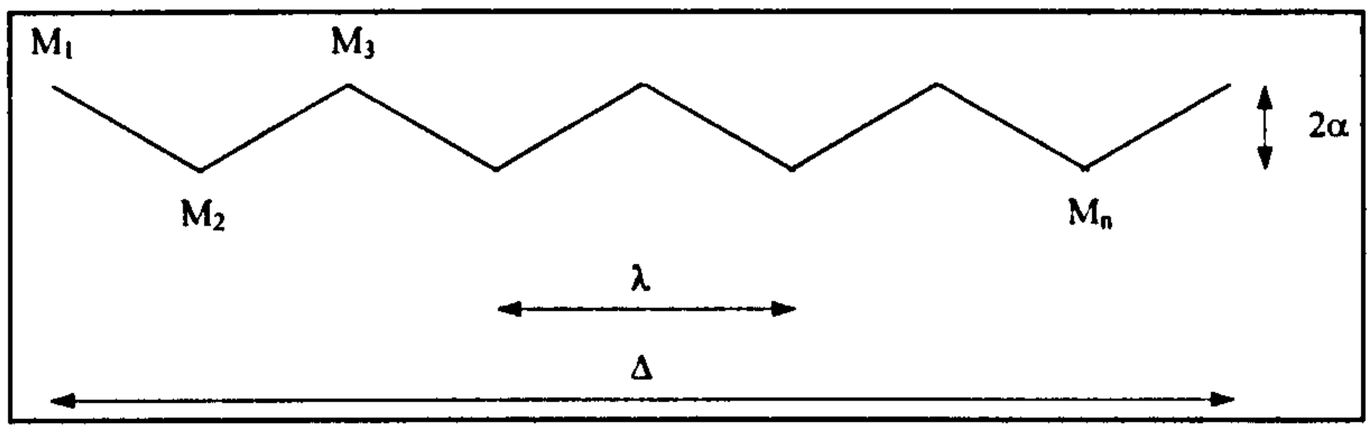

Figure 5.4 Diagram modelling of a roughness profile used by Silfwerbrand[49] for evaluating surface roughness

The wavelength λ and the double amplitude 2α are defined as the surface roughness parameters and are then determined for different values of the distance Δ between consecutive measuring points using the following expressions:

$$2\alpha = \left[\sum_{j=1}^{n-1} |M_{j+1} - M_j|\right] \frac{1}{n-1} \tag{5.12}$$

$$\lambda = \frac{2\Delta}{n-1} = \frac{2[x(M_n) - x(M_1)]}{n-1} \tag{5.13}$$

where:

$M_1, M_2, M_3, \ldots, Mn$	are the (n) extreme values (maximum and minimum values) of the concrete surface
$x(M_n)$	is the extreme point in the longitudinal position
$\Delta = x(M_n) - x(M_1)$	is the distance between first and last extreme points

Based on his results, Silfwerbrand showed that 2α is dependent on the treatment of the surface. However, neither 2α nor α/Δ are independent of Δ. In addition, any sudden or individual drop in the surface that might be caused by a displaced piece of aggregate can distort the values of 2α.

Abu-Tair et al[50] used a 2D profile texture meter to measure and characterise surface roughness. Their 2D profile texture meter consisted of 500 needles spaced 1 mm apart, each 0.8 mm in diameter. The needles were allowed to drop freely to the surface to be measured and thus take up its profile. A photograph was then taken of the profile formed. By enlarging the photograph, readings were obtained which defined the texture depth of concrete samples. Based on their results they suggested an improved method for measuring and characterising surface roughness. In their method the profile of the surface is treated as a series of irregular waves with each wave having its own wavelength and maximum and minimum amplitude. By calculating the values of the double amplitude 2α for each wave a definition of the surface roughness is obtained. If points A, B, C, D and E shown in Figure 5.5 adopted from Abu-Tair et al[50] represent the maximum and minimum heights of the measured surface, then for the wave W_1 the average double amplitude is given by the expression:

$$D_a = \frac{[(A-B)+(C-B)]}{2} \tag{5.14}$$

By dividing the average double amplitude by the wave length W, a better definition of the roughness of the surface can be obtained, since as D_a increases the surface is considered to be rougher and as W increases the surface is considered to be less rough. By averaging the values of D_a for all waves, it is possible to obtain a parameter known as roughness gradient and which defines the roughness more accurately.

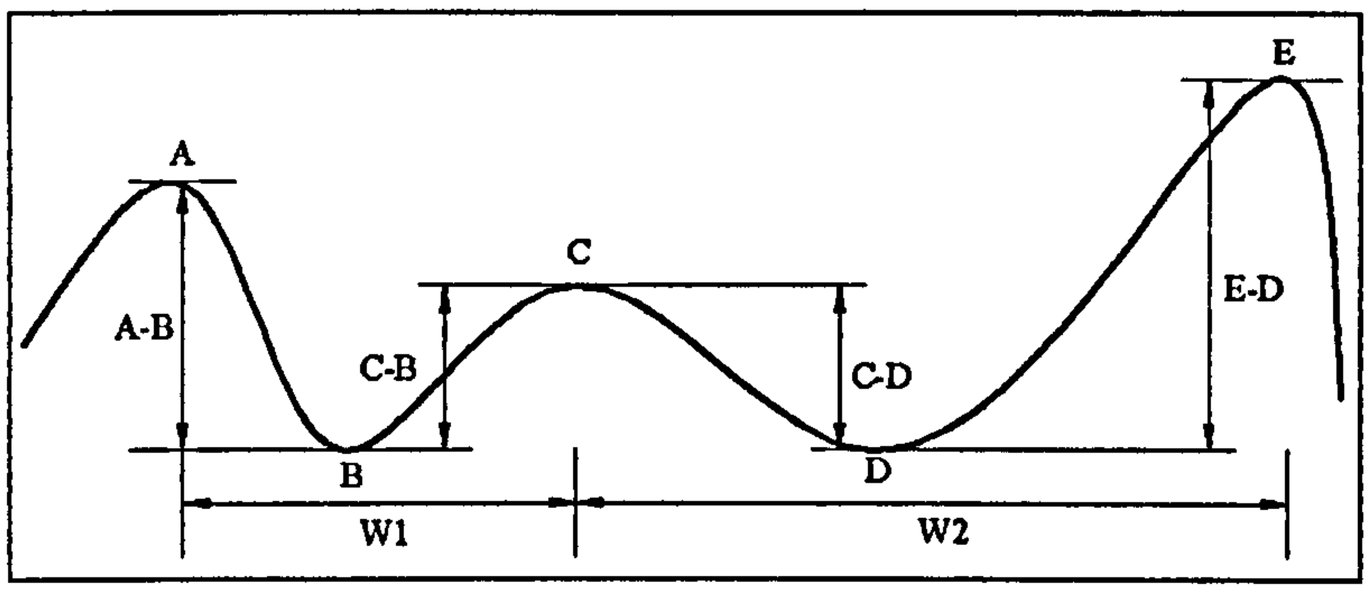

Figure 5.5 Diagram modelling of a roughness profile used by Abu-Tair et al[50] for evaluating surface roughness

Maerz et al[40] developed laser profilometry equipment to measure and characterise the surface roughness of concrete substrates prior to FRP laminate application. The development of the equipment was based on the principles of Schmaltz microscope and the method of shadow profilometry, that uses a laser profiling line rather than a linear beam of light or shadow edge. This method is also known as laser striping. Maerz et al[40] used a striping laser with eleven stripes to illuminate the surface of the concrete substrate at an angle of 45^0. The surface was observed at an angle of 90^0 from the direction of illumination using a high-resolution camera as shown in Figure 5.6 adopted from Maerz et al[40]. The projected slit of light appeared as a straight line if the surface was flat, and as a progressively more undulating line as the roughness of the surface increased. Classical image analysis techniques were employed to transform the image of the laser stripes into a series of eleven profiles in x-y plane. Each profile was then characterised by determining RΔa parameter. Measurements on slab specimens prepared using different levels of sandblasting (progressively increasing the roughness by increasing the duration of sandblasting) confirmed the ability of laser striping to measure the roughness as well as the ability of parameter RΔa to accurately characterise the roughness.

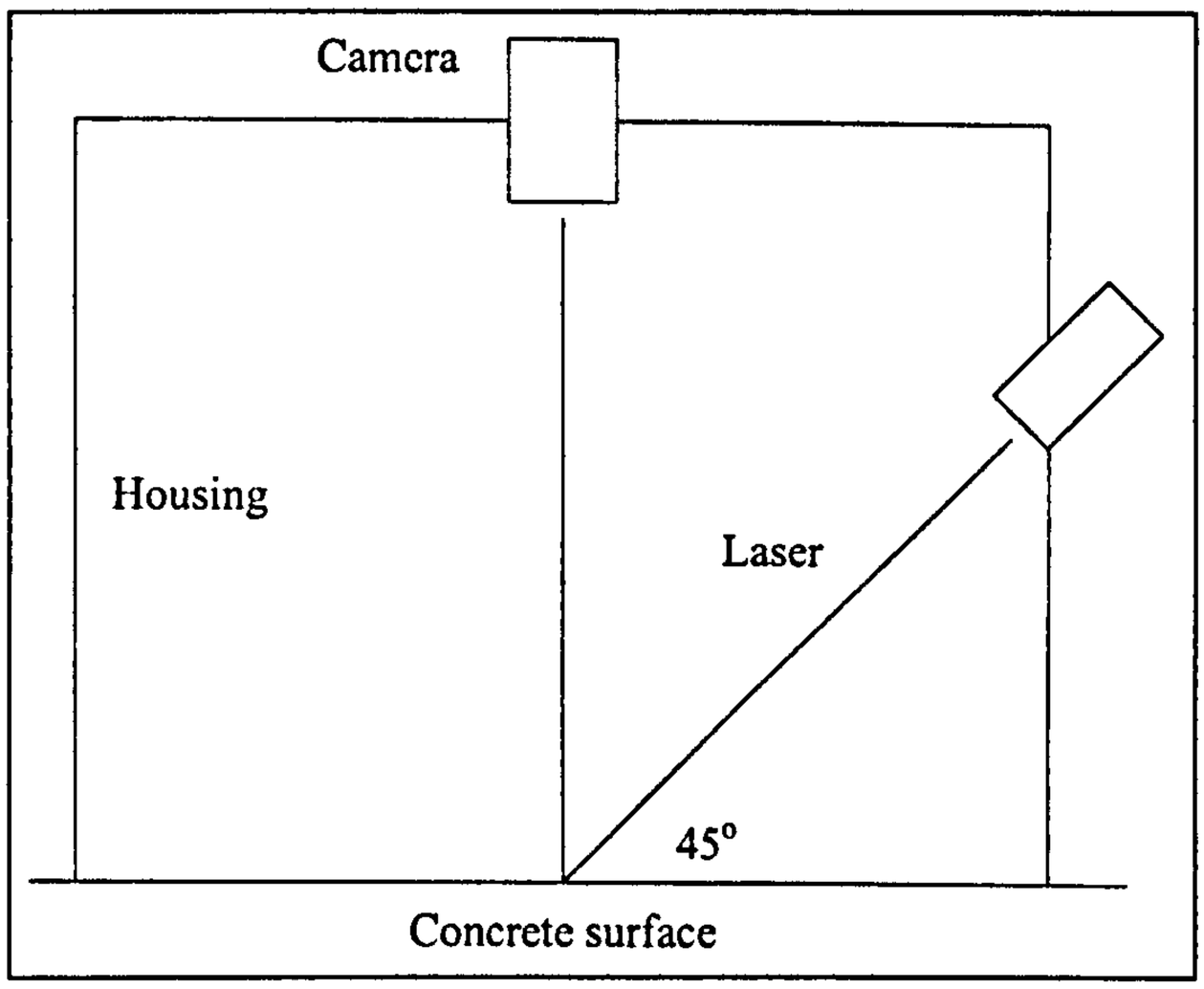

Figure 5.6 Schematic of laser striping method adopted from Maerz et al[40]

A 3D interferometric fringe-based imaging system for surface profiling, positioning and control for space applications was developed by ESA[51]. The method is similar to the one developed by Maerz et al[40] and belongs to a group of techniques known as phase measurement interferometry.

The method is based on using projected fringes having cosine intensity profiles. The pattern of the projected fringe on the surface of an object can then be analysed to find the co-ordinates of points on the surface. The fringes can be produced either by using a suitable mask in a conventional projector or, as in this system, by projecting interference fringes. The aim of using projected fringes, instead of a scanning spot or line, is that data for all points in an image plane can be captured simultaneously, hence reducing the required image acquisition time. The measuring system consists of a fringe projector, a camera, a control system for the laser diode, and a computer for processing the data. A schematic of the system is shown in Figure 5.7 adopted from ESA[51]. The fringe projector illuminates the surface of the object under investigation with a set of vertical interference fringes within an illumination cone as shown in Figure 6.7 adopted

from ESA[51] and the camera captures images of the surface as a set of points $P_1 \ldots P_N$ (where $N \leq$ number of available camera pixels). During measurement the fringe projector, object and camera remain stationary. The fringes have approximately equal angular separation and can be adjusted in phase and spatial frequency by the system. By adjusting the fringes capture of several images of the object with different fringe-phase settings can be achieved. The captured images are then processed to produce a complete fringe-phase map of those parts of the surface which are both illuminated by the projector and visible to the camera. The fringe-phase map is then processed together with details of the system geometry to produce a set of co-ordinates for each point on the surface.

Phase measurements produce wrapped-phase maps consisting of values within a repeating 2π range. These phase maps are then unwrapped to produce the correct phase relationship between all points in the map together with the absolute-phase values. Unwrapping is performed by making a series of 2π corrections to the phase values at the 2π discontinuities in the map to produce a continuous phase surface. Finally, geometric calculations transform the absolute fringe-phase values into 3-dimensional co-ordinates. Figure 5.8 adopted from ESA[51] summarises the various stages involved in the processing of the phase-stepped images

The co-ordinates of the system are shown in Figure 5.9 adopted from ESA[51]. SS′ is the axis of the fringe projector and corresponds to zero fringe-phase. All the projected fringes are assumed to lie on one side of the fringe projector, making all values of θ_S positive. θ_S can be found from the absolute phase Φ and the known angular separation of the fringes. CC′ is the axis of the camera and coincides with the z-axis of the co-ordinate system. θ_X can take both positive and negative values. The camera and the fringe projector are separated by a distance D along the x-axis. θ_A is the angle between

the axis of the fringe projector and the axis of the camera. As it can be seen in Figure 5.9 adopted from ESA[51] knowledge of the angles θ_S, θ_X, and θ_Y allows calculation of the x, y, and z co-ordinates of point P, provided that the fixed parameters of the system geometry are known.

Two software modules (data acquisition module and data processing module) are used to perform all control and data processing activities. Data acquisition module is responsible for controlling the camera, image averaging and phase stepping of the fringe projector. A set of images is then stored for processing. Data processing module is responsible for taking the set of images and performing all necessary calculations to produce the x, y, and z co-ordinates of the surface points.

The data processing can be divided into two areas. These are:

- Phase calculations involving the phase step, fringe-phase and calibration stages
- Geometric calculations, that transform the absolute fringe-phase values into 3-dimensional co-ordinates

The output x, y, and z co-ordinates are finally stored as data files for further use.

The software used is based on a Windows 2000 platform with Visual Basic and MathCAD programmes responsible for system hardware control, image capture and processing. In addition ASCI based commands are used to control the camera.

Finally, the main sources of error include:

- System geometry errors
- Fringe-phase measurement errors
- Fringe-order errors
- Invalid data errors

Sources of system geometry errors include measurement and setting up errors such as the separation distance between the projector and the camera as well as the projector axis to camera axis angle, which result in scaling and distortion errors in the surface geometry calculation.

Fringe-phase measurement is influenced by the characteristics of the projected fringes and the captured images. Hence, phase step errors in the projector and drift of ambient illumination during a measurement reduce the accuracy of phase measurement.

Fringe-order errors contribute to noise in the calculated co-ordinates. If the errors are quite large, then the system is not able to identify the fringe-order in a reliable way resulting in a series of $\pm 2\pi$ errors in the absolute phase values and the analysis breaks down. The magnitude of error required to cause the break down in the analysis is closely related to the number of the fringes projected onto the object. As the number of projected fringes is increased, the system becomes more vulnerable to phase errors. However, when the density of the projected fringes is increased, the potential resolution of the system is improved. Hence, the number of projected fringes is ideally set just bellow the value at which fringe-order errors occur.

When the fringe-phase and phase-step can not be calculated for a pixel element, then the data is not valid and can be removed. There are two possible reasons for this error:

- An image may contain regions that are not illuminated by the fringe-projector. Within these regions, pixel values do not vary between frames.
- Any pixels that receive light from more than one part of the object are likely to give inaccurate phase values. This event can take place when such pixels lie on a discontinuity in the surface image. Errors caused due to this reason, will be localised to the affected pixels and this data can be rejected if necessary.

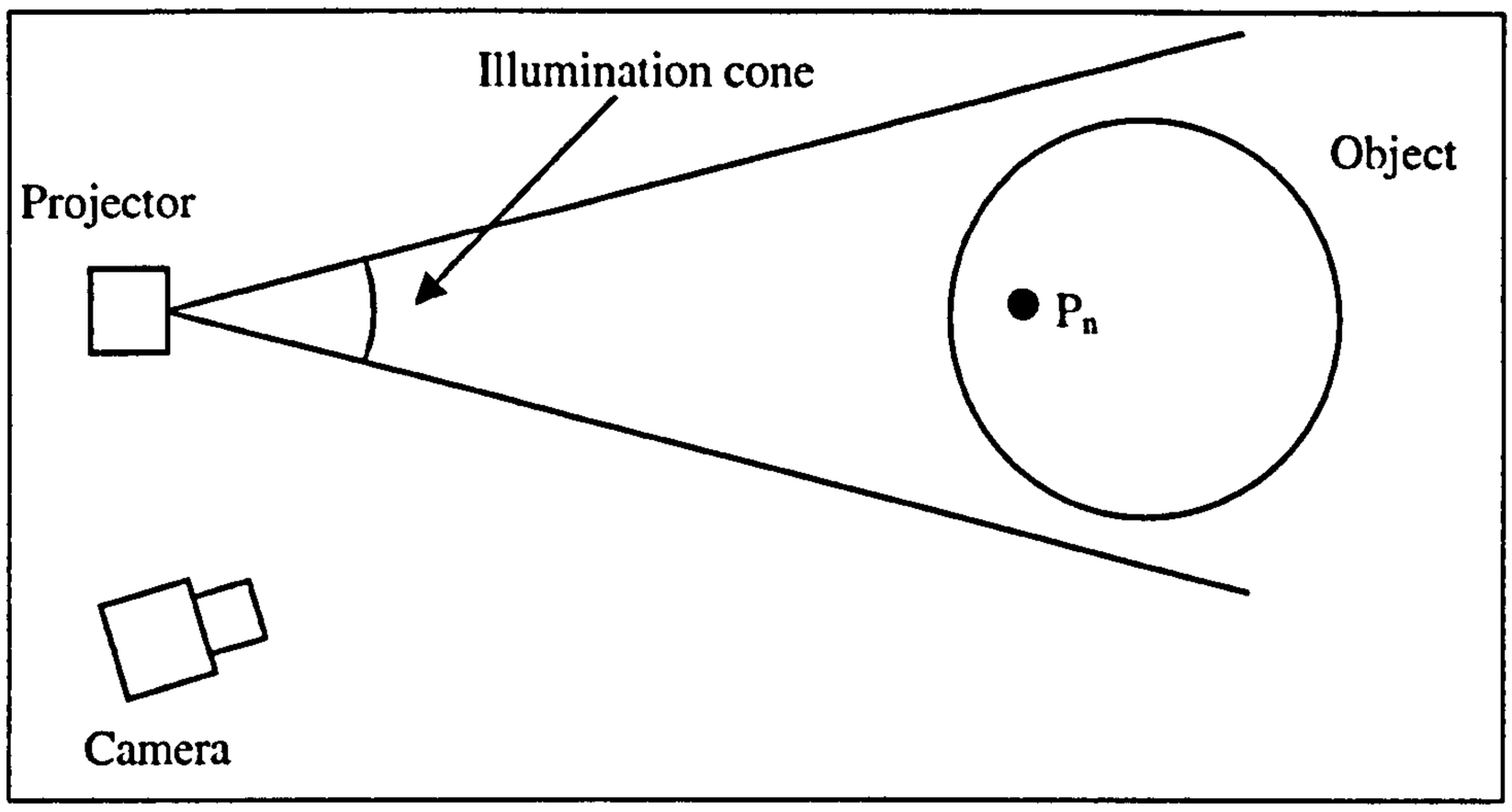

Figure 5.7 Schematic of 3D interferometric fringe-based laser imaging system developed by ESA[51]

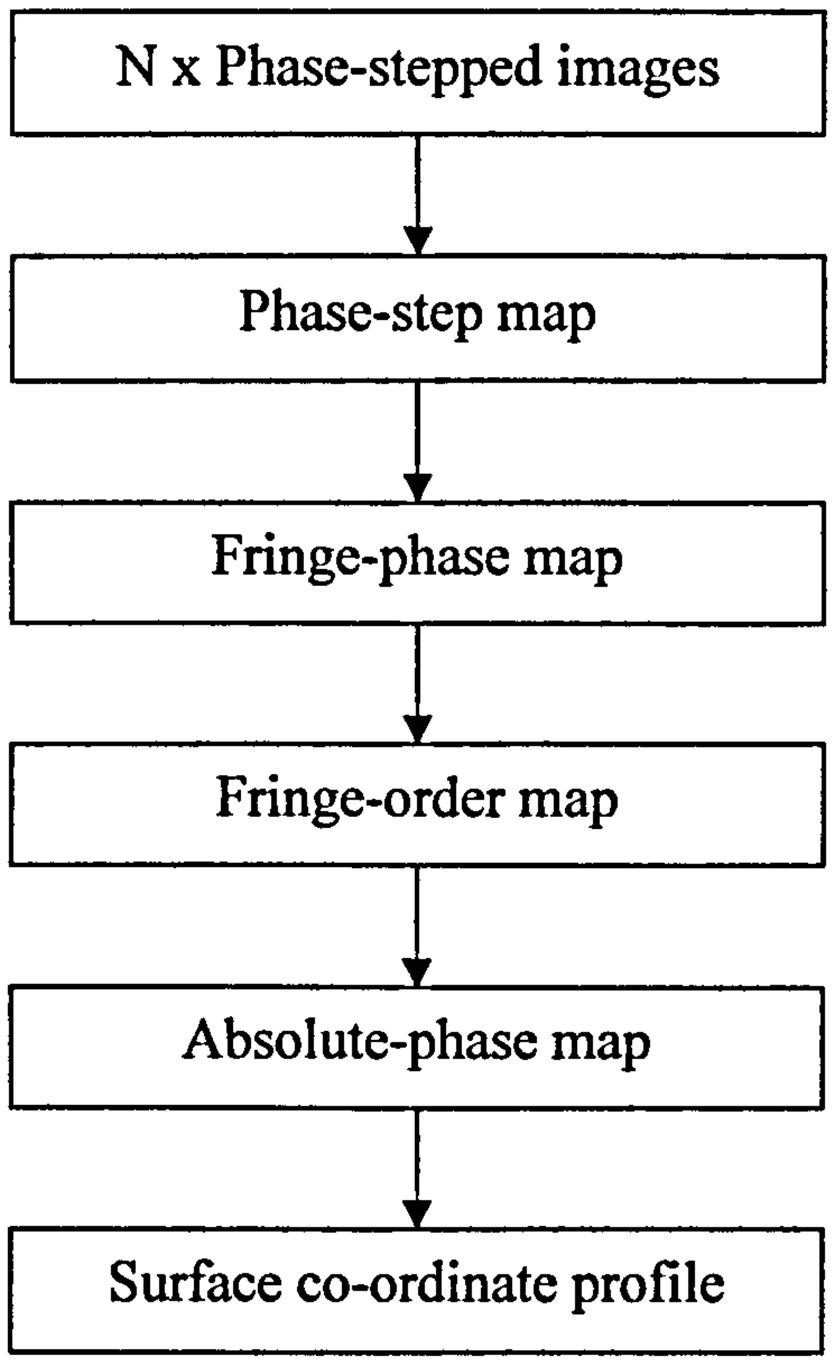

Figure 5.8 Summary of the various stages involved in the processing of the phase-stepped images adopted from ESA[51]

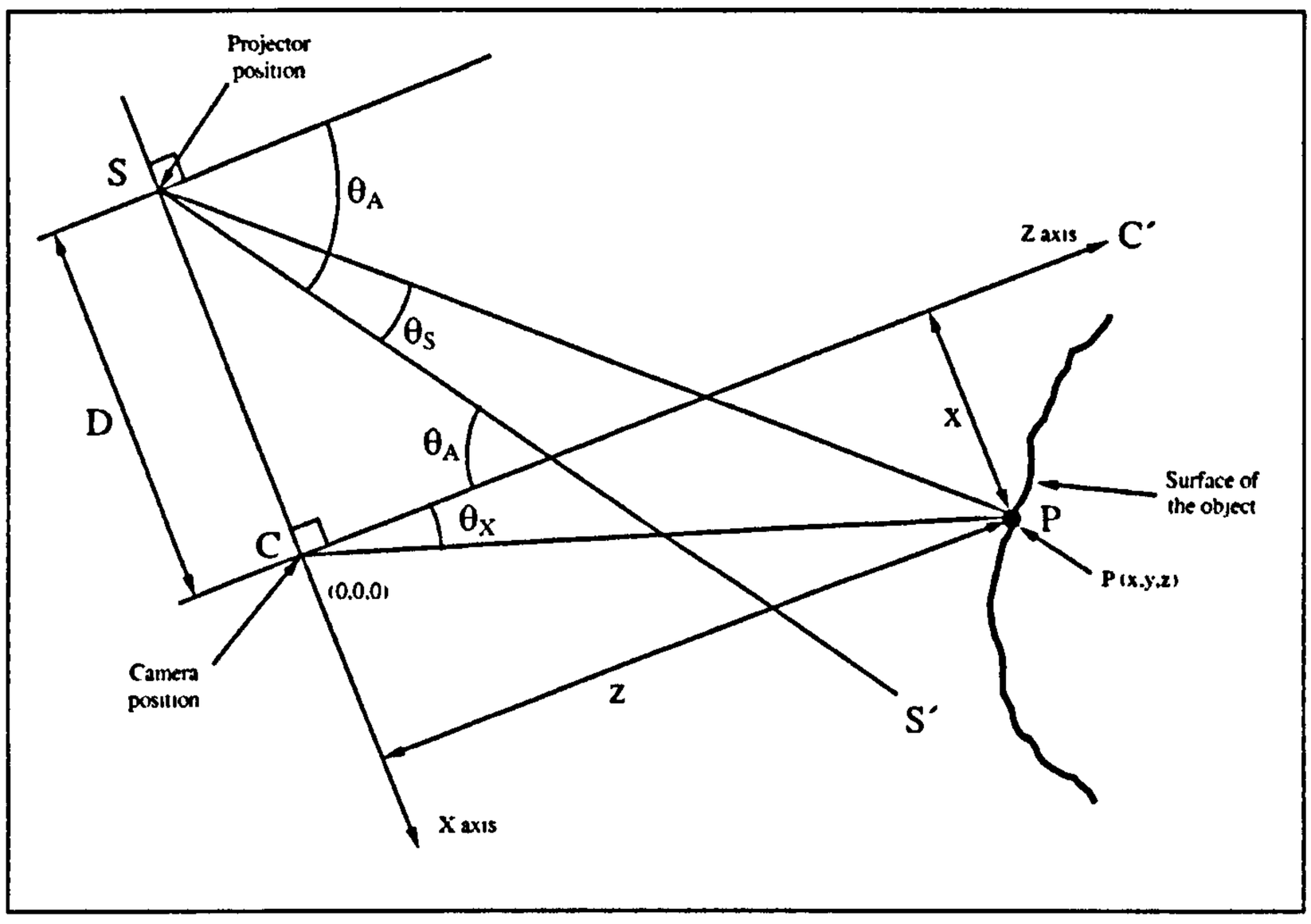

Figure 5.9 Optical system geometry adopted from ESA[51]

5.6 CONCLUSION

In this chapter, a review of the relatively small number of methods developed in the past for measuring and characterising the surface of concrete substrates prior to repair was carried out. From the methods reviewed sand area and fringe based laser interferometry are selected for subsequent use in this research. Selection of sand area method is based on the fact that is quick, easy to perform and is the only method that is about to be standardised. By using sand area method, SRI and Rmean roughness parameters can be determined. However, sand area method is very crude and it can only be used on horizontal surfaces. In order to overcome the above disadvantages, state of the art fringe based laser interferometry will be employed. By using fringe based laser interferometry, a very accurate 3D image of the surface under investigation can be produced. Based on the coordinates of the above 3D image, 2D roughness parameters RΔq, RΔa, Lo and Lr can be evaluated. In addition, 2a and Da/W parameters proposed by Silfwerbrand[49] and Abu-Tair[50] can also be evaluated.

CHAPTER 6

MEASUREMENT AND CHARACTERISATION OF CONCRETE SUBSTRATE SURFACES

6.1 INTRODUCTION

In chapter 5 the effect of surface roughness on the mechanical interlocking and adhesive strength between concrete substrates and repair materials was reviewed. In addition, a review of the relatively small number of methods developed for measuring and characterising surface roughness in the field of concrete repair was carried out. The objective of this chapter is to determine if concrete substrate surfaces produced using pneumatic chipping hammers and remote robotic hydroerosion have different surface roughness classification values. For this reason 2 different methods (sand area method and 3D fringe-based laser interferometry method) are employed for measuring and characterising the surface roughness of concrete substrate specimens produced using the above 2 methods of concrete removal. Selection of sand area method is based on the fact that is quick, easy to perform and is the only method to become standardised, whereas selection of fringe-based laser interferometry method is based on its ability to provide a very accurate 3D image of the surface being investigated. Using sand area method SRI and Rmean roughness parameters will be evaluated, whereas using fringe-based laser interferometry 6 2D roughness parameters (2α, Da/W, RΔa, RΔq, Lo and Lr) will be evaluated on both X and Y axis.

6.2 ROUGHNESS MEASUREMENT AND CHARACTERISATION PROGRAM

6.2.1 Production of concrete substrate surfaces

Forty-eight concrete slab specimens with dimensions of 400x400x110 mm were produced in four groups. Each group had a different w/c ratio and consisted of twelve slabs cast in six different mixes. In total twenty-four mixes were produced. Two slabs and six cubes with dimensions of 100x100x100 mm were produced from each mix. The w/c ratios of groups 1, 2, 3 and 4 were 0.4, 0.45, 0.50 and 0.55 respectively. The specimens were produced using Lafarge Blue Circle OPC CEM-I 42.5 N conforming to BS EN 197 Part 1[30]. Sharp sand with maximum coarse size of 5 mm was used as fine aggregate. River gravel with maximum coarse size of 10 mm was used as coarse aggregate. The mix design of the specimens was based on the guidelines of BRE[31]. The specimens were cast in timber moulds and compacted using a vibrating table. After the concrete had set, the moulds were covered with damp rags. Twenty-four hours after casting the specimens were demoulded and placed in water. After six days in water, the specimens were air-cured in a storage room for 21 days. The storage room temperature was 19 ^{0}C at 50 to 60% relative humidity. Next, a layer of approximately 25-30 mm was removed from the surface of the slabs using a KANGO Type 950 electric hammer which simulated the action of pneumatic chipping hammers used in the construction industry. In addition, to the above slab specimens twelve specimens that were previously used for hydroerosion experiments were used for measuring and characterising surface roughness as well as for pull-off testing. Details of slab specimens produced using the electric hammer are shown in Table 6.1, whereas, specimens produced using hydroerosion are shown in Table 6.2. A view of all specimens is shown in Figure 6.1

Slab group	Mix number	Slab number	Maximum coarse size aggregate (mm)	w/c
1	1	S1	10	0.40
		S2		
	2	S3	10	
		S4		
	3	S5	10	
		S6		
	4	S7	10	
		S8		
	5	S9	10	
		S10		
	6	S11	10	
		S12		
2	7	S13	10	0.45
		S14		
	8	S15	10	
		S16		
	9	S17	10	
		S18		
	10	S19	10	
		S20		
	11	S21	10	
		S22		
	12	S23	10	
		S24		
3	13	S25	10	0.50
		S26		
	14	S27	10	
		S28		
	15	S29	10	
		S30		
	16	S31	10	
		S32		
	17	S33	10	
		S34		
	18	S35	10	
		S36		
4	19	S37	10	0.55
		S38		
	20	S39	10	
		S40		
	21	S41	10	
		S42		
	22	S43	10	
		S44		
	23	S45	10	
		S46		
	24	S47	10	
		S48		

Table 6.1 Details of slab specimens produced using KANGO Type 950 electric hammer

Reference	Max coarse size aggregate (mm)
PL2	10
PL5	20
PL6	20
PL9	10
PL10	10
PL11	10
PL13	10
PL14	10
PL15	10
PL16	10
P1	10
P5	10

Table 6.2 Details of slab specimens produced using remote robotic hydroerosion

Figure 6.1 View of slab substrate specimens produced using either KANGO Type 950 electric hammer or hydroerosion

6.2.2 Sand area method measurements

Initially, an attempt was made to measure and characterise the surface of substrate specimens using the sand area method proposed by prBS EN 1504: Part 10[44] and described in Chapter 5. Surfaces produced using both KANGO Type 950 electric hammer and remote robotic hydroerosion were measured and characterised as shown in Figure 6.2. SRImean and Rmean roughness parameters were measured. Both SRImean and Rmean were calculated as the mean of three measurements from three different circular sand areas distributed across the substrate surface. SRImean and Rmean results are shown in Figures 6.3 and 6.4 respectively. A complete presentation of all measurements is given in **Appendix 6**. For surfaces produced using electric hammer, SRImean values were found to be between 91-111 mm, whereas, Rmean values varied between 5.563-7.691 mm. In the case of slabs produced using remote robotic hydroderosion, SRImean values were found to be between 79-92 mm, whereas, Rmean values varied between 7.525-10.205 mm. Although, measurements clearly indicated that surfaces obtained using hydroerosion had higher roughness compared to those obtained using the electric hammer, the method is crude and not very accurate. Hence, it can only be used as a rough guide for measuring and characterising horizontal surfaces.

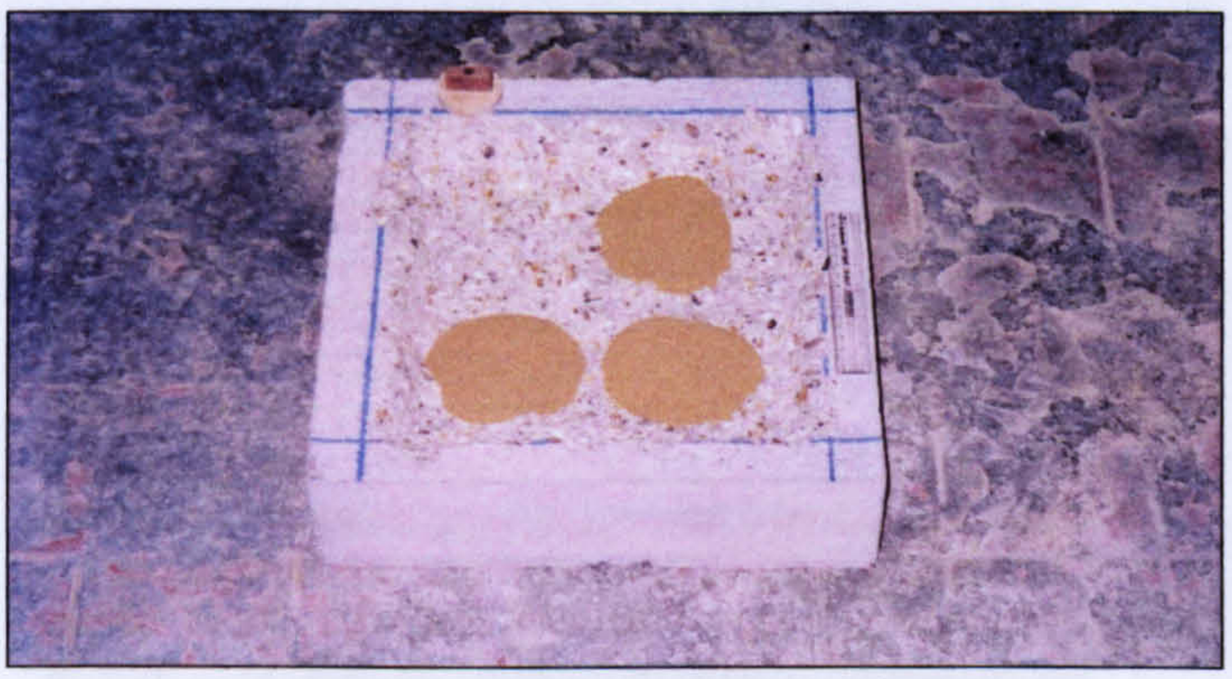

Figure 6.2 Roughness measurement of slab specimen using sand area method

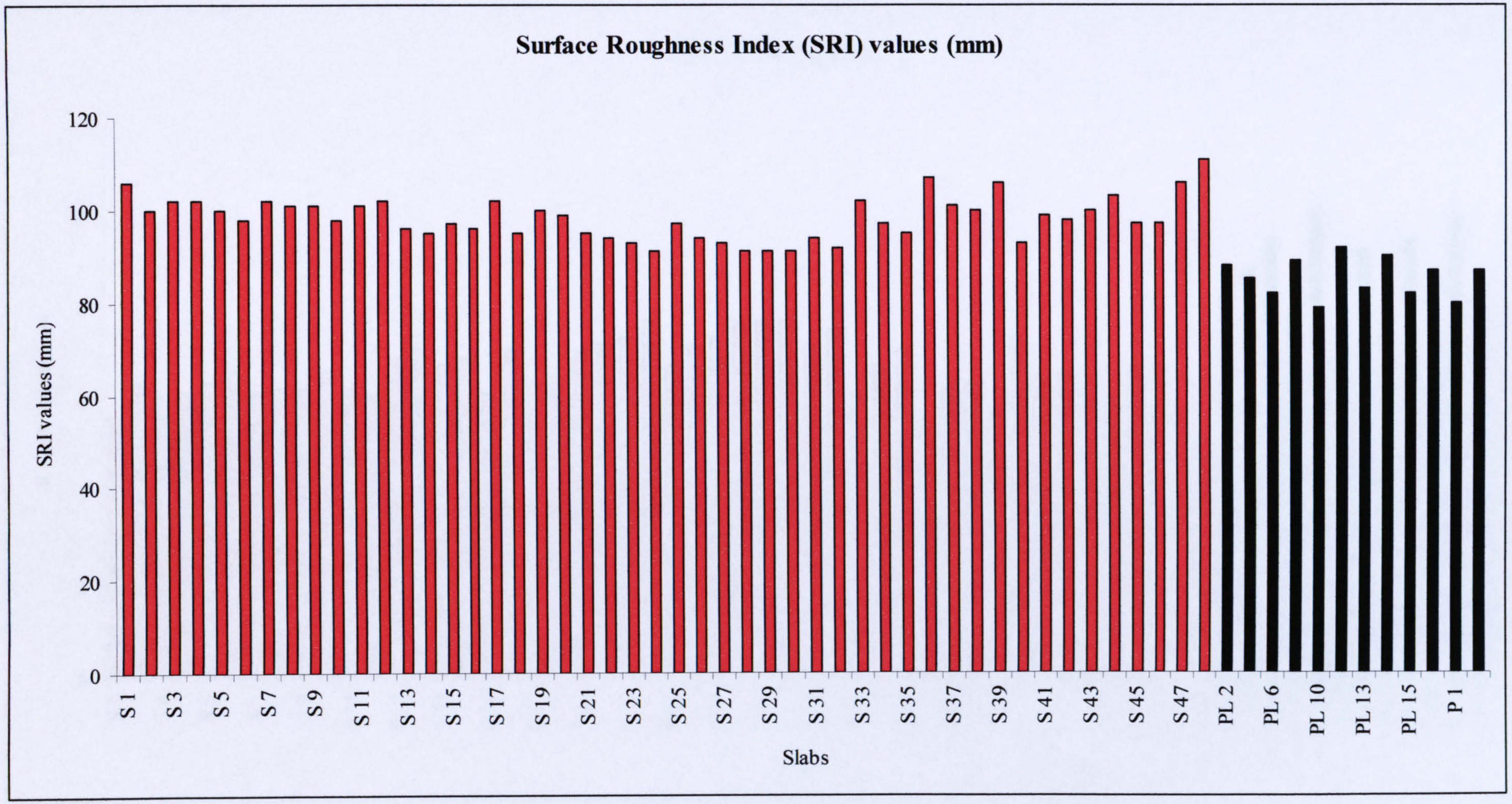

Figure 6.3 SRI mean values

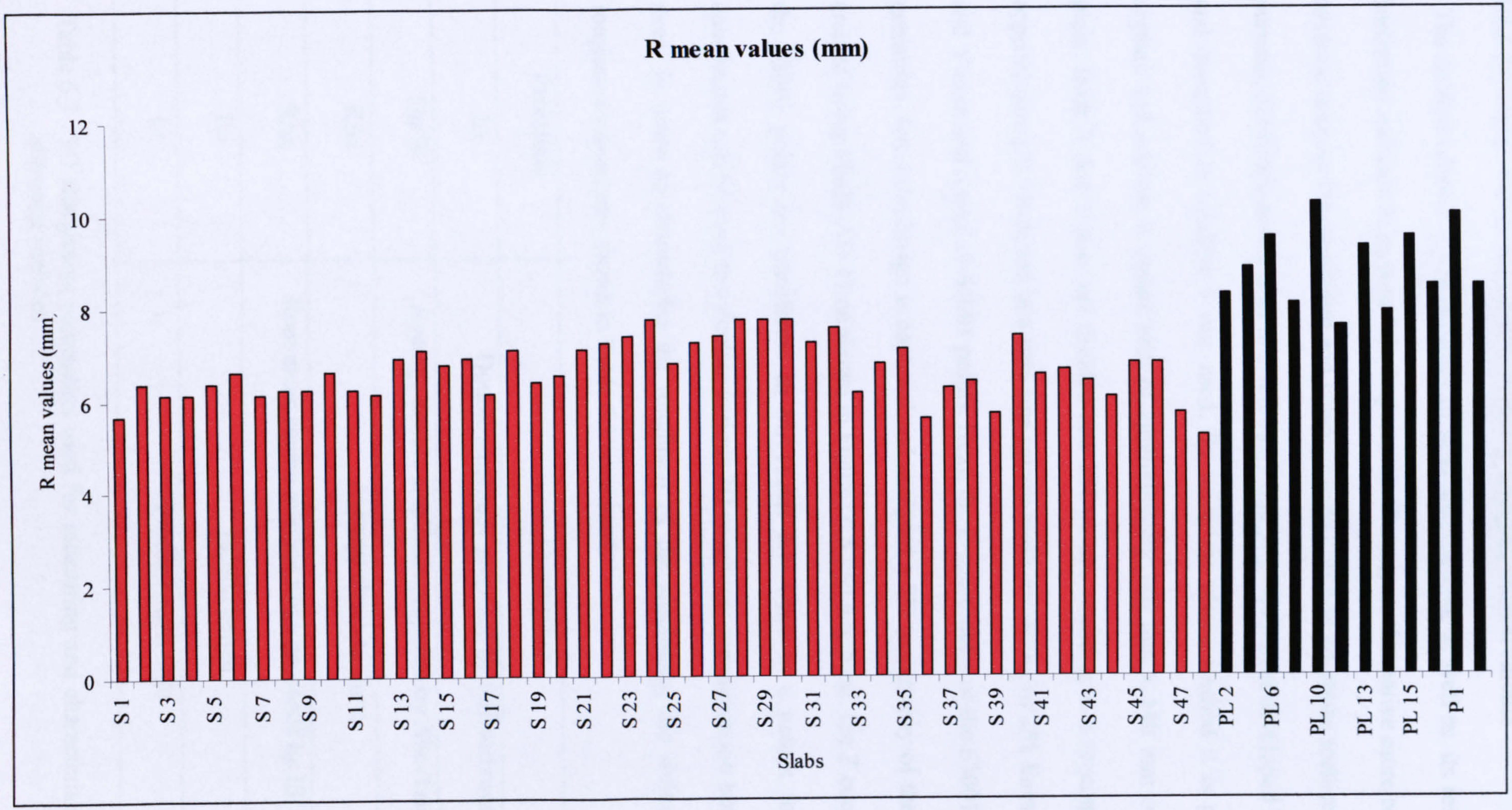

Figure 6.4 Rmean values

6.2.3 3D fringe-based laser interferometry imaging measurements

The limited reliability and accuracy of sand area method, as well as, its restriction to horizontal surfaces emphasized the importance of using an alternative more reliable and accurate method for measuring and characterising concrete substrate surfaces. For this purpose, 3D fringe-based laser interferometry imaging equipment developed by ESA[51] and described in Chapter 5 was used. By using the above method it is possible to capture and analyse a square area of approximately 140 mm x 140 mm on the X-Y plain. Both X and Y axes are divided into 251 points, resulting in a spacing length of approximately 0.5 mm and in a very fine square mesh consisting of 251 lines on both X and Y axes and a total of 63001 points. Next, the Z-coordinates of the 63001 points are generated. Once the image is captured and analysed a 3D topography of the surface is created using MathCAD 11 as shown in Figures 6.5 and 6.6. Next, the Z coordinates of the 63001 points are transferred to MATLAB 5.3. Once in a matrix form the Z-coordinates can be used to calculate various 2D roughness parameters on both X and Y axes. In order to characterise the roughness of the specimens, the following 6 2D roughness parameters shown in Table 6.3 were used:

Parameter	Description
2α	Double amplitude proposed by Silfwerbrand[49]
Da/W	Average double amplitude proposed by Abu-Tair et al[50]
$R\Delta a$	Average absolute slope
$R\Delta q$	Root mean square average slope proposed by ISO 4287[37]
Lo	Profile length
Lr	Profile length ratio

Table 6.3 2D Roughness parameters used for measuring and characterising concrete substrate surfaces

Selection of the above roughness parameters was based on their sensitivity to record changes which influence the amount of surface contact area available, which in turn, influences mechanical interlocking and hence interface bond strength as described in Chapter 5. Each of these parameters was calculated for every line along the X and Y axes and an average roughness parameter value based on the results of the 251 lines was obtained for both X and Y axes. Programming codes written in MATLAB for calculating the above 6 roughness parameters on both X and Y axes are shown in **Appendix 7,** whereas, the topography of all 60 specimens together with the values of all 6 2D parameters on both X and Y axes are presented in **Appendix 8.**

Double amplitude 2α results for both X and Y axes are shown in Figures 6.7 and 6.8 respectively. For surfaces produced using the electric hammer, 2αx values were found to be between 0.4408-0.537 mm, whereas, for surfaces produced using remote robotic hydroerosion, 2αx values varied between 0.5366-0.6938 mm. For surfaces produced using the electric hammer, 2αy values were found to be between 0.4445-0.8801 mm, whereas, for surfaces produced using remote robotic hydroerosion, 2αy values varied between 0.6577-1.2822 mm. In conclusion, double amplitude 2α is able to distinguish between surfaces obtained using different removal methods and confirm the ability of hydroerosion to produce rougher surfaces compared to traditional removal methods such as pneumatic/electric chipping hammers.

Average Double amplitude Da/W results for both X and Y axes are shown in Figures 6.9 and 6.10 respectively. For surfaces produced using the electric hammer, (Da/W)x values were found to be between 0.3955-0.5153, whereas, for surfaces produced using remote robotic hydroerosion, (Da/W)x values varied between 0.4824-0.6236. For surfaces produced using the electric hammer, (Da/W)y values were found to be between 0.4-0.7922, whereas, for surfaces produced using remote robotic hydroerosion, (Da/W)y

values varied between 0.59-1.1521. In conclusion, average double amplitude Da/W is able to distinguish between surfaces obtained using different removal methods and confirm the ability of hydroerosion to produce rougher surfaces compared to traditional removal methods such as pneumatic/electric chipping hammers.

Average absolute slope RΔa results for both X and Y axes are shown in Figures 6.11 and 6.12 respectively. For surfaces produced using the electric hammer, RΔax values were found to be between 0.793-1.032, whereas, for surfaces produced using remote robotic hydroerosion, RΔax values varied between 0.965-1.280. For surfaces produced using the electric hammer, RΔay values were found to be between 0.799-1.583, whereas, for surfaces produced using remote robotic hydroerosion, RΔay values varied between 1.183-2.306. In conclusion, average absolute slope RΔa is able to distinguish between surfaces obtained using different removal methods and confirm the ability of hydroerosion to produce rougher surfaces compared to traditional removal methods such as pneumatic/electric chipping hammers.

Root mean square average slope RΔq results for both X and Y axes are shown in Figures 6.13 and 6.14 respectively. For surfaces produced using the electric hammer, RΔqx values were found to be between 0.793-1.032 $mm^{1/2}$, whereas, for surfaces produced using remote robotic hydroerosion, RΔqx values varied between 0.965-1.280 $mm^{1/2}$. For surfaces produced using the electric hammer, RΔqy values were found to be between 0.799-1.583 $mm^{1/2}$, whereas, for surfaces produced using remote robotic hydroerosion, RΔqy values varied between 1.183-2.306 $mm^{1/2}$. In conclusion, root mean square average slope RΔq is able to distinguish between surfaces obtained using different removal methods and confirm the ability of hydroerosion to produce rougher surfaces compared to traditional removal methods such as pneumatic/electric chipping hammers.

Profile length Lo results for both X and Y axes are shown in Figures 6.15 and 6.16 respectively. For surfaces produced using the electric hammer, Lox values were found to be between 188.83-210.20 mm, whereas, for surfaces produced using remote robotic hydroerosion, Lox values varied between 207.18-239.91 mm. For surfaces produced using the electric hammer, Loy values were found to be between 189.81-277.98 mm, whereas, for surfaces produced using remote robotic hydroerosion, Loy values varied between 232.15-369.58 mm. In conclusion profile length Lo is able to distinguish between surfaces obtained using different removal methods and confirm the ability of hydroerosion to produce rougher surfaces compared to traditional removal methods such as pneumatic/electric chipping hammers.

Profile length ratio Lr results for both X and Y axes are shown in Figures 6.17 and 6.18 respectively. For surfaces produced using the electric hammer, Lrx values were found to be between 1.37-1.53, whereas, for surfaces produced using remote robotic hydroerosion, Lrx values varied between 1.49-1.73. For surfaces produced using the electric hammer, Lry values were found to be between 1.37-2, whereas, for surfaces produced using remote robotic hydroerosion, Lry values varied between 1.67-2.66. In conclusion profile length ratio Lr is able to distinguish between surfaces obtained using different removal methods and confirm the ability of hydroerosion to produce rougher surfaces compared to traditional removal methods such as pneumatic/electric chipping hammers.

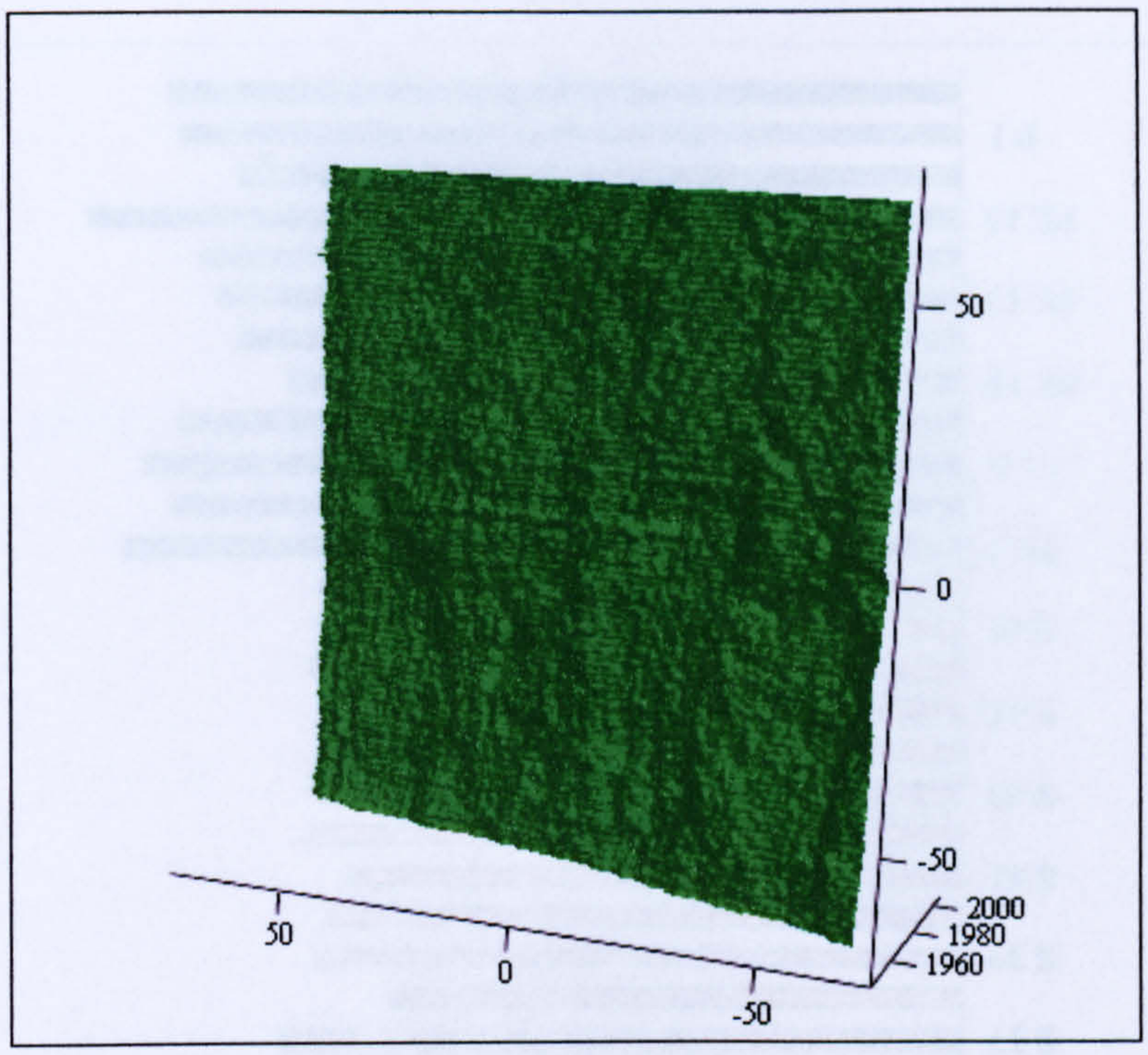

(X, Y, Z)

Figure 6.5 Slab S1 Topography

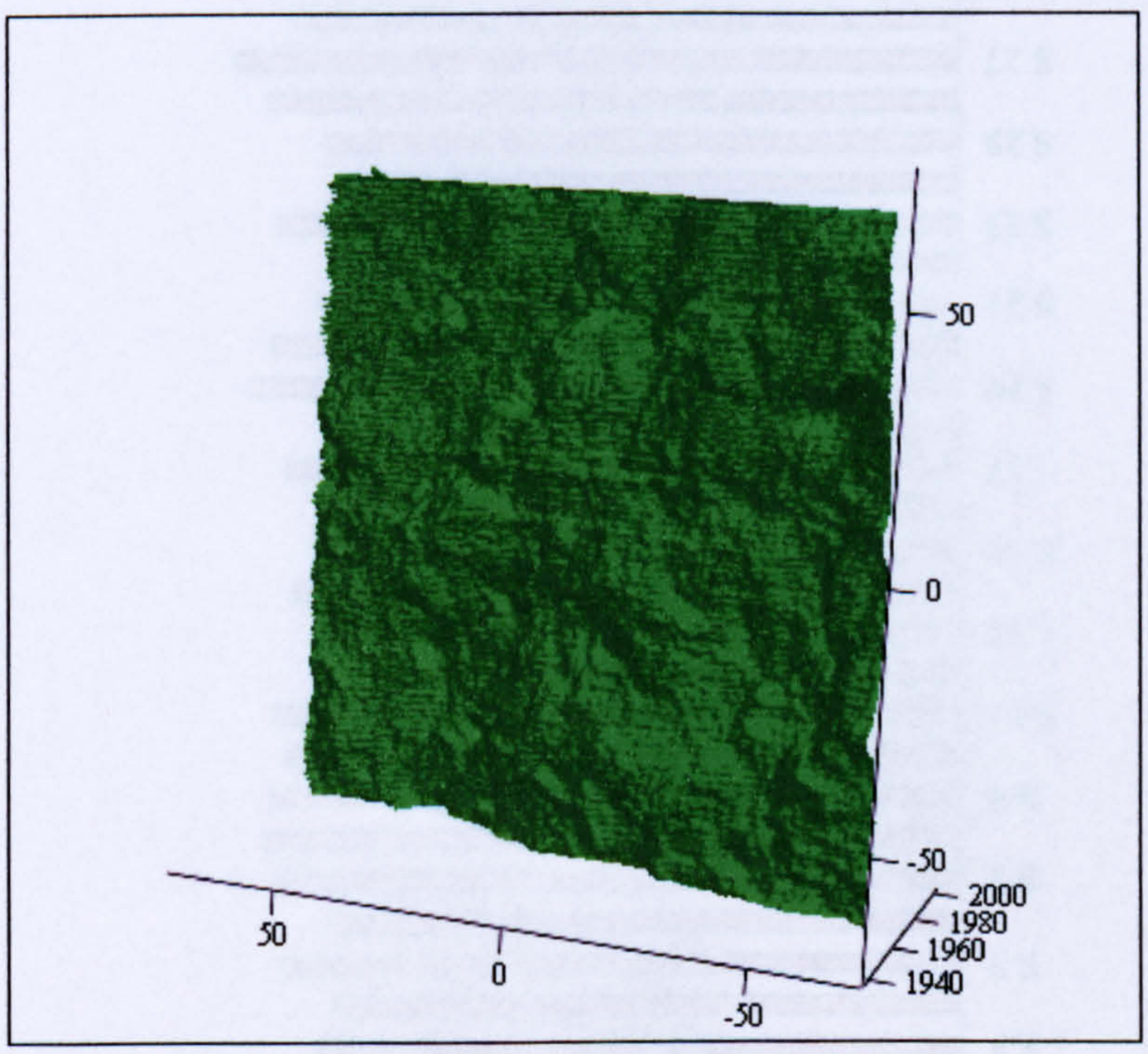

(X, Y, Z)

Figure 6.6 Slab PL2 Topography

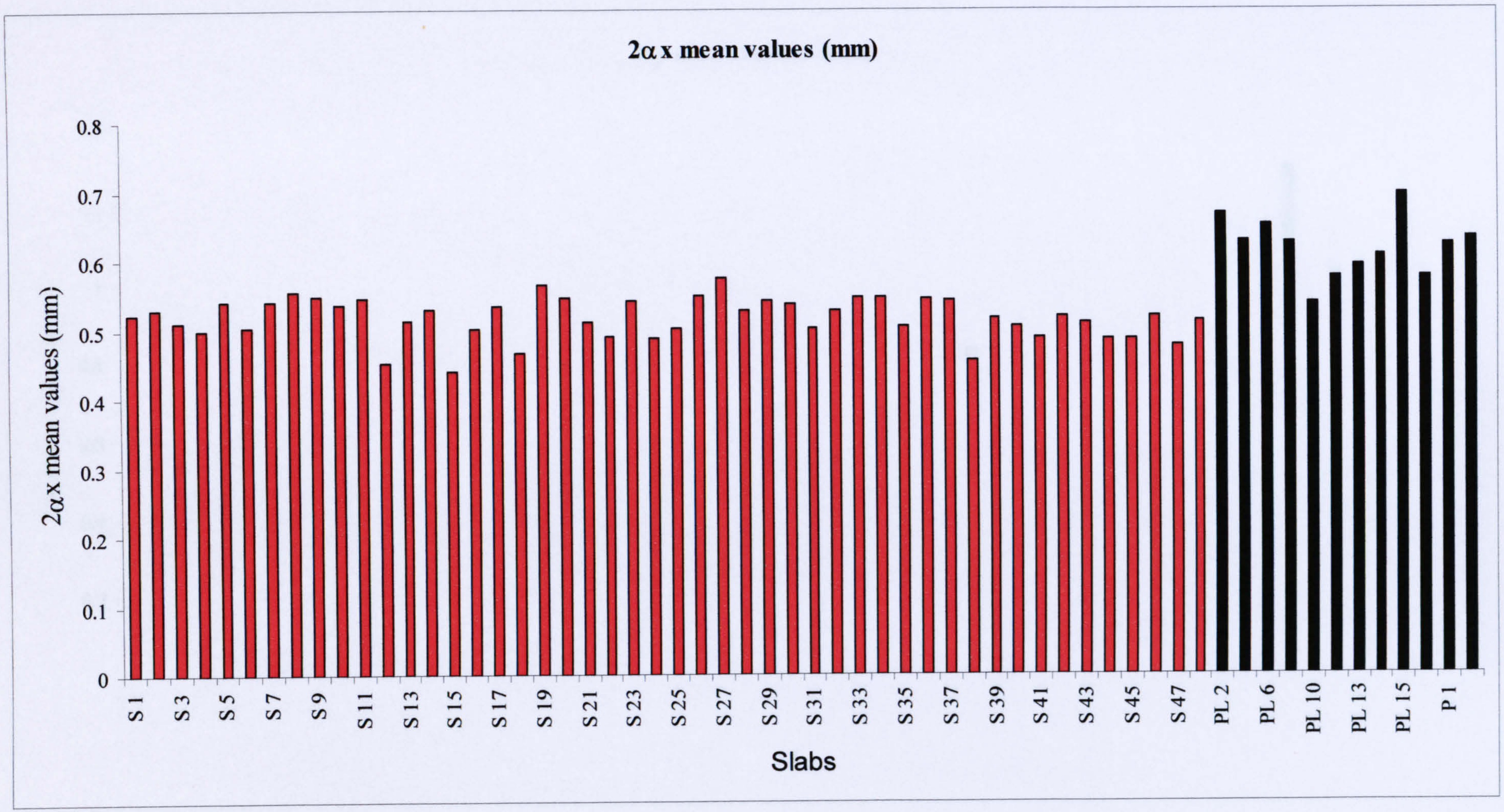

Figure 6.7 Double amplitude 2α mean values measured along the x axis

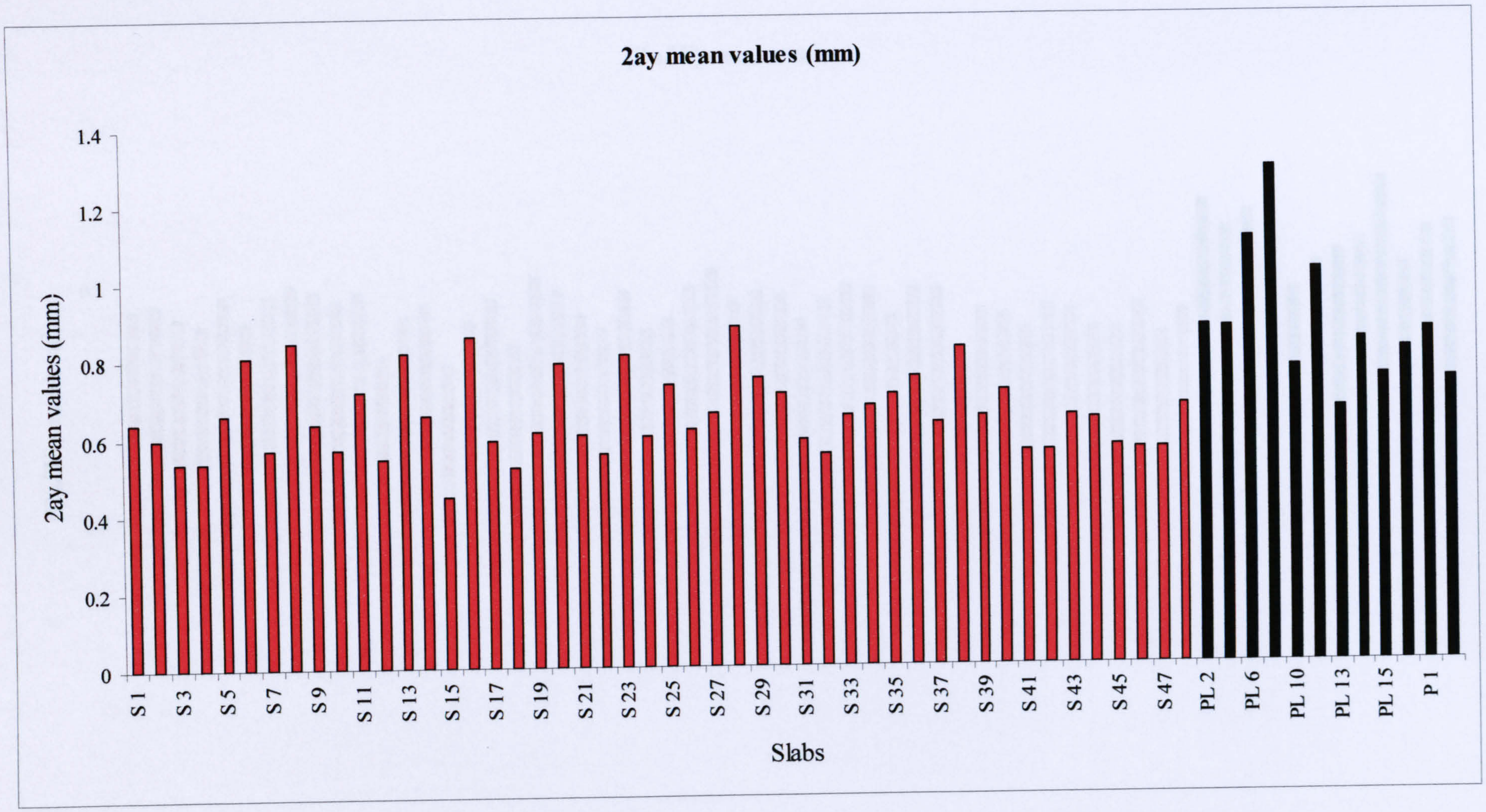

Figure 6.8 Double amplitude 2α mean values measured along the y axis

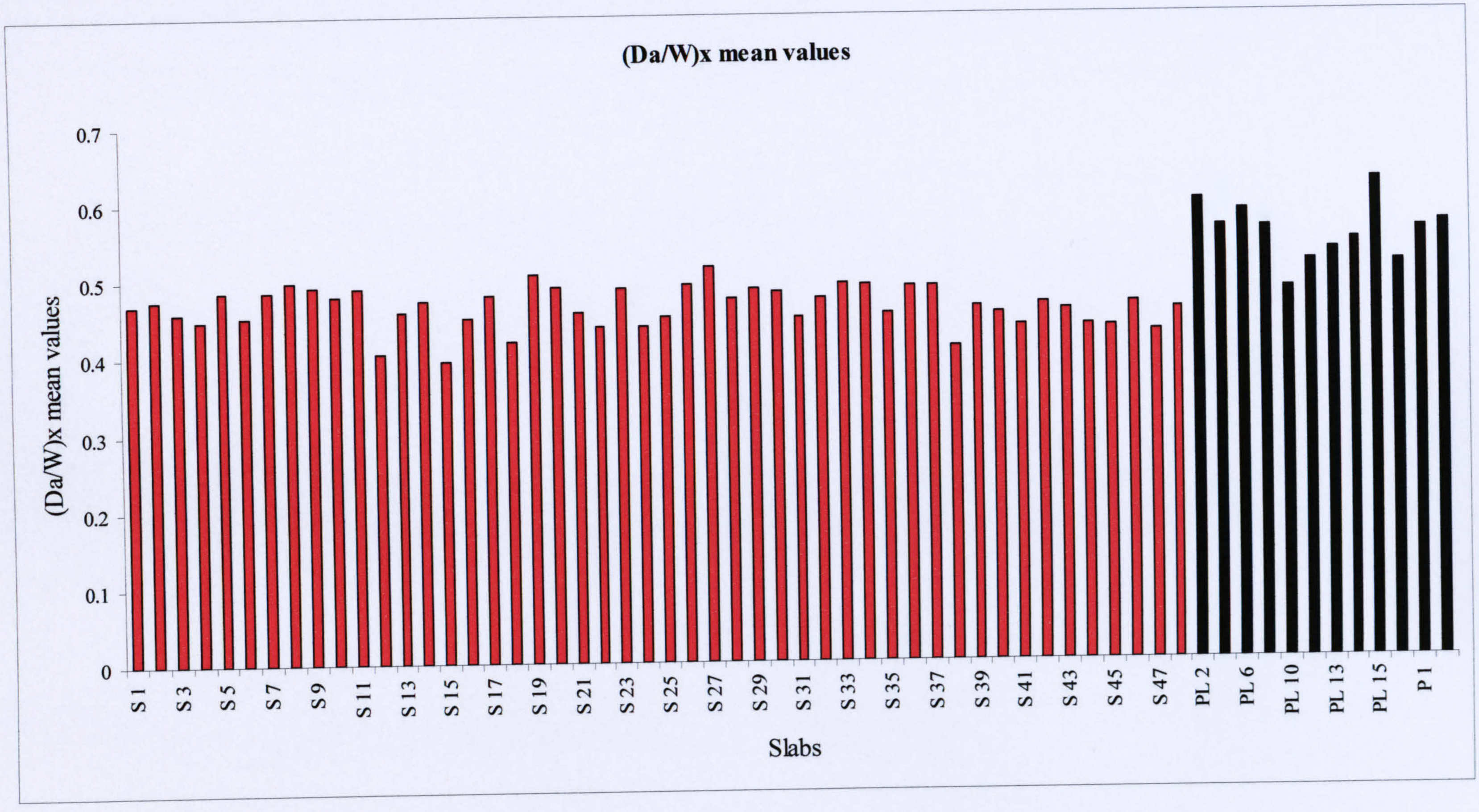

Figure 6.9 Average double amplitude over wavelength Da/W mean values measured along the x axis

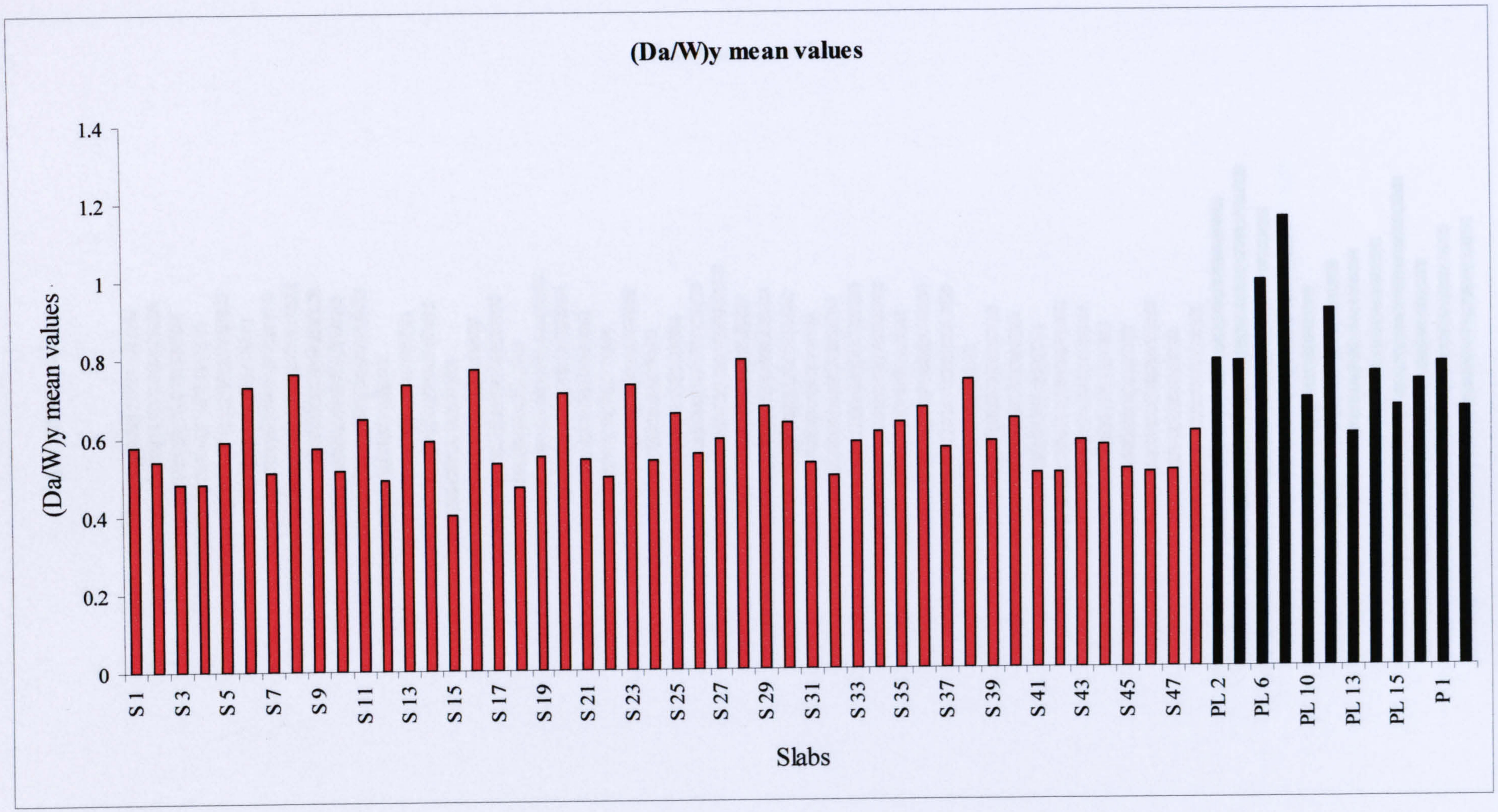

Figure 6.10 Average double amplitude over wavelength Da/W mean values measured along the y axis

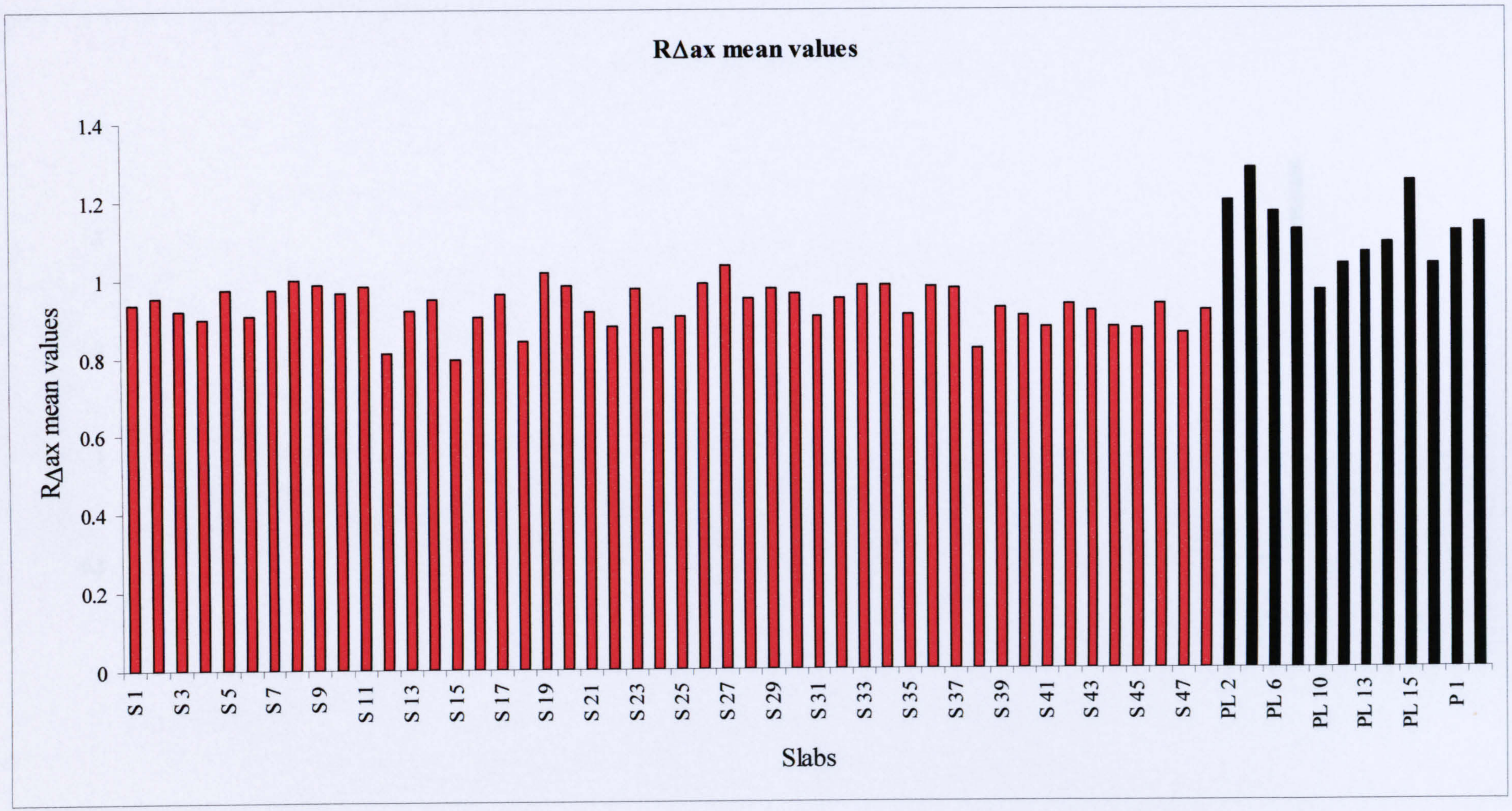

Figure 6.11 Average absolute slope RΔa mean values measured along x axis

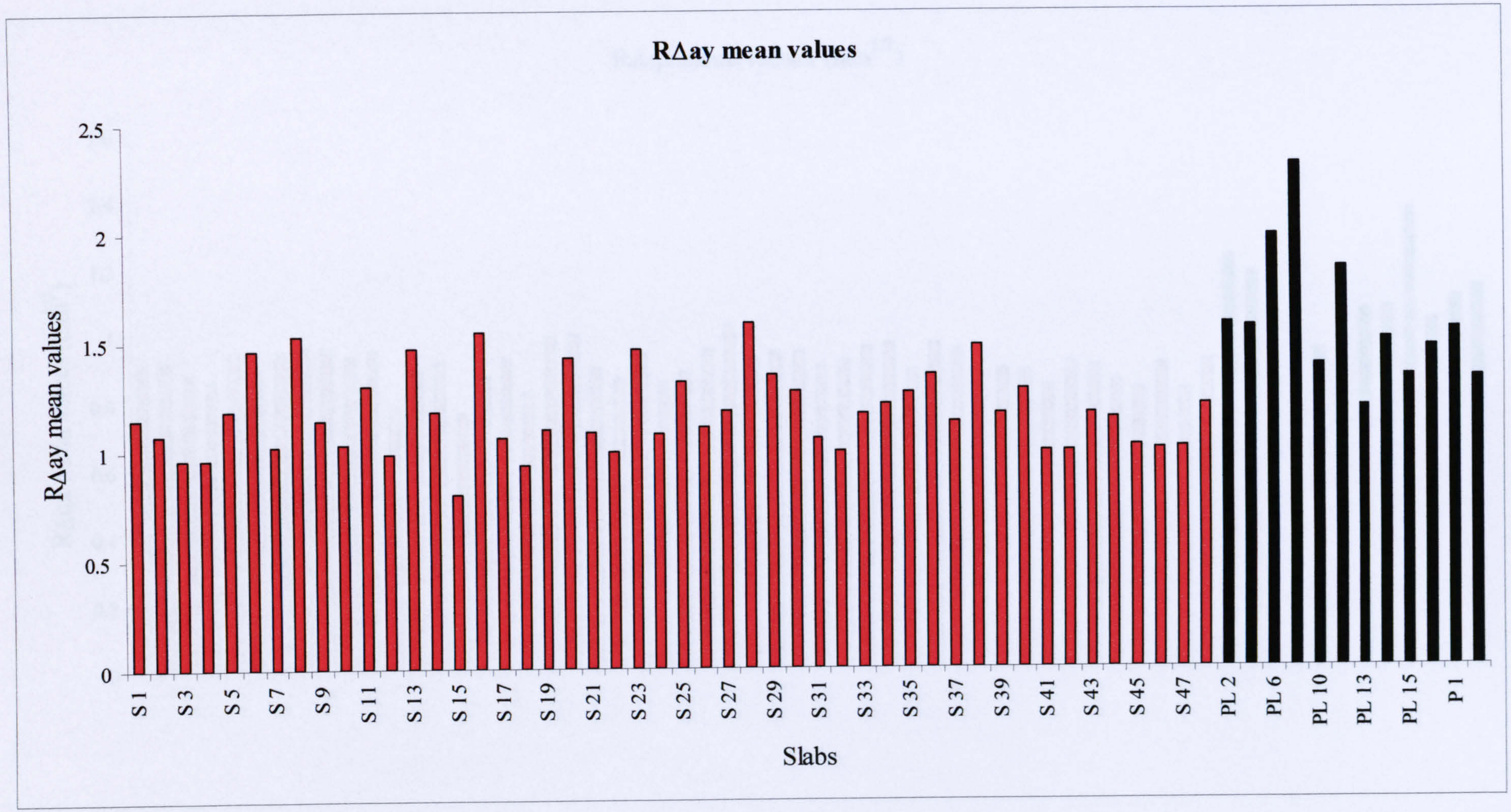

Figure 6.12 Average absolute slope RΔa mean values measured along y axis

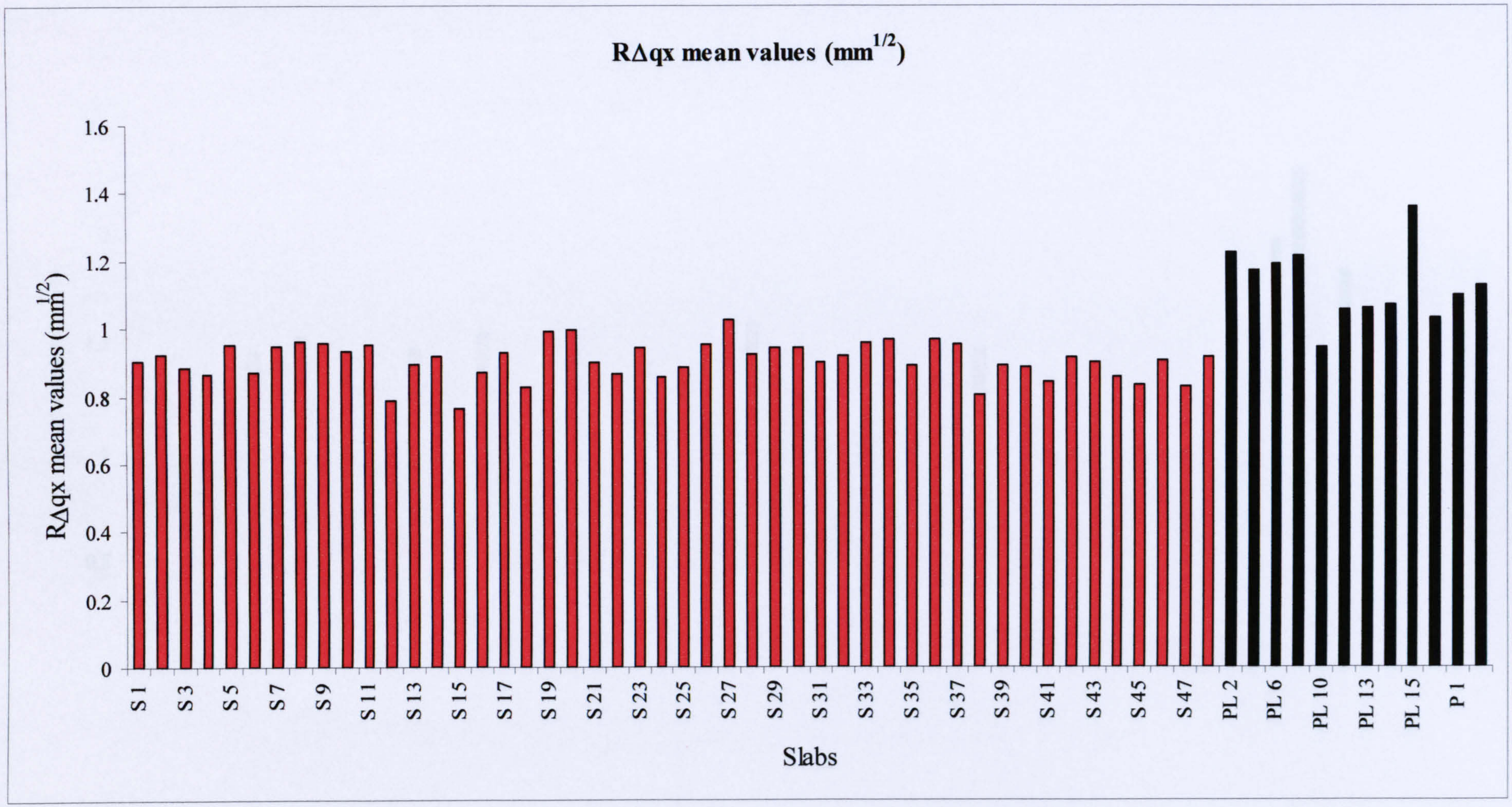

Figure 6.13 Root mean square average slope RΔq mean values measured along the x axis

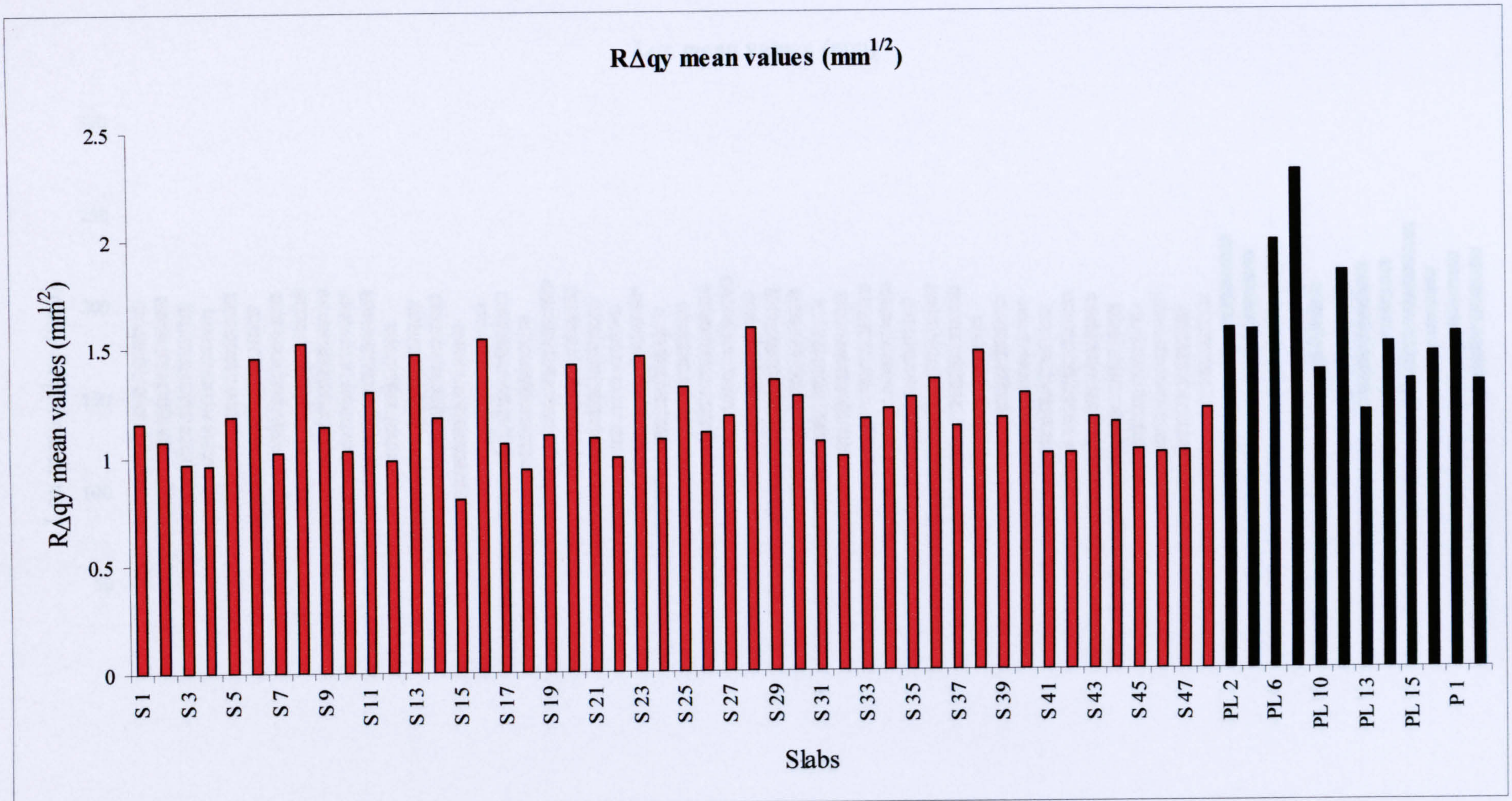

Figure 6.14 Root mean square average slope RΔq mean values measured along the y axis

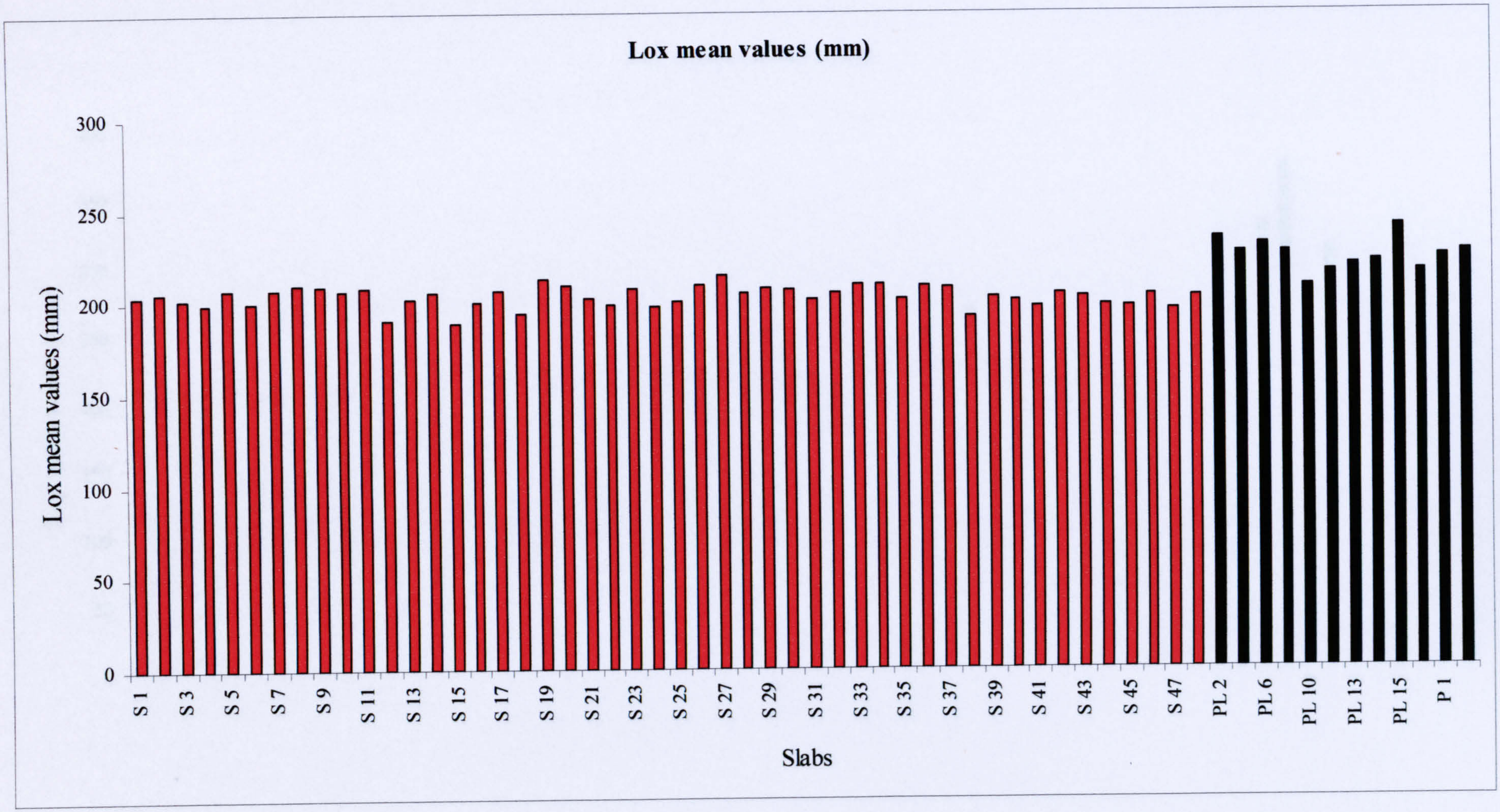

Figure 6.15 Actual profile length Lo mean values measured along the x axis

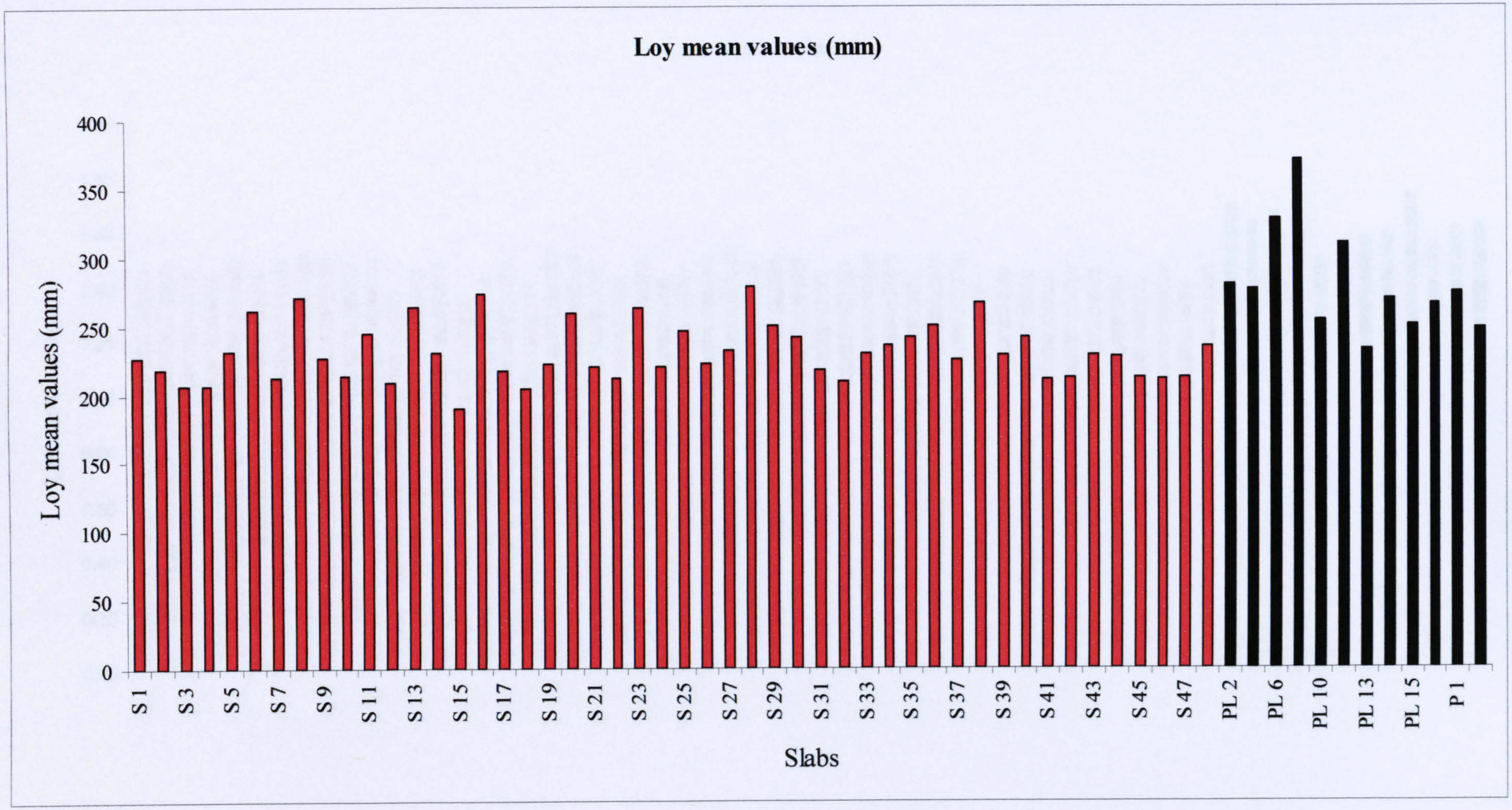

Figure 6.16 Actual profile length Lo mean values measured along the y axis

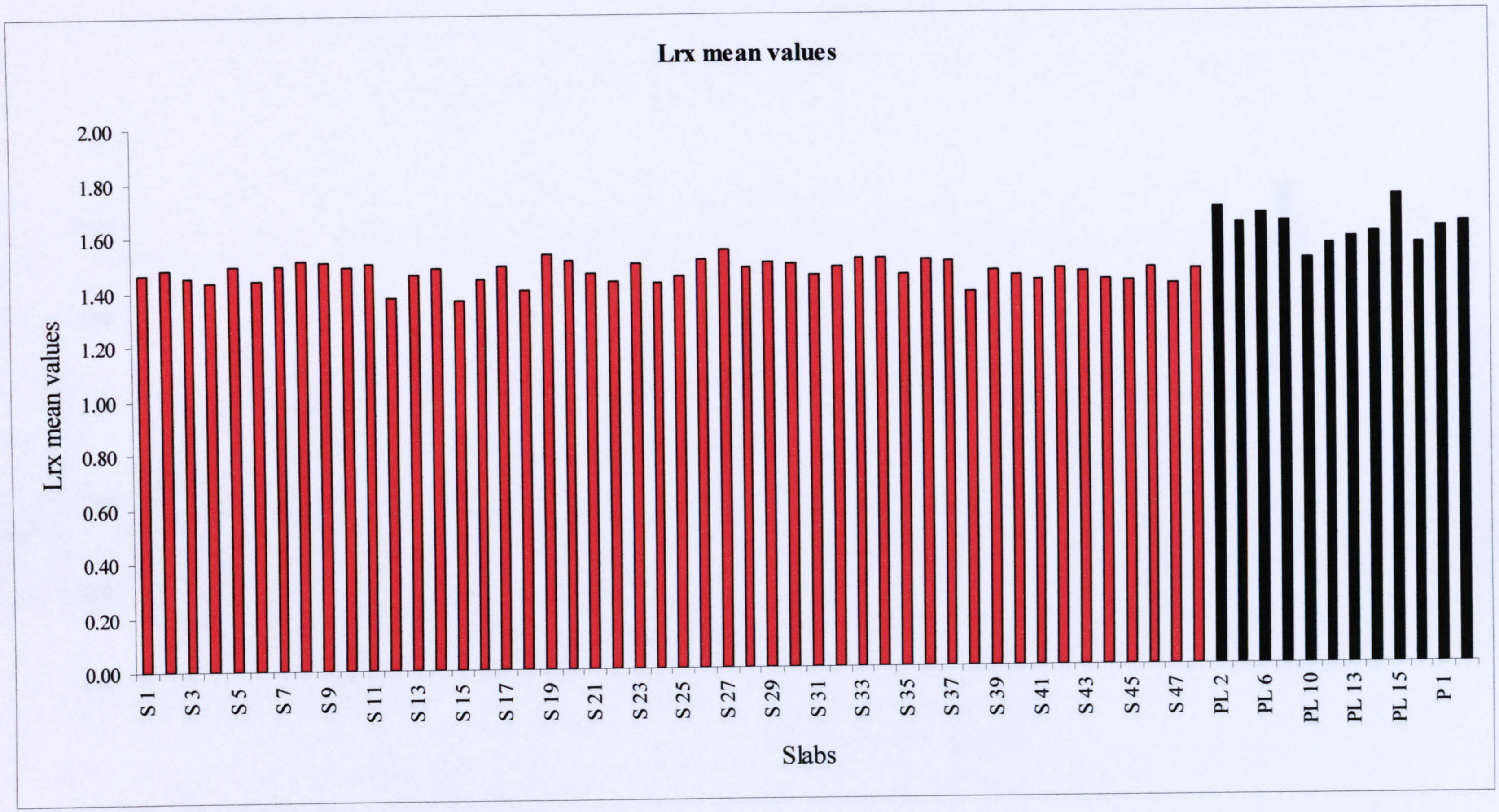

Figure 6.17 Profile length ratio Lr mean values measured along the x axis

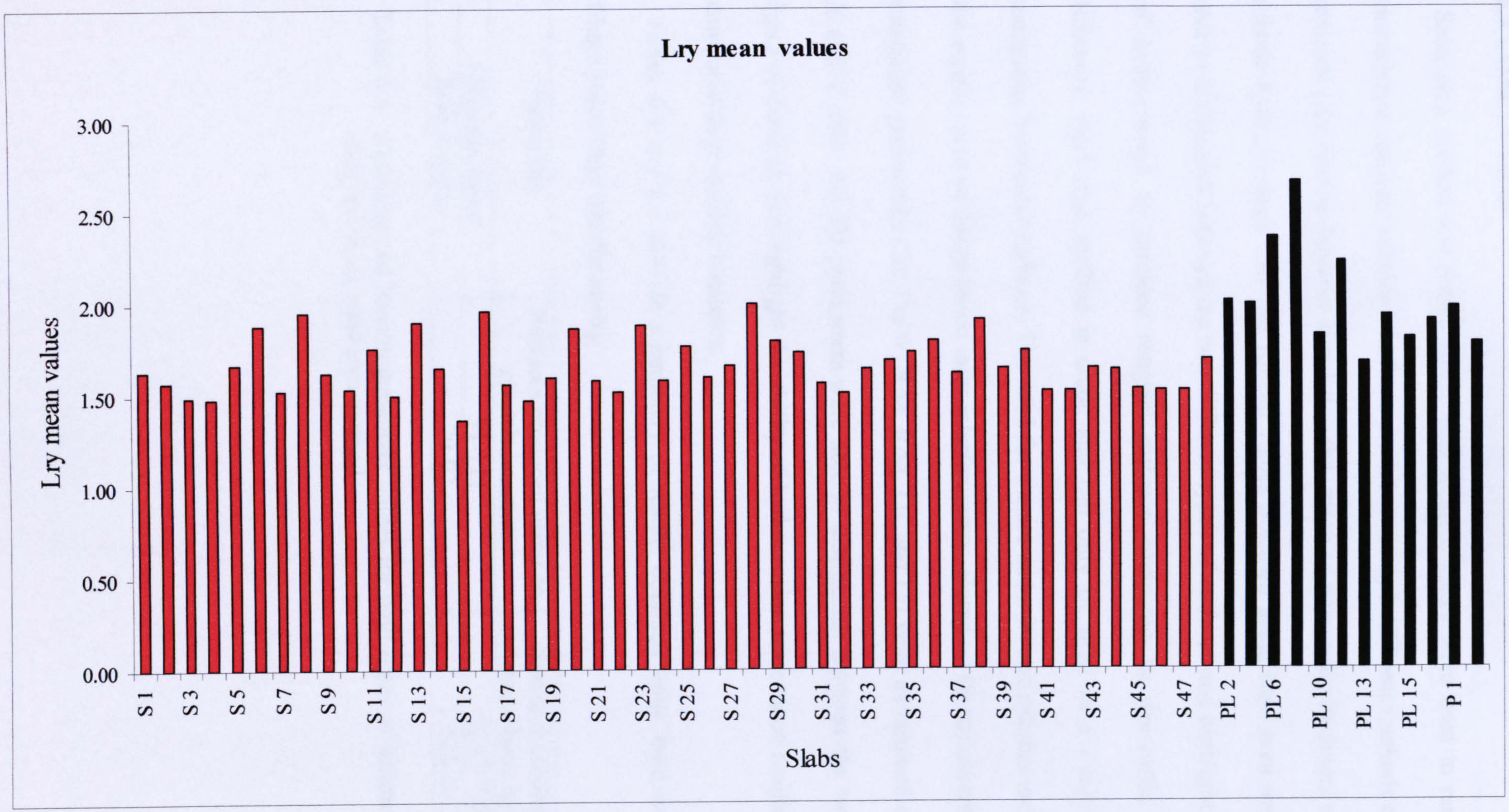

Figure 6.18 Profile length ratio Lr mean values measured along the y axis

6.3 CONCLUSION

Sand area method and fringe based laser interferometry were used to measure and characterise concrete substrate surfaces produced using 2 different methods of concrete removal (An electric hammer simulating the action of pneumatic hammers and remote robotic hydroerosion). SRI and Rmean values obtained using sand area method were able to distinguish between the two different types of surfaces and highlight the ability of hydroerosion to produce rougher surfaces compared to pneumatic hammers. However, sand area method is crude and can only be used as a rough guide for measuring horizontal surfaces. The need for a more accurate and reliable method led to the employment of fringe based laser interferometry. Based on its measurements, 6 2D roughness parameters (2α, Da/W, $R\Delta a$, $R\Delta q$, Lo, and Lr) were determined on both the X and Y axes. All 2D parameters were able to distinguish between the two different types of surfaces and highlight the ability of hydroerosion to produce rougher surfaces compared to pneumatic hammers.

Tables 6.4 and 6.5 provide a summary of results obtained using sand area and 3D fringe based laser interferometry.

Parameter	Surfaces produced using an electric hammer	Surfaces produced using remote robotic hydroerosion
SRImean (mm)	91-111	5.563-7.691
Rmean (mm)	79-92	7.525-10.205

Table 6.4 SRImean and Rmean parameter values for both types of substrate surfaces obtained using sand area method

Parameter	Surfaces produced using an electric hammer	Surfaces produced using remote robotic hydroerosion
2αx (mm)	0.4408-0.5370	0.5366-0.6938
2αy (mm)	0.4445-0.8801	0.6577-1.2822
(Da/W)x	0.3955-0.5153	0.4824-0.6236
(Da/W)y	0.4000-07922	0.5900-1.1521
RΔax	0.7930-1.0320	0.9650-1.2800
RΔay	0.7990-1.5830	1.1830-2.3060
RΔqx ($mm^{1/2}$)	0.7930-1.0320	0.9650-1.2800
RΔqy ($mm^{1/2}$)	0.7990-1.5830	1.1830-2.3060
Lox (mm)	188.83-210.20	207.18-239.91
Loy (mm)	189.81-277.98	232.15-369.58
Lrx	1.37-1.53	1.49-1.73
Lry	1.37-2.00	1.67-2.66

Table 6.5 2α, Da/W, RΔa, RΔq, Lo and Lr parameter values for both X and Y axis and for both types of substrate surfaces obtained using 3D fringe based laser interferometry method

CHAPTER 7

CRITERIA AFFECTING THE SELECTION OF REPAIR MATERIALS

7.1 INTRODUCTION

The next step after the removal of defective concrete and the preparation of steel reinforcement and substrate concrete is the selection and application of the repair material. At present, in the construction industry a large number of different types of repair materials are available, which according to their manufacturers satisfy all the requirements for a durable long lasting repair. The objective of this chapter is to describe the various properties that repair materials must have to satisfy all requirements for a durable long lasting repair and hence select the right type of repair materials for subsequent repair experiments. For this reason the main types of repair materials used in the construction industry are presented. Applications, advantages and limitations of each repair material are briefly described. Finally, reference to primers/bonding agents that are used to protect steel reinforcement and improve adhesive strength between the concrete substrate and the repair material is also made.

7.2 PROPERTIES OF REPAIR MATERIALS

The selection of the appropriate repair materials is a complex process that involves investigating the mechanisms that cause concrete deterioration, predicting service and exposure conditions and anticipating durability, constructibility, aesthetics and cost. After requirements are established and desired material properties are defined, the selection of repair materials can be made. According to Plum[52] repairs can be classified into two categories: non-structural or cosmetic repairs, in which load carrying capacity

is not a major consideration for the repair, and structural repairs, where the repair patch is required to carry the load originally carried by the removed concrete. Similarly, according to Cusson and Mailvaganam[53] non-structural repairs are performed to improve surface appearance, reduce permeability, protect steel reinforcement, or improve abrasion resistance. On the other hand, structural repairs are performed to restore the design load carrying capacity of a damaged member, or improve the load carrying capacity of an under-designed member.

The mechanical properties most often considered during selection of repair materials for structural repairs include:

- Compressive strength
- Tensile strength
- Flexural strength
- Adhesive strength

Compressive, tensile and flexural strength of the repair material should be similar to that of the concrete substrate in order to ensure that there will be no reduction in the ultimate load carrying capacity of the repaired member. Adhesive strength is also of great importance to the durability of patch repair. It should be sufficient to keep the repaired area intact. Concrete Society Technical Report No. 38[54] recommends that an adhesive strength of at least 0.8 N/mm^2 should be achieved. However, compatibility between the repair material and the concrete substrate is equally important. According to Emmons et al[55] compatibility can be defined as a balance of physical, chemical and electrochemical properties and dimensions between a repair material and the existing substrate that will ensure that the repair can withstand all stresses induced by volume changes and chemical and electrochemical effects without distress and deterioration

over a designated period of time. Figure 7.1 adopted from Emmons et al[55] shows the various factors affecting the compatibility of repair materials.

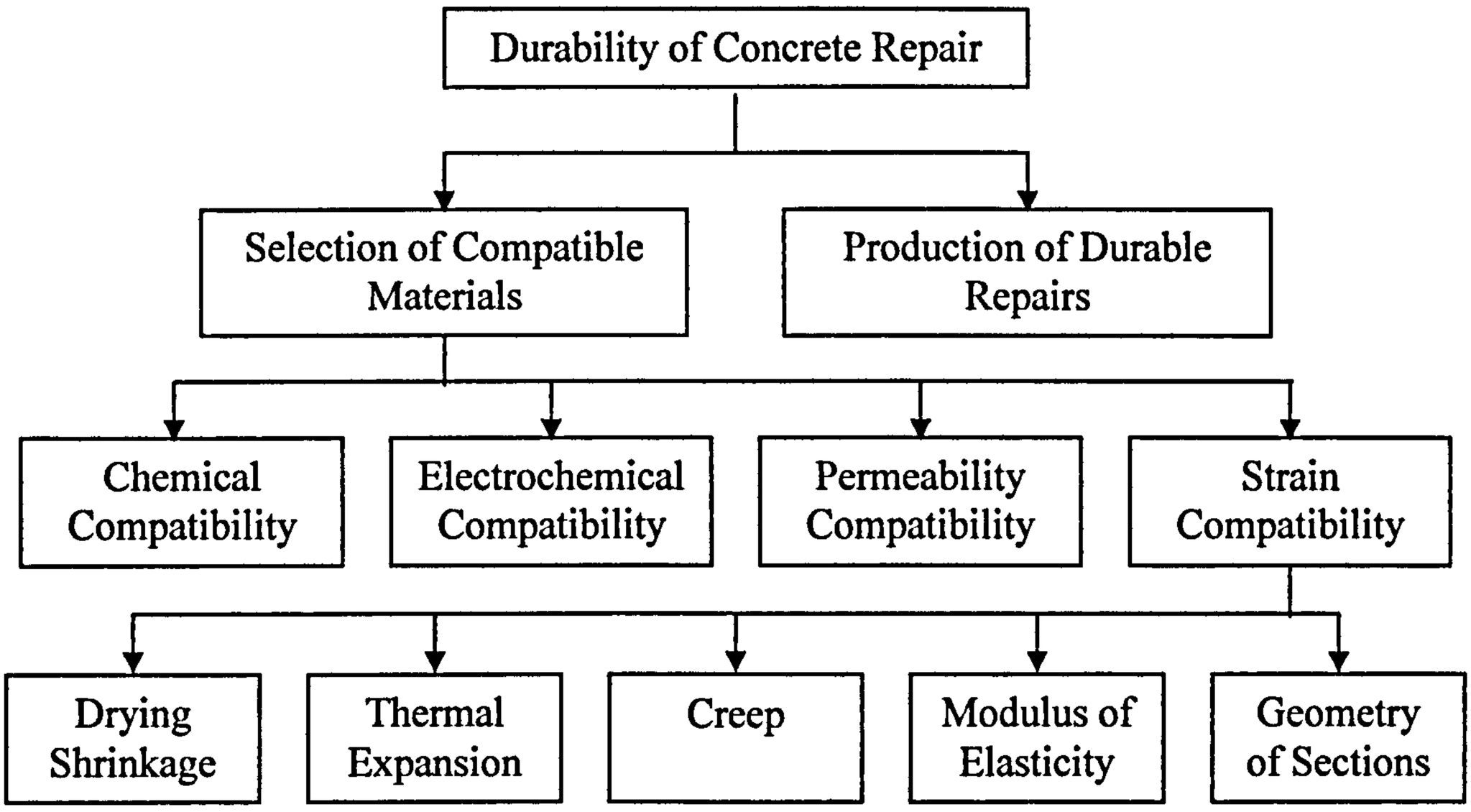

Figure 7.1 Factors affecting durability of concrete repairs adopted from Emmons et al[55]

Chemical compatibility properties include C_3A content, alkali content, and chloride content. During selection of repair materials all aspects of chemical compatibility must be considered. For example, when concrete that is being repaired includes potentially reactive aggregates, a repair material with low alkalinity should be used.

Electrochemical compatibility properties include electrical resistivity and pH. The repair material should prevent corrosion of steel reinforcement, both within the repair area and in the surrounding unrepaired reinforced concrete. Based on published papers considerable controversy exists as to the most appropriate types of repair materials used to ensure electrochemical compatibility. Gulikers and van Mier[56] provide a comprehensive overview of the electrochemical reactions involved in corrosion of steel reinforcement in concrete. They studied the effect of concrete removal from a corroding area and its replacement with different types of repair materials on subsequent corrosion activity in the patches and surrounding concrete. They concluded that strong galvanic

corrosion can develop in unrepaired areas adjacent to the repair patches when repairs are conducted using OPC mortars. On the other hand they found that polymer concretes did not affect corrosion of steel reinforcement in adjacent unrepaired areas. Marossezeky and Wong[57] found that styrene butadiene and acrylic modified mortars provided greater protection against corrosion developing at the boundary of the original concrete and the repaired patch than OPC repair mortars. The above studies suggest that best corrosion protection can be achieved by using polymer-modified concretes or polymer concretes with high electrical resistivity. However, these results are not in agreement with recommendations given by other researchers. According to Emmons et al[58] repair materials that are highly resistive or non-conductive have a tendency to isolate the repaired area from adjacent undamaged areas. Hence, if there is a large permeability or chloride content differential between the repair and the rest of the concrete, the corosion becomes concentrated in a restricted area, and the rate of corrosion may be increased, resulting in a premature failure in either the repair or the adjacent concrete. Dehawah et al[59] support this view, as they found lower corrosion rates in reinforced concrete beams repaired with OPC mortars, compared to beams repaired with polymer-modified cementitious mortars. These conclusions tend to support the use of repair materials of similar composition, density and permeability to the surrounding concrete in the repair area in order to maximise electrochemical compatibility. Other researchers, such as McCurrich et al[60] suggest the use of corrosion inhibiting primers to the exposed steel reinforcement. McCurrich et al[60] studied the influence of a variety of different primers, including OPC mortar slurry, polymer-modified cementitious slurry, non-passivating or passivating epoxies and zinc-rich epoxy on corrosion activity. They found that while the use of no primer, or OPC mortar slurry provided excellent protection to rebar in the repair zone, corrosion of steel

reinforcement in the surrounding concrete could be accelerated. They concluded that a low permeability polymer-modified repair mortar used in conjunction with a zinc rich epoxy rebar primer provided the best anti-corrosion protection to steel reinforcement both in the repair zone and in the adjacent concrete. However, this finding is not supported by the work of Heiman and Koerstz[61], who found that the use of a zinc epoxy primer on the steel reinforcement did not have any beneficial effect as a corrosion inhibitor.

Low permeability of the repair material is of major concern since areas that have been repaired are the most vulnerable to H_2O, O_2, CO_2 and ^-Cl penetration. However, in many cases very low permeability repair materials are not the best option. A small number of cracks in the repair, or its debonding, will significantly reduce the benefit of a very low permeability repair material. Microcracks connected with wider cracks originating from the surface of the repair have a more significant effect in reducing durability than the permeability of the repair itself. Emmons et al[58] emphasised that the insistence on low permeability as a criterion for repair materials can lead to unsuitable choices, incompatibility problems, and eventual failure. They concluded that a bad example was the use of very low permeability repair materials for repairing thousands of bridge columns in North America leading to encapsulation. When the temperature drops, moisture in vapour form migrates toward the barrier and is converted to a liquid form at the dew point. Water solubles are carried along in the migration. The liquid is then turned into ice at freezing temperatures, resulting in freeze-thaw damage at the edge of the barrier. When the temperature is rising again, the moisture is converted back to a vapour form, leaving water solubles behind in a crystalline form since vapour is not capable of making a solution. Repeated cycles can result to severe deterioration from one of these damaging forces. Morgan[62] also emphasised the fact that repair materials

that are impermeable to moisture vapour diffusion should be used with great caution in the repair of hydraulic structures, such as dams and reservoirs, since their use could cause saturation of the substrate concrete behind the repair.

Strain compatibility is one of the most important factors for selecting repair materials. During the last decade a number of research papers by Emberson and Mays[63], Plum[64], Emmons and Vaysburd[65], Decter and Keeley[66], and Emmons et al[67] highlighted the importance of strain compatibility in achieving durable long lasting repairs. Strain compatibility of repair materials is depended upon their strain behaviour relative to the concrete substrate. Relative strain changes cause internal stresses within the repair material, at the interface and in the concrete substrate, and can result in cracking, loss of load carrying capacity, delamination, and deterioration. Cracking is the most important factor affecting the durability of patch repairs, especially in severe environments. The presence of cracks dramatically increases the permeability and the possibility of H_2O, CO_2 and ^-Cl to penetrate through the repair. Even isolated narrow cracks can cause corrosion of steel reinforcement that can lead to the failure of the repair. From a theoretical point of view, an ideal repair should be free of cracks. However, from a practical point of view, the aim is to minimise the amount of cracks. The mechanical properties that determine the strain compatibility of the repair materials with the concrete substrate include:

- Coefficient of thermal expansion
- Modulus of elasticity
- Creep
- Restrained shrinkage

The coefficient of thermal expansion is a measure of the change of length in a material when it is subjected to a change in temperature. For concrete the coefficient of thermal expansion varies between $7.4x10^{-6}$ ^0C to $13x10^{-6}$ ^0C and is dependent on the mix design and the type of aggregate used. If the repair material and the concrete substrate have similar coefficients of thermal expansion then a change in temperature will be evenly distributed through both of them and no stresses will be developed. However, if the repair material has significantly lower or higher coefficient of thermal expansion than the concrete substrate then temperature changes will induce shear stresses at the interface between the repair material and the concrete substrate as shown in Figure 7.2 adopted from Emmons[9]. These stresses can cause failure at the interface or in the lower strength material. BS 6319 Part 12[68], BS EN 1770[69] and ASTM C 531[70] can be used to determine the coefficient of thermal expansion of repair materials.

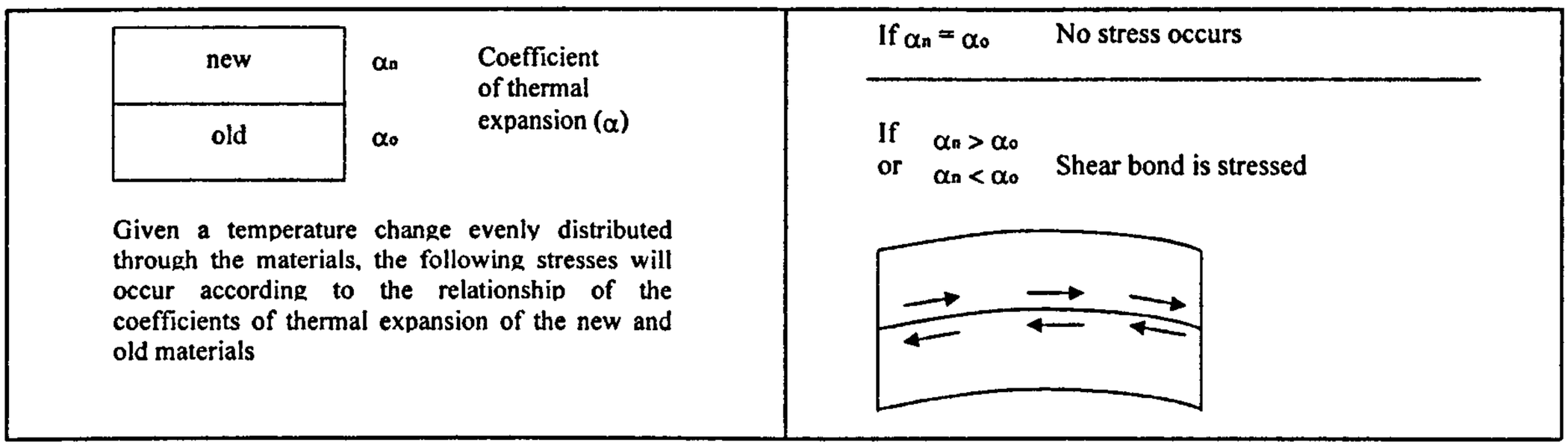

Figure 7.2 Effect of coefficient of thermal expansion on strain compatibility adopted from Emmons[9]

The modulus of elasticity is a measure of rigidity, low modulus materials deform more than those of high modulus under a given load. When the external compressive or tensile load is applied parallel to the bond line, materials with significantly different moduli of elasticity will transfer stresses from the low modulus material to the high modulus material, leading to stress concentration and failure of the high modulus material as shown in Figure 7.3 adopted from Emmons[9]. When the external load is

applied perpendicular to the bond line, the difference in the modulus of elasticity between the two materials is less problematic if the external load is compressive. However, if the perpendicularly applied load is tensile, significant difference between the moduli of the two materials is likely to cause adhesion failure. According to Chidiac and Mailvaganam[71] the ratio of modulus of elasticity of a repair material to that of substrate concrete should be between 0.75-1.25. BS 6319: Part 6[72], BS EN 13412[73] and ASTM C 469[74] can be used to determine the modulus of elasticity of repair materials in compression.

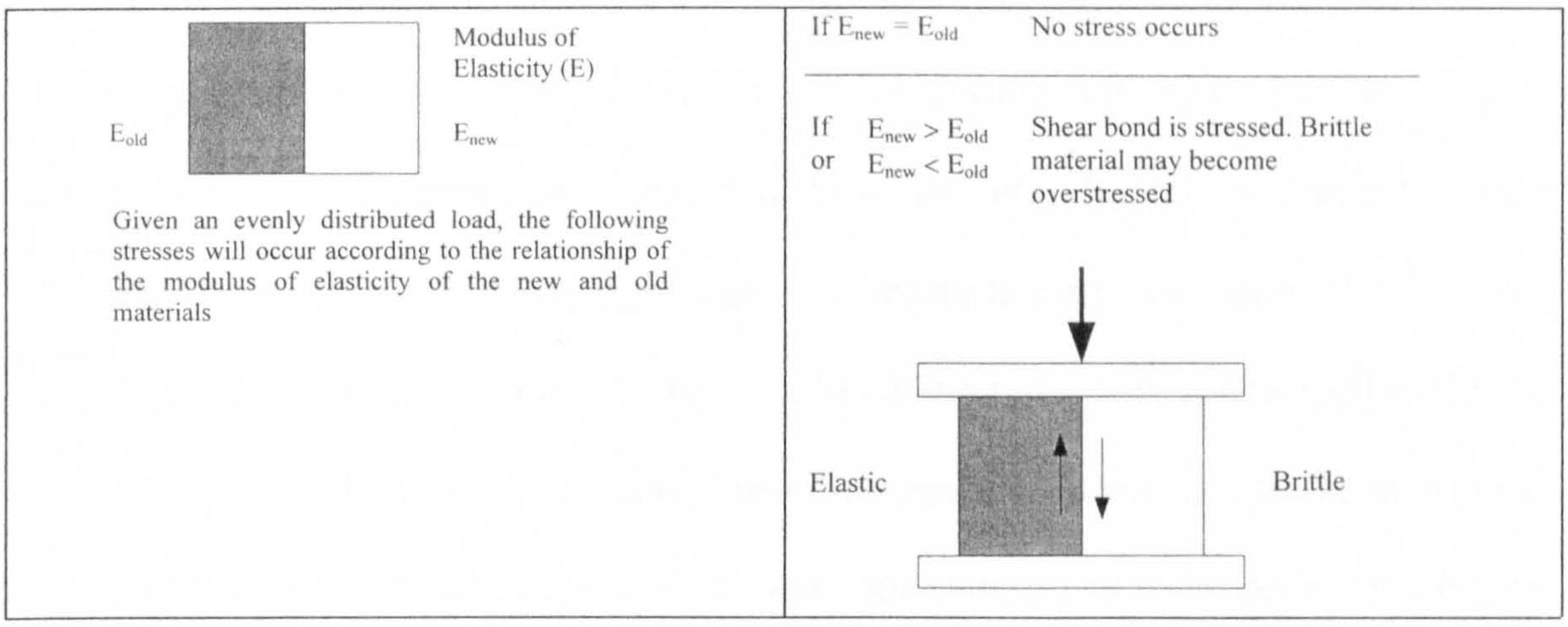

Figure 7.3 Effect of modulus of elasticity on dimensional strain adopted from Emmons[9]

Creep is a time-dependent inelastic deformation that occurs with prolonged application of stress. It can result in reduced load-bearing capacity of the repair material and also result in load transfer from the repair material to the substrate concrete, or to a non-structural element. In the case of patch repairs loaded in compression, the repair material must have very low creep potential as shown in Figure 7.4 adopted from Emmons[9]. In the case of patch repairs loaded in tension, creep can be beneficial, as it can reduce or cancel the adverse effect of shrinkage in the repair material. ASTM C 512[75] and ASTM C 1181[76] can be used to determine creep of repair materials in

compression, whereas, BS 6319 Part 11[77] can be used to determine creep of repair materials in compression and tension.

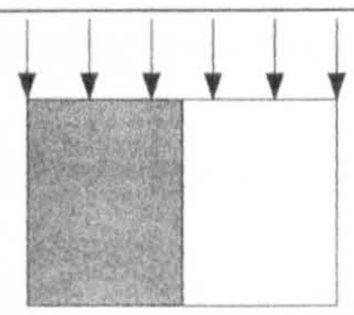

If the old material has already developed a stable creep volume, stresses will develop according to the amount of creep occuring in the new material

If (ε_{cr}) new = 0 No stress occurs

If (ε_{cr}) new > 0 Shear bond is stressed. Loads carried by repair are reduced

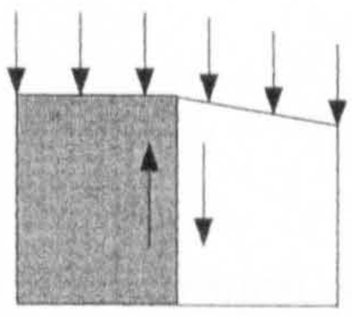

Figure 7.4 Effect of creep on strain compatibility adopted from Emmons[9]

Restrained shrinkage is the most common cause of patch repair failures. Repair materials tend to contract due to moisture loss after they have been hardened. This phenomenon is known as drying shrinkage. According to Emmons[9] most of the drying shrinkage will take place in the first 30 days. In addition, research conducted by Alberta Transportation and Utilities[78] indicated that the majority of shrinkage (more than 50%) occurred during the initial 7 days after casting. However, repair materials are not free to shrink because they are bonded to the concrete substrate. Since drying shrinkage is restrained from occurring by the concrete substrate the repair material will accumulate internal tensile stress as shown in Figure 7.5 adopted from Emmons[9]. The repair material has no tensile strength when first placed, but starts to gain tensile strength as time passes. Although, the repair material is stretched due to restrained shrinkage it also relaxes due to tensile creep that reduces tensile stress to a net stress. If the net tensile stress exceeds the tensile capacity, the repair material will crack. Emmons[9] classified repair materials in three basic categories according to their drying shrinkage performance. Any repair material with shrinkage of less than OPC concrete (0.05%) is considered to be of low shrinkage. Materials with shrinkage values between 0.05% and 0.10% are considered to be of moderate shrinkage. Materials with shrinkage values

greater than 0.10% are considered to be of high shrinkage and should be avoided. Restrained shrinkage can be minimised if during the selection of repair materials the following guidelines are taken into account:

- Use of mixes with maximum aggregate content
- Use of clean and sound aggregates
- Use of aggregate size as large as practical
- Use of minimum required cement content to meet strength requirements
- Use of placement techniques that allow for optimum aggregate loadings
- Use of proper wet curing conditions that reduce early drying shrinkage
- Avoid conditions that can increase water demand, such as high temperature mixes

BS 6319 Part 12[68] can be used to determine unrestrained linear shrinkage, whereas, ASTM C 157[79] and ASTM C 596[80] can be used to determine the drying shrinkage of repair materials. Although, the above methods can be used to measure unrestrained shrinkage, the stresses induced when this shrinkage is restrained and the consequent risk of cracking are more important in the field of concrete repair. Despite the importance of measuring the effects of restrained shrinkage, as opposed to those of unrestrained shrinkage, only a small number of test methods have been developed for this purpose. However, these methods are unsatisfactory for predicting the field performance of patch repairs because they only provide information such as amount and width of cracks but do not provide information regarding the development of stresses. In addition, with the exception of the German angle test[81] no other method has been standardised.

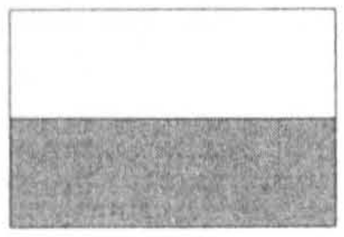

Drying shrinkage (ε_{sh})

ε_{sh}

If the old material has already developed a stable drying shrinkage volume, the following stresses will occur according to the amount of drying shrinkage of the new material

If $\varepsilon_{sh} = 0$ No stress occurs

If $\varepsilon_{sh} > 0$ Shear bond is stressed. Loads carried by repair are reduced; tension in repair material

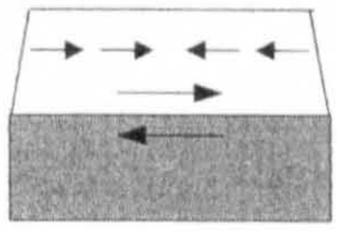

Figure 7.5 Effect of restrained shrinkage on strain compatibility adopted from Emmons[9]

Finally, it should be emphasized that in order to achieve a successful and long-lasting repair all the above compatibility requirements should be considered not only individually, but also as a complete integrated system of components and sub-components known as the total system. The total system or holistic approach is described by Emmons and Vaysburd[82] as an attempt to understand the behaviour of a concrete patch repair not only as the result of the various properties of its components viewed separately, but also, as the net result of the interaction between them. Vaysburd et al[83] recently extended the concept of the total system and described concrete patch repairs as a complex system of materials exposed to both external and internal factors such as mechanical loads, service and environmental exposure conditions, substrate behaviour, and early/mature age behaviour of repair material and their interaction. Ignoring the actual manner in which concrete patch repairs behave can lead to premature failure. Gu et al[84] describe one such example which is the use of very low permeability repair materials in reinforced concrete patch repairs. Although, the aim is to avoid corrosion of steel reinforcement by preventing the passage of external agents such as H_2O, O_2, CO_2 and ^{-}Cl, the use of very low permeability repair materials can lead to accelerated corrosion due to electrochemical incompatibility. Electrochemical incompatibility is developed due to electrochemical potential imbalance (EPI) caused in different sections of the steel reinforcement bar because of the dissimilar environments

created by the concrete patch repair. When the existing concrete substrate adjacent to the patch repair is porous and the oxygen permeability is quite high, the corrosion potential of the steel in such an area, Esb, is higher than the corrosion potential Erp, of the steel area covered by the patch repair. The electrochemical potential difference $|Esb - Erp|$ occurs due to the uneven oxygen availability caused by porosity or density differences between the existing concrete substrate and the patch repair and its amplitude represents the magnitude of electrochemical incompatibility. The result of electrochemical potential imbalance (EPI) is the creation of an oxygen corrosion macrocell. The section of the steel reinforcement embedded in the denser repair material develops a local "anodic area" where corrosion is accelerated. Oxygen reduction takes place at local "cathodic areas" in the adjacent porous concrete substrate where the oxygen concentration is high.

7.3 TYPES OF REPAIR MATERIALS

A large number of repair materials are available for shallow or deep structural patch repairs. The most common repair materials used for structural patch repairs in the construction industry include:

- Ordinary Portland Cement (OPC) mortar
- Ordinary Portland Cement (OPC) concrete
- Rapid Hardening Cement (RHC) concrete
- High strength concrete
- Polymer-modified cement concrete
- Polymer concrete
- Preplaced-aggregate concrete
- Shotcrete

- Fibre-reinforced concretes and shotcretes

CS-MR-4.5[85] describes the various types of generic repair materials used in the construction industry.

OPC mortars are low cost, general purpose repair materials that are typically used for both sallow and deep repairs up to 100 mm. Most OPC mortars can achieve a compressive strength of approximately 30 N/mm^2 at 28 days and satisfy the requirements for load carrying capability. In addition, the coefficient of thermal expansion and the modulus of elasticity are equal to that of the concrete substrate. However, moderate levels of restrained shrinkage induce stresses in the repair and may lead to the reduction in load carrying capacity of the repair and in the formation of cracks.

OPC concrete is a low cost, general purpose repair material that is typically used for deep repairs greater than 50 mm. Most OPC concretes can achieve a minimum compressive strength of approximately 30 N/mm^2 at 28 days and satisfy the requirements for load carrying capability. In addition, the coefficient of thermal expansion and the modulus of elasticity are equal to that of the concrete substrate. However, proper curing of OPC concrete is critical in reducing restrained shrinkage and for future long-term durability of the repair.

RHC concrete is used to minimise out-of-service time of repaired pavements and bridge decks. The depth and volume of the repair are usually small due to the high cost and rapid heat generation of RHC. Most RHC concretes can achieve a compressive strength of approximately 21 N/mm^2 at 4 hours. In addition, the coefficient of thermal expansion and the modulus of elasticity are equal to that of the concrete substrate. However, proper curing of RHC concrete is critical in controlling restrained shrinkage

which may induce stresses and lead to the reduction of load carrying capacity of the repair and in the formation of cracks.

High strength concrete is attractive as a potential repair material of structural concrete because of its high strength and durability while requiring minimal out-of-service time in carrying out the repair. Special types of cement or RHC can be used to produce high strength concrete. When RHC is used an accelerator may be required to achieve the specified minimum compressive strength at 24 hours. High strength concretes have a maximum w/c ratio of 0.35 and a minimum compressive strength of 50-100 N/mm^2 at 28 days. Many high strength concretes require a retarding admixture to control rapid stiffening in even moderate temperatures due to high cement contents. In some cases mineral admixtures such as PFA and GGBS are used to improve the strength and durability characteristics of high strength concrete.

Polymer-modified cement concrete is based on OPC concrete in which a water soluble or emulsified polymer has been added during the mixing process. Polymer modifiers are used to enhance the properties of the repair material. Latex (SBR) is the most common polymer modifier and is used to reduce permeability, increase adhesive strength with the substrate, and reduce modulus of elasticity. Polymer-modified concretes are typically used for shallow repairs up to 50 mm deep in situations where a less permeable, higher tensile strength material than conventional concrete is required. For repairs of greater depth the repair material must be placed in lifts. The properties and application of Polymer-modified concretes vary widely depending on the type and the amount of polymer used during the mixing process. Some of these concretes have coefficients of thermal expansion and moduli of elasticity close to commonly used structural concretes. However, Plum[86] demonstrated that the addition of latex (SBR) to

modify OPC concrete can cause the flexural creep value to dramatically increase under high humidity conditions.

Polymer concretes are typically used for shallow repairs up to 50 mm deep in pavements and bridge decks where a fast curing, high strength, and low permeability repair material is required. For repairs of greater depth the repair material must be placed in lifts. However, the cost for using Polymer concretes in deep repairs will likely result in another repair material being selected. Polymers used to produce concrete mixtures include epoxy resigns, polyesters, vinylesters, acrylics, styrenes, and polyurethanes. Application of these repair materials varies significantly. Some of them require a dry surface, some a moist surface, and some are not sensitive to moisture.

Preplaced-aggregate concrete is used for repairing large areas where low volume change is required. For repairs to vertical and overhead surfaces, the surface must be formed and aggregate tightly packed within the form. The preplaced aggregate is gap graded to exclude fines and typically has a 40% to 50% void ratio after the aggregate is packed. Care must be taken in preplacing coarse aggregate to avoid breakage and segregation of the aggregate. This becomes more difficult when the nominal maximum size aggregate increases or when two or more sizes are blended. Intrusion grout mixtures should be proportioned to obtain the specified consistency, air content, and compressive strength. A grout fluidifier is commonly used to offset bleeding, to reduce water/cement ratio and still provide a given consistency, and to retard stiffening so that handling times can be extended. Preplaced-aggregate concretes usually have coefficients of thermal expansion and moduli of elasticity equal to the concrete substrate. In addition the levels of drying shrinkage are very low.

Shotcrete mixtures are typically used to repair large spalled areas in vertical and overhead surfaces where the depth of repair is less than 150 mm. Conventional shotcrete

is the most common form of shotcrete used in the construction industry. It is pneumatically applied using a dry or wet mix process. Dry mix shotcrete process involves the premixing of binder and aggregates, which are then fed into a special mechanical feeder metering the premixed materials into a hose. The material is conveyed through the hose with compressed air to a nozzle which is outfitted with a water ring where additional water is mixed with the binder and the aggregates. The mix is jetted from the nozzle at high velocity onto the substrate. Wet mix shotcrete process involves premixing of all ingredients including binder, aggregates, admixtures, and mixing water. The premixed repair materials are deposited into a pump or pressure vessel which transports the repair materials to an exit nozzle, where compressed air is introduced. The repair material is propelled onto the substrate with compressed air. The properties of shotcrete are largely dependent on the conditions under which it placed, equipment used, and experience of the application staff. Shotcrete typically has a compressive strength in the range of 20 N/mm^2 to 48 N/mm^2. The coefficient of thermal expansion and modulus of elasticity are equal to that of the concrete substrate. However, drying shrinkage is usually within moderate levels.

Fibre-reinforced concretes and shotcretes are used to repair concrete where increased tensile strength is required. Steel or plastic fibres are the most common and are used to increase tensile strength, control shrinkage cracking and enhance toughness to impact and abrasion. The more common steel fibre shapes include straight, crimped, surface-deformed, and hooked ends. The straight steel fibres provide the least amount of toughness for the same volume concentration. Fibres are usually described by their aspect ratio, which is fibre length to diameter. Steel fibre-reinforced concretes usually have higher higher cement and fine aggregate contents and smaller nominal maximum aggregate size than conventional concretes. Nominal maximum size aggregate for these

concretes is usually 20 mm or less. The practical upper limit for most steel fibres is generally considered to be 2% by volume of the total concrete mixture. Pozzolans are often used to reduce the cement content in the mixture.

7.4 TYPES OF PRIMERS/BONDING AGENTS

In most repair projects adequate adhesive strength can be obtained by placing repair materials directly against properly prepared concrete. Bonding agents can be used to improve adhesive strength between the repair material and the concrete substrate. However, according to Silfwerbrand and Paulsson[87] bonding agents should normally be avoided. Use of bonding agents leads to two interfaces resulting in the creation of two possible planes of weakness instead of one. In addition, a grout often has a high water/cement ratio leading to a low strength and the risk of cohesive failure within the bonding agent itself. On the other hand bonding agents may have an ability to absorb loose particles on an insufficiently prepared surface. This absorption may increase the adhesive strength for this particular case. Three main types of bonding agents are frequently used:

- Cement-based slurries
- Latex emulsions
- Epoxy resigns

In the case of OPC mortar or concrete repair materials cement or sand/cement slurry is used as a bonding agent. After the substrate has been prepared, and immediately before placing the repair material, a thin coating of grout must be vigorously applied into the prepared substrate concrete surface.

In the case of polymer-modified concrete repair materials commercial blended latex-modified cement slurry bonding agents that are mixed with water on site and applied on the prepared substrate concrete surface should be used. Commercial latex bonding agents should follow the requirements of various standards such as ASTM C 1059[88]. In addition, manufacturer's instructions should be strictly followed when using latex products because not all of them are compatible with concrete.

A large number of epoxy resign based commercial products are available for use as bonding agents. These materials should follow the requirements of various standards such as ASTM C 881[89]. However, use of an epoxy resign agent may produce a vapour barrier, resulting in the failure of the bond. In addition epoxy resins have poor creep properties and should be avoided when the repair is subject to constant loading.

7.5 CONCLUSION

In this chapter a review of the various properties that repair materials must have to satisfy all requirements for a durable long lasting repair was carried out. In addition, a review of the various types of repair materials used in the construction industry was performed. The purpose of the above studies was to give a basis for the selection of repair materials to be used in the subsequent repair experiments of this research. For this reason the following 3 types of generic repair materials: a) Ordinary Portland Cement (OPC) mortar, b) Ordinary Portland Cement (OPC) concrete and c) polymer modified cement concrete are selected in order to be used in subsequent repair experiments.

Selection of OPC mortar is based on its ability to satisfy all requirements for strength (compressive, tensile, flexural and adhesive strength). In addition, it is chemically and electrochemically compatible to substrate concrete. It can also achieve similar water permeability properties to that of substrate concrete by using the right w/c ratio. Finally,

it can satisfy most aspects of strain compatibility since its coefficient of thermal expansion and modulus of elasticity are equal to that of substrate concrete. However, it has moderate levels of restrained shrinkage which can induce stresses in the repair and may lead to the reduction of load carrying capacity of the repair and in the formation of cracks.

Selection of OPC concrete is based on its ability to satisfy all requirements for strength (compressive, tensile, flexural and adhesive strength). In addition, it is chemically and electrochemically compatible to substrate concrete. It can also achieve similar water permeability properties to that of substrate concrete by using the right w/c ratio. Finally, it can satisfy most aspects of strain compatibility since its coefficient of thermal expansion and modulus of elasticity are equal to that of substrate concrete. However, proper curing is critical in reducing restrained shrinkage.

Selection of polymer modified cement concrete is based on data published by manufacturers which claims to meet all required mechanical properties and satisfy all aspects of compatibility.

Finally, the ability of cement-based slurry primers/bonding agents to protect steel reinforcement and at the same time promote adhesive strength will also be investigated.

CHAPTER 8

TEST METHODS FOR EVALUATING THE QUALITY OF PATCH REPAIRS

8.1 INTRODUCTION

Adhesion of the repair material to the concrete substrate is generally considered to be an important criterion in assessing the success and long-term durability of patch repairs. However, lack of standard procedures and test methods has resulted in the development of many different types of tests for measuring the adhesive strength. Development of such tests should be based on the following parameters:

- Ability to simulate actual site conditions
- Ability to expose only the bond to environmental conditions
- Ability to simulate the stress state of reinforced concrete members
- Highly sensitive to variation of adhesive strength
- Ability to assess in-situ adhesive strength
- Reproducibility of test results

There is no single test method that can satisfy all the above parameters. Hence selection should be based on the importance of each of the above parameters under a specific case.

The objective of this chapter is to describe the various test methods used for evaluating the adhesive strength of patch repairs and hence select the most appropriate test method for use in subsequent repair experiments. The test methods discussed include:

- tensile bond tests
- shear bond tests

- slant shear tests
- patch repair tests

In addition, an initial study on the use of ultrasonic pulse velocity method for assessing the quality of the bond interface between repair materials and concrete substrates is also described. The procedure for performing each test is briefly described and the advantages and limitations of each test are highlighted. Finally, particular reference to pull-off test is made, since it is the only test that can be used in-situ to evaluate the quality of concrete repairs and the one that will be used in this thesis.

8.2 TENSILE BOND TESTS

Tensile bond tests can be divided into direct and indirect. Direct tensile bond tests include the pull-off test, pipe nipple grip uniaxial tensile bond test, friction grip tensile bond test, and dumb-bell briquette test. Indirect tensile bond tests have been used on a small scale and include flexural tests and tensile split tests.

8.2.1 Direct tensile bond tests

8.2.1.1 Pull-off test

Pull-off test is used to assess the in-situ tensile or compressive strength of concrete. It can also be used to assess the adhesive strength between concrete substrates and repair materials. The first modern development of the pull-off concept for assessing the in-situ strength of concrete was undertaken independently in the UK by Long and Murray[90], and in Austria, by Stehno and Mall[91], where it was called tear-off test. BS 1881: Part 207[92] gives recommendations on the use of pull-off test for assessing the in-situ tensile or compressive strength of concrete, whereas, BS EN 1542[93] and ASTM D 4541[94]

give recommendations for measuring the adhesive strength between concrete substrates and repair materials. A number of different types of commercial pull-off test devices have been developed for assessing the adhesive strength of concrete patch repairs and overlays. McLeish[95] provides a detailed review of these devices. Although there are variations in the equipment and methods of performing pull-off tests the general test procedure can be described as follows:

A partial core is drilled perpendicular to the surface of the concrete. According to BS EN 1542[93] the partially drilled core should extend 10-20 mm beyond the bonding interface between the repair material and the substrate. A metal block (dolly) of the same nominal diameter is then attached to the top of the partially drilled core with the aid of a suitable epoxy resign. When the resign has achieved sufficient strength, a purely perpendicular force is applied to the metal block by means of a device, which in turn reacts with the surrounding area. The load is applied at a constant rate and the ultimate load at failure is recorded. The pull-off strength is given by the expression:

$$S_{PO} = \frac{F_T}{A_f} \tag{8.1}$$

where:

S_{PO} is the pull-off strength

F_T is the tensile (pull-off) force

A_f is the area of the fractured surface

A schematic of the pull-off test for assessing the adhesive strength is shown in Figure 8.1.

Cleland and Long[96] and Cleland and Misra[97] reviewed the factors that influence the variability of the pull-off test. These are:

- Disc material and thickness

- Core depth
- Core perpendicularity
- Moisture condition
- Loading rate

Disc material and thickness are important in order to achieve a satisfactory uniform stress distribution in the concrete. Bungey and Madandoust[98] investigated the effect of disc material and thickness on the pull-off strength of uniform concrete using experiments and finite element analyses. They concluded that the disc should be at least 20 mm thick for steel and 30 mm for aluminium. Austin et al[99] studied the effect of steel and aluminium discs using two different types of generic repair materials. They concluded that the disc thickness is less critical when testing the adhesive strength of patch repairs since the stresses are distributed through the depth of the repair material resulting in a more uniform stress distribution at the interface than at the surface of the repair material. However, when testing the adhesive strength of shallow patch repairs or thin overlays the thickness of the disc will be as critical as for testing the strength of uniform concrete.

The effect of core depth was investigated by Cleland and Long[96], Bungey and Madandoust[98] and Vaysburd and McDonald[100]. In the first two studies it was found that for core depths of 5 mm or more, the failure load is independent of core depth, but is less than that at the surface. For core depths of 20 mm or more the reduction in tensile strength between the base of the core and the surface can be up to 25%. According to Cleland and Long[96] the reason for this difference in tensile strength is that for shallow cores the combination of the stress concentration at the periphery of the core and the higher stress toward the centre, near the point of the application of the load, gives rise to

a more uniform state of stress and therefore a higher failure load. Finite element analyses carried out by Austin et al[99] showed that the stress concentration around the periphery of the core is minimal when the core extends at least 10 mm into the substrate. Since the stress concentration at the periphery can be avoided by extending the drilled core at least 10 mm into the substrate uneven stresses can only be occur in thin repairs due to the proximity of the applied point load. Hence, for testing patch repairs the base of the partially drilled core should extend sufficiently below the interface to ensure uniform stress distribution at the interface. In addition, the load at which failure occurs may be lower for shallow repairs of less than 10 mm. Vaysburd and McDonald[100] carried out field experiments in three different sites using three different types of commercial pull-off testing equipment and nine types of generic repair materials. Part of their research was aimed at studying the effect of the core depth on pull-off test results. Three different partial core depths were investigated. Finite element analyses were also performed. Results from both experiments and finite element analyses emphasised the importance of the core depth on pull-off test results. Based on their findings they suggested that the core depth should extend a minimum of 25 mm or one-half of the core diameter, whichever is larger into the substrate concrete.

Core perpendicularity is an important factor since pull-off testing requires the application of a purely axial load without bending. Although, various types of commercial pull-off testing equipment satisfy this requirement eccentricity can arise due to inaccurate coring of the specimen as shown in Figure 8.2 adopted from Cleland and Long[96]. According to Cleland and Long[96] by combining the direct tensile stress with that due to eccentricity, it can be shown that for small values of the angle α, the ratio of the failure load for any angle α to the failure load at $\alpha = 0$ is equal to

$$\frac{F_T \text{ at } \alpha}{F_T \text{ at } \alpha = 0} = \frac{1}{\left[1 + \frac{8\alpha}{D} y\right]} \tag{8.2}$$

where:

α is the inclination angle of the core

D is the diameter of the core

y is the depth of the core

Experiments carried out with cores of up to 40 mm and with axes at angles of up to 20^0 to the vertical confirmed the validity of the above relationship. Core perpendicularity is much more important when testing concrete repairs since the depth to the interface can be well in excess of 30 mm. This means that for the error to be less than 10% when testing a 50 mm deep repair, the axis of the applied load and the core must be within 0.7^0 of the perpendicular to the interface.

Cleland and Long[96] investigated the effect of moisture in the variability of pull-off test. Experimental results showed that pull-off test is not significantly influence by the moisture condition of the repair material.

According to Bungey and Madandoust[98] there is no evidence that the rate of loading critically influences pull-off test results. However, BS EN 1542[93] states that a constant loading rate of 0.05 ± 0.01 MPa/s should be used.

Based on the above BS EN 1542[93] states that the metal blocks should be either from steel or aluminium. The diameter of the metal blocks should be 50 mm. For aluminium blocks a thickness/diameter ratio of 60% should be used to ensure uniform stress distribution in the concrete. The loading system should be capable of applying a force to the block normal to the concrete surface through a bearing ring or tripod. Five pull-off tests should be carried out at each location. The arrangement of the test positions, the

sequence of the tests and the numbering system to be used is shown in Figure 8.3. A constant loading rate of 0.05 ± 0.01 MPa/s should be used.

When assessing the adhesive strength of patch repairs it is important to note the type and location of the failure since only those occurring at the interface are direct measurements of the adhesive strength. Failures occurring either at the repair material or at the concrete substrate are lower bound estimates of the adhesive strength. Finally, failures occurring at the dolly indicate the use of low strength adhesive materials or inadequate preparation of the repair material surface. For failures occurring at the interface the percentage of failure surface between the substrate and the repair material should also be recorded as shown in Figure 8.4 adopted from McLeish[95].

Pull-off test is considered to be by most researchers the best method available in evaluating the adhesive strength and hence the quality of patch repairs and overlays due to the following reasons:

- Ability to represent the actual site conditions
- Ability to assess the in-situ adhesive strength of patch repairs and overlays
- Ability to provide a measure of adhesive strength and identify the mode of failure
- Non-destructive form of testing

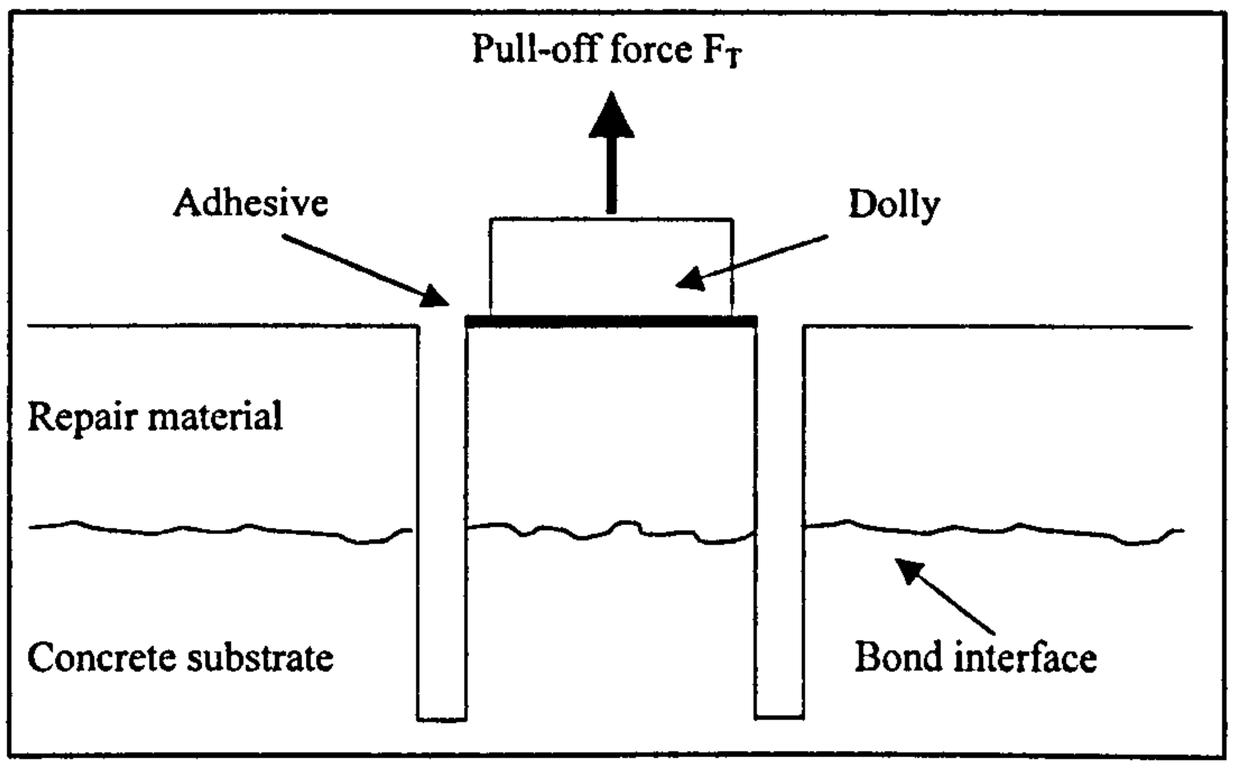

Figure 8.1 Schematic of pull-off test for assessing adhesive strength

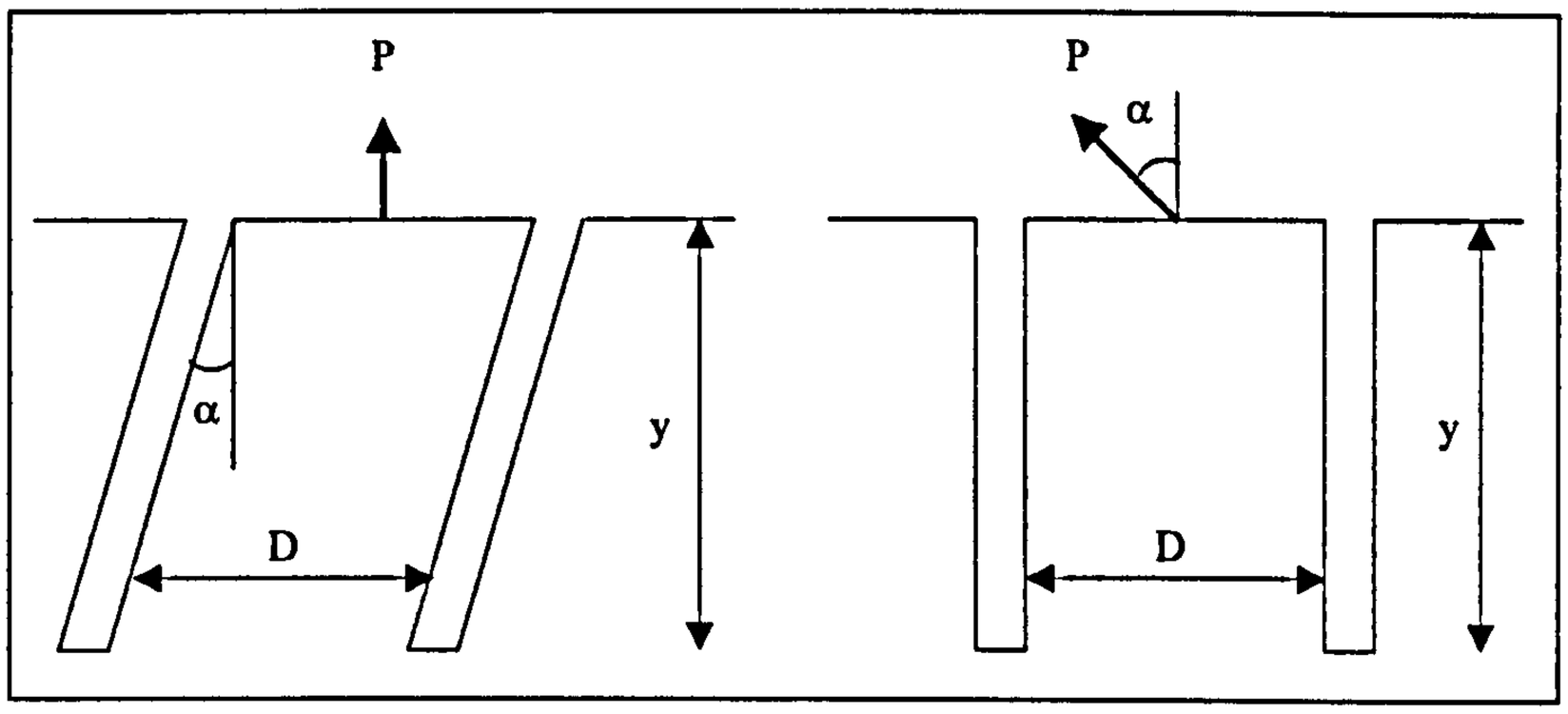

Figure 8.2 Causes of eccentricity adopted from Cleland and Long[96]

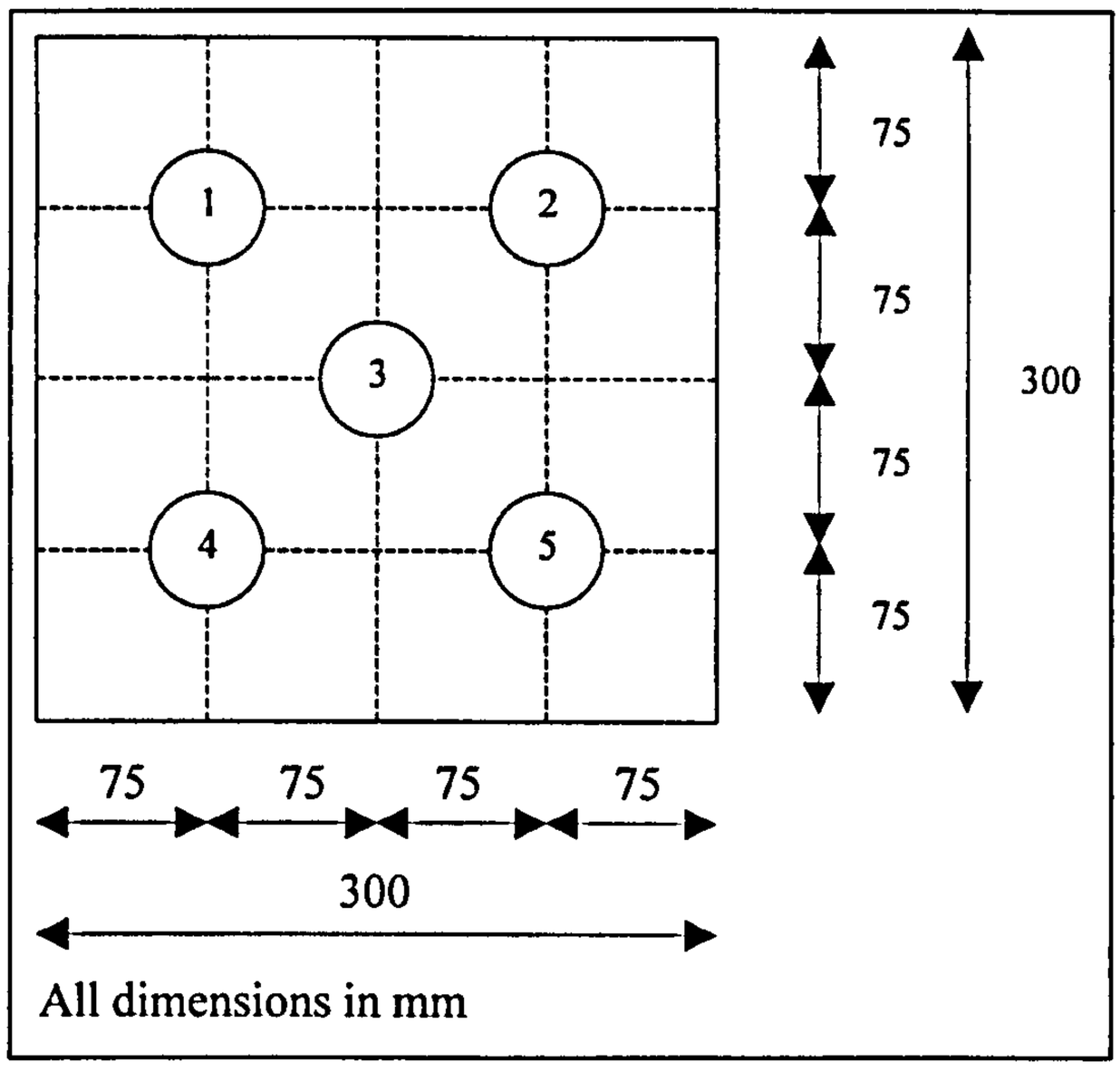

Figure 8.3 Schematic of pull-off test positions according to BS EN 1542[93]

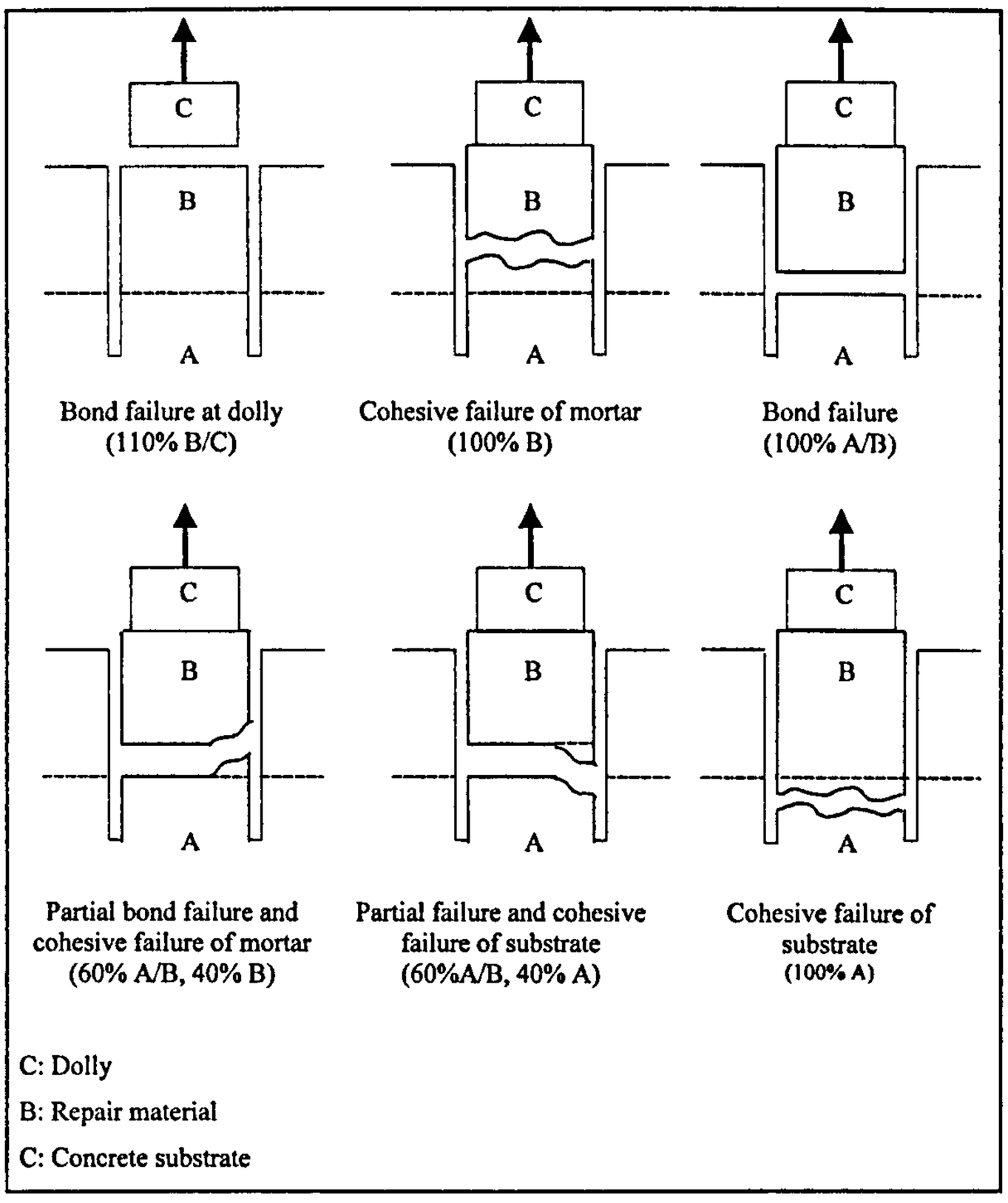

Figure 8.4 Pull-off test core failure modes adopted from McLeish[95]

8.2.1.2 Pipe nipple grip/friction grip tensile bond tests

The pipe nipple grip and the friction grip tensile bond tests are essentially the same except the shear force transfer mechanism is different. In both tests the specimen consists of a 76 mm diameter by 76 mm long cylinder of repair material bonded to a 76 mm diameter by 76 mm long cylinder of substrate concrete.

In the case of the pipe nipple grip test, the lateral circumference of the substrate concrete cylinder with a sawn surface is bonded with epoxy resin inside a nominal 76 mm inside diameter by 76 mm long black steel pipe nipple. After the epoxy has cured, the specimen is inverted and an empty steel pipe of the same size is mounted on the top of the base concrete, with a rubber O-ring being placed in between the pipes. The rubber O-ring provides approximately 4.8 mm of spacing between the pipes at the bond

interface. The repair material is then poured into the empty steel pipe nipple. After curing, the repair material has bonded to the sawn surface of the substrate concrete and to the inside of the pipe nipple into which it has been poured. The specimen is then attached to the testing machine with the aid of pipe caps with special attachments, which are screwed onto the pipes at both ends.

In the case of the friction grip test two identical split pipe pieces (friction grip) are used, one to grip the substrate concrete the other to grip the repair material. By closing together the sides of the steel pipe which has been split parallel to its longitudinal axis the required friction around the lateral surface area of the bond strength specimen to transfer external load to the bond interface is developed. A schematic of both tests is shown in Figure 8.5.

Knab and Spring[101] performed tests to evaluate pipe nipple grip/friction grip tensile bond tests and slant shear test. Three types of generic repair materials were used. A substantial difference in failure stress values between the pipe nipple grip/friction grip tensile bond tests and slant shear test was recorded. However, results were not directly comparable because in each test the bond interface had different geometry and was subjected to different loading conditions and stress states. They concluded that the pipe nipple grip bond test is more suitable compared to the friction-grip tensile bond test because of its higher average failure stress and better relative precision.

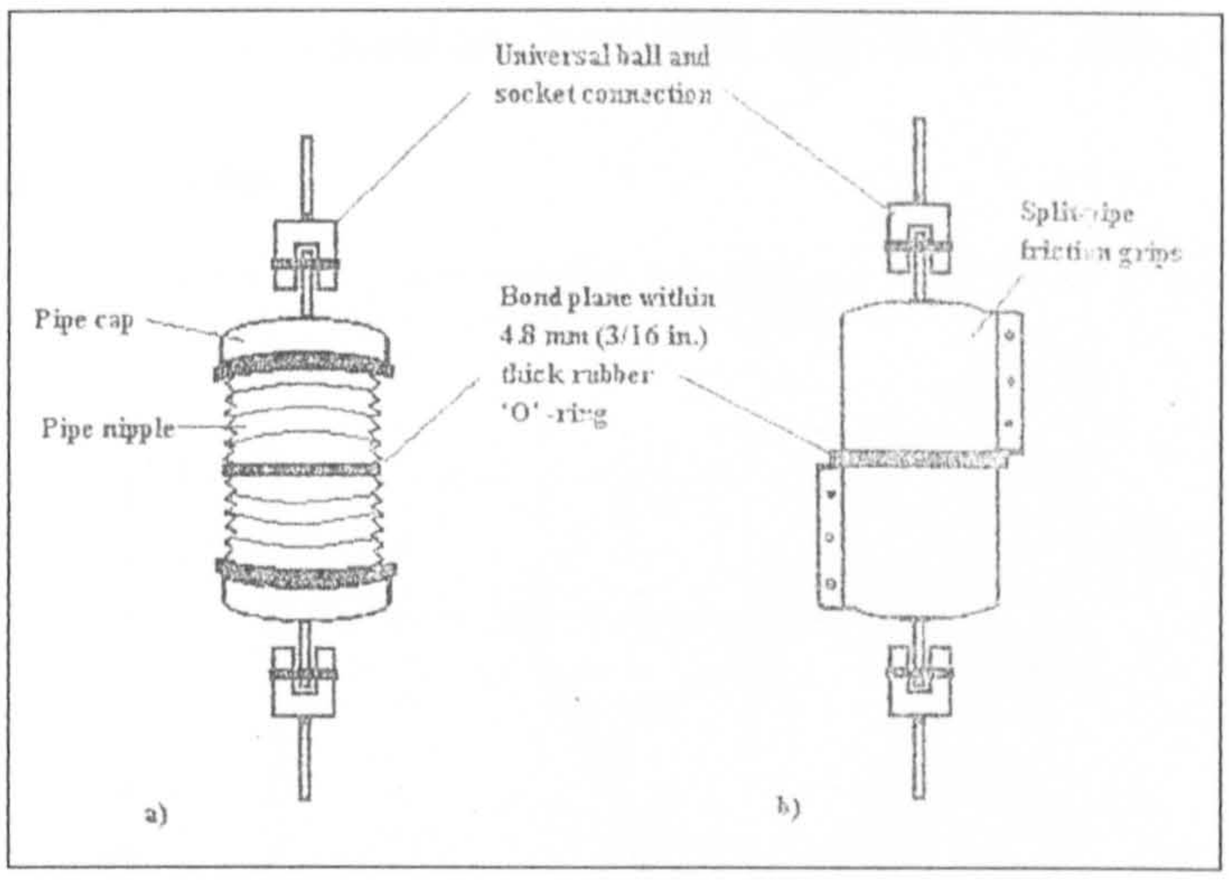

Figure 8.5 a) Pipe-nipple grip tensile bond test b) Friction-grip tensile test

8.2.1.3 Dumb-bell briquette test (dog-bone test)

Dumb-bell briquette test is also known as dog-bone test. BS 6319: Part 7[102] gives recommendations for measuring the tensile bond strength using the dump-bell briquette test. The test specimen is cast in a dumb-bell briquette shaped mould giving a cross sectional area at the waist of 645 mm^2 as shown in Figure 8.6. The geometry is such that during testing the specimen can be held at each end using specially shaped jaws and under tension will break across the narrowest width. Judge et al[103] carried out dumb-bell briquette and pull-off tests. Results showed that failure stresses from the dumb-bell briquette test were much higher than that from the pull-off test. The difference in failure stresses may be partly attributed to different types of surface preparation. The substrate surfaces for pull-off tests were acid etched, well washed and wire brushed, whereas for dumb-bell briquette tests broken surfaces were used. Ohama et al[104] also performed dumb-bell briquette tests to investigate the effect of polymer addition on tensile bond strength together with other types of tests. Results showed that failure stresses from dumb-bell briquette tests were higher than that from another direct tensile test in the same paper shown in Figure 8.7. Dumb-bell briquette test is economical and easy to

perform. However, it is a laboratory test and can not be used for assessing the performance of repairs on site.

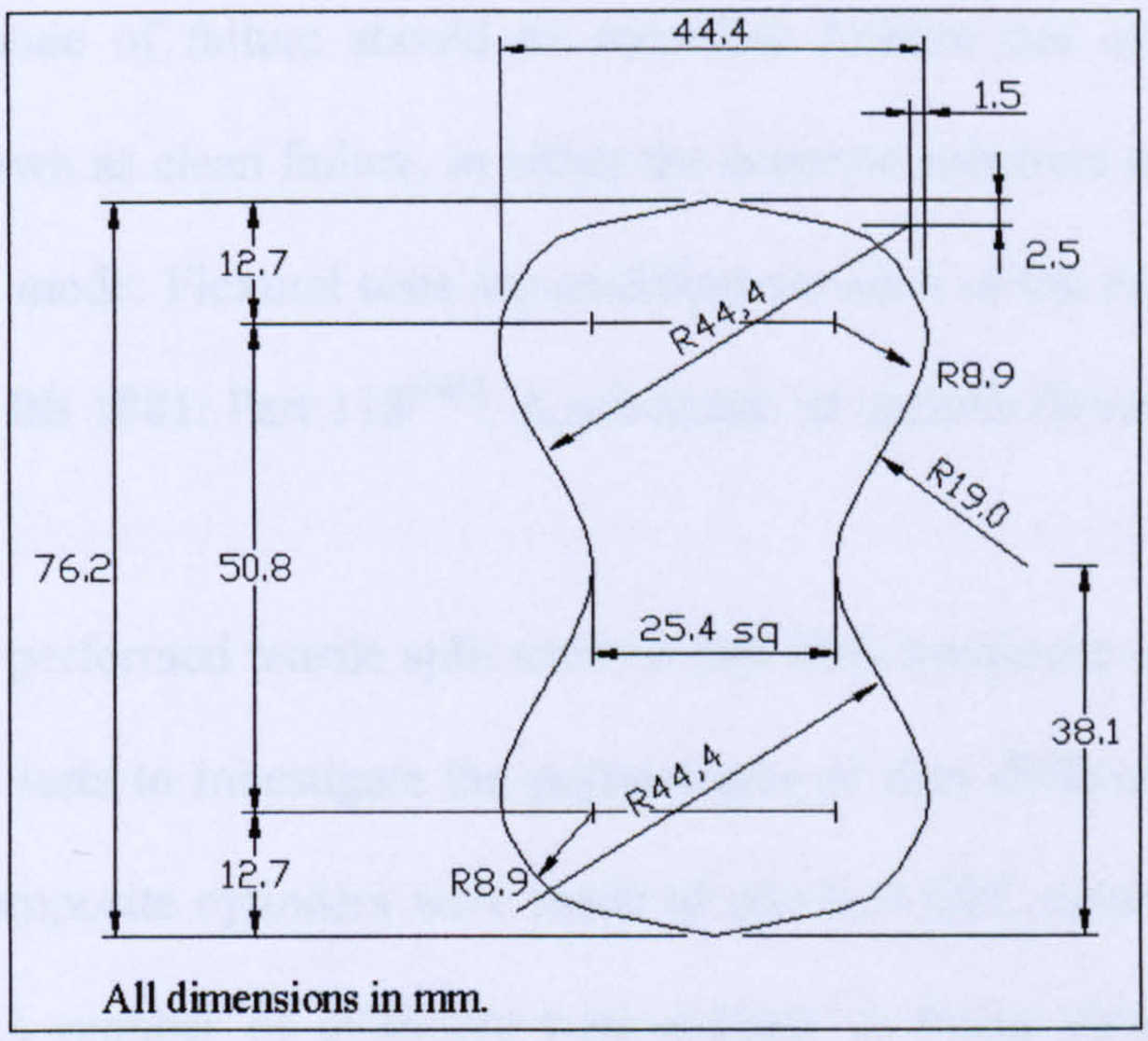

Figure 8.6 Schematic of dumb-bell briquette test specimen

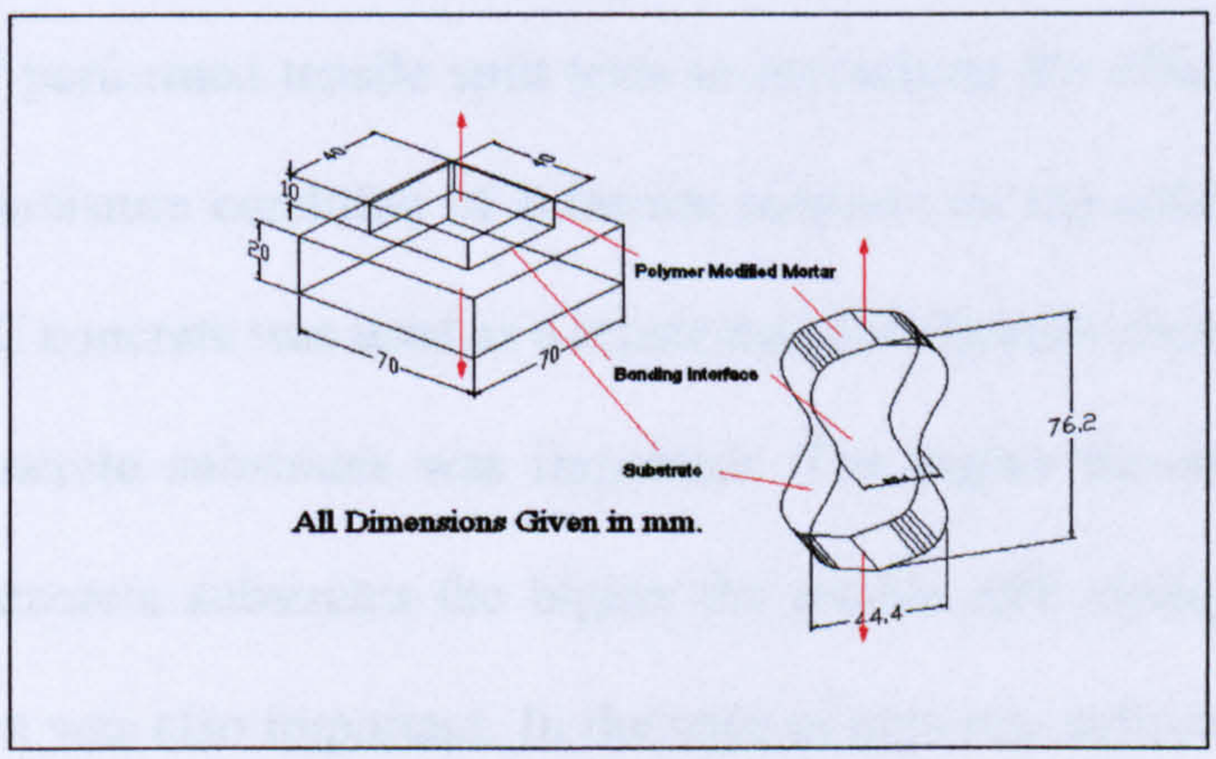

Figure 8.7 Schematic of a direct tensile test and dumb-bell briquette test performed by Ohama et al[104]

8.2.2 Indirect tensile bond tests

A small number of indirect tensile bond tests have been performed but only on a very limited scale. Indirect tensile bond tests include tensile split tests and flexural tests. Tensile split tests are modified versions of the tensile split method described by BS

1881: Part 117[105] and they can be performed in either repaired cubes or cylinders as shown in Figure 8.8. When tensile split tests are performed the maximum tensile split stress and the mode of failure should be recorded. Failure can occur in the bond interface also known as clean failure, in either the concrete substrate or repair material, or in a combined mode. Flexural tests are modified versions of the modulus of rapture test described by BS 1881: Part 118[106]. A schematic of various flexural tests is shown in Figure 8.9.

Ramey et al[107] performed tensile split tests on 3x6 inch composite cylinders together with direct shear tests to investigate the performance of four different types of repair materials. The composite cylinders were made of one-half OPC concrete and one-half repair material. A number of cylinders were subject to freeze-thaw cycles. Results showed that coefficients of variation from tensile split tests were smaller compared to direct shear tests.

Geissert et al[108] performed tensile split tests to investigate the effects of age, freeze-thaw cycles and moisture condition of substrate concrete on the adhesive strength and failure mode. OPC concrete was used as a repair material. Results showed that the effect of age of the concrete substrates was important. The higher the age and hence the strength of the concrete substrates the higher the tensile split strength. The effect of freeze-thaw cycles was also important. In the case of concrete substrates that were wet during the application of the repair material the average tensile split strength of the freeze-thaw specimens was 20% lower than the continuously water cured specimens of the same age. However, when the concrete substrates were dry during the application of the repair material no significant decrease in the average tensile split strength was recorded by the use of freeze-thaw cycles. Failure modes were also recorded. In most specimens failure occurred at the bond interface.

Wall et al[109] used two types of flexural tests (Figure 8.8 c and d), tensile split test and the slant shear test to investigate the effects of various parameters on the adhesive strength. The following parameters were investigated: w/c ratio of OPC mortar repair material, thickness of the bond layer, different curing conditions, wetting of the substrate concrete surface prior to the application of OPC mortar bonding agent, and delay between mixing a polymer bonding agent and its application to substrate concrete. Although a reduction in adhesive strength was observed using polymer agent compared to the OPC mortar the relative decrease in adhesive strength detected by the indirect tensile tests (flexural tests and tensile split test) was not as sensitive as the slant shear test.

Abu-Tair et al[110] performed another type of flexural test together with slant shear tests. Flexural test specimens were cast in 100x100x500 mm moulds and then cut in two halves using a diamond saw. The repair material of approximately 25 mm in thickness was sandwiched between the two halves as seen in Figure 8.10. The composite specimens obtained using the above procedure were then tested using the standard modulus of rapture test shown in Figure 8.11. Three types of repair materials were used: OPC concrete, polymer-modified concrete and epoxy resign. Four surface preparation methods smooth as-sawn, wire-brushed, needle-gunned and hand-chiseled, were used to prepare the samples. Specimens from both tests were subjected to both static and cyclic loading. Results showed that the flexure test was more sensitive to the effects of different repair materials on the adhesive strength, whereas the slant shear test was more sensitive to the effects of different surface preparations.

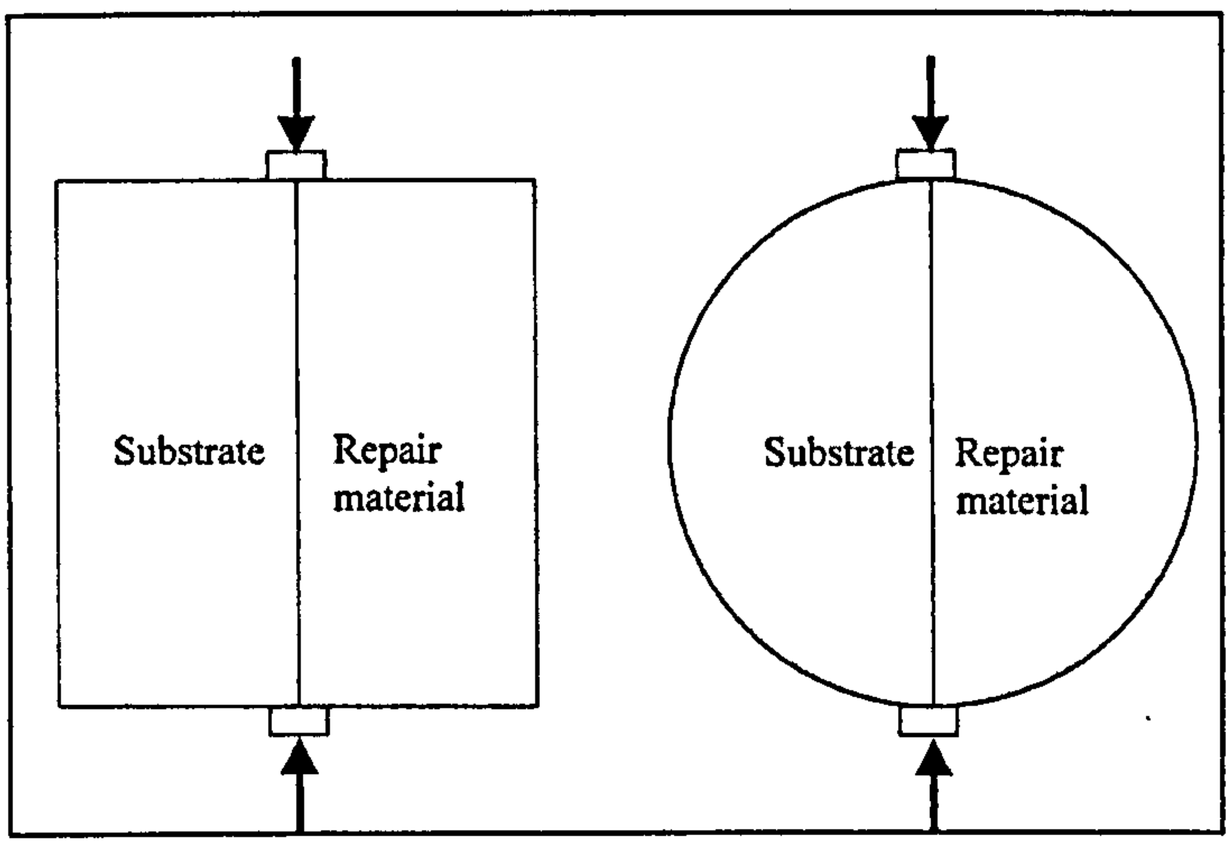

Figure 8.8 Schematic of tensile split tests

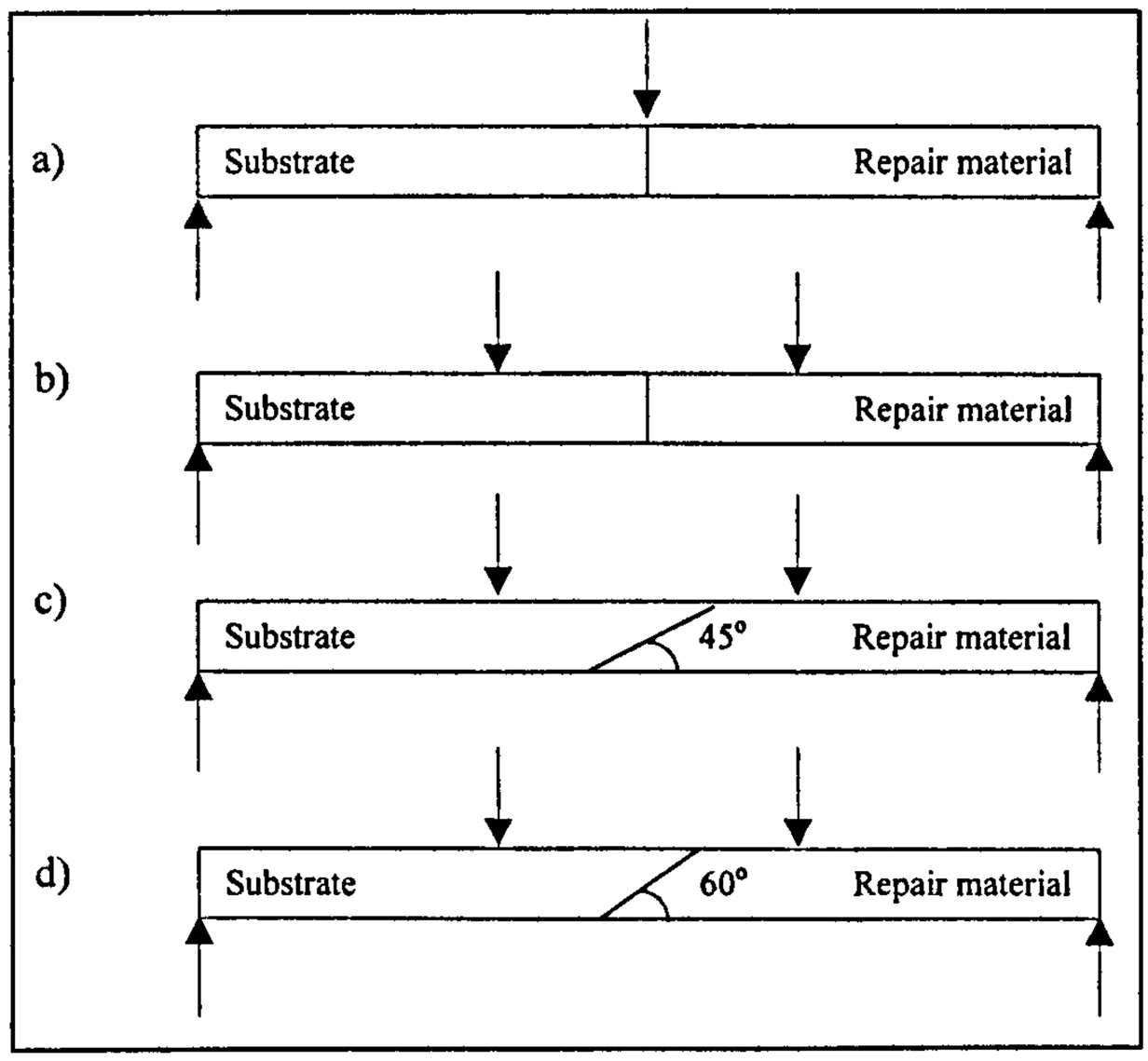

Figure 8.9 Schematic of different types of flexural tests

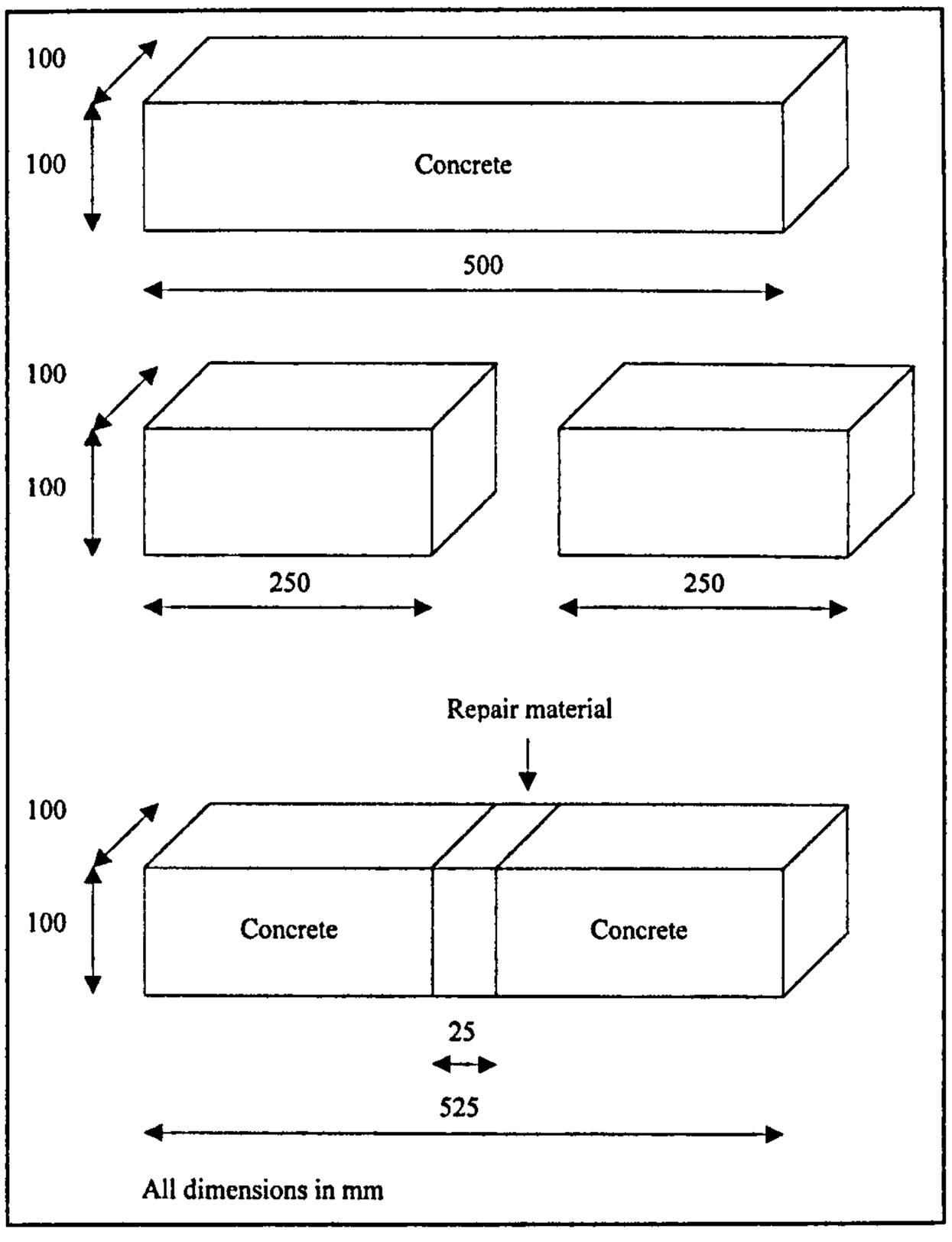

Figure 8.10 Production of flexural test specimens used by Abu-Tair[110]

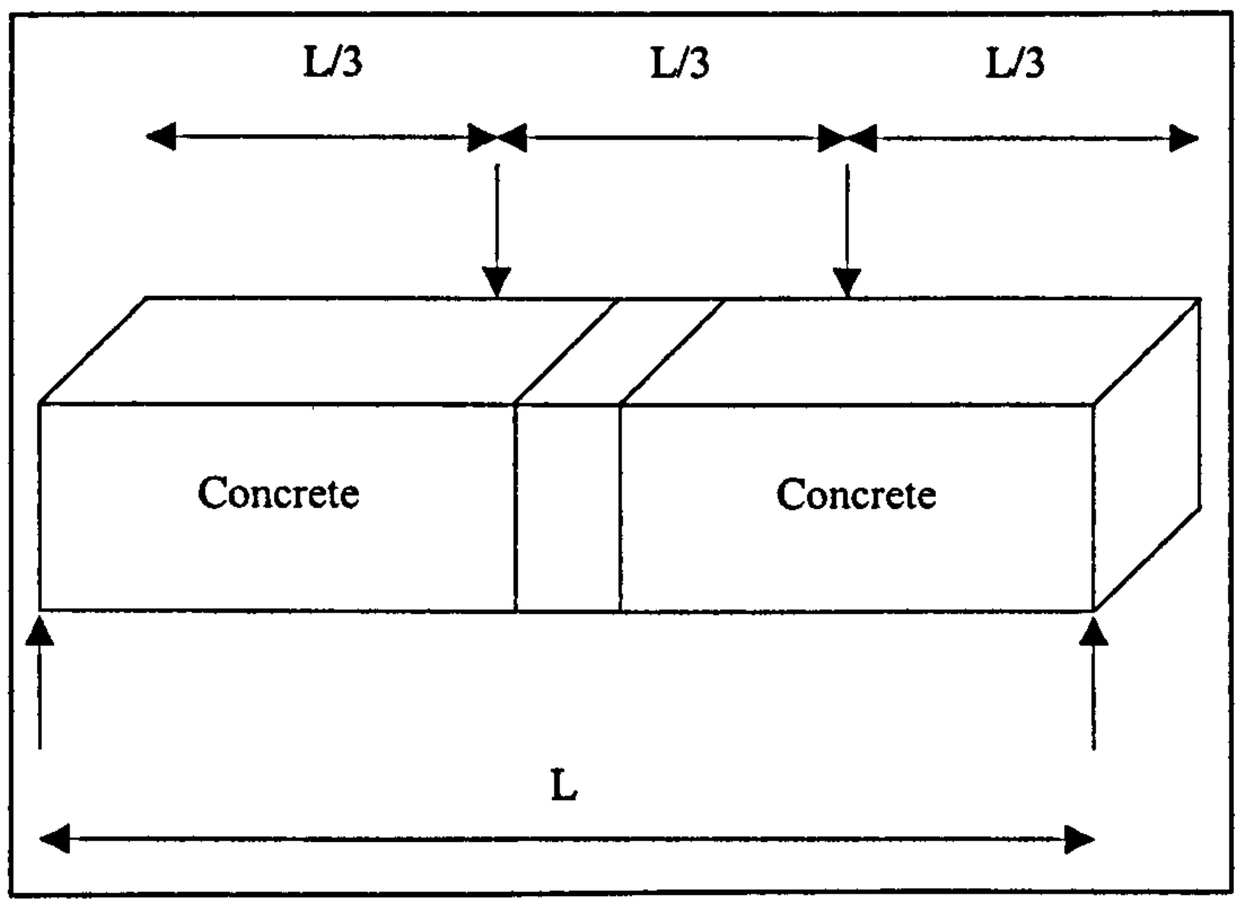

Figure 8.11 Flexural test performed by Abu-Tair et al[110]

8. 3 SHEAR BOND TESTS

Shear bond tests can be performed either by applying a shear force or a torque over the bond interface. In the first case, a more uniform shear stress distribution is achieved over the bond interface, while in the second case, a high shear stress gradient will be developed.

Ohama et al[104] performed two types of direct shear bond tests using circular and rectangular cross-section specimens as shown in Figure 8.12. Results showed that circular cross-section specimens produced higher shear bond strength compared to square specimens. However, since the loading positions are not known, it is not clear whether the difference in shear bond strength can be attributed to secondary bending effects or shape effects of the bond area.

Tayabji[111] reported shear bond tests on a bridge deck. Cores of approximately 94 mm in diameter were cut from test positions of the repaired bridge deck. The cores were tested using direct shear test equipment. Results showed a decrease of the shear bond strength with an increase of the removal depth of concrete achieved using hydrojetting. It appears that the findings of this research contradict the generally established belief that for a real case of repair such as this one, increased removal depth by hydroblasting would produce stronger, at least not weaker bond strength. No explanation was given.

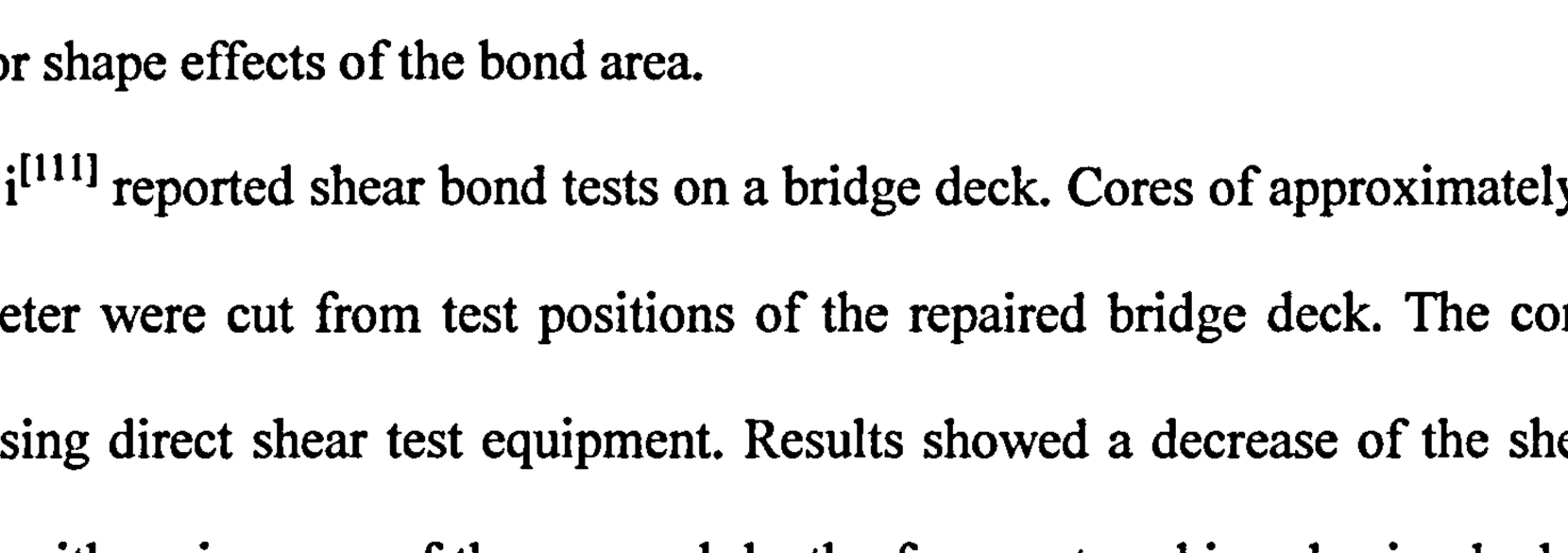

Figure 8.12 Direct shear bond tests

Cleland et al[112] developed a twist-off shear test to study the effect of curing conditions on bond strength. A schematic of the twist-off shear test is shown in Figure 8.13. The test procedure is basically the same as the pull-off test except a torque is applied instead of a tensile force. In their research, the twist-off test was used together with the pull-off test to study the effect of substrate concrete surface preparation. The surfaces of the concrete substrates were obtained using two different methods: saw cut and split/chisel hammered. Results from the pull-off test showed a significant decrease in adhesive strength on split/chisel hammered surfaces whereas results from the twist-off test hardly showed any difference.

Yeoh et al[113] used both twist-off and pull-off tests to investigate the effect of different curing conditions and different repair materials. Good correlation and similar trends were observed.

Ali et al[114] also used twist-off and pull-off tests to study the effect of different bonding agents and different types of substrate concrete surface preparation. Initially, experiments were carried out on three-month-old OPC mortar slabs with a new layer of cement mortar cast on them. Next, experiments were carried out on OPC concrete slabs with a new layer of concrete cast on them. Finally, experiments were carried out on precast concrete slabs stiffened with steel pipes with a new layer of concrete cast on them. Surface treatment of OPC mortar slabs included grinding, chipping, shot blasting hydroblasting and no treatment. Surface treatment of OPC concrete slabs included fine grinding, coarse grinding, chipping, shot blasting, dry ice-blasting, and no treatment. For OPC mortar slabs the bonding agents used were cement slurry, epoxy resign and no bonding agent whereas, for OPC concrete slabs the bonding agents used were polymer (Styrene Butadiene), epoxy resign and no bonding agent. Results showed that when no bonding agent was used, the influence of the surface roughness on the adhesive shear

strength was very significant. Rougher surfaces produced higher adhesive shear strengths. When OPC mortar was used as a bonding agent, the adhesive shear strength was low and failure occurred at the interface between the substrate and the repair material. Finally, when polymer mortar and epoxy resign were used as bonding agents the value of the adhesive shear strength was improved significantly. Epoxy resign produced very high adhesive shear strengths and failure of specimens occurred at the interface. Polymer mortar also gave high adhesive strength values but most failures occurred at the interface.

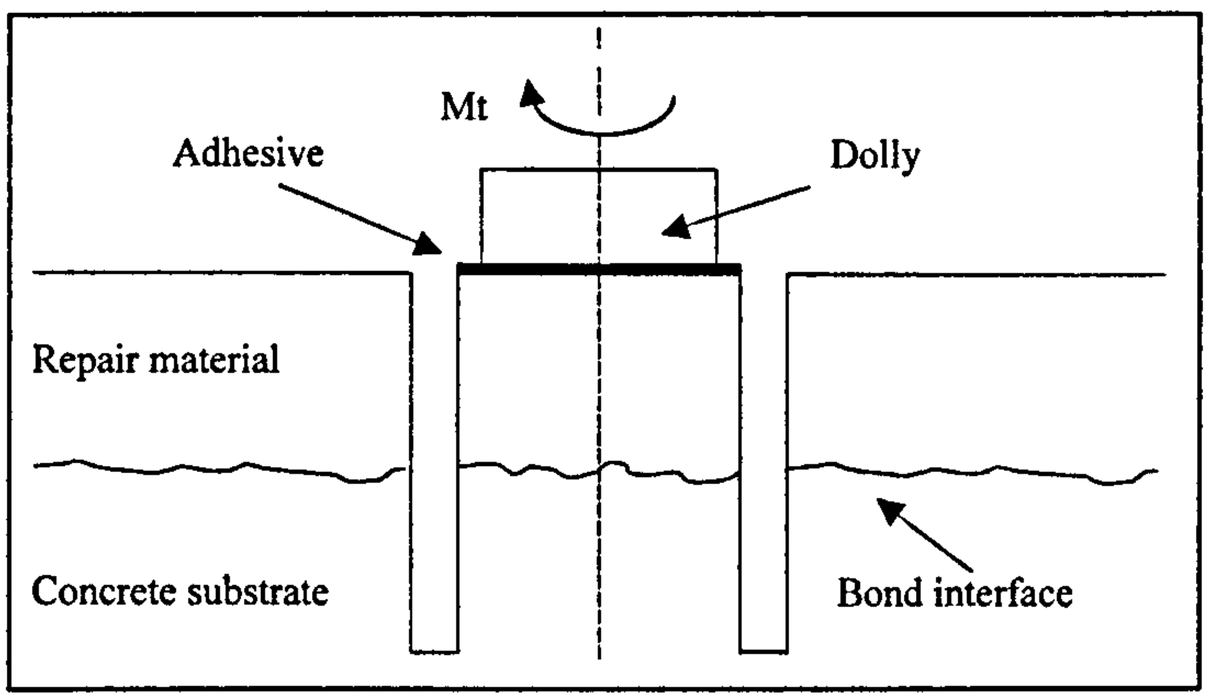

Figure 8.13 Schematic of twist-off test

8.4 SLANT SHEAR TEST

The first test of this type was the Arizona slant shear test which was developed by Kreigh[115]. The test was based on comparing the strength of repaired 6x12 inch concrete cylinders against standard concrete specimens. According to Kreigh[115] this type of test represents a more realistic situation in terms of the actual mode of failure of concrete. However, this type of test suffers from difficulties in producing the specimens and is only of practical use for assessing large quantities of repair materials and bonding agents. In order to overcome these problems a simplified version was developed by Tabor[116]. Today the slant shear test is the most common type of test used by manufacturers of repair materials to evaluate product performance. BS 6319: Part 4[117],

BS EN 12615[118] and ASTM C 882[119] describe the use of the slant shear test version developed by Tabor[116] for assessing the adhesive strength between epoxy-resign repair materials and substrate concrete.

The test is based on applying a compressive load to a specimen in the form of a composite prism with a bond line running diagonally through it. The bond is subjected to a combination of shear and compressive stresses which according to some researchers is more closer to that encountered in concrete structures. As the angle between the bond line and the vertical axis decreases the ratio of shear to compressive stresses increases. For prisms of modest dimensions an angle of 30^{o} has found to be the shallowest practical angle at which a joint can be formed.

In order to perform a slant shear test a high strength concrete plaque is cast. The plaque should have dimensions of 150x150x55 mm. After the plaque is demoulded and cured for 28 days it is sawn in two halves. Repair material is applied at each halve-plaque to obtain a composite plaque of 150x150x55 mm as shown in Figure 8.14. After the repair material is cured the composite plaque is sawn in three sections as shown in Figure 8.15. The outer sections of the sawn composite plaque are discarded and the middle section is used as the test prism. The composite test prism is then placed in a compression machine and is tested under a compressive load. The failure stress is obtained by dividing the load at failure by the cross-sectional area of the composite prism. Both the failure stress and mode of failure are recorded.

Wall et al[109], Rizzo et al[120] Climacao et al[121] prefer the slant shear test because they claim that it closely represents the actual stress state of in-situ repairs. Judge et al[103], Ohama et al[104], Abu-Tair et al[110], Naderi et al[122], Al-Mandil et al[123], Austin and Robins[124], Sausier et al[125], Wade et al[126], and Pan[127] included the slant shear test in their research to compare its reliability against other types of tests. In many of the above

studies a significant scatter of slant shear test results or conflict between slant shear test results and other test results were observed raising questions regarding the credibility of slant shear test.

Ohama et al[104] measured the adhesive strength of polymer modified materials using different types of tests. By varying the polymer/cement ratio, the adhesive strength was measured from each type of test and plotted against the polymer/cement ratio. All types of tests except the slant shear test showed an increase in the adhesive strength with an increase in the polymer/cement ratio up to 20%. The slant shear test showed a decrease in the adhesive strength with an increase of polymer/cement ratio up to 5%.

Naderi et al[122] also obtained conflicting results between pull-off and slant shear tests. They reported that the slant shear test gave less consistent results. The conflicting results made them question the reliability of the slant shear test.

Austin and Robins[124] concluded that the results obtained using the slant shear test may not be representative of the actual adhesive strength of patch repairs. They emphasised the fact that the test is significantly influenced by the mechanical interlock at the bond plane and the compressive strength of the weaker material.

Pan[127] concluded that the direction of the bond line in the slant shear test may vary slightly depending on the method used to produce the substrate. If the direction of the actual bond line is significantly diverted from the direction of the critical bond line at which the required external stress to produce a shear bond failure is minimum, high variation in the failure load can be expected.

Slant shear test is economical and easy to perform, however, it is a laboratory test and can not be used for assessing the performance of repairs on site.

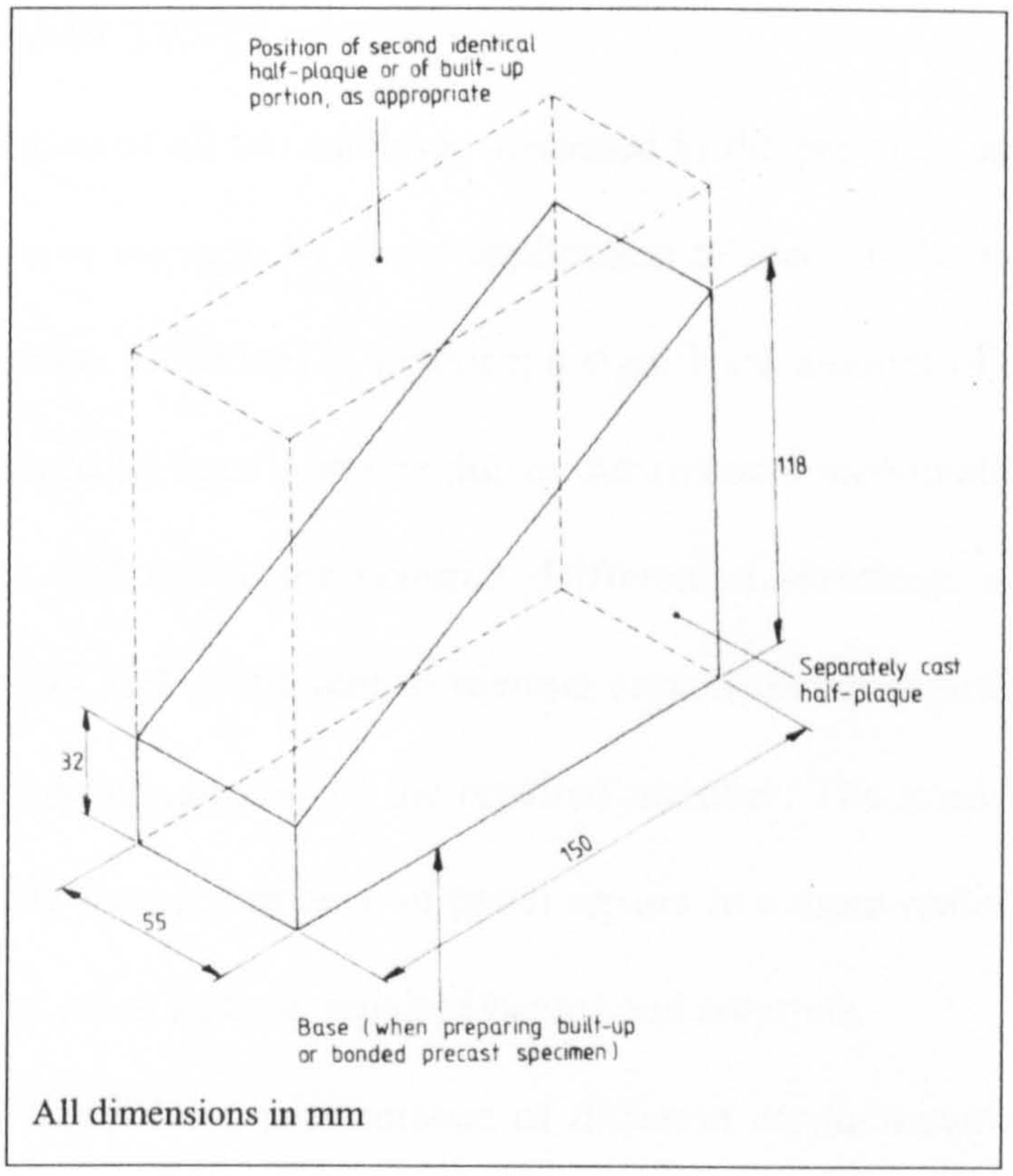

Figure 8.14 Schematic of 150x150x55 mm composite plaque

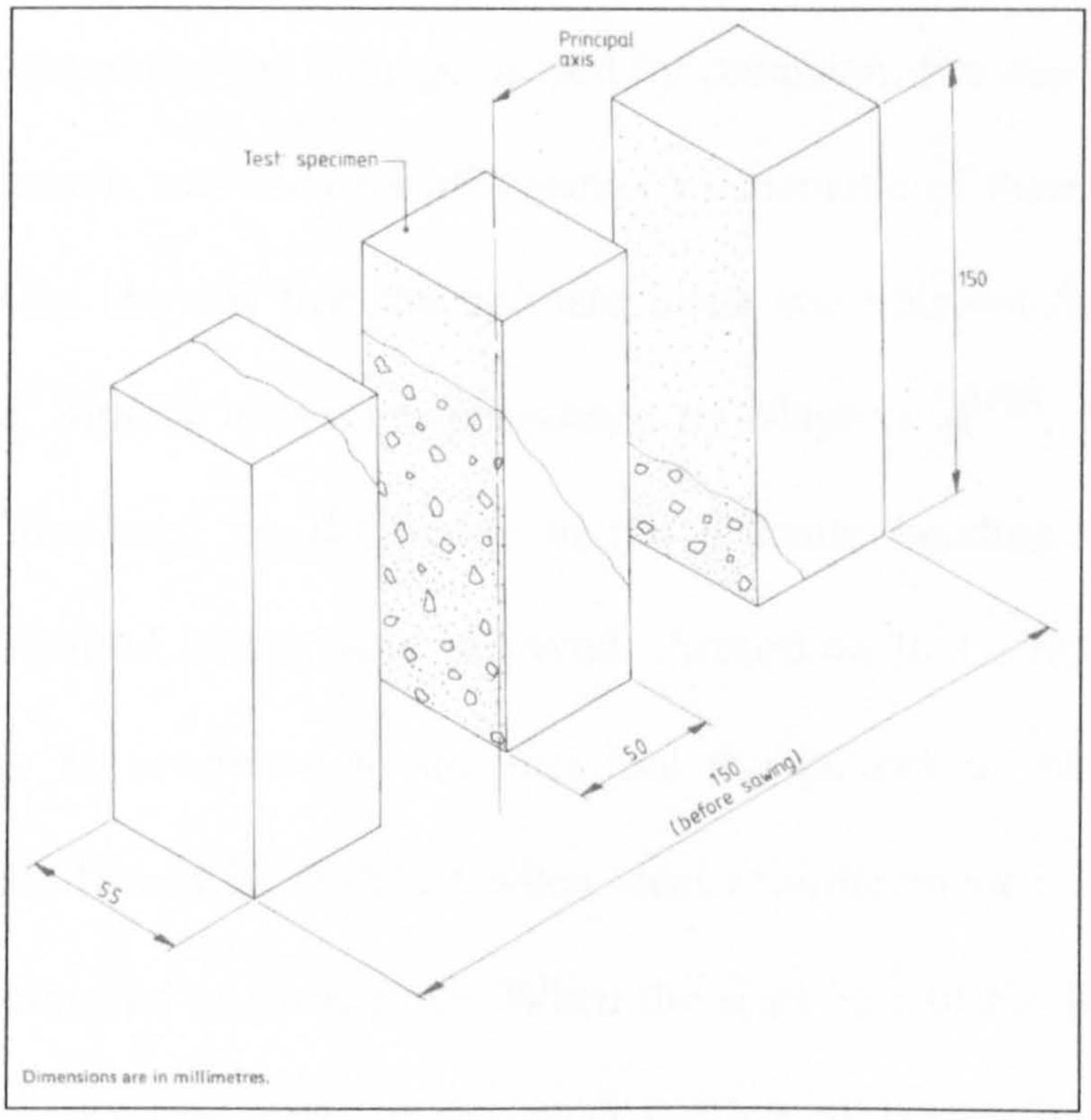

Figure 8.15 Schematic of composite test prism

8.5 PATCH REPAIR TESTS

The major limitation of all test methods discussed in the previous sections is that they measure the adhesive strength by direct application of load on the repair material and the concrete substrate. However, in practice, a significant amount of the loading of the repair will be induced by tensile strains due to dimensional incompatibility between the concrete substrate and the repair material. Differential shrinkage and differences in modulus of elasticity and coefficient of thermal expansion can significantly reduce the long-term load carrying capacity of the repaired member. The need to develop a new type of test to study the performance of patch repairs in a more realistic way has led to the development of patch tests on repaired beams and columns.

Burley et al[128] studied the performance of different repair materials using flexural tests. A number of reinforced concrete beams with dimensions of 2500x205x104 mm were cast either with no performed faults or with three different types of performed faults. The faults simulated the damage caused by corrosion, fire and impact. The same mode of reinforcement was used for all beams. A schematic of these tests is shown in Figure 8.16. Results showed that the ultimate loads were almost the same including unrepaired beams. Similar tests were performed by Mays et al[129], Kudlapur et al[130] and Cairns[131]. Similarly, no difference in the ultimate bending capacity between repaired and unrepaired beams was observed. According to Cairns and Zao[132] the above results can be attributed to the fact that the pattern of stress and strain in reinforced concrete beams is modified when steel reinforcement is exposed within a length of beam subjected to shear force. When the steel bars of the beam are exposed, the maximum compressive strain at the cross-section of largest bending moment is increased and the distance from the compression face of the beam to the neutral surface is reduced. Away from the section of largest bending moment, depth to the neutral

surface will be increased and the normal pattern of strains may even be reversed, with tension strains developing on the compression face. Reinforced concrete beams may be capable of carrying a significant amount of their load capacity even where steel reinforcement is exposed over a major proportion of the span. Shear failures do not occur where all steel bars in the cross-section are exposed. The risk of anchorage failure immediately outside of the exposed length is increased. Compression failures may occur on the tension face of a beam if the exposed length extends close to the supports. Results obtained using numerical calculations based on a non-linear finite strip technique developed by Lin and Raoof[133] were in good agreement with the above findings.

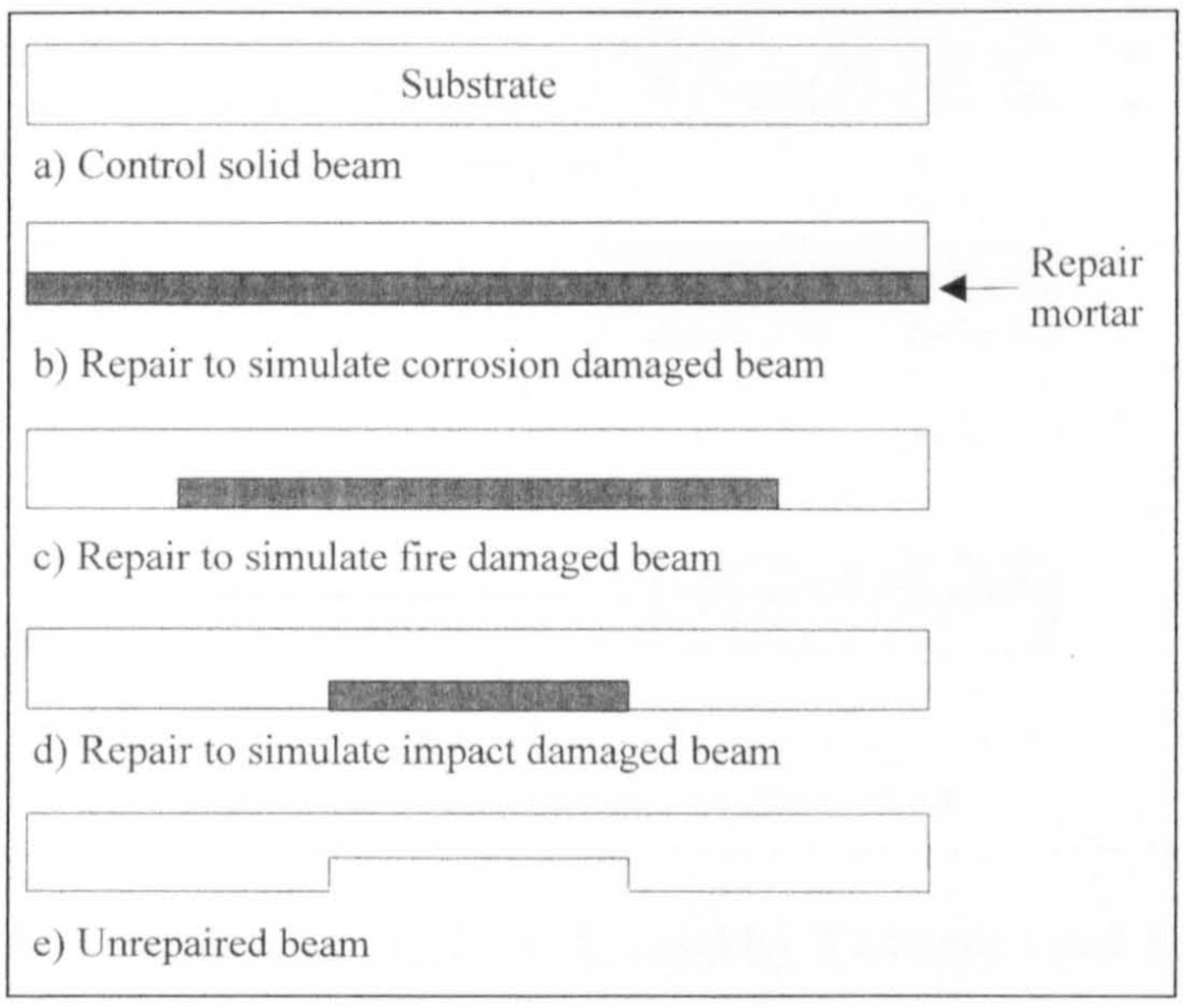

Figure 8.16 Flexural tests

Ramirez et al[134] performed repairs of concrete columns with localised partial loss of corners or cover. Their research was focused on improving column strengths. Repaired columns showed increased strength, and failure occurred due to the debonding of the repair material.

Emberson and Mays[135] investigated the effect of dissimilar elastic properties (Modulus of elasticity and Poisson's ratio) between repair materials and substrate

concrete using axially loaded patch repair tests. Their research was divided into three stages: direct transferring of stress, indirect transferring of stresses in a plain concrete substrate, and indirect transferring of stresses in a reinforced concrete substrate. A schematic of these tests is shown in Figure 8.17. Results showed that the Young's modulus E value of the repair material is of paramount importance in reinforced patch repairs. Poisson's ratio ν is more influential in unreinforced than in reinforced patch repairs. Finally, comparison of experimental results with those obtained using finite element analysis showed good agreement within the elastic range, provided that interfacial adhesion failure did not occur.

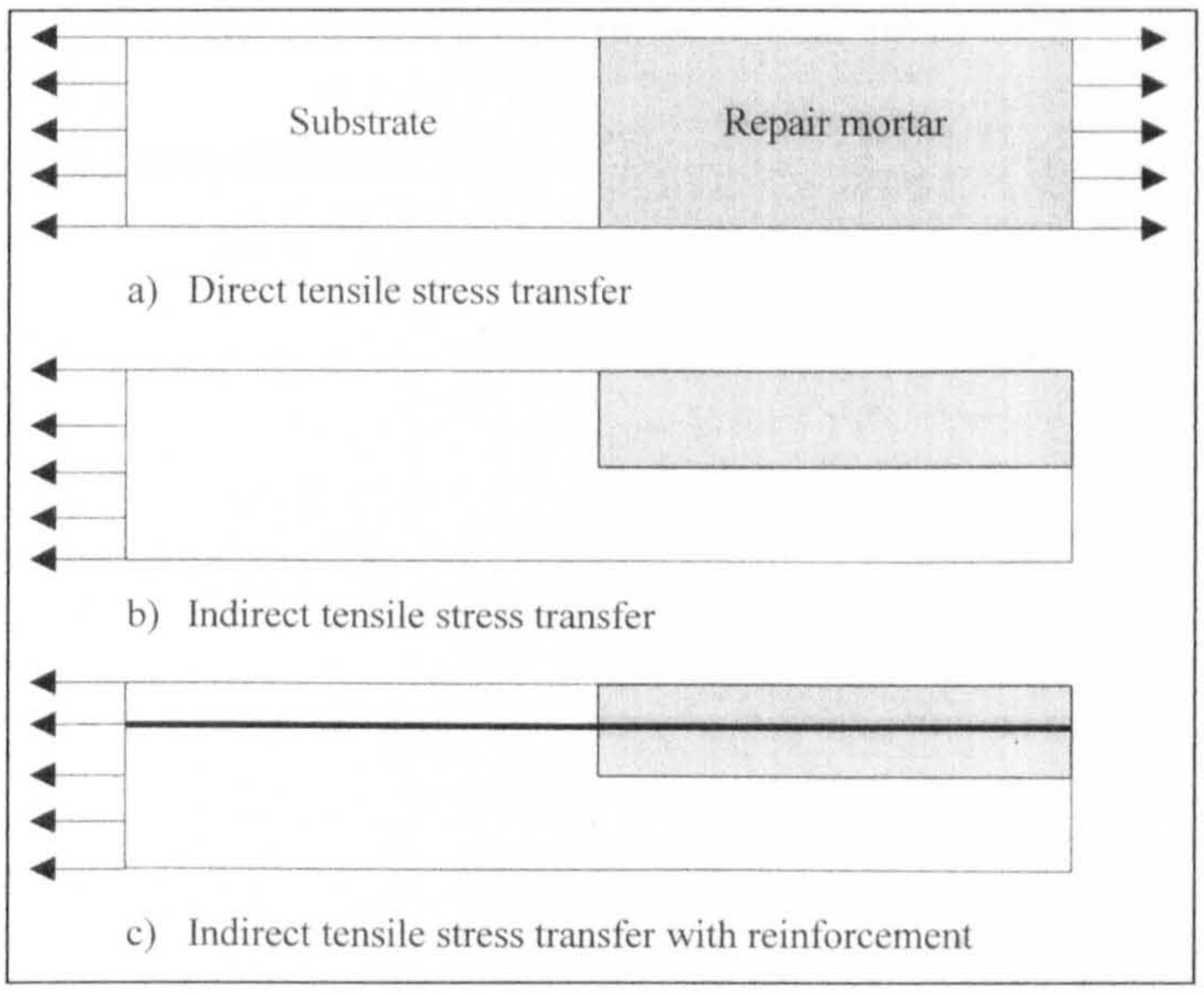

Figure 8.17 Patch repair tests performed by Emberson and Mays[135]

Austin and Robins[136] developed a patch test specially designed to simulate the stress environment that occurs in reinforced concrete members loaded in compression, flexure or pre-loaded compression-tension. A schematic of the different loading arrangements is shown in Figure 8.18. Compression tests produced both composite and debonding failure modes. The debonding loads were sensitive to the type of repair material, the roughness of the substrate and the moisture conditions at the time of repair. However, in flexural tests all specimens failed by a vertical crack through the repair material into the

substrate, indicating composite behaviour. Linear elastic finite element analysis was also performed to investigate the effect of modulus of elasticity on stress distribution. Results showed that stresses transferred to the repair material were decreasing when the modulus of elasticity was decreasing.

In an other paper Austin and Robins[137] presented the results of pull-off tests and slant shear tests performed simultaneously with patch repair tests. Results obtained from these three tests for a particular combination of repair material, concrete substrate and concrete substrate surface were not directly comparable because each test produced different stress states along the bond interface. In order to overcome this problem a bond failure envelope based on Coulomb theory was used which enabled meaningful comparison of results from different tests.

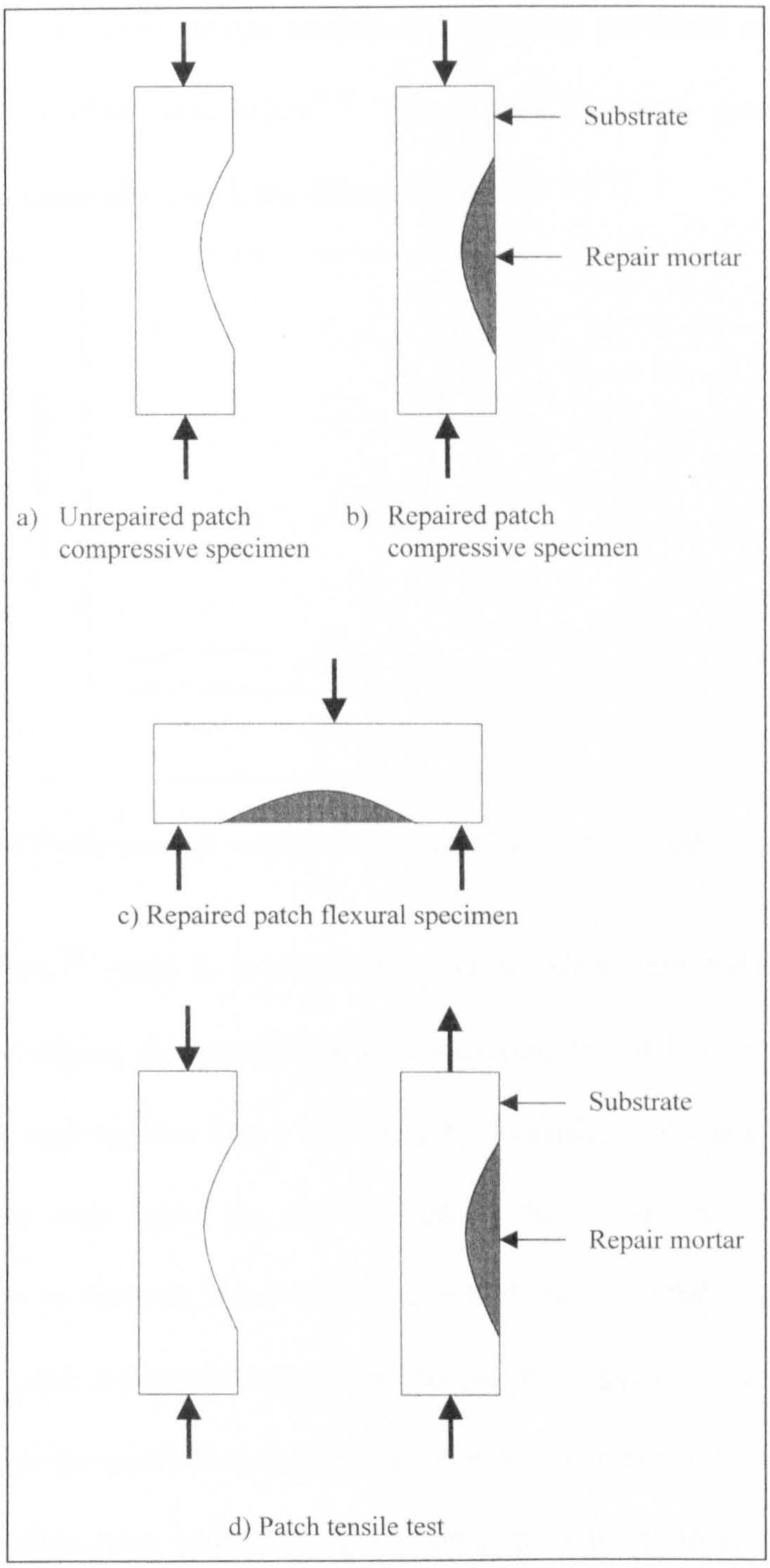

a) Unrepaired patch compressive specimen

b) Repaired patch compressive specimen

c) Repaired patch flexural specimen

d) Patch tensile test

Figure 8.18 Different types of patch repair tests developed by Austin and Robins[137]

8.6 ULTRASONIC PULSE VELOCITY METHOD

Recently, Andrews et al[138], Krause et al[139] and Yamaguchi et al[140] used ultrasonic pulse velocity measurements to locate objects in concrete such as steel reinforcement bars and voids. In their case the interest is still in time of flight but of that part of the pulse reflected at the discontinuity. If an excitation pulse is received after reflection at a

discontinuity a plot of pulse energy against depth can be produced as shown in Figure 8.19 adopted from Cleland and Misra[97]. This results to a clear peak in the reflected energy for a depth coinciding with the discontinuity.

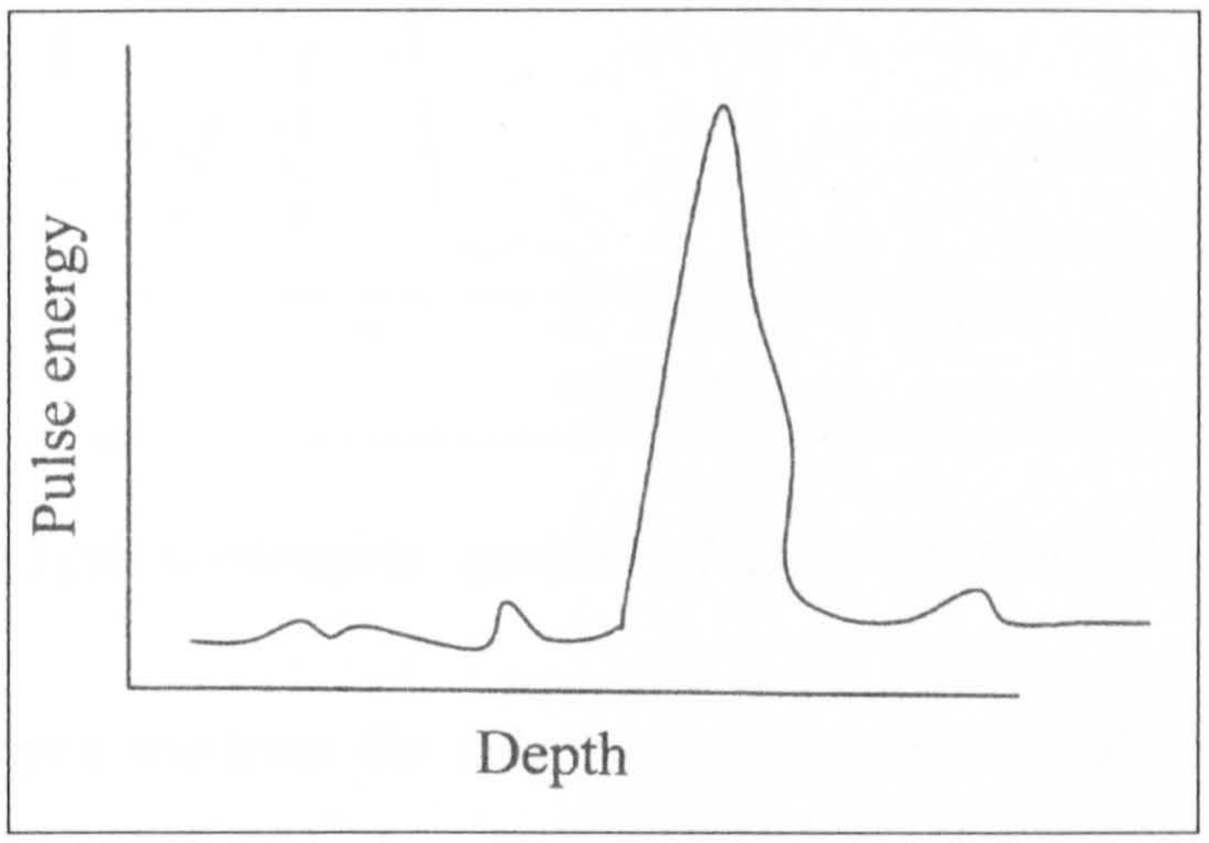

Figure 8.19 Pulse energy versus depth adopted from Cleland and Misra[97]

Cleland and Misra[97] used a modified version of ultrasonic pulse velocity testing equipment to investigate the possibility of measuring the adhesive strength between substrate concrete and various repair materials by assessing the extent of discontinuity. Their investigation was based on the hypothesis that lower adhesion strengths are associated with more discrete bond interfaces which in turn lead to an increase in the magnitude of the peak reflected energy. For this purpose discrete ultrasonic pulses were transmitted through the repaired specimen in order for the reflected pulse to arrive at the receiver before subsequent pulses were transmitted. The pulse reflected from bond interface was then analysed using Fast Fourier Transform (FFT) and a frequency spectrum was obtained as shown in Figure 8.20.

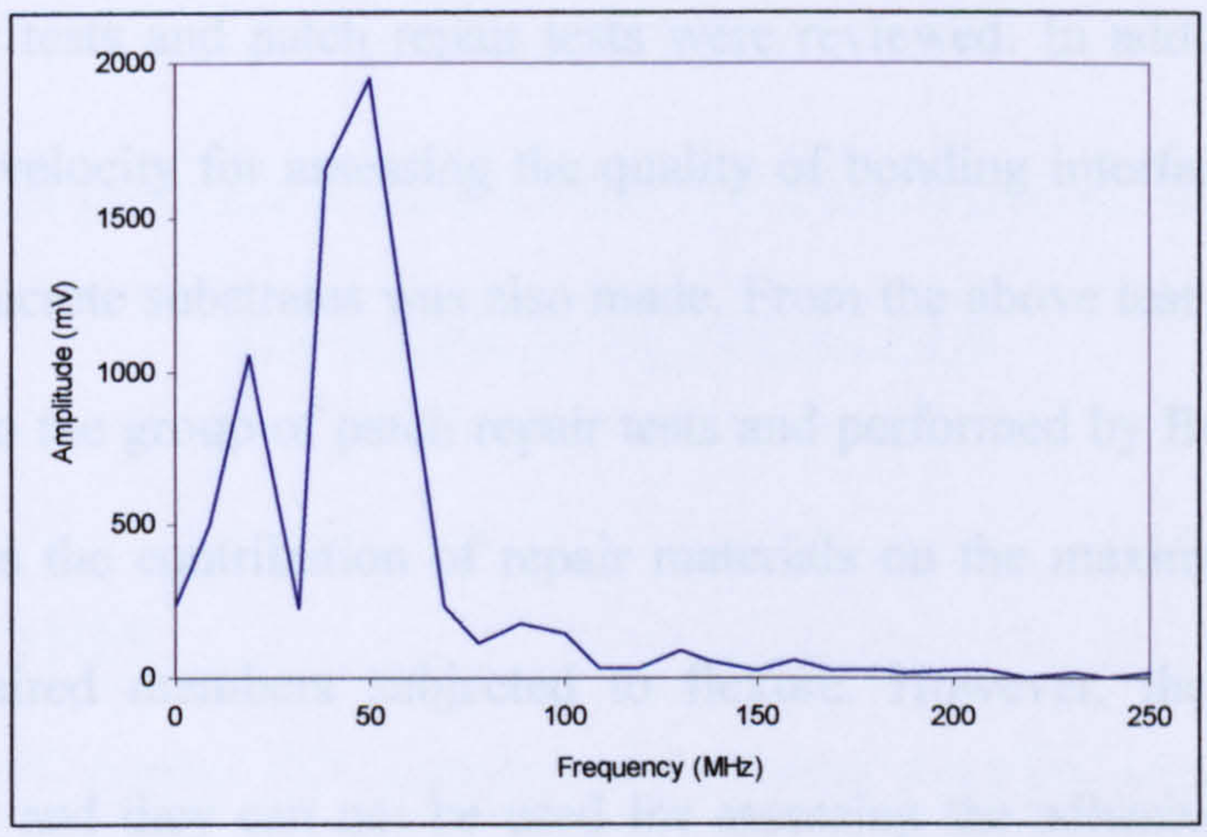

Figure 8.20 Typical frequency spectrum adopted from Cleland and Misra[97]

From the frequency spectrum the magnitude of the peak amplitude was compared against the adhesive strength obtained using the pull-off test method as shown in Figure 8.21.

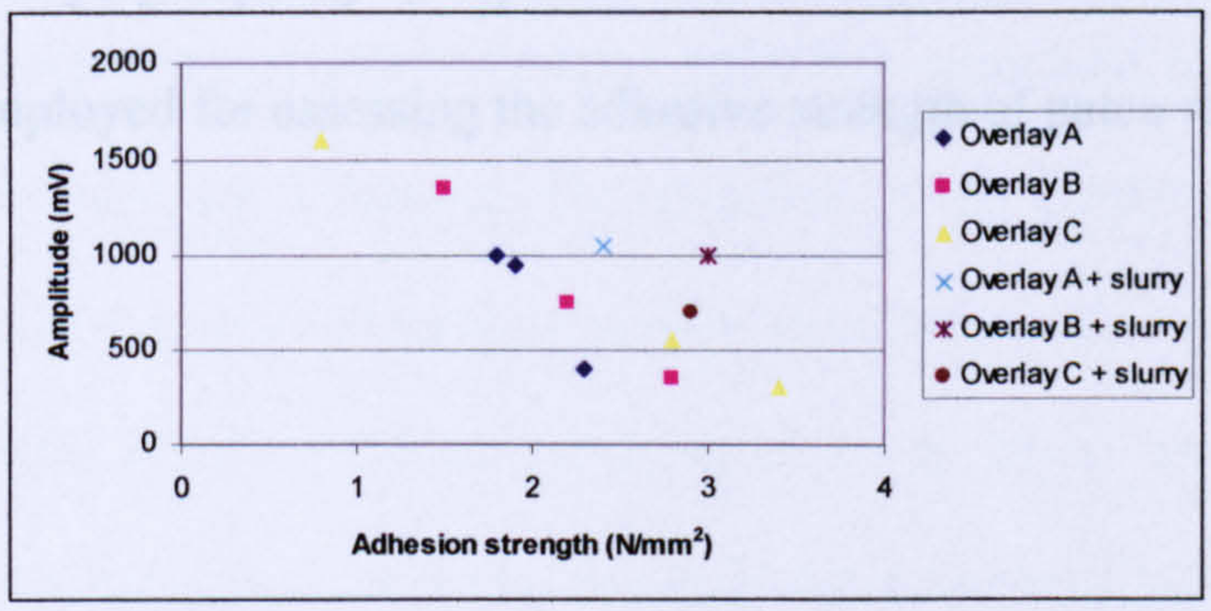

Figure 8.21 Correlation between ultrasonic pulse amplitude and adhesive strength adopted from Cleland and Misra[97]

Results indicated a reasonable correlation when OPC concrete was used as a repair material. When cement slurry was used as a repair material the results were less accurate.

8.7 CONCLUSION

In this chapter a review of the various test methods used for evaluating the adhesive strength of patch repairs and overlays was performed. Tensile bond tests, shear bond

tests, slant shear tests and patch repair tests were reviewed. In addition, reference to ultrasonic pulse velocity for assessing the quality of bonding interface between repair materials and concrete substrates was also made. From the above test methods, flexural tests belonging to the group of patch repair tests and performed by Burley et al[128] can be used to assess the contribution of repair materials on the maximum load carrying capacity of repaired members subjected to flexure. However, the above tests are laboratory based and they can not be used for assessing the adhesive strength of real patch repairs. In order to overcome this problem pull-off test can be employed. It is quick, easy, inexpensive and most important of all is the only method that can be used to evaluate the adhesive strength of real repairs. Based on the above, a decision is made to employ flexural tests in order to evaluate the contribution of repair materials on the maximum load carrying capacity of repaired beams subjected to flexure, whereas pull-off test will be employed for assessing the adhesive strength of patch repairs.

CHAPTER 9

EXPERIMENTAL EVALUATION OF FLEXURAL BEHAVIOUR OF REPAIR MATERIALS

9.1 INTRODUCTION

In chapter 7 OPC mortar, OPC concrete and polymer modified cement concrete were chosen as the most appropriate types of repair materials for the patch repair study. Their selection was based on their ability to satisfy all requirements for strength (compressive, tensile, flexural and adhesive strength) and all aspects of compatibility (chemical, electrochemical, permeability and dimensional compatibility). In chapter 8 flexural tests on repaired composite beams were chosen as the most appropriate type of tests for assessing the contribution of repair materials on the maximum load carrying capacity of repaired members subjected to flexure. The objective of this chapter is to evaluate the performance of different types of repair materials when subjected to tension/flexure and confirm the material selection for the patch repair study. Most repair materials, like substrate concrete seem to be very strong in compression but relatively weak in tension. Hence, the need for assessing the contribution of repair materials to the maximum load carrying capacity of repaired composite members when subjected to tension/flexure is of great importance. For this reason, the contribution of 6 types of generic repair materials (OPC mortar w/c = 0.4, OPC mortar w/c = 0.5, OPC concrete w/c = 0.4, OPC concrete w/c = 0.5, polymer modified cement concrete MonoTop 615 and polymer modified cement concrete reinforced with glass fibres Zentifix GM 25) on the maximum load carrying capacity of repaired composite unreinforced beams subjected to flexure in accordance to BS 1881 Part 118[106] will be investigated.

9.2 REPAIR MATERIAL FLEXURAL BEHAVIOUR RESEARCH PROGRAM

9.2.1 Production of concrete substrate beam specimens

In order to evaluate the tensile/flexural behaviour of various types of generic repair materials 160 beam specimens were produced in 4 groups. Every group consisted of 2 mixes. Every mix consisted of 4 solid beams with dimensions 100x100x500 mm, 16 unrepaired beams and 4 cubes with dimensions of 100x100x100 mm. All unrepaired beams had the same length 500 mm and the same width 100 mm. However, the depth of the unrepaired beams for groups 1, 2, 3, and 4 was 50, 60, 70, and 80 mm, respectively. The specimens were produced using Lafarge Blue Circle OPC CEM-I 42.5 N conforming to BS EN 197 Part 1[30]. Sharp sand with maximum coarse size of 5 mm was used as fine aggregate. River gravel with maximum coarse size of 20 mm was used as coarse aggregate. The mix design of the specimens was based on the guidelines of BRE[31]. All specimens had the same w/c of 0.45. The specimens were cast in timber moulds and compacted using a vibrating table. After 3 to 4 hours of casting the surface of the unrepaired beams was peeled off using a wire brush which was able to remove the cement paste and expose the coarse aggregate. The above process was performed in order to create an artificially roughened surface and promote the adhesion between the substrate concrete and the repair material. When the concrete had set, the moulds were covered with damp rags. Twenty-four hours after casting the specimens were demoulded and placed in water for 27 days. Next, the substrate specimens were taken out of the water and placed inside their moulds and were filled using different types of generic repair materials. Twenty-four hours after the installation of the repair material the repaired composite beams were demoulded and placed in water. After 6 days in water, the specimens were air-cured in a storage room for 21 days. The storage room temperature was approximately 19 ^{0}C at 50-60% relative humidity. Details of solid and

unrepaired beams are shown in Table 9.1. Photographs during the production of the beams are shown in **Appendix 9,** whereas, compressive strength values obtained from crushing cubes during testing of the beams are shown in **Appendix 10.**

Group Number	Mix Number	Number of Beams	Beam Dimensions (mm)
1	1	4	100x100x500
		16	50x100x500
	2	4	100x100x500
		16	50x100x500
2	3	4	100x100x500
		16	60x100x500
	4	4	100x100x500
		16	60x100x500
3	5	4	100x100x500
		16	70x100x500
	6	4	100x100x500
		16	70x100x500
4	7	4	100x100x500
		16	80x100x500
	8	4	100x100x500
		16	80x100x500

Table 9.1 Details of solid and unrepaired beam specimens

Six types of generic repair materials were used.

- Ordinary Portland Cement Concrete (OPCC w/c = 0.4)
- Ordinary Portland Cement Concrete (OPCC w/c = 0.5)
- Ordinary Portland Cement Mortar (OPCM w/c = 0.4)
- Ordinary Portland Cement Mortar (OPCM w/c = 0.5)
- Polymer-modified cement mortar (SIKA MonoTop 615)
- Polymer-modified cement mortar reinforced with glass fibres (MC Chemicals Zentrifix GM 25)

Selection of the first 4 types of generic repair materials was based on their ability to satisfy all requirements regarding mechanical behaviour such as compressive, tensile,

flexural, and adhesive strength. In addition, their similar chemical, electrochemical, dimensional, and permeability properties with those of the substrate concrete can satisfy all aspects of compatibility. Selection of the last 2 types of generic repair materials was based on data published by manufacturers which claims to meet all required mechanical properties and satisfy all aspects of compatibility.

All specimens were tested following the guidelines of BS 1881: Part 118[106]. A view of the specimens during testing is shown in Figure 9.1. All repaired composite beams were tested with their repair material subjected to flexure as shown in Figure 9.2.

Figure 9.1 Solid and repaired composite beams during testing

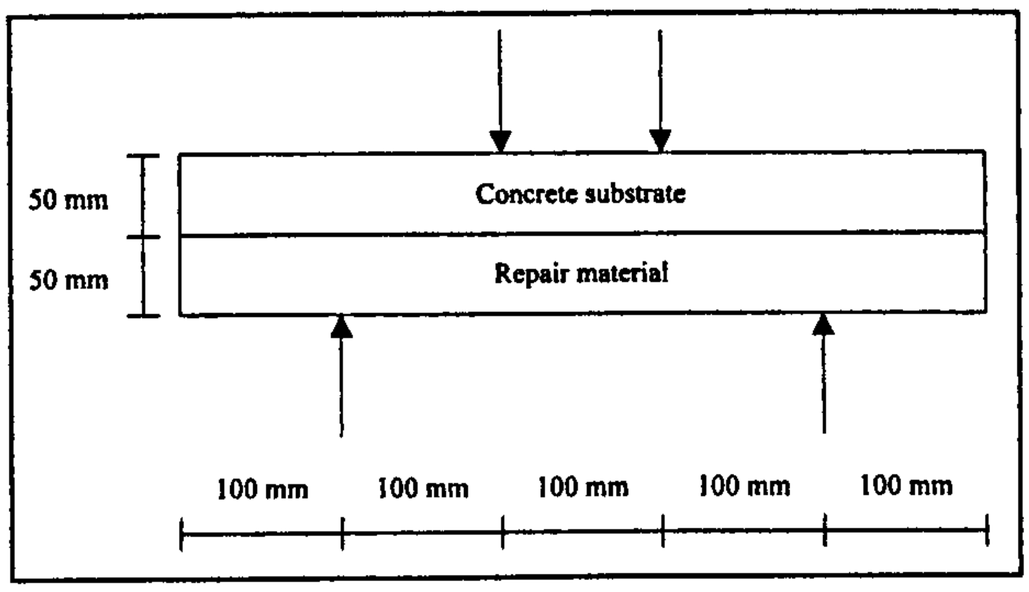

a) Loading arrangement for group 1 repaired composite beams

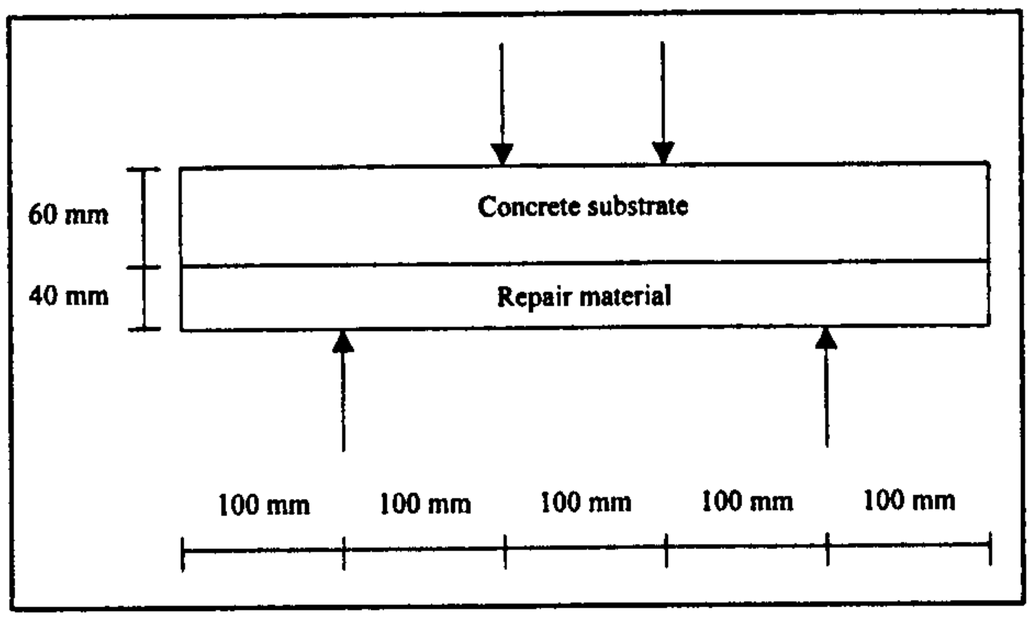

b) Loading arrangement for group 2 repaired composite beams

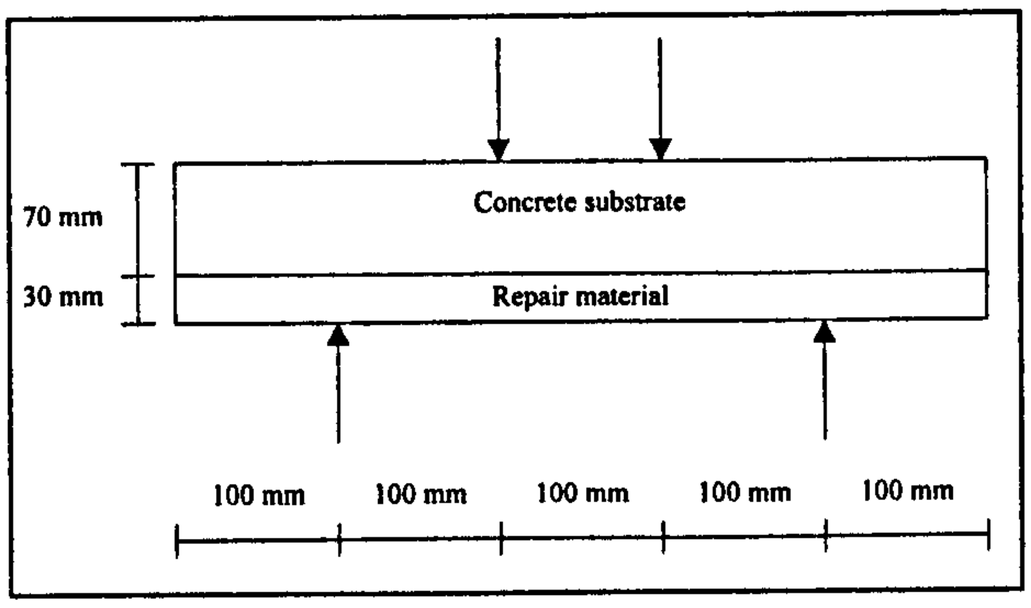

c) Loading arrangement for group 3 repaired composite beams

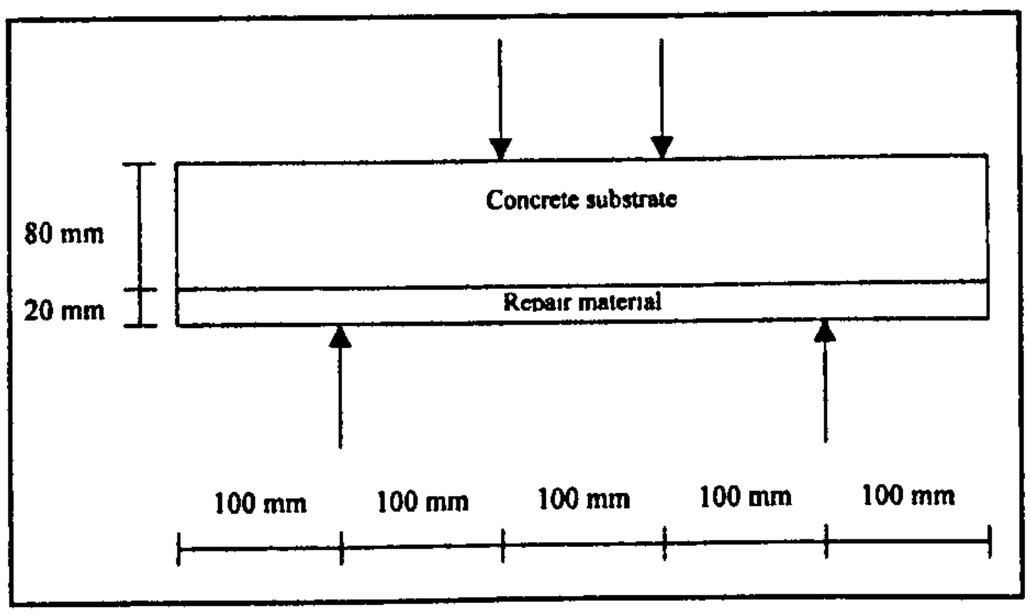

d) Loading arrangement for group 4 repaired composite beams

Figure 9.2 Schematic of flexural test performed on repaired composite beams

9.2.2 Flexure test results

The effects of different types of generic repair materials at different repair depths on the maximum load carrying capacity of composite repaired beams are described below:

1) For repair depths of 50 mm (50% of the overall cross-section of the composite repaired beams) the performance of different types of generic repair materials is presented in Table 9.2. More detailed information is provided in Tables 9.6 and 9.7.

Mix	Maximum average load (Solid beams) (kN)	Repair material	Maximum average load (Repaired beams) (kN)
1	17.43	OPCC (w/c = 0.4)	20.57
		OPCM (w/c = 0.4)	20.32
		Zentrifix GM 25	17.61
2	17.49	OPCC (w/c = 0.5)	16.38
		OPCM (w/c = 0.5)	17.14
		MonoTop 615	11.09

Table 9.2 Maximum average load results for 50 mm repairs (mixes 1 and 2)

From Tables 9.2, 9.6 and 9.7 it is obvious that beams repaired using OPCC (w/c = 0.4), OPCM (w/c = 0.4), and Zentrifix GM 25 exceeded the maximum average load capacity of solid beams. Beams repaired using OPCC (w/c = 0.5) and OPCM (w/c = 0.5) significantly increased their maximum average load capacity when compared to unrepaired beams and they reached 93.65% and 97.99% of the maximum average load capacity of solid beams, respectively. Finally, beams repaired using MonoTop 615 were able to increase their maximum average load capacity by 112.86% when compared to unrepaired beams (from 5.21 kN to 11.09 kN). However, the maximum load capacity achieved was 36.59% lower when compared to solid beams (11.09 kN against 17.49 kN).

2) For repair depths of 40 mm (40% of the overall cross-section of the composite repaired beams) the performance of different types of generic repair materials is presented in Table 9.3. More detailed information is provided in Tables 9.8 and 9.9.

Mix	Maximum average load (Solid beams) (kN)	Repair material	Maximum average load (Repaired beams) (kN)
3	17.32	OPCC (w/c = 0.4)	19.75
		OPCM (w/c = 0.4)	17.13
		Zentrifix GM 25	15.23
4	19.16	OPCC (w/c = 0.5)	18.30
		OPCM (w/c = 0.5)	16.28
		MonoTop 615	9.19

Table 9.3 Maximum average load results for 40 mm repairs (mixes 3 and 4)

From Tables 9.3, 9.8 and 9.9 it is obvious that beams repaired using OPCC (w/c = 0.4) exceeded the maximum average load capacity of solid beams. Beams repaired using OPCM (w/c = 0.4), Zentrifix GM 25, OPCC (w/c = 0.5), and OPCM (w/c = 0.5) significantly increased their maximum average load capacity when compared to unrepaired beams and they reached 98.90%, 87.93%, 95.51%, and 84.96% of the maximum average load capacity of solid beams, respectively. Finally, beams repaired using MonoTop 615 were able to increase their maximum average load capacity by 24.02% when compared to unrepaired beams (from 7.41 kN to 9.19 kN). However, the maximum load capacity achieved was 52.03% lower when compared to solid beams (9.19 kN against 19.16 kN).

3) For repair depths of 30 mm (30% of the overall cross-section of the composite repaired beams) the performance of different types of generic repair materials is presented in Table 9.4. More detailed information is provided in Tables 9.10 and 9.11.

Mix	Maximum average load (Solid beams) (kN)	Repair material	Maximum average load (Repaired beams) (kN)
5	16.88	OPCC (w/c = 0.4)	19.35
		OPCM (w/c = 0.4)	16.67
		Zentrifix GM 25	15.33
6	18.73	OPCC (w/c = 0.5)	17.77
		OPCM (w/c = 0.5)	14.69
		MonoTop 615	12.46

Table 9.4 Maximum average load results for 30 mm repairs (mixes 5 and 6)

From Tables 9.4, 9.10 and 9.11 it is obvious that beams repaired using OPCC (w/c = 0.4) exceeded the maximum average load capacity of solid beams. Beams repaired using OPCM (w/c = 0.4), Zentrifix GM 25, OPCC (w/c = 0.5), and OPCM (w/c = 0.5) significantly increased their maximum average load capacity when compared to unrepaired beams and they reached 98.75%, 90.81%, 94.87%, and 78.43% of the maximum average load capacity of solid beams, respectively. Finally, beams repaired using MonoTop 615 increased their maximum average load capacity by 25.73% when compared to unrepaired beams (from 9.91 kN to 12.46 kN). However, the maximum load capacity achieved was 33.47% lower when compared to solid beams (12.46 kN against 18.73 kN).

4) For repair depths of 20 mm (20% of the overall cross-section of the composite repaired beams) the performance of different types of generic repair materials is presented in Table 9.5. More detailed information is provided in Tables 9.12 and 9.13.

Mix	Maximum average load (Solid beams) (kN)	Repair material	Maximum average load (Repaired beams) (kN)
7	17.34	OPCC (w/c = 0.4)	23.59
		OPCM (w/c = 0.4)	20.62
		Zentrifix GM 25	19.56
8	17.90	OPCC (w/c = 0.5)	20.49
		OPCM (w/c = 0.5)	19.10
		MonoTop 615	14.62

Table 9.5 Maximum average load results for 20 mm repairs (mixes 7 and 8)

From Tables 9.5, 9.12 and 9.13 it is obvious that beams repaired using OPCC (w/c = 0.4), OPCM (w/c = 0.4), Zentrifix GM 25, OPCC (w/c = 0.5), and OPCM (w/c = 0.5) exceeded the maximum average load capacity of solid beams. Beams repaired using MonoTop 615 increased their maximum average load capacity by 37.53% when compared to unrepaired beams (from 10.63 kN to 14.62 kN). However, the maximum load capacity achieved was 18.32% lower when compared to solid beams (14.62 kN against 17.90 kN).

Finally, it should be noted that all beams specimens (both solid and repaired composite beam specimens) failed in flexure. No failures at the bonding interface between concrete substrates and repair materials were observed.

Beam no	Substrate dimensions (mm)	Substrate average compressive strength (N/mm^2)	Repair material	Repair dimensions (mm)	Repair average compressive strength (N/mm^2)	Max load (kN)	Max average load (kN)
1	100 x 100 x 500	56.64	N/A	N/A	N/A	18.31	17.43
2	100 x 100 x 500		N/A	N/A		17.02	
3	100 x 100 x 500		N/A	N/A		15.12	
4	100 x 100 x 500		N/A	N/A		19.28	
5	50 x 100 x 500		N/A	N/A		5.38	5.15
6	50 x 100 x 500		N/A	N/A		4.62	
7	50 x 100 x 500		N/A	N/A		5.46	
8	50 x 100 x 500		N/A	N/A		5.15	
9	50 x 100 x 500		OPC Concrete (w/c = 0.4)	50 x 100 x 500	53.78	20.89	20.57
10	50 x 100 x 500		OPC Concrete (w/c = 0.4)	50 x 100 x 500		19.61	
11	50 x 100 x 500		OPC Concrete (w/c = 0.4)	50 x 100 x 500		21.58	
12	50 x 100 x 500		OPC Concrete (w/c = 0.4)	50 x 100 x 500		20.18	
13	50 x 100 x 500		OPC Mortar (w/c = 0.4)	50 x 100 x 500	50.63	18.54	20.32
14	50 x 100 x 500		OPC Mortar (w/c = 0.4)	50 x 100 x 500		19.95	
15	50 x 100 x 500		OPC Mortar (w/c = 0.4)	50 x 100 x 500		21.14	
16	50 x 100 x 500		OPC Mortar (w/c = 0.4)	50 x 100 x 500		21.66	
17	50 x 100 x 500		Zentrifix GM 25	50 x 100 x 500	26.77	16.40	17.61
18	50 x 100 x 500		Zentrifix GM 25	50 x 100 x 500		16.64	
19	50 x 100 x 500		Zentrifix GM 25	50 x 100 x 500		18.54	
20	50 x 100 x 500		Zentrifix GM 25	50 x 100 x 500		18.85	

Table 9.6 Mix 1 test results

Beam no	Substrate dimensions (mm)	Substrate average compressive strength (N/mm^2)	Repair material	Repair dimensions (mm)	Repair average compressive strength (N/mm^2)	Max load (kN)	Max average load (kN)
1	100 x 100 x 500	54.07	N/A	N/A	N/A	15.95	17.49
2	100 x 100 x 500		N/A	N/A		19.23	
3	100 x 100 x 500		N/A	N/A		16.03	
4	100 x 100 x 500		N/A	N/A		18.73	
5	50 x 100 x 500		N/A	N/A		5.20	5.21
6	50 x 100 x 500		N/A	N/A		4.52	
7	50 x 100 x 500		N/A	N/A		5.32	
8	50 x 100 x 500		N/A	N/A		5.80	
9	50 x 100 x 500		OPC Concrete (w/c = 0.5)	50 x 100 x 500	40.50	18.73	16.38
10	50 x 100 x 500		OPC Concrete (w/c = 0.5)	50 x 100 x 500		16.26	
11	50 x 100 x 500		OPC Concrete (w/c = 0.5)	50 x 100 x 500		15.45	
12	50 x 100 x 500		OPC Concrete (w/c = 0.5)	50 x 100 x 500		15.06	
13	50 x 100 x 500		OPC Mortar (w/c = 0.5)	50 x 100 x 500	41.86	16.50	17.14
14	50 x 100 x 500		OPC Mortar (w/c = 0.5)	50 x 100 x 500		17.03	
15	50 x 100 x 500		OPC Mortar (w/c = 0.5)	50 x 100 x 500		18.27	
16	50 x 100 x 500		OPC Mortar (w/c = 0.5)	50 x 100 x 500		16.75	
17	50 x 100 x 500		Sika MonoTop 615	50 x 100 x 500	24.79	12.09	11.09
18	50 x 100 x 500		Sika MonoTop 615	50 x 100 x 500		11.92	
19	50 x 100 x 500		Sika MonoTop 615	50 x 100 x 500		11.26	
20	50 x 100 x 500		Sika MonoTop 615	50 x 100 x 500		9.09	

Table 9.7 Mix 2 test results

Beam no	Substrate dimensions (mm)	Substrate average compressive strength (N/mm^2)	Repair material	Repair dimensions (mm)	Repair average compressive strength (N/mm^2)	Max load (kN)	Max average load (kN)
1	100 x 100 x 500	53.81	N/A	N/A	N/A	19.42	17.32
2	100 x 100 x 500		N/A	N/A		18.35	
3	100 x 100 x 500		N/A	N/A		14.96	
4	100 x 100 x 500		N/A	N/A		16.56	
5	60 x 100 x 500		N/A	N/A		7.17	7.31
6	60 x 100 x 500		N/A	N/A		7.11	
7	60 x 100 x 500		N/A	N/A		6.73	
8	60 x 100 x 500		N/A	N/A		8.21	
9	60 x 100 x 500		OPC Concrete (w/c = 0.4)	40 x 100 x 500	53.99	20.80	19.75
10	60 x 100 x 500		OPC Concrete (w/c = 0.4)	40 x 100 x 500		20.60	
11	60 x 100 x 500		OPC Concrete (w/c = 0.4)	40 x 100 x 500		17.91	
12	60 x 100 x 500		OPC Concrete (w/c = 0.4)	40 x 100 x 500		19.67	
13	60 x 100 x 500		OPC Mortar (w/c = 0.4)	40 x 100 x 500	45.47	18.31	17.13
14	60 x 100 x 500		OPC Mortar (w/c = 0.4)	40 x 100 x 500		16.07	
15	60 x 100 x 500		OPC Mortar (w/c = 0.4)	40 x 100 x 500		17.43	
16	60 x 100 x 500		OPC Mortar (w/c = 0.4)	40 x 100 x 500		16.69	
17	60 x 100 x 500		Zentrifix GM 25	40 x 100 x 500	25.35	16.09	15.23
18	60 x 100 x 500		Zentrifix GM 25	40 x 100 x 500		13.81	
19	60 x 100 x 500		Zentrifix GM 25	40 x 100 x 500		15.11	
20	60 x 100 x 500		Zentrifix GM 25	40 x 100 x 500		15.89	

Table 9.8 Mix 3 test results

Beam no	Substrate dimensions (mm)	Substrate average compressive strength (N/mm^2)	Repair material	Repair dimensions (mm)	Repair average compressive strength (N/mm^2)	Max load (kN)	Max average load (kN)
1	100 x 100 x 500	52.73	N/A	N/A	N/A	21.13	19.16
2	100 x 100 x 500		N/A	N/A		19.61	
3	100 x 100 x 500		N/A	N/A		17.98	
4	100 x 100 x 500		N/A	N/A		17.93	
5	60 x 100 x 500		N/A	N/A		7.73	7.41
6	60 x 100 x 500		N/A	N/A		7.23	
7	60 x 100 x 500		N/A	N/A		7.11	
8	60 x 100 x 500		N/A	N/A		7.57	
9	60 x 100 x 500		OPC Concrete (w/c = 0.5)	40 x 100 x 500	42.33	17.47	18.30
10	60 x 100 x 500		OPC Concrete (w/c = 0.5)	40 x 100 x 500		20.02	
11	60 x 100 x 500		OPC Concrete (w/c = 0.5)	40 x 100 x 500		17.89	
12	60 x 100 x 500		OPC Concrete (w/c = 0.5)	40 x 100 x 500		17.81	
13	60 x 100 x 500		OPC Mortar (w/c = 0.5)	40 x 100 x 500	40.45	16.20	16.28
14	60 x 100 x 500		OPC Mortar (w/c = 0.5)	40 x 100 x 500		15.49	
15	60 x 100 x 500		OPC Mortar (w/c = 0.5)	40 x 100 x 500		17.21	
16	60 x 100 x 500		OPC Mortar (w/c = 0.5)	40 x 100 x 500		16.21	
17	60 x 100 x 500		Sika MonoTop 615	40 x 100 x 500	25.36	8.85	9.19
18	60 x 100 x 500		Sika MonoTop 615	40 x 100 x 500		8.90	
19	60 x 100 x 500		Sika MonoTop 615	40 x 100 x 500		9.65	
20	60 x 100 x 500		Sika MonoTop 615	40 x 100 x 500		9.34	

Table 9.9 Mix 4 test results

Beam no	Substrate dimensions (mm)	Substrate average compressive strength (N/mm^2)	Repair material	Repair dimensions (mm)	Repair average compressive strength (N/mm^2)	Max load (kN)	Max average load (kN)
1	100 x 100 x 500	48.08	N/A	N/A	N/A	15.41	16.88
2	100 x 100 x 500		N/A	N/A		17.24	
3	100 x 100 x 500		N/A	N/A		16.03	
4	100 x 100 x 500		N/A	N/A		18.84	
5	70 x 100 x 500		N/A	N/A		9.88	9.56
6	70 x 100 x 500		N/A	N/A		9.34	
7	70 x 100 x 500		N/A	N/A		9.56	
8	70 x 100 x 500		N/A	N/A		9.46	
9	70 x 100 x 500		OPC Concrete (w/c = 0.4)	30 x 100 x 500	55.08	20.79	19.35
10	70 x 100 x 500		OPC Concrete (w/c = 0.4)	30 x 100 x 500		18.19	
11	70 x 100 x 500		OPC Concrete (w/c = 0.4)	30 x 100 x 500		20.27	
12	70 x 100 x 500		OPC Concrete (w/c = 0.4)	30 x 100 x 500		18.14	
13	70 x 100 x 500		OPC Mortar (w/c = 0.4)	30 x 100 x 500	52.70	16.09	16.67
14	70 x 100 x 500		OPC Mortar (w/c = 0.4)	30 x 100 x 500		18.61	
15	70 x 100 x 500		OPC Mortar (w/c = 0.4)	30 x 100 x 500		15.60	
16	70 x 100 x 500		OPC Mortar (w/c = 0.4)	30 x 100 x 500		16.36	
17	70 x 100 x 500		Zentrifix GM 25	30 x 100 x 500	25.71	15.60	15.33
18	70 x 100 x 500		Zentrifix GM 25	30 x 100 x 500		15.48	
19	70 x 100 x 500		Zentrifix GM 25	30 x 100 x 500		15.49	
20	70 x 100 x 500		Zentrifix GM 25	30 x 100 x 500		14.76	

Table 9.10 Mix 5 test results

Beam no	Substrate dimensions (mm)	Substrate average compressive strength (N/mm^2)	Repair material	Repair dimensions (mm)	Repair average compressive strength (N/mm^2)	Max load (kN)	Max average load (kN)
1	100 x 100 x 500	57.22	N/A	N/A	N/A	18.91	18.73
2	100 x 100 x 500		N/A	N/A		18.96	
3	100 x 100 x 500		N/A	N/A		18.28	
4	100 x 100 x 500		N/A	N/A		18.77	
5	70 x 100 x 500		N/A	N/A		11.03	9.91
6	70 x 100 x 500		N/A	N/A		9.99	
7	70 x 100 x 500		N/A	N/A		9.19	
8	70 x 100 x 500		N/A	N/A		9.43	
9	70 x 100 x 500		OPC Concrete (w/c = 0.5)	30 x 100 x 500	47.38	19.31	17.77
10	70 x 100 x 500		OPC Concrete (w/c = 0.5)	30 x 100 x 500		16.03	
11	70 x 100 x 500		OPC Concrete (w/c = 0.5)	30 x 100 x 500		17.86	
12	70 x 100 x 500		OPC Concrete (w/c = 0.5)	30 x 100 x 500		17.88	
13	70 x 100 x 500		OPC Mortar (w/c = 0.5)	30 x 100 x 500	42.19	14.82	14.69
14	70 x 100 x 500		OPC Mortar (w/c = 0.5)	30 x 100 x 500		14.77	
15	70 x 100 x 500		OPC Mortar (w/c = 0.5)	30 x 100 x 500		15.53	
16	70 x 100 x 500		OPC Mortar (w/c = 0.5)	30 x 100 x 500		13.62	
17	70 x 100 x 500		Sika MonoTop 615	30 x 100 x 500	24.32	12.42	12.46
18	70 x 100 x 500		Sika MonoTop 615	30 x 100 x 500		12.13	
19	70 x 100 x 500		Sika MonoTop 615	30 x 100 x 500		12.02	
20	70 x 100 x 500		Sika MonoTop 615	30 x 100 x 500		13.28	

Table 9.11 Mix 6 test results

Beam no	Substrate dimensions (mm)	Substrate average compressive strength (N/mm^2)	Repair material	Repair dimensions (mm)	Repair average compressive strength (N/mm^2)	Max load (kN)	Max average load (kN)
1	100 x 100 x 500	55.65	N/A	N/A	N/A	15.80	17.34
2	100 x 100 x 500		N/A	N/A		17.65	
3	100 x 100 x 500		N/A	N/A		18.50	
4	100 x 100 x 500		N/A	N/A		17.40	
5	80 x 100 x 500		N/A	N/A		13.43	12.06
6	80 x 100 x 500		N/A	N/A		10.51	
7	80 x 100 x 500		N/A	N/A		12.28	
8	80 x 100 x 500		N/A	N/A		12.00	
9	80 x 100 x 500		OPC Concrete (w/c = 0.4)	20 x 100 x 500	61.83	23.71	23.59
10	80 x 100 x 500		OPC Concrete (w/c = 0.4)	20 x 100 x 500		25.56	
11	80 x 100 x 500		OPC Concrete (w/c = 0.4)	20 x 100 x 500		21.69	
12	80 x 100 x 500		OPC Concrete (w/c = 0.4)	20 x 100 x 500		23.41	
13	80 x 100 x 500		OPC Mortar (w/c = 0.4)	20 x 100 x 500	60.90	23.54	20.62
14	80 x 100 x 500		OPC Mortar (w/c = 0.4)	20 x 100 x 500		20.64	
15	80 x 100 x 500		OPC Mortar (w/c = 0.4)	20 x 100 x 500		21.72	
16	80 x 100 x 500		OPC Mortar (w/c = 0.4)	20 x 100 x 500		16.58	
17	80 x 100 x 500		Zentrifix GM 25	20 x 100 x 500	28.12	16.56	19.56
18	80 x 100 x 500		Zentrifix GM 25	20 x 100 x 500		21.40	
19	80 x 100 x 500		Zentrifix GM 25	20 x 100 x 500		20.03	
20	80 x 100 x 500		Zentrifix GM 25	20 x 100 x 500		20.26	

Table 9.12 Mix 7 test results

Beam no	Substrate dimensions (mm)	Substrate average compressive strength (N/mm^2)	Repair material	Repair dimensions (mm)	Repair average compressive strength (N/mm^2)	Max load (kN)	Max average load (kN)
1	100 x 100 x 500	52.17	N/A	N/A	N/A	18.08	17.90
2	100 x 100 x 500		N/A	N/A		18.16	
3	100 x 100 x 500		N/A	N/A		17.08	
4	100 x 100 x 500		N/A	N/A		18.27	
5	80 x 100 x 500		N/A	N/A		10.59	10.63
6	80 x 100 x 500		N/A	N/A		10.11	
7	80 x 100 x 500		N/A	N/A		11.54	
8	80 x 100 x 500		N/A	N/A		10.27	
9	80 x 100 x 500		OPC Concrete (w/c = 0.5)	20 x 100 x 500	47.20	22.70	20.49
10	80 x 100 x 500		OPC Concrete (w/c = 0.5)	20 x 100 x 500		18.78	
11	80 x 100 x 500		OPC Concrete (w/c = 0.5)	20 x 100 x 500		19.38	
12	80 x 100 x 500		OPC Concrete (w/c = 0.5)	20 x 100 x 500		21.09	
13	80 x 100 x 500		OPC Mortar (w/c = 0.5)	20 x 100 x 500	42.55	19.23	19.10
14	80 x 100 x 500		OPC Mortar (w/c = 0.5)	20 x 100 x 500		18.01	
15	80 x 100 x 500		OPC Mortar (w/c = 0.5)	20 x 100 x 500		18.54	
16	80 x 100 x 500		OPC Mortar (w/c = 0.5)	20 x 100 x 500		20.60	
17	80 x 100 x 500		MonoTop 615	20 x 100 x 500	27.01	14.98	14.62
18	80 x 100 x 500		MonoTop 615	20 x 100 x 500		13.13	
19	80 x 100 x 500		MonoTop 615	20 x 100 x 500		14.71	
20	80 x 100 x 500		MonoTop 615	20 x 100 x 500		15.66	

Table 9.13 Mix 8 test results

9.3 CONCLUSION

Structural elements repaired with OPCC (w/c = 0.4), OPCM (w/c = 0.4), Zentrifix GM 25, OPCC (w/c = 0.5), and OPCM (w/c = 0.5) are able to satisfy flexural compatibility. Structural elements repaired with Monotop 615, although, are able to increase their maximum load carrying capacity between 24.02%-112.86%, they are not able to fully achieve their initial maximum load capacity. Hence, for elements subjected to flexure one of the above five materials is the best option. For reinforced concrete elements the above recommendation is not so important since most of the flexural stress is taken by the steel reinforcement.

In the next chapter, the above 6 repair materials will be further experimentally evaluated and their water permeability properties investigated.

CHAPTER 10

EXPERIMENTAL EVALUATION OF PERMEABILITY PROPERTIES OF REPAIR MATERIALS

10.1 INTRODUCTION

In chapter 9, 6 different types of generic repair materials (OPC mortar w/c = 0.4, OPC mortar w/c = 0.5, OPC concrete w/c = 0.4, OPC concrete w/c = 0.5, polymer modified cement concrete MonoTop 615 and polymer modified cement concrete reinforced with glass fibres Zentrifix GM 25) were investigated for use in subsequent repair experiments. The objective of this chapter is to further experimentally evaluate and compare the water permeability properties of the above 6 types of generic repair materials. Many concrete disintegration mechanisms involve the penetration of aggressive substances, such as O_2, SO_2, CO_2 and Cl^-. In many cases, H_2O is also required to sustain the disintegration mechanisms. Hence, repair materials that have a surface zone that is highly resistant to the ingress of H_2O will theoretically produce durable repairs. In order to study water permeability, absorption by immersion test and ISAT described in BS 1881 Part 122[141] and BS 1881 Part 208[142], respectively, were used.

10.2 PENETRABILITY METHODS

10.2.1 General

Penetrability methods are used to assess the ability of the surface zone of the concrete to restrict the passage of external agents such as water, sulphates, chlorides, and carbon dioxide that may lead to direct deterioration of the concrete or to depassivation and corrosion of the steel reinforcement.

There are three main transport mechanisms by which external agents can penetrate into concrete:

- Absorption
- Permeation
- Diffusion

Absorption is described as the passage of fluids due to capillary forces. Contaminants, such as Cl^- and SO_3^- are transported within the fluid. The term sorptivity is used to describe the tendency of a solid to absorb a fluid. For one-dimensional water absorption into an initially dry porous solid the volume of an absorbed fluid can be related to time by the following empirical equation

$$V = As\sqrt{t} \tag{10.1}$$

where:

V is the volume of fluid absorbed (m^3)

A is the wetted area (m^2)

s is the sorptivity ($m/\sqrt{s}$)

t is the time (s)

Permeation can be described as the flow of a fluid under the action of a pressure head. For steady-state, unidirectional flow of a fluid through a saturated porous solid, the flow rate is given by Darcy's law:

$$Q = kAI \tag{10.2}$$

where:

Q is the flow rate (m^3/s)

k is the coefficient of permeability (m/s)

A is the cross-sectional area of flow (m^2)

I is the hydraulic gradient (m/m)

The coefficient of permeability depends on both the structure of the solid and the properties of the fluid. In the case of concrete, the coefficient of permeability depends mainly on the mix design, the w/c ratio and the age of concrete.

Diffusion can be described as the movement of molecular or ionic substances from regions of higher concentration to regions of lower concentration of the substances. The rate of movement of the substance is given by Fick's first law of diffusion:

$$F = \frac{\partial m}{\partial t}\frac{1}{A} = -D\frac{\partial C}{\partial x} \tag{10.3}$$

where:

F is the mass flux (kg/m^2s)

m is the mass of flowing substance (kg)

t is the time (s)

A is the area (m^2)

D is the diffusion coefficient (m^2/s)

C is the concentration (kg/m^3)

x is the distance (m)

Various penetrability tests have been developed for assessing the durability of a concrete surface. Most of these tests are based on one of the above transport mechanisms. Penetrability tests can be divided into three groups:

- Water absorption tests
- Water-permeability tests

- Air permeability tests

10.2.2 Water absorption tests

Water absorption tests measure the absorption rate of the water into the concrete under a relatively low water pressure head. The absorption rate of the water is a function of the capillary porosity, which in turn is a function of w/c ratio and curing history. Water absorption tests include:

- Absorption by immersion test which is described by BS 1881: Part 122[141]
- Initial surface-absorption test (ISAT) which is described by BS 1881: Part 208[142]
- Figg water-absorption test
- Covercrete-absorption test

Absorption by immersion test is used to measure the ease with which a fluid can penetrate concrete. Tests can be performed on either cores or cubes. In order for the specimens to achieve a constant mass they should be oven dried for 72 ± 2 h at a temperature of 105 ± 5 ^{0}C before testing. After cooling the specimens are weight and immersed in water. The temperature of the water used for testing should be maintained at 20 ± 1 ^{0}C. The specimens are placed on supports in a dish with a flat base and are completely immersed in a head of water 25 ± 5 mm. After 30 ± 0.5 min the specimens are surfaced dried and weight. The same procedure is repeated after 24 hours when the test will end. The 24 hours duration of the test gives sufficient results for analysing the water absorption properties of concrete. Finally, the absorption of each specimen is expressed as a percentage increase in weight compared to its dry weight. Absorption by immersion test is simple and very easy to perform but in practise is not frequently used. Fluid flow is very complex during the test so the method is usually treated empirically.

In addition, the drying regime of the specimen significantly influences the results. For specimens dried at high temperatures results are much higher compared to specimens made of the same mix but dried at lower temperatures. This is mainly due to the fact that drying at high temperatures may cause removal of the combined water compared to drying at low temperatures. In most good quality concretes water absorption is well below 10% by mass.

ISAT is used to measure the initial surface absorption of concrete, which, can be defined as the rate of flow of water into concrete per unit area at a stated interval from the start of the test and at a constant applied head. In order to perform the test a watertight circular cap with a minimum surface area of 5000 mm^2 is sealed to the concrete surface and connected by means of flexible tubes to a reservoir. The reservoir is filled with water so that the water level is 200 mm above the concrete surface. The applied pressure of 200 mm head of water is worse than the severest weather exposure in the UK due to driving rain. The watertight circular cup is also connected to a capillary tube with a scale which is positioned horizontally at the same height as the water in the reservoir. Prior to testing cube specimens are oven dried at a temperature of $105 \pm 5\ ^0C$ until constant mass is achieved, i.e. not more than 0.1% weight change over any 24 h drying period. After cooling the cap is fixed on the concrete surface and the specimen is subjected to a head of water of 200 mm. At specific intervals (10 min, 30 min, and 1 h) from the start of the test, the valve below the reservoir is closed and the movement of water in the capillary tube is used to measure the rate at which water is absorbed into concrete. ISAT is simple and inexpensive to perform. In addition, it is sensitive to changes in concrete quality. However, it is only able to measure the absorption of the outer 10 -15 mm of concrete and is affected by surface coatings. In addition, it is unreliable for concretes with a high sorptivity surface layer. This is

because the flow of water through the concrete specimen in the ISAT test is not one-directional, but for concretes with a low surface sorptivity, it may be considered to be one-dimensional. However, as the sorptivity of the surface layer increases, radial movement governs the flow of water in the specimen.

Figg's water absorption test as the name suggests was developed by Figg[143] in 1973. The test is based on drilling a 5.5 mm diameter hole into concrete to a depth of 30 mm. The hole is cleaned, a disc of rigid polymeric foam is pushed into the hole to a depth of 20 mm from the surface and the hole is sealed using silicone rubber. Next, a hypodermic needle is inserted through the silicone rubber seal and connected to a syringe and a horizontal capillary through a series of connectors. A water head of 100 mm is then applied and the time taken for the meniscus to travel 50 mm in the horizontal capillary is recorded. The value obtained is known as the water absorption index and is measured in seconds. The higher the absorption index the lower the water absorption of concrete.

The main limitation of ISAT is that it can only measure the water absorption of the outer 10-15 mm of concrete, whereas the main limitation of Figg's test is that it can only measure the water absorption of concrete deeper than 20 mm. The covercrete-absorption test was developed by Dhir[144] to overcome the above limitations by providing an integrated water absorption of the surface zone to a depth of 50 mm. The test is based on drilling a 13 mm diameter hole into concrete to a depth of 50 mm. A gasketted cap is placed over the hole and a tube connected to a reservoir passes through the cap and empties into the hole. The cap contains a second tube which is connected to a horizontal capillary. The reservoir and the capillary are placed in such a way that a water head of 200 mm is maintained above the centre of the hole. The tube connected to

the reservoir is closed and the movement of the meniscus in the capillary is measured between 10 and 11 minutes after initial contact with water.

10.2.3 Water-permeability tests

Water-permeability tests provide information on the permeability of concrete under a low water pressure head. Water-permeability tests include:

- CLAM test
- Steinert method

CLAM test is used to measure the flow of water into the concrete surface under a fixed pressure. Montgomery and Adams[145] and Basheer et al[146] provide a detailed description of the test. The method is based on attaching a specially designed cap to the concrete surface. Pressurized water is provided by a micrometer-screw piston. A pressure gauge in the chamber monitors the water pressure. In order to perform the test, the chamber is filled with water, the micrometer screw is turned so as to maintain a constant water pressure of about 150 kPa above atmospheric pressure and the movement of the piston through the cylinder is recorded at constant intervals for 20-30 minutes. By measuring the movement of the piston through the cylinder the volume of water that penetrates into the concrete can be determined. Plotting the volume of water versus time information regarding the permeability of concrete can be obtained. Since the flow of water into the concrete is not unidirectional and a steady-state condition is not achieved, a permeability index is obtained rather than the true permeability.

Steinert method as the name suggests was developed by Steinert[147] in 1979. The test is based on the guard ring principle to achieve a better approximation of unidirectional flow under pressure. A cap, which is made of 2 concentric chambers separated by a

circular rubber seal, is attached to the concrete surface. The concentric chambers are filled with water and pressurized to 600 kPa using compressed air. Flow under the inner chamber is approximately unidirectional. Hence, monitoring of flow as a function of time is easier to interpret compared to CLAM test

10.2.4 Air-permeability tests

Air-permeability tests are similar to water-permeability tests and provide information on the flow of air, or other gases through concrete. Relationships exist between air permeability of concrete and durability factors such as water/cement ratio, compressive strength, and curing efficiency. Air-permeability tests are usually easier to perform than water-permeability tests. Air-permeability tests include:

- Figg air-permeability test
- Schonlin test

Figg's air permeability test as the name suggests was developed by Figg[143] in 1973. The test is based on drilling a 5.5 mm diameter hole into concrete to a depth of 30 mm. The hole is cleaned, a disc of rigid polymeric foam is pushed into the hole to a depth of 20 mm from the surface and the hole is sealed using silicone rubber. Next, a hypodermic needle is inserted through the silicone rubber seal and connected to a vacuum pump. The vacuum pump is turned on until the pressure inside the hole is decreased to -85 kPa below atmospheric pressure. The valve is then closed and the flow of air inside the hole results in a reduction of the vacuum. The time taken to obtain a 5 kPa increase in the hole is known as the air permeability index and is measured in seconds. The higher the air permeability index the lower the air absorption of concrete.

The main disadvantage of Figg's air permeability test is that a hole needs to be drilled. In order to avoid drilling a hole, Schonlin test was developed. A description of the test is provided by Schonlin and Hilsdorf[148]. The method is based on the use of a 50 mm in diameter chamber of known volume which is attached to the concrete surface. Next, a vacuum pump is used to evacuate the chamber to a pressure less than -99 kPa. The valve is then closed and the time when the vacuum pressure reaches -95 kPa is taken as the start of the test. The time required for the value of vacuum pressure to increase from -95 kPa to -70 kPa is measured. When dense concrete is investigated, the vacuum pressure change during 120 seconds is measured instead. Based on the above measurements and the known volume of the chamber, a permeability index measured in m^2/s is obtained.

10.3 REPAIR MATERIAL WATER PERMEABILITY RESEARCH PROGRAM

10.3.1 Production of specimens

In order to evaluate the water permeability properties of the 6 generic repair materials selected in the previous Chapter, 72 cubes and 24 cylinders were produced in 6 mixes. Each mix was made from a different generic repair material and consisted of 12 cubes and 4 cylinders. The cubes had dimensions of 100x100x100 mm, whereas, the length of the cylinders was 200 mm and their diameter 100 mm. Cylinders were produced in order to determine tensile strength. From the 12 cubes of each mix, 4 cubes were used to determine compressive strength, 4 cubes were used to perform the absorption by immersion test and the last 4 cubes were used to perform the ISAT. The specimens were cast in steel moulds and compacted using a vibrating table. Twenty-four hours after casting the specimens were demoulded and placed in water. After 6 days in water, the specimens were air-cured in a storage room for 21 days. The storage room temperature

was approximately 19 ^{0}C at 50-60% relative humidity. Photographs during the production of the specimens are shown in **Appendix 11**, whereas, compressive and tensile strength values obtained from splitting cylinders and crushing cubes are shown in **Appendix 12**.

10.3.2 Absorption by immersion test results

Results of the absorption by immersion tests performed on the 6 generic repair materials selected in Chapter 9 are shown in Table 10.1. More detailed information is provided in Table 10.3.

Repair material	Average water absorption (%)	
	Time (0.5 h)	Time (24 h)
OPC Concrete (w/c = 0.4)	2.31	5.53
OPC Concrete (w/c = 0.5)	2.97	6.78
OPC Mortar (w/c = 0.4)	4.50	9.35
OPC Mortar (w/c = 0.5)	6.45	12.14
Zentrifix GM 25	5.91	12.76
MonoTop 615	3.35	9.71

Table 10.1 Absorption by immersion test results

From Tables 10.1 and 10.3 it is obvious that OPCC (w/c = 0.4) gives the best results, with an average water absorption of 2.31% and 5.53% at 0.5 and 24 hours, respectively. OPCC (w/c = 0.5) is ranked in the second place with slightly higher water absorption values of 2.97% and 6.78% at 0.5 and 24 hours, respectively. In the third place, at 0.5 hours is ranked MonoTop 615 with an average water absorption of 3.35%, while, at 24 hours OPCM (w/c = 0.4) is ranked in the third place with an average water absorption of 9.35%. In the fourth place, at 0.5 hours is ranked OPCM (w/c = 0.4) with an average water absorption of 4.50%, while, at 24 hours MonoTop 615 is ranked in the fourth place with an average water absorption of 9.71%. In the fifth place, at 0.5 hours is

ranked Zentrifix GM 25 with an average water absorption of 5.91%, while, at 24 hours OPCM (w/c = 0.5) is ranked in the fifth place with an average water absorption of 12.14%. Finally, in the sixth place, at 0.5 hours is ranked OPCM (w/c = 0.5) with an average water absorption of 6.45%, while, at 24 hours Zentrifix GM 25 is ranked in the sixth place with an average water absorption of 12.76%. Based on the above results OPCC (w/c = 0.4) and OPCC (w/c = 0.5) can be classified as repair materials having low water absorption, OPCM (w/c = 0.4) and MonoTop 615 can be classified as repair materials having moderate water absorption, and OPCM (w/c = 0.5) and Zetrifix GM 25 can be classified as repair materials having high water absorption. Figure 10.1 summarises the above results.

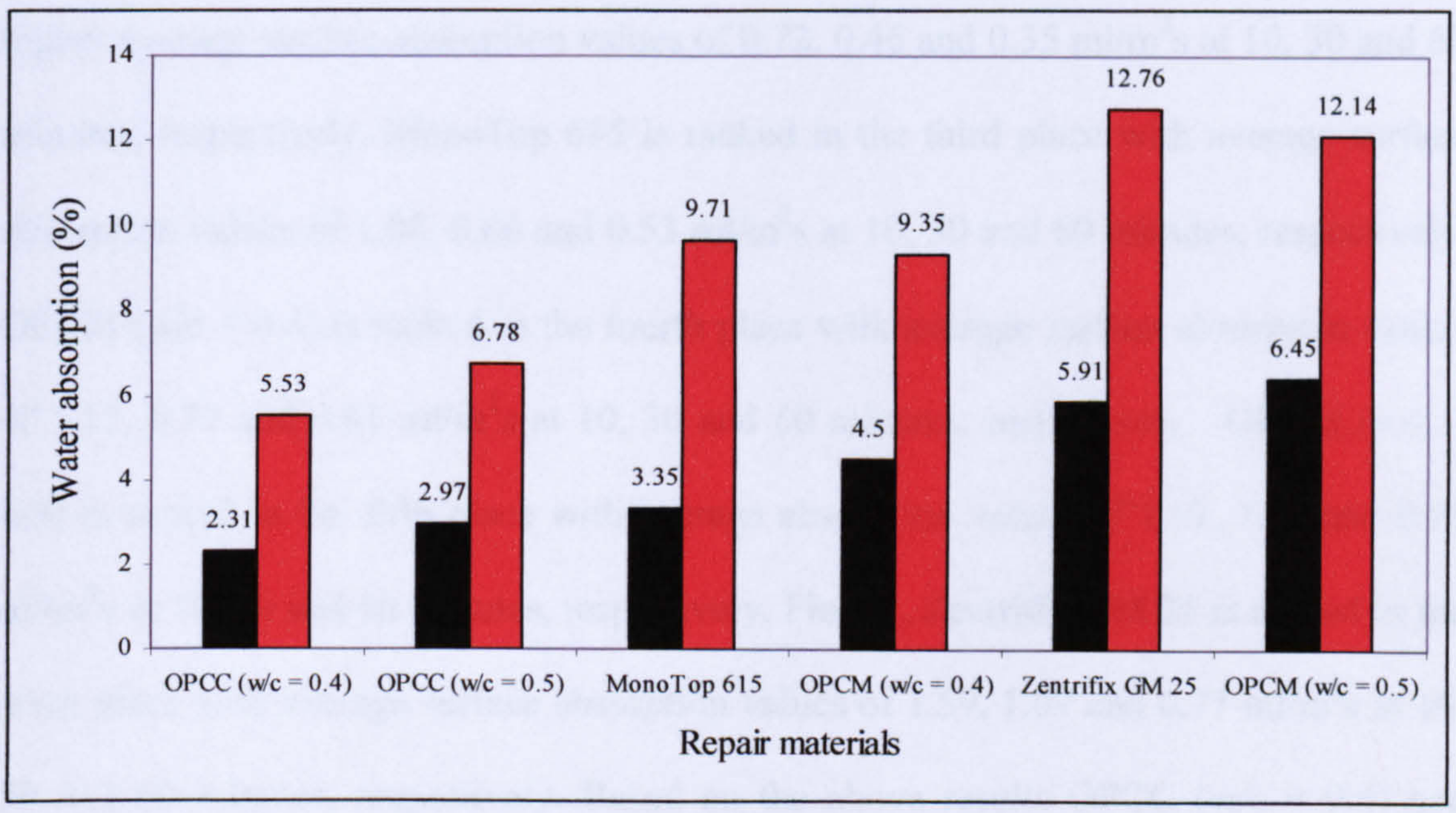

Figure 10.1 Absorption by immersion test results

10.3.3 Initial surface absorption test (ISAT) results

Results of the initial surface absorption tests performed on the 6 generic repair materials selected in Chapter 9 are shown in Table 10.2. More detailed information is provided in Table 10.4.

Repair material	Average surface absorption (ml/m^2s)		
	10 min	30 min	60 min
OPCC (w/c = 0.4)	0.61	0.36	0.26
OPCC (w/c = 0.5)	0.72	0.46	0.35
OPCM (w/c = 0.4)	1.15	0.77	0.61
OPCM (w/c = 0.5)	1.57	1.00	0.79
Zentrifix GM 25	1.59	1.07	0.77
MonoTop 615	1.00	0.66	0.53

Table 10.2 Initial surface absorption test results

From Tables 10.2 and 10.4 it is obvious that OPCC (w/c = 0.4) gives the best results, with an average surface absorption of 0.61, 0.36 and 0.26 ml/m^2s at 10, 30 and 60 minutes, respectively. OPCC (w/c = 0.5) is ranked in the second place with slightly higher average surface absorption values of 0.72, 0.46 and 0.35 ml/m^2s at 10, 30 and 60 minutes, respectively. MonoTop 615 is ranked in the third place with average surface absorption values of 1.00, 0.66 and 0.53 ml/m^2s at 10, 30 and 60 minutes, respectively. OPCM (w/c = 0.4) is ranked in the fourth place with average surface absorption values of 1.15, 0.77 and 0.61 ml/m^2s at 10, 30 and 60 minutes, respectively. OPCM (w/c = 0.5) is ranked in the fifth place with average absorption values of 1.57, 1.00 and 0.79 ml/m^2s at 10, 30 and 60 minutes, respectively. Finally, Zentrifix GM 25 is ranked in the sixth place with average surface absorption values of 1.59, 1.07 and 0.77 ml/m^2s at 10, 30 and 60 minutes, respectively. Based on the above results OPCC (w/c = 0.4) and OPCC (w/c = 0.5) can be classified as repair materials having low water surface absorption, MonoTop 615 and OPCM (w/c = 0.4) can be classified as repair materials having moderate water surface absorption, and OPCM (w/c = 0.5) and Zetrifix GM 25 can be classified as repair materials having high water surface absorption. Figure 10.2 summarises the above results.

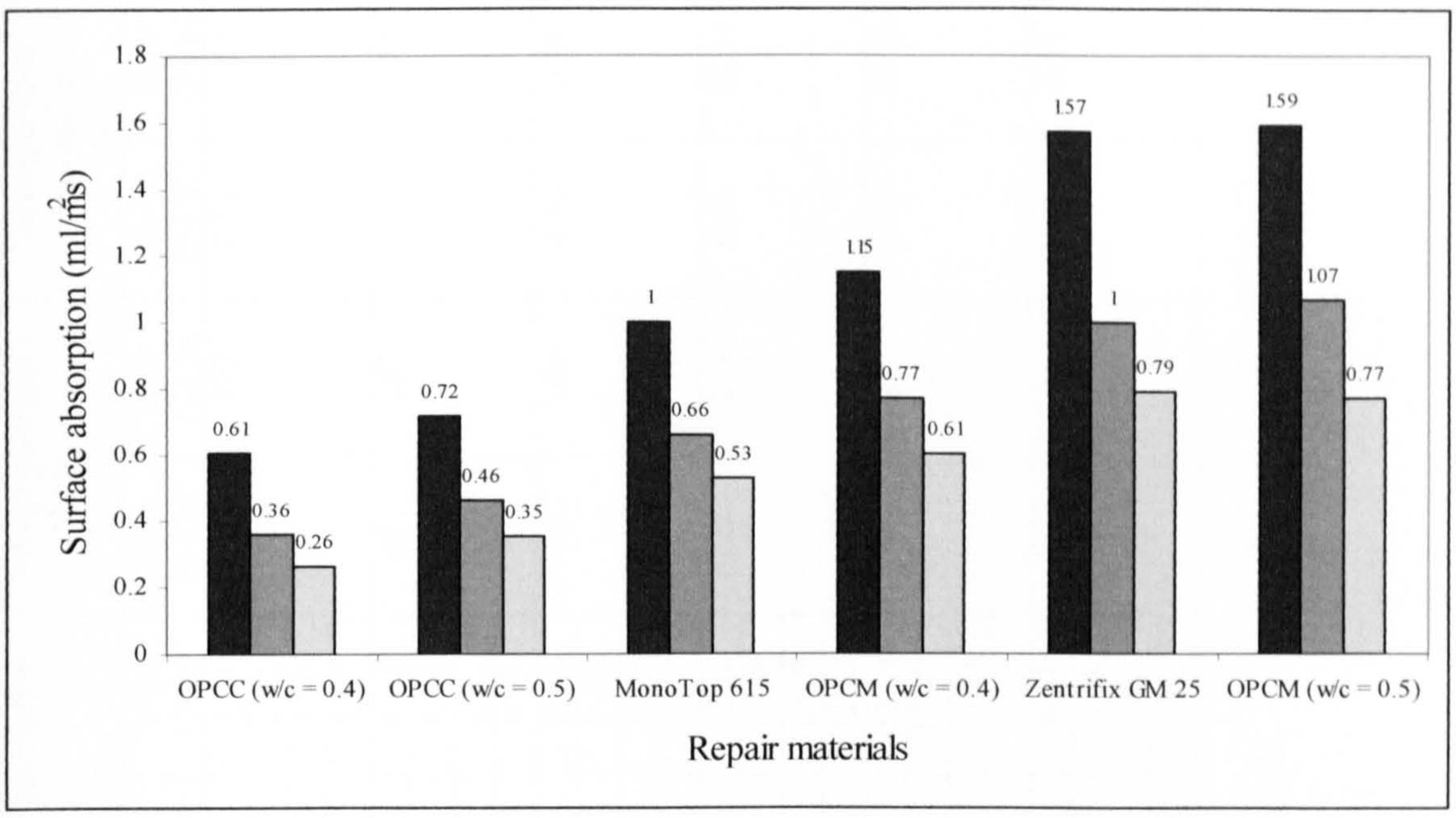

Figure 10.2 Initial surface absorption test results

Repair material	Average compressive strength (N/mm^2)	Average tensile strength (N/mm^2)	Cube no	Weight (gr)			Water absorption (gr)		Water absorption (%)		Average water absorption (gr)		Average water absorption (%)	
				Time (0 h)	Time (0.5 h)	Time (24 h)	Time (0.5 h)	Time (24 h)	Time (0.5 h)	Time (24 h)	Time (0.5 h)	Time (24 h)	Time (0.5 h)	Time (24 h)
OPC Concrete (w/c = 0.4)	64.24	5.16	1	2224	2275	2348	51	124	2.29	5.58	52	123	2.31	5.53
			2	2250	2302	2372	52	122	2.31	5.42				
			3	2237	2289	2360	52	123	2.32	5.50				
			4	2209	2260	2333	51	124	2.31	5.61				
OPC Concrete (w/c = 0.5)	44.93	4.51	1	2204	2270	2350	66	146	2.99	6.62	65	147	2.97	6.78
			2	2150	2214	2298	64	148	2.98	6.88				
			3	2161	2225	2309	64	148	2.96	6.85				
			4	2164	2228	2310	64	146	2.96	6.75				
OPC Mortar (w/c = 0.4)	50.89	5.16	1	2017	2109	2205	92	188	4.56	9.32	91	189	4.50	9.35
			2	2026	2118	2217	92	191	4.54	9.43				
			3	2018	2106	2202	88	184	4.36	9.12				
			4	2008	2099	2199	91	191	4.53	9.51				
OPC Mortar (w/c = 0.5)	34.74	3.99	1	1884	2006	2115	122	231	6.48	12.26	122	229	6.45	12.14
			2	1904	2021	2128	117	224	6.14	11.76				
			3	1888	2013	2120	125	232	6.62	12.29				
			4	1880	2003	2110	123	230	6.54	12.23				
Zentrifix GM 25	26.43	2.56	1	1641	1734	1841	93	200	5.67	12.19	97	209	5.91	12.76
			2	1622	1717	1834	95	212	5.86	13.07				
			3	1638	1738	1851	100	213	6.11	13.01				
			4	1647	1746	1857	99	210	6.01	12.75				
MonoTop 615	25.33	2.81	1	1534	1580	1674	46	140	2.99	9.13	51	146	3.35	9.71
			2	1458	1508	1603	50	145	3.43	9.95				
			3	1515	1568	1665	53	150	3.50	9.90				
			4	1522	1575	1672	53	150	3.48	9.86				

Table 10.3 Detailed absorption by immersion test results

Repair material	Average compressive strength (N/mm^2)	Average tensile strength (N/mm^2)	Cube no	10 min surface absorption (ml/m^2s)	10 min average surface absorption (ml/m^2s)	30 min surface absorption (ml/m^2s)	30 min average surface absorption (ml/m^2s)	60 min surface absorption (ml/m^2s)	60 min average surface absorption (ml/m^2s)
OPC Concrete (w/c = 0.4)	64.24	5.16	1	0.53	0.61	0.32	0.36	0.23	0.26
			2	0.56		0.32		0.22	
			3	0.66		0.43		0.30	
			4	0.67		0.38		0.28	
OPC Concrete (w/c = 0.5)	44.93	4.51	1	0.66	0.72	0.42	0.46	0.32	0.35
			2	0.69		0.42		0.31	
			3	0.70		0.47		0.36	
			4	0.83		0.53		0.39	
OPC Mortar (w/c = 0.4)	50.89	5.16	1	1.12	1.15	0.82	0.77	0.64	0.61
			2	1.08		0.73		0.57	
			3	1.17		0.75		0.59	
			4	1.22		0.78		0.63	
OPC Mortar (w/c = 0.5)	34.74	3.99	1	1.46	1.57	0.94	1.00	0.75	0.79
			2	1.56		1.02		0.81	
			3	1.60		1.04		0.76	
			4	1.64		1.01		0.85	
Zentrifix GM 25	26.43	2.56	1	1.44	1.59	1.00	1.07	0.72	0.77
			2	1.60		1.04		0.75	
			3	1.60		1.12		0.80	
			4	1.70		1.13		0.81	
MonoTop 615	25.33	2.81	1	1.00	1.00	0.66	0.66	0.53	0.53
			2	0.95		0.61		0.48	
			3	1.00		0.66		0.53	
			4	1.04		0.70		0.57	

Table 10.4 Detailed initial surface absorption test results

10.4 CONCLUSION

Both the absorption by immersion and initial surface absorption tests rank OPCC (w/c = 0.4) and OPCC (w/c = 0.5) as low water absorption repair materials, OPCM (w/c =0.4) and Montop 615 as moderate water absorption repair materials, and OPCM (w/c = 0.5) and Zentrifix GM 25 as high water absorption repair materials. Increased water absorption values of the last 4 repair materials can be attributed to the absence of coarse size aggregate. Finally, it should be emphasized that selection of very low water permeability repair materials is not always the best option. As mentioned in chapter 7, in the case of reinforced concrete patch repairs the use of very low permeability repair materials can lead to accelerated corrosion due to electrochemical incompatibility. Hence, if the surrounding concrete is very porous selection of one of the last 4 repair materials is the best option.

On the basis of the material experimentation performed in chapters 9 and 10, the following 3 repair materials: OPCC (w/c = 0.4), OPCM (w/c = 0.4) and Zentrifix GM 25 are to be used in the subsequent patch repair study.

CHAPTER 11

EXPERIMENTAL EVALUATION OF CONCRETE PATCH REPAIRS

11.1 INTRODUCTION

As mentioned in chapter 8, adhesion of the repair material to the concrete substrate is generally considered to be an important criterion in assessing the success and long-term durability of patch repairs. Pull-off test is the only experimental method that can be used to assess the adhesive strength of real patch repairs on site. The objective of this chapter is to perform a parametric study and investigate the various parameters influencing the adhesive strength of patch repairs. The parameters investigated include: a) influence of substrate surface on the average adhesive strength, b) influence of substrate strength on the average adhesive strength, c) influence of type of generic repair material on the average adhesive strength and d) influence of the use of bonding agent/ primer on the average adhesive strength.

11.2 PULL-OFF TESTING RESEARCH PROGRAM

11.2.1 Production of repaired slab specimens

In order to evaluate the adhesive strength of repaired slab specimens the 60 substrate slab specimens produced in chapter 6 for the purposes of measuring and characterising substrate surface roughness were repaired. The substrate specimens were divided into 5 groups. Every group consisted of 12 slabs. The first 4 groups consisted of substrates produced using an electric hammer, whereas, the last group consisted of substrates produced using remote robotic hydroerosion. Based on their flexural strength and water

absorption performance determined in chapters 9 and 10 the following 3 repair materials were used:

- Ordinary Portland Cement Concrete (OPCC w/c = 0.4)
- Ordinary Portland Cement Mortar (OPCM w/c = 0.4)
- Polymer-modified cement concrete reinforced with glass fibres (MC Chemicals Zentrifix GM 25)

In addition, cement based slurry bonding agent/primer MC Chemicals Zentrifix KMH was used in the repair of 30 specimens.

Prior to repair, the substrates were placed in water for 24 hours. Next, the substrates were taken from the water and left for 5 minutes to dry. Any excess water was removed using a dry piece of cloth. Next, the substrates were placed inside timber moulds and repaired using the above 3 types of generic repair materials. Each group of slabs was divided into 3 sub-groups. Each sub-group consisted of 4 slabs. In every group of slabs one sub-group was repaired using OPCC (w/c = 0.4), one sub-group was repaired using OPCM (w/c = 0.4), and one sub-group was repaired using Zentrifix GM25. Every sub-group was further divided into 2 sub-sub-groups each one consisting of 2 slabs. In every sub-group one sub-sub-group was repaired using the bonding agent/primer Zentrifix KMH, whereas, the other sub-sub-group was repaired without the use of the bonding agent. In the case of specimens repaired using the bonding agent/primer Zentrifix KMH, the repair material was installed immediately after the application of the bonding agent/primer in accordance with the guidelines provided by the bonding agent manufacturer. Twenty-four hours after the installation of the repair material the repaired slabs were demoulded and placed in water. After 6 days in water, the slabs were taken

out of the water and were air-cured in a storage room for 21 days. The storage room temperature was approximately 19 ^{0}C at 50-60% relative humidity. Details of all repaired slabs are shown in Tables 11.1 and 11.2. Photographs during the repair of the slabs are shown in **Appendix 13.**

Slab Group	w/c	Mix Number	Slab Number	Repair Material	Bonding Agent
1	0.40	1	S1	Zentrifix GM 25	N/A
			S2		
		2	S3		Zentrifix KMH
			S4		
		3	S5	OPCM (w/c = 0.40)	Zentrifix KMH
			S6		
		4	S7		N/A
			S8		
		5	S9	OPCC (w/c = 0.40)	Zentrifix KMH
			S10		
		6	S11		N/A
			S12		
2	0.45	7	S13	OPCC (w/c = 0.40)	N/A
			S14		
		8	S15		Zentrifix KMH
			S16		
		9	S17	OPCM (w/c = 0.40)	N/A
			S18		
		10	S19		Zentrifix KMH
			S20		
		11	S21	Zentrifix GM25	Zentrifix KMH
			S22		
		12	S23		N/A
			S24		
3	0.50	13	S25	OPCC (w/c = 0.40)	N/A
			S26		
		14	S27		Zentrifix KMH
			S28		
		15	S29	OPCM (w/c = 0.40)	N/A
			S30		
		16	S31		Zentrifix KMH
			S32		
		17	S33	Zentrifix GM25	Zentrifix KMH
			S34		
		18	S35		N/A
			S36		
4	0.55	19	S37	OPCC (w/c = 0.40)	N/A
			S38		
		20	S39		Zentrifix KMH
			S40		
		21	S41	OPCM (w/c = 0.40)	Zentrifix KMH
			S42		
		22	S43		N/A
			S44		
		23	S45	Zentrifix GM25	Zentrifix KMH
			S46		
		24	S47		N/A
			S48		

Table 11.1 Repair of substrate slabs produced using an electric hammer

Slab Group	Slab Number	Repair Material	Bonding Agent
5	P5	OPCC (w/c = 0.40)	N/A
	PL14		
	PL15		Zentrifix KMH
	PL16		
	PL11	OPCM (w/c = 0.40)	N/A
	PL13		
	P1		Zentrifix KMH
	PL2		
	PL9	Zentrifix GM25	N/A
	PL10		
	PL5		Zentrifix KMH
	PL6		

Table 11.2 Repair of substrate slabs produced using remote robotic hydroerosion

After curing was completed 5 partial cores were drilled perpendicular to the surface of each repaired slab in accordance to BS EN 1542[93]. The partially drilled cores extended at least 25 mm beyond the bonding interface between the repair material and the substrate. Next, aluminium discs (dollies) were attached at the top of the partially drilled cores using a two part (resign-hardener) adhesive. Forty-eight hours after the installation of the aluminium discs pull-off tests were performed to evaluate the adhesive strength of the repaired specimens. Five pull-off tests were performed on each slab and a total of 300 on all 60 slabs. Photographs during drilling of cores and pull-off testing are shown in **Appendix 14.**

11.2.2 Pull-off test results

Modes of failure, values of adhesive strength and values of average adhesive strength obtained by performing 300 pull-off tests on 60 repaired slab specimens are shown in Tables 11.3-11.17 and in Figure 11.1. Compressive strength values for both the substrates and the repair materials are shown in **Appendix 15.**

Mix Number	w/c	Slab Number	Substrate Average Compressive Strength (N/mm^2)	Bonding Agent	Repair Material	Repair Average Compressive Strength (N/mm^2)	Core Position	Adhesive Strength (N/mm^2)	Mode of Failure	Average Adhesive Strength (N/mm^2)
1	0.40	S1	57.77	N/A	Zentrifix GM 25	27.16	1	1.19	100% Interface	1.19
							2	1.22	100% Interface	
							3	1.02	100% Interface	
							4	0.99	100% Interface	
							5	1.53	100% Interface	
		S2					1	0.71	100% Interface	0.93
							2	1.02	100% Interface	
							3	0.71	100% Interface	
							4	0.89	100% Interface	
							5	1.30	100% Interface	
2	0.40	S3	53.94	Zentrifix KMH	Zentrifix GM 25	27.16	1	1.20	100% Interface	0.99
							2	0.92	100% Interface	
							3	1.32	100% Interface	
							4	0.46	100% Interface	
							5	1.07	100% Interface	
		S4					1	0.82	100% Interface	1.11
							2	1.35	100% Interface	
							3	1.30	100% Interface	
							4	0.92	100% Interface	
							5	1.15	100% Interface	

Table 11.3 Modes of failure, adhesive strength and average adhesive strength values for slabs S1-S4

Mix Number	w/c	Slab Number	Substrate Average Compressive Strength (N/mm^2)	Bonding Agent	Repair Material	Repair Average Compressive Strength (N/mm^2)	Core Position	Adhesive Strength (N/mm^2)	Mode of Failure	Average Adhesive Strength (N/mm^2)
3	0.40	S5	57.04	Zentrifix KMH	OPCM (w/c = 0.40)	51.60	1	0.97	100% Interface	1.12
							2	0.61	100% Interface	
							3	1.43	100% Interface	
							4	1.25	100% Interface	
							5	1.32	100% Interface	
		S6					1	1.58	100% Interface	1.19
							2	1.30	100% Interface	
							3	0.92	100% Interface	
							4	1.43	100% Interface	
							5	0.74	100% Interface	
4	0.40	S7	58.13	N/A	OPCM (w/c = 0.40)	51.60	1	0.92	100% Interface	1.11
							2	0.94	100% Interface	
							3	1.45	100% Interface	
							4	0.92	100% Interface	
							5	1.32	100% Interface	
		S8					1	1.38	100% Interface	1.34
							2	1.53	100% Interface	
							3	1.22	100% Interface	
							4	1.43	100% Interface	
							5	1.12	100% Interface	

Table 11.4 Modes of failure, adhesive strength and average adhesive strength values for slabs S5-S8

Mix Number	w/c	Slab Number	Substrate Average Compressive Strength (N/mm^2)	Bonding Agent	Repair Material	Repair Average Compressive Strength (N/mm^2)	Core Position	Adhesive Strength (N/mm^2)	Mode of Failure	Average Adhesive Strength (N/mm^2)
5	0.40	S9	56.29	Zentrifix KMH	OPCC (w/c = 0.40)	57.93	1	1.02	100% Interface	1.16
							2	1.02	100% Interface	
							3	1.02	100% Interface	
							4	1.43	100% Interface	
							5	1.32	100% Interface	
		S10					1	1.02	100% Interface	1.02
							2	1.02	100% Interface	
							3	0.82	100% Interface	
							4	1.63	100% Interface	
							5	0.61	100% Interface	
6	0.40	S11	55.98	N/A	OPCC (w/c = 0.40)	57.93	1	1.12	100% Interface	1.19
							2	1.38	100% Interface	
							3	1.12	100% Interface	
							4	1.22	100% Interface	
							5	1.12	100% Interface	
		S12					1	0.95	100% Interface	0.95
							2	0.71	100% Interface	
							3	0.95	100% Interface	
							4	1.43	100% Interface	
							5	0.71	100% Interface	

Table 11.5 Modes of failure, adhesive strength and average adhesive strength values for slabs S9-S12

Mix Number	w/c	Slab Number	Substrate Average Compressive Strength (N/mm^2)	Bonding Agent	Repair Material	Repair Average Compressive Strength (N/mm^2)	Core Position	Adhesive Strength (N/mm^2)	Mode of Failure	Average Adhesive Strength (N/mm^2)
7	0.45	S13	53.59	N/A	OPPC (w/c = 0.40)	48.30	1	0.82	100% Interface	0.98
							2	1.15	100% Interface	
							3	1.40	100% Interface	
							4	0.71	100% Interface	
							5	0.82	100% Interface	
		S14					1	0.61	100% Interface	1.06
							2	1.22	100% Interface	
							3	1.80	100% Interface	
							4	0.84	100% Interface	
							5	0.82	100% Interface	
8	0.45	S15	50.44	Zentrifix KMH	OPCC (w/c = 0.40)	48.30	1	1.32	100% Interface	1.07
							2	1.07	100% Interface	
							3	0.82	100% Interface	
							4	1.07	100% Interface	
							5	1.07	100% Interface	
		S16					1	0.82	100% Interface	1.07
							2	1.32	100% Interface	
							3	1.07	100% Interface	
							4	1.07	100% Interface	
							5	1.07	100% Interface	

Table 11.6 Modes of failure, adhesive strength and average adhesive strength values for slabs S13-S16

Mix Number	w/c	Slab Number	Substrate Average Compressive Strength (N/mm^2)	Bonding Agent	Repair Material	Repair Average Compressive Strength (N/mm^2)	Core Position	Adhesive Strength (N/mm^2)	Mode of Failure	Average Adhesive Strength (N/mm^2)
9	0.45	S17	47.41	N/A	OPCM (w/c = 0.40)	47.66	1	0.92	100% Interface	0.87
							2	0.97	100% Interface	
							3	0.99	100% Interface	
							4	0.70	100% Interface	
							5	0.75	100% Interface	
		S18					1	0.71	100% Interface	0.87
							2	0.99	100% Interface	
							3	0.74	100% Interface	
							4	0.92	100% Interface	
							5	0.97	100% Interface	
10	0.45	S19	50.19	Zentrifix KMH	OPCM (w/c = 0.40)	47.66	1	0.20	100% Interface	0.71
							2	1.04	100% Interface	
							3	0.66	100% Interface	
							4	0.71	100% Interface	
							5	0.94	100% Interface	
		S20					1	0.51	100% Interface	0.89
							2	1.22	100% Interface	
							3	1.07	100% Interface	
							4	0.71	100% Interface	
							5	0.94	100% Interface	

Table 11.7 Modes of failure, adhesive strength and average adhesive strength values for slabs S17-S20

Mix Number	w/c	Slab Number	Substrate Average Compressive Strength (N/mm^2)	Bonding Agent	Repair Material	Repair Average Compressive Strength (N/mm^2)	Core Position	Adhesive Strength (N/mm^2)	Mode of Failure	Average Adhesive Strength (N/mm^2)
11	0.45	S21	53.54	Zentrifix KMH	Zentrifix GM 25	29.52	1	0.46	100% Interface	0.72
							2	0.82	100% Interface	
							3	0.46	100% Interface	
							4	1.22	100% Interface	
							5	0.66	100% Interface	
		S22					1	0.82	100% Interface	0.85
							2	1.17	100% Interface	
							3	0.82	100% Interface	
							4	0.94	100% Interface	
							5	0.51	100% Interface	
12	0.45	S23	52.56	N/A	Zentrifix GM 25	29.52	1	0.61	100% Interface	0.67
							2	1.02	100% Interface	
							3	0.25	100% Interface	
							4	0.76	100% Interface	
							5	0.69	100% Interface	
		S24					1	0.82	100% Interface	0.88
							2	0.56	100% Interface	
							3	1.12	100% Interface	
							4	0.71	100% Interface	
							5	1.17	100% Interface	

Table 11.8 Modes of failure, adhesive strength and average adhesive strength values for slabs S21-S24

Mix Number	w/c	Slab Number	Substrate Average Compressive Strength (N/mm^2)	Bonding Agent	Repair Material	Repair Average Compressive Strength (N/mm^2)	Core Position	Adhesive Strength (N/mm^2)	Mode of Failure	Average Adhesive Strength (N/mm^2)
13	0.50	S25	42.42	N/A	OPCC (w/c = 0.40)	52.04	1	1.12	100% Interface	0.71
							2	0.41	100% Interface	
							3	0.61	100% Interface	
							4	0.41	100% Interface	
							5	1.02	100% Interface	
		S26					1	0.61	100% Interface	0.83
							2	1.32	100% Interface	
							3	1.02	100% Interface	
							4	0.84	100% Interface	
							5	0.38	100% Interface	
14	0.50	S27	43.72	Zentrifix KMH	OPCC (w/c = 0.40)	52.04	1	0.71	100% Interface	0.89
							2	0.89	100% Interface	
							3	0.82	100% Interface	
							4	1.02	100% Interface	
							5	1.02	100% Interface	
		S28					1	1.17	100% Interface	1.17
							2	1.17	100% Interface	
							3	1.07	100% Interface	
							4	1.12	100% Interface	
							5	1.32	100% Interface	

Table 11.9 Modes of failure, adhesive strength and average adhesive strength values for slabs S25-S28

Mix Number	w/c	Slab Number	Substrate Average Compressive Strength (N/mm^2)	Bonding Agent	Repair Material	Repair Average Compressive Strength (N/mm^2)	Core Position	Adhesive Strength (N/mm^2)	Mode of Failure	Average Adhesive Strength (N/mm^2)
15	0.50	S29	46.23	N/A	OPCM (w/c = 0.40)	48.77	1	1.02	100% Interface	0.83
							2	0.82	100% Interface	
							3	0.99	100% Interface	
							4	0.51	100% Interface	
							5	0.82	100% Interface	
		S30					1	1.25	100% Substrate	0.97
							2	0.92	100% Interface	
							3	0.46	100% Interface	
							4	1.02	100% Interface	
							5	1.22	100% Interface	
16	0.50	S31	42.94	Zentrifix KMH	OPCM (w/c = 0.40)	48.77	1	0.46	100% Interface	0.76
							2	1.22	100% Interface	
							3	0.38	100% Interface	
							4	0.61	100% Interface	
							5	1.15	100% Interface	
		S32					1	1.32	100% Interface	1.08
							2	1.20	100% Interface	
							3	1.15	100% Interface	
							4	0.92	100% Interface	
							5	0.79	100% Interface	

Table 11.10 Modes of failure, adhesive strength and average adhesive strength values for slabs S29-S32

Mix Number	w/c	Slab Number	Substrate Average Compressive Strength (N/mm^2)	Bonding Agent	Repair Material	Repair Average Compressive Strength (N/mm^2)	Core Position	Adhesive Strength (N/mm^2)	Mode of Failure	Average Adhesive Strength (N/mm^2)
17	0.50	S33	43.50	Zentrifix KMH	Zentrifix GM 25	23.81	1	0.82	100% Interface	0.91
							2	1.17	100% Interface	
							3	0.94	100% Interface	
							4	0.71	100% Interface	
							5	0.91	100% Interface	
		S34					1	1.02	100% Interface	1.00
							2	0.99	100% Interface	
							3	0.92	100% Interface	
							4	1.32	100% Interface	
							5	0.74	100% Interface	
18	0.50	S35	41.10	N/A	Zentrifix GM 25	23.81	1	0.61	100% Interface	0.70
							2	0.71	100% Interface	
							3	0.61	100% Interface	
							4	0.70	100% Interface	
							5	0.87	100% Interface	
		S36					1	0.96	100% Interface	0.96
							2	1.10	100% Interface	
							3	0.71	100% Interface	
							4	1.02	100% Interface	
							5	0.99	100% Interface	

Table 11.11 Modes of failure, adhesive strength and average adhesive strength values for slabs S33-S36

Mix Number	w/c	Slab Number	Substrate Average Compressive Strength (N/mm^2)	Bonding Agent	Repair Material	Repair Average Compressive Strength (N/mm^2)	Core Position	Adhesive Strength (N/mm^2)	Mode of Failure	Average Adhesive Strength (N/mm^2)
19	0.55	S37	40.39	N/A	OPCC (w/c = 0.40)	54.98	1	0.82	100% Interface	0.90
							2	0.51	100% Interface	
							3	0.87	100% Interface	
							4	1.43	100% Interface	
							5	0.87	100% Interface	
		S38					1	1.02	100% Interface	0.62
							2	0.61	100% Interface	
							3	0.32	100% Interface	
							4	0.64	100% Interface	
							5	0.51	100% Interface	
20	0.55	S39	40.27	Zentrifix KMH	OPCC (w/c = 0.40)	54.98	1	1.05	100% Interface	1.05
							2	1.12	100% Interface	
							3	1.27	100% Interface	
							4	0.82	100% Interface	
							5	0.97	100% Interface	
		S40					1	1.20	100% Interface	1.12
							2	1.12	100% Interface	
							3	1.02	100% Interface	
							4	0.92	100% Interface	
							5	1.32	100% Interface	

Table 11.12 Modes of failure, adhesive strength and average adhesive strength values for slabs S37-S40

Mix Number	w/c	Slab Number	Substrate Average Compressive Strength (N/mm^2)	Bonding Agent	Repair Material	Repair Average Compressive Strength (N/mm^2)	Core Position	Adhesive Strength (N/mm^2)	Mode of Failure	Average Adhesive Strength (N/mm^2)
21	0.55	S41	39.49	Zentrifix KMH	OPCM (w/c = 0.40)	49.27	1	0.38	100% Interface	0.82
							2	1.07	100% Interface	
							3	1.10	100% Interface	
							4	0.71	100% Interface	
							5	0.82	100% Interface	
		S42					1	1.12	100% Interface	0.87
							2	0.38	100% Interface	
							3	1.02	100% Interface	
							4	1.07	100% Interface	
							5	0.76	100% Interface	
22	0.55	S43	37.14	N/A	OPCM (w/c = 0.40)	49.27	1	0.92	100% Interface	0.69
							2	0.25	100% Interface	
							3	0.66	100% Interface	
							4	1.17	100% Interface	
							5	0.46	100% Interface	
		S44					1	0.51	100% Interface	0.54
							2	0.71	100% Interface	
							3	0.51	100% Interface	
							4	0.71	100% Interface	
							5	0.25	100% Interface	

Table 11.13 Modes of failure, adhesive strength and average adhesive strength values for slabs S41-S44

Mix Number	w/c	Slab Number	Substrate Average Compressive Strength (N/mm^2)	Bonding Agent	Repair Material	Repair Average Compressive Strength (N/mm^2)	Core Position	Adhesive Strength (N/mm^2)	Mode of Failure	Average Adhesive Strength (N/mm^2)
23	0.55	S45	41.15	Zentrifix KMH	Zentrifix GM 25	28.41	1	0.97	100% Interface	0.79
							2	0.76	100% Interface	
							3	0.97	100% Interface	
							4	0.79	100% Interface	
							5	0.46	100% Interface	
		S46					1	0.97	100% Interface	0.86
							2	0.97	100% Interface	
							3	0.61	100% Interface	
							4	0.71	100% Interface	
							5	1.02	100% Interface	
24	0.55	S47	39.14	N/A	Zentrifix GM 25	28.41	1	0.79	100% Interface	0.62
							2	0.51	100% Interface	
							3	0.51	100% Interface	
							4	0.56	100% Interface	
							5	0.71	100% Interface	
		S48					1	0.82	100% Interface	0.74
							2	0.56	100% Interface	
							3	0.66	100% Interface	
							4	0.92	100% Interface	
							5	0.74	100% Interface	

Table 11.14 Modes of failure, adhesive strength and average adhesive strength values for slabs S45-S48

Slab Number	Substrate Average Compressive Strength (N/mm^2)	Bonding Agent	Repair Material	Repair Average Compressive Strength (N/mm^2)	Core Position	Adhesive Strength (N/mm^2)	Mode of Failure	Average Adhesive Strength (N/mm^2)
P5	51.75	N/A	OPCC (w/c = 0.40)	52.98	1	1.30	100% Interface	1.56
					2	1.78	100% Interface	
					3	1.56	100% Interface	
					4	1.94	100% Interface	
					5	1.22	100% Interface	
PL14	64.20			52.98	1	0.71	100% Interface	1.19
					2	0.84	100% Interface	
					3	1.25	100% Interface	
					4	2.45	100% Adhesive	
					5	0.71	100% Interface	
PL15	47.81	Zentrifix KMH	OPCC (w/c = 0.40)	52.98	1	1.53	100% Interface	2.18
					2	2.04	100% Interface	
					3	2.55	100% Adhesive	
					4	2.75	100% Interface	
					5	2.04	100% Interface	
PL16					1	1.48	100% Interface	1.98
					2	1.58	100% Adhesive	
					3	2.04	100% Interface	
					4	2.24	100% Interface	
					5	2.55	100% Repair	

Table 11.15 Modes of failure, adhesive strength and average adhesive strength values for slabs P5, PL14, PL15 and PL16

Slab Number	Substrate Average Compressive Strength (N/mm^2)	Bonding Agent	Repair Material	Repair Average Compressive Strength (N/mm^2)	Core Position	Adhesive Strength (N/mm^2)	Mode of Failure	Average Adhesive Strength (N/mm^2)
PL11	51.28	N/A	OPCM (w/c = 0.40)	47.02	1	1.04	100% Interface	1.23
					2	1.53	100% Interface	
					3	1.02	100% Interface	
					4	1.02	100% Interface	
					5	1.53	100% Interface	
PL13					1	0.71	100% Interface	0.83
					2	1.02	100% Interface	
					3	1.02	100% Interface	
					4	0.71	100% Interface	
					5	0.71	100% Interface	
P1	53.75	Zentrifix KMH	OPCM (w/c = 0.40)	47.02	1	1.58	100% Interface	1.39
					2	0.82	100% Interface	
					3	1.39	100% Interface	
					4	2.45	100% Interface	
					5	0.71	100% Interface	
PL2	57.35			47.02	1	0.71	100% Interface	1.03
					2	1.32	100% Interface	
					3	0.71	100% Interface	
					4	1.68	100% Interface	
					5	0.74	100% Interface	

Table 11.16 Modes of failure, adhesive strength and average adhesive strength values for slabs PL11, PL13, P2 and PL2

Slab Number	Substrate Average Compressive Strength (N/mm^2)	Bonding Agent	Repair Material	Repair Average Compressive Strength (N/mm^2)	Core Position	Adhesive Strength (N/mm^2)	Mode of Failure	Average Adhesive Strength (N/mm^2)
PL9	50.08	N/A	Zentrifix GM 25	26.77	1	0.61	100% Interface	0.94
					2	1.30	100% Interface	
					3	0.94	100% Interface	
					4	0.92	100% Interface	
					5	0.94	100% Interface	
PL10					1	0.51	100% Interface	0.91
					2	1.12	100% Interface	
					3	0.38	100% Interface	
					4	1.63	100% Adhesive	
					5	0.91	100% Interface	
PL5	52.95	Zentrifix KMH	Zentrifix GM 25	26.77	1	1.32	100% Interface	0.99
					2	1.15	100% Interface	
					3	0.87	100% Interface	
					4	0.99	100% Interface	
					5	0.61	100% Interface	
PL6					1	0.71	100% Interface	0.96
					2	0.66	100% Interface	
					3	1.32	100% Interface	
					4	1.40	100% Interface	
					5	0.71	100% Interface	

Table 11.17 Modes of failure, adhesive strength and average adhesive strength values for slabs PL9, PL10, PL5 and PL6

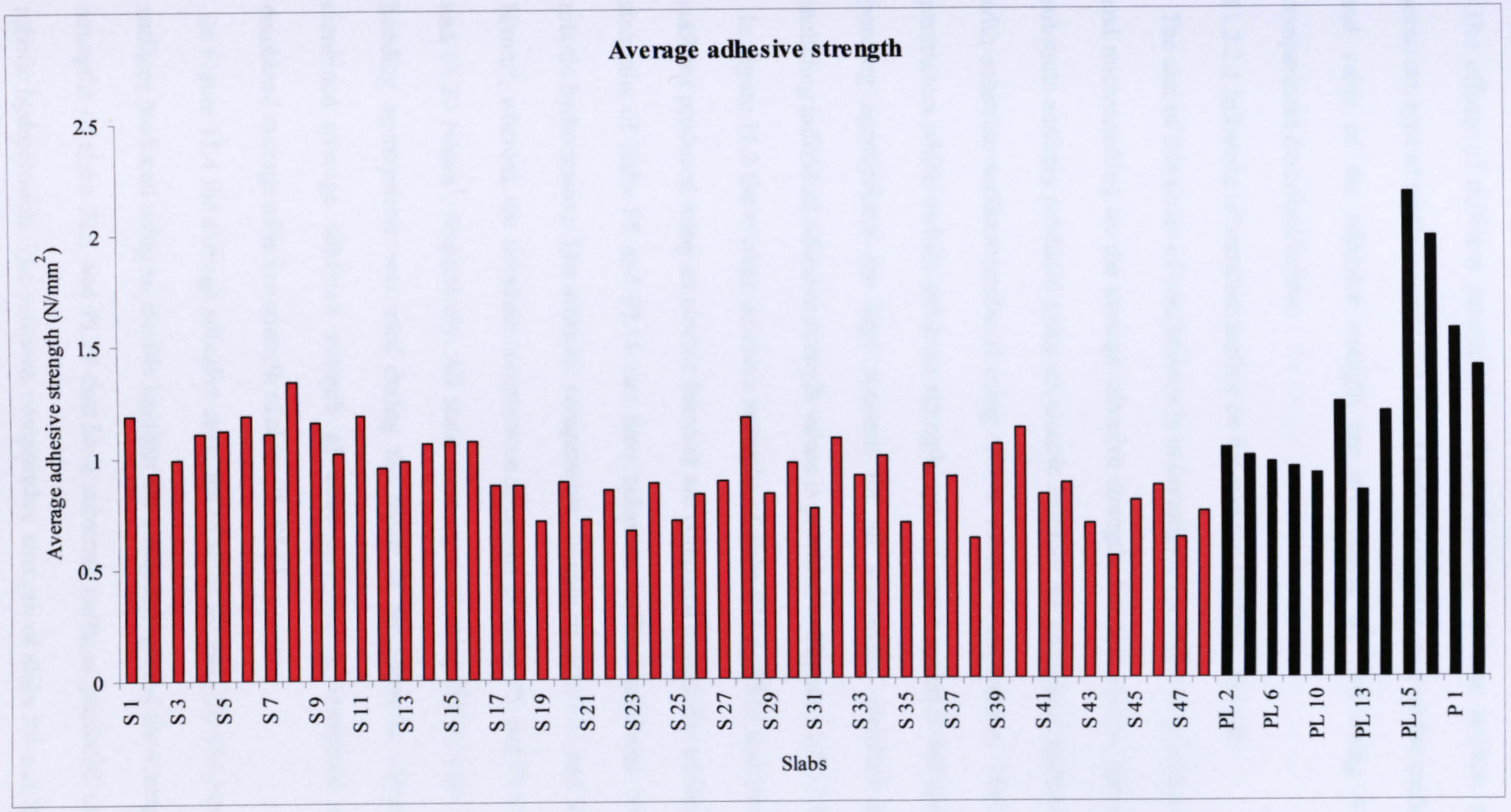

Figure 11.1 Average adhesive strength values

reinforcement in the surrounding concrete could be accelerated. They concluded that a low permeability polymer-modified repair mortar used in conjunction with a zinc rich epoxy rebar primer provided the best anti-corrosion protection to steel reinforcement both in the repair zone and in the adjacent concrete. However, this finding is not supported by the work of Heiman and Koerstz[61], who found that the use of a zinc epoxy primer on the steel reinforcement did not have any beneficial effect as a corrosion inhibitor.

Low permeability of the repair material is of major concern since areas that have been repaired are the most vulnerable to H_2O, O_2, CO_2 and ^-Cl penetration. However, in many cases very low permeability repair materials are not the best option. A small number of cracks in the repair, or its debonding, will significantly reduce the benefit of a very low permeability repair material. Microcracks connected with wider cracks originating from the surface of the repair have a more significant effect in reducing durability than the permeability of the repair itself. Emmons et al[58] emphasised that the insistence on low permeability as a criterion for repair materials can lead to unsuitable choices, incompatibility problems, and eventual failure. They concluded that a bad example was the use of very low permeability repair materials for repairing thousands of bridge columns in North America leading to encapsulation. When the temperature drops, moisture in vapour form migrates toward the barrier and is converted to a liquid form at the dew point. Water solubles are carried along in the migration. The liquid is then turned into ice at freezing temperatures, resulting in freeze-thaw damage at the edge of the barrier. When the temperature is rising again, the moisture is converted back to a vapour form, leaving water solubles behind in a crystalline form since vapour is not capable of making a solution. Repeated cycles can result to severe deterioration from one of these damaging forces. Morgan[62] also emphasised the fact that repair materials

N/mm^2, whereas, the substrate strength of slabs PL15 and PL16 is 47.81 N/mm^2. All slabs were repaired using OPCC (w/c = 0.4). Zentrifix KMH was used as a bonding agent during the repair of all 4 slabs. In Figure 11.5 the combined average adhesive strength of slabs S9+S10 is compared against the combined average adhesive strength of slabs PL15+PL16.

In Figure 11.6 the average adhesive strengths of slabs S17 and S18 that have substrate surfaces produced using an electric hammer are compared against the average adhesive strengths of slabs PL11 and PL13 that have substrate surfaces produced using remote robotic hydroerosion. The substrate compressive strength of slabs S17 and S18 is 47.41 N/mm^2, whereas, the substrate strength of slabs PL11 and PL13 is 51.28 N/mm^2. All slabs were repaired using OPCM (w/c = 0.4). No bonding agent/primer was used during the repair of the slabs. In Figure 11.7 the combined average adhesive strength of slabs S17+S18 is compared against the combined average adhesive strength of slabs PL11+PL13.

In Figure 11.8 the average adhesive strengths of slabs S5 and S6 that have substrate surfaces produced using an electric hammer are compared against the average adhesive strengths of slabs P1 and PL2 that have substrate surfaces produced using remote robotic hydroerosion. The substrate compressive strength of slabs S5 and S6 is 57.04 N/mm^2, whereas, the substrate strengths of slabs P1 and PL2 are 53.75 and 57.35 N/mm^2, respectively. All slabs were repaired using OPCM (w/c = 0.4). Zentrifix KMH was used as a bonding agent during the repair of all 4 slabs. In Figure 11.9 the combined average adhesive strength of slabs S5+S6 is compared against the combined average adhesive strength of slabs P1+PL2.

In Figure 11.10 the average adhesive strengths of slabs S23 and S24 that have substrate surfaces produced using an electric hammer are compared against the average

adhesive strengths of slabs PL9 and PL10 that have substrate surfaces produced using remote robotic hydroerosion. The substrate compressive strength of slabs S23 and S24 is 52.56 N/mm^2, whereas, the substrate strength of slabs PL9 and PL10 is 50.08 N/mm^2. All slabs were repaired using Zentrifix GM 25. No bonding agent/primer was used during the repair of the slabs. In Figure 11.11 the combined average adhesive strength of slabs S23+S24 is compared against the combined average adhesive strength of slabs PL9+PL10.

In Figure 11.12 the average adhesive strengths of slabs S21 and S22 that have substrate surfaces produced using an electric hammer are compared against the average adhesive strengths of slabs PL5 and PL6 that have substrate surfaces produced using remote robotic hydroerosion. The substrate compressive strength of slabs S21 and S22 is 53.54 N/mm^2, whereas, the substrate strengths of slabs PL5 and PL6 is 52.95 N/mm^2. All slabs were repaired using Zentrifix GM 25. Zentrifix KMH was used as a bonding agent during the repair of all 4 slabs. In Figure 11.13 the combined average adhesive strength of slabs S21+S22 is compared against the combined average adhesive strength of slabs PL5+PL6.

From the above comparisons it is quite clear that substrate surfaces produced using remote robotic hydroerosion provide higher adhesive strength values compared to substrate surfaces produced using an electric hammer. The average adhesive strength values for substrate surfaces obtained using remote robotic hydroerosion varied between 0.83-2.18 N/mm^2, whereas, the average adhesive strength values for substrate surfaces produced using an electric hammer varied between 0.54-1.34 N/mm^2. The reason for the better performance of substrate surfaces produced using remote robotic hydroerosion can be attributed to a combination of 2 factors:

- Higher roughness values as proved in Chapter 6 by the use of 2 different measurement methods (sand-area method and fringe-based laser interferometry) which promote the mechanical interlocking between the substrate and the repair material and hence increase the capacity of the bonding interface
- Absence or very limited introduction of microcracks at the top 9-10 mm of the substrate which does not significantly reduce the capacity of the bonding interface

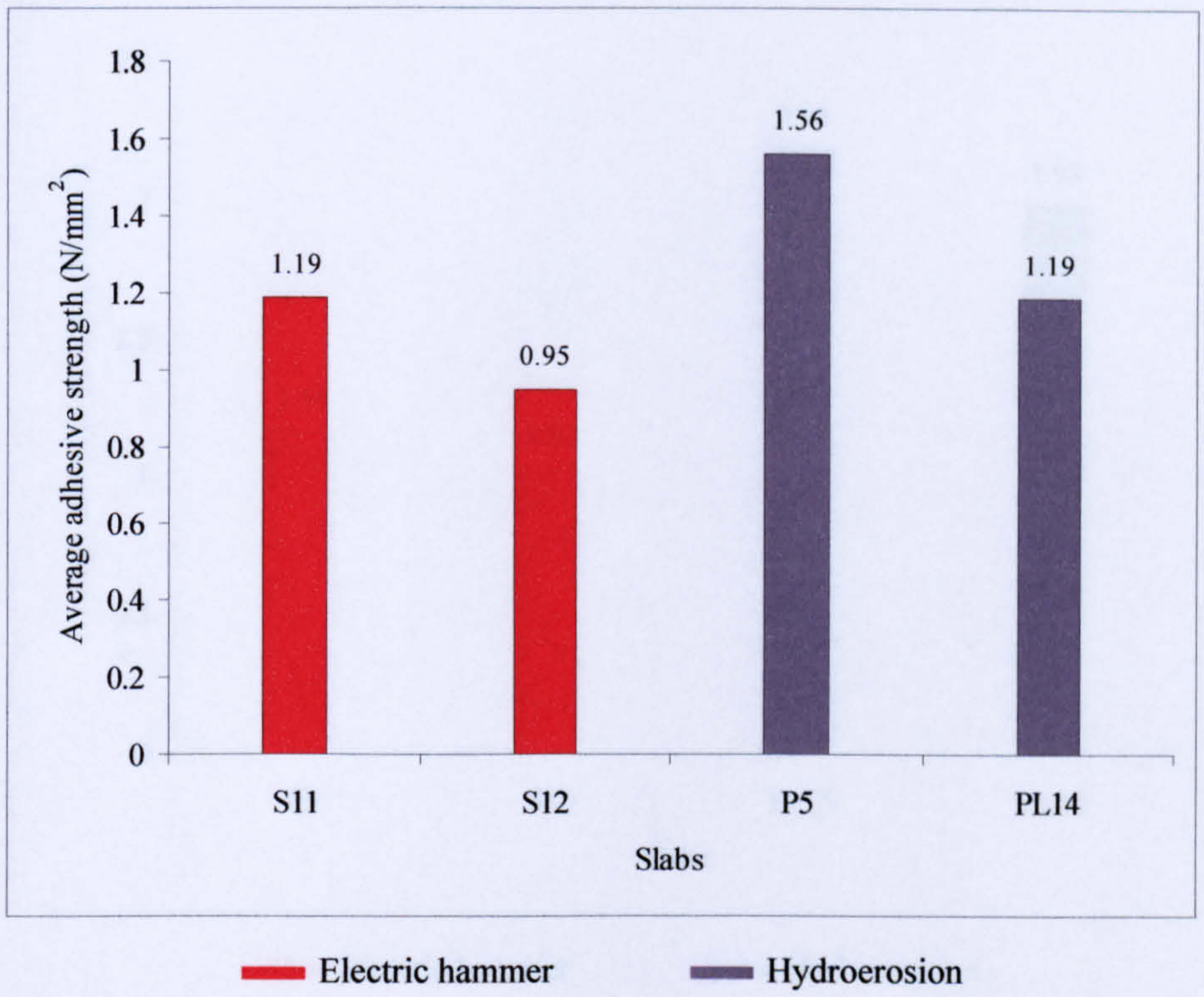

Figure 11.2 Influence of different types of substrate surface on the average adhesive strength of slabs S11, S12, P5 and PL14

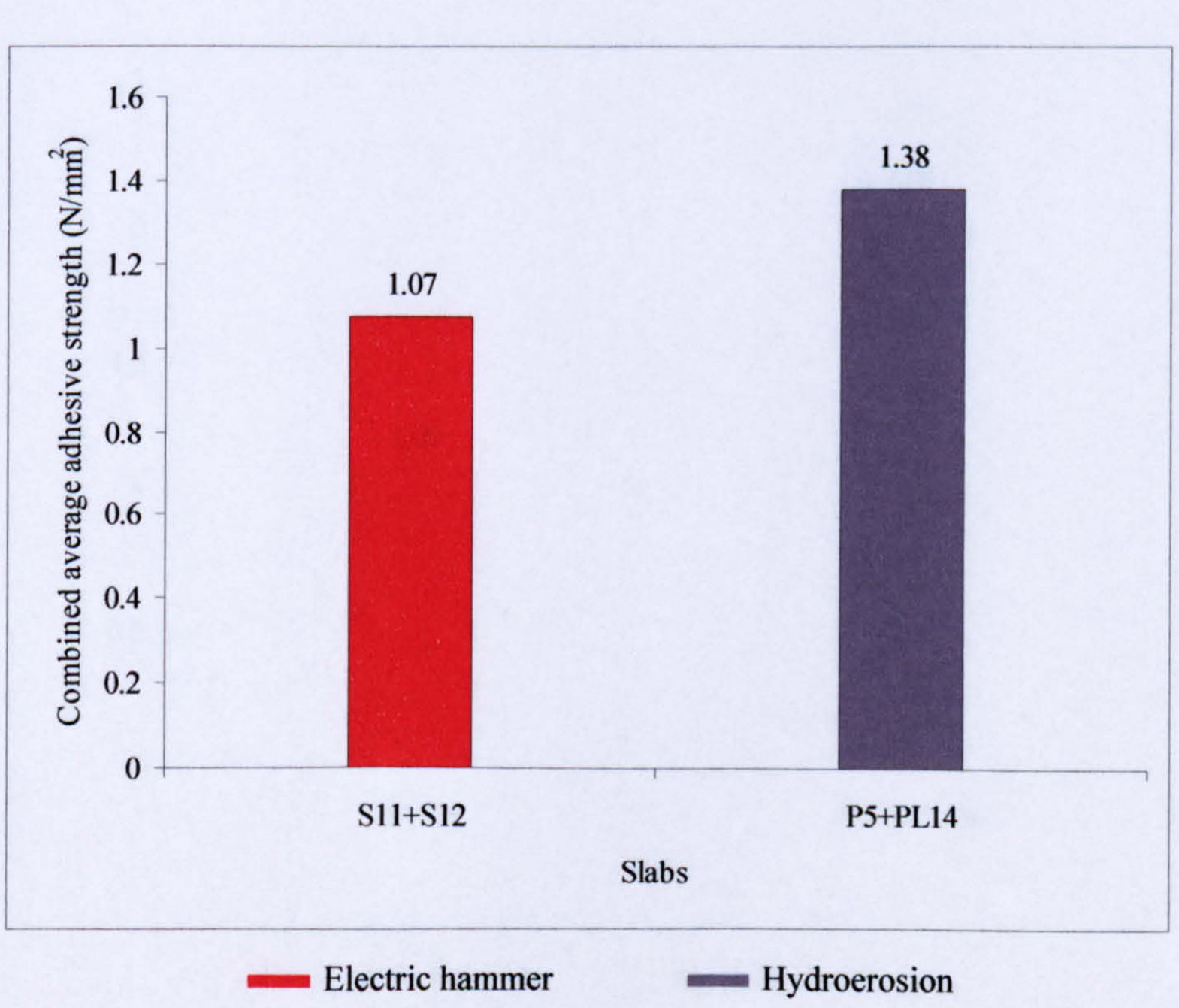

Figure 11.3 Influence of different types of substrate surface on the combined average adhesive strength of slabs S11+S12 and P5+PL14

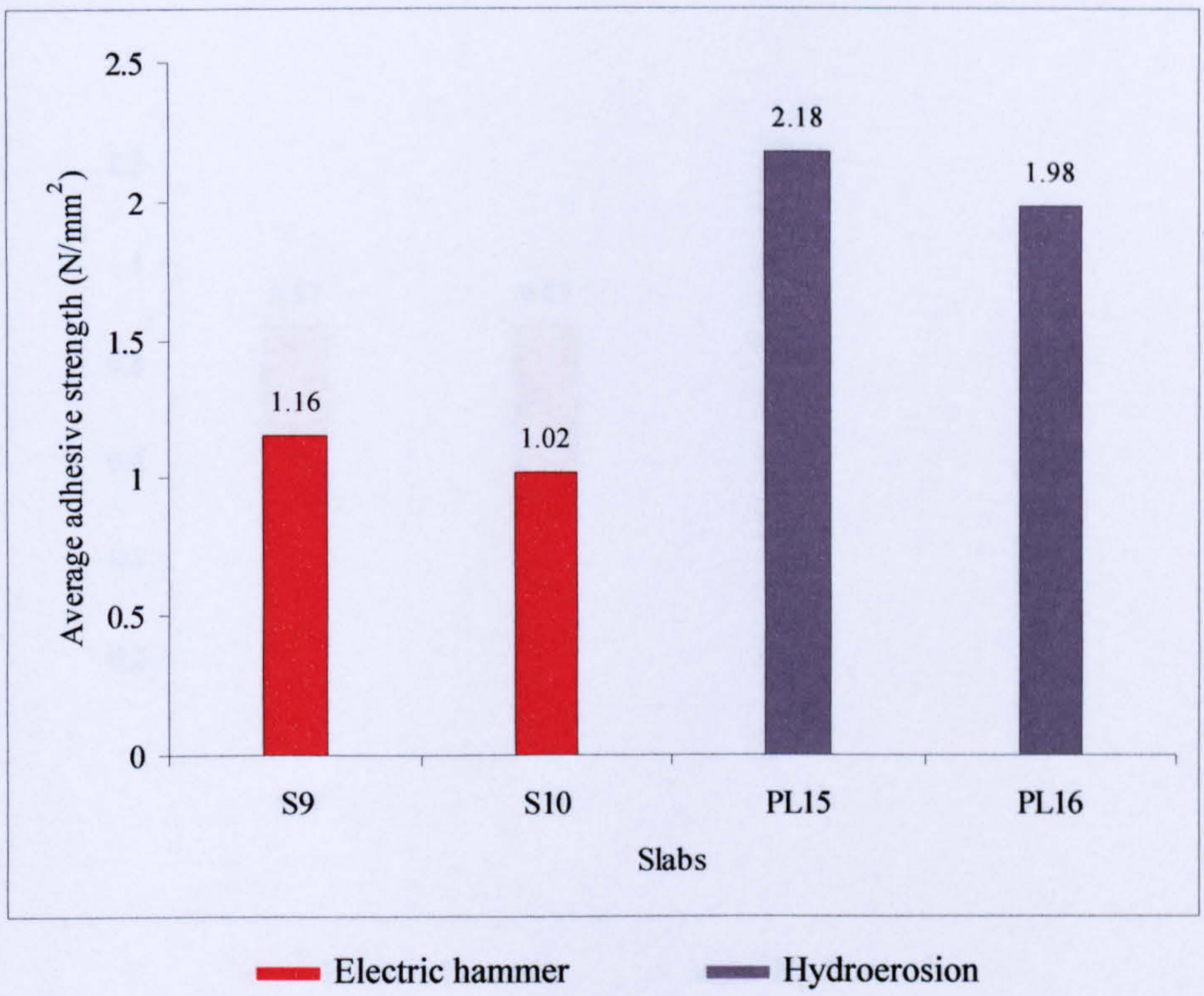

Figure 11.4 Influence of different types of substrate surface on the average adhesive strength of slabs S9, S10, PL15 and PL16

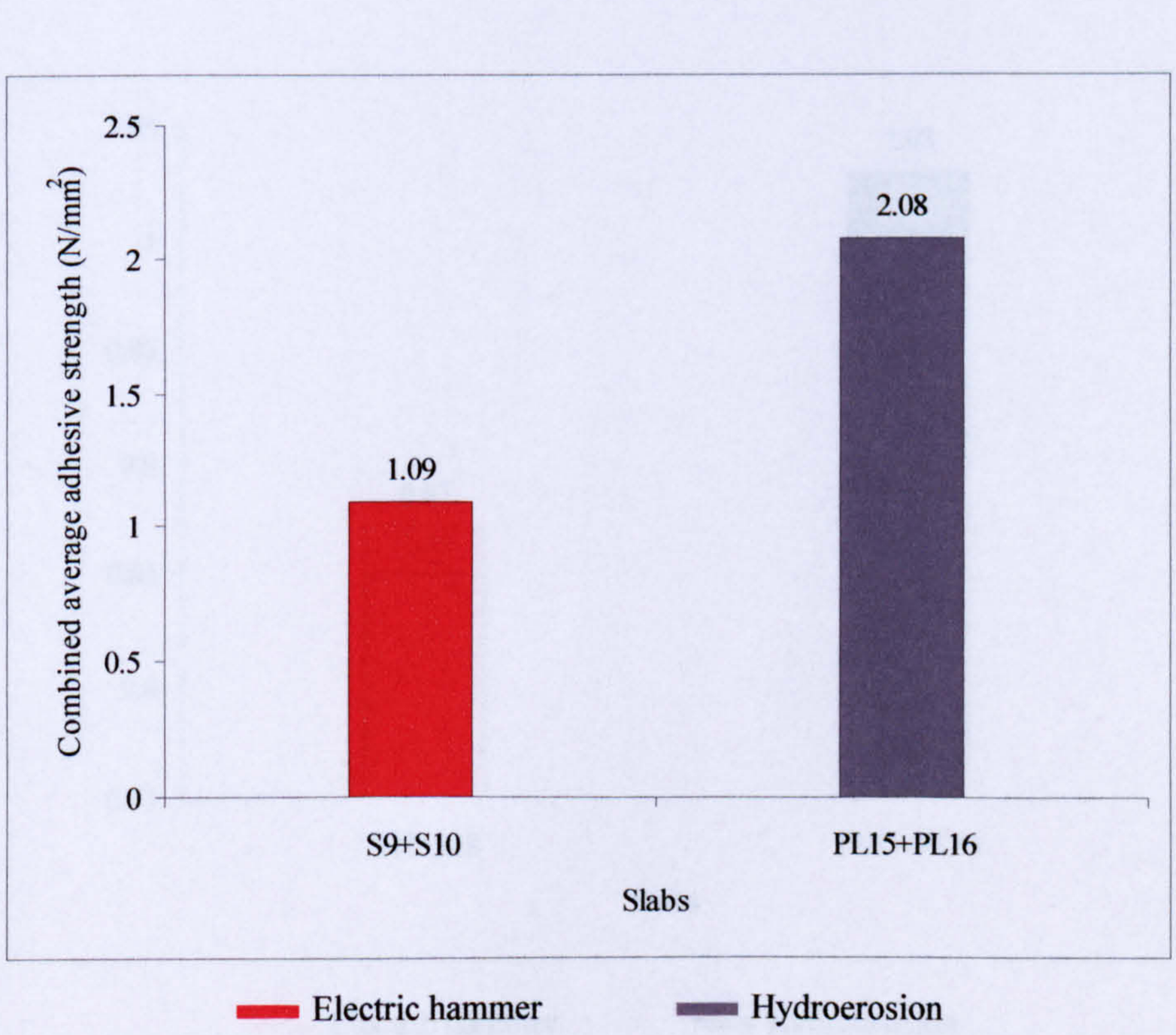

Figure 11.5 Influence of different types of substrate surface on the combined average adhesive strength of slabs S9+S10 and PL15+PL16

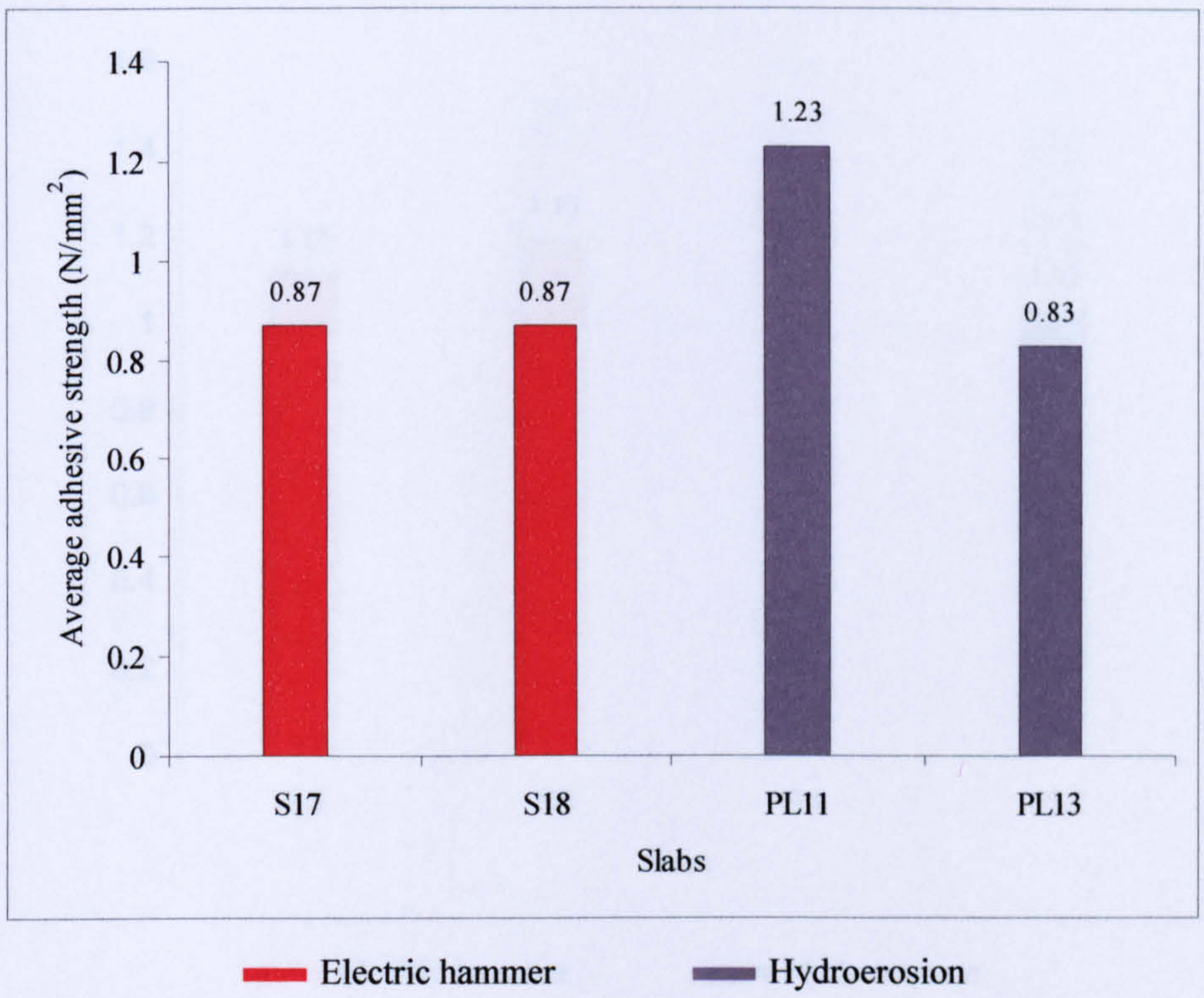

Figure 11.6 Influence of different types of substrate surface on the average adhesive strength of slabs S17, S18, PL11 and PL13

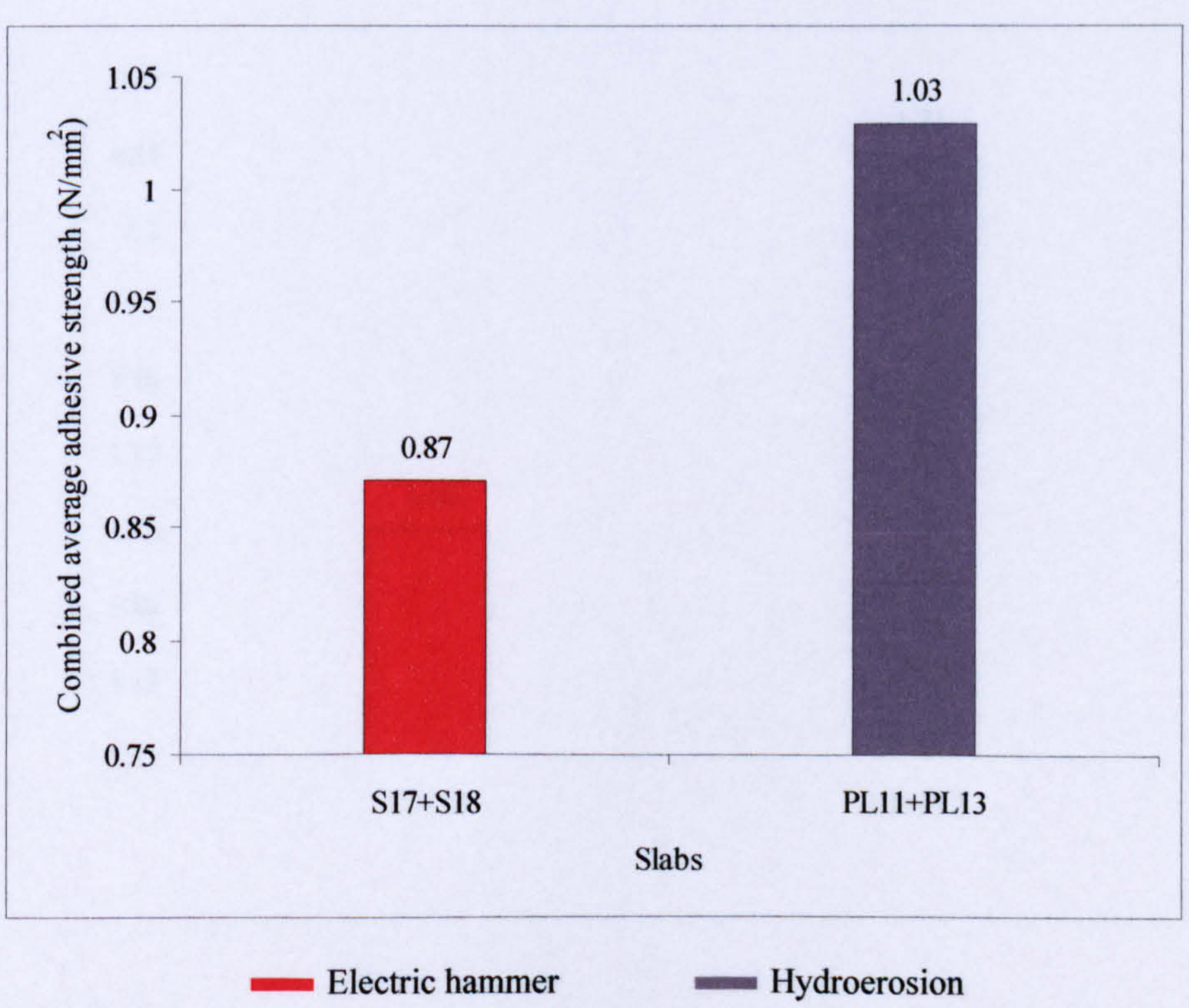

Figure 11.7 Influence of different types of substrate surface on the combined average adhesive strength of slabs S17+S18 and PL11+PL13

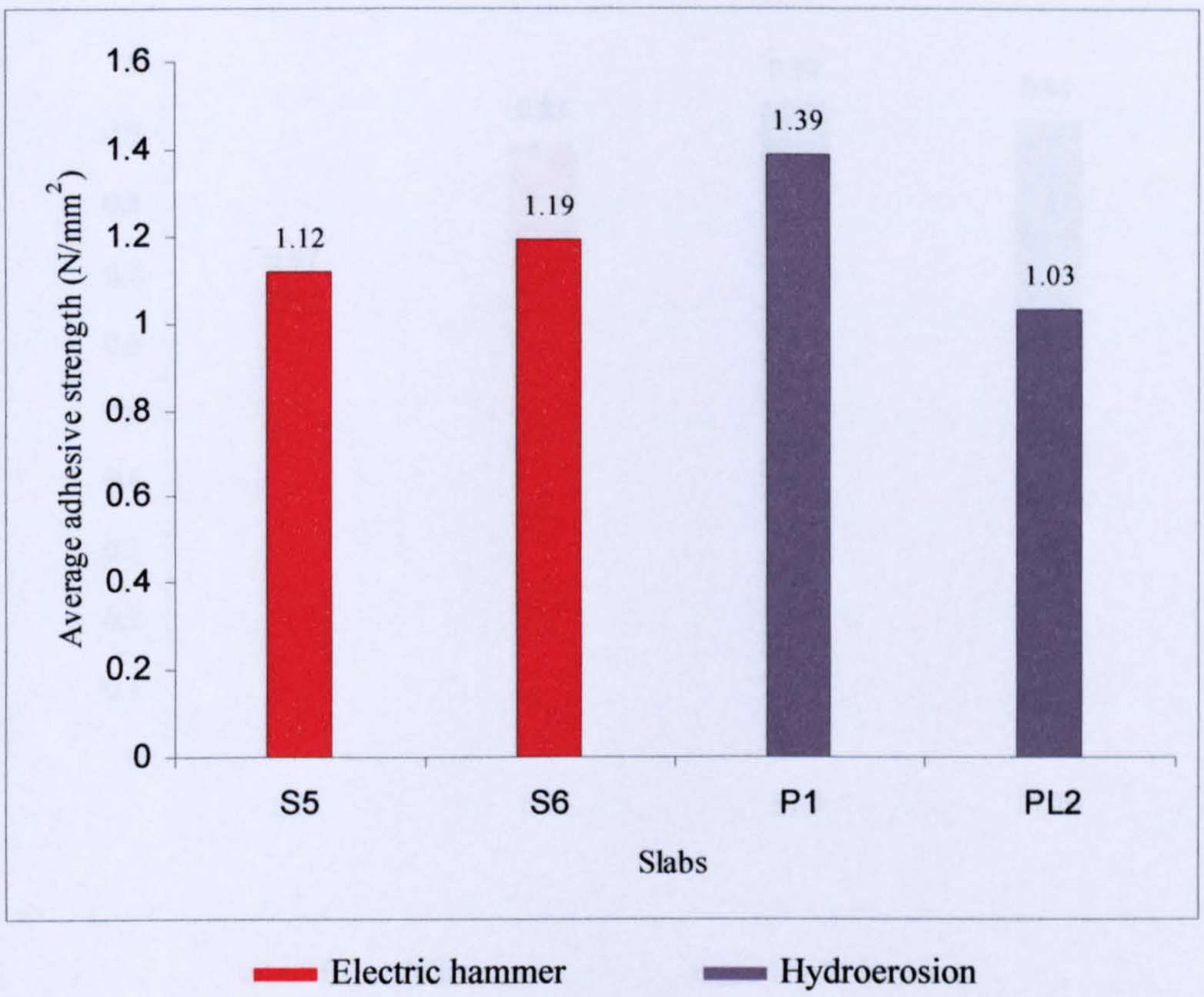

Figure 11.8 Influence of different types of substrate surface on the average adhesive strength of slabs S5, S6, P1 and PL2

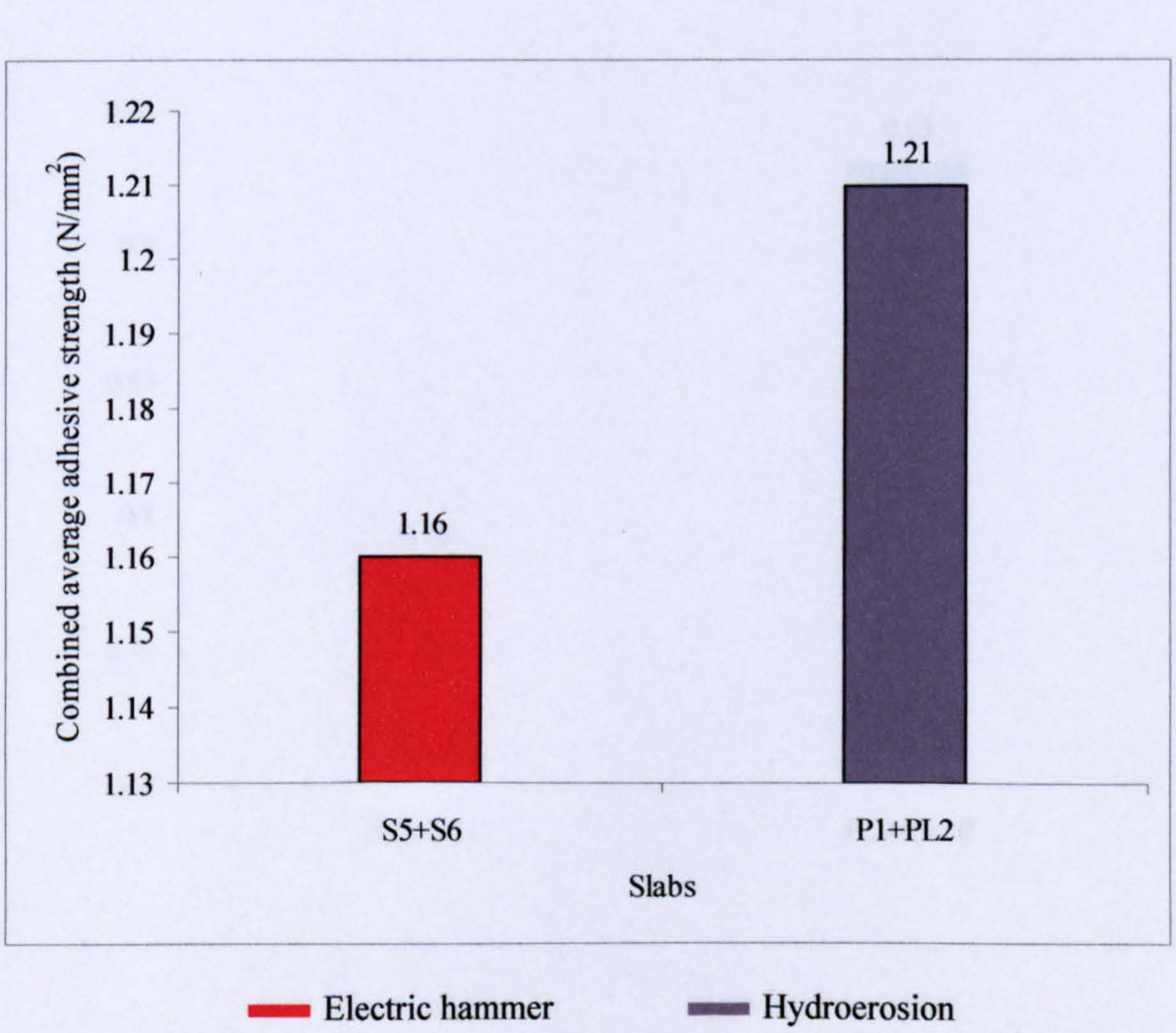

Figure 11.9 Influence of different types of substrate surface on the combined average adhesive strength of slabs S5+S6 and P1+PL2

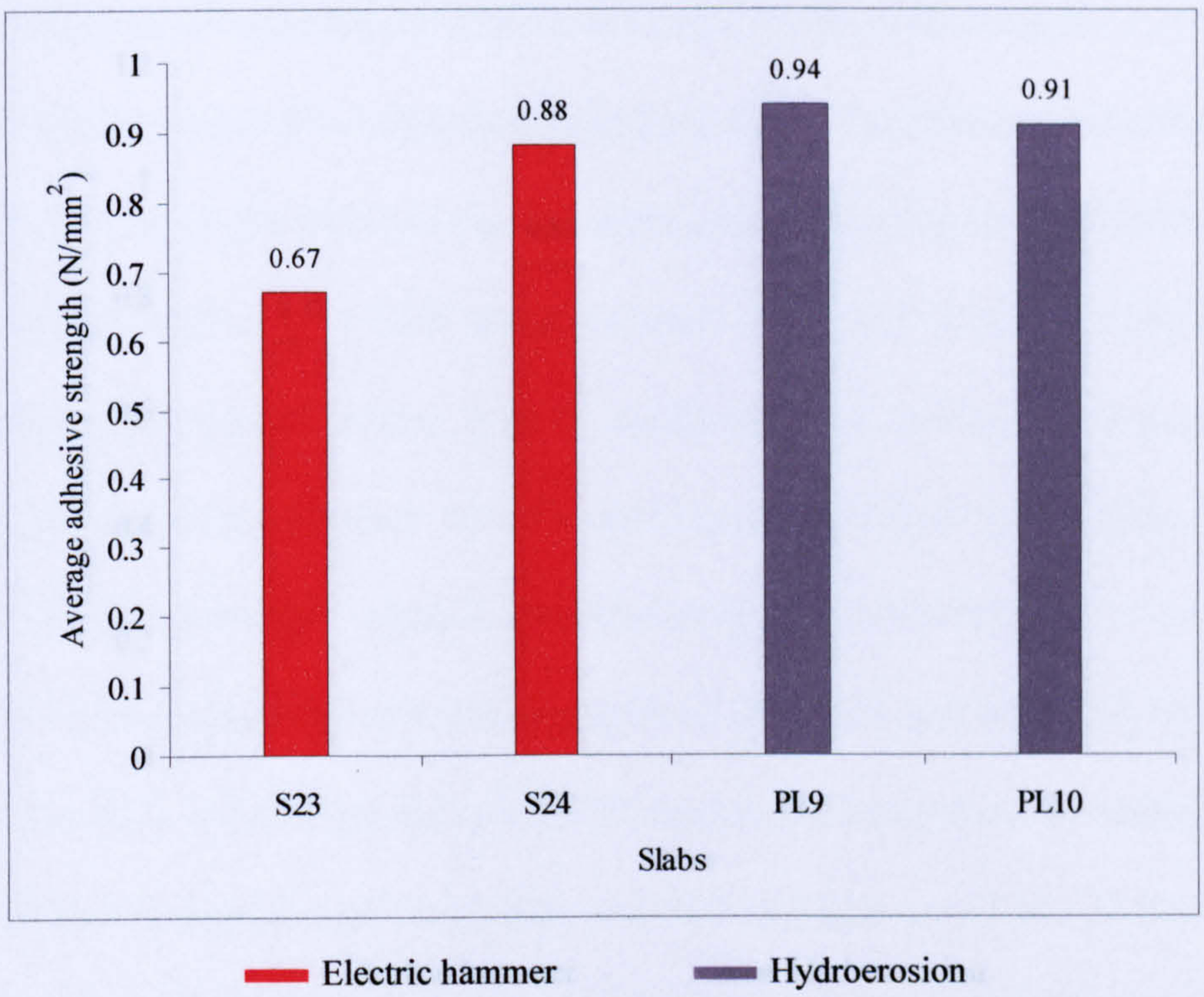

Figure 11.10 Influence of different types of substrate surface on the average adhesive strength of slabs S23, S24, PL9 and PL10

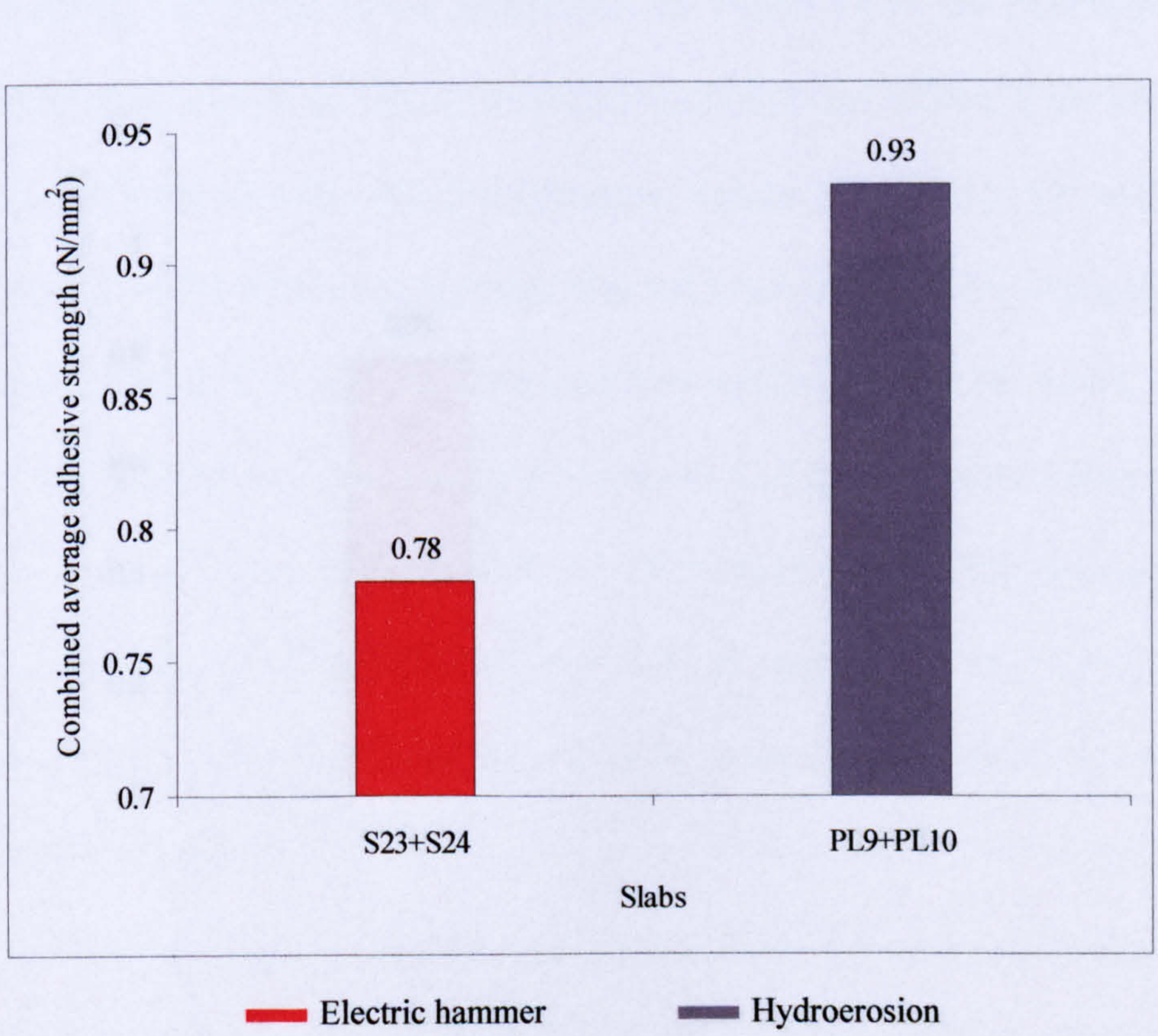

Figure 11.11 Influence of different types of substrate surface on the combined average adhesive strength of slabs S23+S24 and PL9+PL10

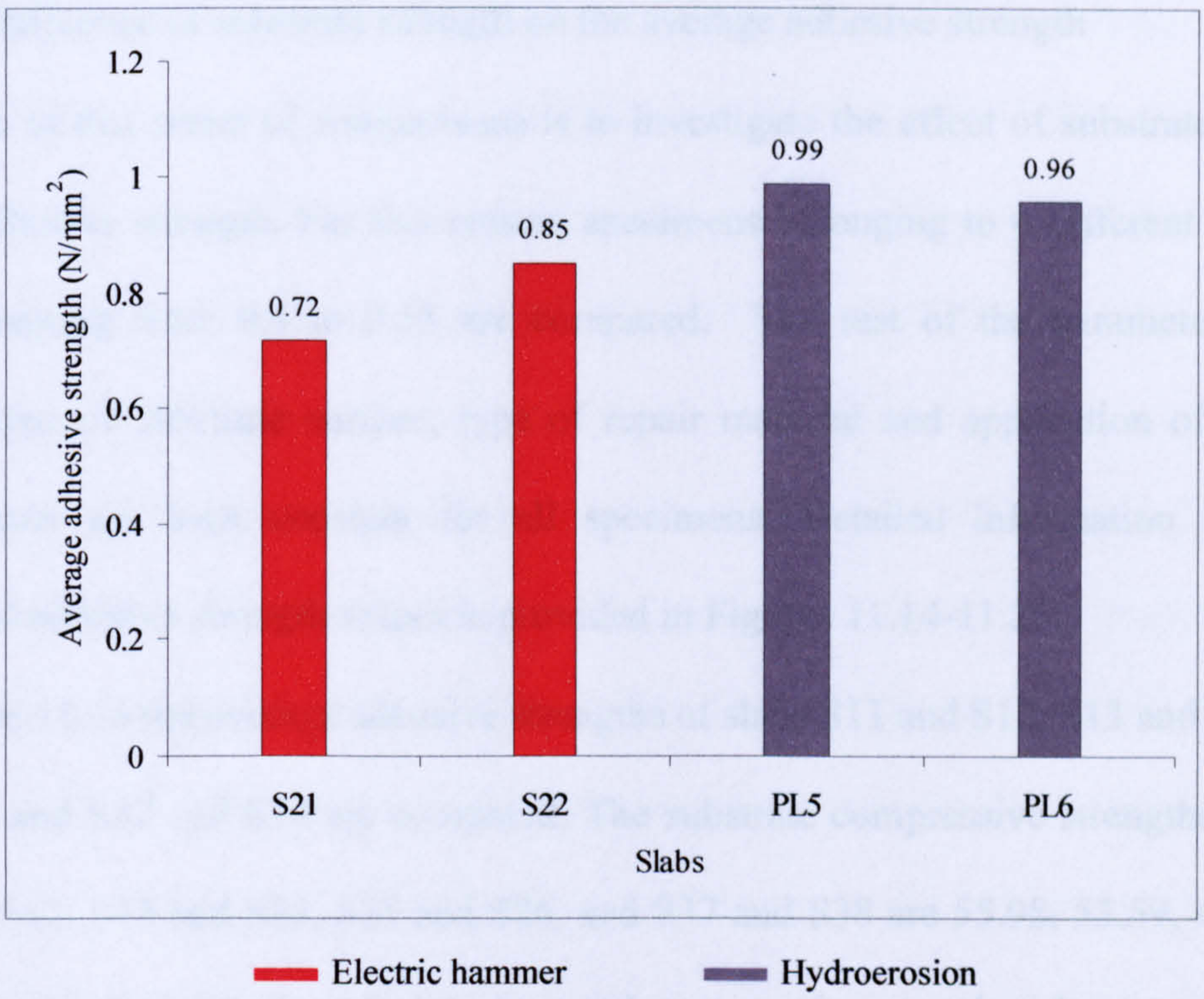

Figure 11.12 Influence of different types of substrate surface on the average adhesive strength of slabs S21, S22, PL5 and PL6

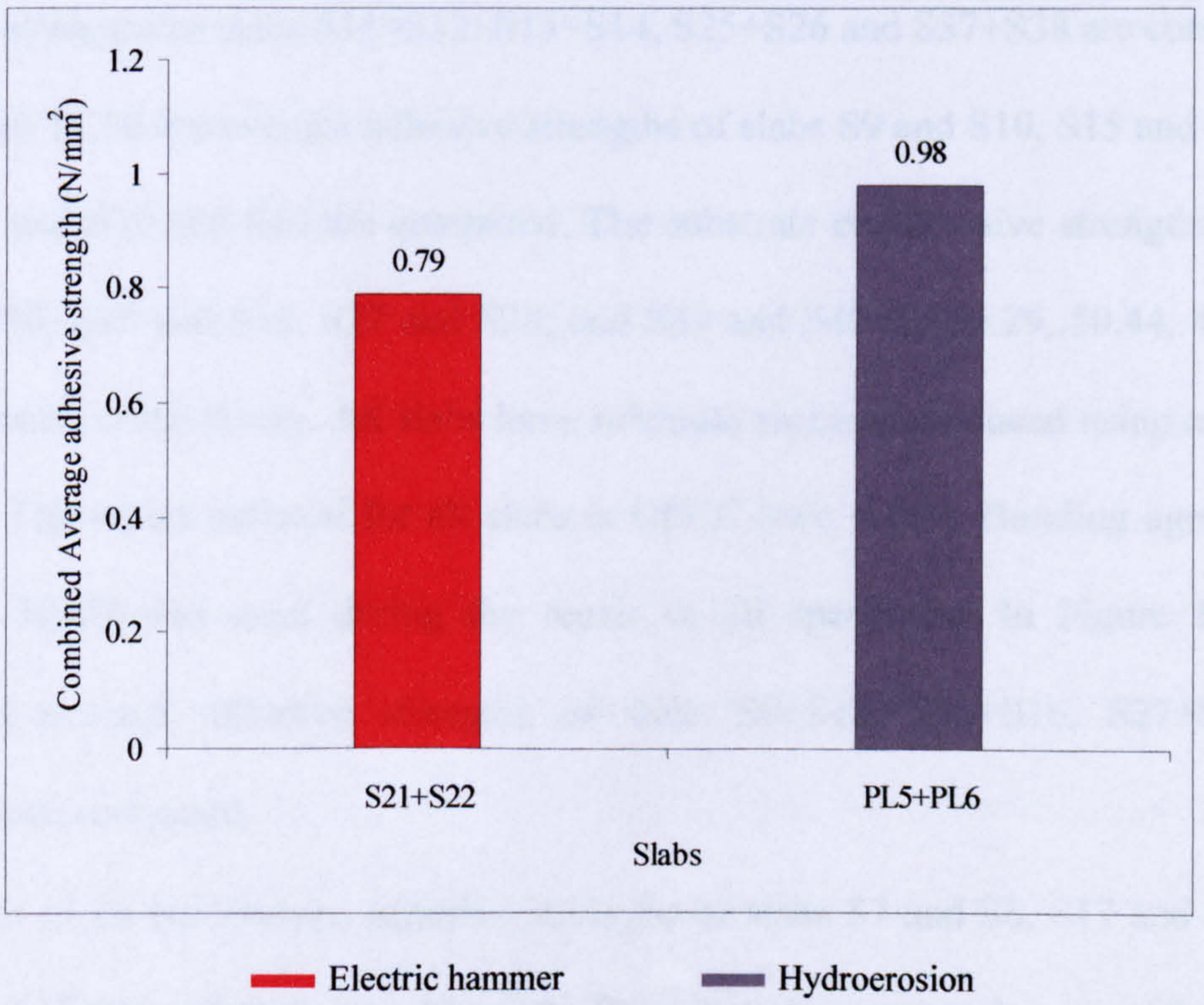

Figure 11.13 Influence of different types of substrate surface on the combined average adhesive strength of slabs S21+S22 and PL5+PL6

11.2.2.2 Influence of substrate strength on the average adhesive strength

The aim of this series of comparisons is to investigate the effect of substrate strength on the adhesive strength. For this reason, specimens belonging to 4 different w/c ratio groups ranging from 0.4 to 0.55 are compared. The rest of the parameters which include type of substrate surface, type of repair material and application of bonding agent/primer are kept constant for all specimens. Detailed information including individual adhesive strength values is provided in Figures 11.14-11.25.

In Figure 11.14 the average adhesive strengths of slabs S11 and S12, S13 and S14, S25 and S26, and S37 and S38 are compared. The substrate compressive strengths of slabs S11 and S12, S13 and S14, S25 and S26, and S37 and S38 are 55.98, 53.59, 42.42 and 40.34 N/mm^2, respectively. All slabs have substrate surfaces produced using an electric hammer. The repair material for all slabs is OPCC (w/c = 0.4). No bonding agent/primer was used during the repair of the specimens. In Figure 11.15 the combined average adhesive strengths of slabs S11+S12, S13+S14, S25+S26 and S37+S38 are compared.

In Figure 11.16 the average adhesive strengths of slabs S9 and S10, S15 and S16, S27 and S28, and S39 and S40 are compared. The substrate compressive strengths of slabs S9 and S10, S15 and S16, S27 and S28, and S39 and S40 are 56.29, 50.44, 43.72 and 40.27 N/mm^2, respectively. All slabs have substrate surfaces produced using an electric hammer. The repair material for all slabs is OPCC (w/c = 0.4). Bonding agent/primer Zentrifix KMH was used during the repair of all specimens. In Figure 11.17 the combined average adhesive strengths of slabs S9+S10, S15+S16, S27+S28, and S39+S40 are compared.

In Figure 11.18 the average adhesive strengths of slabs S7 and S8, S17 and S18, S29 and S30, and S43 and S44 are compared. The substrate compressive strengths of slabs S7 and S8, S117 and S18, S29 and S30, and S43 and S44 are 58.13, 47.41, 46.23 and

37.14 N/mm^2, respectively. All slabs have substrate surfaces produced using an electric hammer. The repair material for all slabs is OPCM (w/c = 0.4). No bonding agent/primer was used during the repair of the specimens. In Figure 11.19 the combined average adhesive strengths of slabs S7+S8, S17+S18, S29+S30 and S43+S44 are compared.

In Figure 11.20 the average adhesive strengths of slabs S5 and S6, S19 and S20, S31 and S32, and S41 and S42 are compared. The substrate compressive strengths of slabs S5 and S6, S19 and S20, S31 and S32, and S41 and S42 are 57.04, 50.19, 42.94 and 39.49 N/mm^2, respectively. All slabs have substrate surfaces produced using an electric hammer. The repair material for all slabs is OPCM (w/c = 0.4). Bonding agent/primer Zentrifix KMH was used during the repair of all specimens. In Figure 11.21 the combined average adhesive strengths of slabs S5+S6, S19+S20, S31+S32 and S41+S42 are compared.

In Figure 11.22 the average adhesive strengths of slabs S1 and S2, S23 and S24, S35 and S36, and S47 and S48 are compared. The substrate compressive strengths of slabs S1 and S2, S23 and S24, S35 and S36, and S47 and S48 are 57.77, 52.56, 41.10 and 39.14 N/mm^2, respectively. All slabs have substrate surfaces produced using an electric hammer. The repair material for all slabs is Zentrifix GM 25. No bonding agent/primer was used during the repair of all specimens. In Figure 11.23 the combined average adhesive strengths of slabs S1+S2, S23+S24, S35+S36 and S47+S48 are compared.

In Figure 11.24 the average adhesive strengths of slabs S3 and S4, S21 and S22, S33 and S34, and S45 and S46 are compared. The substrate compressive strengths of slabs S3 and S4, S21 and S22, S33 and S34, and S45 and S46 are 53.94, 53.54, 43.50 and 41.15 N/mm^2, respectively. All slabs have substrate surfaces produced using an electric hammer. The repair material for all slabs is Zentrifix GM 25. Bonding agent/primer

37.14 N/mm^2, respectively. All slabs have substrate surfaces produced using an electric hammer. The repair material for all slabs is OPCM (w/c = 0.4). No bonding agent/primer was used during the repair of the specimens. In Figure 11.19 the combined average adhesive strengths of slabs S7+S8, S17+S18, S29+S30 and S43+S44 are compared.

In Figure 11.20 the average adhesive strengths of slabs S5 and S6, S19 and S20, S31 and S32, and S41 and S42 are compared. The substrate compressive strengths of slabs S5 and S6, S19 and S20, S31 and S32, and S41 and S42 are 57.04, 50.19, 42.94 and 39.49 N/mm^2, respectively. All slabs have substrate surfaces produced using an electric hammer. The repair material for all slabs is OPCM (w/c = 0.4). Bonding agent/primer Zentrifix KMH was used during the repair of all specimens. In Figure 11.21 the combined average adhesive strengths of slabs S5+S6, S19+S20, S31+S32 and S41+S42 are compared.

In Figure 11.22 the average adhesive strengths of slabs S1 and S2, S23 and S24, S35 and S36, and S47 and S48 are compared. The substrate compressive strengths of slabs S1 and S2, S23 and S24, S35 and S36, and S47 and S48 are 57.77, 52.56, 41.10 and 39.14 N/mm^2, respectively. All slabs have substrate surfaces produced using an electric hammer. The repair material for all slabs is Zentrifix GM 25. No bonding agent/primer was used during the repair of all specimens. In Figure 11.23 the combined average adhesive strengths of slabs S1+S2, S23+S24, S35+S36 and S47+S48 are compared.

In Figure 11.24 the average adhesive strengths of slabs S3 and S4, S21 and S22, S33 and S34, and S45 and S46 are compared. The substrate compressive strengths of slabs S3 and S4, S21 and S22, S33 and S34, and S45 and S46 are 53.94, 53.54, 43.50 and 41.15 N/mm^2, respectively. All slabs have substrate surfaces produced using an electric hammer. The repair material for all slabs is Zentrifix GM 25. Bonding agent/primer

Zentrifix GM 25 was used during the repair of all specimens. In Figure 11.25 the combined average adhesive strengths of slabs S3+S4, S21+S22, S33+S34 and S45+S46 are compared.

Although, results obtained from the above comparisons are not conclusive some general comments can be made regarding the influence of substrate compressive strength on the average adhesive strength of repaired slabs. In all 6 comparison cases repaired slabs having substrates with w/c ratio of 0.4 and hence compressive strength values between 53.94—58.13 N/mm^2 produced the highest average adhesive strength values. In 3 out of 6 comparison cases repaired slabs having substrates with w/c ratio of 0.55 and hence compressive strength values between 37.14—41.15 N/mm^2 produced the lowest average adhesive strength values. In general, average adhesive strength seems to be influenced by the substrate compressive strength. However, when the w/c ratio is linearly increased and hence the compressive strength of the substrate is linearly decreased the average adhesive strength does not follow a linear decrease pattern.

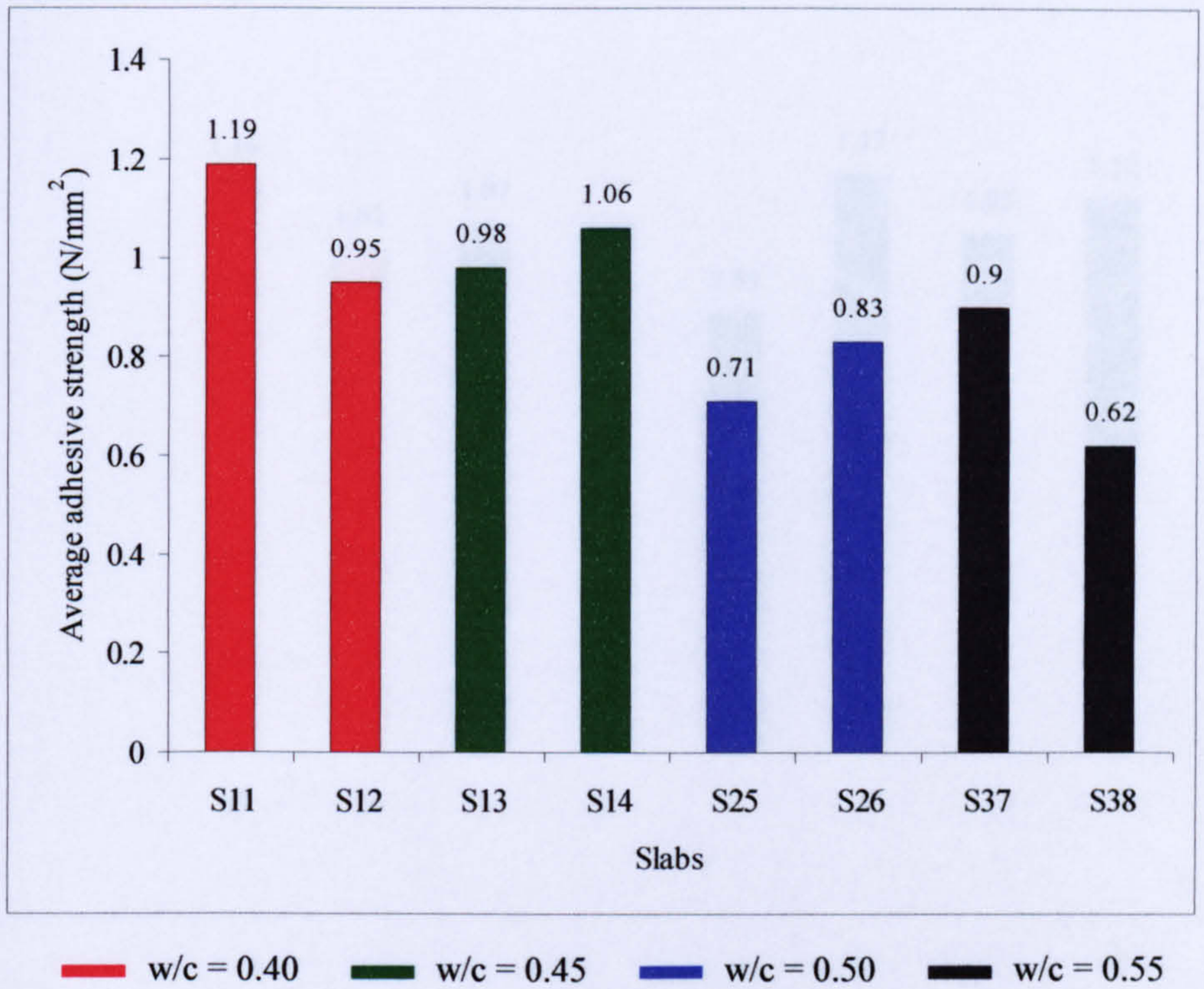

Figure 11.14 Influence of substrate strength on the average adhesive strength of slabs S11and S12, S13 and S14, S25 and S26, and S37 and S38

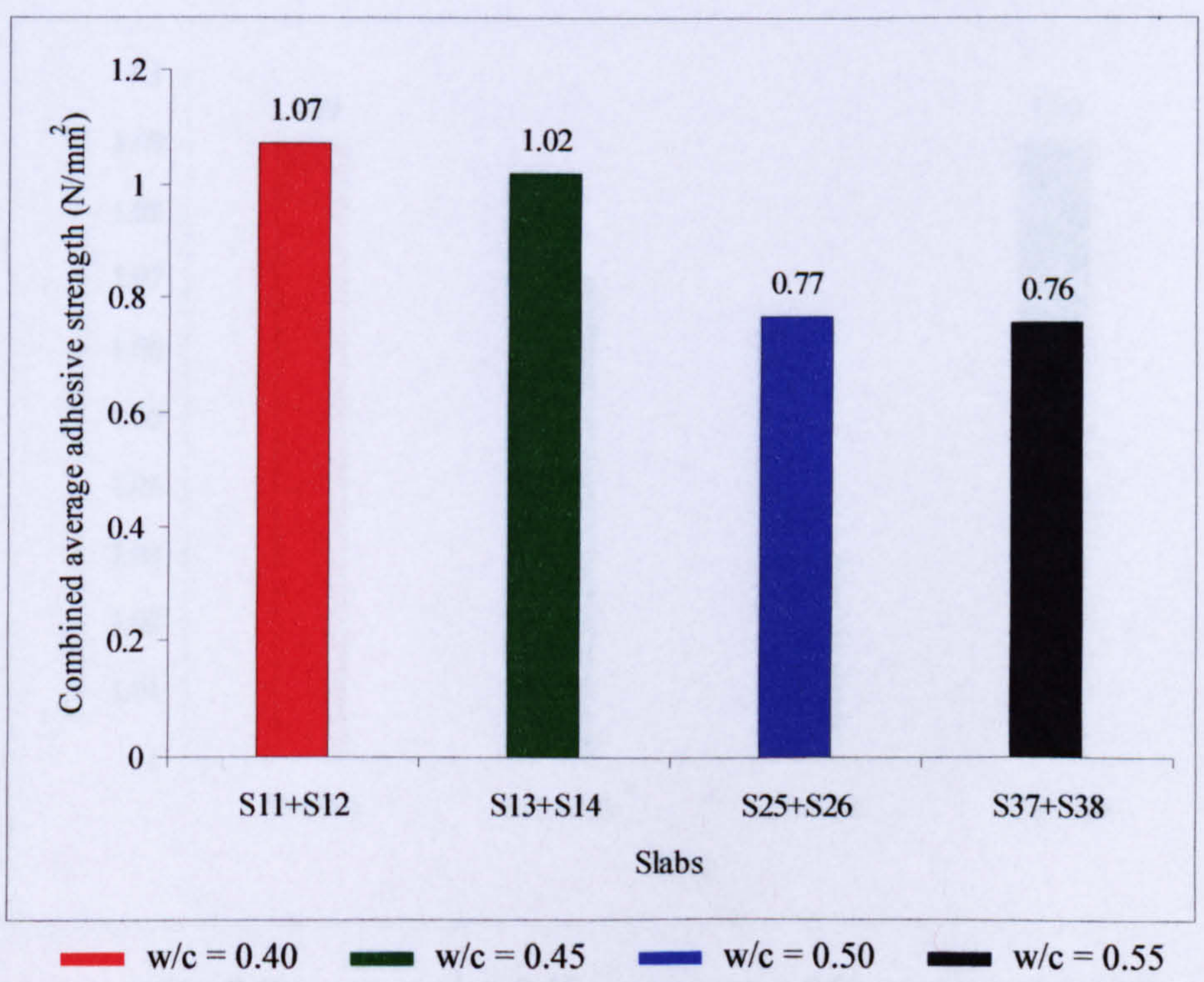

Figure 11.15 Influence of substrate strength on the combined average adhesive strength of slabs S11+S12, S13+S14, S25+S26 and S37+S38

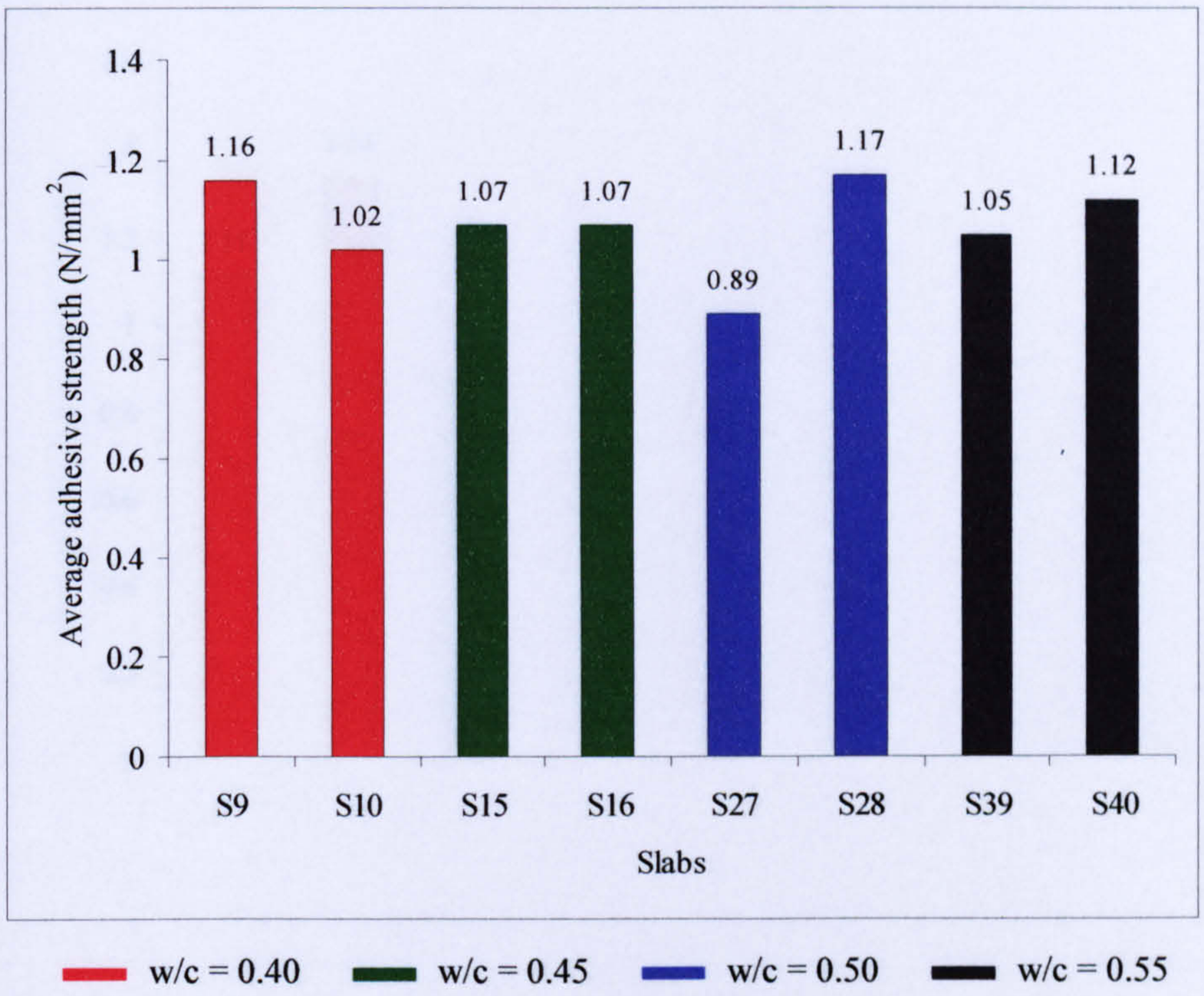

Figure 11.16 Influence of substrate strength on the average adhesive strength of slabs S9 and S10, S15 and S16, S27 and S28, and S39 and S40

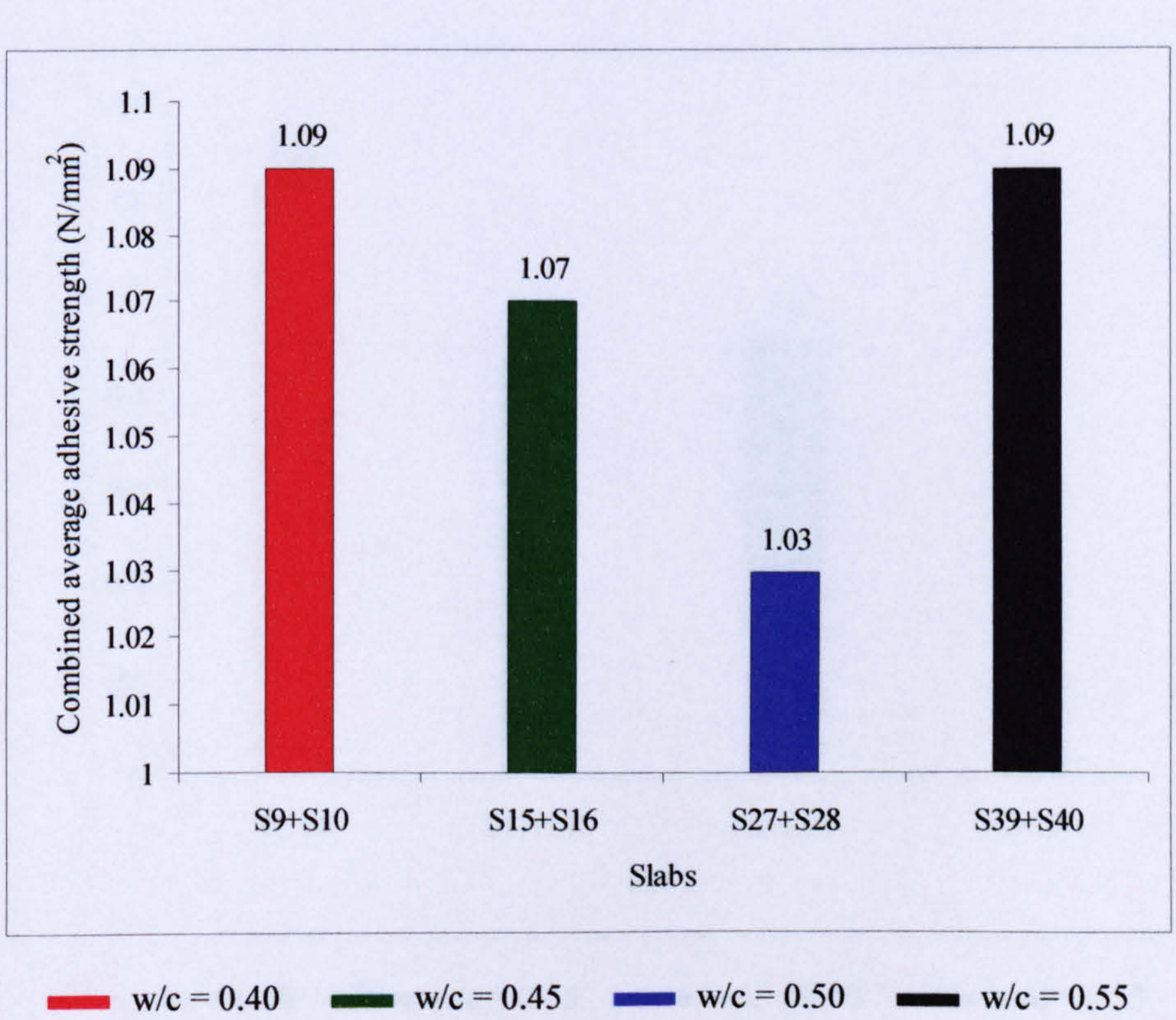

Figure 11.17 Influence of substrate strength on the combined average adhesive strength of slabs S9+S10, S15+S16, S27+S28, and S39+S40

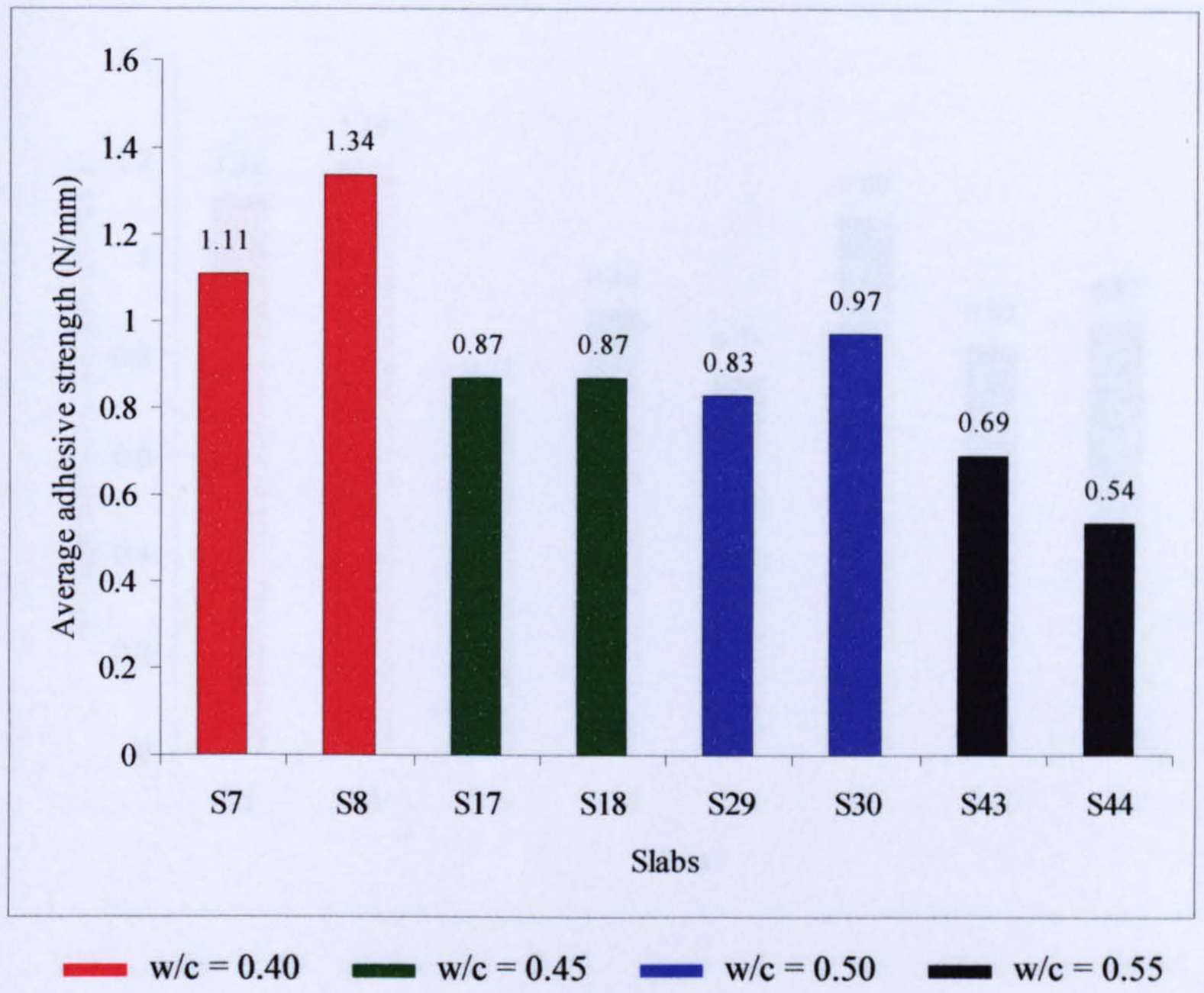

Figure 11.18 Influence of substrate strength on the average adhesive strength of slabs S7 and S8, S17 and S18, S29 and S30, and S43 and S44

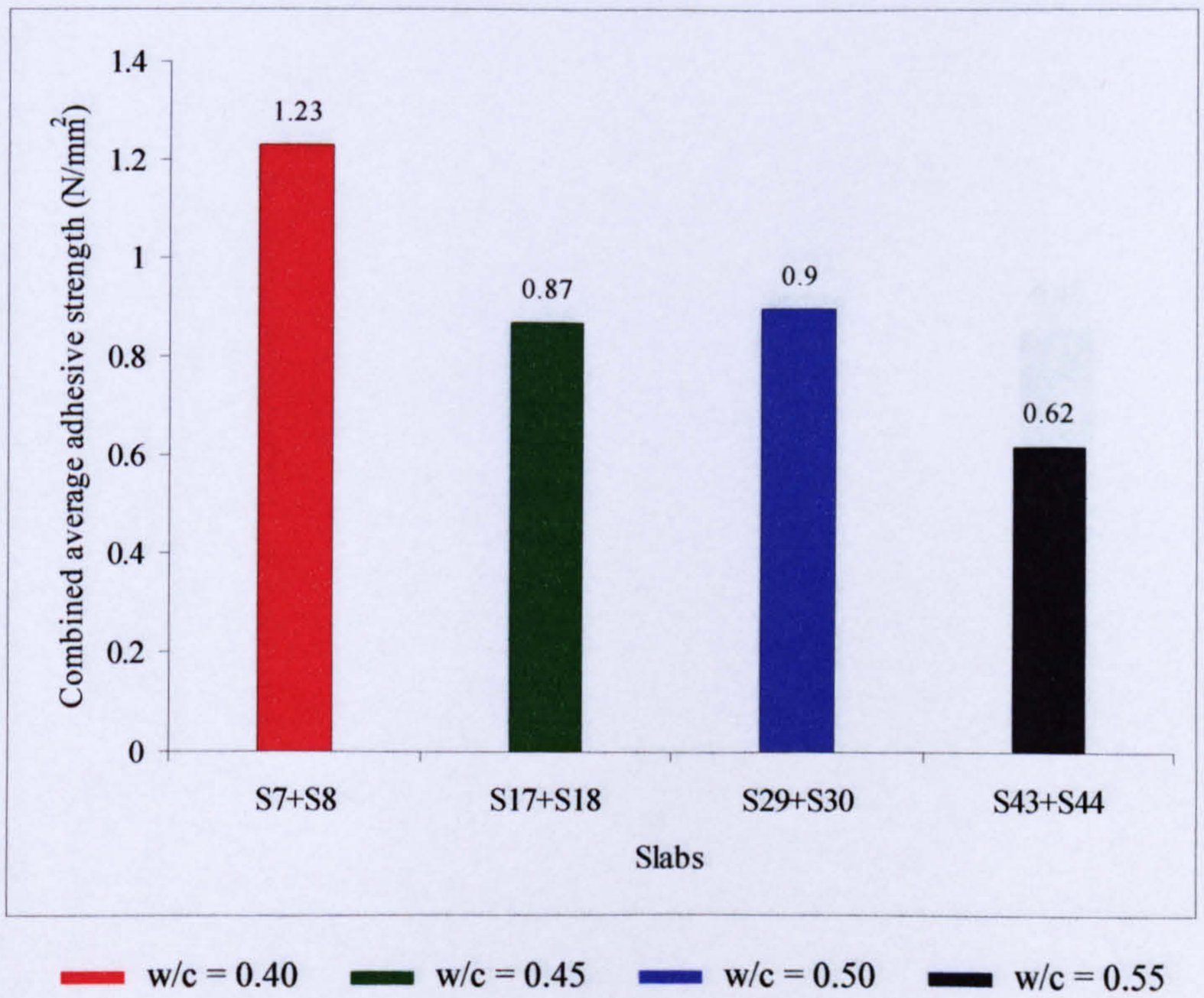

Figure 11.19 Influence of substrate strength on the combined average adhesive strength of slabs S7+S8, S17+S18, S29+S30 and S43+S44

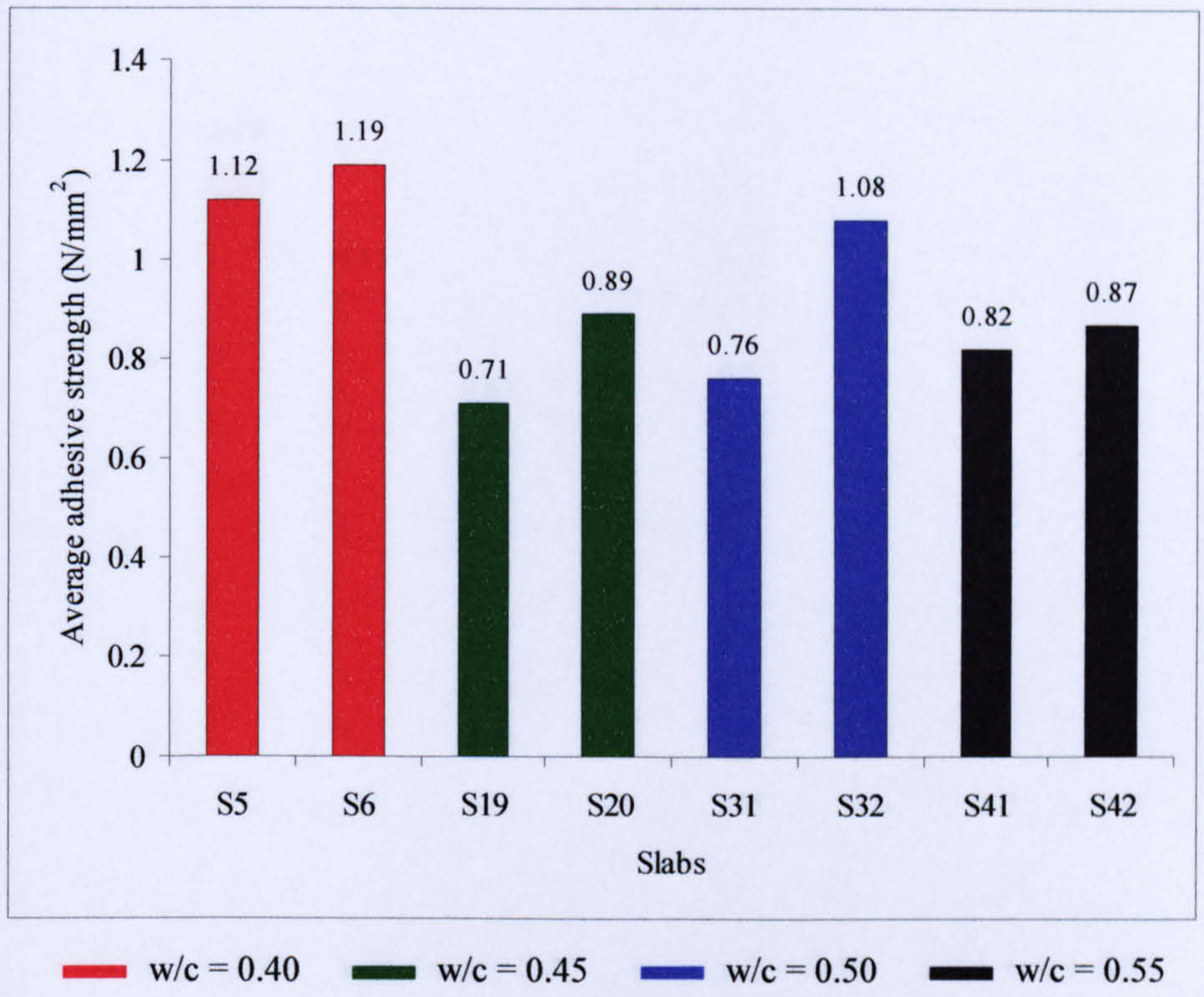

Figure 11.20 Influence of substrate strength on the average adhesive strength of slabs S5 and S6, S19 and S20, S31 and S32, and S41 and S42

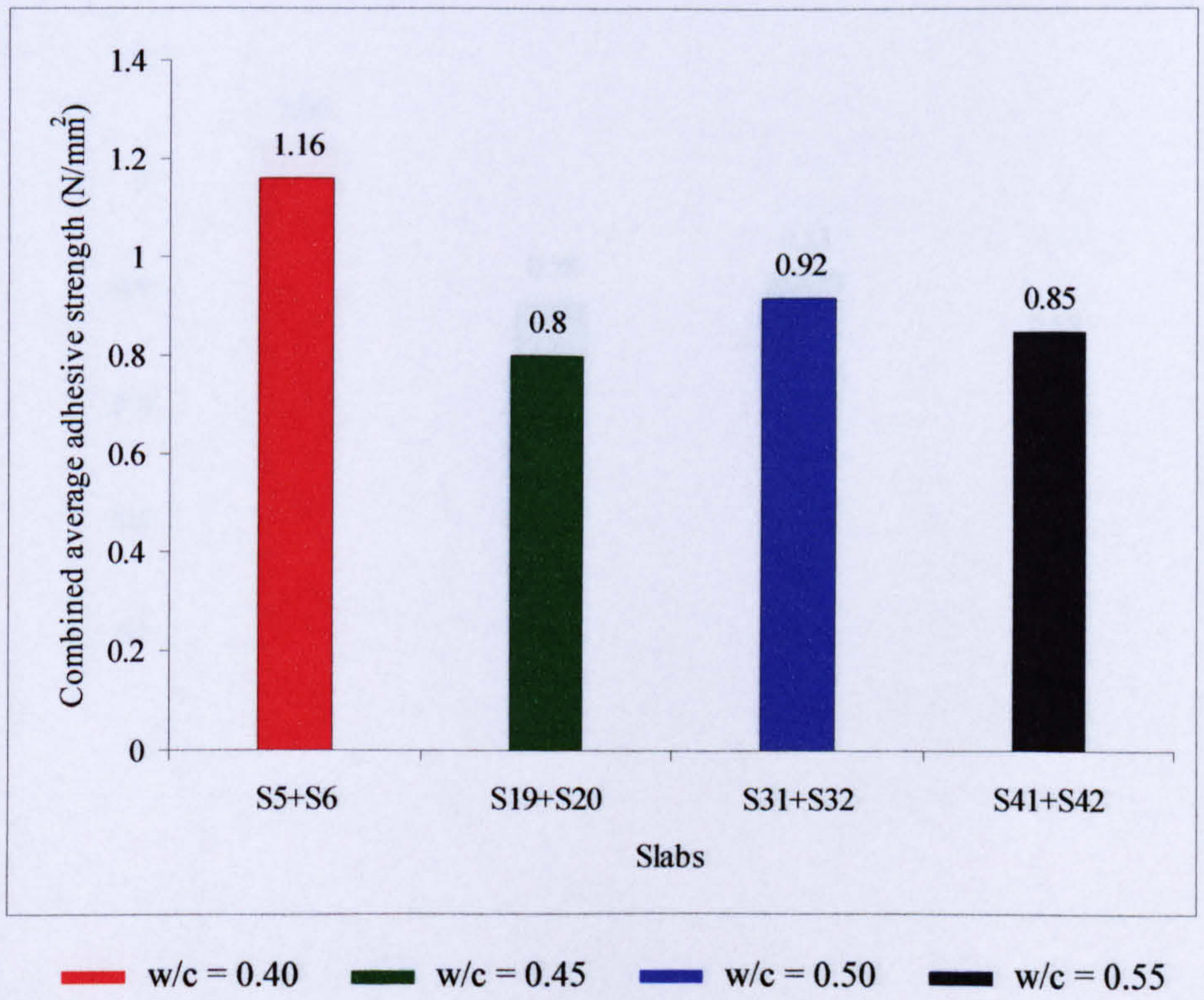

Figure 11.21 Influence of substrate strength on the combined average adhesive strength of slabs S5+S6, S19+S20, S31+S32 and S41+S42

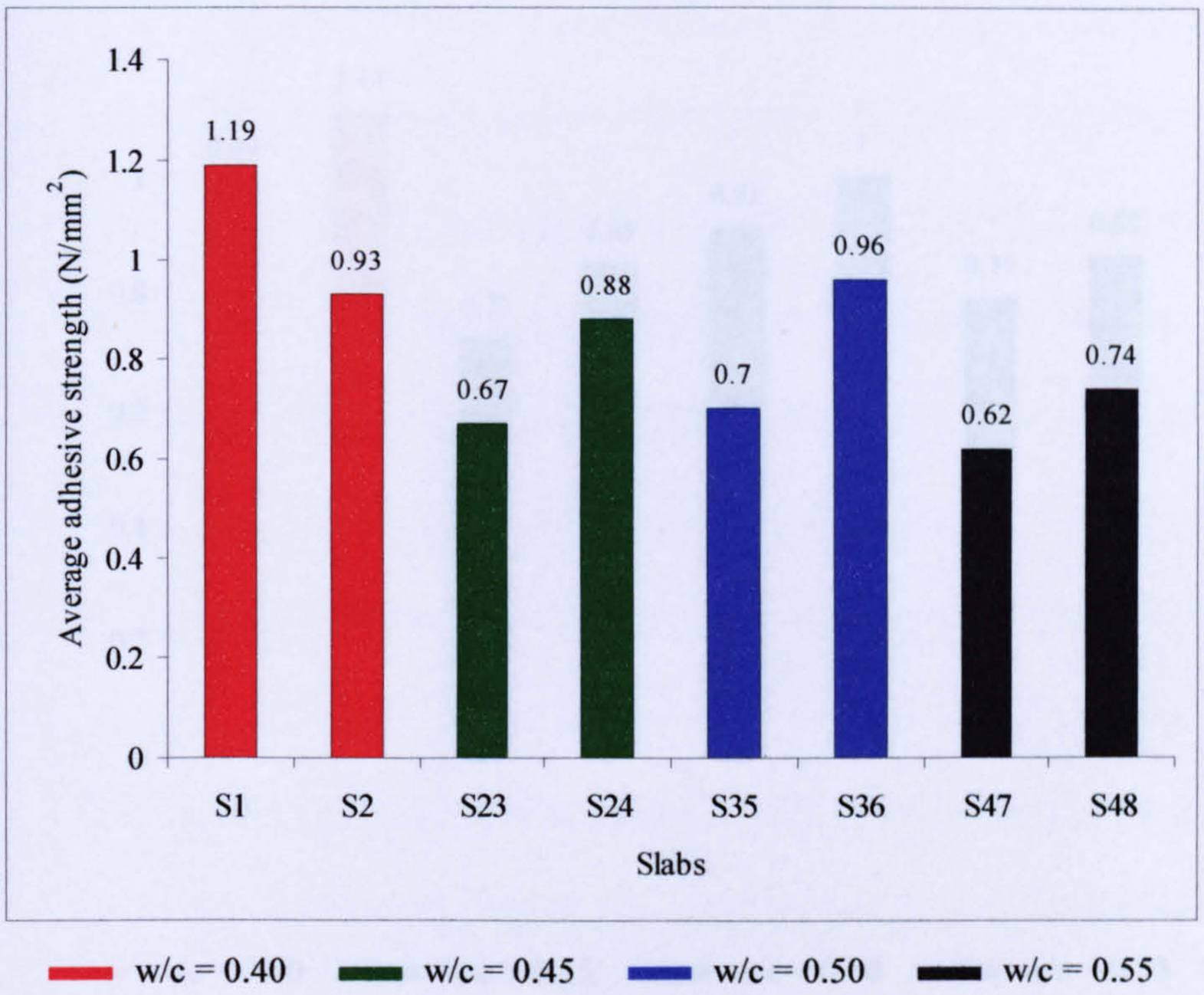

Figure 11.22 Influence of substrate strength on the average adhesive strength of slabs S1 and S2, S23 and S24, S35 and S36, and S47 and S48

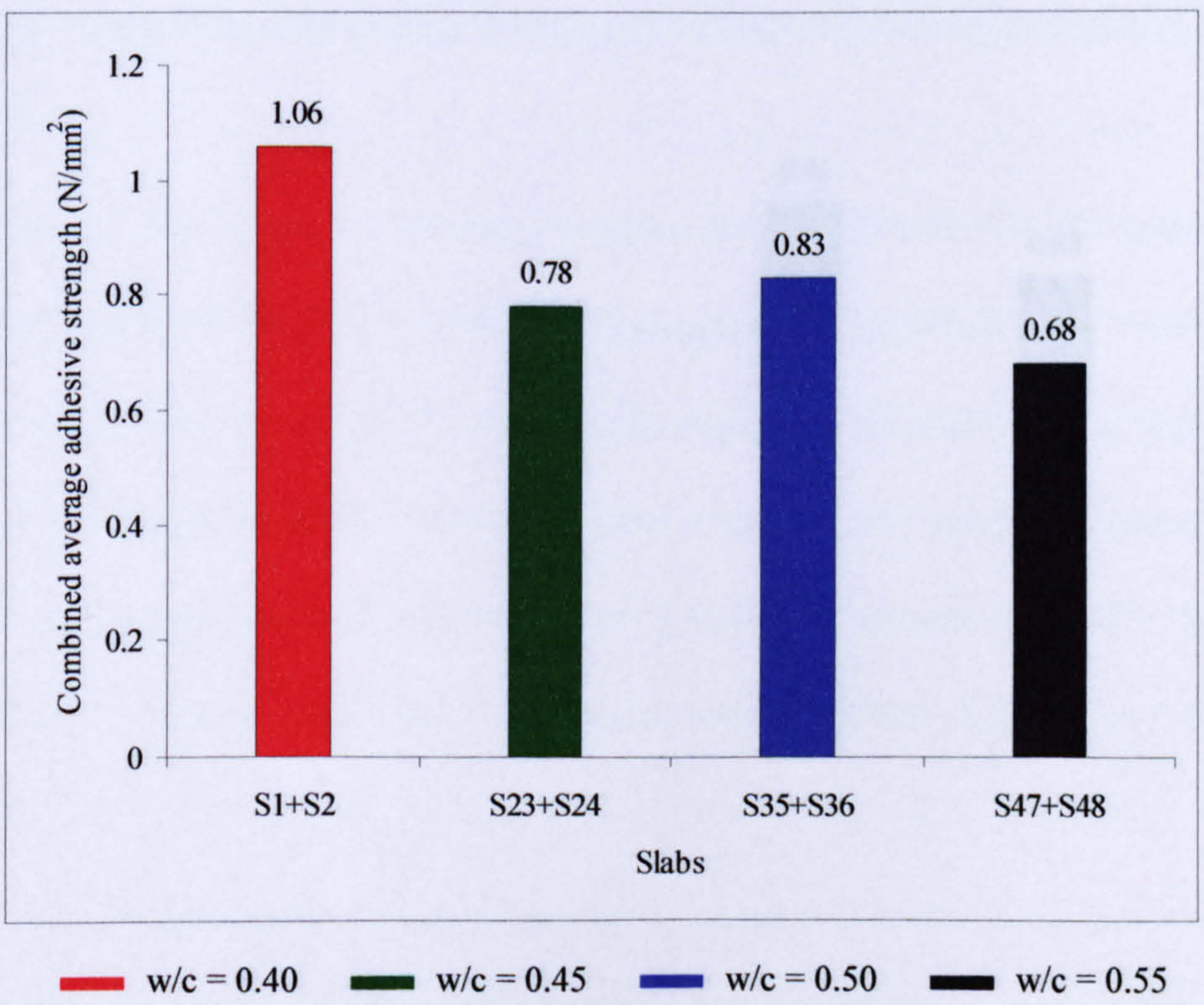

Figure 11.23 Influence of substrate strength on the combined average adhesive strength of slabs S1+S2, S23+S24, S35+S36 and S47+S48

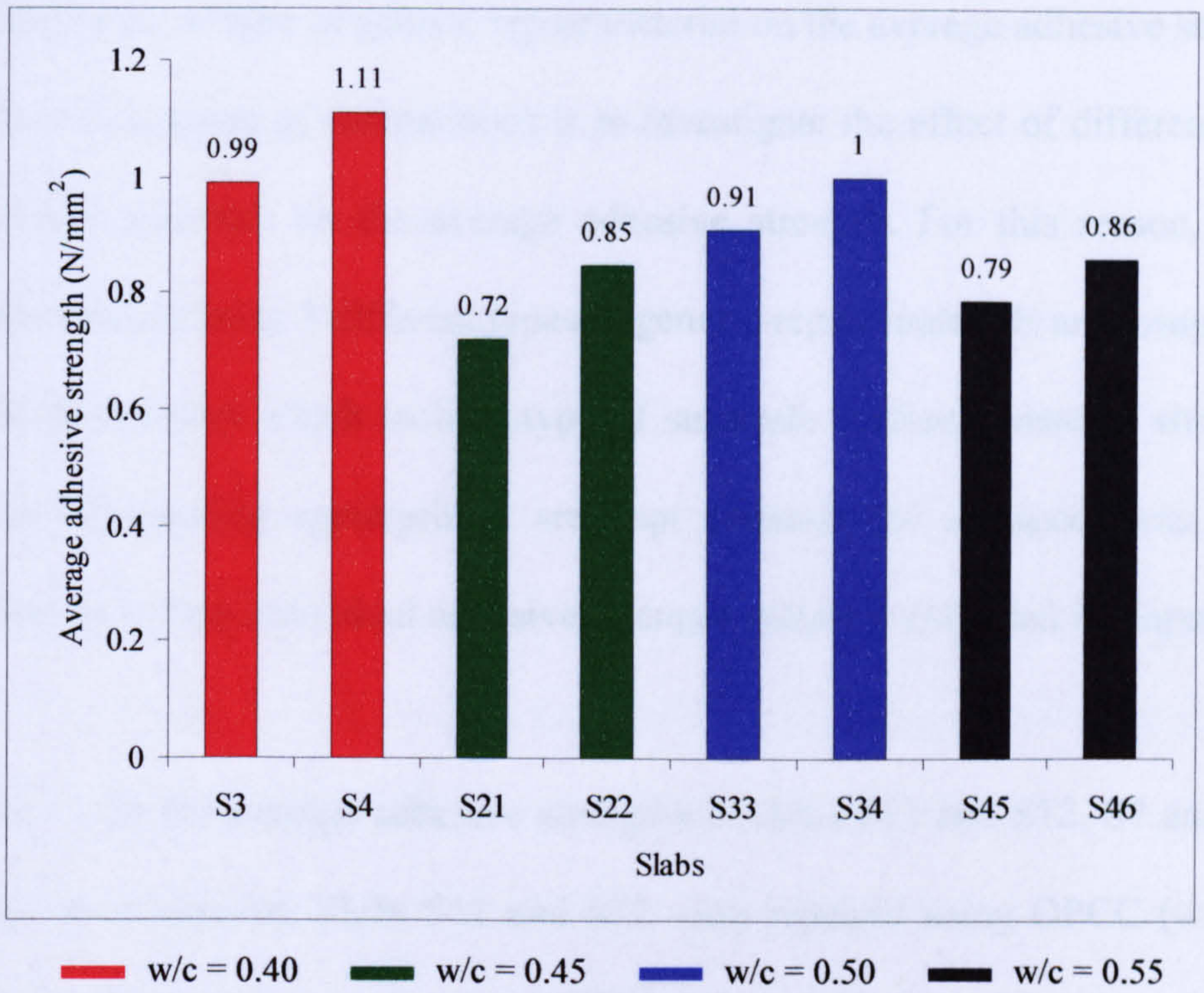

Figure 11.24 Influence of substrate strength on the average adhesive strength of slabs S3 and S4, S21 and S22, S33 and S34, and S45 and S46

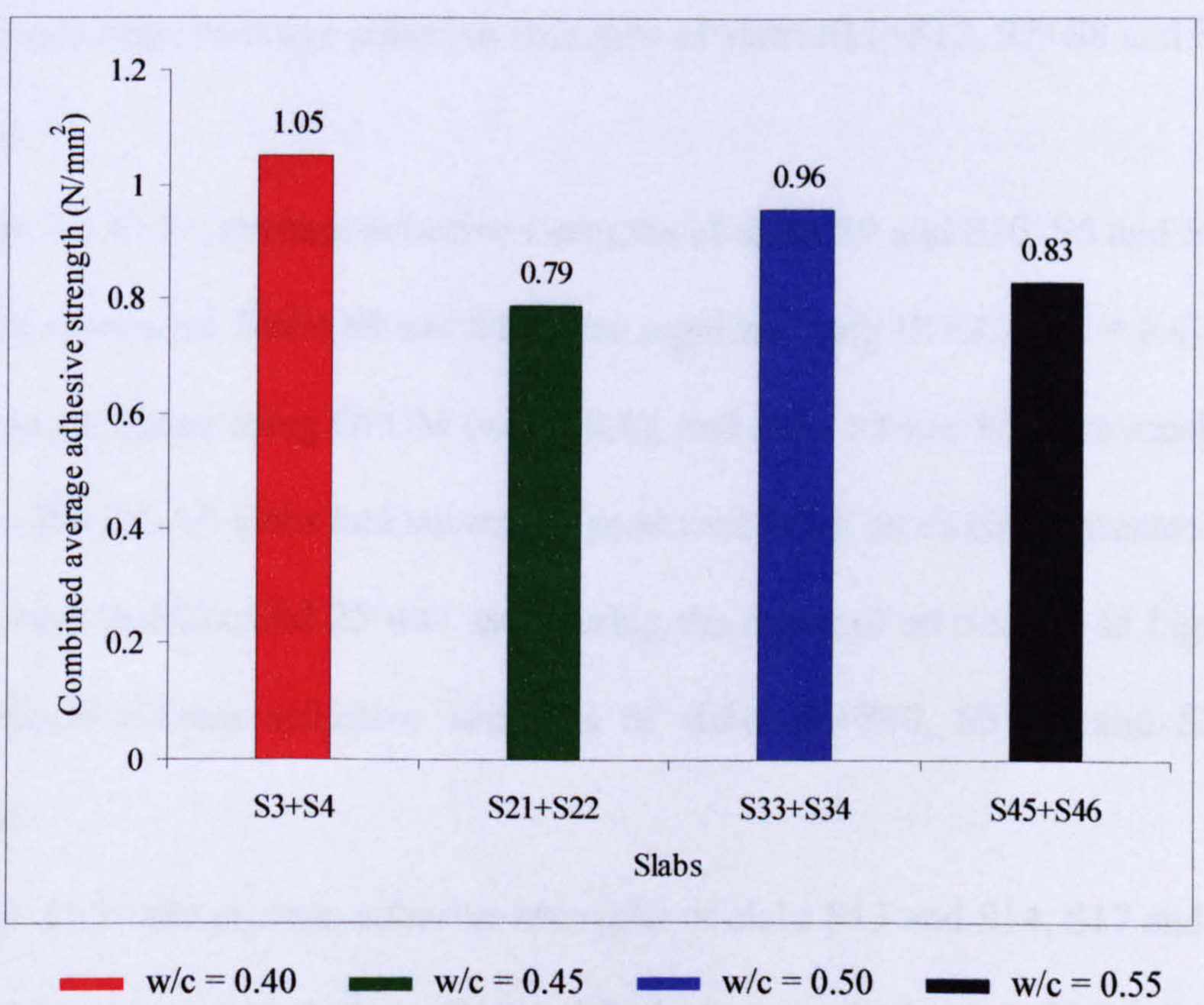

Figure 11.25 Influence of substrate strength on the combined average adhesive strength of slabs S3+S4, S21+S22, S33+S34, and S45+S46

11.2.2.3 Influence of type of generic repair material on the average adhesive strength

The aim of this series of comparisons is to investigate the effect of different types of generic repair materials on the average adhesive strength. For this reason, substrate specimens repaired using 3 different types of generic repair materials are compared. The rest of the parameters which include type of substrate surface, substrate strength and application of bonding agent/primer are kept constant for all specimens. Detailed information including individual adhesive strength values is provided in Figures 11.26-11.45.

In Figure 11.26 the average adhesive strengths of slabs S11 and S12, S7 and S8, and S1 and S2 are compared. Slabs S11 and S12 were repaired using OPCC (w/c = 0.4), slabs S7 and S8 were repaired using OPCM (w/c = 0.4), and slabs S1 and S2 were repaired using Zentrifix GM 25. All slabs had substrates produced using an electric hammer. No bonding agent/primer was used during the repair all 6 slabs. In Figure 11.27 the combined average adhesive strengths of slabs S11+S12, S7+S8 and S1+S2 are compared.

In Figure 11.28 the average adhesive strengths of slabs S9 and S10, S5 and S6, and S3 and S4 are compared. Slabs S9 and S10 were repaired using OPCC (w/c = 0.4), slabs S5 and S6 were repaired using OPCM (w/c = 0.4), and slabs S3 and S4 were repaired using Zentrifix GM 25. All slabs had substrates produced using an electric hammer. Bonding agent/primer Zentrifix GM 25 was used during the repair of all 6 slabs. In Figure 11.29 the combined average adhesive strengths of slabs S9+S10, S5+S6 and S3+S4 are compared.

In Figure 11.30 the average adhesive strengths of slabs S13 and S14, S17 and S18, and S23 and S24 are compared. Slabs S13 and S14 were repaired using OPCC (w/c = 0.4), slabs S17 and S18 were repaired using OPCM (w/c = 0.4), and slabs S23 and S24 were

repaired using Zentrifix GM 25. All slabs had substrates produced using an electric hammer. No bonding agent/primer was used during the repair of all 6 slabs. In Figure 11.31 the combined average adhesive strengths of slabs S13+S14, S17+S18 and S23+S24 are compared.

In Figure 11.32 the average adhesive strengths of slabs S15 and S16, S19 and S20, and S21 and S22 are compared. Slabs S15 and S16 were repaired using OPCC (w/c = 0.4), slabs S19 and S20 were repaired using OPCM (w/c = 0.4), and slabs S21 and S22 were repaired using Zentrifix GM 25. All slabs had substrates produced using an electric hammer. Bonding agent/primer Zentrifix GM 25 was used during the repair of all 6 slabs. In Figure 11.33 the combined average adhesive strengths of slabs S15+S16, S19+S20 and S21+S22 are compared.

In Figure 11.34 the average adhesive strengths of slabs S25 and S26, S29 and S30, and S35 and S36 are compared. Slabs S25 and S26 were repaired using OPCC (w/c = 0.4), slabs S29 and S30 were repaired using OPCM (w/c = 0.4), and slabs S35 and S36 were repaired using Zentrifix GM 25. All slabs had substrates produced using an electric hammer. No bonding agent/primer was used during the repair of all 6 slabs. In Figure 11.35 the combined average adhesive strengths of slabs S25+S26, S29+S30 and S35+S36 are compared.

In Figure 11.36 the average adhesive strengths of slabs S27 and S28, S31 and S32, and S33 and S34 are compared. Slabs S27 and S28 were repaired using OPCC (w/c = 0.4), slabs S31 and S32 were repaired using OPCM (w/c = 0.4), and slabs S33 and S34 were repaired using Zentrifix GM 25. All slabs had substrates produced using an electric hammer. Bonding agent/primer Zentrifix GM 25 was used during the repair of all 6 slabs. In Figure 11.37 the combined average adhesive strengths of slabs S27+S28, S31+S32 and S33+S34 are compared.

In Figure 11.38 the average adhesive strengths of slabs S37 and S38, S43 and S44, and S47 and S48 are compared. Slabs S37 and S38 were repaired using OPCC (w/c = 0.4), slabs S43 and S44 were repaired using OPCM (w/c = 0.4), and slabs S47 and S48 were repaired using Zentrifix GM 25. All slabs had substrates produced using an electric hammer. No bonding agent/primer was used during the repair of all 6 slabs. In Figure 11.39 the combined average adhesive strengths of slabs S37+S38, S43+S44 and S47+S48 are compared.

In Figure 11.40 the average adhesive strengths of slabs S39 and S40, S41 and S42, and S45 and S46 are compared. Slabs S39 and S40 were repaired using OPCC (w/c = 0.4), slabs S41 and S42 were repaired using OPCM (w/c = 0.4), and slabs S45 and S46 were repaired using Zentrifix GM 25. All slabs had substrates produced using an electric hammer. Bonding agent/primer Zentrifix GM 25 was used during the repair of all 6 slabs. In Figure 11.41 the combined average adhesive strengths of slabs S39+S40, S41+S42 and S45+S46 are compared.

In Figure 11.42 the average adhesive strengths of slabs P5 and PL14, PL11 and PL13, and PL9 and PL10 are compared. Slabs P5 and PL14 were repaired using OPCC (w/c = 0.4), slabs PL11 and PL13 were repaired using OPCM (w/c = 0.4), and slabs PL9 and PL10 were repaired using Zentrifix GM 25. All slabs had substrates produced using remote robotic hydroerosion. No bonding agent/primer was used during the repair of all 6 slabs. In Figure 11.43 the combined average adhesive strengths of slabs P5+PL14, PL11+PL13 and PL9+PL10 are compared.

In Figure 11.44 the average adhesive strengths of slabs PL15 and PL16, P1 and PL2, and PL5 and PL6 are compared. Slabs PL15 and PL16 were repaired using OPCC (w/c = 0.4), slabs P1 and PL2 were repaired using OPCM (w/c = 0.4), and slabs PL5 and PL6 were repaired using Zentrifix GM 25. All slabs had substrates produced using remote

robotic hydroerosion. Bonding agent/primer Zentrifix GM 25 was used during the repair of all 6 slabs. In Figure 11.45 the combined average adhesive strengths of slabs PL15+PL16, P1+PL2 and PL5+PL6 are compared.

From the above comparisons it is quite clear that in 7 out of 10 cases specimens repaired using OPCC (w/c = 0.4) provide higher adhesive strength values when compared to specimens repaired using either OPCM (w/c = 0.4) or Zentrifix GM 25. In addition, OPCC (w/c = 0.4) seems to achieve the best results in terms of adhesive strength on both types of substrate surfaces. In the other 3 cases OPCM (w/c = 0.4) provides the highest adhesive strength values. Hence, OPCC (w/c = 0.4) seems to be the best option in terms of its influence on the adhesive strength followed by OPCM (w/c = 0.4) and Zentrifix GM 25.

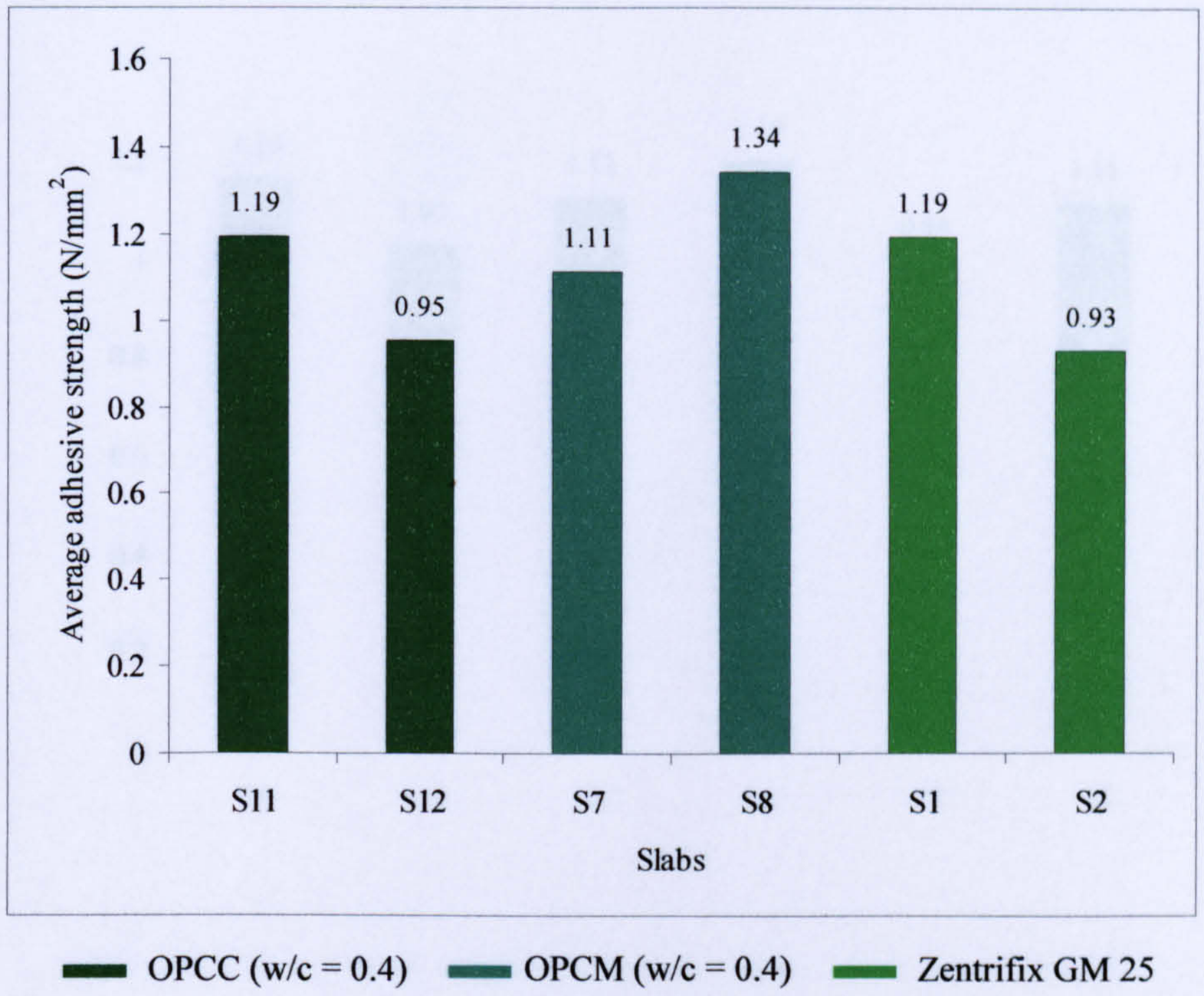

Figure 11.26 Influence of different types of generic repair material on the average adhesive strength of slabs S11 and S12, S7 and S8, and S1 and S2

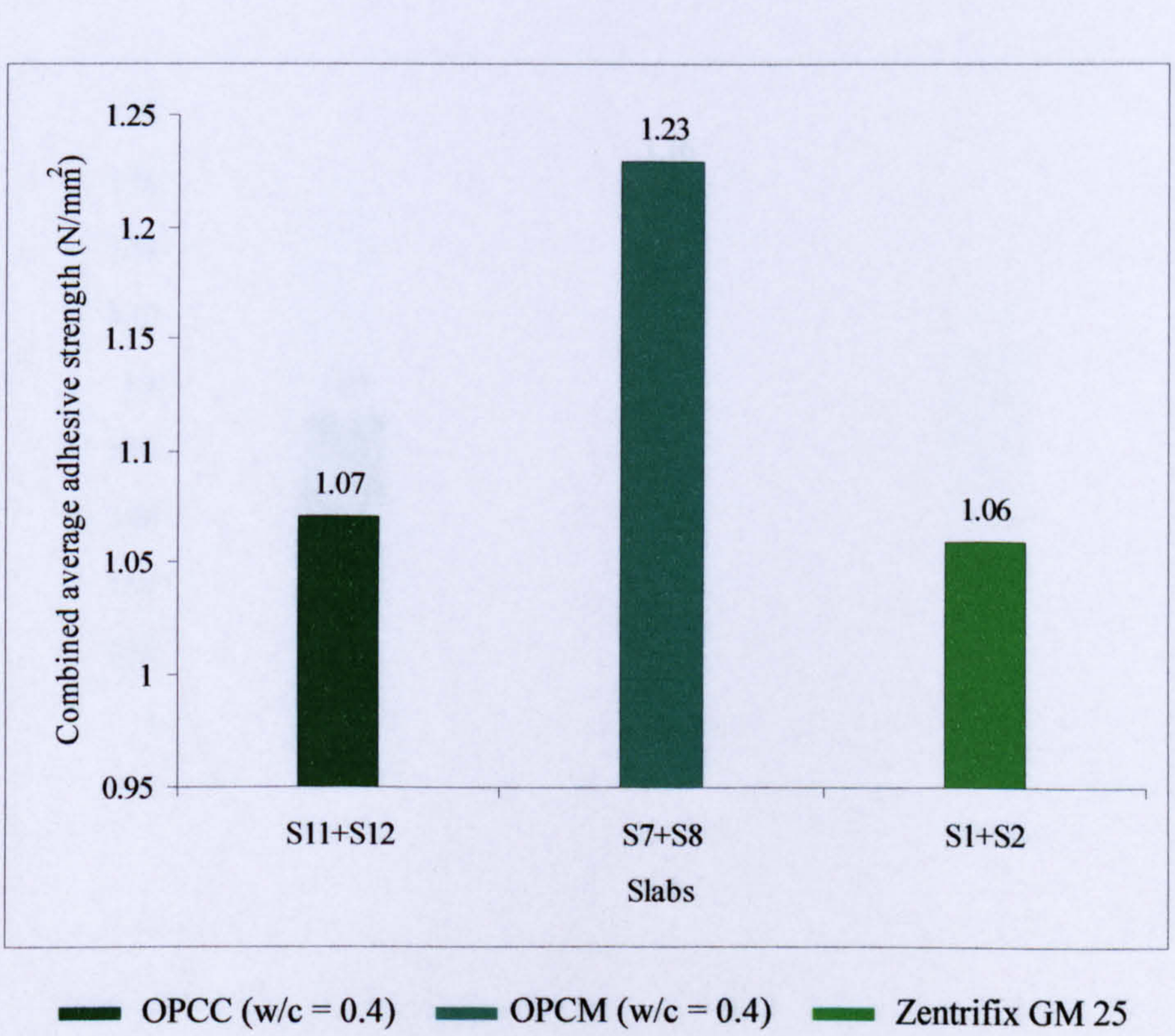

Figure 11.27 Influence of different types of generic repair material on the combined average adhesive strength of slabs S11+S12, S7+S8 and S1+S2

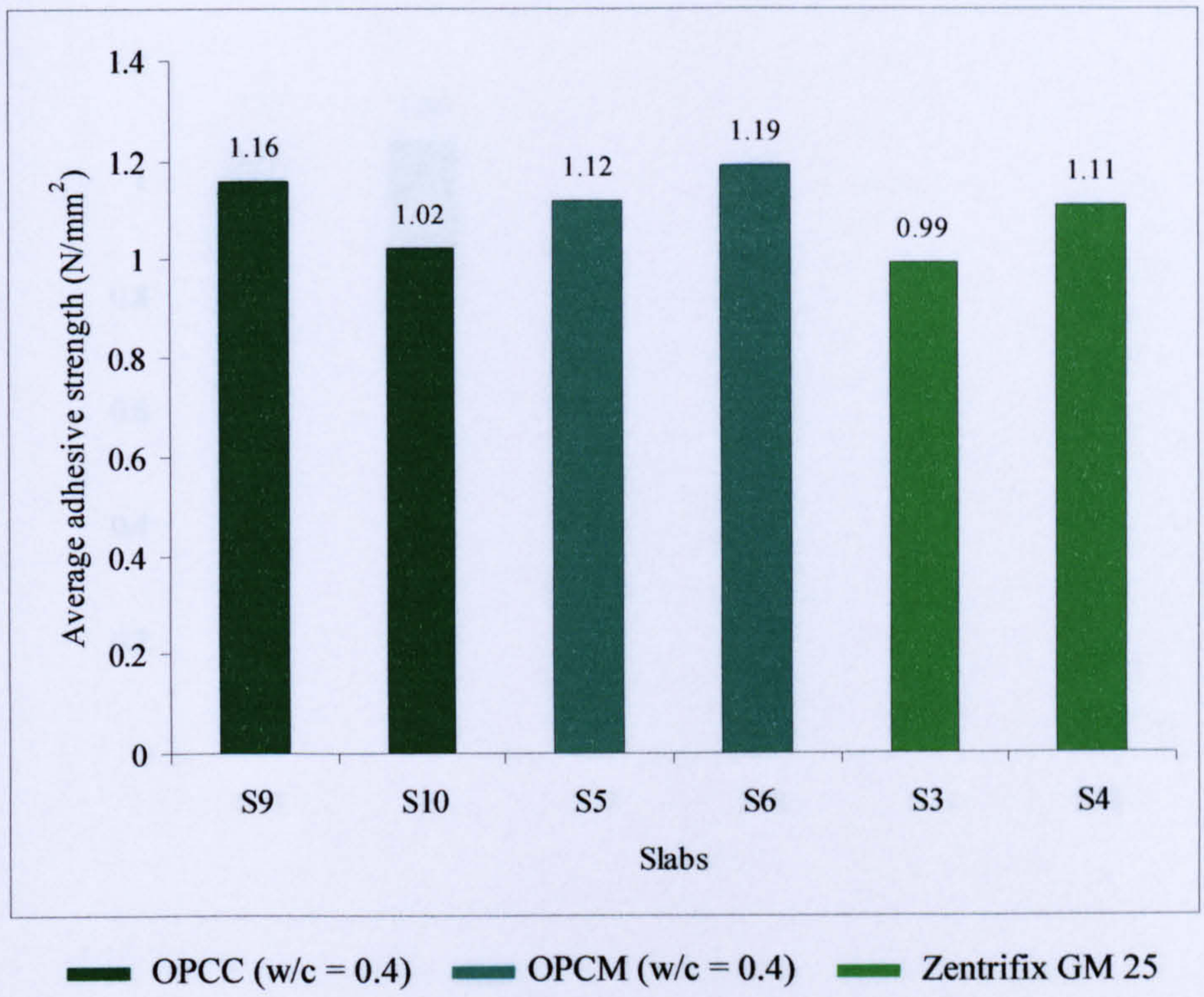

Figure 11.28 Influence of different types of generic repair material on the average adhesive strength of slabs S9 and S10, S5 and S6, and S3 and S4

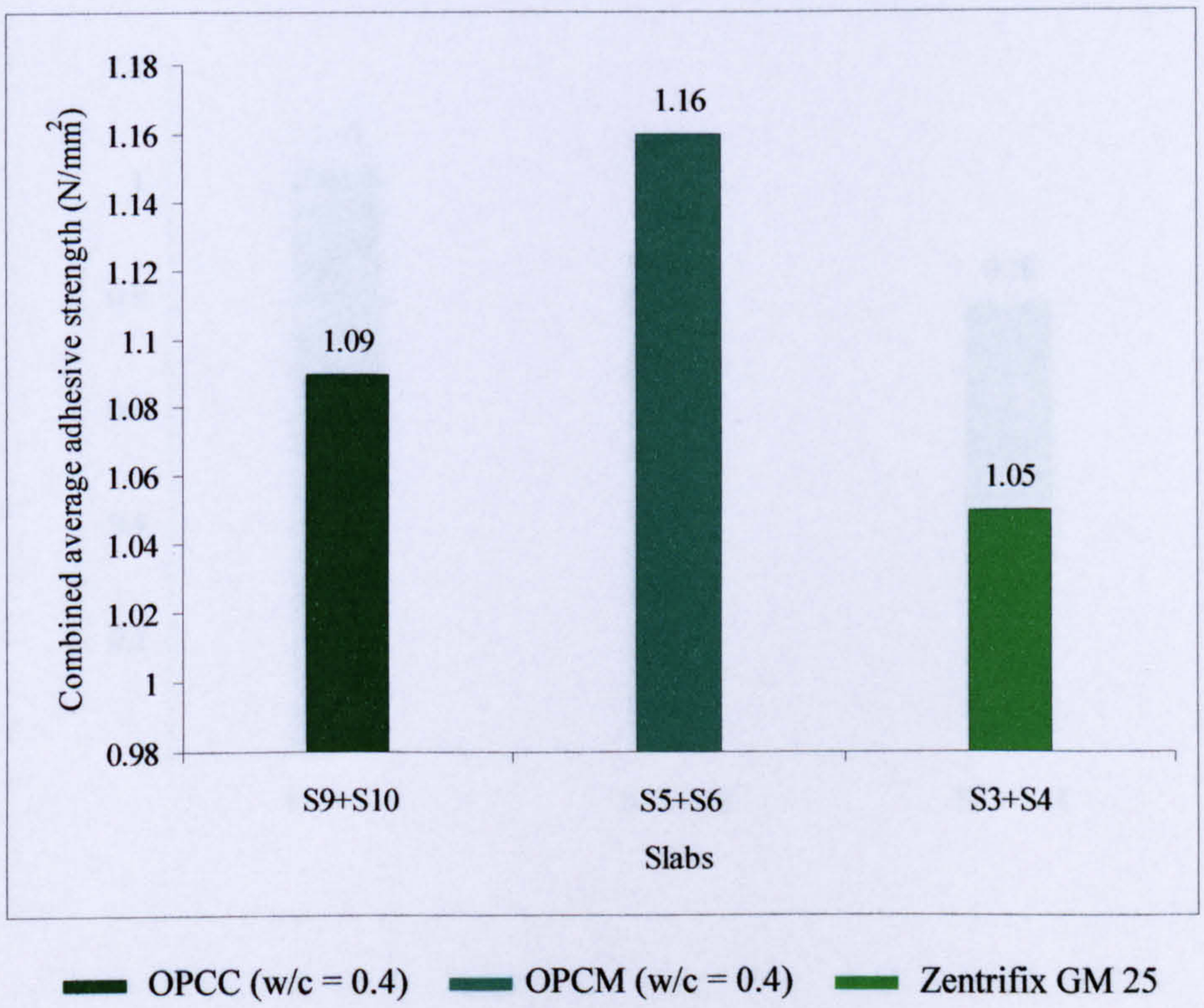

Figure 11.29 Influence of different types of generic repair material on the combined average adhesive strength of slabs S9+S10, S5+S6 and S3+S4

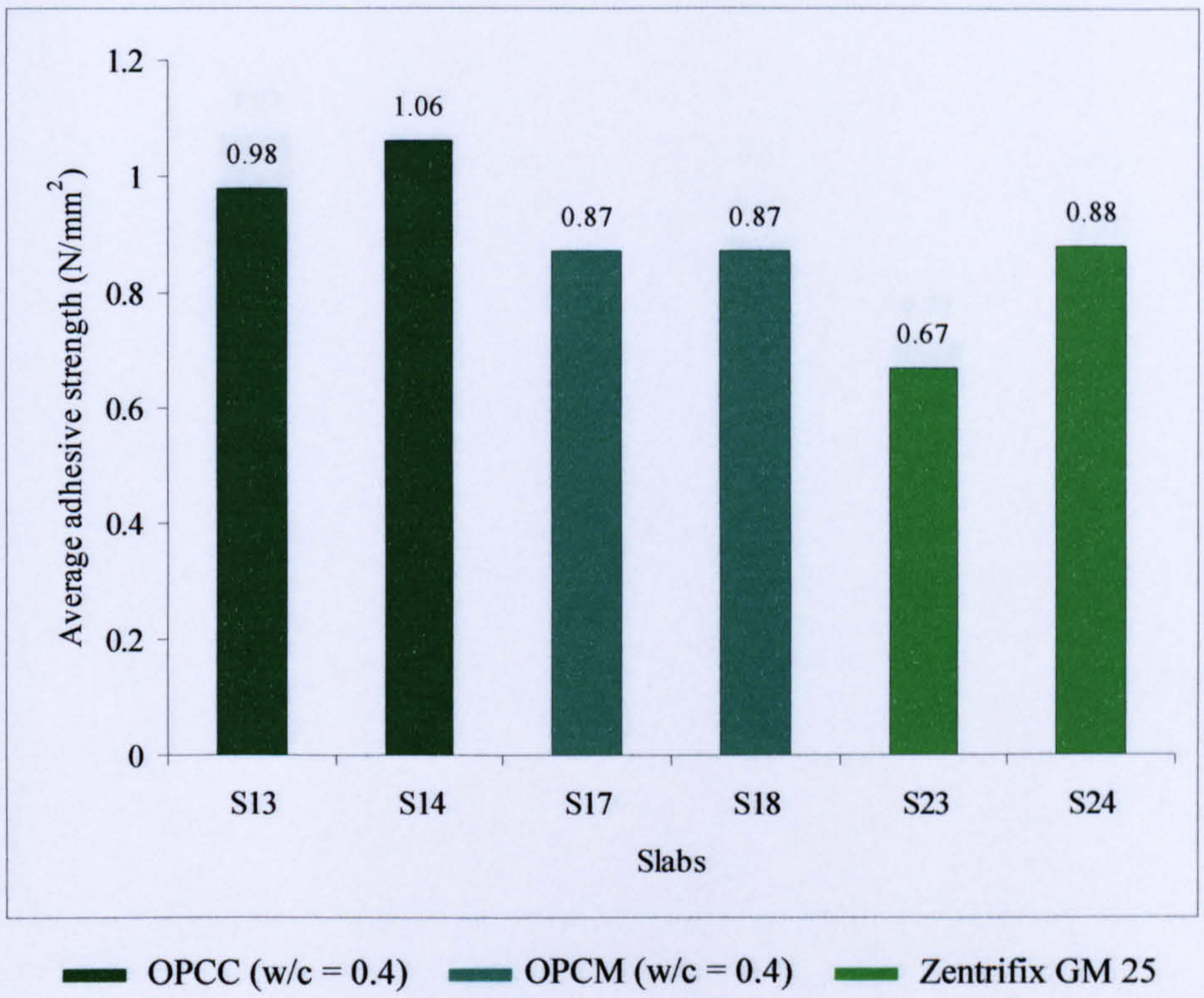

Figure 11.30 Influence of different types of generic repair material on the average adhesive strength of slabs S13 and S14, S17 and S18, and S23 and S24

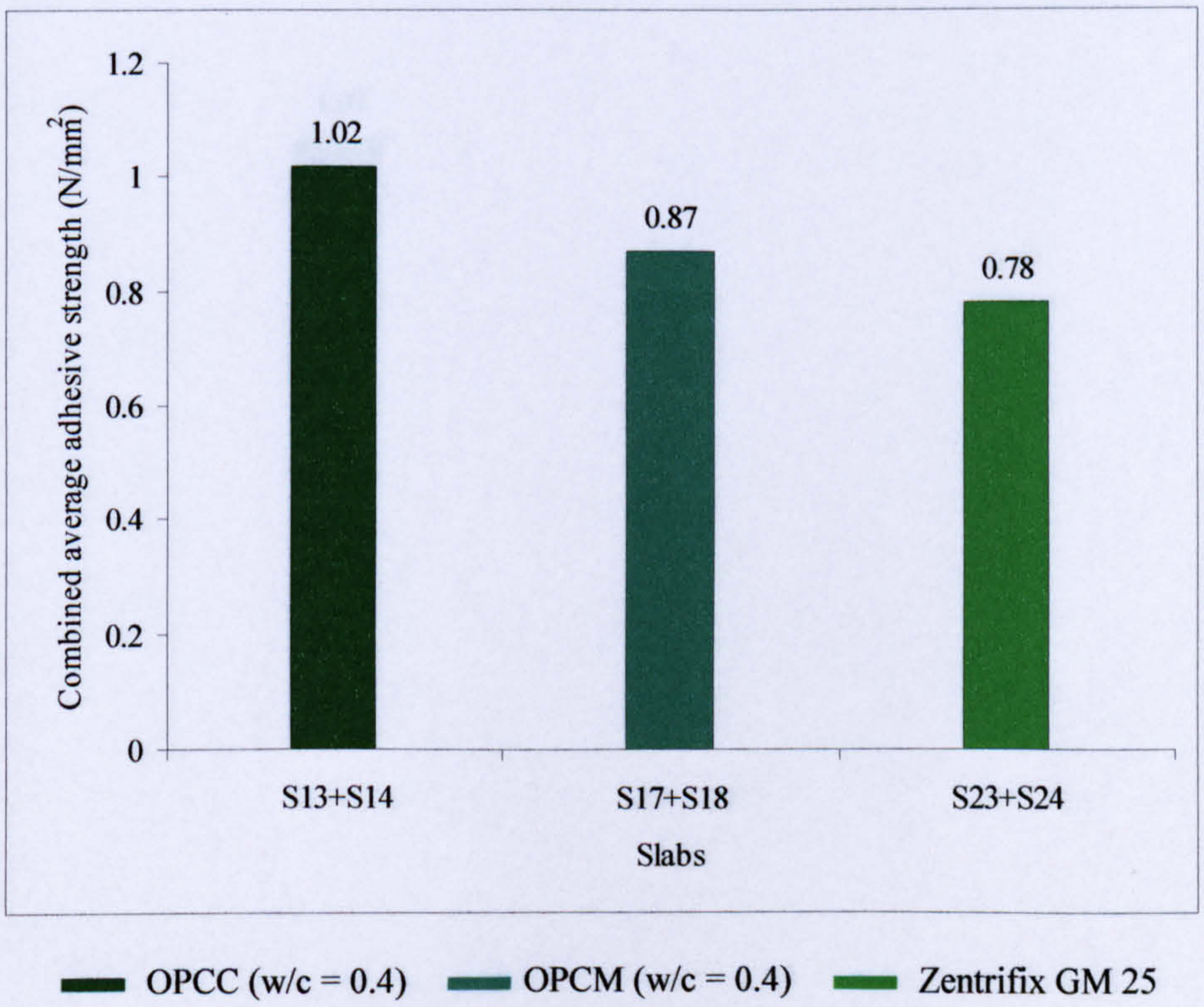

Figure 11.31 Influence of different types of generic repair material on the combined average adhesive strength of slabs S13+S14, S17+S18 and S23+S24

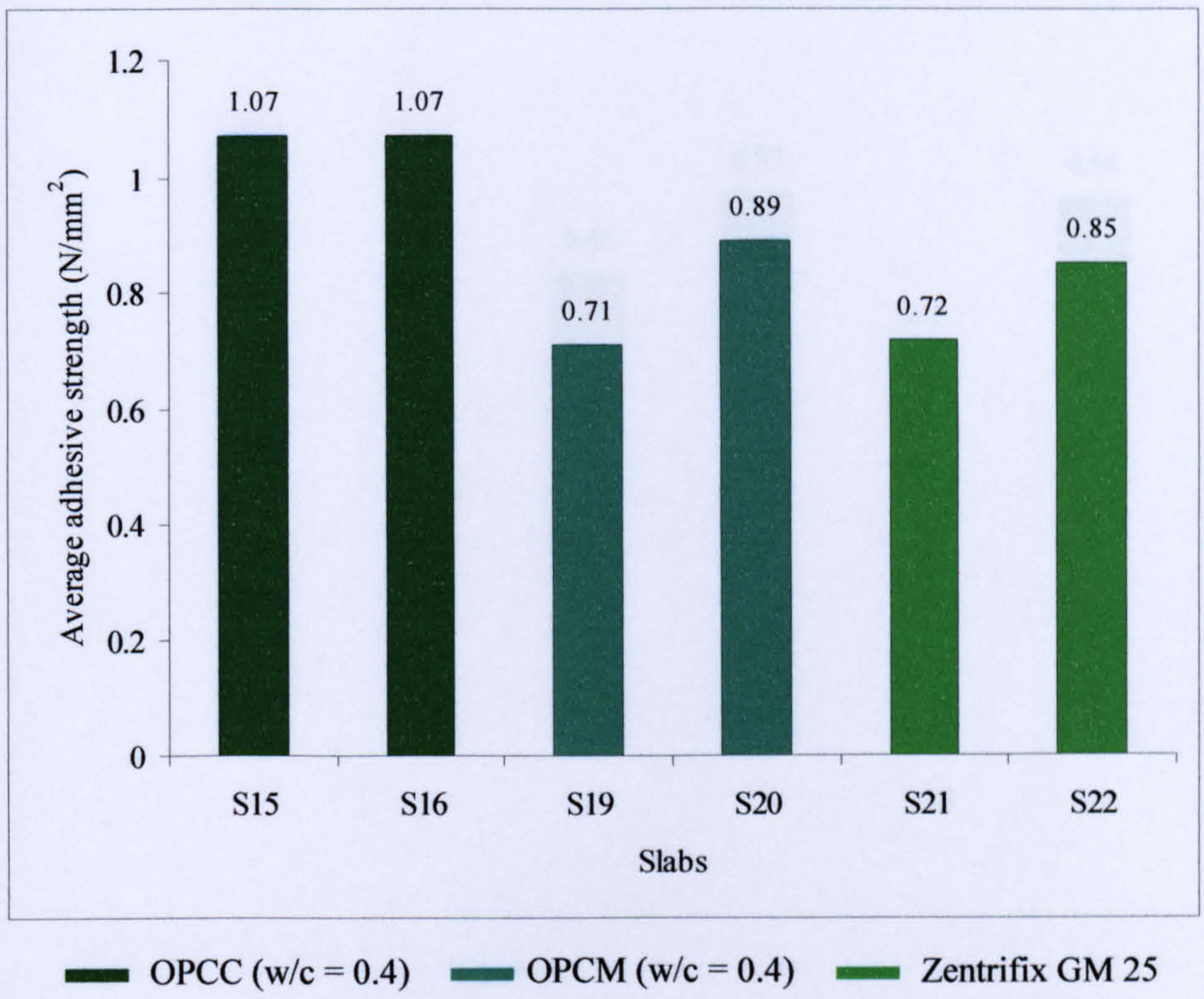

Figure 11.32 Influence of different types of generic repair material on the average adhesive strength of slabs S15 and S16, S19 and S20, and S21 and S22

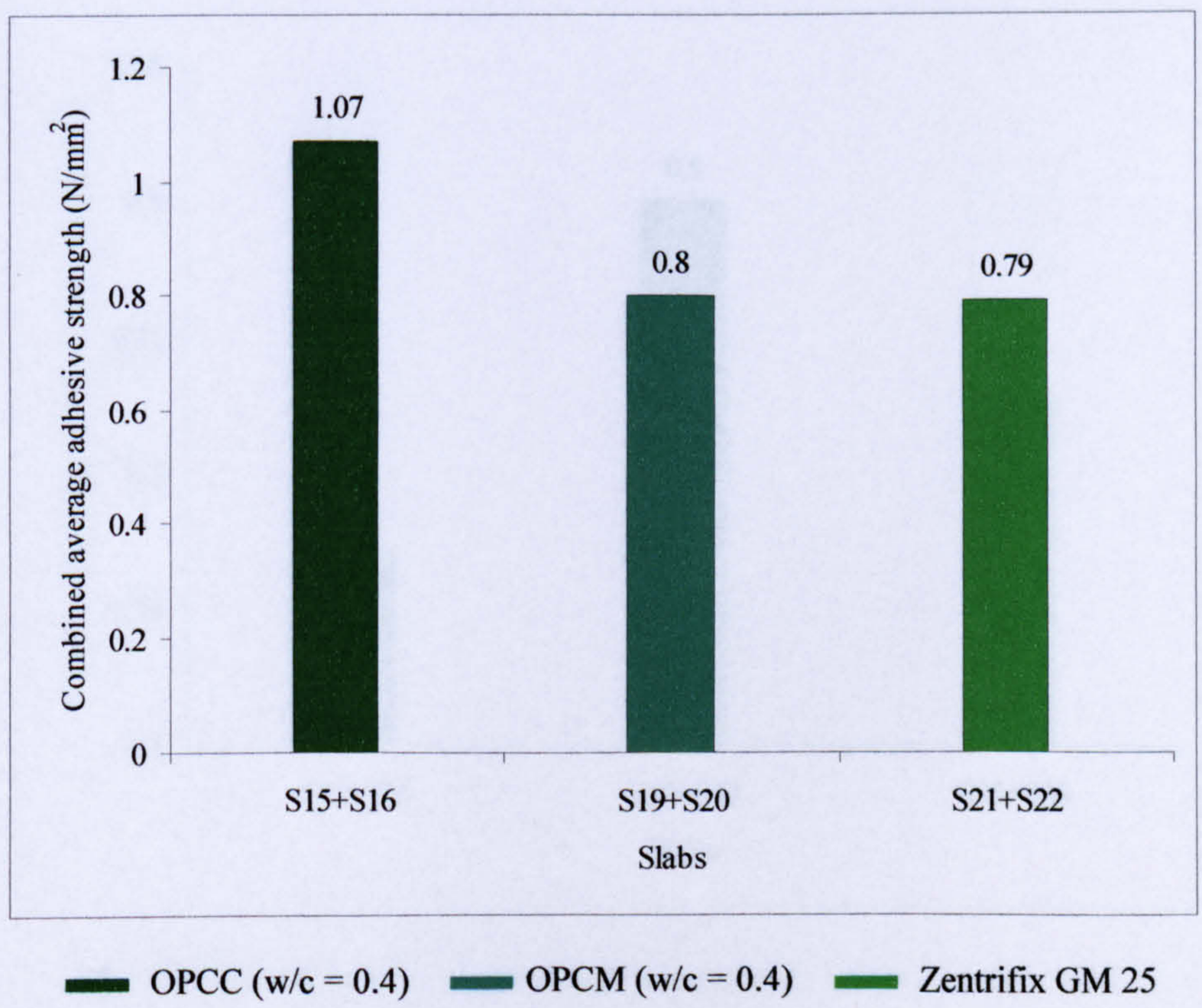

Figure 11.33 Influence of different types of generic repair material on the combined average adhesive strength of slabs S15+S16, S19+S20 and S21+S22

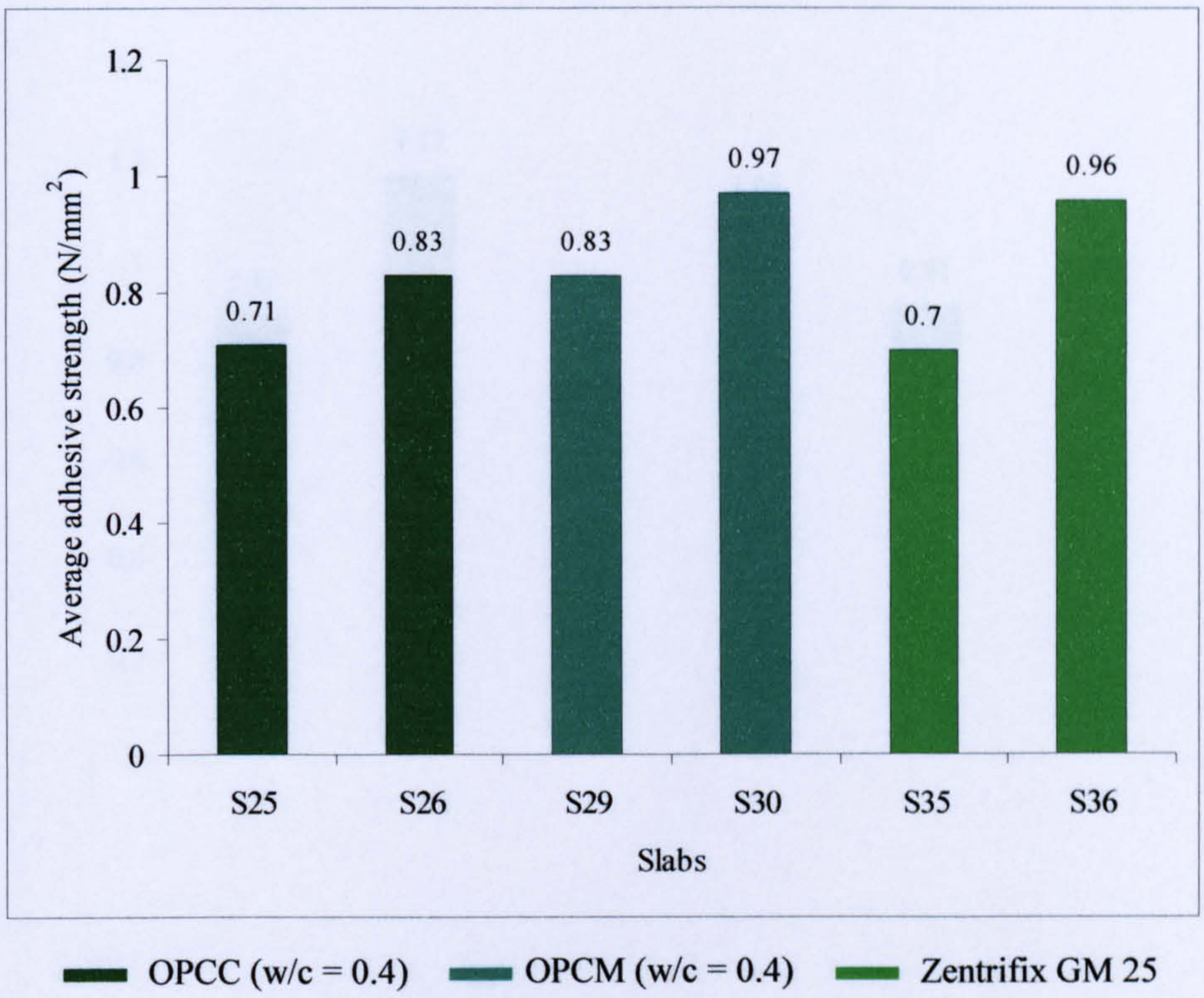

Figure 11.34 Influence of different types of generic repair material on the average adhesive strength of slabs S25 and S26, S29 and S30, and S35 and S36

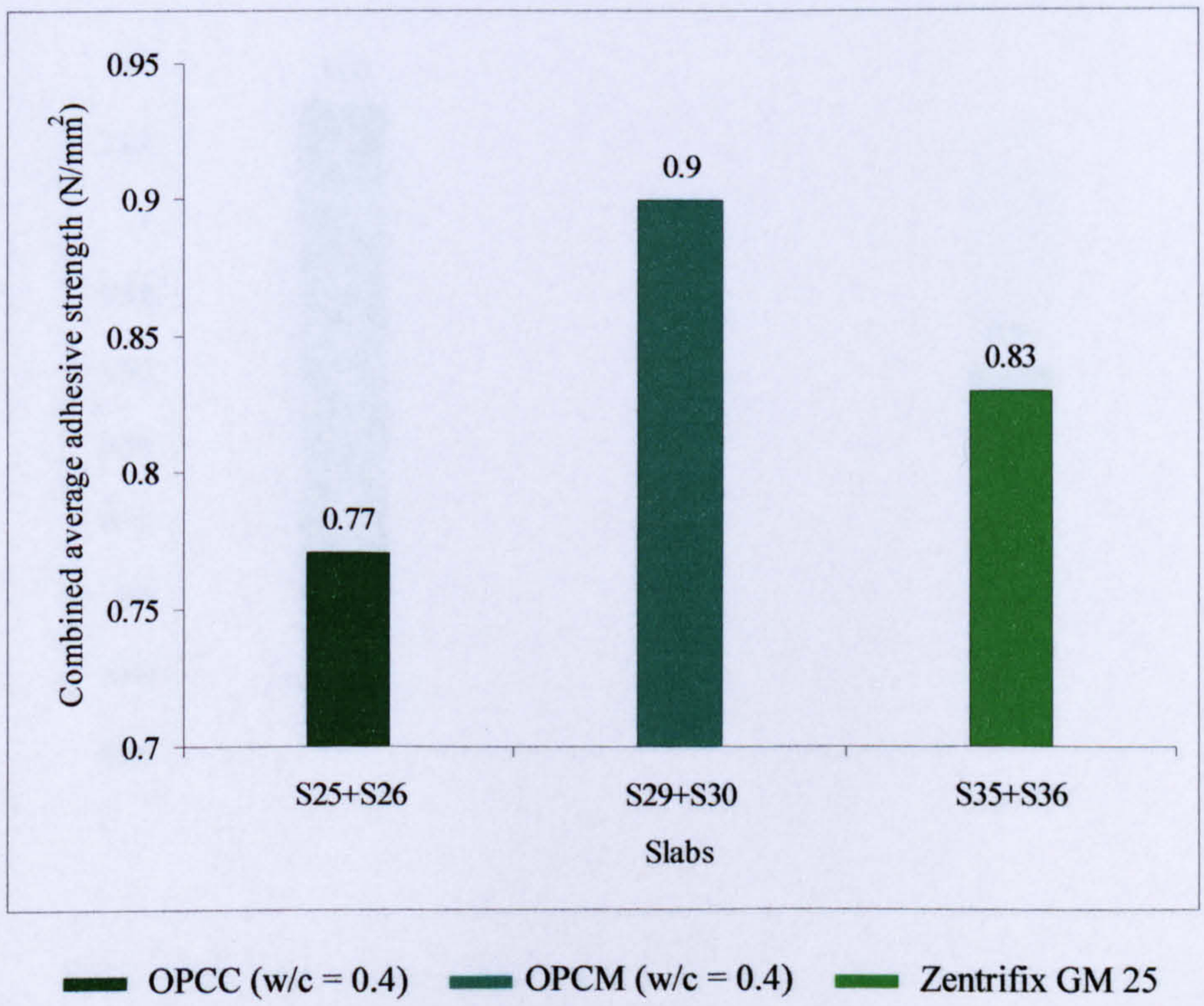

Figure 11.35 Influence of different types of generic repair material on the combined average adhesive strength of slabs S25+S26, S29+S30 and S35+S36

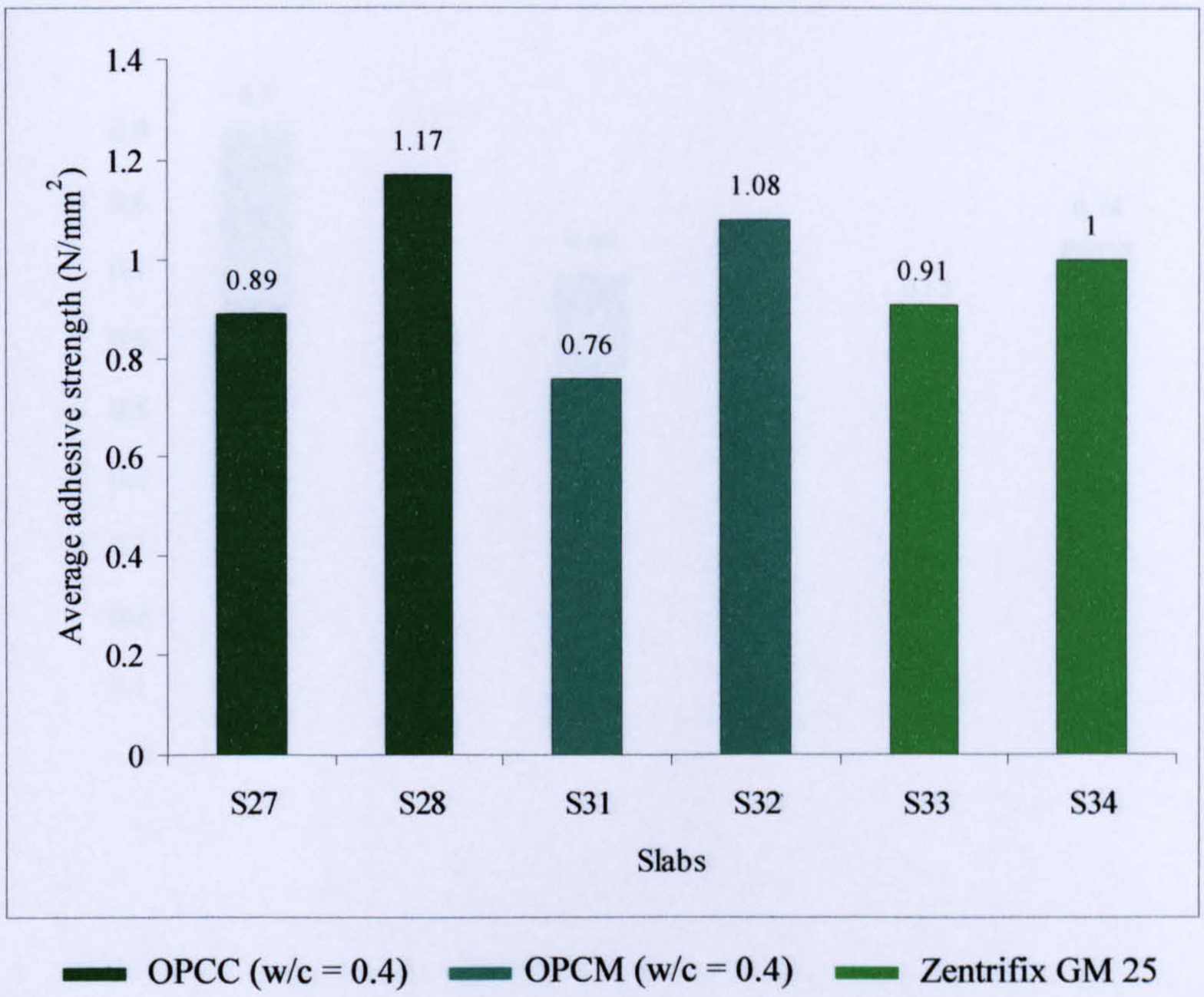

Figure 11.36 Influence of different types of generic repair material on the average adhesive strength of slabs S27 and S28, S31 and S32, and S33 and S34

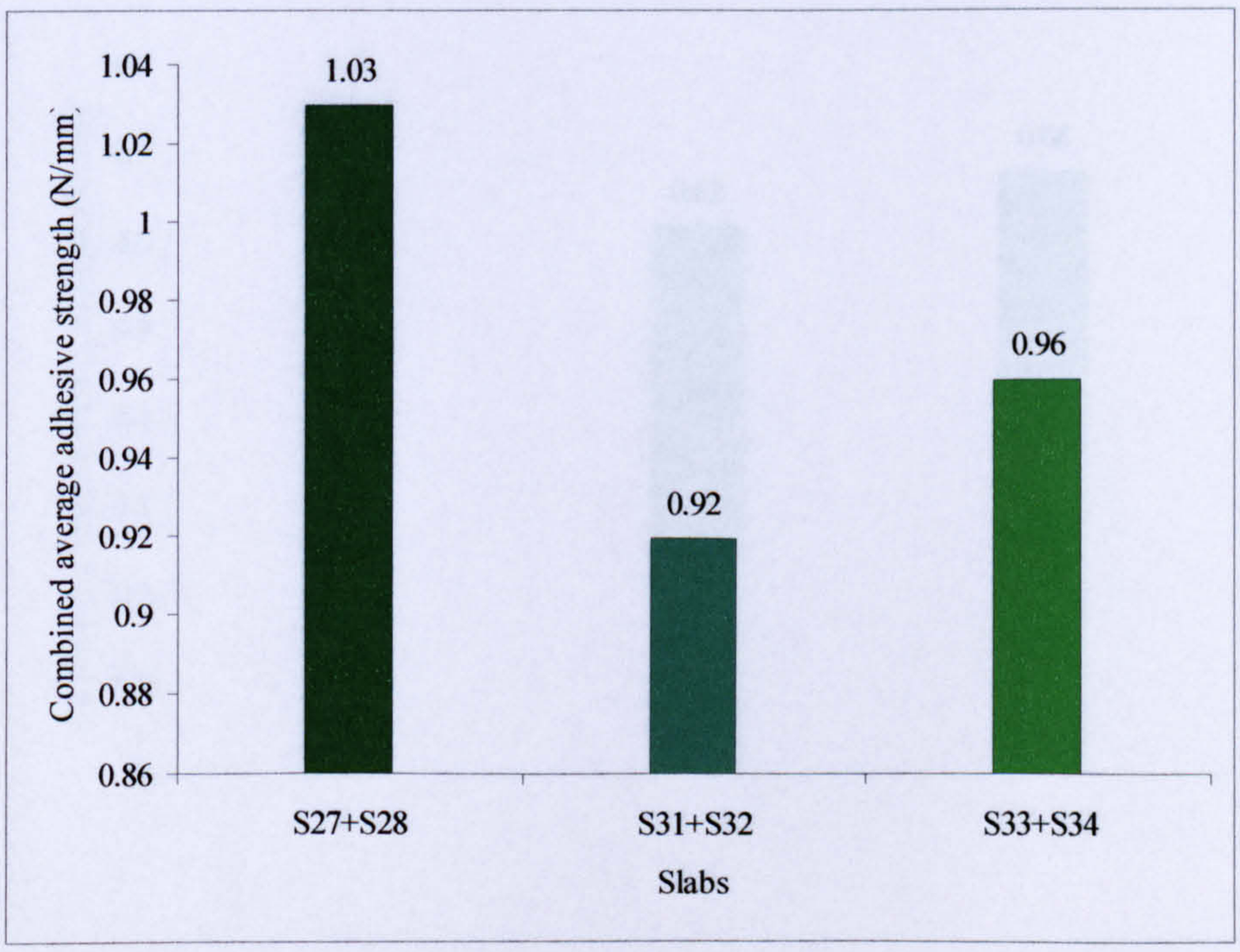

Figure 11.37 Influence of different types of generic repair material on the combined average adhesive strength of slabs S27+S28, S31+S32 and S33+S34

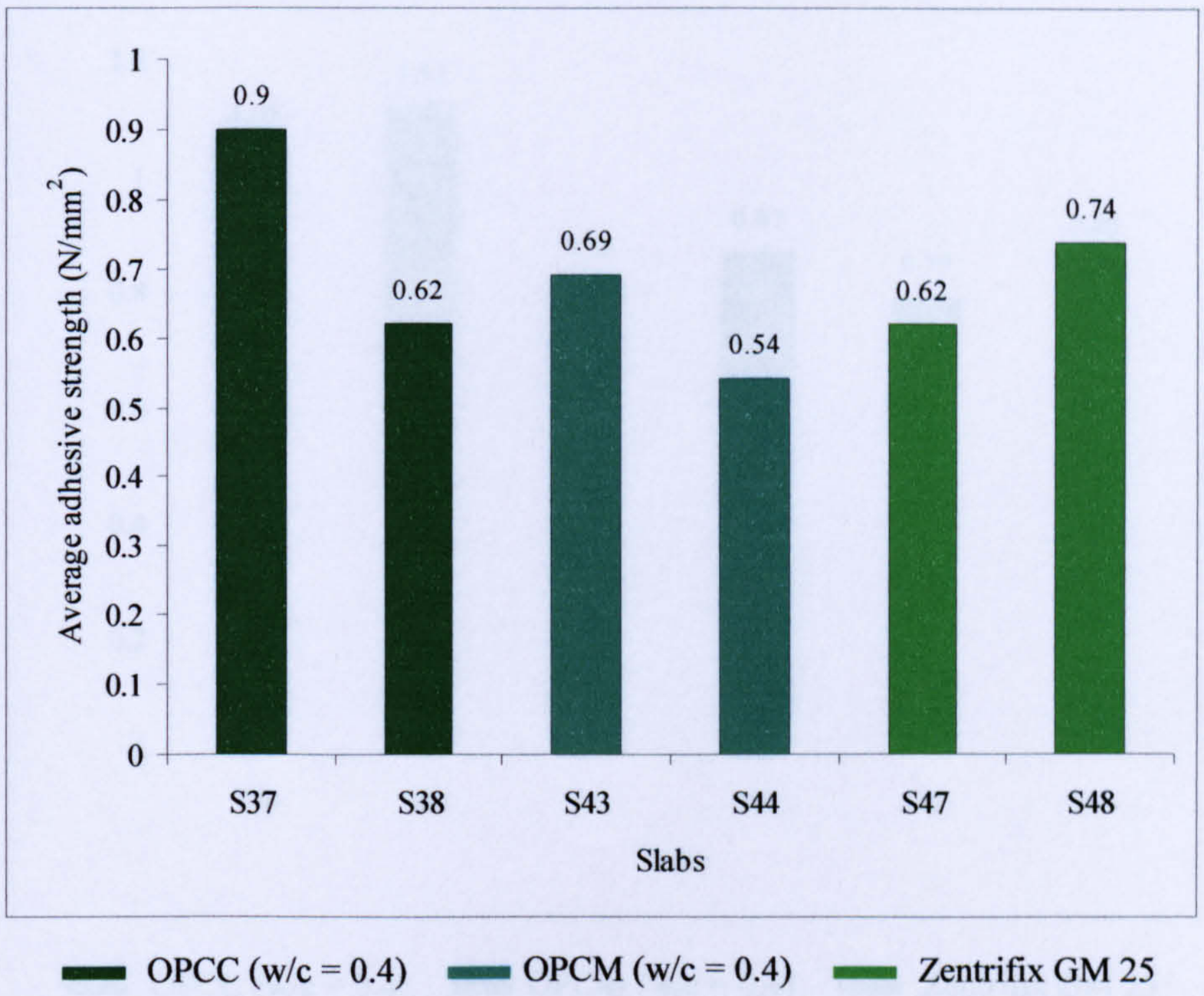

Figure 11.38 Influence of different types of generic repair material on the average adhesive strength of slabs S37 and S38, S43 and S44, and S47 and S48

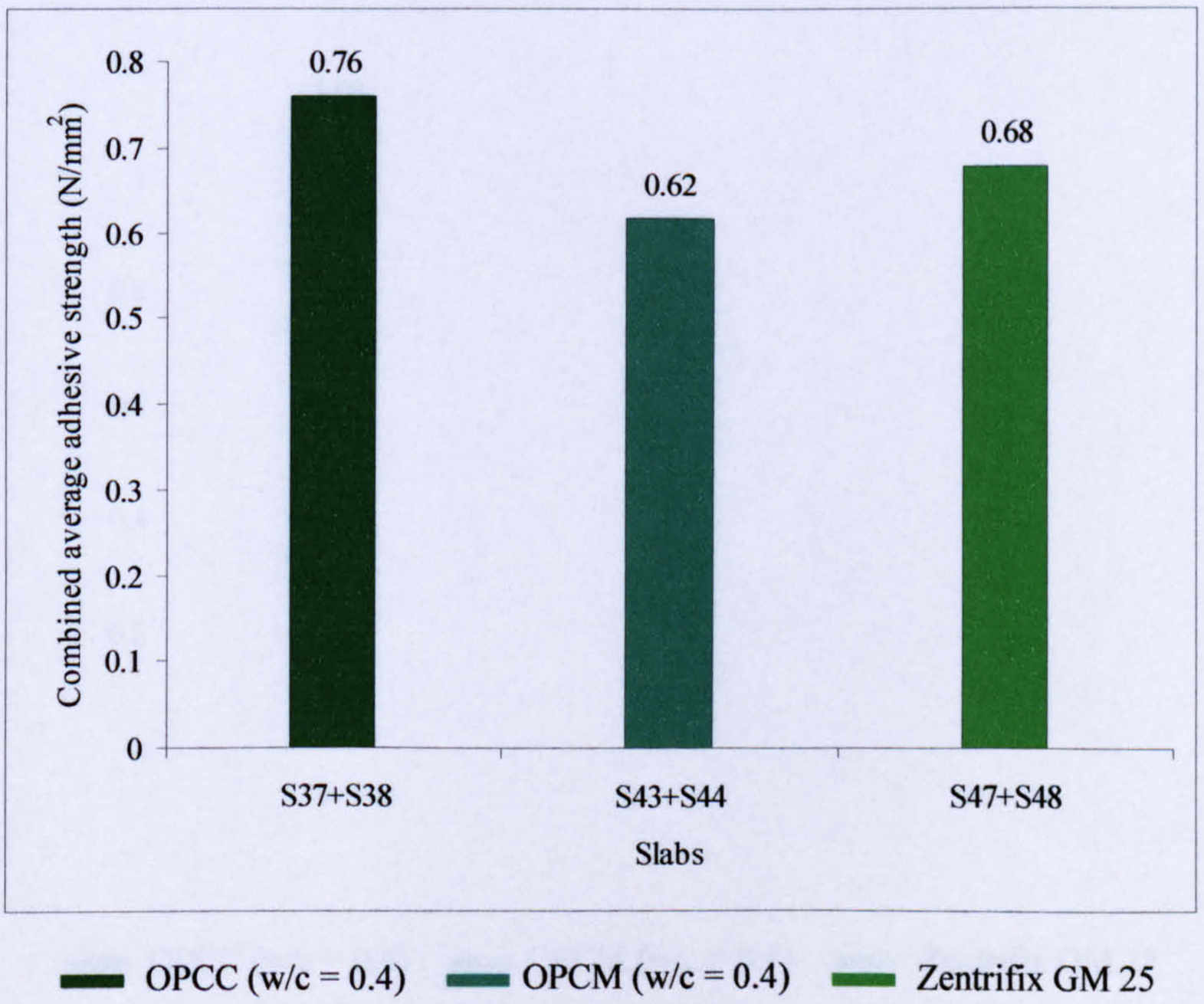

Figure 11.39 Influence of different types of generic repair material on the combined average adhesive strength of slabs S37+S38, S43+S44 and S47+S48

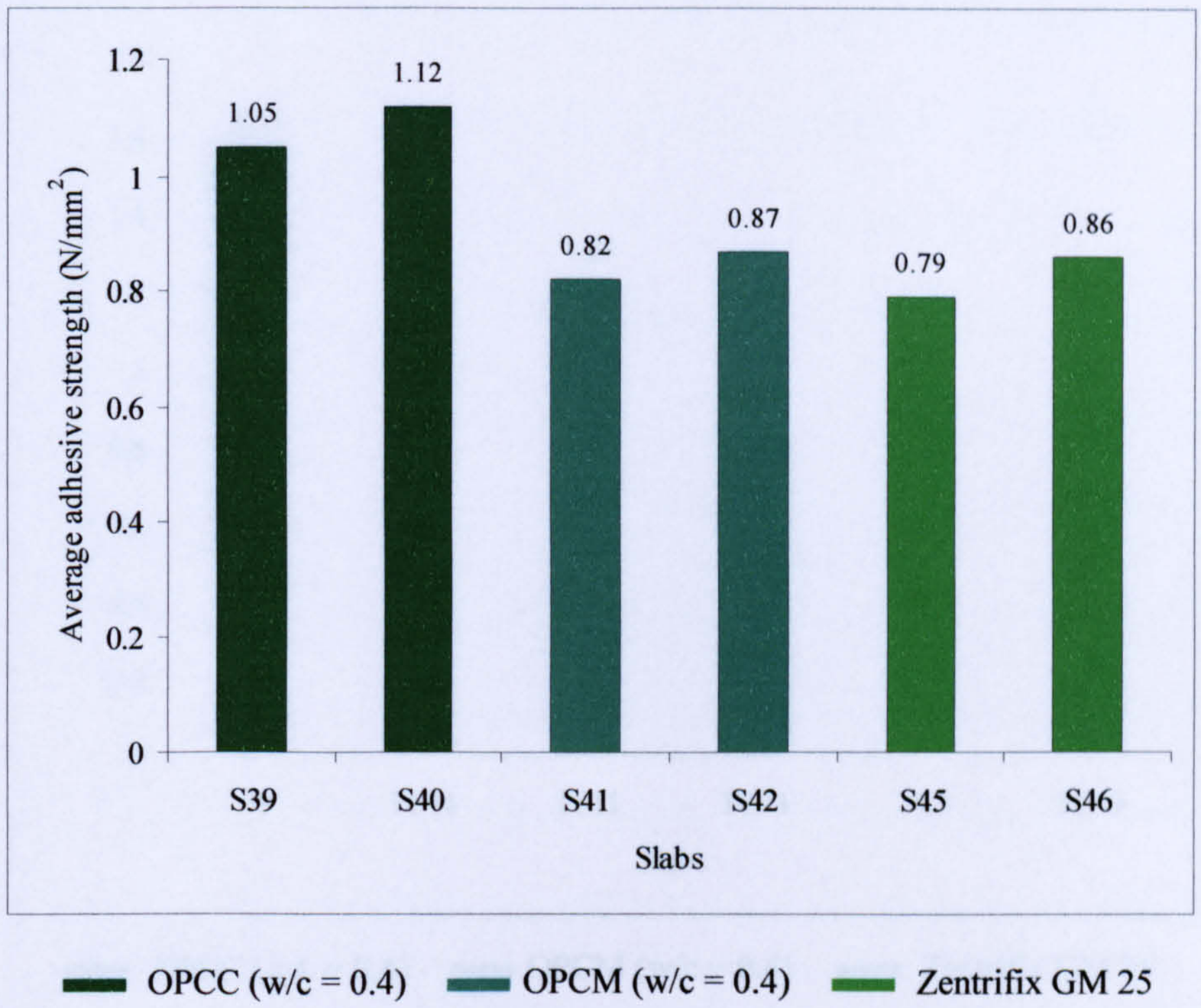

Figure 11.40 Influence of different types of generic repair material on the average adhesive strength of slabs S39 and S40, S41 and S42, and S45 and S46

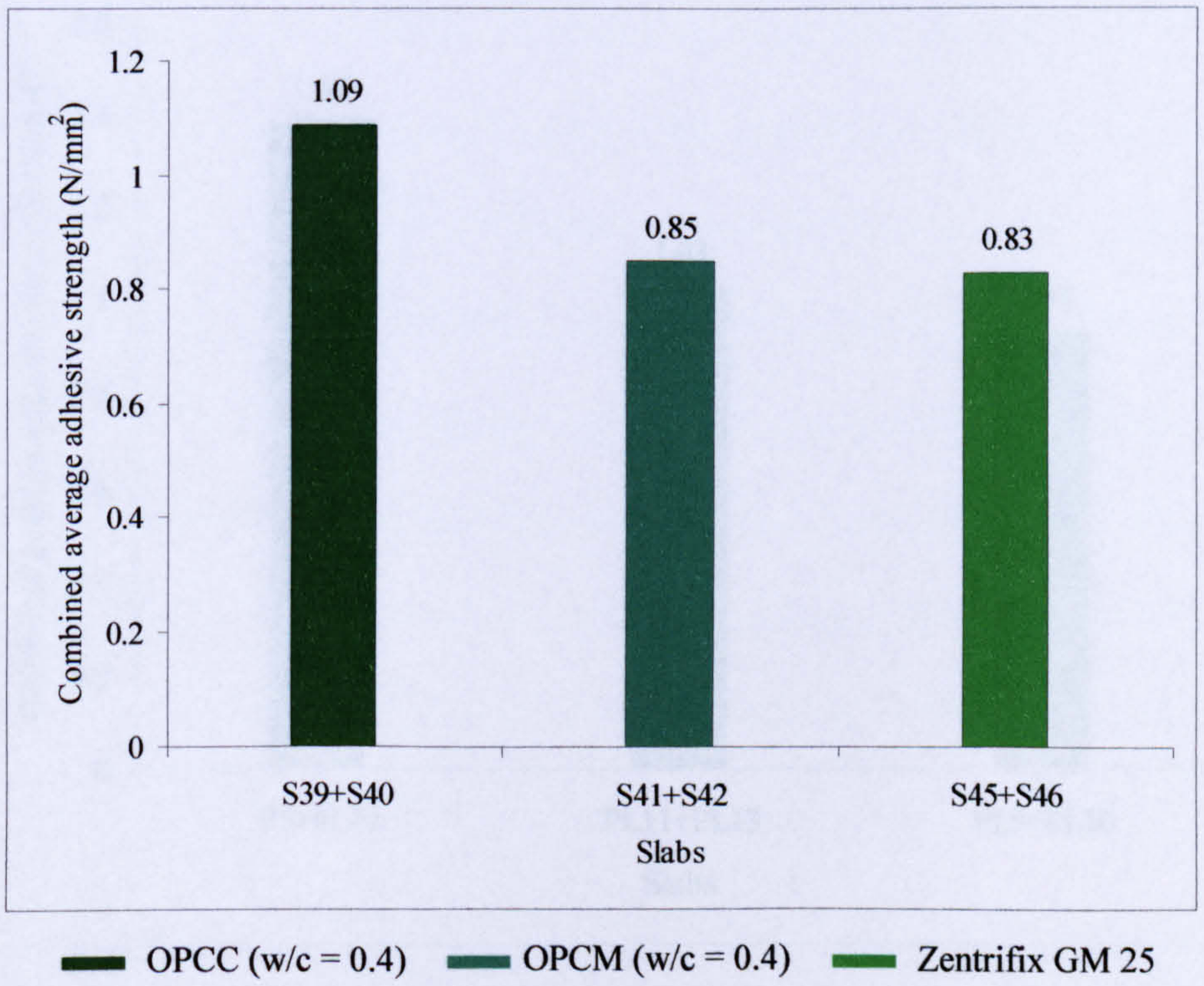

Figure 11.41 Influence of different types of generic repair material on the combined average adhesive strength of slabs S37+S38, S43+S44 and S47+S48

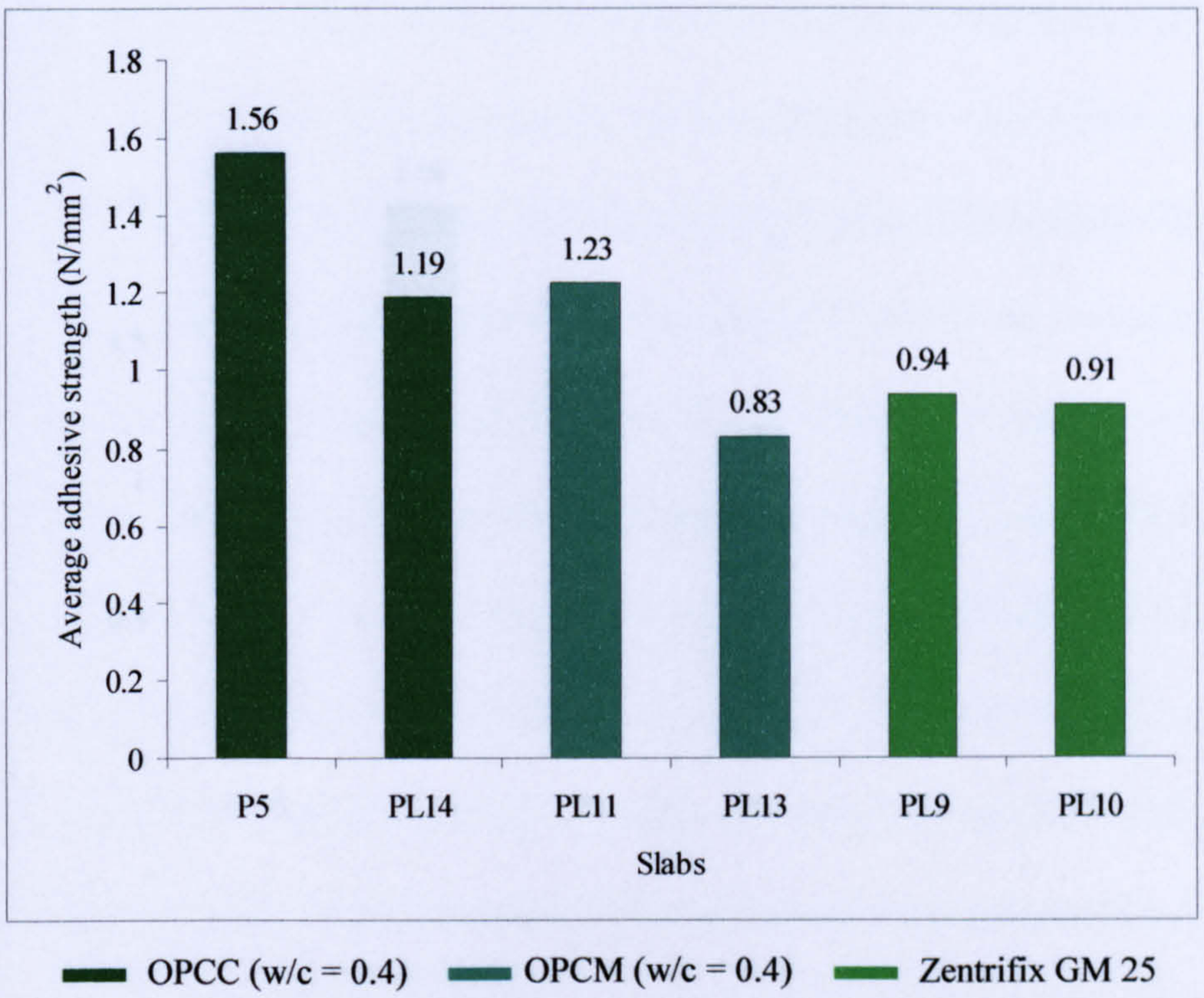

Figure 11.42 Influence of different types of generic repair material on the average adhesive strength of slabs P5 and PL14, PL11 and PL13, and PL9 and PL10

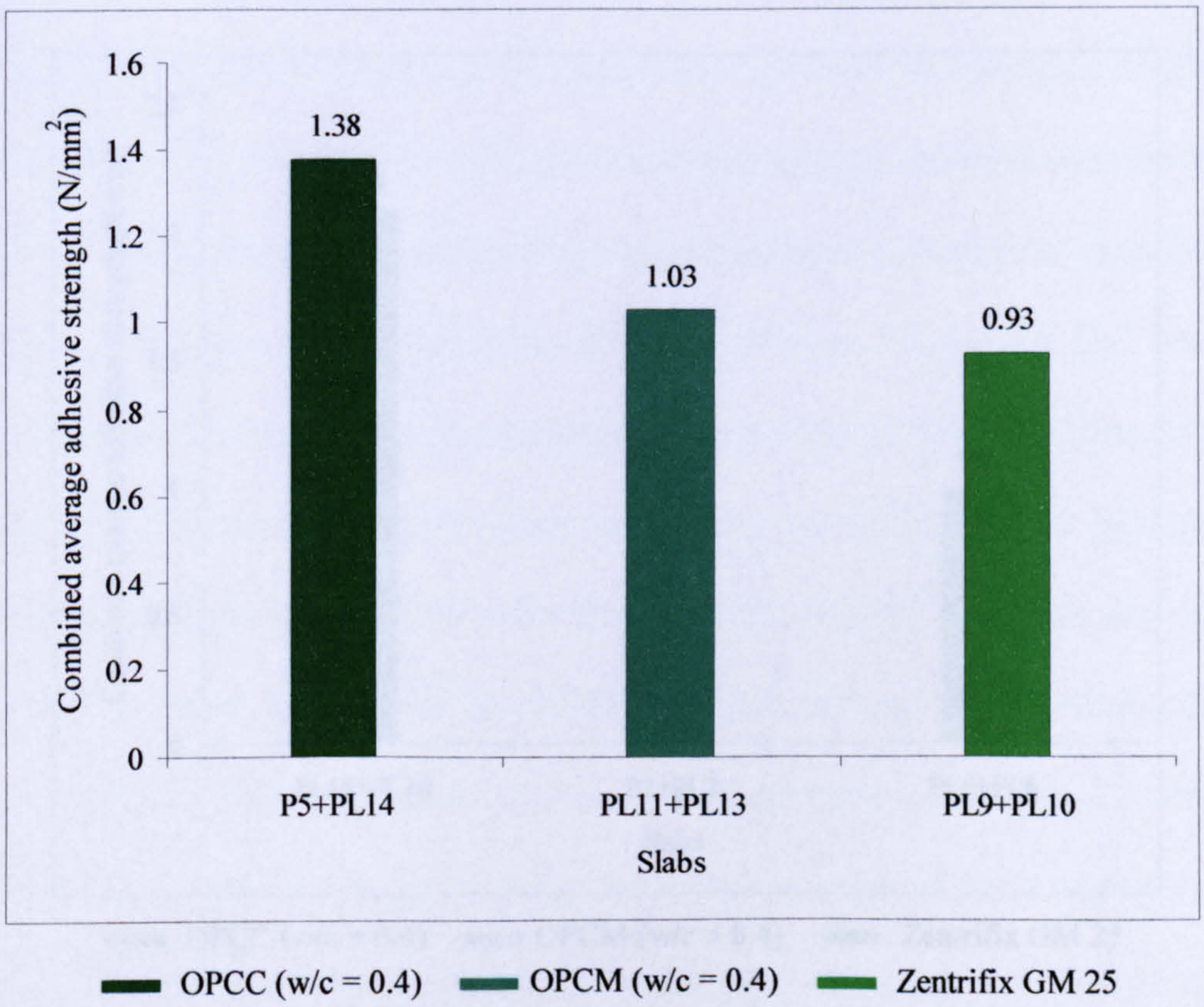

Figure 11.43 Influence of different types of generic repair material on the combined average adhesive strength of slabs P5+PL14, PL11+PL13 and PL9+PL10

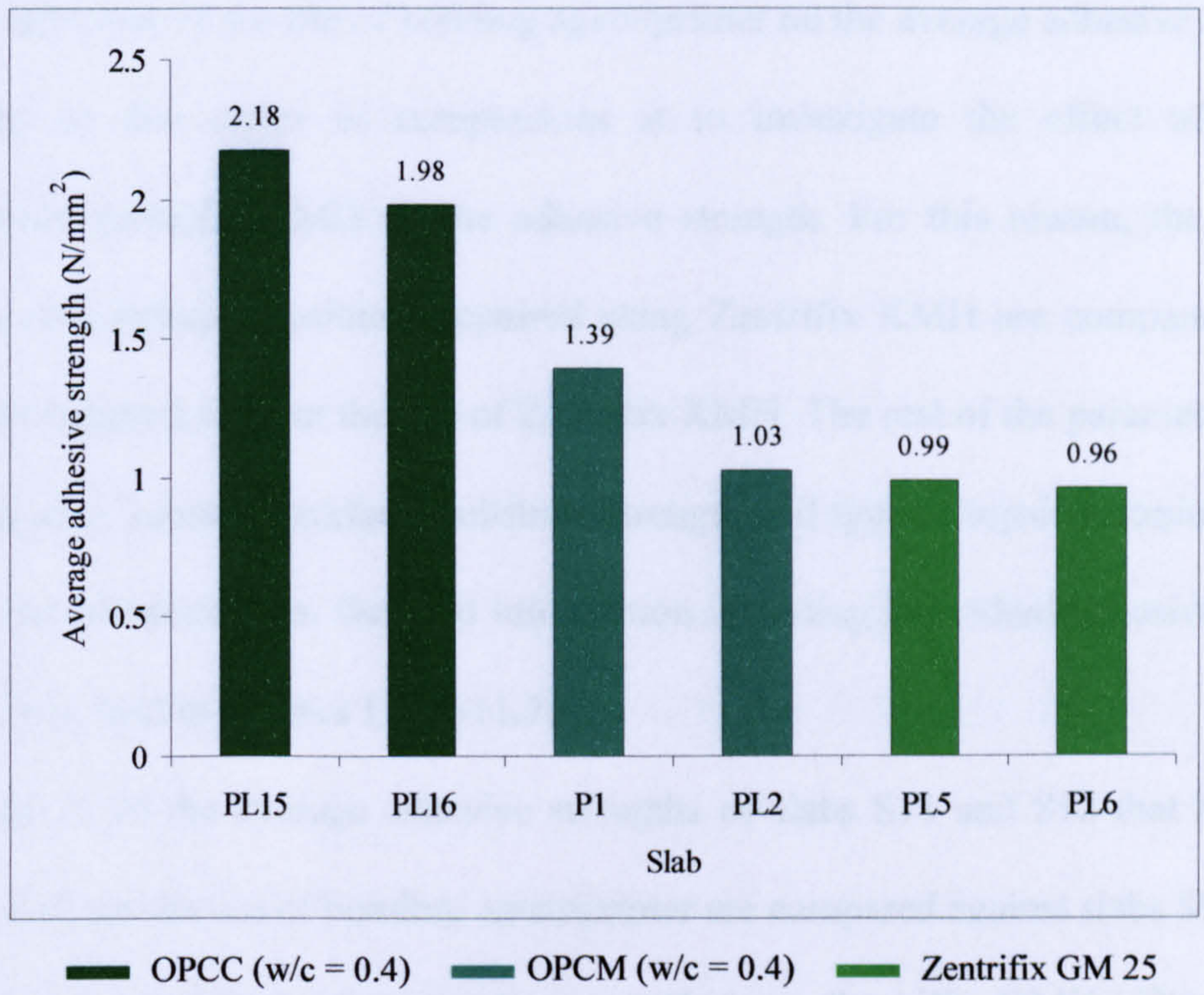

Figure 11.44 Influence of different types of generic repair material on the average adhesive strength of slabs PL15 and PL16, P1 and PL2, and PL5 and PL6

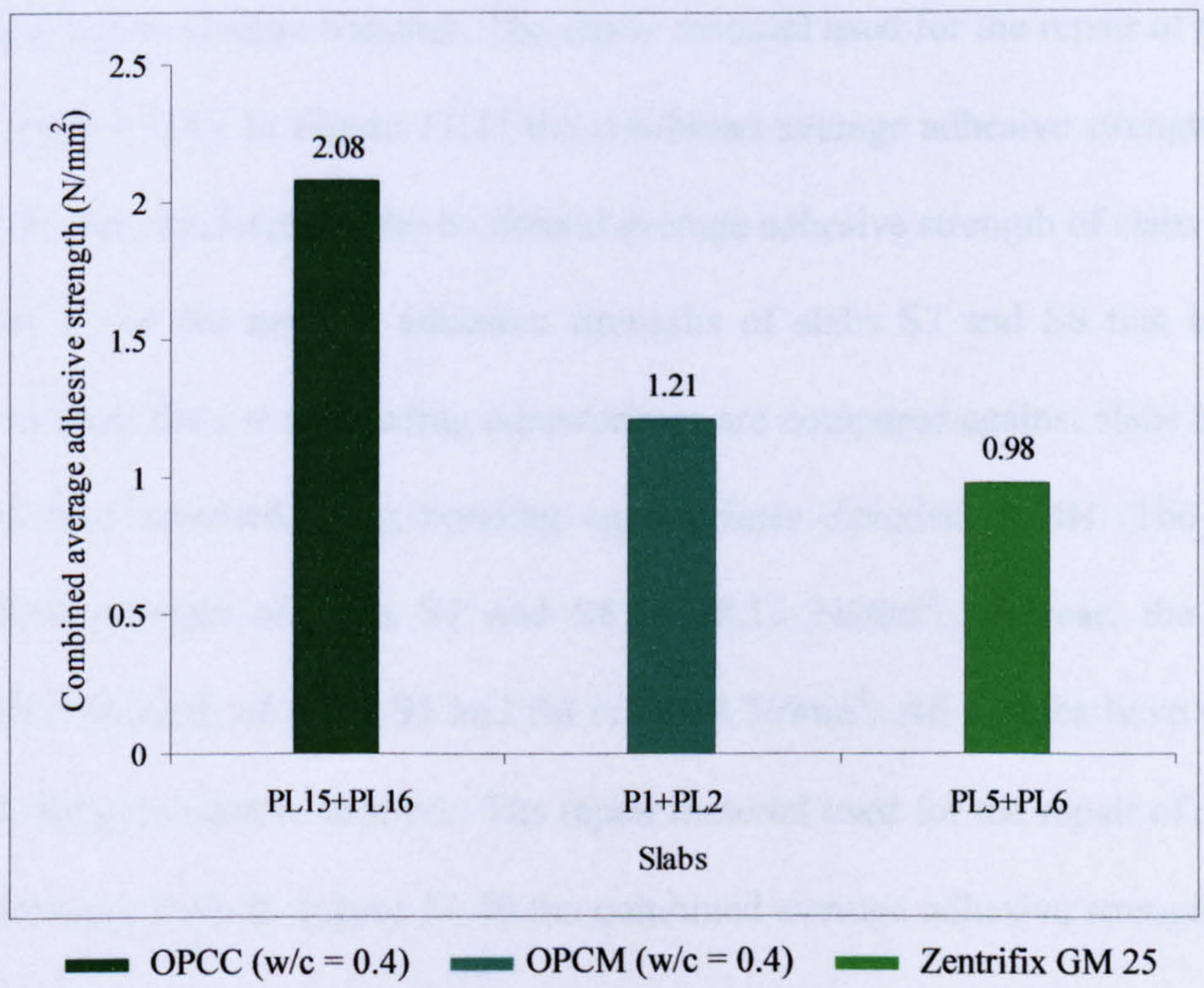

Figure 11.45 Influence of different types of generic repair material on the combined average adhesive strength of slabs PL15+PL16, P1+PL2 and PL5+PL6

11.2.2.4 Influence of the use of bonding agent/primer on the average adhesive strength

The aim of this series of comparisons is to investigate the effect of bonding agent/primer Zentrifix KMH on the adhesive strength. For this reason, the adhesive strengths of substrate specimens repaired using Zentrifix KMH are compared against specimens repaired without the use of Zentrifix KMH. The rest of the parameters which include type of substrate surface, substrate strength and type of repair material are kept constant for all specimens. Detailed information including individual adhesive strength values is provided in Figures 11.46-11.75.

In Figure 11.46 the average adhesive strengths of slabs S11 and S12 that have been repaired without the use of bonding agent/primer are compared against slabs S9 and S10 that have been repaired using bonding agent/primer Zentrifix KMH. The substrate compressive strength of slabs S11 and S12 is 55.98 N/mm^2, whereas, the substrate compressive strength of slabs S9 and S10 is 56.29 N/mm^2. All 4 slabs have substrates produced using an electric hammer. The repair material used for the repair of all 4 slabs is OPCC (w/c = 0.4). In Figure 11.47 the combined average adhesive strength of slabs S11+S12 is compared against the combined average adhesive strength of slabs S9+S10.

In Figure 11.48 the average adhesive strengths of slabs S7 and S8 that have been repaired without the use of bonding agent/primer are compared against slabs S5 and S6 that have been repaired using bonding agent/primer Zentrifix KMH. The substrate compressive strength of slabs S7 and S8 is 58.13 N/mm^2, whereas, the substrate compressive strength of slabs S5 and S6 is 57.04 N/mm^2. All 4 slabs have substrates produced using an electric hammer. The repair material used for the repair of all 4 slabs is OPCM (w/c = 0.4). In Figure 11.49 the combined average adhesive strength of slabs S7+S8 is compared against the combined average adhesive strength of slabs S5+S6.

In Figure 11.50 the average adhesive strengths of slabs S1 and S2 that have been repaired without the use of bonding agent/primer are compared against slabs S3 and S4 that have been repaired using bonding agent/primer Zentrifix KMH. The substrate compressive strength of slabs S1 and S2 is 57.77 N/mm^2, whereas, the substrate compressive strength of slabs S3 and S4 is 53.94 N/mm^2. All 4 slabs have substrates produced using an electric hammer. The repair material used for the repair of all 4 slabs is Zentrifix GM 25. In Figure 11.51 the combined average adhesive strength of slabs S1+S2 is compared against the combined average adhesive strength of slabs S3+S4.

In Figure 11.52 the average adhesive strengths of slabs S13 and S14 that have been repaired without the use of bonding agent/primer are compared against slabs S15 and S16 that have been repaired using bonding agent/primer Zentrifix KMH. The substrate compressive strength of slabs S13 and S14 is 53.59 N/mm^2, whereas, the substrate compressive strength of slabs S15 and S16 is 50.44 N/mm^2. All 4 slabs have substrates produced using an electric hammer. The repair material used for the repair of all 4 slabs is OPCC (w/c = 0.4). In Figure 11.53 the combined average adhesive strength of slabs S13+S14 is compared against the combined average adhesive strength of slabs S15+S16.

In Figure 11.54 the average adhesive strengths of slabs S17 and S18 that have been repaired without the use of bonding agent/primer are compared against slabs S19 and S20 that have been repaired using bonding agent/primer Zentrifix KMH. The substrate compressive strength of slabs S17 and S18 is 47.41 N/mm^2, whereas, the substrate compressive strength of slabs S19 and S20 is 50.19 N/mm^2. All 4 slabs have substrates produced using an electric hammer. The repair material used for the repair of all 4 slabs is OPCM (w/c = 0.4). In Figure 11.55 the combined average adhesive strength of slabs

S17+S18 is compared against the combined average adhesive strength of slabs S19+S20.

In Figure 11.56 the average adhesive strengths of slabs S23 and S24 that have been repaired without the use of bonding agent/primer are compared against slabs S21 and S22 that have been repaired using bonding agent/primer Zentrifix KMH. The substrate compressive strength of slabs S23 and S24 is 52.56 N/mm^2, whereas, the substrate compressive strength of slabs S21 and S22 is 53.54 N/mm^2. All 4 slabs have substrates produced using an electric hammer. The repair material used for the repair of all 4 slabs is Zentrifix GM 25. In Figure 11.57 the combined average adhesive strength of slabs S23+S24 is compared against the combined average adhesive strength of slabs S21+S22.

In Figure 11.58 the average adhesive strengths of slabs S25 and S26 that have been repaired without the use of bonding agent/primer are compared against slabs S27 and S28 that have been repaired using bonding agent/primer Zentrifix KMH. The substrate compressive strength of slabs S25 and S26 is 42.42 N/mm^2, whereas, the substrate compressive strength of slabs S27 and S28 is 43.72 N/mm^2. All 4 slabs have substrates produced using an electric hammer. The repair material used for the repair of all 4 slabs is OPCC (w/c = 0.4). In Figure 11.59 the combined average adhesive strength of slabs S25+S26 is compared against the combined average adhesive strength of slabs S27+S28.

In Figure 11.60 the average adhesive strengths of slabs S29 and S30 that have been repaired without the use of bonding agent/primer are compared against slabs S31 and S32 that have been repaired using bonding agent/primer Zentrifix KMH. The substrate compressive strength of slabs S29 and S30 is 46.23 N/mm^2, whereas, the substrate compressive strength of slabs S31 and S32 is 42.92 N/mm^2. All 4 slabs have substrates

produced using an electric hammer. The repair material used for the repair of all 4 slabs is OPCM (w/c = 0.4). In Figure 11.61 the combined average adhesive strength of slabs S29+S30 is compared against the combined average adhesive strength of slabs S31+S32.

In Figure 11.62 the average adhesive strengths of slabs S33 and S34 that have been repaired without the use of bonding agent/primer are compared against slabs S35 and S36 that have been repaired using bonding agent/primer Zentrifix KMH. The substrate compressive strength of slabs S33 and S34 is 43.50 N/mm^2, whereas, the substrate compressive strength of slabs S35 and S36 is 41.10 N/mm^2. All 4 slabs have substrates produced using an electric hammer. The repair material used for the repair of all 4 slabs is Zentrifix GM 25. In Figure 11.63 the combined average adhesive strength of slabs S33+S34 is compared against the combined average adhesive strength of slabs S35+S36.

In Figure 11.64 the average adhesive strengths of slabs S37 and S38 that have been repaired without the use of bonding agent/primer are compared against slabs S39 and S40 that have been repaired using bonding agent/primer Zentrifix KMH. The substrate compressive strength of slabs S37 and S38 is 40.39 N/mm^2, whereas, the substrate compressive strength of slabs S39 and S40 is 40.27 N/mm^2. All 4 slabs have substrates produced using an electric hammer. The repair material used for the repair of all 4 slabs is OPCC (w/c = 0.4). In Figure 11.65 the combined average adhesive strength of slabs S37+S38 is compared against the combined average adhesive strength of slabs S39+S40.

In Figure 11.66 the average adhesive strengths of slabs S43 and S44 that have been repaired without the use of bonding agent/primer are compared against slabs S41 and S42 that have been repaired using bonding agent/primer Zentrifix KMH. The substrate

compressive strength of slabs S43 and S44 is 37.14 N/mm^2, whereas, the substrate compressive strength of slabs S41 and S42 is 39.49 N/mm^2. All 4 slabs have substrates produced using an electric hammer. The repair material used for the repair of all 4 slabs is OPCM (w/c = 0.4). In Figure 11.67 the combined average adhesive strength of slabs S43+S44 is compared against the combined average adhesive strength of slabs S41+S42.

In Figure 11.68 the average adhesive strengths of slabs S47 and S48 that have been repaired without the use of bonding agent/primer are compared against slabs S45 and S46 that have been repaired using bonding agent/primer Zentrifix KMH. The substrate compressive strength of slabs S47 and S48 is 39.14 N/mm^2, whereas, the substrate compressive strength of slabs S45 and S46 is 41.15 N/mm^2. All 4 slabs have substrates produced using an electric hammer. The repair material used for the repair of all 4 slabs is Zentrifix GM 25. In Figure 11.69 the combined average adhesive strength of slabs S47+S48 is compared against the combined average adhesive strength of slabs S45+S46.

In Figure 11.70 the average adhesive strengths of slabs P5 and PL14 that have been repaired without the use of bonding agent/primer are compared against slabs PL15 and PL16 that have been repaired using bonding agent/primer Zentrifix KMH. The substrate compressive strengths of slabs P5 and PL14 are 51.75 and 64.20 N/mm^2, respectively. The substrate compressive strength of slabs PL15 and PL16 is 47.81 N/mm^2. All 4 slabs have substrates produced using remote robotic hydroerosion. The repair material used for the repair of all 4 slabs is OPCC (w/c = 0.4). In Figure 11.71 the combined average adhesive strength of slabs P5+PL14 is compared against the combined average adhesive strength of slabs PL15+PL16.

In Figure 11.72 the average adhesive strengths of slabs PL11 and PL13 that have been repaired without the use of bonding agent/primer are compared against slabs P1 and PL2 that have been repaired using bonding agent/primer Zentrifix KMH. The substrate compressive strength of slabs PL11 and PL13 is 51.28 N/mm^2, whereas, the substrate compressive strengths of slabs P1 and PL2 are 53.75 and 57.35 N/mm^2, respectively. All 4 slabs have substrates produced using remote robotic hydroerosion. The repair material used for the repair of all 4 slabs is OPCM (w/c = 0.4). In Figure 11.73 the combined average adhesive strength of slabs PL11+PL13 is compared against the combined average adhesive strength of slabs P1+PL2.

In Figure 11.74 the average adhesive strengths of slabs PL9 and PL10 that have been repaired without the use of bonding agent/primer are compared against slabs PL5 and PL6 that have been repaired using bonding agent/primer Zentrifix KMH. The substrate compressive strength of slabs PL9 and PL10 is 50.08 N/mm^2, whereas, the substrate compressive strengths of slabs PL5 and PL6 is 52.95 N/mm^2. All 4 slabs have substrates produced using remote robotic hydroerosion. The repair material used for the repair of all 4 slabs is Zentrifix GM 25. In Figure 11.75 the combined average adhesive strength of slabs PL9+PL10 is compared against the combined average adhesive strength of slabs PL5+PL6.

From the above comparisons it is clear that in 11 out of 15 cases specimens repaired using bonding agent/primer Zentrifix KMH provide higher adhesive strength values when compared to specimens repaired without the use of bonding agent/primer. In addition, bonding agent/primer Zentrifix KMH seems to improve adhesive strength when applied to both types of substrate surfaces. However, it should be noted that the use of bonding agents/primers should closely follow the manufacturer's guidelines. This

usually means that the repair material should be applied immediately after the application of the bonding/agent primer when the bonding agent/primer is still wet.

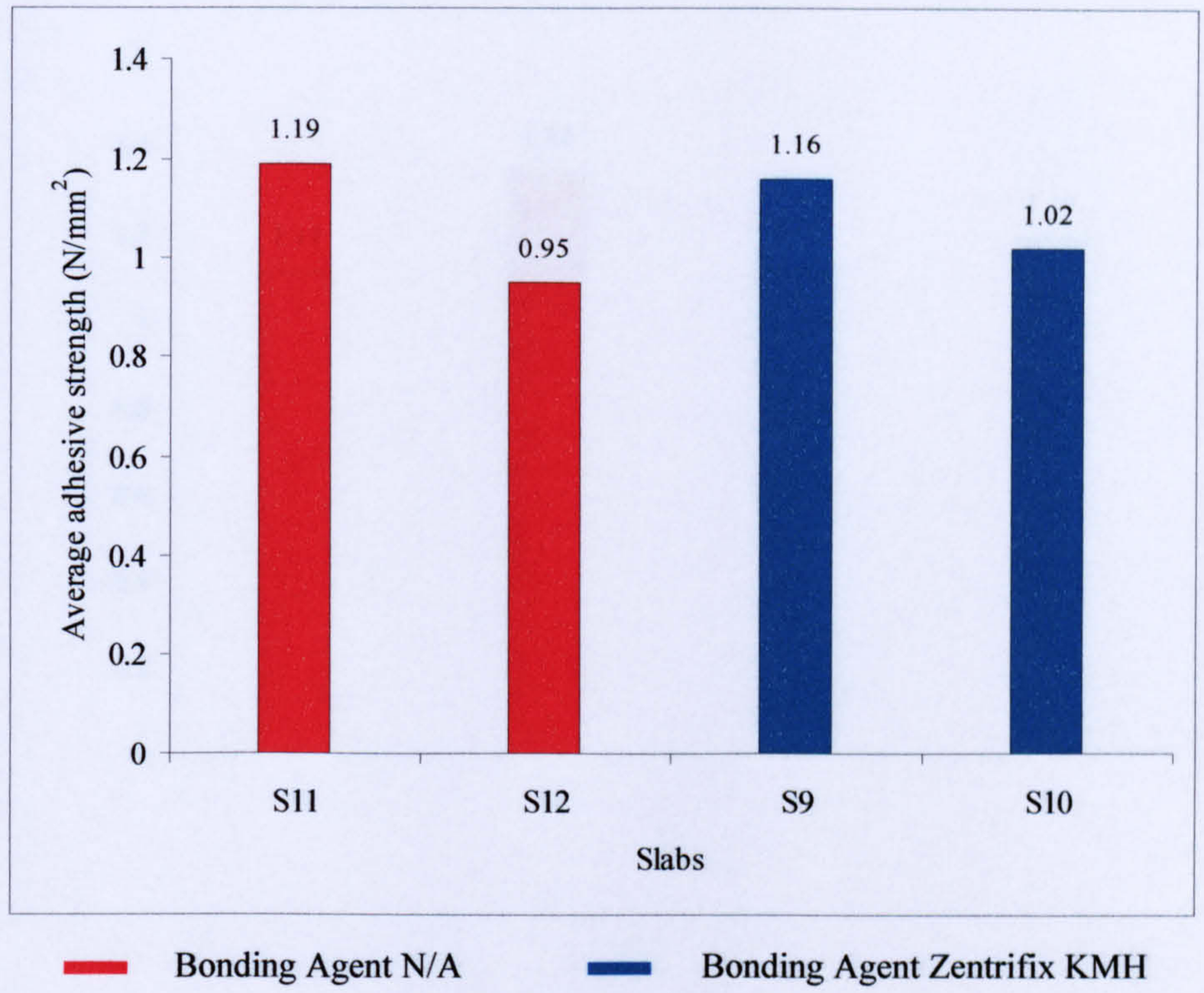

Figure 11.46 Influence of bonding agent Zentrifix KMH on the average adhesive strength of slabs S11, S12, S9 and S10

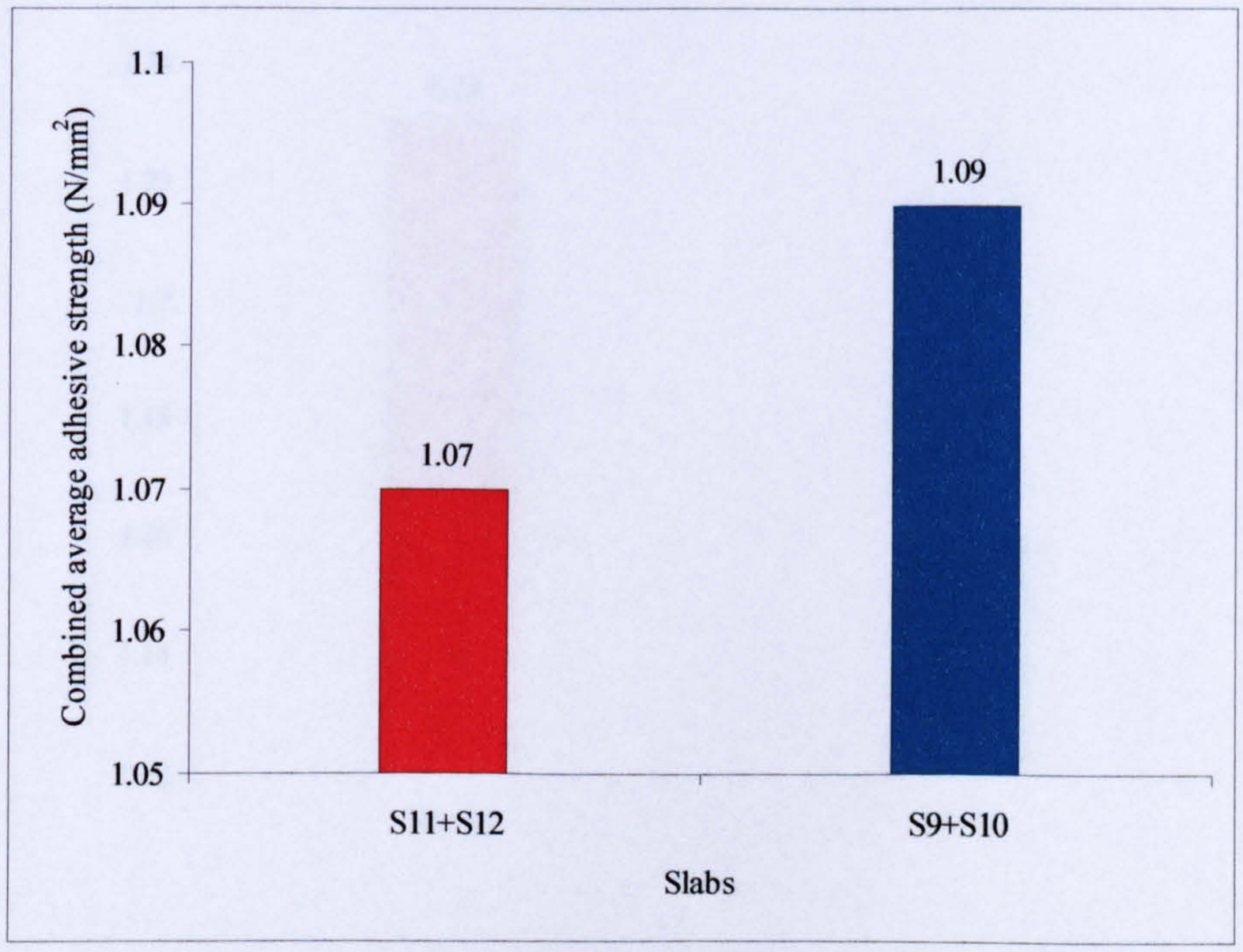

Figure 11.47 Influence of bonding agent Zentrifix KMH on the combined average adhesive strength of slabs S11+S12 and S9+S10

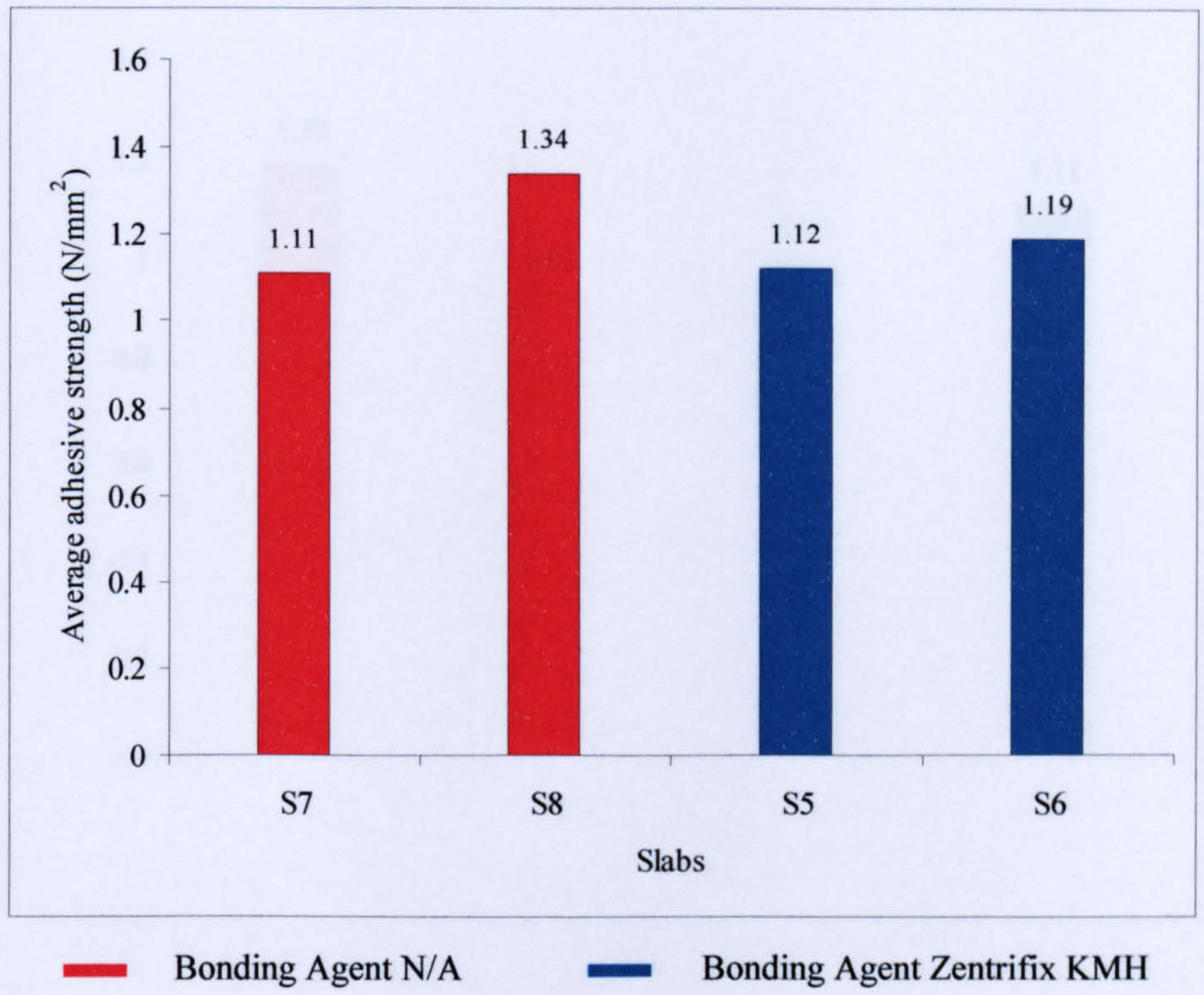

Figure 11.48 Influence of bonding agent Zentrifix KMH on the average adhesive strength of slabs S7, S8, S5 and S6

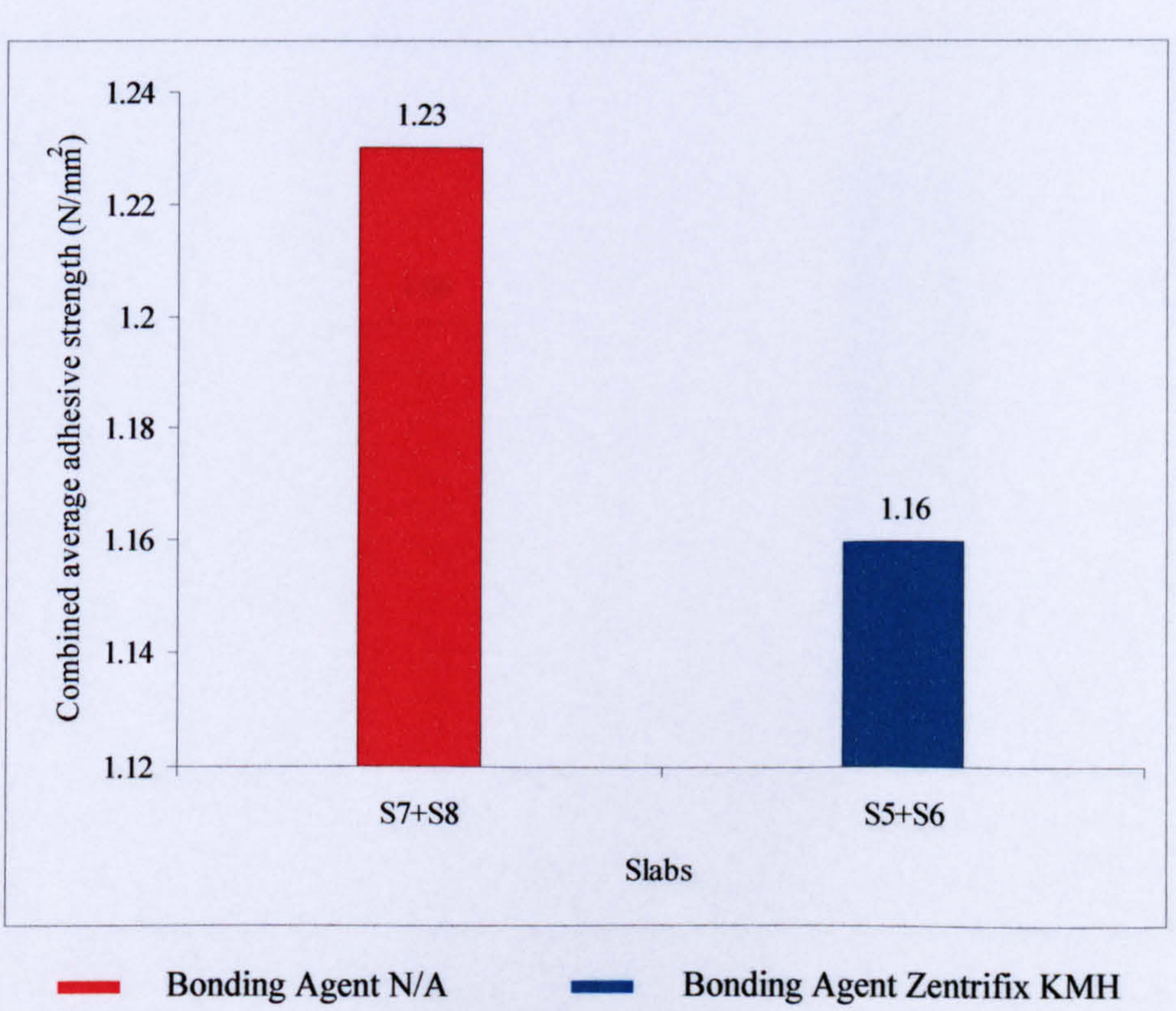

Figure 11.49 Influence of bonding agent Zentrifix KMH on the combined average adhesive strength of slabs S7+S8 and S5+S6

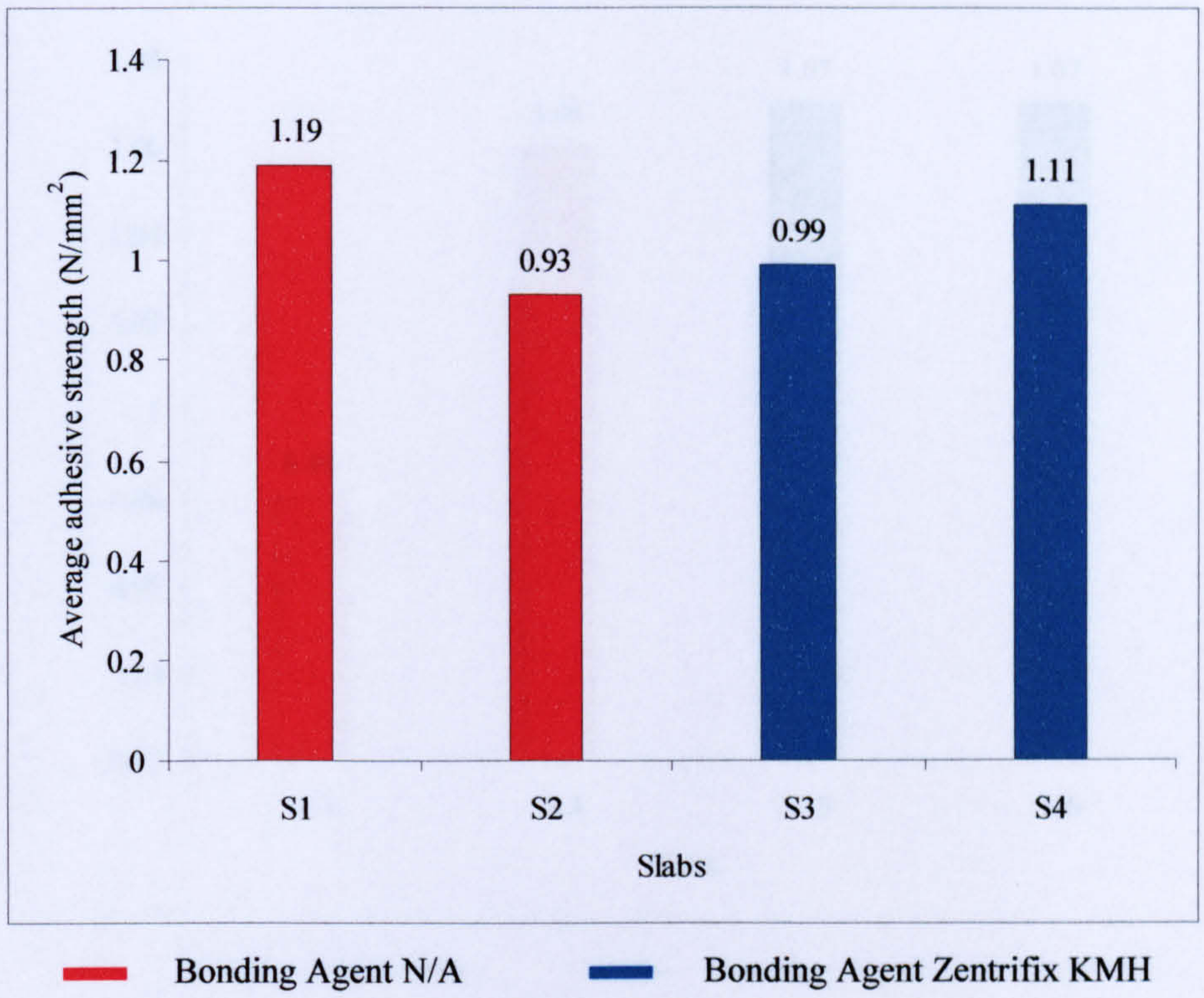

Figure 11.50 Influence of bonding agent Zentrifix KMH on the average adhesive strength of slabs S1, S2, S3 and S4

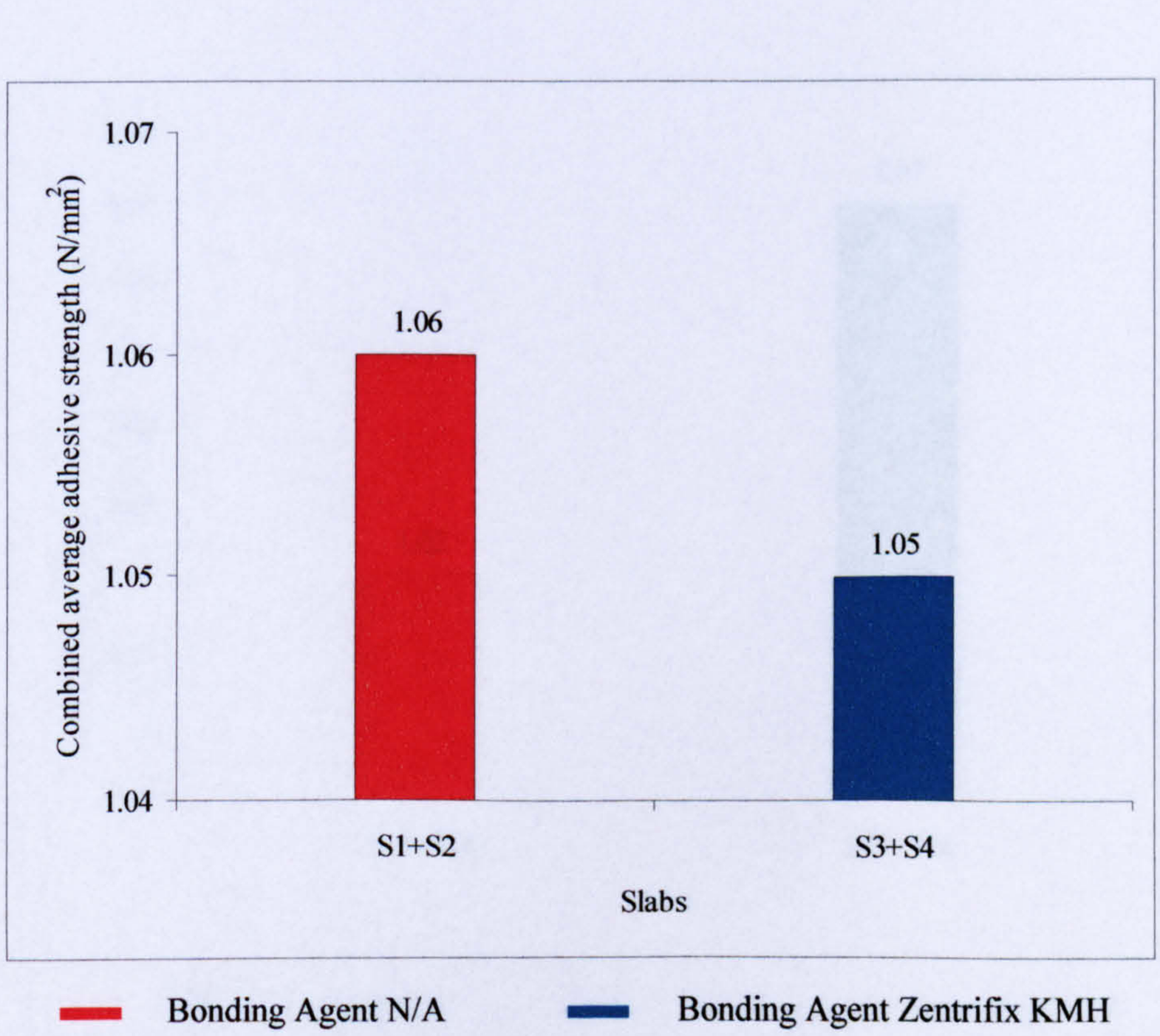

Figure 11.51 Influence of bonding agent Zentrifix KMH on the combined average adhesive strength of slabs S1+S2 and S3+S4

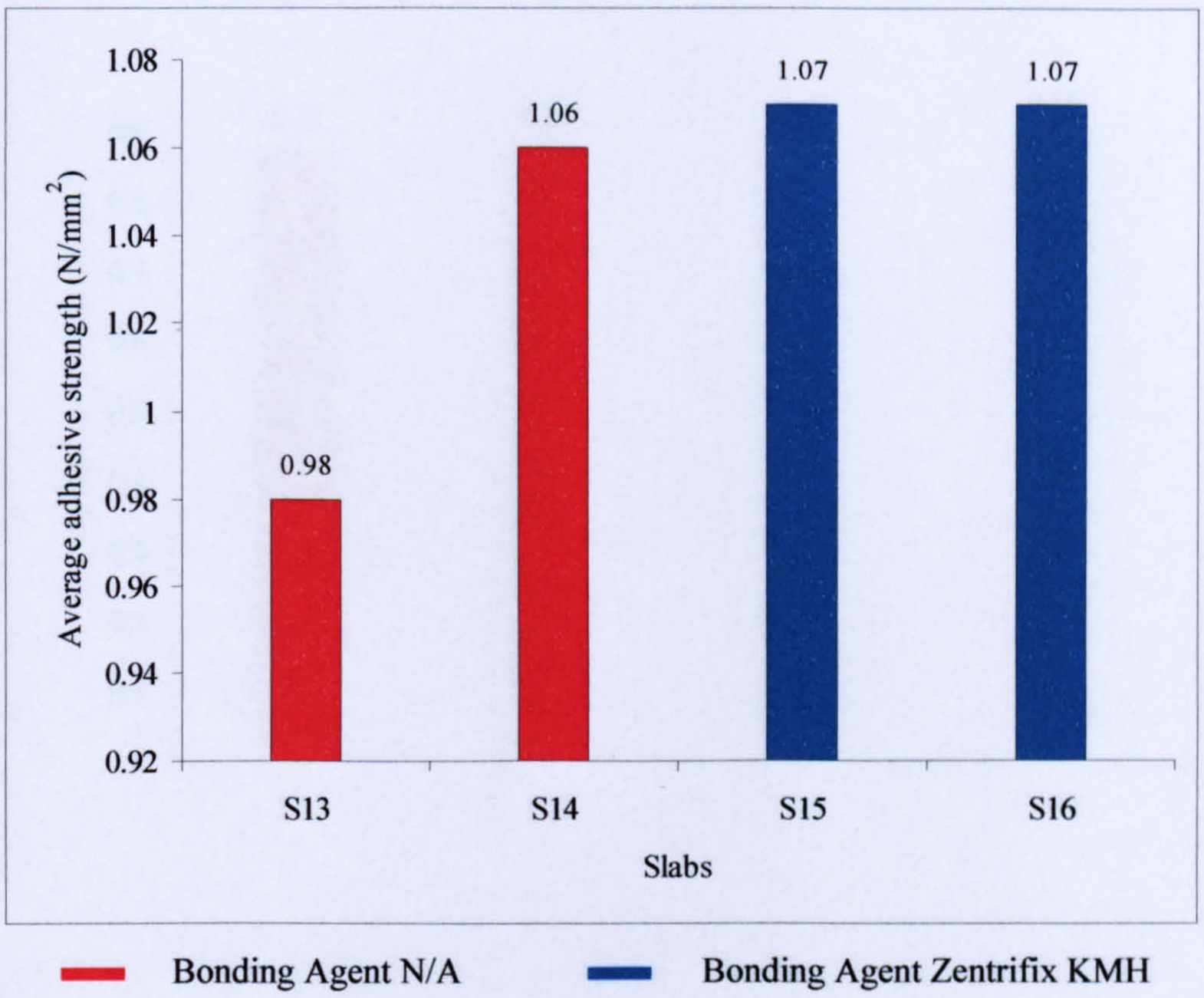

Figure 11.52 Influence of bonding agent Zentrifix KMH on the average adhesive strength of slabs S13, S14, S15 and S16

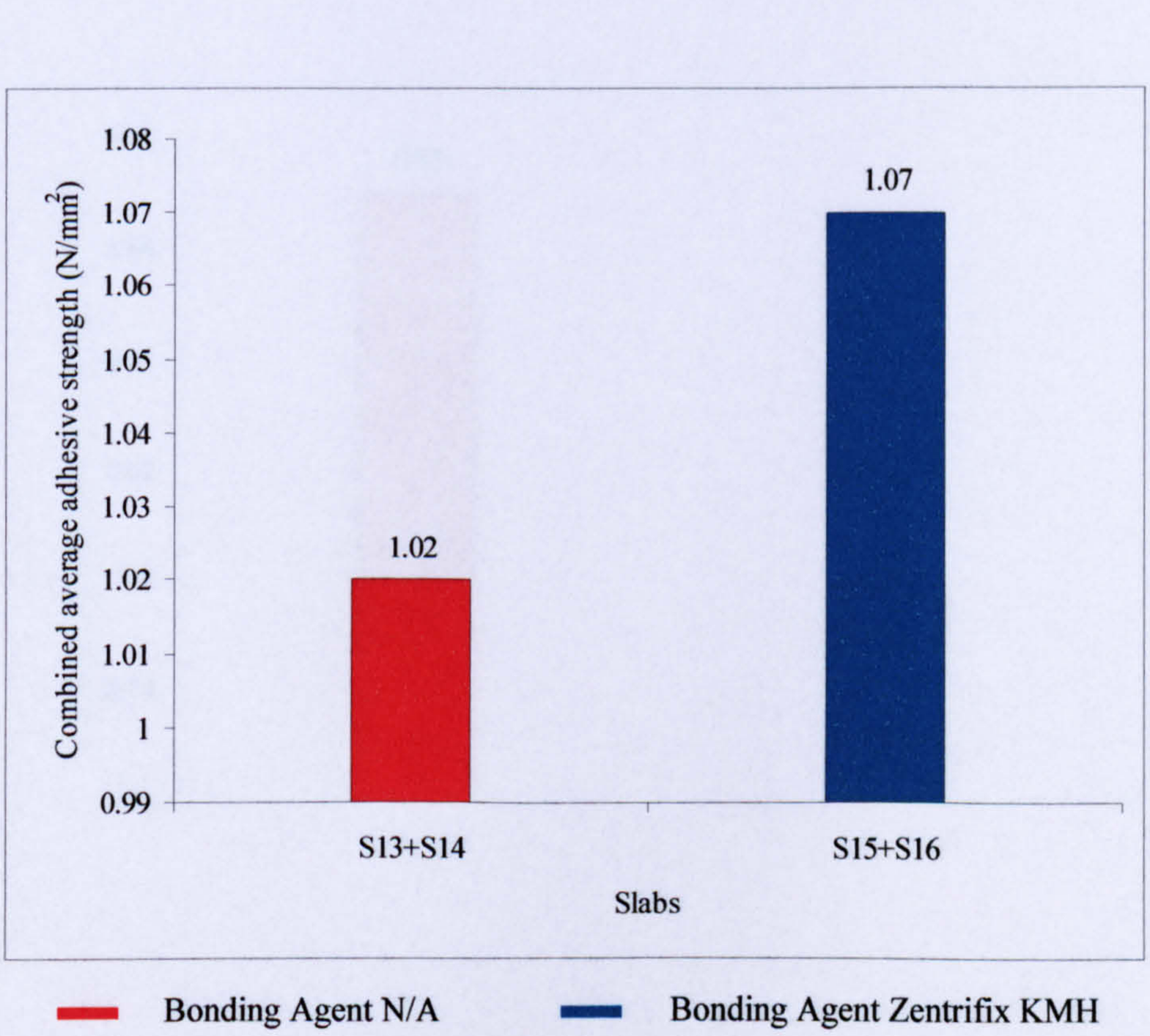

Figure 11.53 Influence of bonding agent Zentrifix KMH on the combined average adhesive strength of slabs S13+S14 and S15+S16

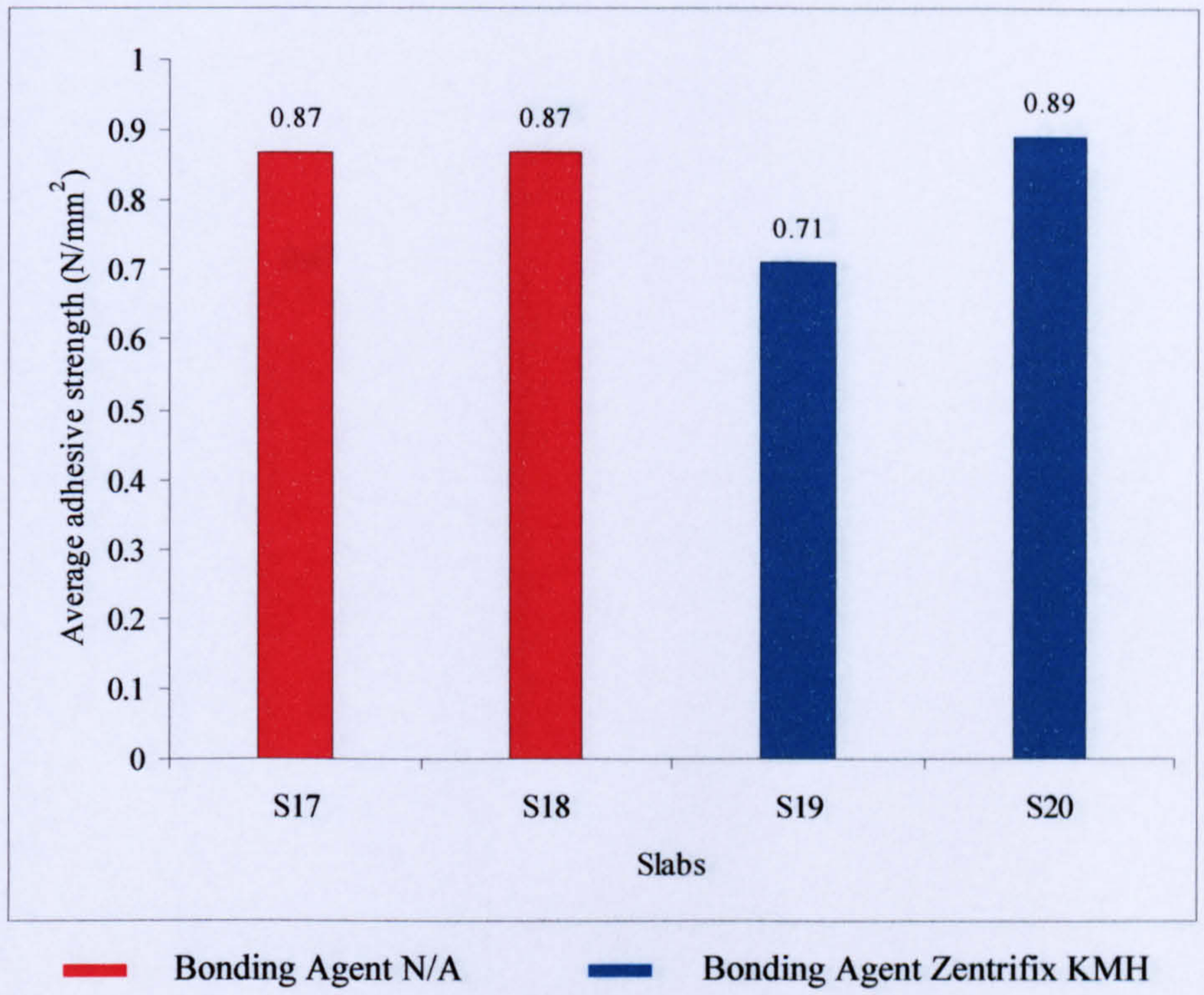

Figure 11.54 Influence of bonding agent Zentrifix KMH on the average adhesive strength of slabs S17, S18, S19 and S20

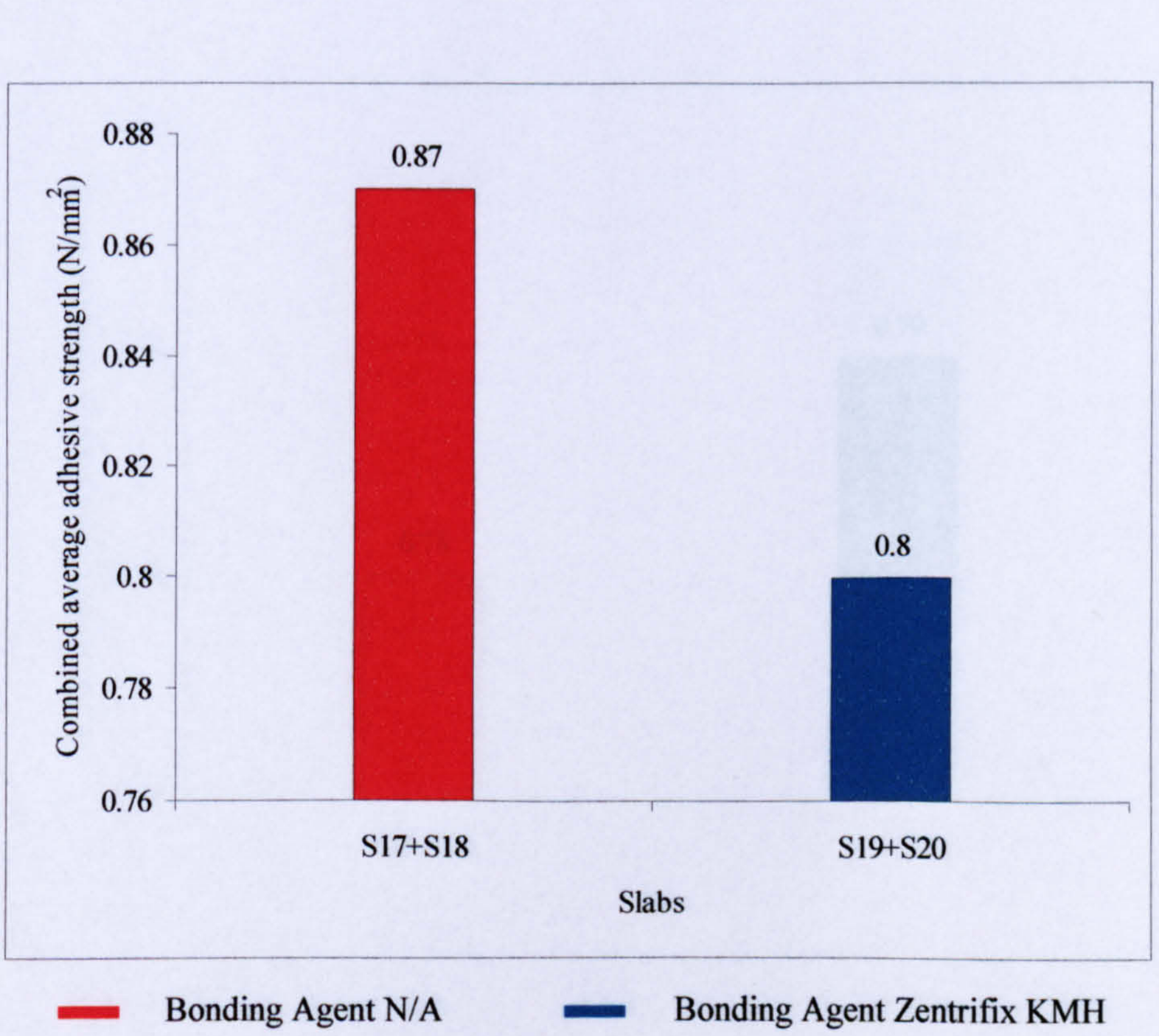

Figure 11.55 Influence of bonding agent Zentrifix KMH on the combined average adhesive strength of slabs S17+S18 and S19+S20

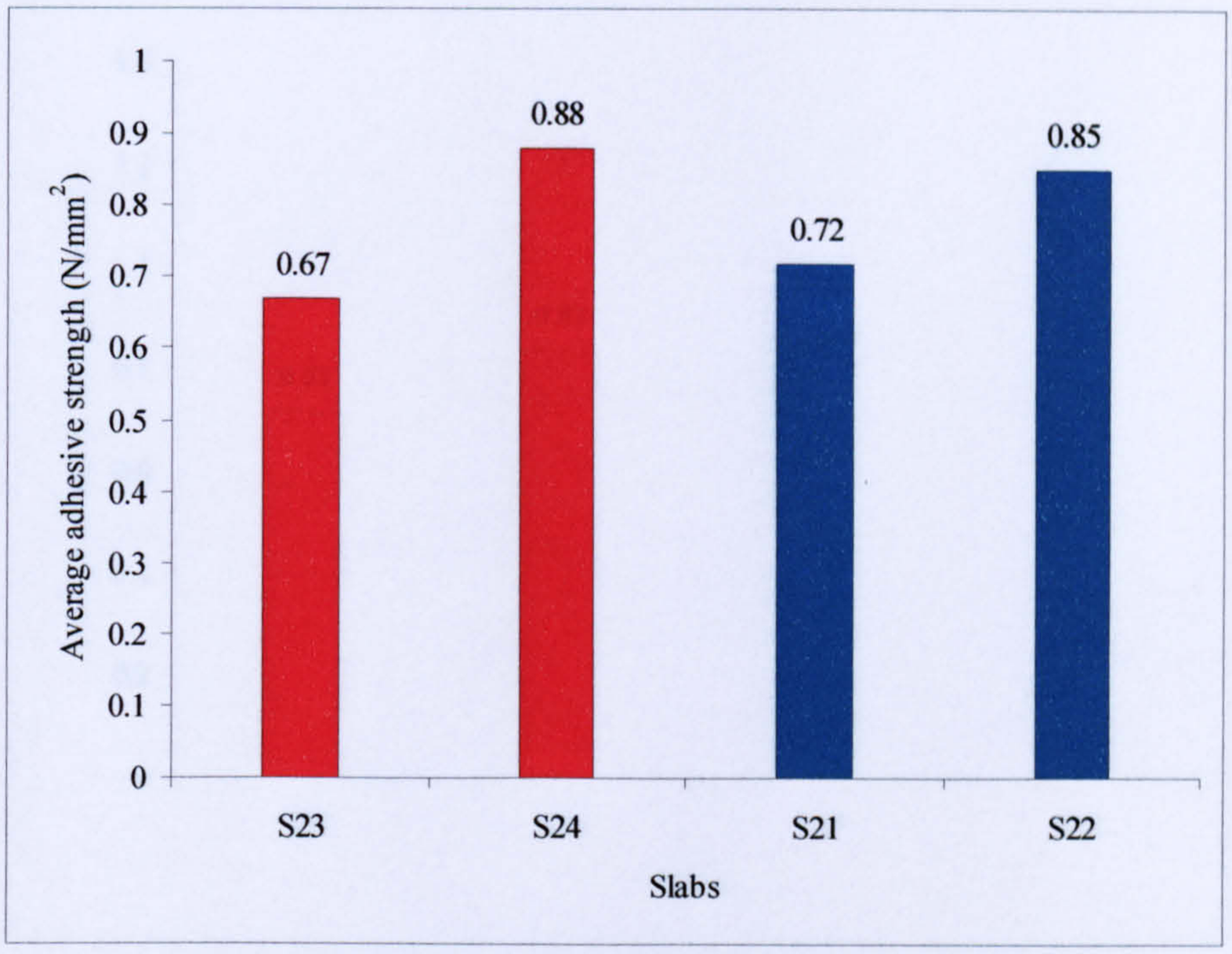

Figure 11.56 Influence of bonding agent Zentrifix KMH on the average adhesive strength of slabs S23, S24, S21 and S22

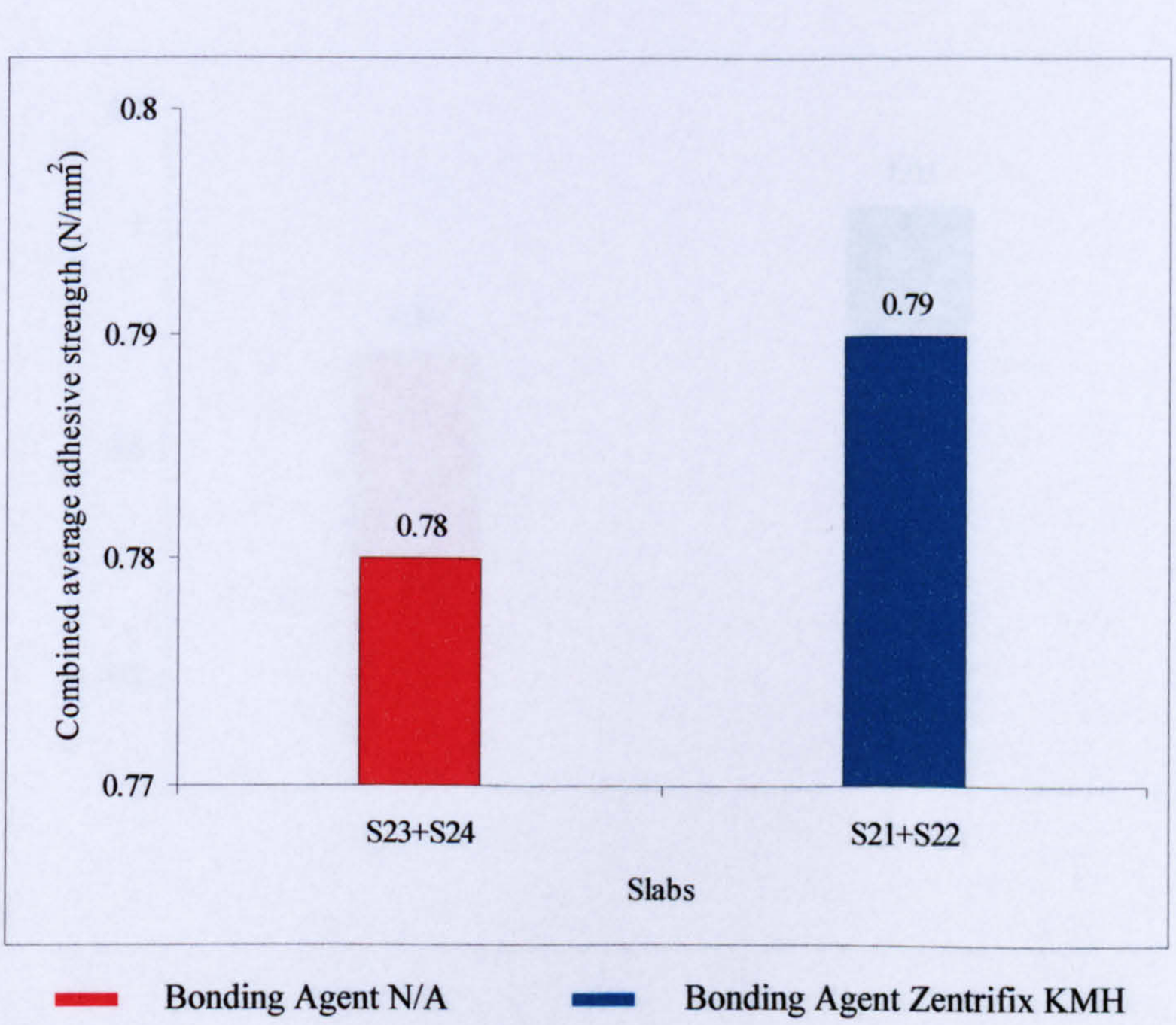

Figure 11.57 Influence of bonding agent Zentrifix KMH on the combined average adhesive strength of slabs S23+S24 and S21+S22

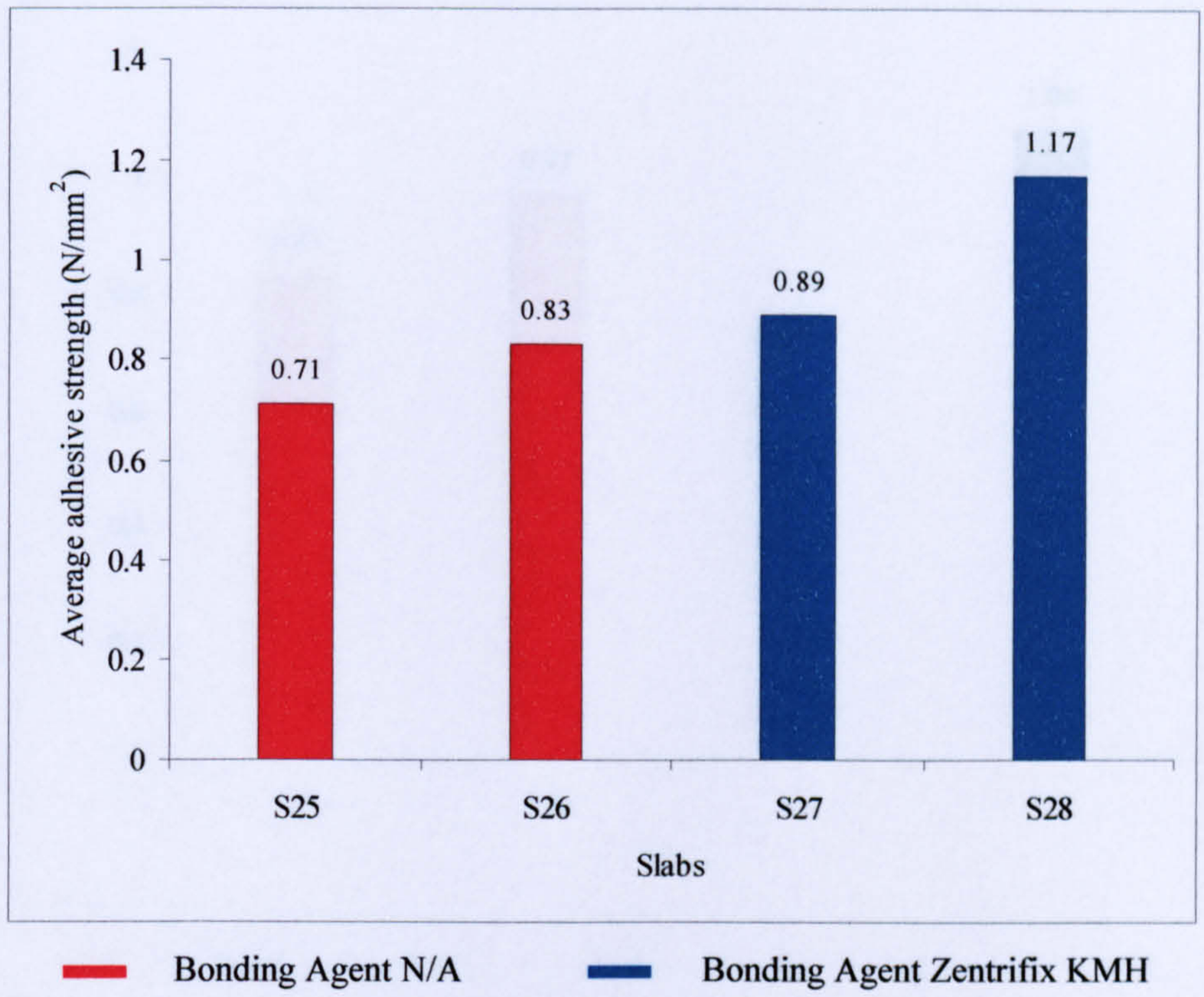

Figure 11.58 Influence of bonding agent Zentrifix KMH on the average adhesive strength of slabs S25, S26, S27 and S28

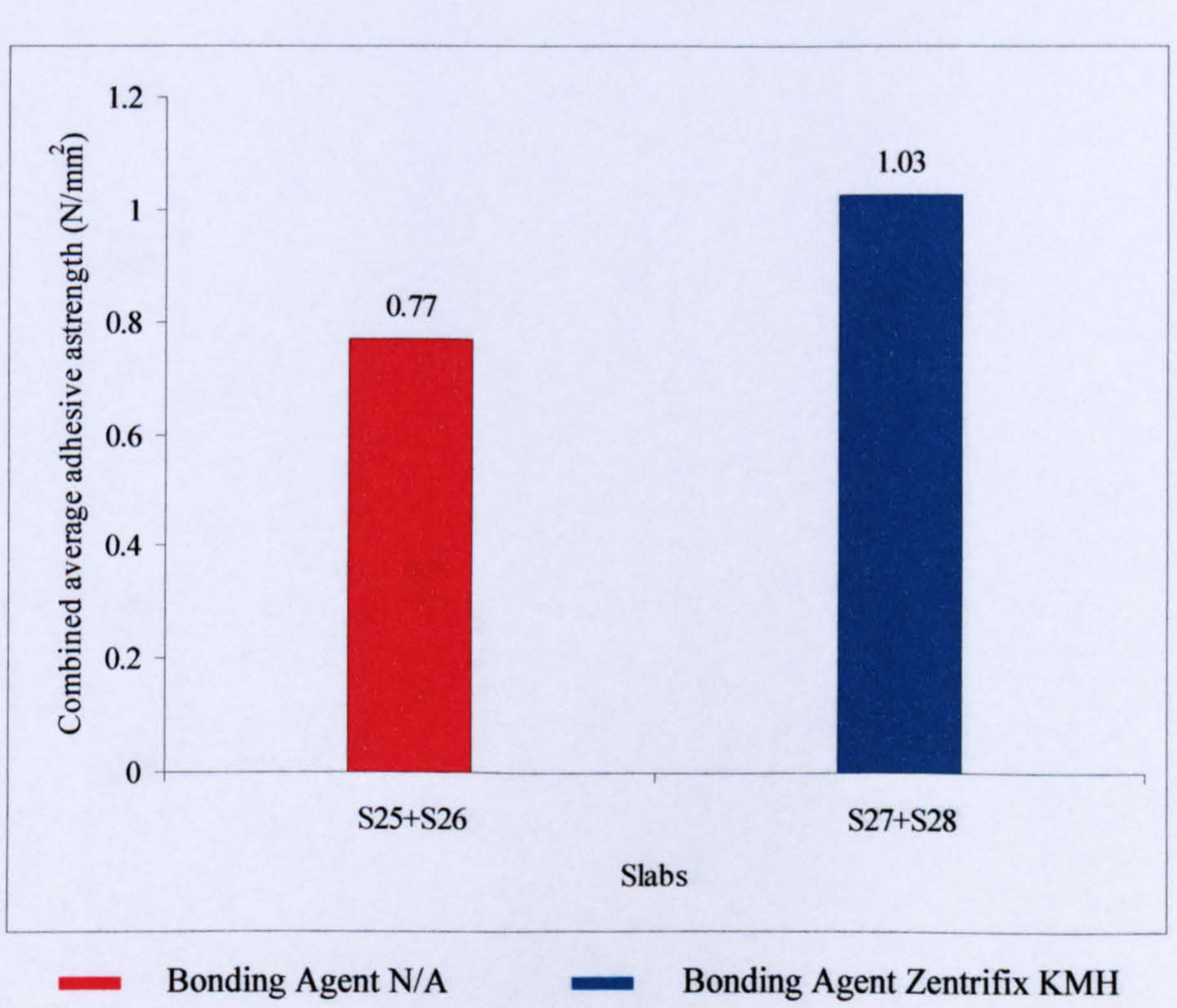

Figure 11.59 Influence of bonding agent Zentrifix KMH on the combined average adhesive strength of slabs S25+S26 and S27+S28

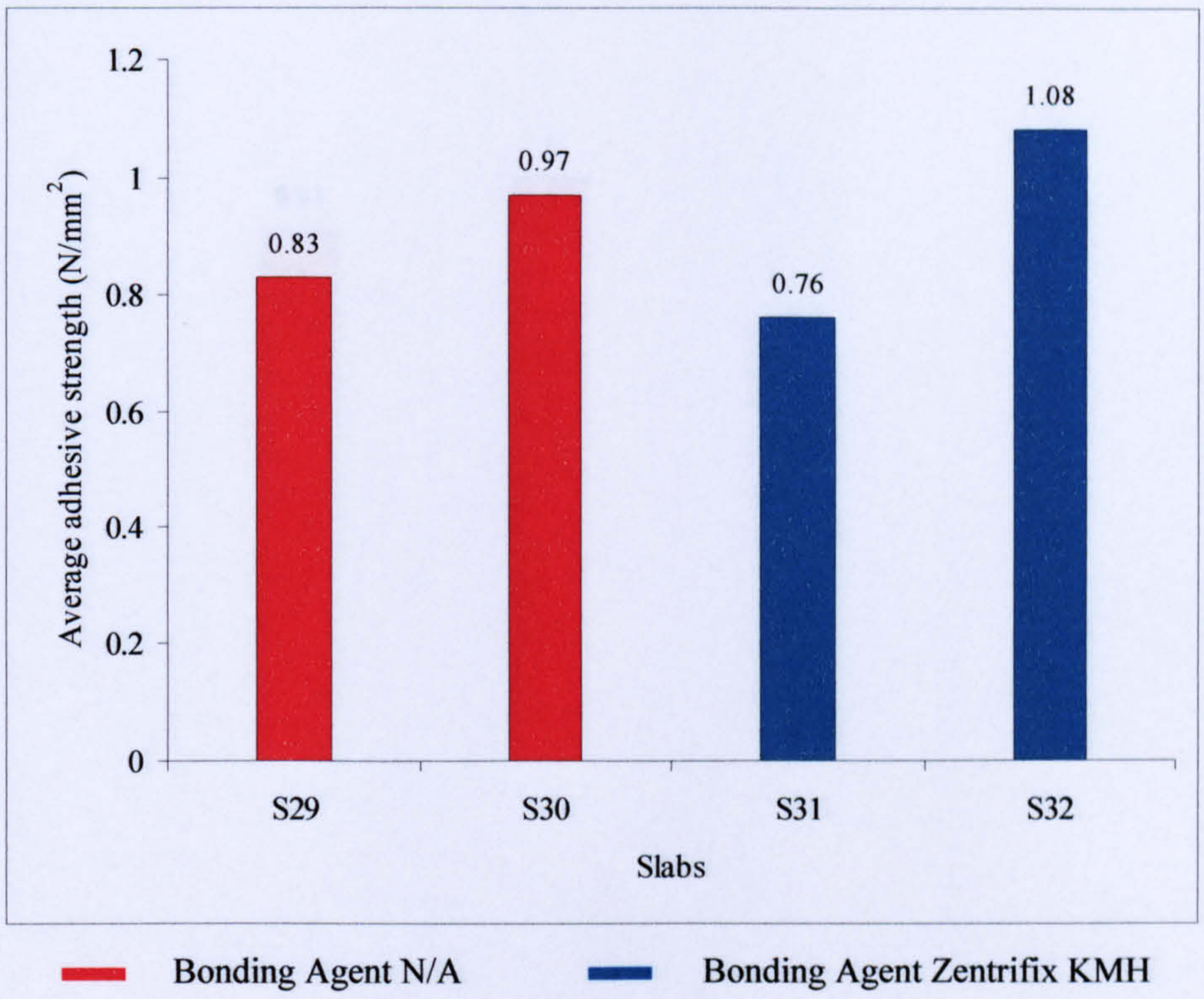

Figure 11.60 Influence of bonding agent Zentrifix KMH on the average adhesive strength of slabs S29, S30, S31 and S32

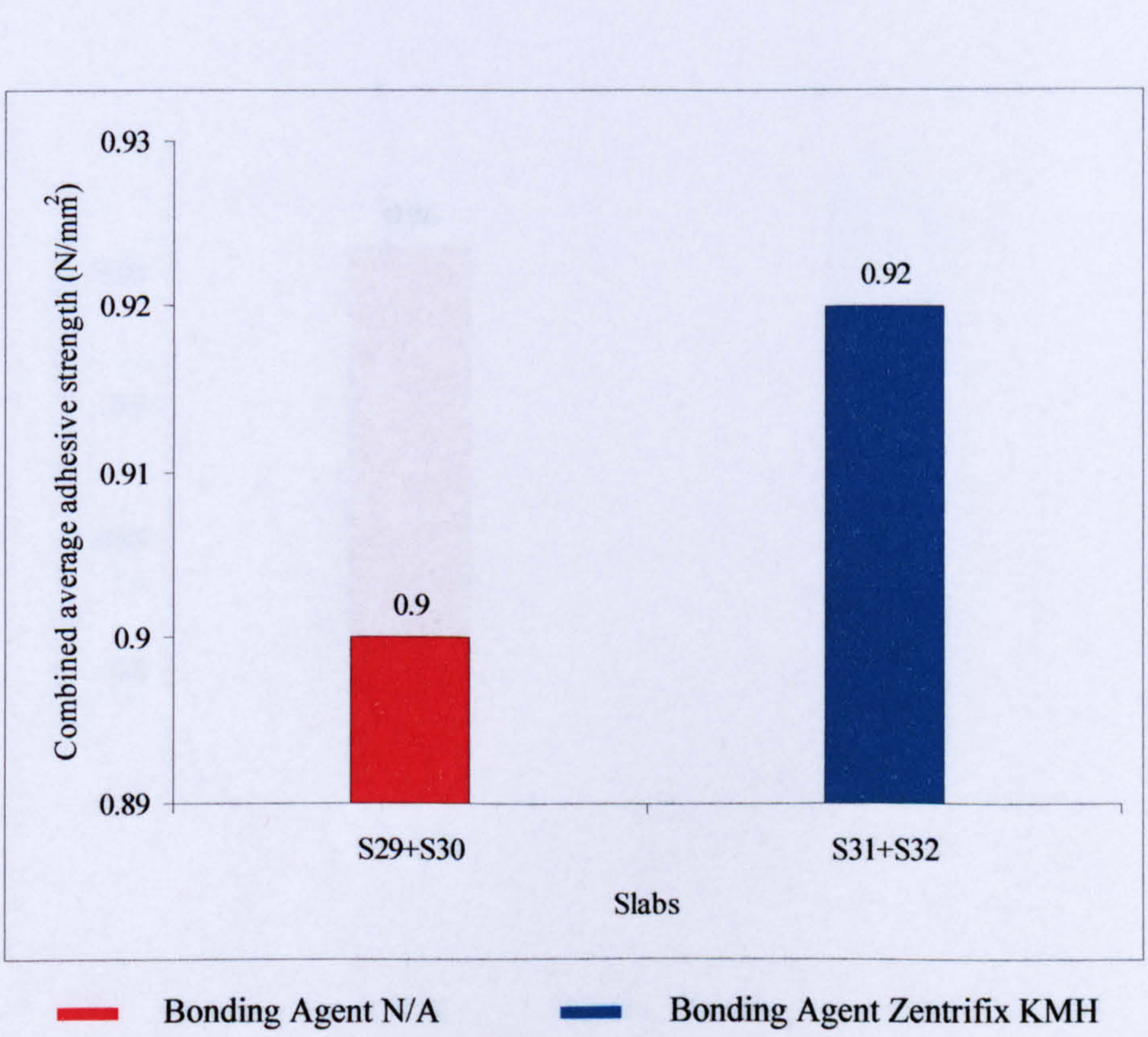

Figure 11.61 Influence of bonding agent Zentrifix KMH on the combined average adhesive strength of slabs S29+S30 and S31+S32

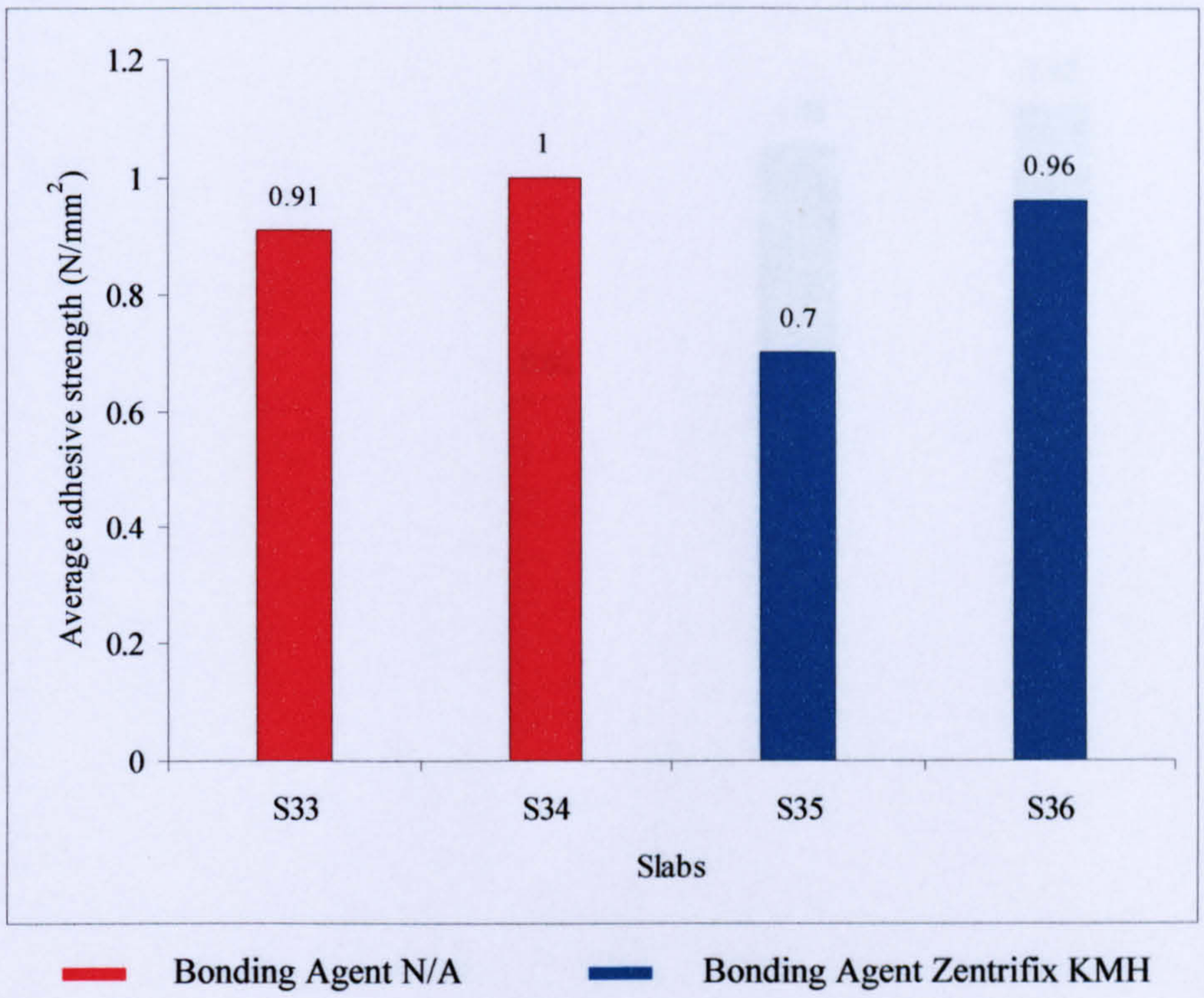

Figure 11.62 Influence of bonding agent Zentrifix KMH on the average adhesive strength of slabs S33, S34, S35 and S36

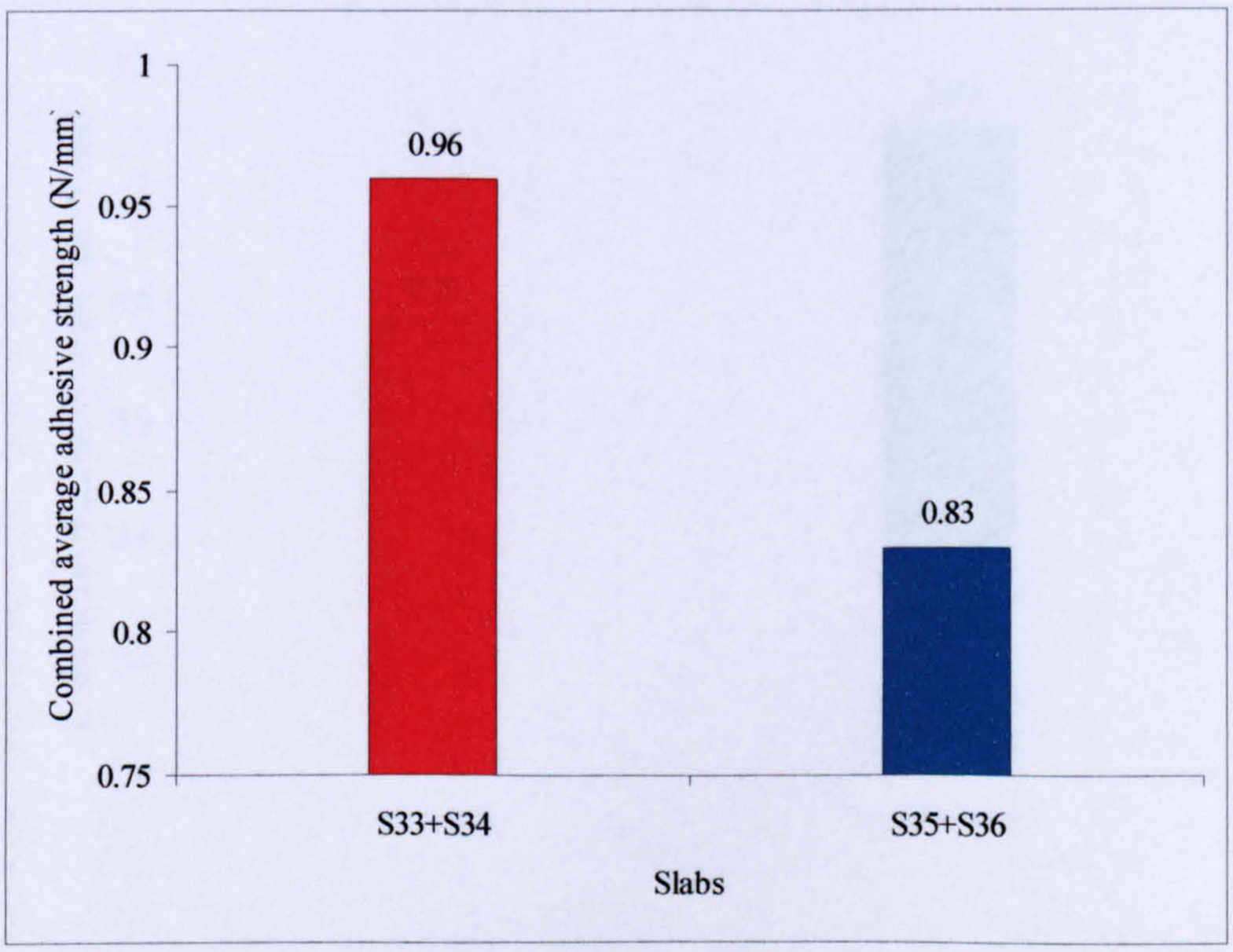

Figure 11.63 Influence of bonding agent Zentrifix KMH on the combined average adhesive strength of slabs S33+S34 and S35+S36

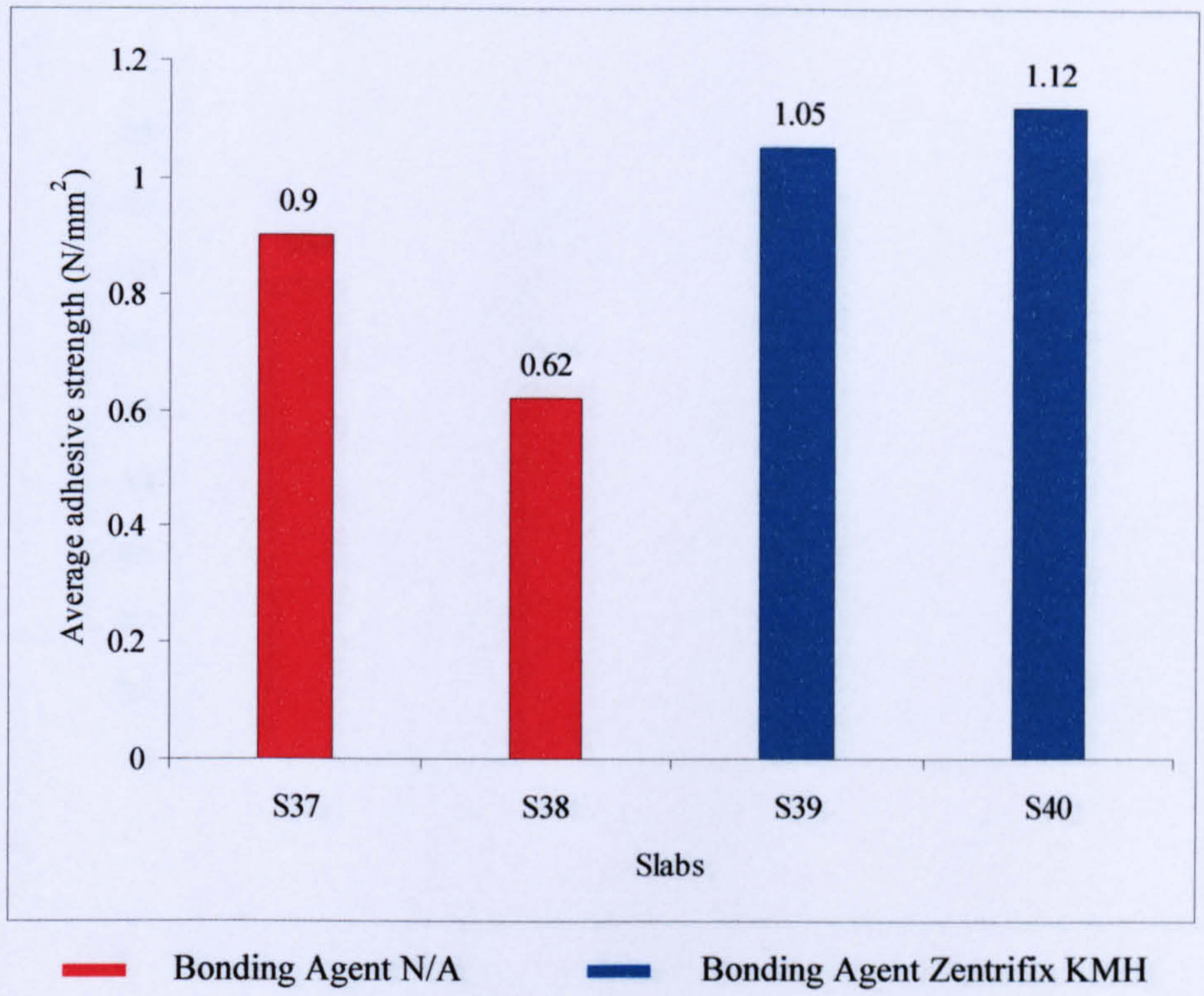

Figure 11.64 Influence of bonding agent Zentrifix KMH on the average adhesive strength of slabs S37, S38, S39 and S40

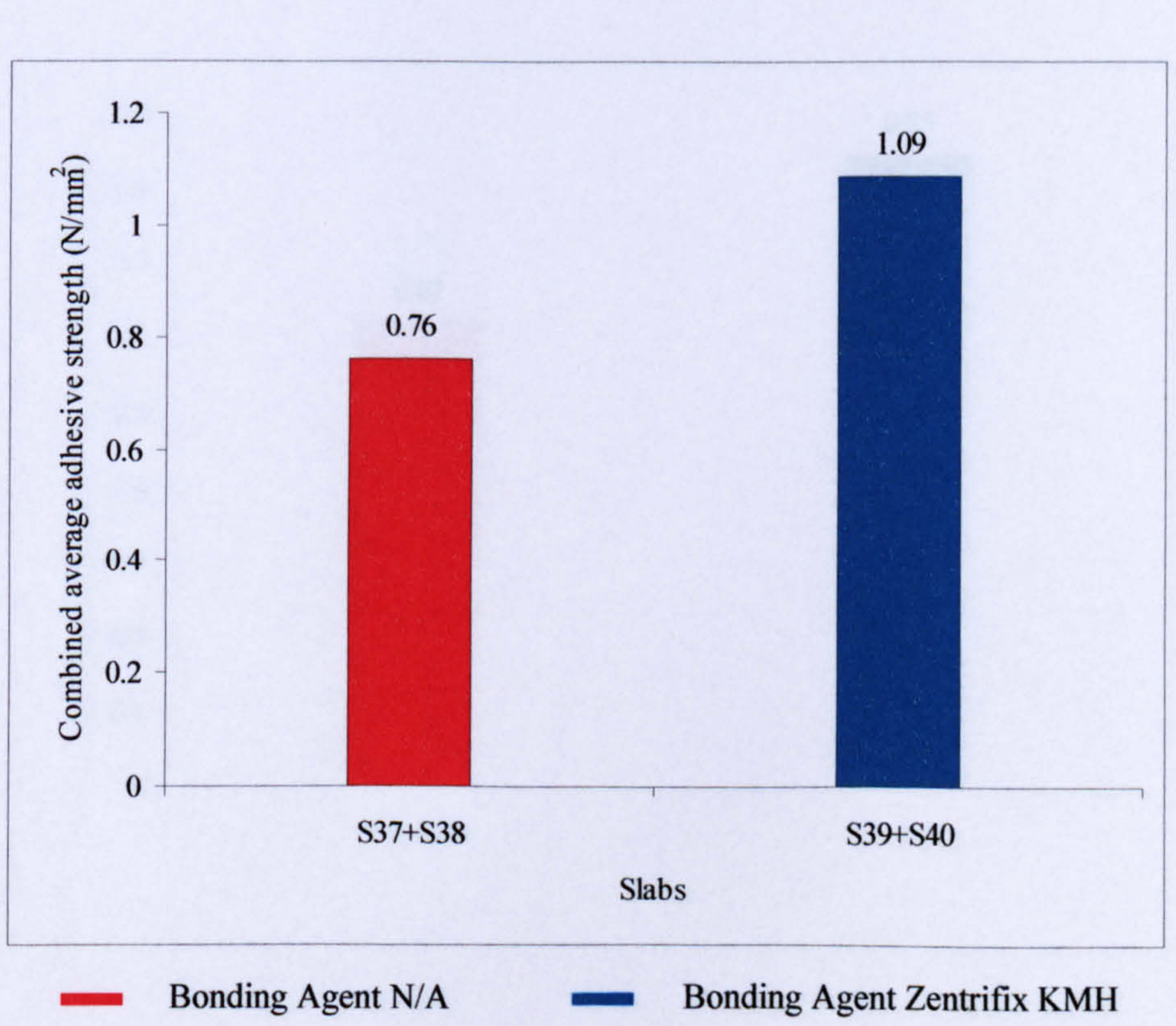

Figure 11.65 Influence of bonding agent Zentrifix KMH on the combined average adhesive strength of slabs S37+S38 and S39+S40

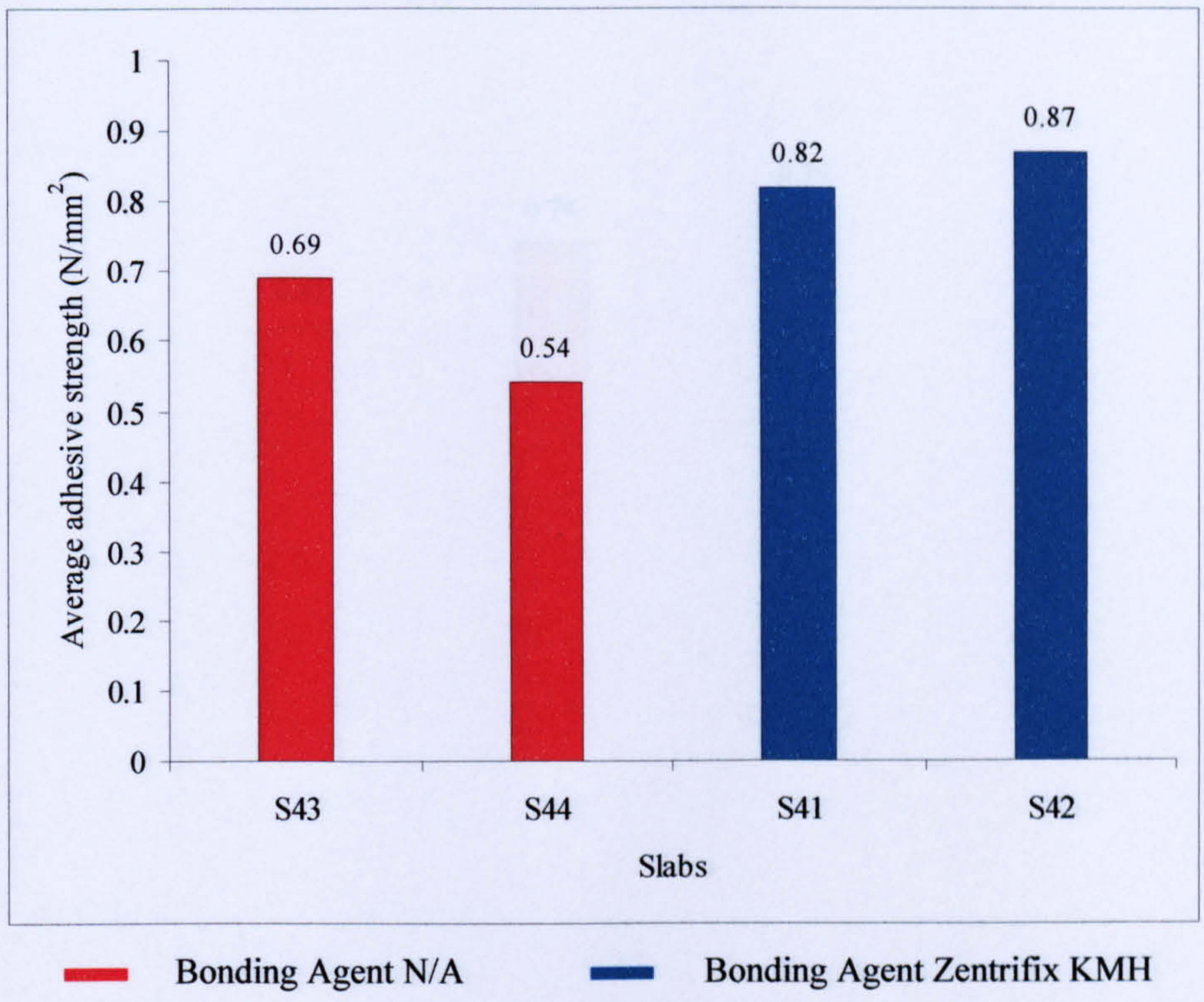

Figure 11.66 Influence of bonding agent Zentrifix KMH on the average adhesive strength of slabs S43, S44, S41 and S42

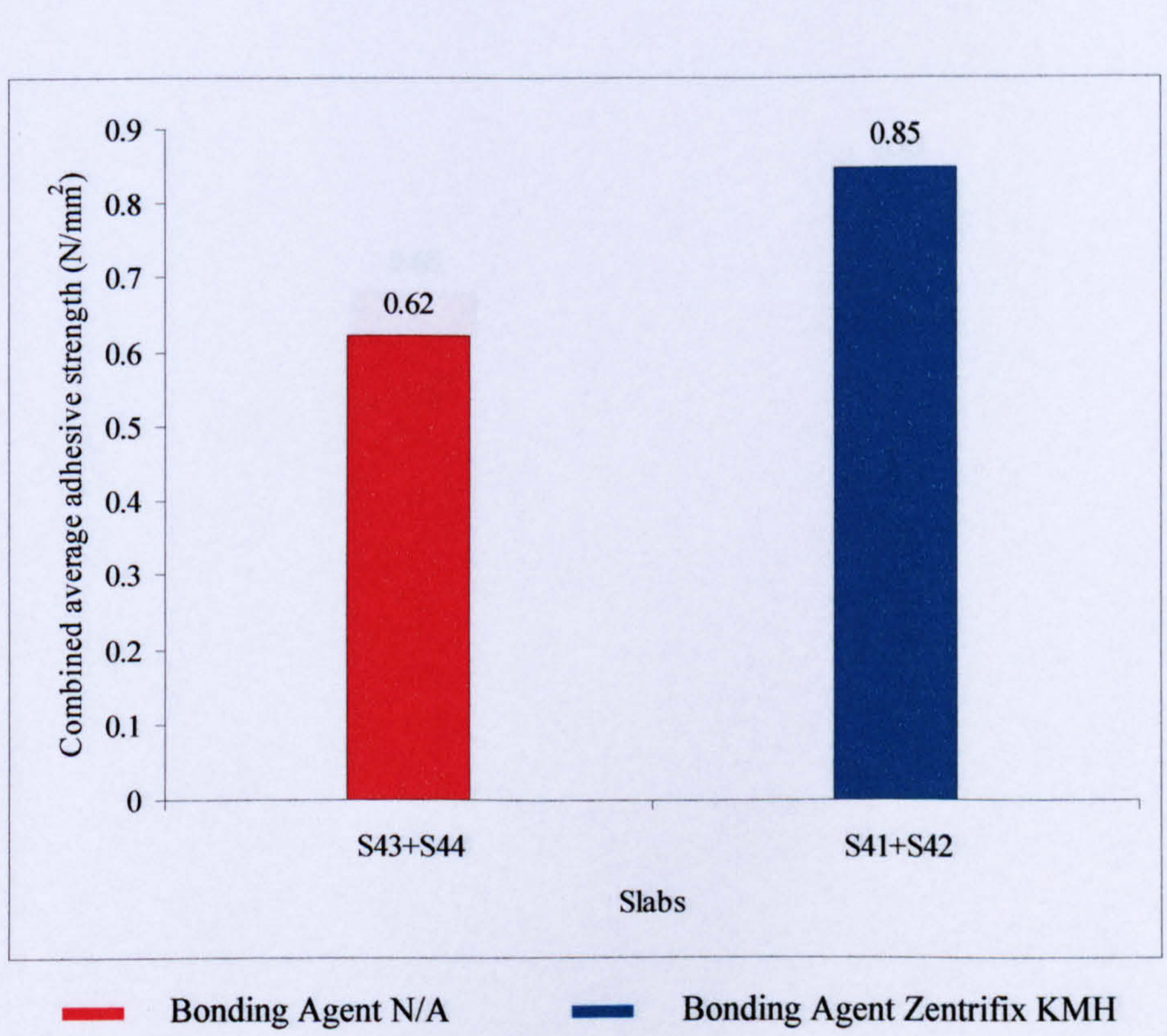

Figure 11.67 Influence of bonding agent Zentrifix KMH on the combined average adhesive strength of slabs S43+S44 and S41+S42

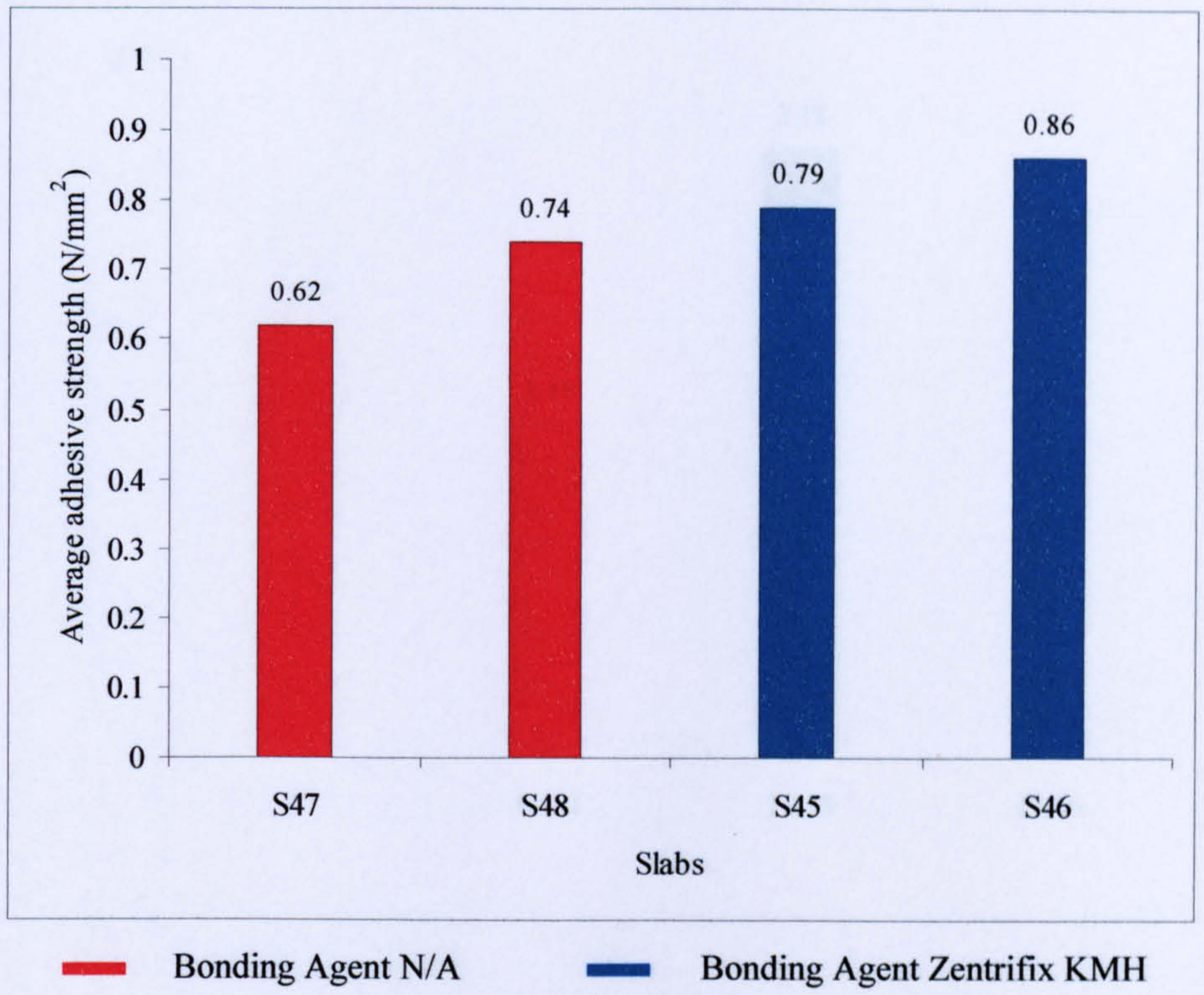

Figure 11.68 Influence of bonding agent Zentrifix KMH on the average adhesive strength of slabs S47, S48, S45 and S46

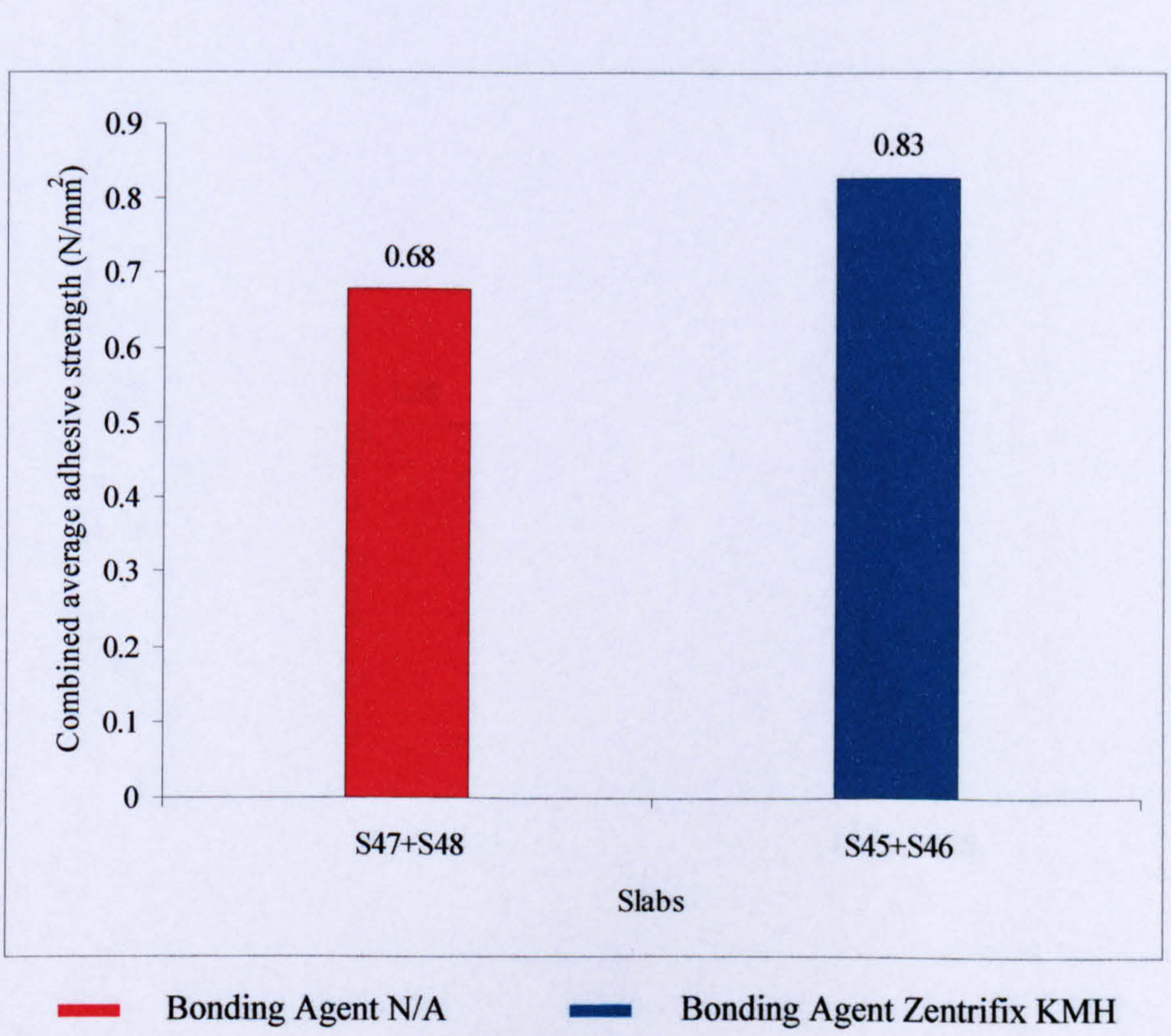

Figure 11.69 Influence of bonding agent Zentrifix KMH on the combined average adhesive strength of slabs S47+S48 and S45+S46

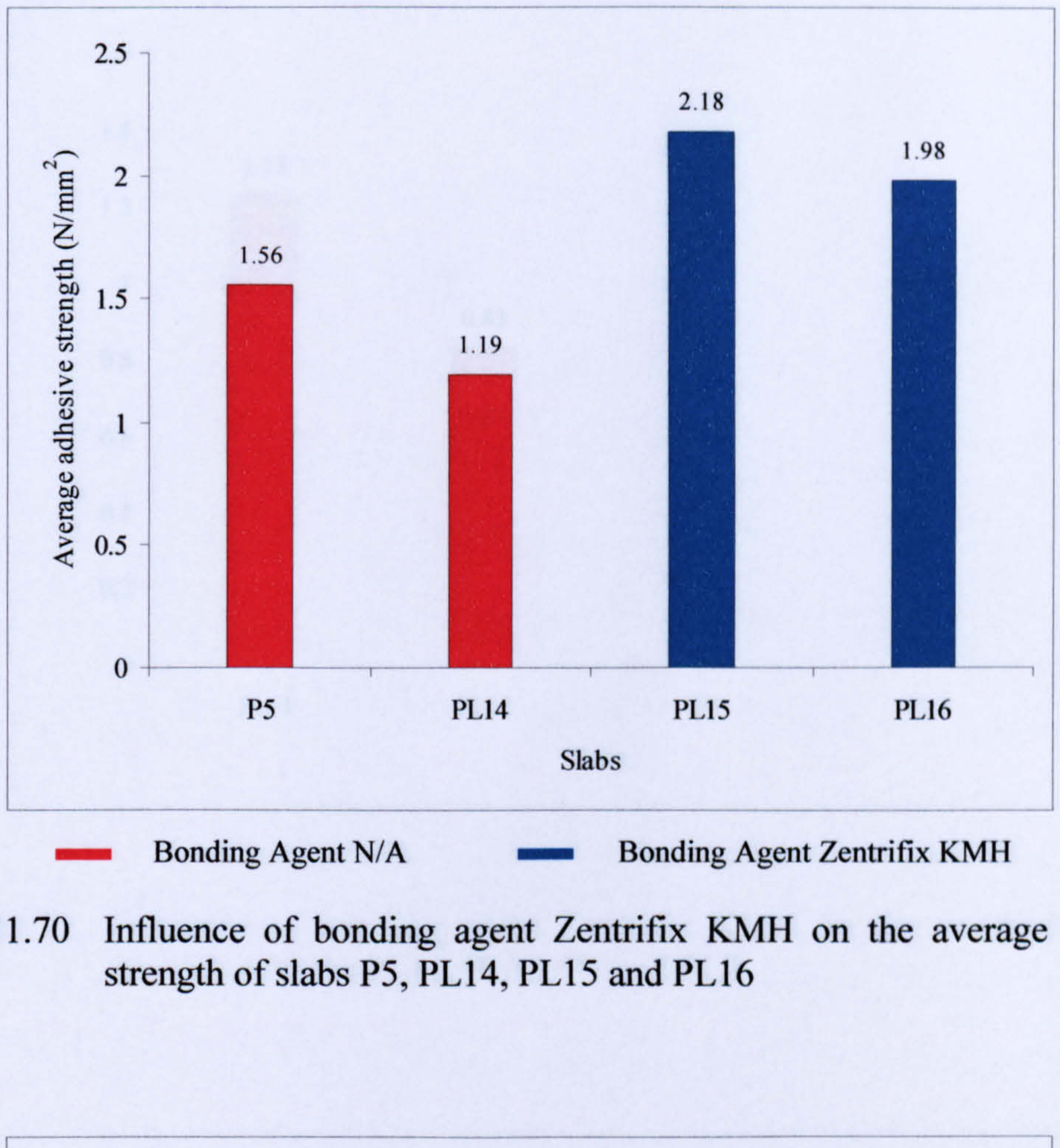

Figure 11.70 Influence of bonding agent Zentrifix KMH on the average adhesive strength of slabs P5, PL14, PL15 and PL16

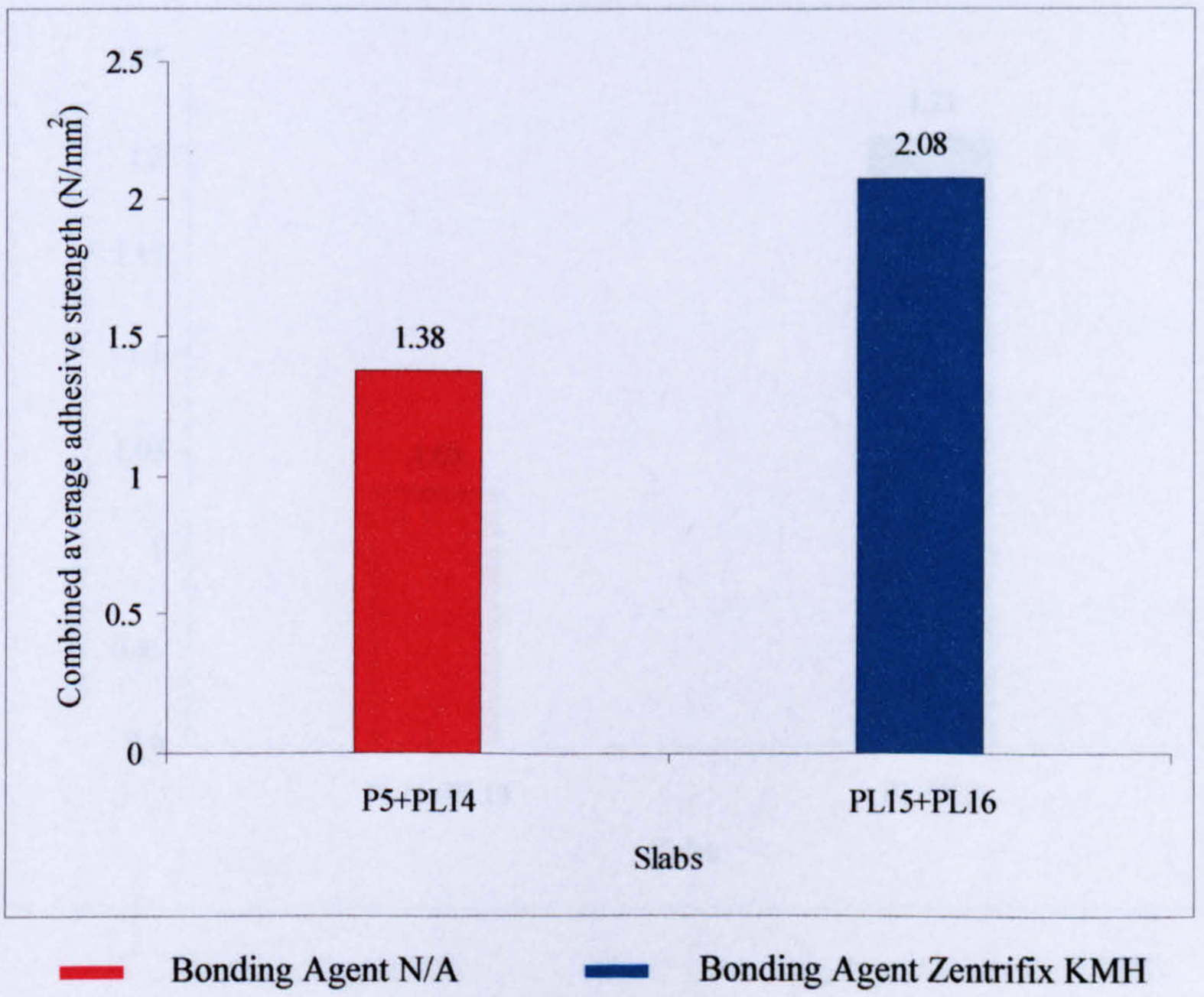

Figure 11.71 Influence of bonding agent Zentrifix KMH on the combined average adhesive strength of slabs P5+PL14 and PL15+PL16

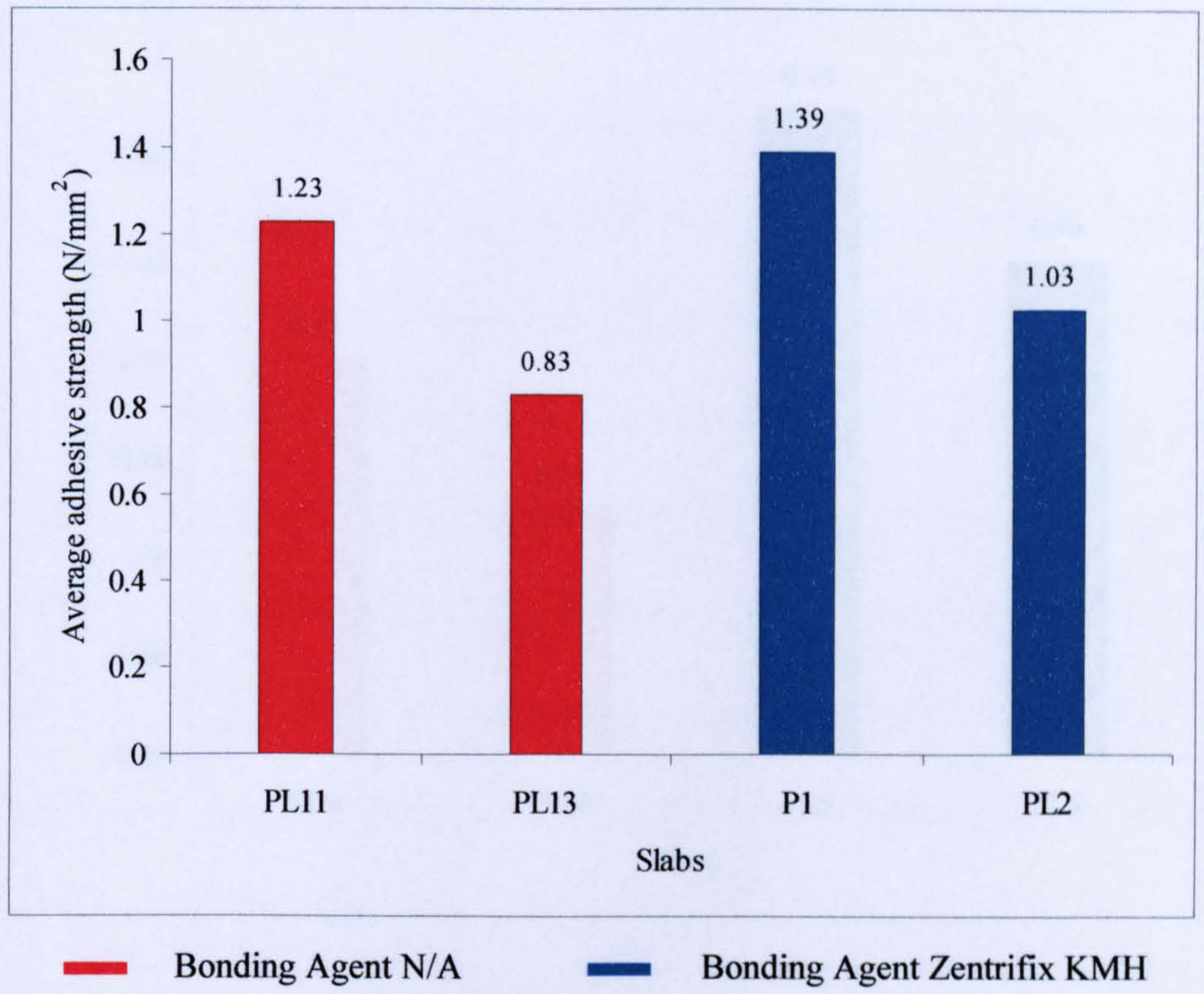

Figure 11.72 Influence of bonding agent Zentrifix KMH on the average adhesive strength of slabs PL11, PL13, P1 and PL2

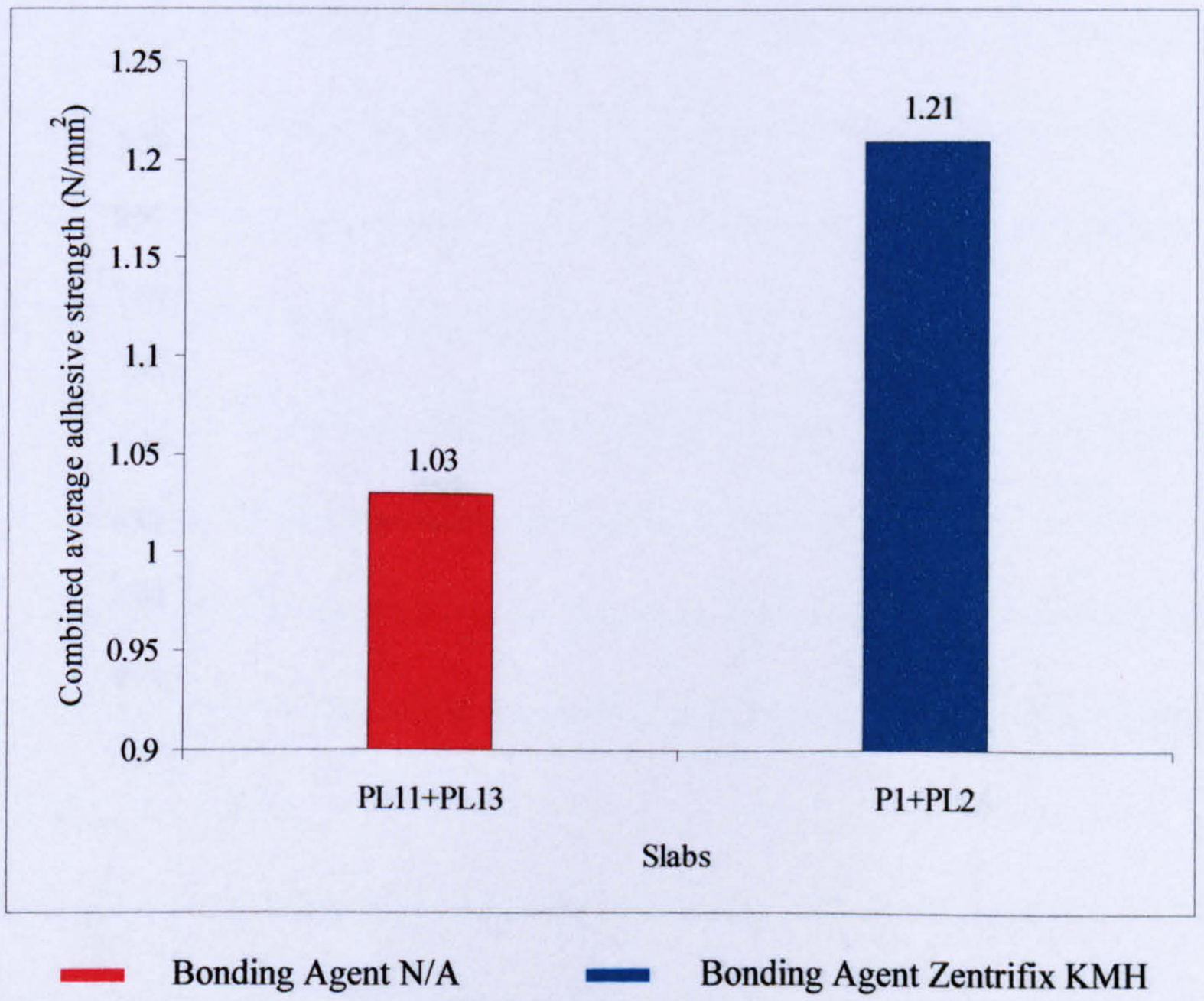

Figure 11.73 Influence of bonding agent Zentrifix KMH on the combined average adhesive strength of slabs PL11+PL13 and P1+PL2

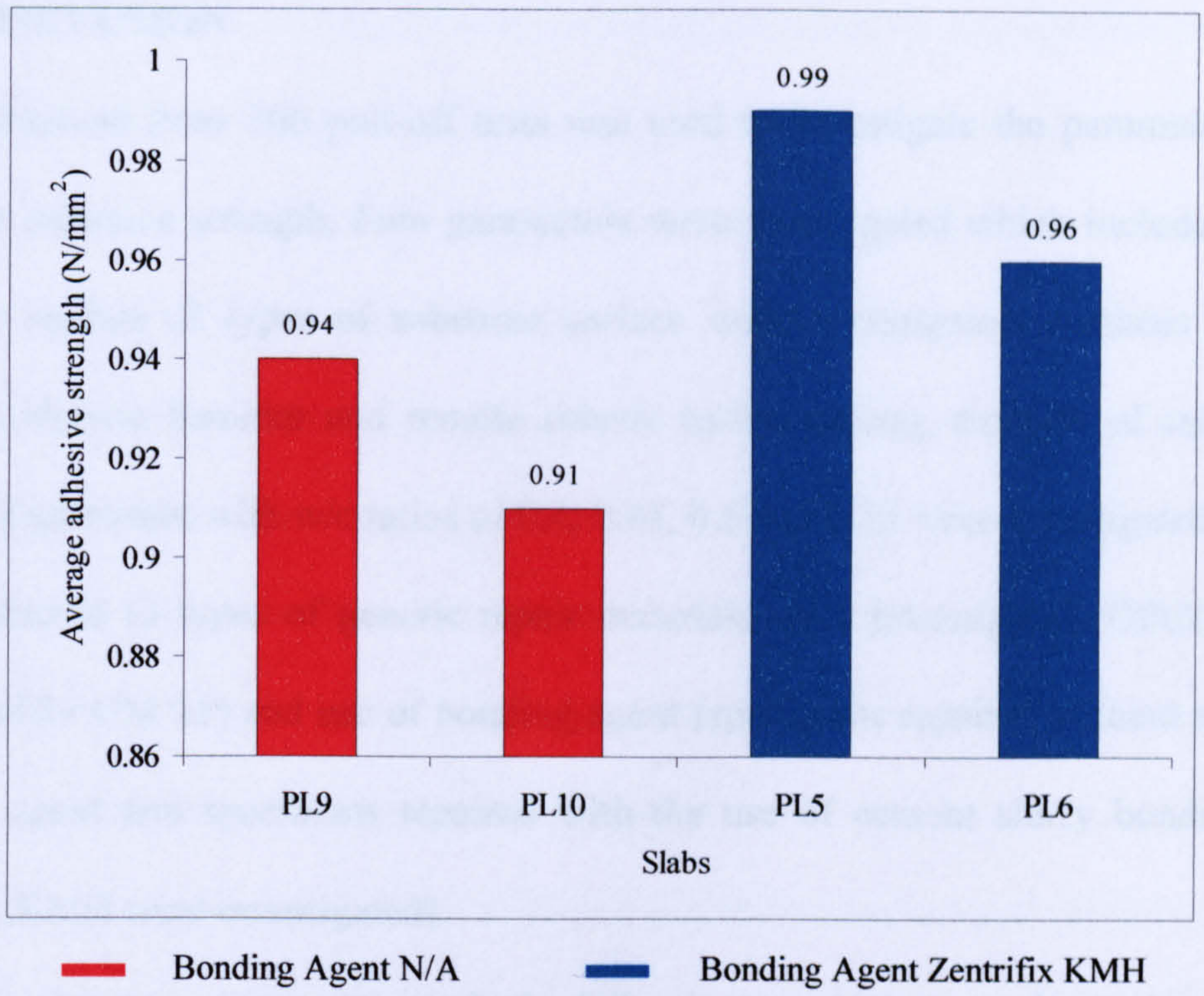

Figure 11.74 Influence of bonding agent Zentrifix KMH on the average adhesive strength of slabs PL9, PL10, PL5 and PL6

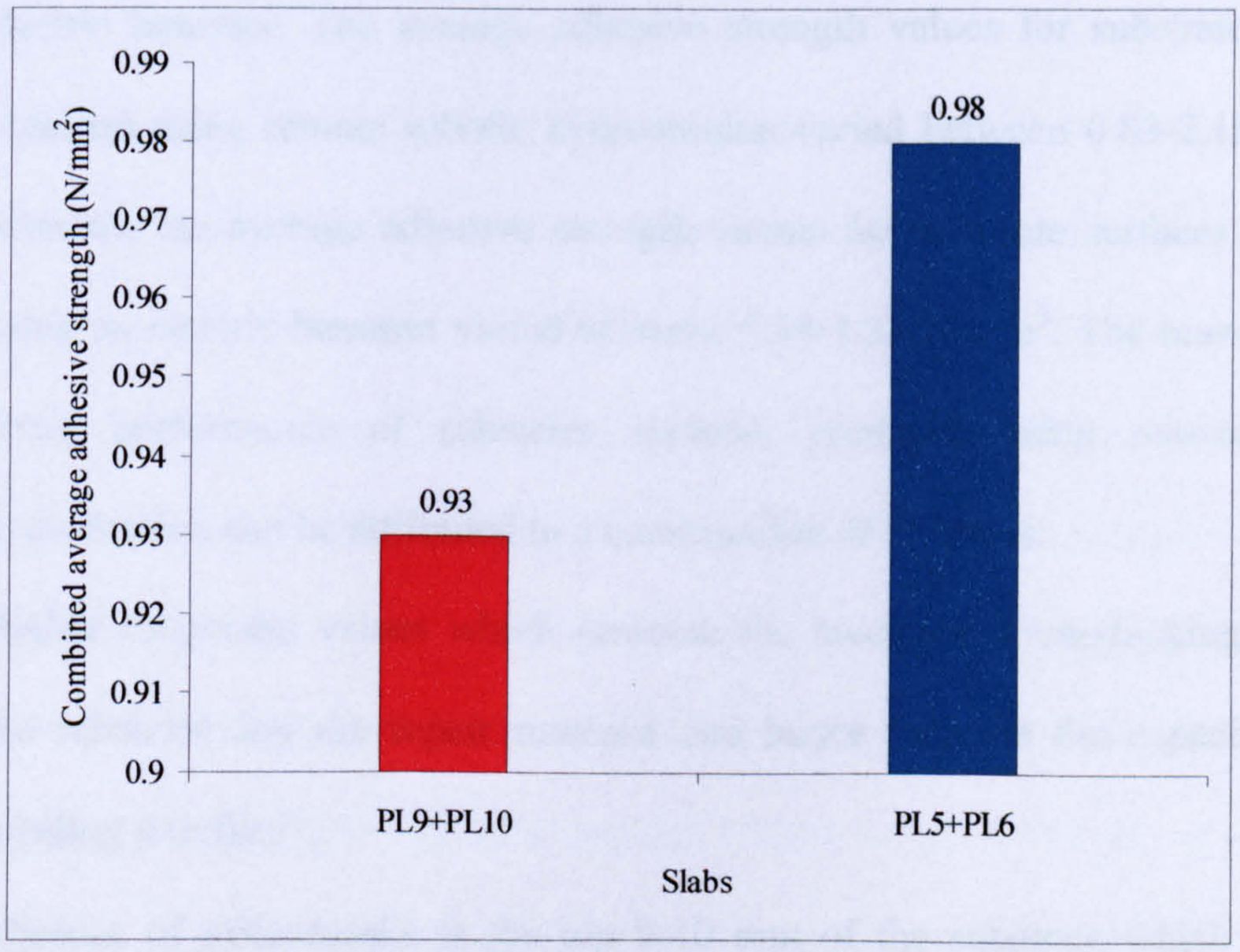

Figure 11.75 Influence of bonding agent Zentrifix KMH on the combined average adhesive strength of slabs PL9+PL10 and PL5+PL6

11.3 CONCLUSION

Data obtained from 300 pull-off tests was used to investigate the parameters which influence adhesive strength. Four parameters were investigated which included type of substrate surface (2 types of substrate surface were investigated: surfaces produced using an electric hammer and remote robotic hydroerosion), strength of substrate (4 groups of substrates with w/c ratios of 0.4, 0.45, 0.5 and 0.55 were investigated), type of repair material (3 types of generic repair materials were investigated: OPCC, OPCM and Zentrifix GM 25) and use of bonding agent (specimens repaired without the use of bonding agent and specimens repaired with the use of cement slurry bonding agent Zentrifix KMH were investigated).

Based on the above parametric study the following conclusions can be made:

1) Substrate surfaces produced using remote robotic hydroerosion provide higher adhesive strength values compared to substrate surfaces produced using an electric hammer. The average adhesive strength values for substrate surfaces obtained using remote robotic hydroerosion varied between 0.83-2.18 N/mm^2, whereas, the average adhesive strength values for substrate surfaces produced using an electric hammer varied between 0.54-1.34 N/mm^2. The reason for the better performance of substrate surfaces produced using remote robotic hydroerosion can be attributed to a combination of 2 factors:

- Higher roughness values which promote the mechanical interlocking between the substrate and the repair material and hence increase the capacity of the bonding interface
- Absence of microcracks at the top 9-10 mm of the substrate which does not significantly reduce the capacity of the bonding interface.

2) Although, results regarding the influence of substrate compressive strength on the average adhesive strength are not conclusive the following comments can be made: In all 6 comparison cases repaired slabs that have the lowest w/c ratio of 0.4 and hence the highest compressive strength values (53.94-58.13 N/mm^2) produced the highest average adhesive strength values. In 3 out of 6 cases repaired slabs that have the highest w/c ratio of 0.55 and hence the lowest compressive strength values (37.14-41.15 N/mm^2) produced the lowest average adhesive strength values. In general, average adhesive strength values seem to be influenced by the substrate compressive strength. However, when the w/c ratio is linearly increased and hence the compressive strength of the substrate is linearly decreased the average adhesive strength does not follow a linear decrease pattern.

3) In 7 out of 10 cases specimens repaired using OPCC (w/c = 0.4) provide higher adhesive strength values when compared to specimens repaired using either OPCM (w/c = 0.4) or Zentrifix GM 25. In addition, OPCC (w/c = 0.4) seems to achieve the best results in terms of adhesive strength on both types of substrate surfaces. In the other 3 cases OPCM (w/c = 0.4) provides the highest adhesive strength values. Hence, OPCC (w/c = 0.4) seems to be the best option in terms of its influence on the adhesive strength followed by OPCM (w/c = 0.4) and Zentrifix GM 25.

4) In 11 out of 15 cases specimens repaired using bonding agent/primer Zentrifix KMH provide higher adhesive strength values when compared to specimens repaired without the use of bonding agent/primer. In addition, bonding agent/primer Zentrifix KMH seems to improve adhesive strength when applied to both types of substrate surfaces. However, it should be noted that the use of

bonding agents/primers should closely follow the manufacturer's guidelines. This usually means that the repair material should be applied immediately after the application of the bonding/agent primer when the bonding agent/primer is still wet.

5) Finally, it should be noted that the effect of substrate and repair material strength on the mode of failure of pull-off tests is shown in Tables 11.3-11.17. From the above data it is quite clear that almost all failures (except 5) occurred at the bonding interface between the concrete substrate and the repair material. The importance of this observation is that the values of almost all pull-off tests correspond to the true adhesive strength values. The reason for this pattern is the fact that both the substrates and the repair materials used in this study had quite high strength values. Substrate compressive strength values varied between 37.14-58.13 N/mm^2, whereas, compressive strength values for the 3 repair materials OPCC (w/c = 0.4), OPCM (w/c = 0.4) and Zentrifix GM 25 varied between 48-57.93, 47.02-51.60 and 23.81-29.52 N/mm^2, respectively. Since the bonding interface was the weakest plane along the entire length of the core almost all failures took place at this plane.

CHAPTER 12

CONCLUSIONS AND SUGGESTIONS FOR FUTURE WORK

12.1 INTRODUCTION

This chapter deals with the work carried out on this dissertation against the objectives stated in Chapter 1. For convenience each sub-objective is stated prefacing the corresponding conclusions. In addition, recommendations for future experimental work in the field of concrete patch repairs are also made.

12.2 CONCLUSSIONS AND DISCUSSION

Sub-objective: To review the effect of disintegration mechanisms, abnormal loading and poor workmanship on the long-term durability of concrete structures.

This objective has been successfully achieved. Information regarding the effects of disintegration mechanisms, abnormal loading and poor workmanship on the long-term durability of concrete structures has been obtained and presented on this thesis.

Sub-objective: To review the various methods used for the removal of defective concrete and highlight the advantages of hydrodemolition/hydroerosion over traditional methods of concrete removal.

This objective has been successfully achieved. Information regarding machine-mounted demolishing attachments, mechanical or chemical splitting, sawing and cutting methods, pneumatic chipping hammers, thermal demolition methods, and hydrodemolition has been obtained and presented on this thesis. In addition, the advantages of hydrodemolition over traditional methods of concrete removal were highlighted.

Sub-objective: To investigate the significant influence of adequate preparation of steel reinforcement and concrete substrate surface on the long-term success of the repair.

This objective has been successfully achieved. Information regarding the correct approach on the preparation of steel reinforcement and concrete substrate surface prior to the installation of repair materials has been obtained and presented on this thesis.

Sub-objective: To carry out remote robotic hydroerosion experiments and determine the parameters that influence the efficiency and quality of the operation.

This objective has been achieved to a satisfactory level. Experiments carried out at City University using a MENASA three dimensional cartesian robot demonstrated the advantages of remote robotic hydroerosion over traditional methods of concrete removal. In addition, some of the experimental results confirmed the influence of various factors on the quality and efficiency of hydroerosion

Sub-objective: To investugate the importance of the substrate surface roughness on the adhesive strength of the repair and review the various methods used for measuring and characterising the roughness of substrate concrete surfaces prior to repair.

This objective has been successfully achieved. Information regarding the importance of the substrate surface roughness on the adhesive strength of concrete patch repairs has been obtained and presented on this thesis. In addition, a review of the relatively small number of methods developed for measuring and characterising the surface of concrete substrates prior to repair was also included.

Sub-objective: To measure and characterise the roughness of concrete substrate surfaces prior to repair.

This objective has been successfully achieved. The surface roughness of 48 specimens produced using an electric hammer and the surface roughness of 12 specimens produced using remote robotic hydroerosion were measured and characterised using 2 different methods: sand area method described in prBS EN 1504: Part 10[44] and fringe based laser interferometry. Based on the measurements of fringe based laser interferometry 3D topographies off all surfaces were also produced.

Sub-objective: To compare the roughness of concrete substrate surfaces obtained using different methods of concrete removal (remote robotic hydroerosion and pneumatic chipping hammers) and demonstrate the ability of remote robotic hydroerosion to produce rougher surfaces.

This objective has been successfully achieved. SRI and Rmean values obtained using sand area method clearly indicated the ability of remote robotic hydroerosion to produce rougher surfaces. However, the need for more precise and reliable measurement of the surface roughness led to the employment of fringe based laser interferometry. Based on its measurements, 6 2D roughness parameters (2α, $D\alpha/W$, $R\Delta\alpha$, $R\Delta q$, Lo and Lr) were calculated on both the X and Y axes for both types of surface roughness specimens. All 6 2D roughness parameters clearly indicated the ability of remote robotic hydroerosion to produce rougher substrate surfaces.

Sub-objective: To investigate and critically assess the factors affecting the selection of repair materials.

This objective has been successfully achieved. Information regarding the factors affecting the selection of repair materials such as mechanical properties (compressive, tensile, flexural, and adhesive strength) and compatibility requirements (chemical, electrochemical, permeability, and strain compatibility) of repair materials has been obtained and presented on this thesis. In addition, information regarding the uses, advantages and limitations of the most commonly used repair materials (OPC concrete and mortar, RHC concrete, high strength concrete, polymer-modified concrete, polymer concrete, preplaced-aggregate concrete, shotcrete, and fibre-reinforced concretes and shotcretes) and bonding agents has also been obtained and presented on this thesis.

Sub-objective: To review and select for experimentation the various test methods used for evaluating the quality of patch repairs.

This objective has been successfully achieved. Information regarding the various test methods (tensile bond, shear bond, slant shear, and patch repair tests) used for assessing the adhesive strength of patch repairs has been obtained and presented on this thesis. Advantages and limitations of each test are highlighted.

Sub-objective: To measure and compare the flexural strength behaviour of different types of generic repair materials by performing flexural strength tests on repaired unreinforced concrete beam specimens and thus give a basis of selection.

This objective has been successfully achieved. 6 types of generic repair materials (OPCC w/c = 0.4, OPCC w/c = 0.5, OPCM w/c = 0.4, OPCM w/c = 0.5, Zentrifix GM 25, and MonoTop 615) were used to repair beam substrate specimens. Standard flexural

tests performed on 160 solid and repaired beams confirmed the ability of the first 5 repair materials to achieve flexural compatibility. Beams repaired using MonoTop 615, although were able to significantly increase their maximum load capacity, they were not able to fully achieve the maximum load capacity of solid beams.

Sub-objective: To determine the permeability properties between different types of generic repair materials by performing absorption by immersion and initial surface absorption tests on cubes.

This objective has been successfully completed. The permeability properties of the 6 types of generic repair materials selected above, were evaluated using absorption by immersion test described by BS 1881: Part 122[141] and ISAT described by BS 1881: Part 208[142]. Both absorption by immersion test and ISAT ranked OPCC w/c = 0.4 and OPCC w/c = 0.5 as low water absorption repair materials, OPCM w/c = 0.4 and MonoTop 615 as moderate water absorption repair materials, and OPCM w/c = 0.5 and Zentrifix GM 25 as high water absorption repair materials.

Sub-objective: To repair the above two different types of concrete substrate surface slab specimens using 3 different types of generic repair materials (OPCC, OPCM and Polymer Modified Concrete)

This objective has been successfully completed. Forty-eight slabs produced using an electric hammer and twelve slabs produced using remote robotic hydrodemolition were repaired using 3 different types of generic repair materials (OPCC, OPCM and Zentrifix GM 25). During the repair of half of the above slabs bonding agent/primer Zentrifix KMH was used.

Sub-objective: To measure the adhesive strength of the patch repaired slab specimens using the pull-off test

This objective has been successfully completed. A total of 300 pull-off tests (5 on each repaired slab in accordance to BS 1542[93]) were performed.

Sub-objective: To investigate the effect of different types of substrate surface roughness produced by different methods of concrete removal on the adhesive strength of patch repairs

This objective has been successfully completed. Results clearly indicated the ability of substrate surfaces produced using remote robotic hydroerosion to provide higher adhesive strength values when compared to substrate surfaces produced using an electric hammer. The average adhesive strength values for substrate surfaces obtained using remote robotic hydroerosion varied between 0.83-2.18 N/mm^2, whereas, the average adhesive strength values for substrate surfaces produced using an electric hammer varied between 0.54-1.34 N/mm^2. The reason for the better performance of substrate surfaces produced using remote robotic hydroerosion can be attributed to a combination of higher roughness values and absence or very limited introduction of microcracks at the top 9-10 mm of the substrate.

Sub-objective: To investigate the effect of substrate compressive strength on the adhesive strength of patch repairs

This objective has been achieved to a satisfactory level. Although, results are not conclusive some general comments can be made regarding the influence of substrate compressive strength on the average adhesive strength of repaired slabs. In general, average adhesive strength seems to be influenced by the substrate compressive strength.

However, when the w/c ratio is linearly increased and hence the compressive strength of the substrate is linearly decreased the average adhesive strength does not follow a linear decrease pattern.

Sub-objective: To investigate the effect of different types of generic repair materials on the adhesive strength of patch repairs

This objective has been successfully achieved. In 70% of cases, specimens repaired using OPCC (w/c = 0.4) provide higher adhesive strength values when compared to specimens repaired using either OPCM (w/c = 0.4) or Zentrifix GM 25. In addition, the ability of OPCM (w/c = 0.4) to achieve the best results in terms of adhesive strength does not seem to be influenced by different types of substrate surfaces. In the rest 30% of cases OPCM (w/c = 0.4) provides the highest adhesive strength values. Hence, OPCC (w/c = 0.4) seems to be the best option in terms of its influence to the adhesive strength followed by OPCM (w/c = 0.4) and Zentrifix GM 25.

Sub-objective: To investigate the effect of cement based slurry bonding agents/primers on the adhesive strength patch repairs

This objective has been successfully achieved. In 73% of cases, specimens repaired using bonding agent/primer Zentrifix KMH provide higher adhesive strength values when compared to specimens repaired without the use of bonding agent/primer. In addition, the ability of bonding agent/primer Zentrifix KMH to improve adhesive strength does not seem to be influenced by different types of substrate surfaces.

12.3 SUGGESTIONS FOR FUTURE WORK

In Chapters 9 and 10, experimental evaluation of flexural behaviour of repair materials and experimental evaluation of permeability properties of repair materials have been presented. Because of the limitations on resources and time, strain compatibility of repair materials was not experimentally investigated. An in-depth experimental study of strain compatibility of repair materials and their interaction with concrete substrates needs to be carried out. Based on the work carried out in this thesis and similar work at other research institutions and organisations, the following areas of strain compatibility are considered needing further research:

- Drying shrinkage
- Thermal expansion
- Creep
- Modulus of elasticity

From the above areas of strain compatibility the most important is the drying/restrained shrinkage of repair materials. Although various research studies have been reported on the unrestrained shrinkage of concrete and other repair materials and the factors influencing it, the stresses induced due to restrained shrinkage and the consequent risk of cracking are of greater importance in repaired concrete structures. Restrained shrinkage occurs due to a number of reasons, such as: monolithic construction, presence of adjacent structural members, steel reinforcement or different moisture gradient. It is the strain induced due to restrained shrinkage rather than the magnitude of unrestrained shrinkage that can lead to cracking. As a result of restrained shrinkage, cracks occur when the induced tensile strain, relieved by creep, exceeds the tensile strain capacity of

the material. A number of test methods are available for testing restrained shrinkage. These include:

- Linear restrained shrinkage test
- Plate type test
- Ring test

The main disadvantage of all the above methods is that although they provide information related to the amount and width of the cracks they do not provide any information regarding the developed stress. In addition, none of the above methods is able to evaluate restrained shrinkage in repairs exposed to real environmental conditions. Hence, research that will attempt to develop test methods which will be able to provide information regarding the development of stress in repairs exposed to real environmental conditions is necessary.

BIBLIOGRAPHY

1. BS 8110: Part 1: 1985 Structural use of concrete. Code of practice for design and construction, BSI, UK, 1985
2. BS EN 206: Part 1: 2000 Concrete. Specification, performance, production and conformity, BSI, UK, 2000
3. ACI 318-99 Building Code Requirements for Structural Concrete, ACI Committee 318, USA, 1999
4. BS 1881: Part 120: 1983 Testing concrete. Method for determination of compressive strength of concrete cores, BSI, UK, 1983
5. BS EN 12504: Part 1:2000 Testing concrete in structures. Cored specimens. Taking, examining and testing in compression, BSI, UK, 2000
6. ASTM C 42-99 Standard Test Method for Obtaining and Testing Drilled Cores and Sawed Beams of Concrete, ASTM, USA, 1999
7. ACI 228.1R-95 In-Place Methods to Estimate Concrete Strength, ACI Committee 228, USA, 1995
8. ACI 228.2R-98 Nondestructive Test Methods for Evaluation of Concrete in Structures, ACI Committee 228, USA, 1998
9. Emmons, P. H., Concrete repair and Maintenance Illustrated, pub. R. S. Means Co. Inc. Maryland USA, 1994
10. HEROIC (Hydro-Erosion-for-Repair-of-Insitu-Concrete), Brite/EuRam project BES2-2783, task-1 report, 2001
11. D. A. Chamberlain, E. Gambao, S. E. McCormac, M. A. Garcia, T. McCulloch, C. A. A. Seibert, P. Souretis and A. White, 16th ISARC, 1998

12. Osama Abudayyeh, Anil Sawhney, Hossam El-Bibany, and David Buchanan, Concrete bridge demolition methods and equipment, Journal of Bridge Engineering, August 1998

13. Chapter 5, Concrete Removal and Preparation for Repair, EM 1110-2-2002, June 1995

14. Hindo, K. R., In-Plane Bond Testing and Surface Preparation of Concrete, Concrete International, V 12 No 4, April 1990, pp. 46-48

15. www.conjet.com

16. J. Silfwerbrand, Improving Concrete Bond in Repaired Bridge Decks, Concrete International, V 12 No 9, September 1990, pp. 61-66

17. Ingvarsson, H., and Eriksson, B., Hydrodemolition for Bridge Repairs, Nordisk Betong, Stockholm, No 2-3, 1988, pp. 49-54

18. A. W. Momber, Water jet applications in construction engineering, Pub. A.A. Balkema/Rotterdam, Netherlands, 1998

19. Warner, J., Hydrodemolition for Removing Concrete, Concrete International, V. 20 No. 8, Aug. 1998, pp. 47-50

20. Lohrey, E., C., Use of Hydrodemolition To Remove Deteriorated Concrete from Bridge Decks, Transportation Research Record 1490, 1995

21. A. M. Vaysbund, G. M. Sabnis, P. H. Emmons and J. E McDonald, Interfacial bond and surface preparation in concrete repair, Indian Concrete Journal, January 2001

22. No. 03730-Surface Preparation for the Repair of Deteriorated Concrete Resulting from Reinforcing Steel Corrosion, ICRI

23. C. H. Holl and S. A. O'Connor, Cleaning and Preparing Concrete before Repair Concrete International, V. 19 No 3, March 1997, pp. 60-63

24. ASTM D 4258-83, Standard Practice for Surface Cleaning Concrete for Coating, ASTM, USA, 1983

25. ASTM D 4261-83, Standard Practice for Surface Cleaning Concrete Unit Masonry for Coating, ASTM, USA, 1983

26. ASTM D 4262-83, Standard Test Method for pH of Chemically Cleaned or Etched Concrete Surfaces, ASTM, USA, 1983

27. ASTM D 4259-88, Standard Practice for Abrading Concrete, ASTM, USA, 1988

28. ASTM D 4285-83, Standard Test Method for Indicating Oil or Water in Compressed Air, ASTM, USA, 1983

29. ASTM D 4260-88, Standard Practice for Acid Etching Concrete, ASTM, USA, 1988

30. BS EN 197: Part 1: 2000 Cement. Composition, specifications and conformity criteria for common cements, BSI, UK, 2000

31. Design of normal concrete mixes, BRE report, UK, 1988

32. Brian Griffiths, Manufacturing Surface Technology, Penton Press, London, 2001

33. Surface Texture, Waviness and Lay, ANSI, New York, 1978

34. T. R.Thomas, Rough Surfaces, Longman, London, New, 1982

35. N. Maerz, Photoanalysis of rock fabric, Ph.D Thesis, University of Waterloo, 1990

36. www.predev.com

37. ISO 4287: 1997 Surface Texture: Profile Method-Terms, Definitions and Surface Texture Parameters, 1997

38. ISO 13565: Part 2: 1996 Surface Texture: Profile Method-Surfaces having Stratified Functional Properties, Part 2, Height Characterisation using the Linear Material Ratio Curve, 1996

39. ISO 12085: 1996 Surface Texture: Profile Method-Motif Parameters, 1996

40. N. H. Maerz, A. Nanni, J. J. Mayers and G. Galecki, Laser Profilometry for Concrete Substrate Characterisation Prior to FRP Laminate Application, Concrete Repair Bulletin, May/June 2001, pp. 4-8

41. Stout K. J., Matthia T., Sullivan P. J., Dong W. P., Mainsah E., Luo N., and Zahouani H., Development of Methods for the Characterisation of Roughness in Three Dimensions, Report EUR 15178 EN, EC Brussels, ISBN 0 7044 13132, Penton Press, London, 2000

42. Standsurf 2000, Standsurf Project Web site parameter description pages, University of Huddersfield, 2000
www.hud.ac.uk/schools/engineering/research/ultrap/surface/project_open.html

43. N. J. Dellate Jr., D. W. Fowler, B.F. McCullough, and S. F. Gratter, Investigating performance of bonded concrete overlays, Journal of performance of constructed facilities, May 1998

44. prBS EN 1504: Part10:1999. Products and systems for the protection and repair of concrete structures. Definitions, requirements, quality control and evaluation of conformity. Site application of products and systems and quality control of the works, BSI, UK, 1999

45. Selecting and specifying concrete surface preparation for sealers, coating, and polymer overlays, Technical Guideline No. 03732, 1997, pp 41, ICRI, USA, 1997

46. Holt F. B, and Musgrove G. R., Surface texture classification: a guide to

pavement skid resistance. ASTM Special publication, 1982, pp. 31-44

47. Fiebrich, M. H., Scientific aspects of adhesion phenomena in the interface mineral substrate-polymers, in Adherance of young and old concrete, Proceedings of 2nd Bolomey Workshop, Unterengstringen, 1994, pp. 25-28

48. Vaneevelt, B., Etude de l'endommagement cree dans le beton sain lors de operations de decapage, Travail de fin d'etudes, Universite de Liege, 1991

49. Silfwerbrand, J., Bonding between old and new concrete in structures loaded by static and time-dependent load. Proceedings of the International Conference on Adhesion between polymers and concrete, France 1986, pp. 309-314

50. A. I. Abu-Tair, D. Lavery, A. Nadjay, S. R. Rigden, T.M.A. Ahmed, A new method for evaluating the surface roughness of concrete cut for repair or strengthening, Construction and Building Materials, Vol 14, No 3, 2000, pp. 171-176

51. A New Self-Calibrating 3D Interferometric Fringe-Based Imaging System for Profiling, Positioning and Control in Space, Summary Report, ESA Contract 15787, 2002

52. Plum, D., Materials-what to specify, Constr. Maint. Repair Dig. July/August, 1991, pp 3-7

53. D. Cusson and N. Mailvaganam, Durability of Repair Materials, Concrete International V. 18 No. 3, March 1996, pp 34-38

54. The Concrete Society (UK), Patch repair of reinforced concrete. Model specification and method of measurement. Concrete Society Technical Report No. 38, London 1991

55. Peter H. Emmons, Alexander M. Vaysburd, and James E. McDonald, A Rational Approach to Durable Concrete Repairs, Concrete International, V. 15 No. 9, September 1993, pp. 40-45

56. Gulikers, J. J. W., and van Mier, J. G. M., The Effect of Patch Repairs on the Corrosion of Steel Reinforcement in Concrete, Second Canmet/ACI International Conference on Durability of Concrete, Supplementary Papers, Montreal, Canada, 1991, pp. 445-460

57. Marosszeky, M., and Wang, D., The Study of the Effect of Various Factors on Subsequent Bar Corrosion in Concrete, Second Canmet/ACI International Conference on Durability of Concrete, Supplementary Papers, Montreal, Canada, 1991, pp. 585-606

58. P. H. Emmons, A. M. Vaysburd, and J. E. McDonald, Concrete Repair In The FutureTurn Of The Century-Any Problems?, Concrete International, V. 16 No. 3, March 1994, pp. 42-49

59. Dehawah, H. A. F., Basanbul, I. A., Maslehuddin, M., Al-Sulaimani, G. J. and Baluch, M. H., Durability performance of repaired reinforced concrete beams, ACI Materials Journal, March/April 1994, pp 167-172

60. McCurrich, L. H., Cheriton, L. W., and Little, D. R., Repair systems for preventing further corrosion in damaged reinforced concrete. In: 1st International Conference on Deterioration and Repair of Reinforced Concrete in the Arabian Gulf, Bahrain, October 26-29, 1985, pp. 151-168

61. Heiman, J. L. and Koerstz, P., Performance of polymer-modified cementitious mortars in chloride contaminated concrete, Trans. Inst. Eng. Austral. Civ. Eng. Vol. 33, No. 3, 1991, pp. 169-175

62. D. R. Morgan, Compatibility of concrete repair materials and systems, Construction and Building Materials, Vol 10 No 1, 1996, pp. 57-67

63. N. K. Emberson and G. C. Mays, Significance of property mismatch in the patch repair of structural concrete - Part 1: Properties of repair systems, Magazine of Concrete Research, Vol. 42 No. 152, September 1990, pp 147-160

64. Plum, D. R., The Behaviour of Polymer Materials in Concrete Repair and Factors Influencing Selection, The Structural Engineer, September 1990, pp. 337-345

65. Emmons, P. H., and Vaysburd, A. M., Compatibility Considerations for Durable Concrete Repairs, Transportation Research Record No 13, 1993, pp. 13-19

66. M. H. Decter, C. Keely, Durable concrete repair-importance of compatibility and low shrinkage, Construction and Building Materials, Vol. 11, Nos 5-6, 1997, pp. 267-273

67. P. H. Emmons, A. M. Vaysburd, J. E. McDonald, R. W. Poston, and K. E. Kesner, Selecting Durable Repair Materials: Performance Critiria, Concrete International, V. 22 No. 3, March 2000, pp. 38-45

68. BS 6319: Part 12: 1992 Testing of resign and polymer/cement compositions for use in construction. Methods for measurement of unrestrained linear shrinkage and coefficient of thermal expansion, BSI, UK, 1992

69. BS EN 1770: 1998 Products and systems for the protection and repair of concrete structures. Test methods. Determination of the coefficient of thermal expansion, BSI, UK, 1998

70. ASTM C 531-00 Standard Test Method for Linear Shrinkage and Coefficient of Thermal Expansion of Chemical-Resistant Mortars, Grouts, Monolithic Surfacings, and Polymer Concretes, ASTM, USA, 2000

71. Samir E. Chidiac and Noel P. Mailvaganam, Finite Element Analysis of Patch Repair in a Concrete Flat Slab, Innovations in Urban Infrastructure, 1999

72. BS 6319: Part 6: 1984 Testing of resign and polymer/cement compositions for use in construction. Method for determination of modulus of elasticity in compression, BSI, UK, 1984

73. BS EN 13412: 2002 Products and systems for the protection and repair of concrete structures. Test methods. Determination of modulus of elasticity in compression, BSI, UK, 2002

74. ASTM C 469-02 Standard Test Method for Static Modulus of Elasticity and Poisson's Ratio of Concrete in Compression, ASTM, USA, 2002

75. ASTM C 512-02 Standard Test Method for Creep of Concrete in Compression, ASTM, USA, 2002

76. ASTM C 1181-00 Standard Test Method for Compressive Creep of Chemical-Resistant Polymer Machinery Grouts, ASTM, USA, 2000

77. BS 6319: Part 11: 1993 Testing of resin and polymer/cement compositions for use in construction. Methods for determination of creep in compression and tension, BSI, UK, 1993

78. Alberta Transportation and Utilities, Specification for evaluation of length change of bridge concrete patching materials, Specification B-391, Edmonton, Canada

79. ASTM C 157-03 Standard Test Method for Length Change of Hardened Hydraulic-Cement, Mortar, and Concrete, ASTM, USA, 2003

80. ASTM C 596-01 Standard Test Method for Drying Shrinkage of Mortar Containing Hydraulic Cement, ASTM, USA, 2001

81. Technical test regulations for concrete substitution systems made of cement mortar/concrete with a plastic additive (PCC), German Federal Ministry for Transport, Highway Construction Department, 1990

82. Peter H. Emmons and Alexander M. Vaysburd, The Total System Concept-Necessary for Improving the Performance of Repaired Structures, Concrete International, V. 17 No 3, March 1995, pp. 31-36

83. Alexander M. Vaysburd, Peter H. Emmons, Noel P. Mailvaganam, James E. McDonald, and Benoit Bissonnette, Concrete Repair Technology-A Revised Approach is Needed, Concrete International, V. 26 No 1, January 2004, pp. 59-65

84. Ping Gu, J. J. Beaudoin, P. J. Tumidajski, and N. P. Mailvaganam, Electrochemical Incompatibility of Patches in Reinforced Concrete, Concrete International, V. 19 No 8, August 1997, pp. 68-72

85. Spall Repair, Repair, Technical Note CS-MR-4.5, REMR, 1994

86. Plum, D. R., Materials-Why They Fail, Construction Maintenance & Repair, Sept.-Oct. 1991, pp. 3-6

87. Silfwerbrand and J. Paulsson, Better Bonding of Bridge Deck Overlays, Concrete International, V. 20 No 10, October 1998, pp. 56-61

88. ASTM C 1059-99, Standard Specification for Latex Agents for Bonding Fresh to Hardened Concrete, ASTM, USA, 1999

89. ASTM C 881-99, Standard Specification for Epoxy-Resign-Base Bonding Systems for Concrete, ASTM, USA, 1999

90. Long, A. E., and Murrey, A., The pull-off partially destructive test for concrete, ACI SP-82, PP 327-350, 1986

91. Stehno, G. and Mall, G., The tear-off method-a new way to determine the quality of concrete in structures on site, RILEM International, Symposium on Testing In Situ of Concrete Structures, Budapest 1977, pp. 335-347

92. BS 1881: Part 207: 1992 Testing concrete. Recommendations for the assessment of concrete strength by near-to-surface tests, BSI, UK, 1992

93. BS EN 1542: 1999 Products and systems for the protection and repair of concrete structures. Test methods. Measurement of bond strength by pull-off, BSI, UK, 1999

94. ASTM D 4541-95 Standard Test Method for Pull-Off strength of Coatings Using Portable Adhesion Testers, ASTM, USA, 1995

95. McLeish, A., Standard tests for repair materials and coatings for concrete pull-off testing, CIRIA 1992, Report 139

96. D. J. Cleland and A. E. Long, The pull-off test for concrete patch repairs, Proceedings, Institution of Civil Engineers, Structures and Buildings, V. 103 November 1997, pp. 451-460

97. D. J. Cleland and A. Misra, In-situ adhesion testing of concrete surface repairs, Fifth CANMET/ACI International Conference on Recent Advances in Concrete Technology, Singapore, 2001

98. Bungey J. H. and Madandoust R., Factors influencing pull-off tests on concrete. Magazine of Concrete Research, Vol 44 No. 158, March 1992, pp. 21-30

99. Austin S., Robins, P. and Pan Y., Tensile bond testing of concrete repairs. Materials and Structures Vol 28 No. 179, 1995, pp. 249-259

100. A. M. Vaysburd and J. E. Mcdonald, An Evaluation of Equipment and Procedures for Tensile Bond Testing of Concrete Repairs, Technical Report REMR-CS-61, June 1999

101. L. I. Knab and C. B. Spring, Evaluation of Test Methods for Measuring the Bond Strength of Portland Cement Based Repair Materials to Concrete, Cement, Concrete and Aggregate, Vol. 11, No. 1, Summer 1989, pp. 3-14

102. BS 6319: Part 7: 1985 Testing of resign and polymer /cement compositions for use in construction. Method for measurement of tensile strength, BSI, UK, 1985

103. Judge, A. I., Cheriton, L. W., and Lambe, R. W., Bonding Systems for Concrete Repair-An Assessment of Commonly Used Materials, Proceedings, RILEM Symposium on Adhesion Between Polymers and Concrete, (Aix-en-Provence, September 1986) Chapman and Hall Ltd, London 1986, pp. 661-681

104. Y. Ohama, K. Demura, H. Nagao, and T. Ogi, Adhesion of Polymer-Modified Mortars to Ordinary Portland Cement Mortar by Different Test Methods, Proceedings, RILEM Symposium on Adhesion Between Polymers and Concrete, (Aix-en-Provence, September 1986) Chapman and Hall Ltd, London 1986, pp. 719-729

105. BS 1881: Part 117: 1983. Testing concrete. Method for determination of tensile splitting strength, BSI, UK, 1983

106. BS 1881: Part 118: 1983. Testing concrete. Method for determination of flexural strength, BSI, UK, 1983

107. Ramey, G. E., and Strickland, M., An Experimental Evaluation of Rapid-Setting Materials Used in the Repair of Concrete Bridges and Pavements, FHWA Report AL-88/97B, Alabama Highway Research, Auburn University, Alabama, August, 1984

108. D. G. Geissert, S. E. Li, G. C. Frantz, and J. E. Stephens, Splitting Prism Test Method to Evaluate Concrete-to-Concrete Bond Strength, ACI Materials Journal, V. 96 May/June 1999, pp. 359-366

109. Wall, J. S., Shrive, N. G., and Gamble, B. R., Testing of Bond Between Fresh and Hardened Concrete, Proceedings, RILEM Symposium on Adhesion Between Polymers and Concrete, (Aix-en-Provence, September 1986) Chapman and Hall Ltd, London 1986, pp. 335-344

110. A. I. Abu-Tair, S. R. Rigden, and E. Burley, Testing the Bond between Repair Materials and Concrete Substrate, ACI Materials Journal, V. 93 November/December 1996, pp. 553-558

111. S. D. Tayabji, Bridge Deck and garage Floor Scarification by Hydrojetting. Concrete International, V. 8 No 5, May 1986, pp. 43-48

112. D. J. Cleland, M. Naderi, and A. E. Long, Bond Strength of Patch Repair Mortars for Concrete, Proceedings, RILEM Symposium on Adhesion Between Polymers and Concrete, (Aix-en-Provence, September 1986) Chapman and Hall Ltd, London 1986, pp. 235-244

113. K. M. Yeo, D. J. Cleland, and A. E. Long, The Effect of Environmental Conditions on Interface Adhesion Properties of Concrete Patch Repairs. Proceedings of 2nd International Conference on Inspection, Appraisal, Repair and Maintenance of Buildings and Structures, Jakarta, 1993, pp. 237-244

114. M. Ali, S. Kurihara and S. Matsui, Bonding Shear Strength at the Interface between Old and New Concrete, Department of Civil Engineering, Osaka University, 1998

115. Kreigh, J. D., Arizona Slant Shear Test: A Method to Determine Epoxy Bond Strength, ACI Journal, July 1976

116. Tabor, L. J., The Evaluation of Resign Systems for Concrete Repair, Magazine of Concrete Research, Vol 30 No. 103 Dec. 1978, pp. 221-225

117. BS 6319: Part 4: 1984 Testing of resign compositions for use in construction. Method for measurement of bond strength (slant shear method), BSI, UK, 1984

118. BS EN 12615: 1999 Products and systems for the protection and repair of concrete structures. Test methods. Determination of slant shear strength, BSI, UK, 1999

119. ASTM C 882-99 Standard Test Method for Bond Strength of Epoxy-Resign Systems Used with Concrete by Slant Shear, ASTM, USA, 1999

120. E. M. Rizzo and M. B. Sobelman, Selection Criteria for Concrete Repair Materials, Concrete International, V. 11 No 9, October 1989, pp. 46-49

121. J. C. T. S. Climacao and P. E. Regan, Evaluation of Bond Strength between Old and New Concrete, Proceedings, The International Conference on Structural Faults and Repair, 27-29 June 1989, London, Ed. M. C. Forde, Engineering Technics Press, Vol.1 pp. 115-122

122. M. Naderi, D. Cleland, and A. Long, Polymer Modified Repair-Materials-Strength and Durability, Proceedings of the 5th International Congress on Polymers in Concrete, Brighton, England, 22-24 September 1987. Ed. Barry W. Staynes pp. 309-313

123. Al-Mandil, M, Y., Performance of Epoxy-Repaired Concrete Under Thermal Cycling, Cement and Concrete Composites, Vol. 12, No. 1, 1990, pp. 47-52

124. S. A. Austin and P. J. Robins, SERC Grant Final Report, The Behaviour of Concrete Patch Repairs-An Initial Study, Department of Civil Engineering, Loughborough University of Technology, March 1991

125. F. Sausier, F. Claireaux, D. Cusson, and M. Pigeon, The challenge of numerical modelling of strains and stresses in concrete repairs, Cement and Concrete Research, Vol. 27, No. 8, 1997, pp. 1261-1270

126. Wade, D. M., Fowler, D. W., and McCullough, B. F., Concrete Bond Characteristics for a Bonded Concrete Overlay on IH-10 in El Paso, Research Report 2911-2, Centre for Transportation Research, The University of Texas at Austin, July 1995

127. Y. Pan, Bond strength of concrete patch repairs. An evaluation of test methods and the influence of workmanship and environment, PhD thesis, Loughborough University, 1995

128. E. Burley, et al, The Performance of Different Repair Techniques and Materials under Static Loading, Proceedings, The International Conference on Structural Faults and Repair, 27-29 June 1989, London, Ed. M. C. Forde, Engineering Technics Press, Vol. 1, pp. 79-86

129. G. Mays and W. Wilkinson, Polymer Repairs to Concrete: Their Influence on Structural Performance, Proceedings of Katharine and Bryant Mather International Conference on Concrete Durability, Ed. J. M. Scanlon, ACI SP-100, Atlanda, Georgia, USA 27 April-1 May 1987

130. Kudlapur, et al, Evaluation of Cold-Weather Concrete Patching Materials, ACI Materials Journal, V. 86 January/February 1989, pp 36-44

131. J. Cairns, Consequences of Bond Loss for Behaviour of Reinforced Concrete Beams, Proceedings of the Fifth International Conference on Structural Faults and Repair, Edinburgh, 29 June-1 July 1993, Vol. 3 pp. 149-154

132. J. Cairns and Z. Zhao, Behaviour of concrete beams with exposed reinforcement, Proceedings, Institution of Civil Engineers, Structures and Buildings, V. 99, March 1993, pp. 141-154

133. Z. Lin and M. Raoof, Non-linear finite strip technique applied to concrete structures, Proceedings, Institution of Civil Engineers, Structures and Buildings,

V. 99, November 1993, pp. 387-401

134. Ramirez J. L. et al, Repair of Concrete Columns with Localised Partial Loss of Corners or Cover, Proceedings of the Fifth International Conference on Structural Faults and Repair, Edinburgh, 29 June-1 July 1993, Vol. 3, pp. 195-203

135. N. K. Emberson and G. C. Mays, Significance of property mismatch in the patch repair of structural concrete - Part 2: Axially loaded reinforced concrete members, Magazine of Concrete Research, Vol. 42 No. 152, September 1990, pp. 161-170

136. S. A. Austin and P. J. Robins, Development of patch test to study behaviour of shallow concrete patch repairs, Magazine of Concrete Research, Vol 45 No. 164 Sept. 1993, pp. 221-229

137. P. J. Robins and S. A. Austin, A unified failure envelope from the evaluation of concrete repair bond tests, Magazine of Concrete Research, Vol 47 No. 170 Mar. 1995, pp. 57-68

138. Andrews, D. R. and Hughes, A. M., A novel ultrasonic transducer for inspecting concrete, IEEE Symposium on Ultrasonics & Ferroelectrics, December 1991, Orlando, Florida

139. Krause, M., Mielentz, F., Milman, B., Wiggenhauser, H., Muller, W. and Schmitz, V., Ultrasonic images of concrete members using an array system, Proc, International Symposium on Non-destructive testing in Civil Engineering, Tokyo, Japan, 2000, pp. 303-311

140. Yamaguchi, T. and Yamaguchi, T., Measurements of thickness and crack depth in concrete by ultrasonic methods, Proc, International Symposium on Non-destructive testing in Civil Engineering, Tokyo, Japan, 2000, pp. 331-340

141. BS 1881: Part 122: 1983 Testing concrete. Method for determination of water absorption, BSI, UK, 1983

142. BS 1881: Part 208: 1996 Testing concrete. Recommendations for the determination of the initial surface absorption of concrete, BSI, UK, 1996

143. J. W. Figg, Methods of measuring the air and water permeability of concrete, Magazine of Concrete Research, Vol 25 No. 85 Dec. 1973, pp. 213-219

144. R. K. Dhir, P. C. Hewllett and Y. N. Chan, Near surface characteristics of concrete: assessment and development of in situ test methods, Magazine of Concrete Research, Vol 39 No 141 Dec. 1987, pp. 183-195

145. F. R. Montgomery and A. Adams, Early Experience with a New Concrete Permeability Apparatus, Proceedings Second International Conference on Structural Faults and Repair, Edinburgh, 30 April-2 May 1985, Vol. 2, pp. 359-363

146. P. A. M. Basheer, A. E. Long and F. R. Montgomery, The Autoclam-a new test for permeability, Concrete Journal, Vol 28, No 7, July/August 1994, pp. 27-29

147. J. Steinert, Nondestructive determination of the depth of penetration of water in gravel concrete at the structure, Translation of article in Forschungsbeitrage fur die Baupraxis, 1979, pp. 151-162

148. K. Schonlin and H. Hilsdorf, Evaluation of the Effectiveness of Curing of Concrete Structures, Concrete Durability: Katharine and Bryant Mather International Conference, ACI SP-100, American Concrete Institute, 1987, pp. 207-226

149. BS 1881: Part 202: 1986 Testing concrete. Recommendations for surface hardness testing by rebound hammer, BSI, UK, 1986

150. BS EN 12504: Part 2: 2001 Testing concrete in structures. Non-destructive testing. Determination of rebound number, BSI, UK, 2001

151. ASTM C 805-97 Standard Test Method for Rebound Number of Hardened Concrete, ASTM, USA, 1997

152. ASTM C 803-97 Standard Test Method for Penetration Resistance of Hardened Concrete, ASTM, USA, 1997

153. ASTM C 900-01 Standard Test Method for Pullout Strength of Hardened Concrete, ASTM, USA, 2001

154. ASTM C 1150-96 Standard Test Method for The Break-Off Number of Concrete, ASTM, USA, 1996

155. Whitehurst, E. A., Evaluation of Concrete Properties from Sonic Tests, ACI Monograph No. 2, ACI/Iowa State University Press, USA, 1967

156. Jones, R., The Non-Destructive Testing of Concrete, Magazine of Concrete Research, Vol 3 No 2, June 1949, pp. 67-78

157. Leslie, J. R., and Cheesman W. J., An Ultrasonic Method of Studying Deterioration and Cracking in Concrete Structures, Journal of the American Concrete Institute, V. 21, No. 1, Sept., Proceedings V. 46, 1949, pp. 17-36

158. BS 1881: Part 203: 1986 Testing concrete. Recommendations for measurement of velocity of ultrasonic pulses in concrete, BSI, UK, 1986

159. ASTM C 597-97 Standard Test Method for Pulse Velocity Through Concrete, ASTM, USA, 1997

160. A. M. Alexander and H. T. Thornton, Ultrasonic Pitch-Catch and Pulse-Echo Measurements in Concrete, Nondestructive Testing of Concrete, ACI SP-112, American Concrete Institute, 1989, pp. 21-40

161. Sansalone, M., Impact-Echo The Complete Story, ACI Structural Journal, V. 94,

No 6, Nov-Dec., 1997, pp. 777-786

162. ASTM C 1383-98 Standard Test Method for Measuring the P-Wave Speed and the Thickness of Concrete Plates Using the Impact-Echo Method, ASTM, USA, 1998

163. J. S. Heisey, K. H. Stokoe and A. H. Meyer, Moduli of Pavement Systems From Spectral Analysis of Surface Waves, Transportation Research Record, No 853, Transportation Research Board, Washington D. C., USA, 1982, pp. 22-31

164. V. M. Malhotra, Testing Hardened Concrete: Nondestructive Methods, American Concrete Institute Monograph No 9, ACI, 1976, 204 pp.

165. T. W. Mitchell, Radioactive/Nuclear Methods, Handbook on Nondestructive Testing of Concrete, Chapter 10, CRS Press, Fla., 1991, pp. 227-252

166. ASTM C 1040-93 Standard Test Methods for Density of Unhardened and Hardened Concrete In Place By Nuclear Methods, ASTM, USA, 1993

167. BS 1881: Part 205: 1986 Testing concrete. Recommendations for radiography of concrete, BSI, UK, 1986

168. N. J. Carino, Performance of Electromagnetic Covermeters for Nondestructive Assessment of Steel Reinforcement, NISTIR 4988, National Institute of Standards and Technology, Sept 1992, 130 pp.

169. BS 1881: Part 204: 1988 Testing concrete. Recommendations on the use of electromagnetic covermeters, BSI, UK, 1988

170. ASTM C 876-91 Standard Test Method for Half-Cell Potentials of Uncoated Reinforcing Steel in Concrete, ASTM, USA, 1991

171. P. Rodriguez, E. Ramirez and J. A. Gonzalez, Methods for Studying Corrosion in Reinforced Concrete, Magazine of Concrete Research, Vol 46 No 167 Jun. 1994, pp. 81-90

172. ASTM D 4788-88 Standard Test Method for Detecting Delaminations in Bridge Decks Using Infrared Thermography, ASTM, USA, 1988

173. ASTM D 4748-98 Standard Test Method for Determining the Thickness of Bound Pavement Layers Using Short-Pulse Radar, ASTM, USA, 1998

APPENDIX 1

REVIEW OF NDT METHODS

1.1 INTRODUCTION

This appendix provides a brief review of the various NDT methods for evaluating concrete structures. The methods discussed include visual inspection, strength estimation methods, stress-wave propagation methods, nuclear methods, magnetic and electrical methods, penetrability methods, infrared thermography, and ground penetrating radar. Particular reference to ultrasonic pulse velocity is made, as being under investigation by some researchers for potential use in assessing the quality of bonding interface and hence the adhesive strength between concrete substrates and repair materials. The applications, advantages and limitations of each method are briefly discussed. Reference to existing BS or ASTM standards for proper application of NDT methods that have been standardised is also made. Finally, detailed description of initial surface absorption test (ISAT) and absorption by immersion test is made, since these two methods will be used in this thesis for assessing the water permeability properties of various repair materials.

1.2 VISUAL INSPECTION

Visual inspection is a powerful NDT method and one of the first steps in the evaluation of a concrete structure. It is used to locate distress patterns such as cracking, spalling, scaling, erosion, and construction defects. In many cases, it can provide an experienced engineer with quite accurate information regarding the causes and extent of deterioration. Optical magnification can enhance the accuracy of visual inspection by providing a more detailed view of local defected areas within the structure. A large

variety of instruments can be used for this purpose including: small hand-held glass magnifiers, stereo microscopes, fiberscopes, borescopes, and small digital video cameras. Visual Inspection has the obvious limitation that only visible surfaces of the structure can be inspected. Internal defects such as delaminations and voids go unnoticed and no quantitative information is obtained about the properties of the concrete. For these reasons, a visual inspection is usually supplemented by one or more of the other NDT methods available.

1.3 STRENGTH ESTIMATION METHODS

1.3.1 General

Strength estimation methods include:

- Schmidt hammer
- Penetration resistance
- Pull-out test
- Break-off test
- Pull-off test

The first three methods are used to assess the in-situ compressive strength, whereas, break-off and pull-off tests can be used to assess either the in-situ compressive or tensile strength of concrete. Pull-off test can also be used to assess the adhesive strength between concrete substrates and repair materials. A common feature of the above test methods is that they do not provide a direct measurement of compressive or tensile strength of concrete. Instead, they measure a strength related property of concrete. By testing cubes, cylinders or cores it is possible to obtain empirical correlations that relate the measured property with compressive or tensile strength of concrete.

1.3.2 Schmidt hammer

The oldest and most widely used NDT method for assessing the compressive strength of concrete structures is the Schmidt hammer tester. It was developed in 1948 by Ernst Schmidt and is also known as Swiss or rebound hammer test. Schmidt hammer provides information on the quality and relative uniformity of concrete surface layers up to 30 mm deep, by measuring the surface hardness. Since surface hardness is related to compressive strength an estimate of the compressive strength of the concrete being examined can be made. BS 1881: Part 202[149], BS EN 12504: Part 2[150] and ASTM C 805[151] give recommendations on the use of Schmidt hammers for testing the surface hardness of concrete. Schmidt hammer test is easy to perform, has a high productivity of more than 5 readings per minute, and a variety of commercial devices are available. However, it gives a measure of surface hardness which may not be representative of the interior concrete. In addition, there are many factors other than compressive strength of concrete that influence the accuracy of the test such as: type of cement, cement content, type of aggregate, type of curing and age of concrete, type of surface, moisture condition of the surface, carbonation, and direction of test. Hence, core drilling and testing for obtaining correlation curves is necessary.

1.3.3 Penetration resistance

The penetration resistance test provides information on the quality and relative uniformity of concrete, by measuring the depth of penetration of a steel probe or pin forced into the concrete by means of a driven unit. Steel probes are driven using high energy, powder-actuated drivers, whereas steel pins are smaller in size than probes and are driven by low energy, spring-actuated drivers. BS 1881: Part 207[92] gives recommendations on the use of high energy powder-actuating probe drivers, whereas

ASTM C 803[152] gives recommendations on the use of both high energy powder-actuating probe drivers and low energy spring-actuating pin drivers. The penetration resistance test is based on the concept that the depth of penetration is inversely proportional to the compressive strength of concrete, although no theoretical basis for this has been established. In addition, the relationship between penetration resistance and compressive strength of concrete is significantly influenced by the hardness of the coarse aggregate. Hence, for two different types of concrete which have the same compressive strength but contain coarse aggregate of different hardness, the concrete with the soft coarse aggregate allows greater penetration than the concrete with the hard coarse aggregate. Penetration resistance test is easy to perform and it has the advantage over the Schmidt hammer test, that a greater depth of concrete can be tested. A second advantage over the Schmidt hammer test is that smaller number of valid measurements is required for each test position. However, the cost of the penetration resistance test is much higher when is compared with the cost of the Schmidt hammer test. In addition, the relationship between penetration resistance measurements and compressive strength is significantly influenced by the hardness of the coarse aggregate. Hence, for compressive strength estimation, core drilling and testing is necessary for obtaining correlation curves. Another limitation of the penetration resistance method is that moderate damage of the concrete surface is caused which may require repair.

1.3.4 Pull-out test

Pull-out test provides information on the quality and relative uniformity of concrete. BS 1881: Part 207[92] and ASTM C 900[153] give recommendations on the use of pull-out test for assessing the compressive strength of concrete. The test is based on measuring the maximum tensile force that can be applied to an embedded metal insert

with an enlarge head before the concrete fails. As the metal insert is pulled out, a roughly cone-shaped fragment of the concrete is also extracted. During the last twenty years analytical and experimental studies have been carried out to determine the failure mechanism of the pull-out test. Although, conclusions are differed, it is generally accepted that circumferential cracking begins in the highly stressed region next to the insert head at a pull-out load that is a fraction of the ultimate value. As the load increases, the circumferential cracking propagates toward the reaction ring. However, there is no agreement on the nature of the final failure mechanism governing the magnitude of the ultimate pull-out load. Pull-out test is quick, easy, and relatively inexpensive to perform, and has the advantage that a small number of tests is required for each test position. Another advantage of the pull-out test is that correlation with compressive strength is relatively insensitive to cement and aggregate characteristics such as type (except lightweight concretes), size and proportions. However, pre-planing is required because drilling is necessary when post-installed metal inserts are used. In addition, moderate damage of the concrete surface is caused which may require repair.

1.3.5 Break-off test

Break-off test was developed in Norway by Johansen in 1976 and provides information on the quality and relative uniformity of concrete. The test method is prescribed by BS 1881: Part 207[92] and ASTM C 1150[154] and is based on measuring the maximum load also known as break-off number required to break off a cylindrical core of concrete at its base from a larger concrete mass. Since break-off test is a measure of the in-situ flexural strength of concrete empirical correlations between break-off number and compressive or tensile strength can be obtained by testing cores, cubes or cylinders. Break-off test is quick and relatively easy to perform, and has the

advantage that a small number of tests is required for each test position. However, pre-planing is required when partial coring is used. In addition, it can only be applied to structural members more than 100 mm thick. Another limitation of the break-off test is that substantial damage of the concrete surface is caused which may require repair.

1.3.6 Pull-off test

Pull-off test is used to assess the in-situ tensile or compressive strength of concrete. It can also be used to assess the adhesive strength between concrete substrates and repair materials. BS 1881: Part 207[92] gives recommendations on the use of pull-off test for assessing the in-situ tensile or compressive strength of concrete. The test is based on the principle that the force required to pull a metal block, together with a layer of concrete or mortar, from the surface to which it has been attached, is related to the tensile strength of concrete. Pull-off test is quick, easy and relatively inexpensive to perform, and has the advantage that a small number of tests is required for each test position. However, moderate damage of the surface is caused which may require repair.

1.4 STRESS-WAVE PROPAGATION METHODS

1.4.1 General

Stress-wave propagation methods for evaluating concrete structures include:

- Ultrasonic pulse velocity
- Pulse-echo
- Impact-echo
- Spectral analysis of surface waves (SASW)

Stress-wave propagation methods are based on the principle, that stress waves generated when pressure, is applied suddenly, to the surface of a solid such as concrete. The disturbance propagates through the solid in a manner analogous to how sound travels through the air. Hence, when pressure is applied suddenly at a point on the surface of a solid such as concrete, the disturbance propagates through the solid in the form of three different waves. These are:

- P-wave
- S-wave
- R-wave

The P-wave is also called the dilatational or compression wave. It is associated with the propagation of normal stress, and particle motion is parallel to the propagation direction. The S-wave is also called the shear or transverse wave. It is associated with the propagation of shear stress, and particle motion is perpendicular to the propagation direction. Both P-wave and S-wave propagate into the solid along hemispherical wavefronts. The R-wave is also called Rayleigh or surface wave and travels along the surface away from the disturbance.

When a stress wave travelling through concrete encounters an air void, it is almost totally reflected at the interface. This is the main reason why stress-wave propagation methods have proven to be successful for locating defects within concrete such as cracks, delaminations, voids, and honeycombing.

1.4.2 Ultrasonic pulse velocity method

Ultrasonic Pulse Velocity method is a long-established NDT method for assessing concrete structures. According to Whitehurst[155] it was developed nearly

simultaneously in the late 1940s in the United Kingdom by Jones and Gatfield[156] and in Canada by Leslie and Cheeseman[157]. In the United Kingdom, research was taking place for the development of an instrument to assess the quality of concrete pavements, whereas, in Canada, emphasis was on the development of an instrument to assess the extent of cracks in dams. It can be used to assess the uniformity and relative quality of concrete, to detect the presence and approximate extend of cracks and voids, to estimate the depth of concrete damaged by fire or frost, and to evaluate the quality of patch repairs. It can also be used to measure changes in the properties of concrete occurring with time, and to determine the dynamic modulus of elasticity E_d and dynamic Poisson's ratio ν of concrete. BS 1881: Part 203[158] and ASTM C 597[159] give recommendations for measuring the ultrasonic pulse velocity in concrete. A schematic of the ultrasonic pulse velocity method is shown in Figure 1.1.

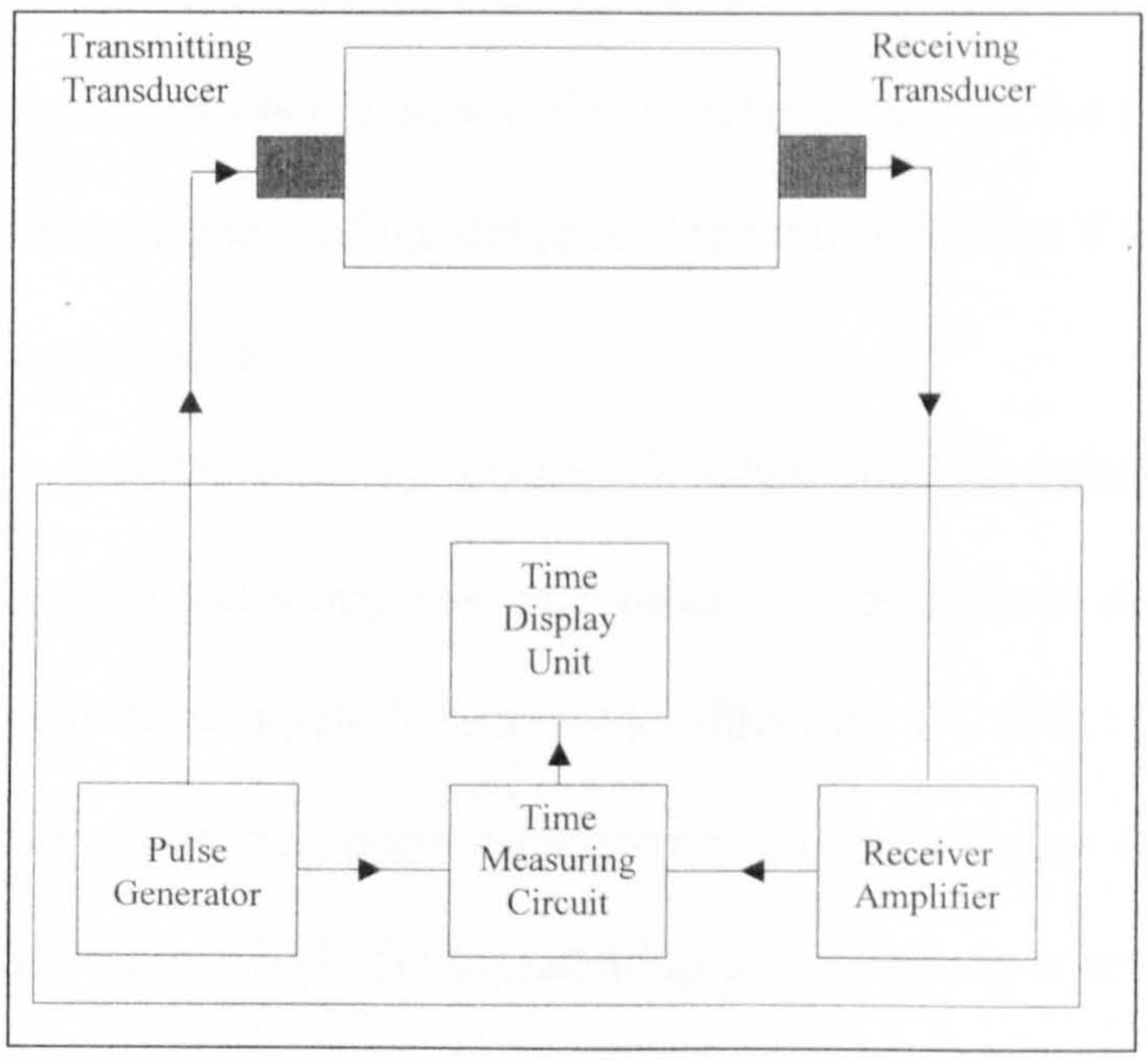

Figure 1.1 Schematic of ultrasonic pulse velocity method

Ultrasonic pulse velocity method is based on the principle that ultrasonic pulses of compressional waves are generated by an electro-acoustical transducer which is held in contact with one surface of the concrete being tested. After traversing through concrete,

the pulses are received and converted into an electrical signal by a second transducer located at a distance L from the transmitting transducer. The time taken for an ultrasonic pulse to travel from the transmitting transducer to the receiving transducer through the concrete is called transit time T, and is measured electronically. The pulse velocity v is given by the following expression:

$$v = \frac{L}{T} \tag{1.1}$$

where:

v is the pulse velocity

L is the distance between the transmitting and the receiving transducers

T is the time taken by the pulse to traverse that distance

When ultrasonic pulse travelling through concrete meets a large void or crack there is negligible transmission of energy across the interface. Instead the ultrasonic pulse is diffracted around the periphery of the defect and the transient time T will be longer than in similar concrete with no defects.

Although energy transfer is at its maximum when the transmitting and receiving transducers are placed directly opposite each other, it is possible to detect pulses which have travelled trough the concrete in some other direction. BS 1881: Part 203[158] states the following three types of transducer arrangement shown in Figure 1.2:

- Direct transmission in which the transmitting and receiving transducers are placed on opposite faces
- Semi-direct transmission in which the transmitting and receiving transducers are placed on adjacent faces
- Indirect or surface transmission in which the transmitting and receiving transducers are placed on the same surface.

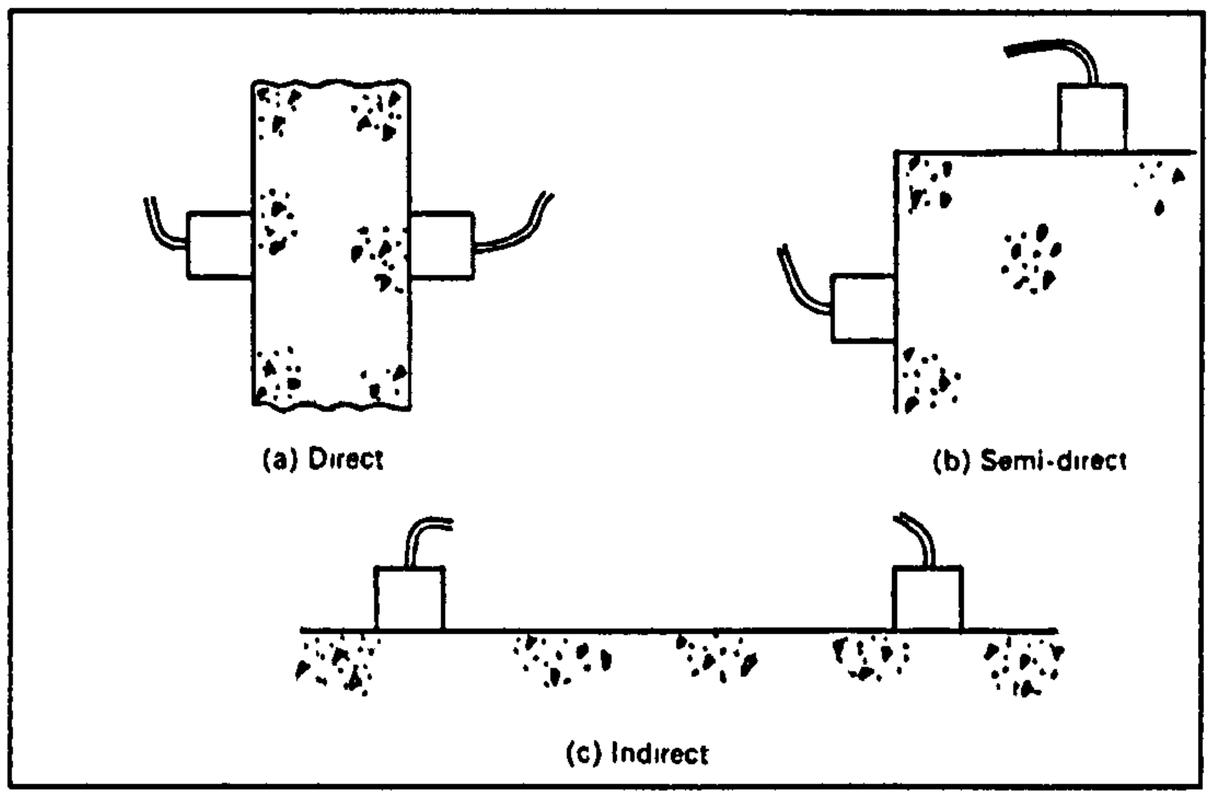

Figure 1.2 Different transducer arrangements

Ultrasonic pulse velocity method is quick and easy to perform and it has a low operational cost. However, operators must be skilled and with experience in the interpretation of results. In addition pulse velocity measurements and their correlations with various physical properties of concrete (compressive strength, dynamic elastic modulus E_d and dynamic Poisson's ratio ν) are influenced by a number of factors (age of concrete, curing conditions, moisture content, mix proportions, type of aggregate and type of cement).

1.4.3 Pulse-echo method

The two main disadvantages of the ultrasonic pulse velocity method are the need for access to both sides of the concrete member being examined and the lack of information regarding the depth of the detected defect. Pulse-echo method was developed to overcome these problems and it can be used for determining the depth of delaminations and voids in relatively thin walls, slabs and pavements. Alexander and Thornton[160] provide a review of the method. The method is based on the principle that a stress wave is introduced into the concrete by a transmitting transducer located at an accessible surface. The pulse propagates into the concrete and is reflected by defects such as voids

and cracks. A separate receiving transducer located next to the transmitting transducer monitors the arrival of the reflected waves. In modern equipment transmitting transducer also acts as a receiving transducer. The output of the receiving transducer is displayed on an oscilloscope as a time-domain waveform. Since the time from the transmission of the pulse to the reception of the echo is measured, the depth of the defect can be determined if the wave speed is known. Pulse-echo method is very successful for locating the depth of delaminations and voids. However, the penetration depth for locating defects is limited, and the accuracy in concrete with large aggregates is not known. In addition, operators must be skilled and with experience in the interpretation of survey results. Finally, pulse-echo equipment is not commercially available and the method has not been standardised by BSI or ASTM.

1.4.4 Impact-echo method

Impact-echo method can be used to measure the thickness of concrete plate structures such as slabs, pavements, bridge decks, and walls. It can also be used to locate voids, cracks, honeycomb, and other defects in structural concrete elements such as slabs, beams and columns. Sansalone[161] describes the history of the development of the method. ASTM C 1383[162] gives recommendations for measuring the P-wave speed and the thickness of concrete plates using the impact-echo method. The method is based on the principle that P-waves are introduced into the concrete by a short-duration mechanical impact. When P-waves travel into concrete are reflected by internal interfaces such as voids and cracks or external boundaries. Multiple reflections of P-waves between the impact surface, defects, and/or other external surfaces give rise to a transient thickness resonance. The arrival of the reflected waves, at the surface where they were generated produces displacements that are measured by a receiving

transducer, located adjacent to the impact point. The output of the receiving transducer is recorded as a time domain waveform. The recorded time domain waveform is transformed into frequency domain using the fast Fourier transform technique and an amplitude spectrum is obtained. The frequency corresponding to the transient thickness resonance is known as thickness frequency and is indicated by a peak in the amplitude spectrum. Impact-echo method is a powerful method for measuring the thickness of plate structures or locating defects in slabs, beams, and columns. It has been standardised by ASTM and has the advantage that access to only one face of the member is needed. However, its application is limited to concrete members less than 2 m thick.

1.4.5 Spectral analysis of surface waves (SASW)

SASW method was developed in the early 1980s. The method can be used to determine the elastic properties and thickness of pavements. It can also be used to detect voids and determine the extent of damage in concrete structures. Heisey[163] provides a review of the method. The method is based on the principle that R-waves are generated by an impact. R-waves travel along the surface of the concrete away from the point of impact. Two receiving transducers spaced a known distance apart, are used to monitor the propagation of R-waves by measuring the vertical surface velocity or acceleration. R-waves contain a range of components of different frequencies. This range depends on the contact time of the impact. Lower frequency components penetrate more deeply into the concrete. Hence, information regarding the properties of the underlying layers can be obtained by monitoring the motion of R-waves. SASW method is a relatively new method for measuring the elastic properties and thickness of pavements. However,

operators must be skilled and with experience in the interpretation of survey results. Its main disadvantage is that involves complex signal processing.

1.5 NUCLEAR METHODS

1.5.1 General

Nuclear methods include radiometry and radiography. Radiometry is used to determine the density of unhardened or hardened concrete. Radiography is used to record on photographic film the intensity of electromagnetic radiation (gamma rays or X-rays) after passing through concrete and is identical to X-rays used for medical purposes. Malhotra[164] and Mitchell[165] provide a review of nuclear methods

1.5.2 Radiometry

Radiometry is used to determine the density of unhardened or hardened concrete. Two radiometry methods are available:

- Direct transmission radiometry
- Backscatter radiometry

The main difference between the two radiometric methods is that direct transmission measures the intensity of high-energy electromagnetic radiation (gamma rays) after passing through concrete, whereas, backscatter measures the intensity of high-energy electromagnetic radiation (gamma rays) that is reflected by the near to surface concrete. ASTM C 1040[166] gives procedures for measuring the density of unhardened concrete by using the direct transmission radiometry method. It also gives procedures for measuring the density of unhardened or hardened concrete using backscatter radiometry method. Both radiometric methods are rapid and portable equipment makes them

suitable for use in the field. Minimal operator skills are required to perform measurements. However, direct transmission radiometry requires access to both sides of the concrete member and commercially available equipment is limited to path lengths of up to 300 mm. In addition, the accuracy of density measurements obtained using backscatter radiometry is lower than direct transmission, and are affected by near to surface material and chemical composition of concrete. Finally, operators must be licensed.

1.5.3 Radiography

Radiography is used to determine the presence of steel reinforcement and its approximate location and size. It can also be used to locate voids and honeycombing. BS 1881: Part 205[167] gives recommendations for radiography of concrete. Radiography is based on the use of special photographic film to record the intensity of electromagnetic radiation (gamma rays or X-rays) after passing through concrete. The method provides an accurate two-dimensional image of the internal structure of the concrete. However, operators must be licensed and highly skilled. In addition heavy and expensive equipment is used, access to both sides of the concrete member is required, measurements take a long time, and extensive safety precautions are needed.

1.6 MAGNETIC AND ELECTRICAL METHODS

1.6.1 General

Magnetic and electrical methods include:

- Covermeter
- Half-cell potential method
- Linear polarisation method

Covermeter is used to locate steel reinforcement bars and to estimate the cover depth. Half-cell potential method is used to provide an indication of probable corrosion activity in a reinforced concrete structure at time of testing. Finally, linear polarisation method is used to provide an indication of corrosion rate at time of testing.

1.6.2 Covermeter

Covermeter is also known as pachometer and can be used to locate steel reinforcement bars and other buried ferromagnetic objects such as water pipes, steel joists and lighting conduits. It can also be used to estimate the cover depth. Carino[168] provides a review of covermeters, whereas BS 1881 Part 204[169] gives recommendations on the use of electromagnetic covermeters. The use of covermeter is based on the principle that the depth of cover can be measured by monitoring the interaction between the bars and a low frequency, electromagnetic field produced by the search head of the covermeter. When a steel bar or other ferromagnetic object lies within this field, the lines of force become distorted. The disturbance caused by the presence of the steel bar in turn produces a local change in field strength which is detected by the search head and is indicated by a meter. The reading of the meter is affected by the orientation and proximity of the steel bar to the search head. Hence, it is possible to locate steel reinforcement bars and determine their orientation. Cover depth may also be determined if a suitable calibration can be obtained for the particular size of bar and the materials under investigation. With some covermeters it is possible, to estimate both bar size and cover when neither is known. Commercial covermeters can be divided into two groups: magnetic reluctance covermeters based on magnetic induction and eddy-current covermeters based on eddy-current effects. Covermeter is lightweight, portable, and easy to use. However, its ability to locate individual steel reinforcement bars and

estimate cover depth is influenced by many factors. In addition, maximum penetration is limited, presence of second layer of reinforcement can not be identified, and high precision estimate of bar diameter is difficult to achieve.

1.6.3 Half-cell potential method

Half-cell potential method can be used to identify regions in a reinforced concrete structure where there is high probability that corrosion is occurring at the time of measurement. ASTM C 876[170] provides procedures for estimating the electrical half-cell potential of uncoated reinforcing steel in concrete. The half-cell potential method is based on measuring the potential difference (voltage) between the steel reinforcement and a standard reference electrode. The measured voltage provides an indication of probable corrosion occurring in the reinforcement at time of testing. Half-cell potential method has the advantage that lightweight and portable equipment is used. However, reliable readings can be obtained only if the concrete is sufficiently moist during testing. In addition, the method can not be applied to concrete with epoxy-coated steel reinforcement. Another limitation of the half-cell potential method is that it does not measure rate of corrosion of steel reinforcement. Finally, testing and interpretation of results should be carried out by well-qualified and experienced operators.

1.6.4 Linear polarisation method

Linear polarisation method provides an indication of corrosion rate at time of testing. Rodriguez[171] provides a review of the method. The method is based on measuring the electrical current required to change by a fixed amount the potential difference between the reinforcement and a standard reference electrode. The measured current and voltage allow determination of the polarisation resistance, which is related to the rate of

corrosion. Linear polarisation method has the advantage that lightweight and portable equipment is used. However, the concrete surface has to be smooth, free of water impermeable coatings or overlays, and free of visible moisture. In addition, the method can not be applied to concrete with epoxy-coated steel reinforcement. Another limitation of the linear polarisation method is that the cover depth must be less than 100 mm. Finally, there are no standard procedures for interpreting results obtained using different devices. Hence, testing and interpretation of results should be carried out by well-qualified and experienced operators.

1.7 PENETRABILITY METHODS

1.7.1 General

Penetrability methods are used to assess the ability of the surface zone of the concrete to restrict the passage of external agents such as water, sulphates, chlorides, and carbon dioxide that may lead to direct deterioration of the concrete or to depassivation and corrosion of the steel reinforcement.

There are three main transport mechanisms by which external agents can penetrate into concrete:

- Absorption
- Permeation
- Diffusion

Absorption is described as the passage of fluids due to capillary forces. Contaminants, such as Cl^- and SO_3^- are transported within the fluid. The term sorptivity is used to describe the tendency of a solid to absorb a fluid. For one-dimensional water absorption

into an initially dry porous solid the volume of an absorbed fluid can be related to time by the following empirical equation

$$V = As\sqrt{t} \tag{1.2}$$

where:

V is the volume of fluid absorbed (m^3)

A is the wetted area (m^2)

s is the sorptivity ($m/\sqrt{s}$)

t is the time (s)

Permeation can be described as the flow of a fluid under the action of a pressure head. For steady-state, unidirectional flow of a fluid through a saturated porous solid, the flow rate is given by Darcy's law:

$$Q = kAI \tag{1.3}$$

where:

Q is the flow rate (m^3/s)

k is the coefficient of permeability (m/s)

A is the cross-sectional area of flow (m^2)

I is the hydraulic gradient (m/m)

The coefficient of permeability depends on both the structure of the solid and the properties of the fluid. In the case of concrete, the coefficient of permeability depends mainly on the mix design, the w/c ratio and the age of concrete.

Diffusion can be described as the movement of molecular or ionic substances from regions of higher concentration to regions of lower concentration of the substances. The rate of movement of the substance is given by Fick's first law of diffusion:

$$F = \frac{\partial m}{\partial t}\frac{1}{A} = -D\frac{\partial C}{\partial x} \tag{1.4}$$

where:

F is the mass flux (kg/m^2s)

m is the mass of flowing substance (kg)

t is the time (s)

A is the area (m^2)

D is the diffusion coefficient (m^2/s)

C is the concentration (kg/m^3)

x is the distance (m)

Various penetrability tests have been developed for assessing the durability of a concrete surface. Most of these tests are based on one of the above transport mechanisms. Penetrability tests can be divided into three groups:

- Water absorption tests
- Water-permeability tests
- Air permeability tests

1.7.2 Water absorption tests

Water absorption tests measure the absorption rate of the water into the concrete under a relatively low water pressure head. The absorption rate of the water is a function of the capillary porosity, which in turn is a function of w/c ratio and curing history. Water absorption tests include:

- Absorption by immersion test which is described by BS 1881: Part 122[141]
- Initial surface-absorption test (ISAT) which is described by BS 1881: Part 208[142]
- Figg water-absorption test
- Covercrete-absorption test

Absorption by immersion test is used to measure the ease with which a fluid can penetrate concrete. Tests can be performed on either cores or cubes. In order for the specimens to achieve a constant mass they should be oven dried for 72 ± 2 h at a temperature of 105 ± 5 ^{0}C before testing. After cooling the specimens are weight and immersed in water. The temperature of the water used for testing should be maintained at 20 ± 1 ^{0}C. The specimens are placed on supports in a dish with a flat base and are completely immersed in a head of water 25 ± 5 mm. After 30 ± 0.5 min the specimens are surfaced dried and weight. The same procedure is repeated after 24 hours when the test will end. The 24 hours duration of the test gives sufficient results for analysing the water absorption properties of concrete. Finally, the absorption of each specimen is expressed as a percentage increase in weight compared to its dry weight. Absorption by immersion test is simple and very easy to perform but in practise is not frequently used. Fluid flow is very complex during the test so the method is usually treated empirically. In addition, the drying regime of the specimen significantly influences the results. For specimens dried at high temperatures results are much higher compared to specimens made of the same mix but dried at lower temperatures. This is mainly due to the fact that drying at high temperatures may cause removal of the combined water compared to drying at low temperatures. In most good quality concretes water absorption is well below 10% by mass.

ISAT is used to measure the initial surface absorption of concrete, which, can be defined as the rate of flow of water into concrete per unit area at a stated interval from the start of the test and at a constant applied head. In order to perform the test a watertight circular cap with a minimum surface area of 5000 mm^2 is sealed to the concrete surface and connected by means of flexible tubes to a reservoir. The reservoir is filled with water so that the water level is 200 mm above the concrete surface. The applied pressure of 200 mm head of water is worse than the severest weather exposure in the UK due to driving rain. The watertight circular cup is also connected to a capillary tube with a scale which is positioned horizontally at the same height as the water in the reservoir. Prior to testing cube specimens are oven dried at a temperature of $105 \pm 5\ ^0C$ until constant mass is achieved, i.e. not more than 0.1% weight change over any 24 h drying period. After cooling the cap is fixed on the concrete surface and the specimen is subjected to a head of water of 200 mm. At specific intervals (10 min, 30 min, and 1 h) from the start of the test, the valve below the reservoir is closed and the movement of water in the capillary tube is used to measure the rate at which water is absorbed into concrete. ISAT is simple and inexpensive to perform. In addition, it is sensitive to changes in concrete quality. However, it is only able to measure the absorption of the outer 10 -15 mm of concrete and is affected by surface coatings. In addition, it is unreliable for concretes with a high sorptivity surface layer. This is because the flow of water through the concrete specimen in the ISAT test is not one-directional, but for concretes with a low surface sorptivity, it may be considered to be one-dimensional. However, as the sorptivity of the surface layer increases, radial movement governs the flow of water in the specimen.

Figg's water absorption test as the name suggests was developed by Figg[143] in 1973. The test is based on drilling a 5.5 mm diameter hole into concrete to a depth of 30 mm.

The hole is cleaned, a disc of rigid polymeric foam is pushed into the hole to a depth of 20 mm from the surface and the hole is sealed using silicone rubber. Next, a hypodermic needle is inserted through the silicone rubber seal and connected to a syringe and a horizontal capillary through a series of connectors. A water head of 100 mm is then applied and the time taken for the meniscus to travel 50 mm in the horizontal capillary is recorded. The value obtained is known as the water absorption index and is measured in seconds. The higher the absorption index the lower the water absorption of concrete.

The main limitation of ISAT is that it can only measure the water absorption of the outer 10-15 mm of concrete, whereas the main limitation of Figg's test is that it can only measure the water absorption of concrete deeper than 20 mm. The covercrete-absorption test was developed by Dhir[144] to overcome the above limitations by providing an integrated water absorption of the surface zone to a depth of 50 mm. The test is based on drilling a 13 mm diameter hole into concrete to a depth of 50 mm. A gasketted cap is placed over the hole and a tube connected to a reservoir passes through the cap and empties into the hole. The cap contains a second tube which is connected to a horizontal capillary. The reservoir and the capillary are placed in such a way that a water head of 200 mm is maintained above the centre of the hole. The tube connected to the reservoir is closed and the movement of the meniscus in the capillary is measured between 10 and 11 minutes after initial contact with water.

1.7.3 Water-permeability tests

Water-permeability tests provide information on the permeability of concrete under a low water pressure head. Water-permeability tests include:

- CLAM test

- Steinert method

CLAM test is used to measure the flow of water into the concrete surface under a fixed pressure. Montgomery and Adams[145] and Basheer et al[146] provide a detailed description of the test. The method is based on attaching a specially designed cap to the concrete surface. Pressurized water is provided by a micrometer-screw piston. A pressure gauge in the chamber monitors the water pressure. In order to perform the test, the chamber is filled with water, the micrometer screw is turned so as to maintain a constant water pressure of about 150 kPa above atmospheric pressure and the movement of the piston through the cylinder is recorded at constant intervals for 20-30 minutes. By measuring the movement of the piston through the cylinder the volume of water that penetrates into the concrete can be determined. Plotting the volume of water versus time information regarding the permeability of concrete can be obtained. Since the flow of water into the concrete is not unidirectional and a steady-state condition is not achieved, a permeability index is obtained rather than the true permeability.

Steinert method as the name suggests was developed by Steinert[147] in 1979. The test is based on the guard ring principle to achieve a better approximation of unidirectional flow under pressure. A cap, which is made of 2 concentric chambers separated by a circular rubber seal, is attached to the concrete surface. The concentric chambers are filled with water and pressurized to 600 kPa using compressed air. Flow under the inner chamber is approximately unidirectional. Hence, monitoring of flow as a function of time is easier to interpret compared to CLAM test

1.7.4 Air-permeability tests

Air-permeability tests are similar to water-permeability tests and provide information on the flow of air, or other gases through concrete. Relationships exist between air permeability of concrete and durability factors such as water/cement ratio, compressive strength, and curing efficiency. Air-permeability tests are usually easier to perform than water-permeability tests. Air-permeability tests include:

- Figg air-permeability test
- Schonlin test

Figg's air permeability test as the name suggests was developed by Figg[143] in 1973. The test is based on drilling a 5.5 mm diameter hole into concrete to a depth of 30 mm. The hole is cleaned, a disc of rigid polymeric foam is pushed into the hole to a depth of 20 mm from the surface and the hole is sealed using silicone rubber. Next, a hypodermic needle is inserted through the silicone rubber seal and connected to a vacuum pump. The vacuum pump is turned on until the pressure inside the hole is decreased to -85 kPa below atmospheric pressure. The valve is then closed and the flow of air inside the hole results in a reduction of the vacuum. The time taken to obtain a 5 kPa increase in the hole is known as the air permeability index and is measured in seconds. The higher the air permeability index the lower the air absorption of concrete.

The main disadvantage of Figg's air permeability test is that a hole needs to be drilled. In order to avoid drilling a hole, Schonlin test was developed. A description of the test is provided by Schonlin and Hilsdorf[148]. The method is based on the use of a 50 mm in diameter chamber of known volume which is attached to the concrete surface. Next, a vacuum pump is used to evacuate the chamber to a pressure less than -99 kPa. The valve is then closed and the time when the vacuum pressure reaches -95 kPa is taken as

the start of the test. The time required for the value of vacuum pressure to increase from -95 kPa to -70 kPa is measured. When dense concrete is investigated, the vacuum pressure change during 120 seconds is measured instead. Based on the above measurements and the known volume of the chamber, a permeability index measured in m^2/s is obtained.

1.8 INFRARED THERMOGRAPHY (IT)

Infrared thermography is used to locate and determine the extent of voids and delaminations in concrete pavements and bridge decks. It can also be used to locate moist insulation in buildings. ASTM D 4788[172] describes the use of infrared thermography for detecting delaminations in bridges. The method is based on the principle that subsurface anomalies such as voids and delaminations result in localised differences in surface temperature caused by different rates of heat transfer at the defect zones. Thermography senses the emission of thermal radiation from the surface of the concrete and produces a visual image from this thermal signal which can be related to the size of an internal defect. Infrared thermography is a global NDT method and permits large concrete surfaces to be inspected in a short period of time. However, if defects are located too deep in concrete or if their diameter is small compared to their depth, the thermal contrast at the surface will be very small due to conduction and hence, such defects may stay undetected. In addition, the depth and thickness of a detected subsurface defect can not be measured. Another limitation of infrared thermography is that measurements of thermal radiation are influenced by environmental conditions.

1.9 GROUND-PENETRATING RADAR (GPR)

GPR was initially developed in 1960s for geophysical applications such as locating buried pipelines, tanks and cables, measuring the thickness of glaciers and sea ice, mapping the bottom of rivers and lakes, and measuring scour around bridge foundations. For evaluating concrete structures, GPR can be used to measure the thickness of pavements, locate metallic embetments such as steel reinforcement, and detect voids, delaminations, and high moisture content regions. Three types of GPR systems have been developed for structural applications: frequency modulation, synthetic-pulse, and short pulse. From these, short-pulse radar systems gained the greatest practical acceptance and are most widely used. Short-pulse radar is analogous to pulse-echo method, except that short-pulse electromagnetic waves are used instead of stress waves. ASTM D 4748[173] gives procedures for using short-pulse radar to determine the thickness of bound pavement layers. Short-pulse radar is based on transmitting short-pulse electromagnetic waves towards the material under examination. The electromagnetic waves travel through concrete and when an interface between two materials with dissimilar dielectric properties is encountered part of the electromagnetic energy is reflected back to the antenna. The antenna receives the reflected electromagnetic energy and generates an output signal proportional to the amount of the reflected electromagnetic energy. An important difference between GPR and stress-wave methods, such as the impact-echo method, is the amount of reflected energy at a concrete-air interface. For stress waves, the reflection is almost 100% because the acoustic impedance of air is negligible compared with concrete. For short-pulse electromagnetic waves however, the reflection is approximately 50%. Hence, GPR is not as sensitive to the detection of concrete-air interfaces as are the stress-waves methods. However, because only 50% of the energy is reflected at a concrete-air

interface, GPR is able to penetrate beyond such an interface and examine features below the interface.

GPR is a very successful method for locating steel reinforcement and detect voids, delaminations and high moisture contents. However, the behaviour of electromagnetic waves propagating through reinforced concrete structures is not completely understood. In addition, electromagnetic waves from high-resolution antennae have limited depth of penetration ranging from 400 up to 750 mm, the region of the concrete irradiated by the antenna is limited to cone-shaped volume directly below the antenna, and congested reinforcement can prevent penetration beyond the reinforcement. Another limitation of the GPR is that cracks and delaminations are not easy to detect unless moisture is also present in the cracks or delamination regions. Finally experienced operators required to operate equipment and interpret large amounts of data obtained during surveys.

APPENDIX 2

PRODUCTION OF REINFORCED POCKET SLABS

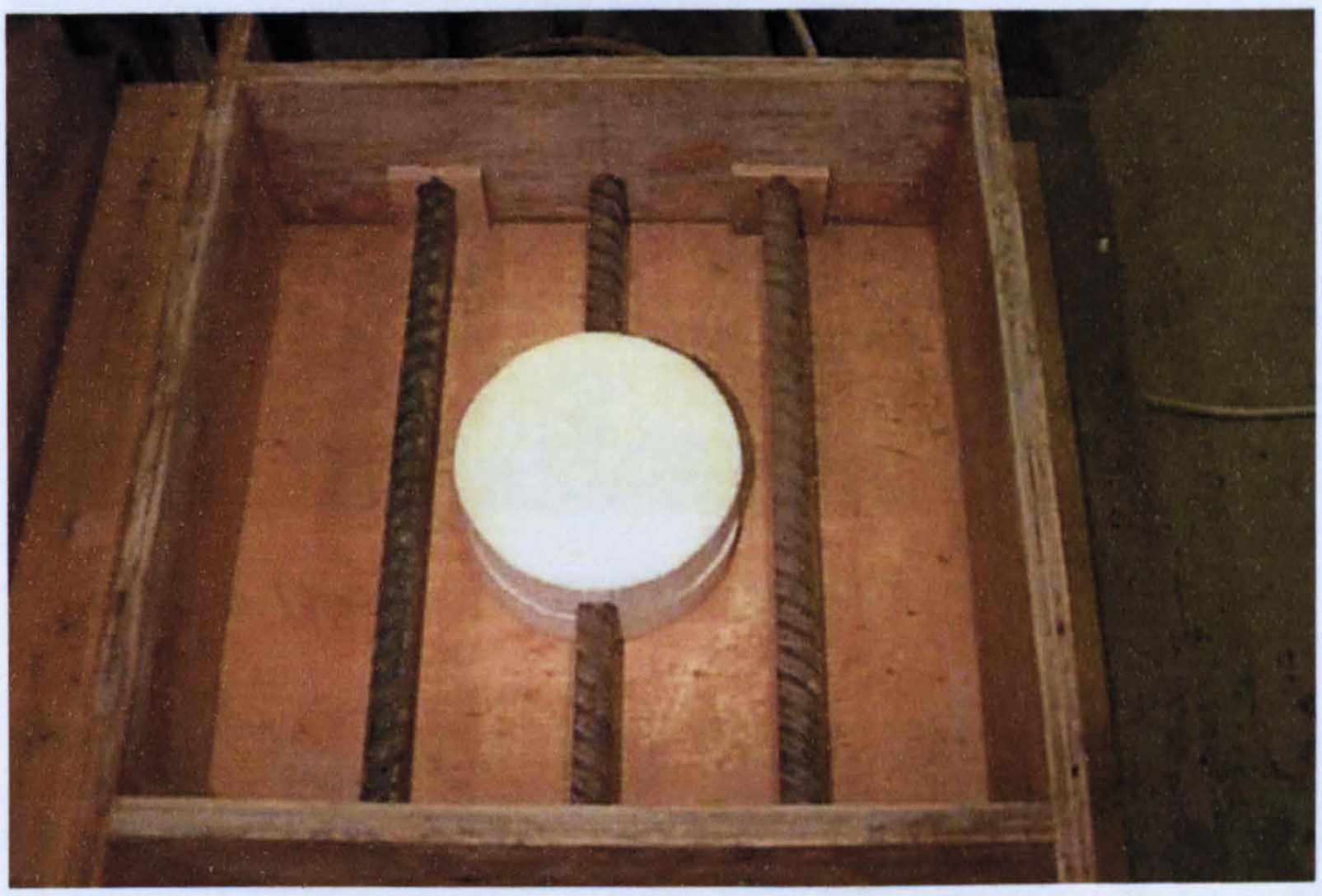

Mould ready for casting reinforced pocket slabs

Reinforced pocket slab after casting

Reinforced pocket slab before filling with low strength concrete

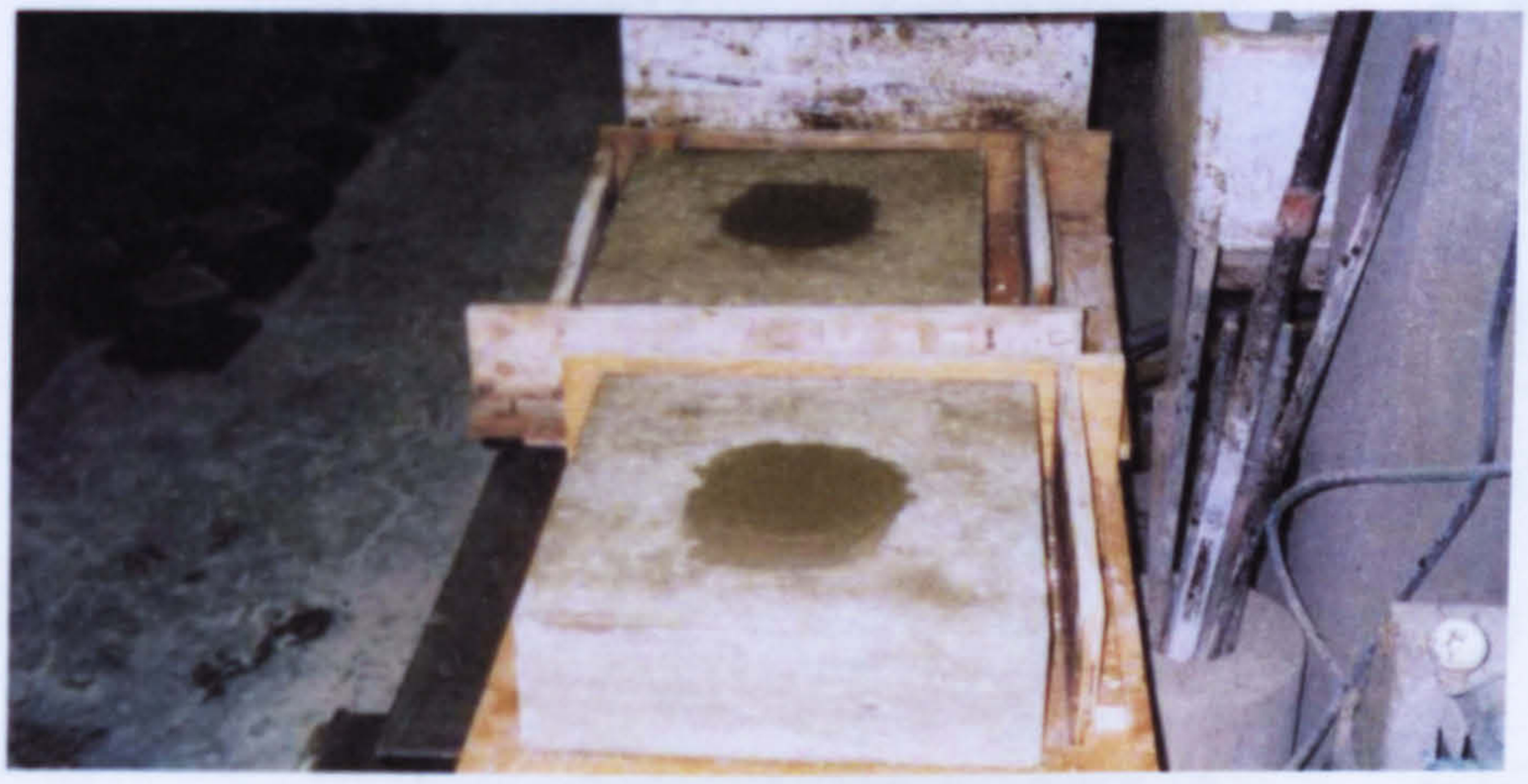

Reinforced pocket slabs after filling with low strength concrete

APPENDIX 3

HYDRODEMOLITION EXPERIMENTS

COMPRESSIVE STRENGTHS

Slab	Cube number	Compressive strength (N/mm^2)	Variation coefficient (%)	Average compressive strength (N/mm^2)
PL1	1	51.01	2.65	52.40
	2	53.80	2.67	
	3	52.40	0	
PL3	1	46.60	2.10	47.60
	2	48.60	2.10	
	3	47.60	0	
PL12	1	55.01	8.87	50.53
	2	49.70	1.64	
	3	46.90	7.18	
PL4	1	48.20	0.52	48.45
	2	48.70	0.52	
	3	48.45	0	
PL7	1	61.20	0.16	61.30
	2	61.40	0.16	
	3	61.30	0	
PL2	1	57.80	0.78	57.35
	2	56.90	0.78	
	3	57.35	0	
PL5 PL6	1	53.90	6.86	57.87
	2	60.40	4.37	
	3	59.30	2.47	
PL9 PL10	1	58.60	3.30	56.73
	2	56.30	0.76	
	3	55.30	2.52	
PL11 PL13	1	48.30	7.60	52.27
	2	51.90	0.71	
	3	56.60	8.28	
PL14	1	65.30	1.71	64.20
	2	65.30	1.71	
	3	62.01	3.41	
PL15 PL16	1	31.78	2.03	32.44
	2	31.95	1.51	
	3	33.14	2.16	
	4	32.87	1.33	
P1 P2	Strong			Strong
	1	60.20	1.20	60.93
	2	61.10	0.28	
	3	61.50	0.94	
	Weak			Weak
	1	30.20	9.12	33.23
	2	34.10	2.62	
	3	35.40	6.53	

P4	Strong			Strong
P5	1	58.50	3.85	56.33
P6	2	50.60	10.17	
	3	65.60	16.46	
	4	48.30	14.26	
	5	57.90	2.79	
	6	57.10	1.37	
	Weak			Weak
	1	25.80	4.97	27.15
	2	27.86	2.62	
	3	26.52	2.32	
	4	28.94	6.59	
	5	26.63	1.92	
	6	27.14	0.04	
RC1	Strong			Strong
	1	60.40	4.55	57.77
	2	57.50	0.47	
	3	55.40	4.10	
	Weak			Weak
	1	30.80	2.65	31.64
	2	33.74	6.64	
	3	30.38	3.98	
RC3	Strong			Strong
	1	52.00	4.42	49.80
	2	50.00	0.40	
	3	47.40	4.82	
	Weak			Weak
	1	28.20	6.72	30.23
	2	32.70	8.17	
	3	29.79	1.46	
P3	Strong			Strong
	1	59.00	2.37	60.43
	2	62.50	3.43	
	3	59.80	1.04	
	Weak			Weak
	1	35.20	4.67	33.63
	2	32.78	2.53	
	3	32.90	2.17	
RC4	Strong			Strong
RC5	1	49.20	1.99	50.20
	2	51.20	1.99	
	3	50.20	0	
	Weak			Weak
	1	33.27	6.36	31.28
	2	29.28	6.39	
	3	31.28	0	

RC6	Strong			Strong
	1	64.40	0.36	64.17
	2	65.40	1.92	
	3	62.70	2.29	
	Weak			Weak
	1	44.80	2.55	45.97
	2	45.65	0.70	
	3	47.48	3.28	

APPENDIX 4

PROFILES OF EXCAVATIONS

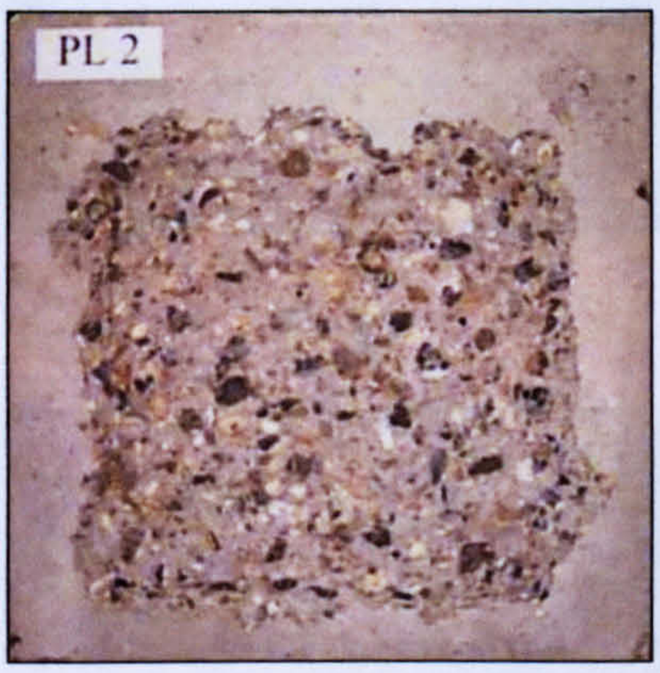

PL 2

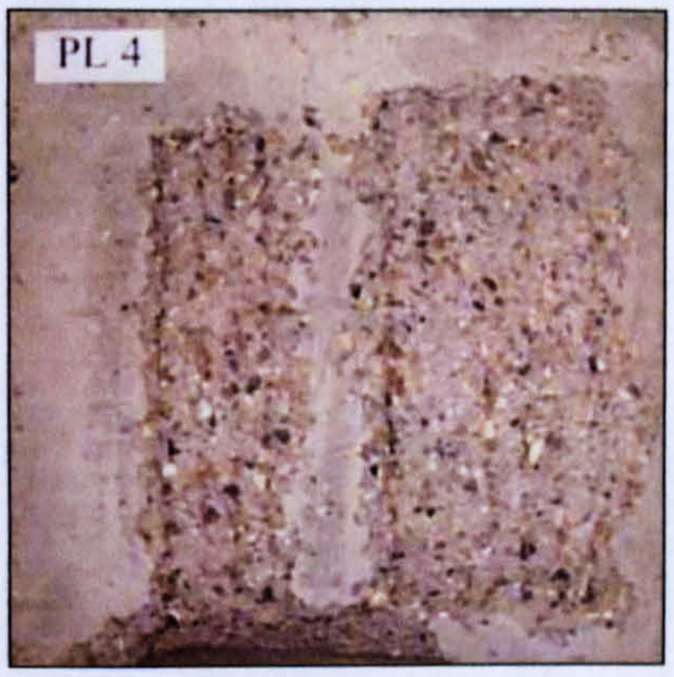

PL 4

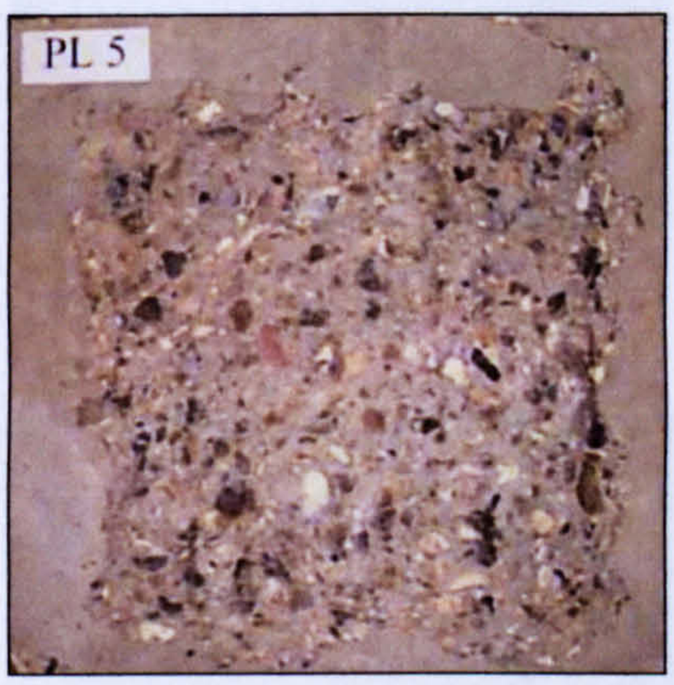

PL 5

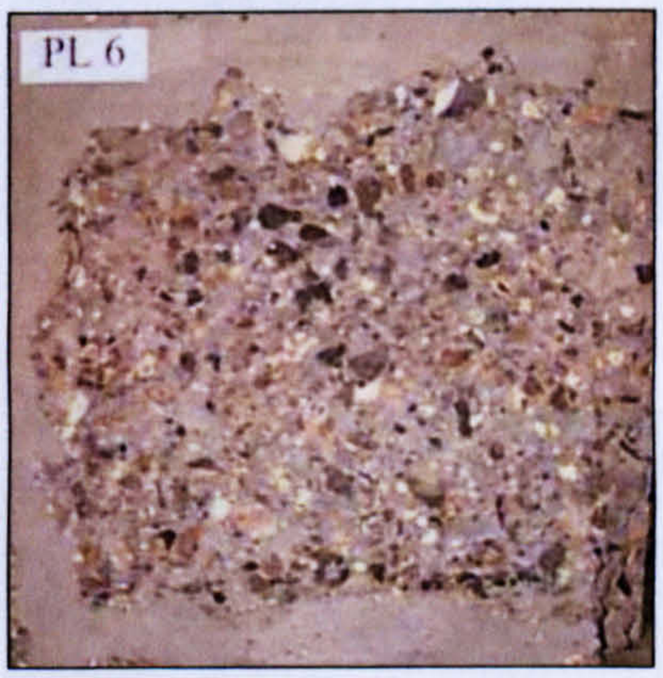

PL 6

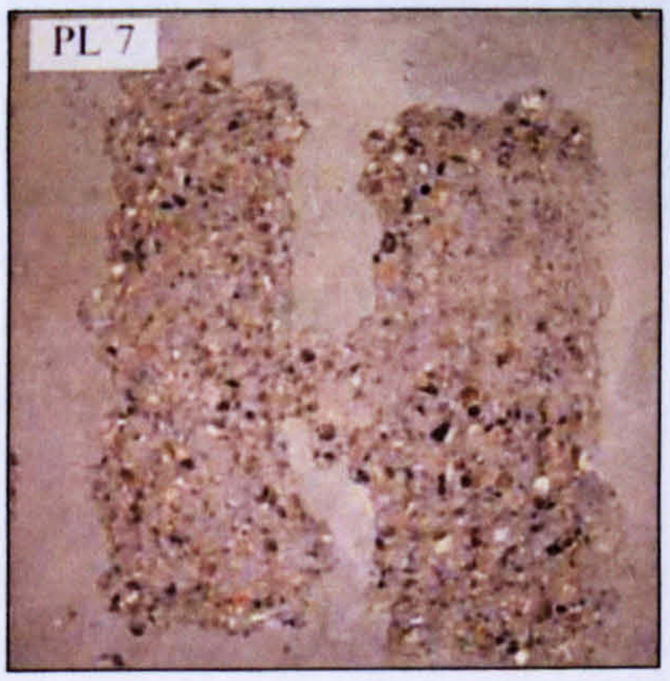

PL 7

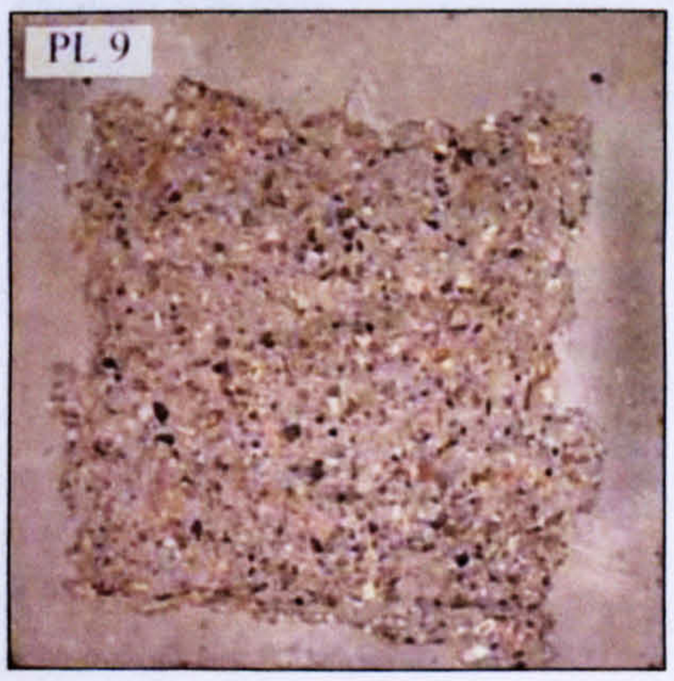

PL 9

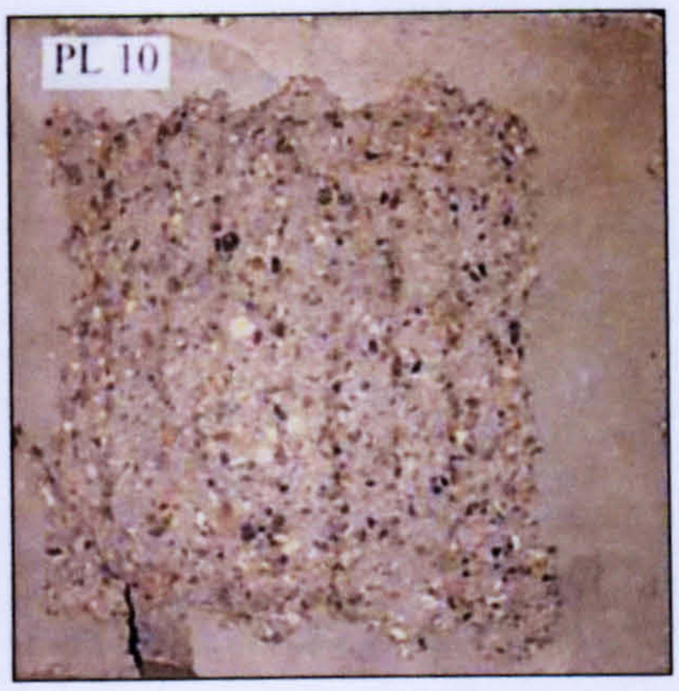

PL 10

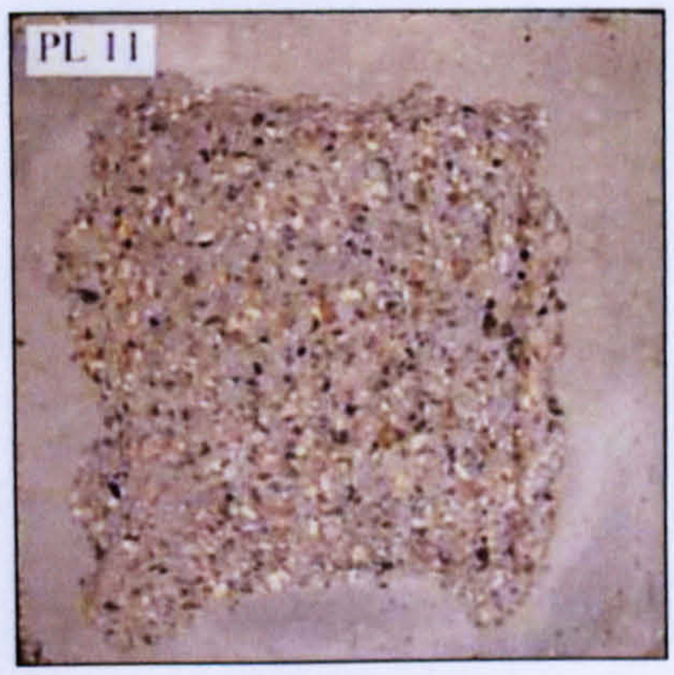

PL 11

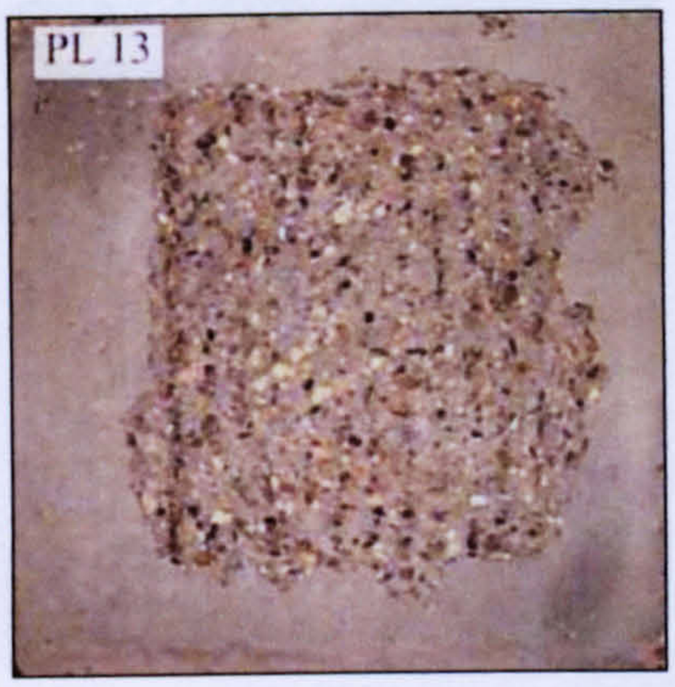

PL 13

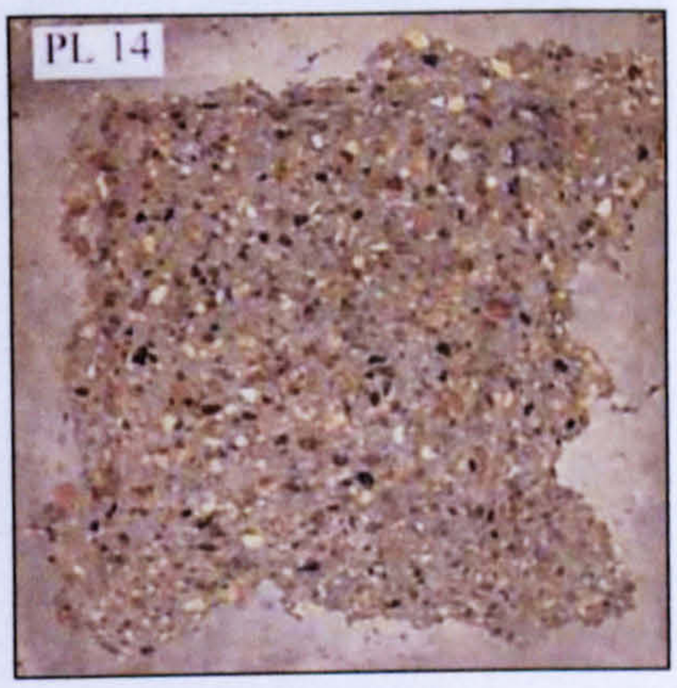

PL 14

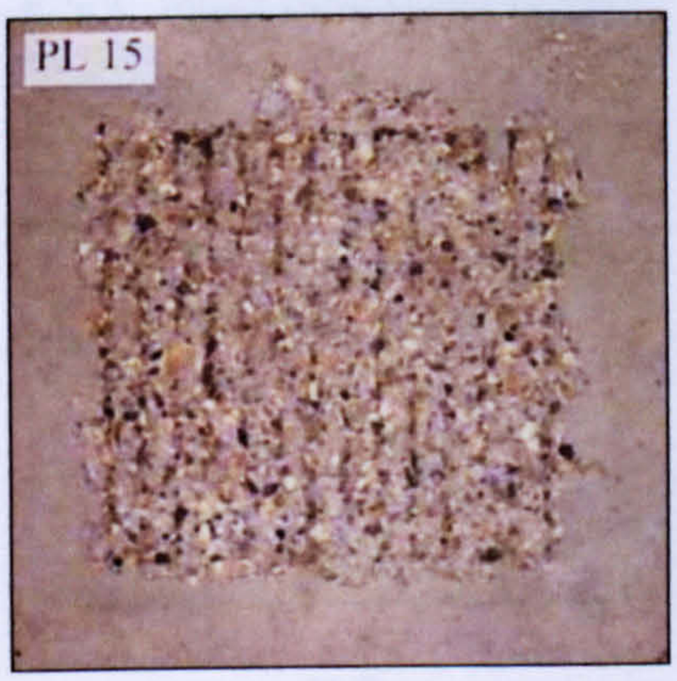

PL 15

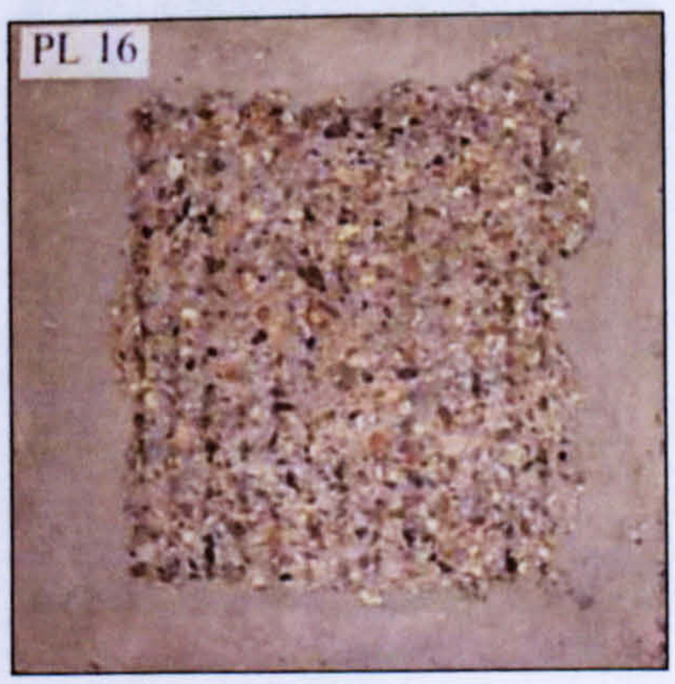

PL 16

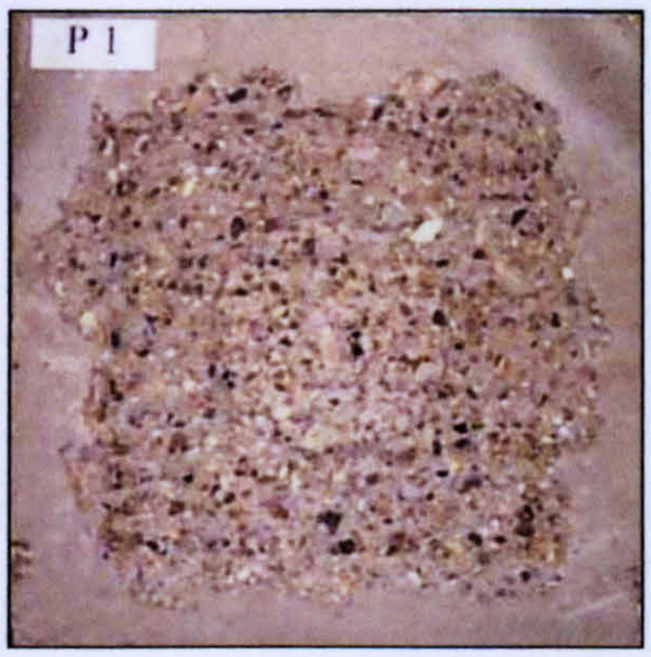

P 1

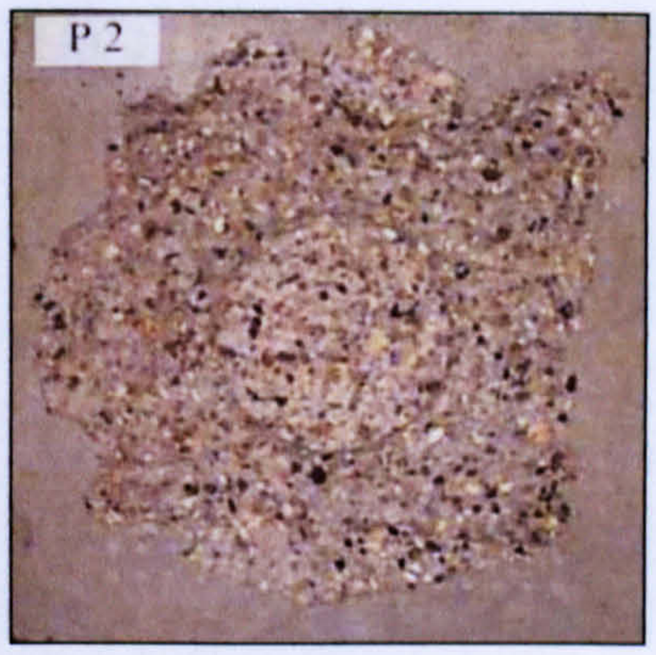

P 2

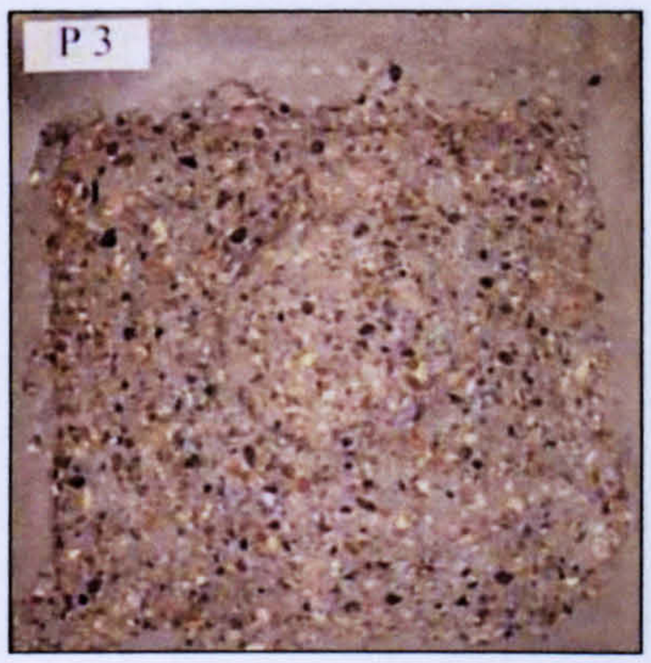

P 3

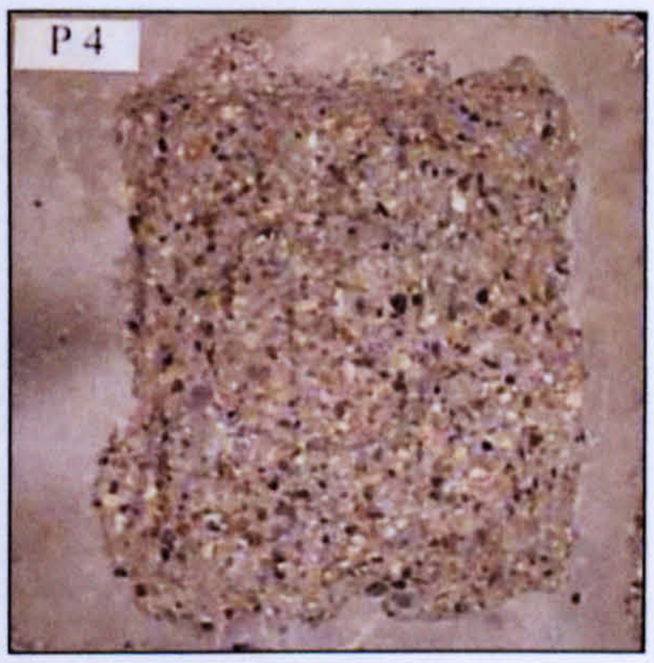

P 4

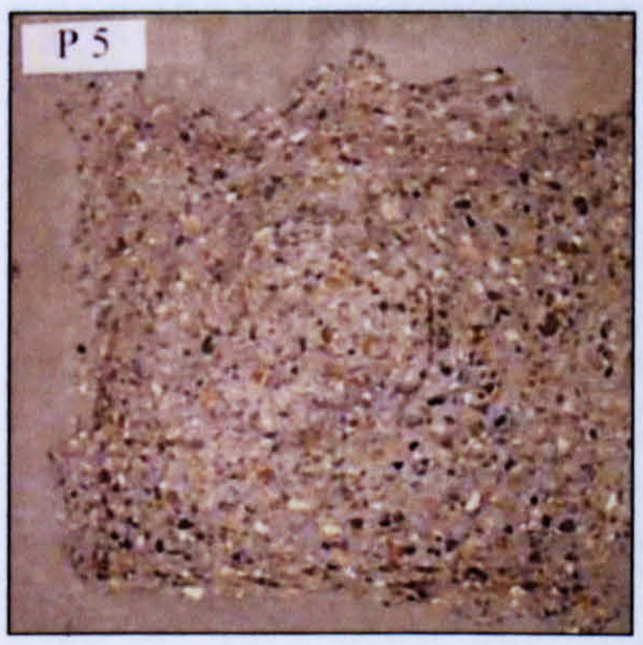

P 5

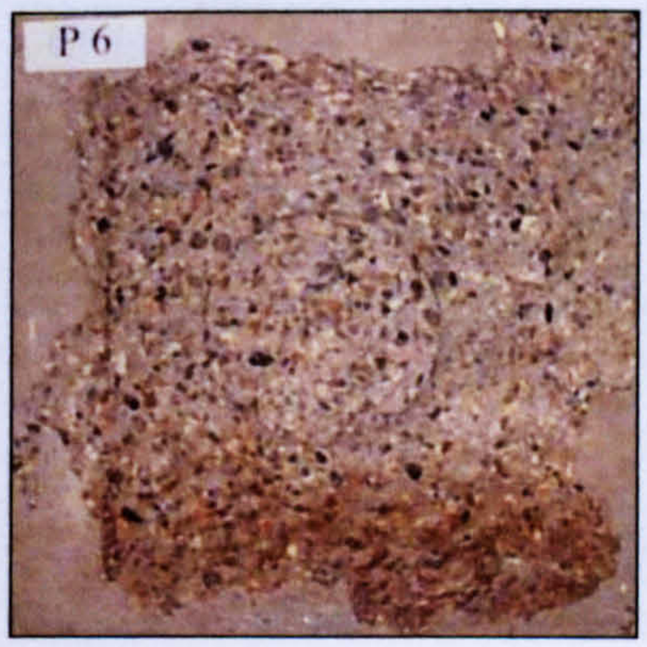

P 6

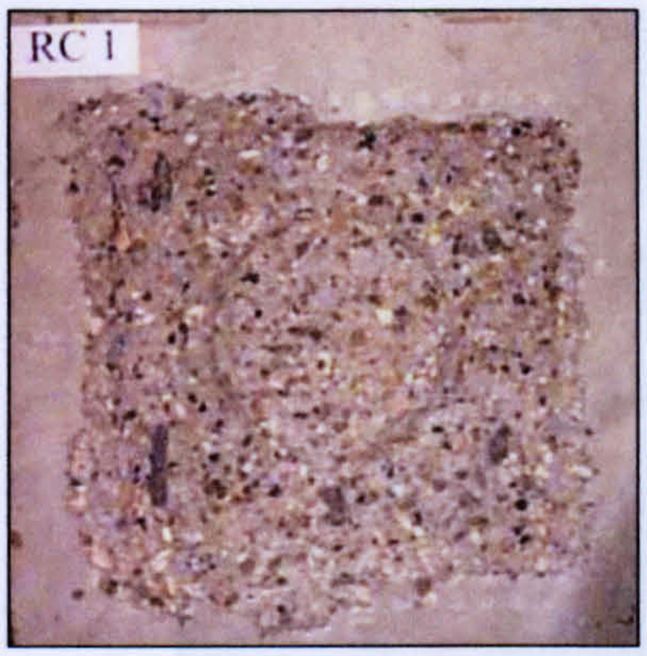

RC 1

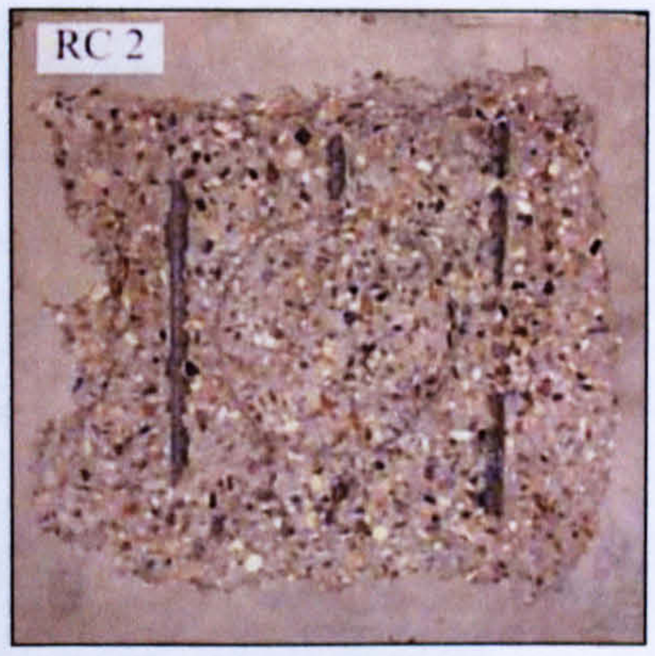

RC 2

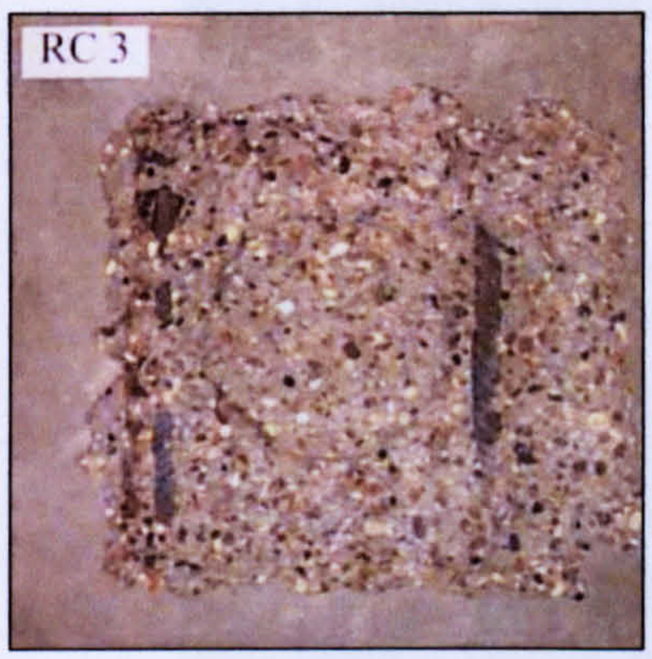

RC 3

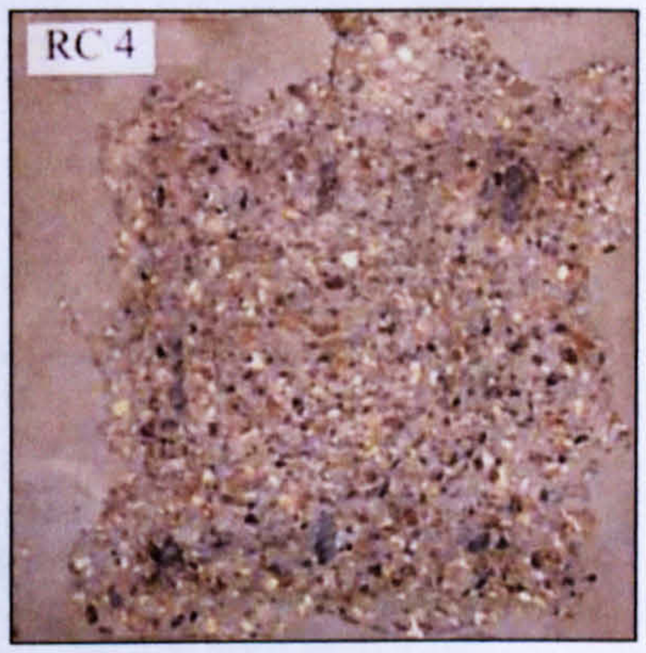

RC 4

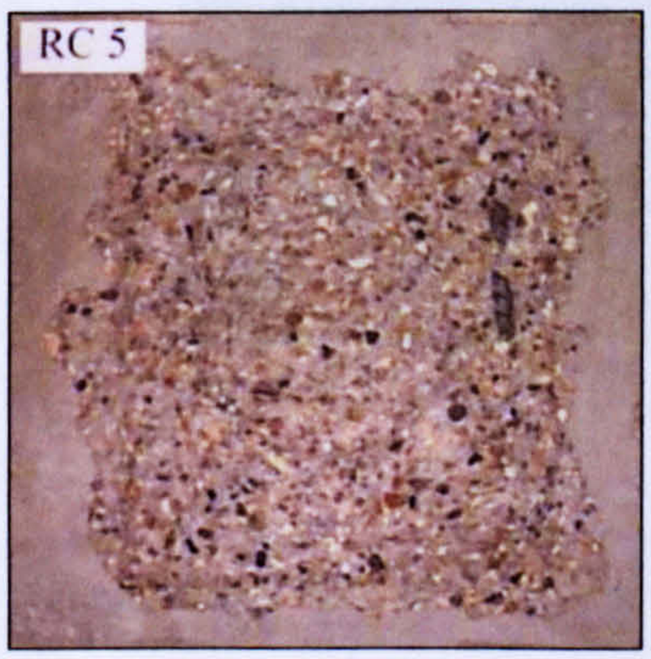

RC 5

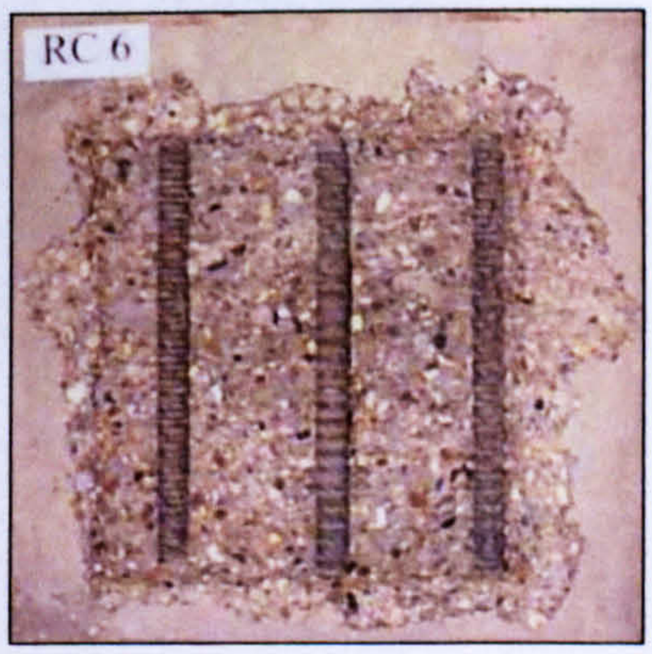

RC 6

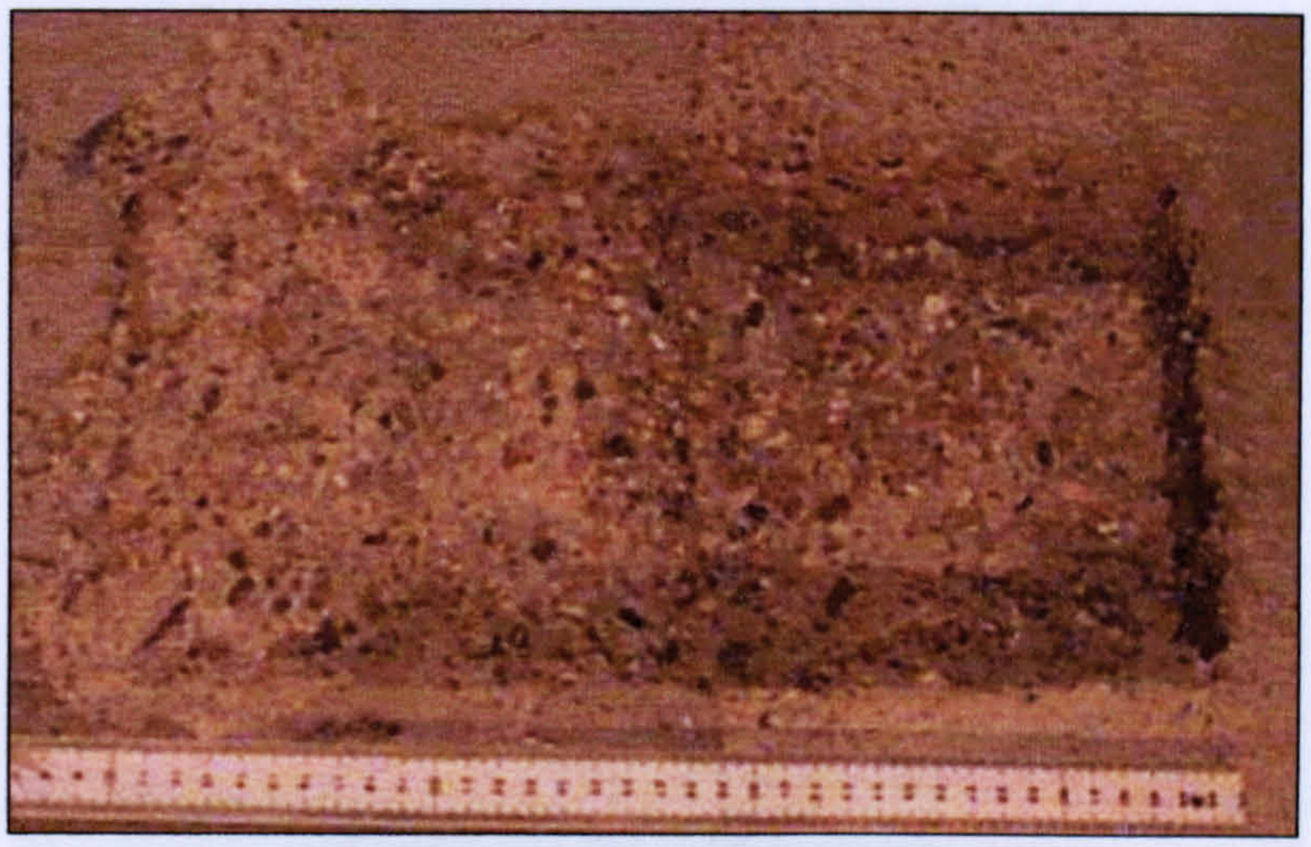

ST 1-00

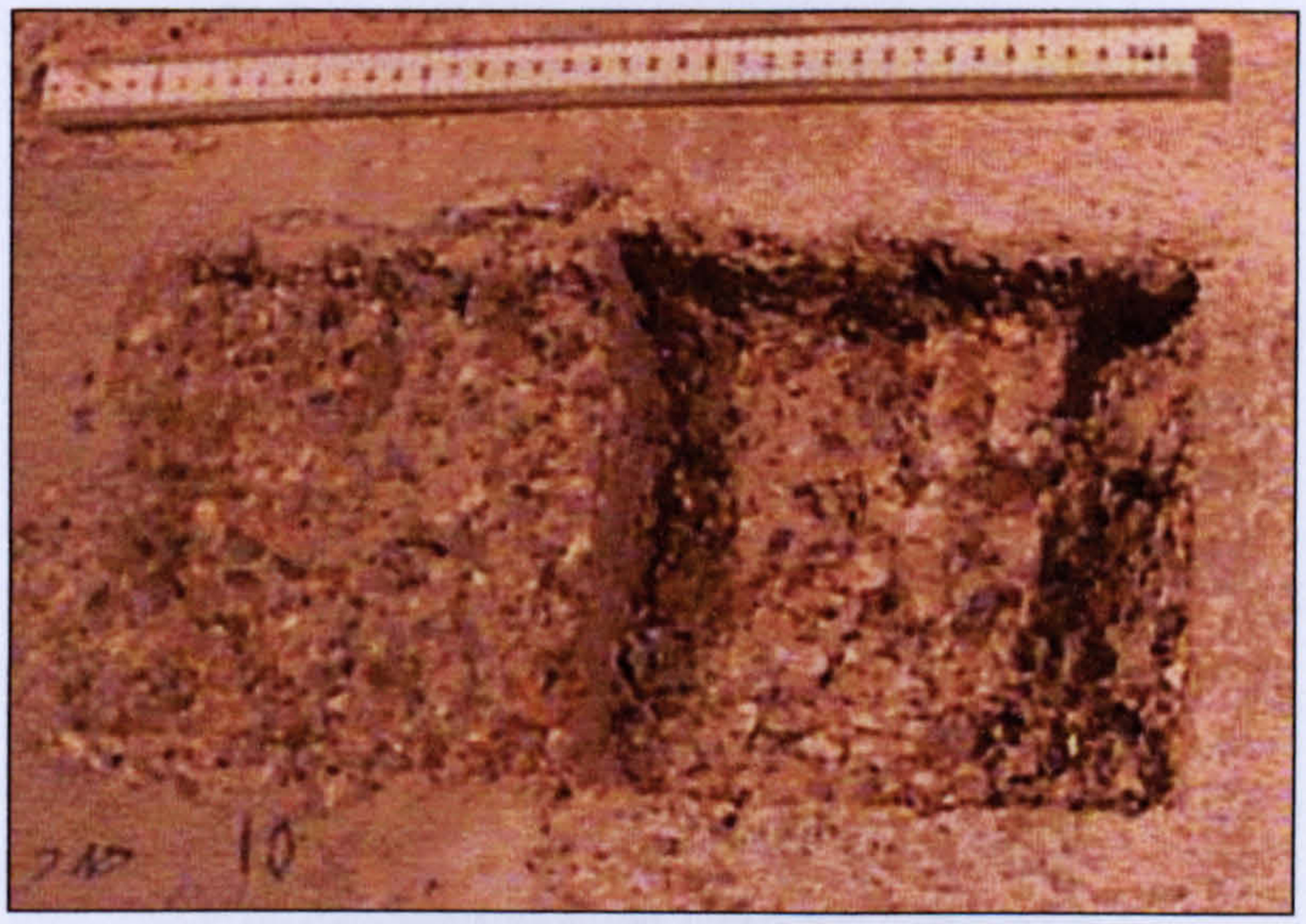

ST 1-10

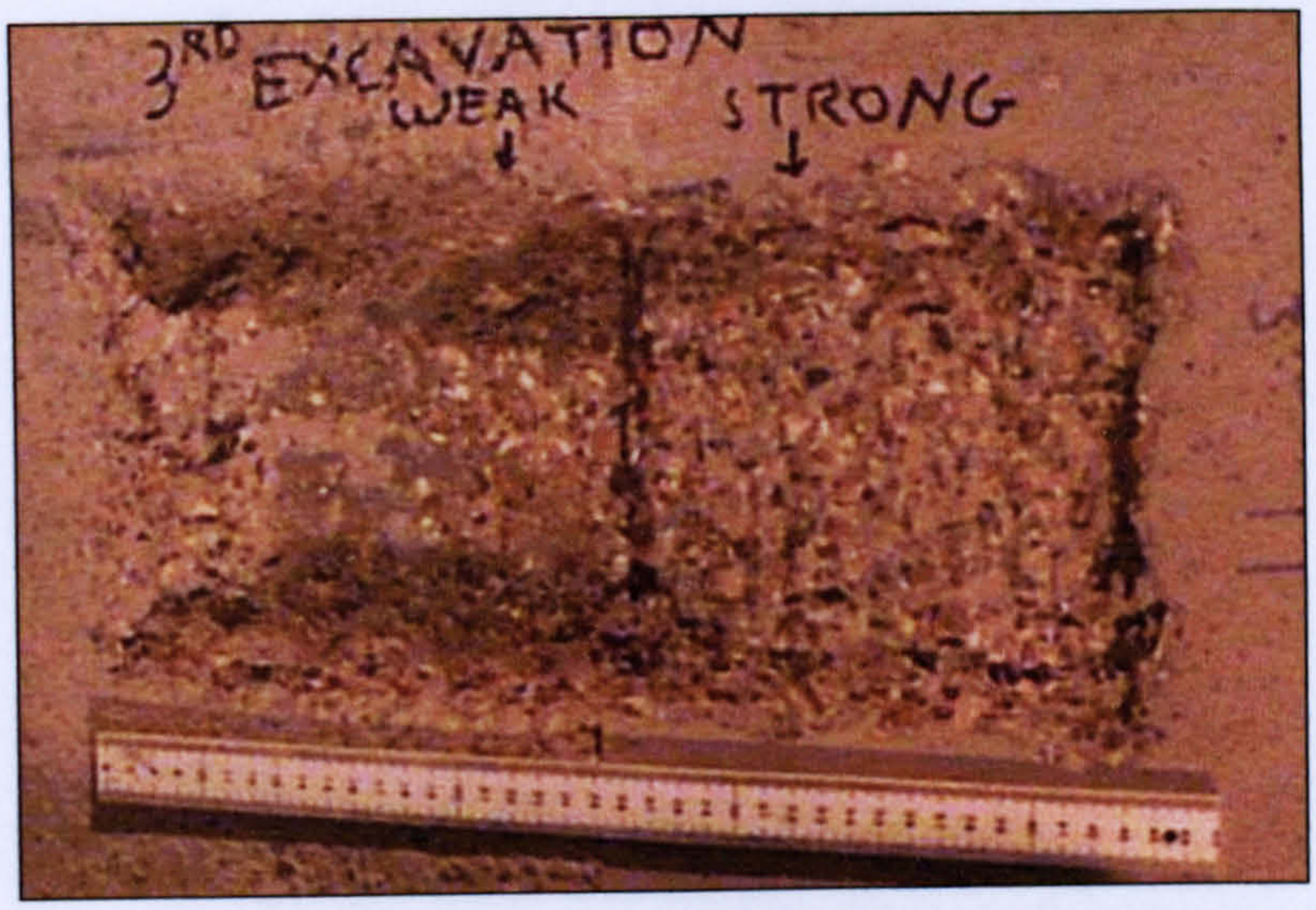

ST 1-11

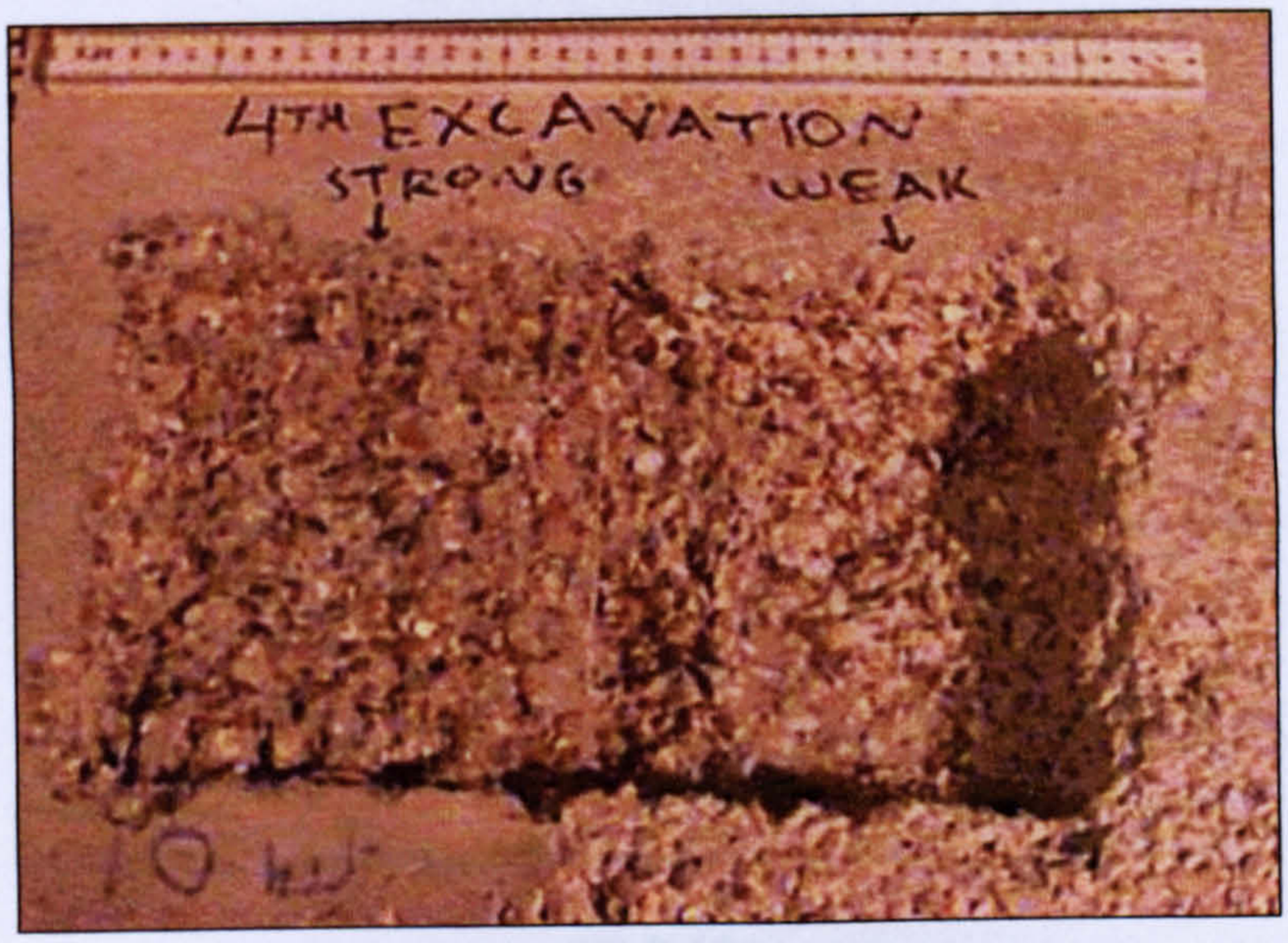

ST 1-01

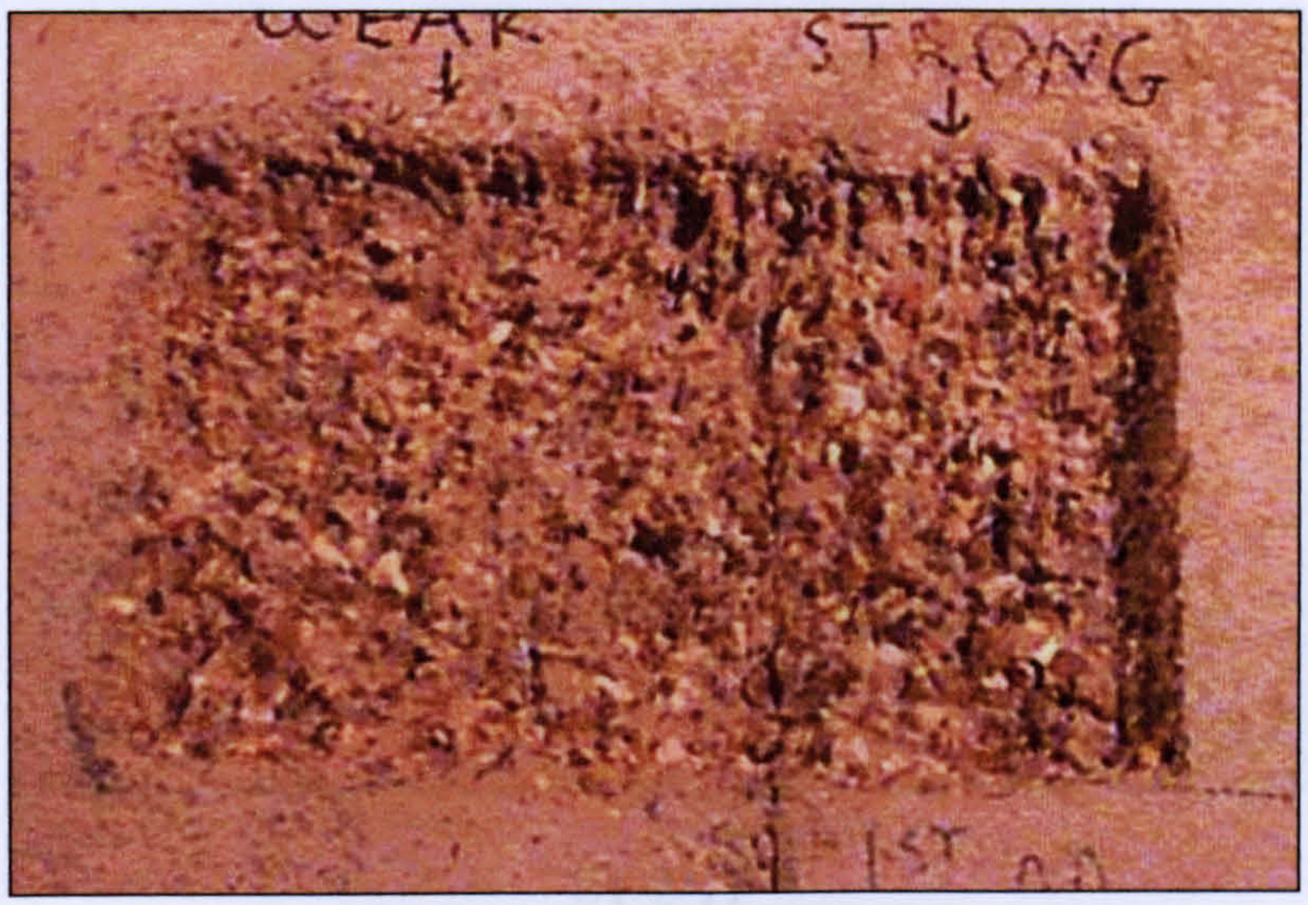

ST 2-00

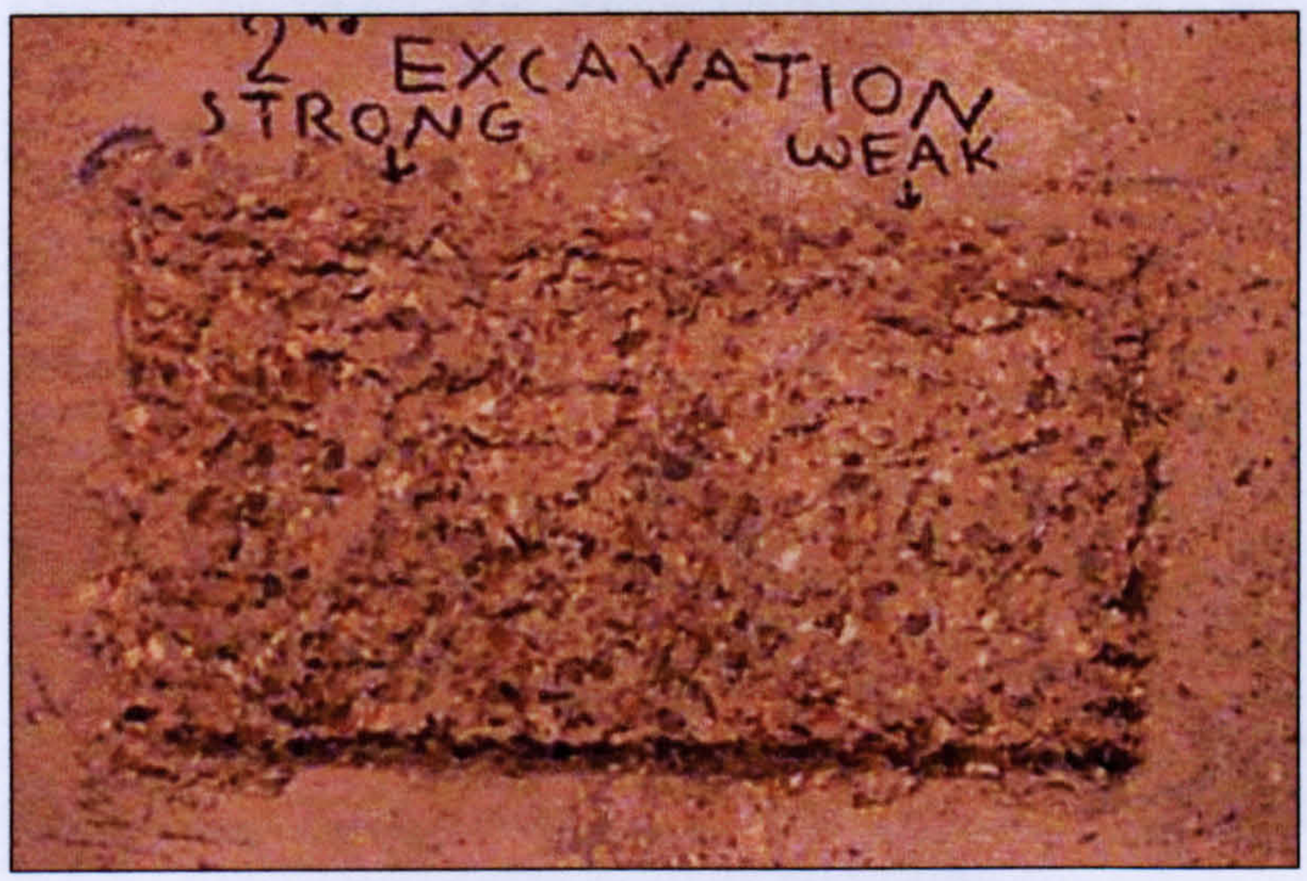

ST 2-10

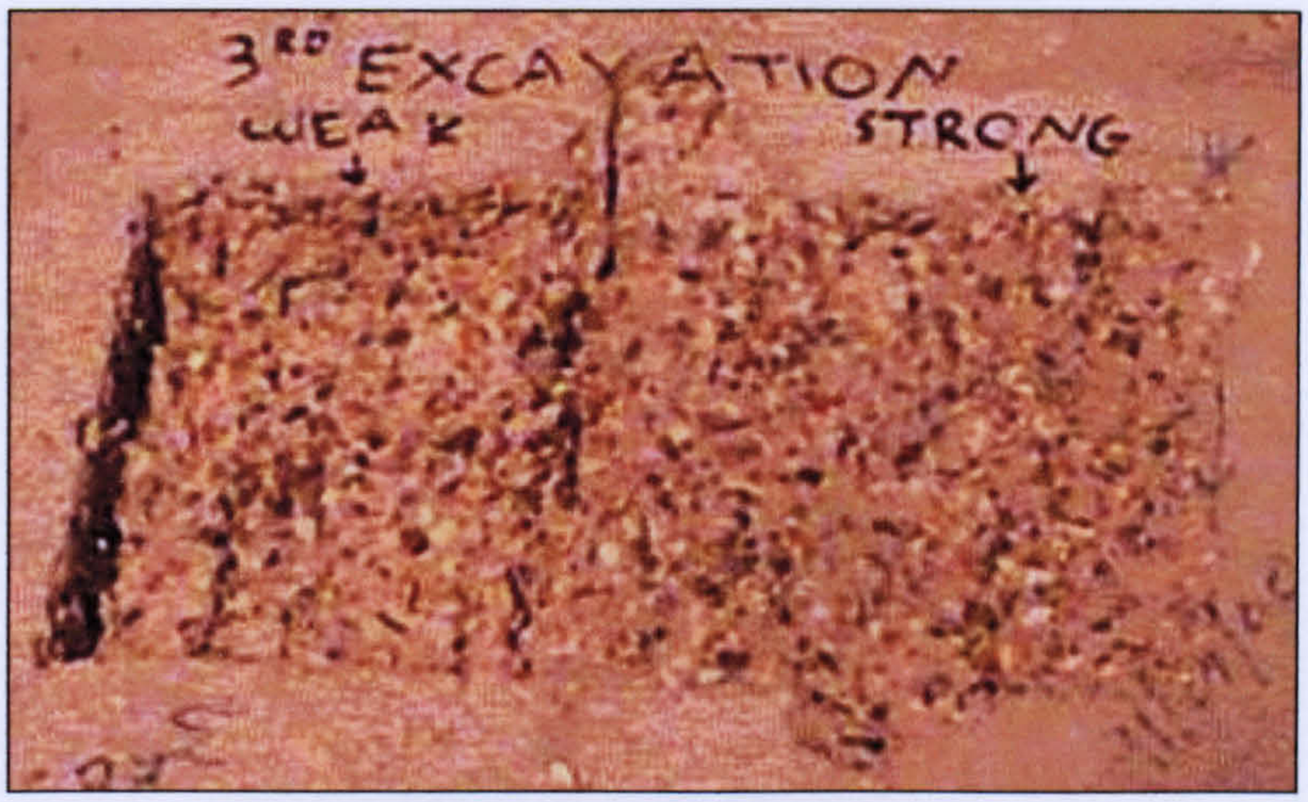

ST 2-11

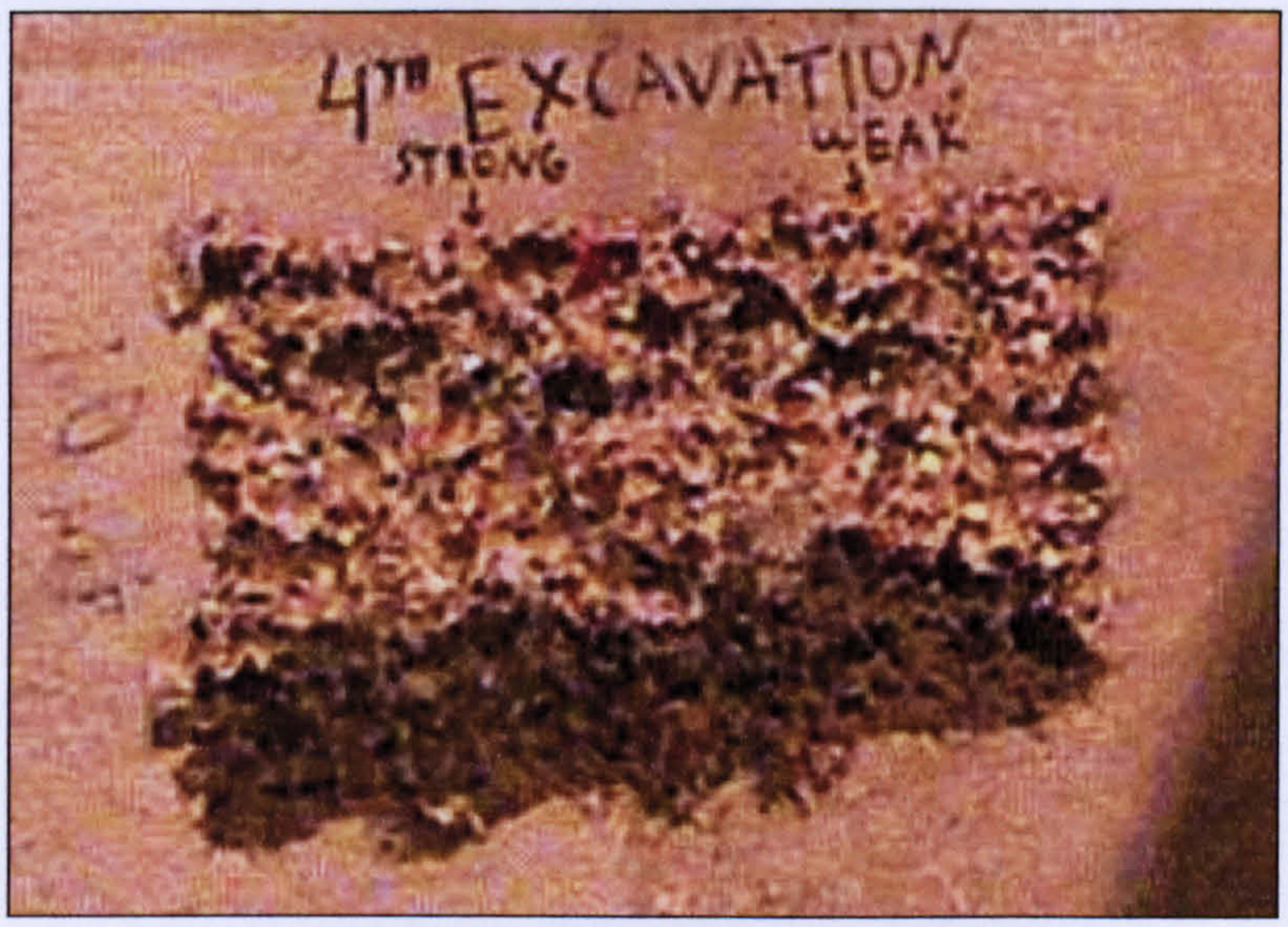

ST 2-01

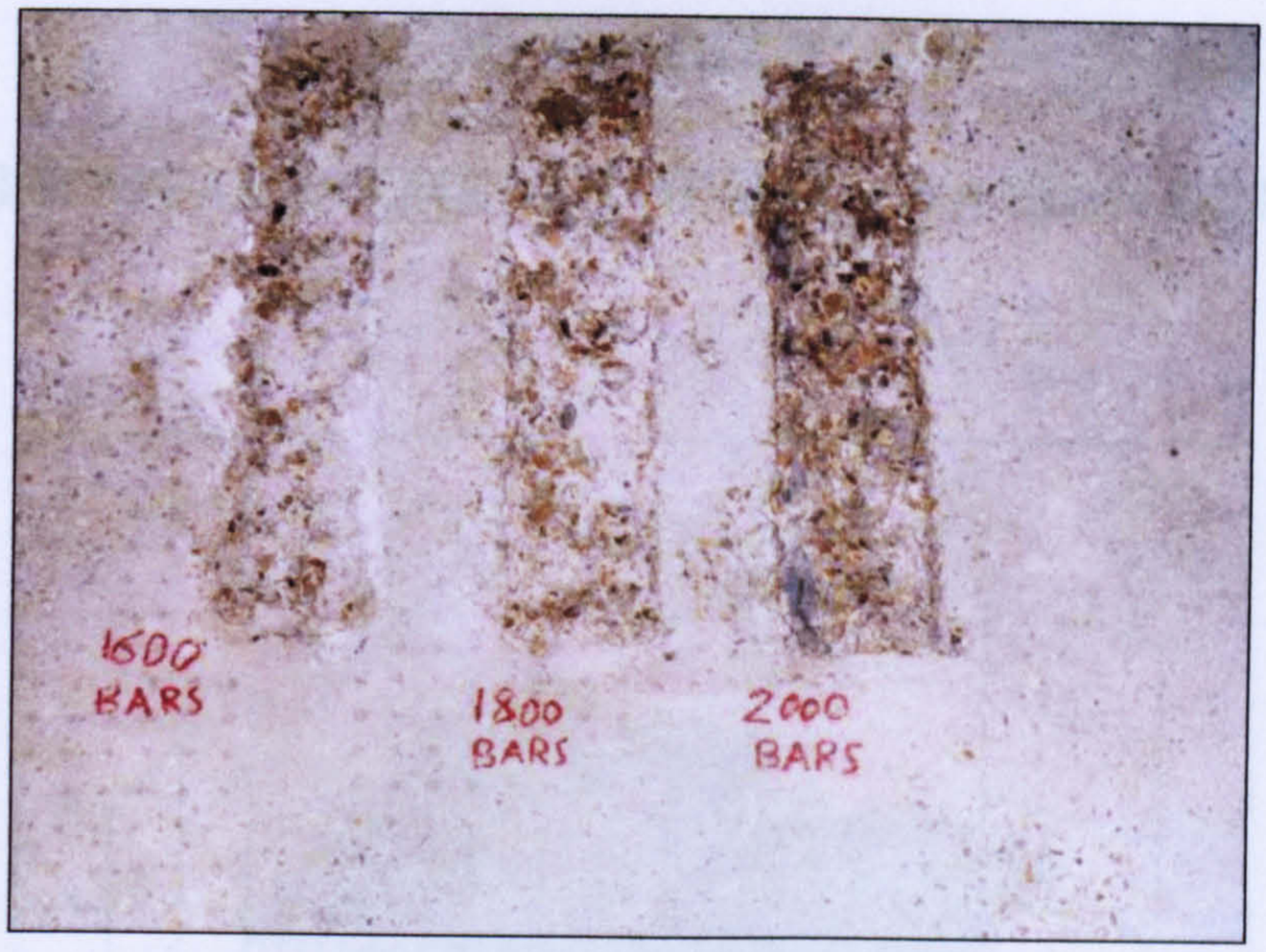

Excavations obtained using different water pressures

APPENDIX 5

LASER MEASUREMENTS OF EXCAVATION DEPTHS

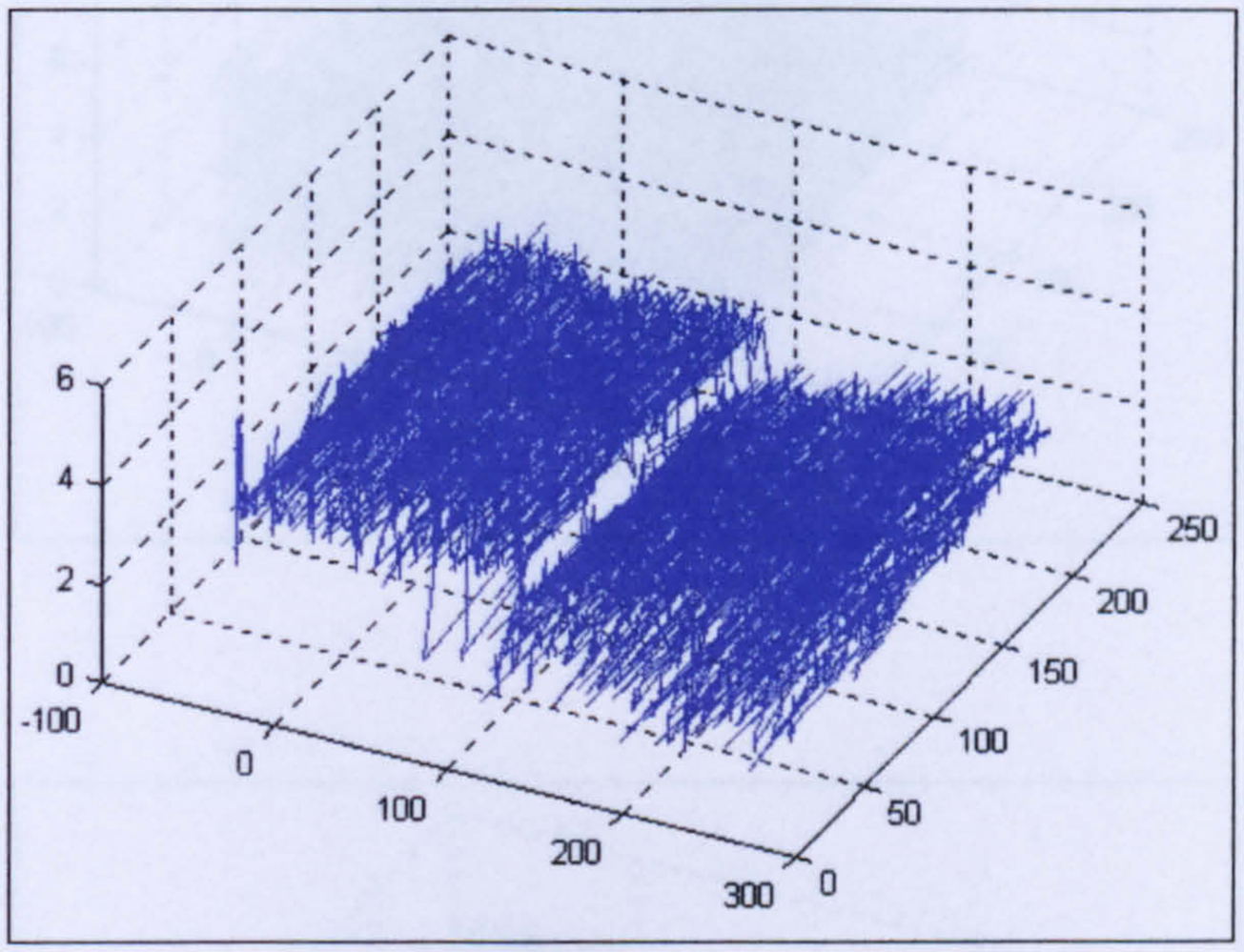

ST 1-00

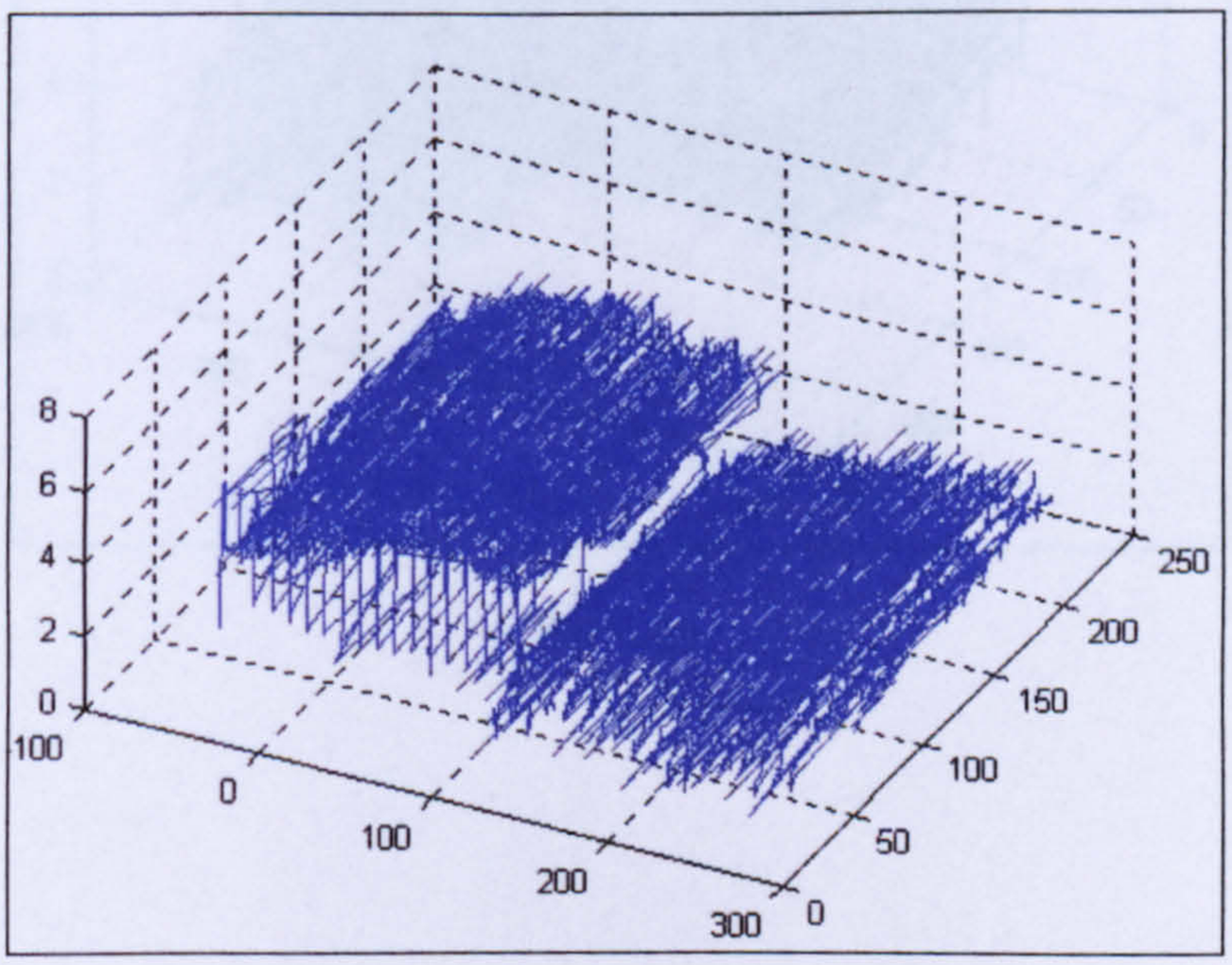

ST 1-10

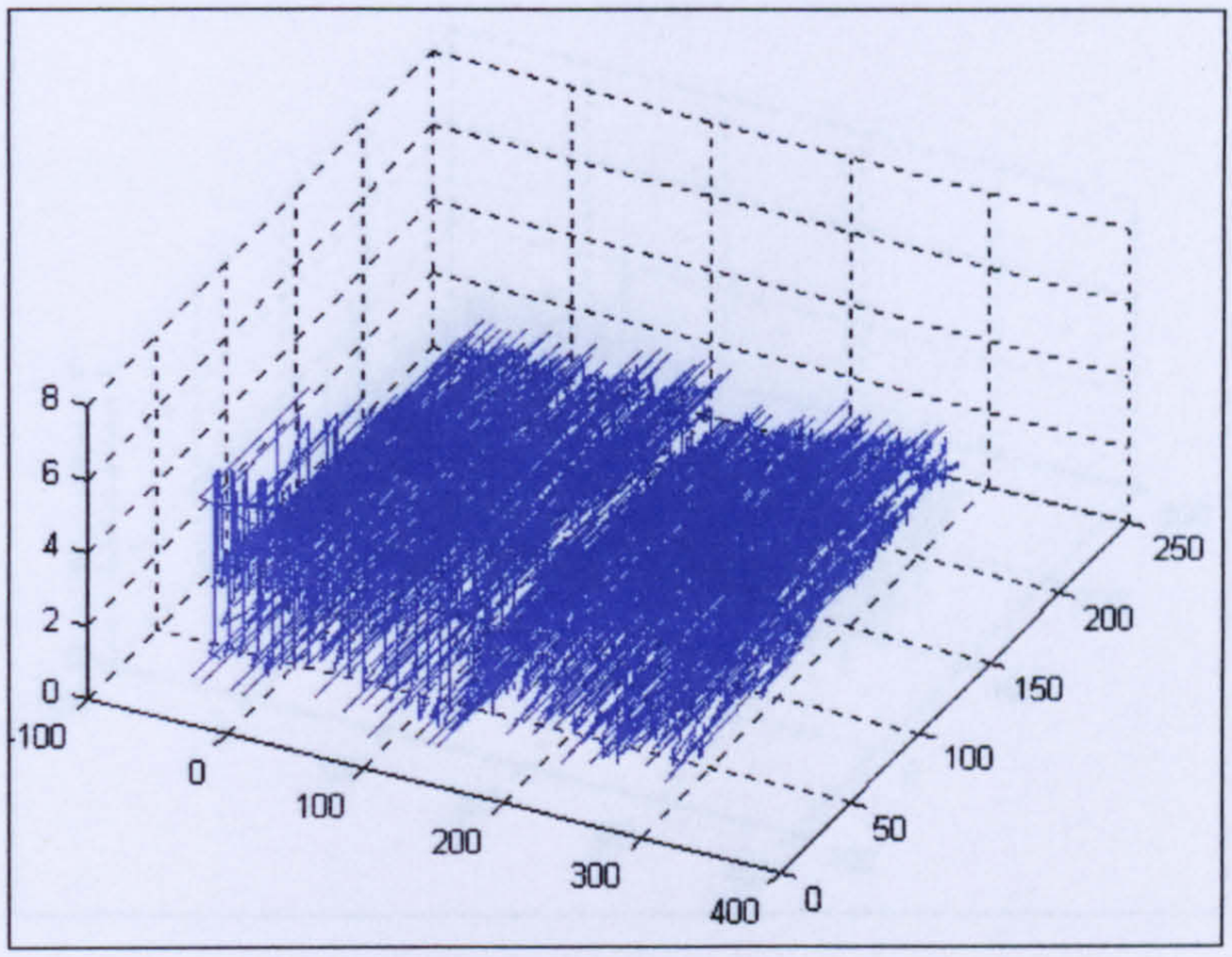
8
6
4
2
0
-100
0
100
200
300
400
0
50
100
150
200
250

ST 1-11

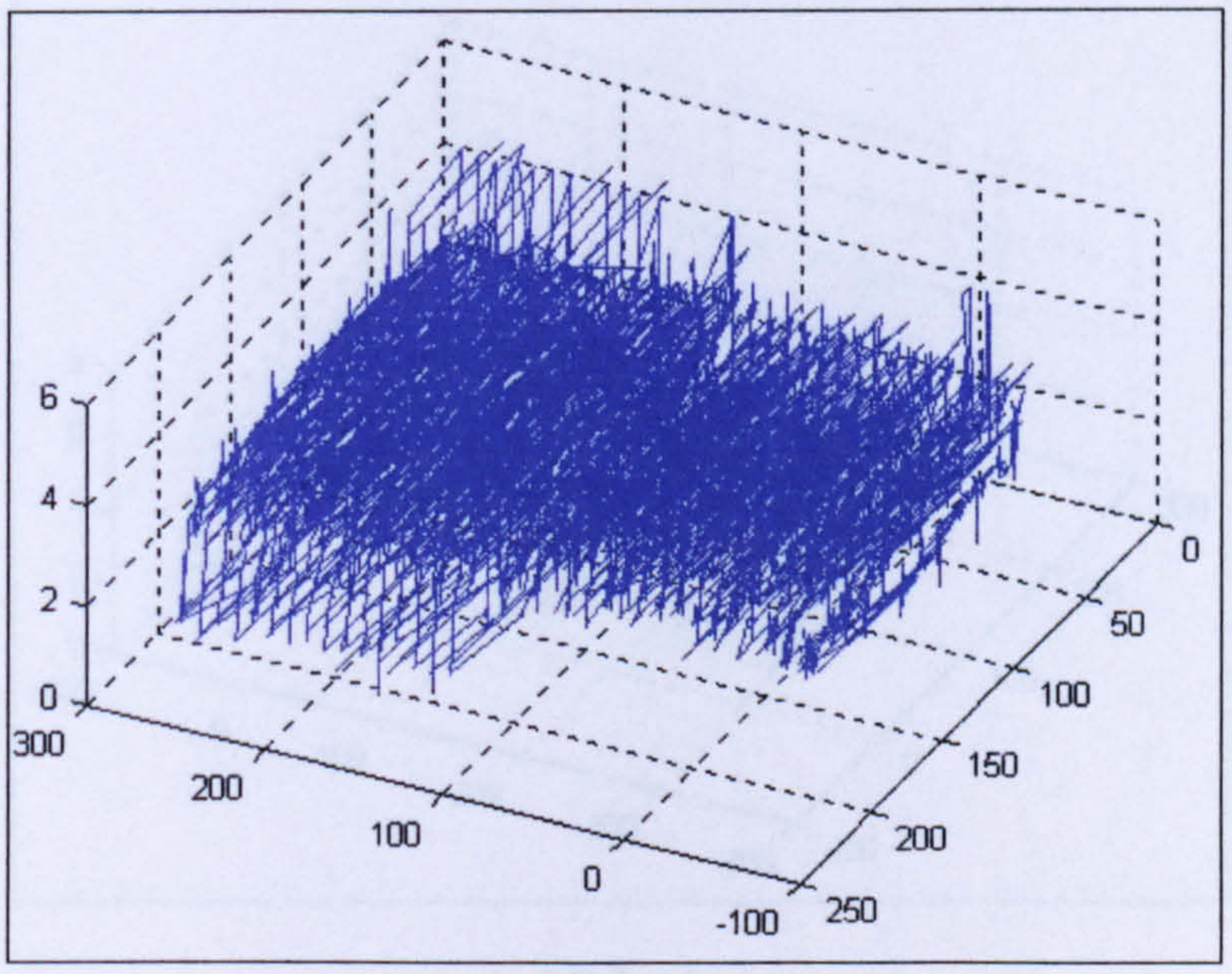
6
4
2
0
300
200
100
0
-100
0
50
100
150
200
250

ST 1-01

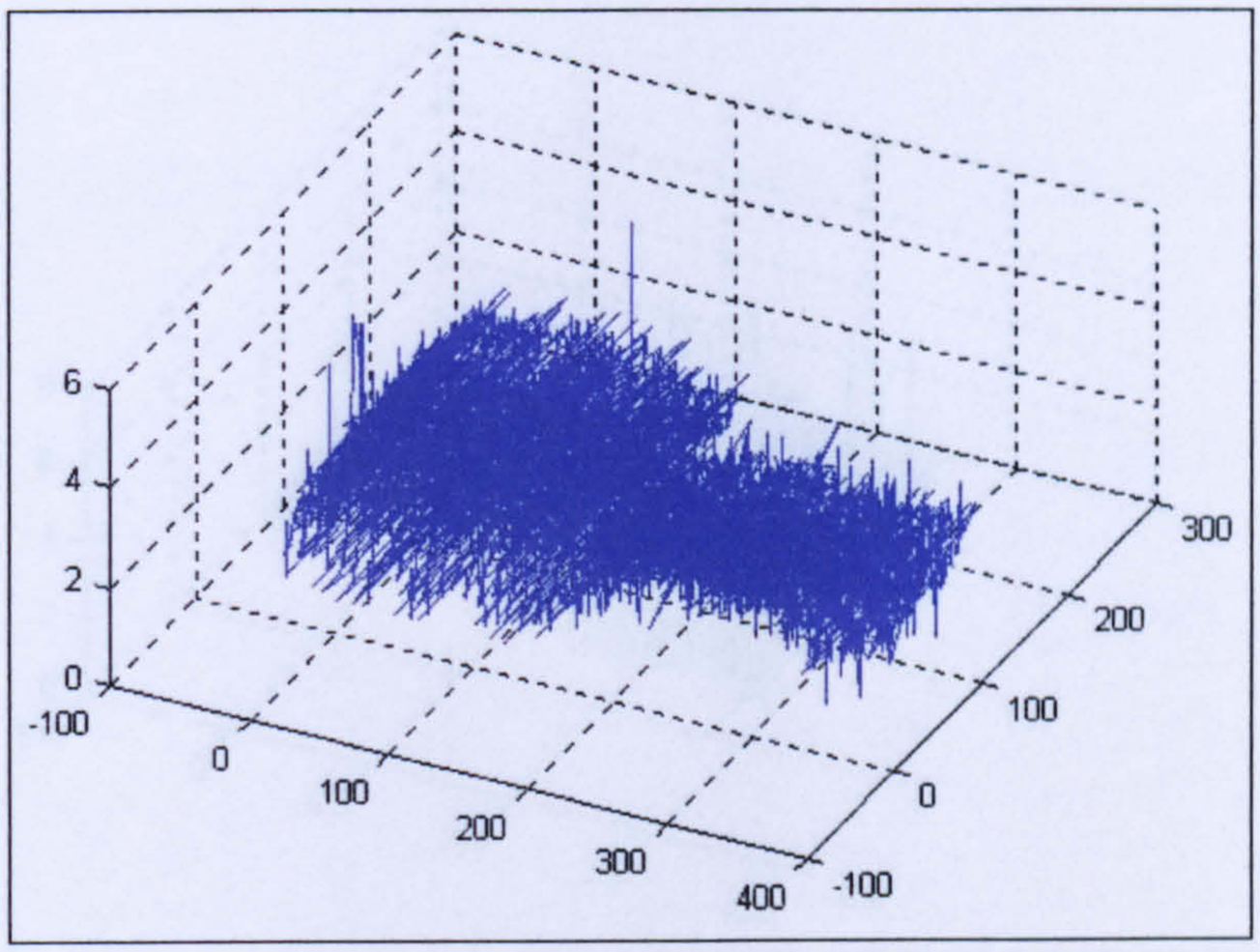
6
4
2
0
-100
0
100
200
300
400
-100
0
100
200
300

ST 2-00

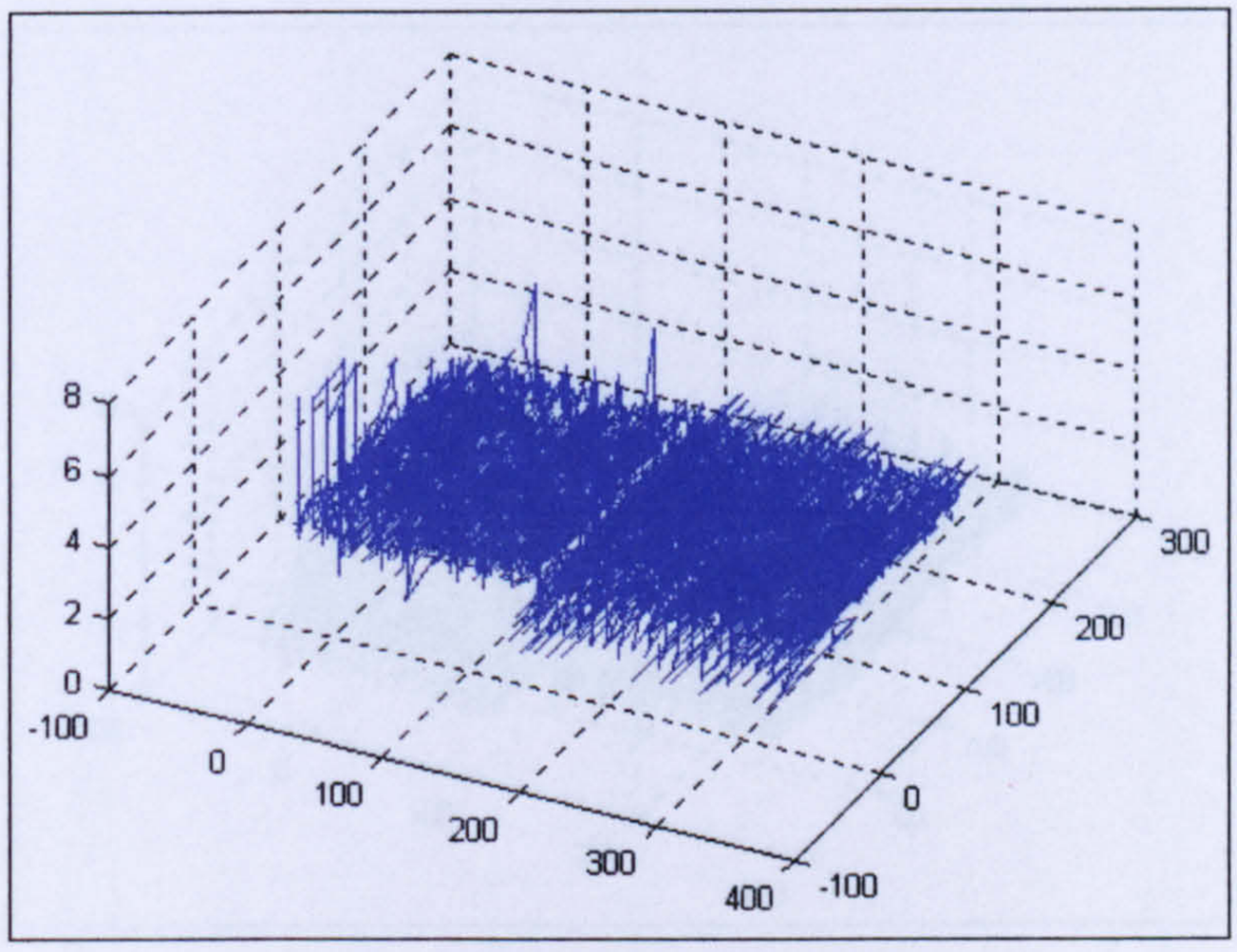
8
6
4
2
0
-100
0
100
200
300
400
-100
0
100
200
300

ST 2-10

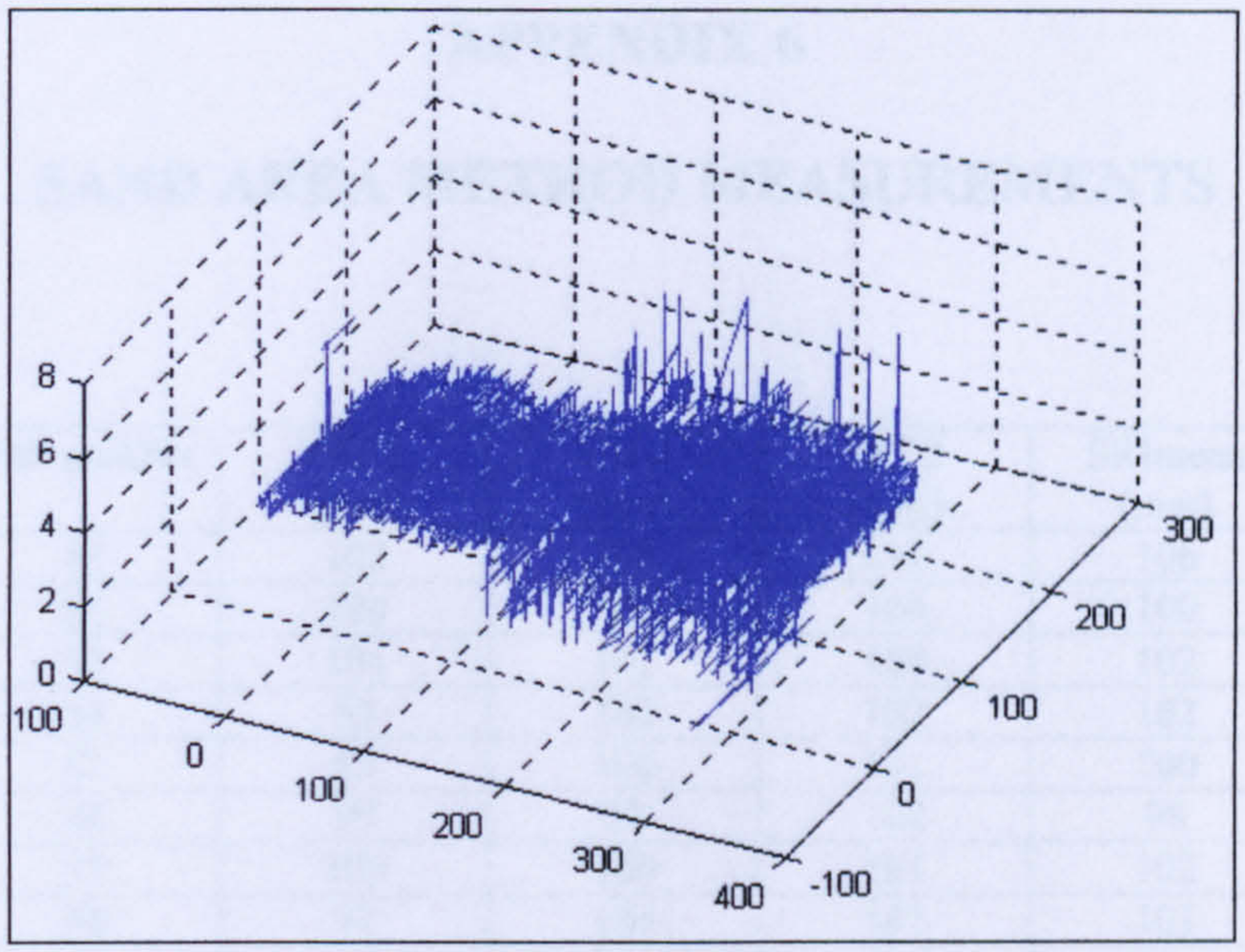
8
6
4
2
0
100
0
100
200
300
400
-100
0
100
200
300

ST 2-11

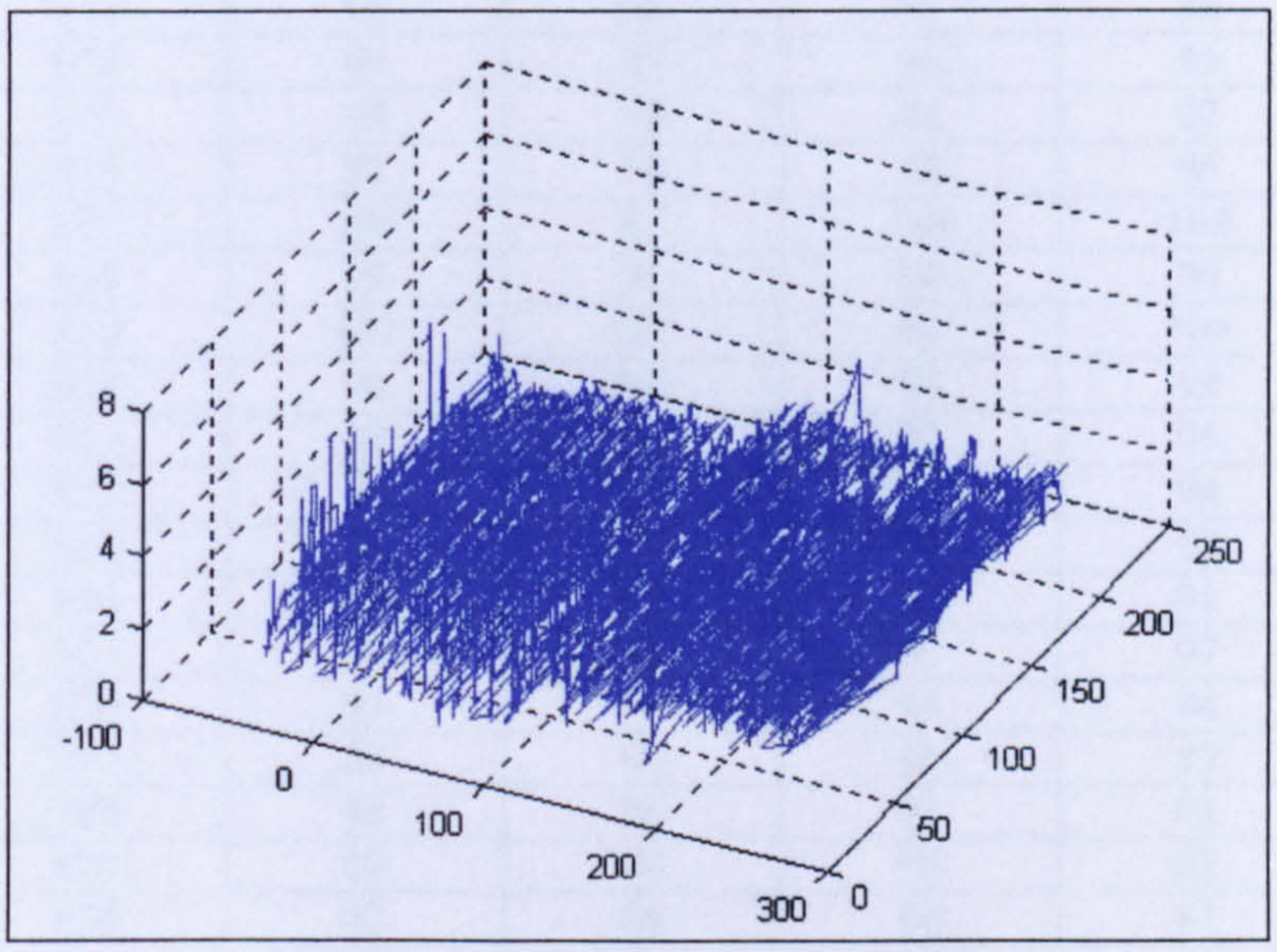
8
6
4
2
0
-100
0
100
200
300
0
50
100
150
200
250

ST 2-01

APPENDIX 6

SAND AREA METHOD MEASUREMENTS

Mix number	Slab number	SRI 1 (mm)	SRI 2 (mm)	SRI 3 (mm)	SRImean (mm)	Rmean (mm)
1	S1	102	105	111	106	5.668
	S2	100	99	100	100	6.369
2	S3	104	101	100	102	6.122
	S4	99	106	102	102	6.122
3	S5	93	106	101	100	6.369
	S6	99	92	102	98	6.632
4	S7	105	100	101	102	6.122
	S8	97	106	101	101	6.243
5	S9	102	103	98	101	6.243
	S10	100	96	97	98	6.632
6	S11	102	101	101	101	6.243
	S12	104	103	100	102	6.122
7	S13	95	96	97	96	6.911
	S14	94	95	96	95	7.057
8	S15	99	98	94	97	6.769
	S16	92	98	98	96	6.911
9	S17	105	97	104	102	6.122
	S18	99	93	94	95	7.057
10	S19	102	101	97	100	6.369
	S20	98	101	98	99	6.498
11	S21	97	96	93	95	7.057
	S22	90	94	98	94	7.208
12	S23	93	92	94	93	7.364
	S24	89	93	92	91	7.691
13	S25	96	98	97	97	6.769
	S26	93	93	95	94	7.208
14	S27	85	99	96	93	7.364
	S28	86	94	93	91	7.691
15	S29	82	98	94	91	7.691
	S30	92	86	96	91	7.691
16	S31	93	94	95	94	7.208
	S32	93	90	92	92	7.525
17	S33	99	105	102	102	6.122
	S34	94	100	96	97	6.769
18	S35	96	95	94	95	7.057
	S36	108	110	103	107	5.563
19	S37	101	103	100	101	6.243
	S38	97	106	98	100	6.369
20	S39	105	108	105	106	5.668
	S40	95	90	94	93	7.364
21	S41	107	96	95	99	6.498
	S42	95	99	101	98	6.632
22	S43	92	105	104	100	6.369
	S44	103	104	103	103	6.003
23	S45	95	100	97	97	6.769
	S46	97	91	102	97	6.769
24	S47	92	106	119	106	5.668
	S48	107	107	118	111	5.169

Slab number	SRI 1 (mm)	SRI 2 (mm)	SRI 3 (mm)	SRImean (mm)	Rmean (mm)
PL2	90	96	79	88	8.224
PL5	85	86	85	85	8.815
PL6	79	85	82	82	9.472
PL9	85	87	95	89	8.041
PL10	77	82	78	79	10.205
PL11	93	90	92	92	7.525
PL13	79	90	80	83	9.245
PL14	92	91	87	90	7.863
PL15	71	91	85	82	9.472
PL16	87	83	91	87	8.415
P2	97	89	75	87	8.415
P5	95	92	84	90	7.863

APPENDIX 7

PROGRAMMING CODES IN MATLAB 5.3 FOR EVALUATING ROUGHNESS PARAMETERS

PROGRAM FOR EVALUATING 2a ROUGHNESS PARAMETER IN BOTH X AND Y AXES

```
function [2αx, 2αxmean, 2αy, 2αymean]=2αresults(filename)
z=textread(filename,'%f');
z1=reshape(z,251,251);
z1 =z1';
2αx=zeros(1,251);
2αy=zeros(1,251);

for i=1:251,
   a=0;
   for j=1:250,
      a=z1(i,j+1)-z1(i,j);
      2αx(i)=2αx(i)+abs(a);
   end;
end;
2αx=2αx/250;
2αxmean=mean(2αx);

for j=1:251,
   b=0;
   for i=1:250,
      b=z1(i+1,j)-z1(i,j);
      2αy(j)=2αy(j)+abs(b);
   end;
end;
2αy=2αy/250;
2αymean=mean(2αy);
```

PROGRAM FOR EVALUATING $\frac{Da}{W}$ ROUGHNESS PARAMETER IN BOTH X AND Y AXES

```
function [Da/W x, Da/W xmean, Da/W y, Da/W ymean]= Da/W results(filename)
z=textread(filename,'%f');
z1=reshape(z,251,251);
z1 =z1';
Da/W x=zeros(1,251);
Da/W y=zeros(1,251);

for i=1:251,
   a=0;
   for j=1:249,
      a=(abs(z1(i,j+1)-z1(i,j))+abs(z1(i,j+2)-z1(i,j+1)))/2.22;
      Da/W x(i)= Da/W x(i)+a;
   end;
end;
Da/W x=Da/W x/249;
Da/W xmean=mean(Da/W x);

for j=1:251,
   b=0;
   for i=1:249,
      b=(abs(z1(i+1,j)-z1(i,j))+abs(z1(i+2,j)-z1(i+1,j)))/2.22;
      Da/W y(j)= Da/W y(j)+b;
   end;
end;
Da/W y=Da/W y/249;
Da/W ymean=mean(Da/W y);
```

PROGRAM FOR EVALUATING RΔa ROUGHNESS PARAMETER IN BOTH X AND Y AXES

```
function [RΔax, RΔaxmean, RΔay, RΔaymean]= RΔaresults(filename)
z=textread(filename,'%f');
z1=reshape(z,251,251);
z1 =z1';
RΔax=zeros(1,251);
RΔay=zeros(1,251);

for i=1:251,
   a=0;
   for j=1:250,
      a=z1(i,j+1)-z1(i,j);
      RΔax(i)= RΔax(i)+abs(a);
   end;
end;
RΔax=RΔax/139;
RΔaxmean=mean(RΔax);

for j=1:251,
   b=0;
   for i=1:250,
      b=z1(i+1,j)-z1(i,j);
      RΔay(j)= RΔay(j)+abs(b);
   end;
end;
RΔay=RΔay/139;
RΔaymean=mean(RΔay);
```

PROGRAM FOR EVALUATING RΔq ROUGHNESS PARAMETER IN BOTH X AND Y AXES

```
function [RΔqx, RΔqxmean, RΔqy, RΔqymean]=RΔqresults(filename)
z=textread(filename,'%f');
z1=reshape(z,251,251);
z1 =z1';
RΔqx=zeros(1,251);
RΔqy=zeros(1,251);

for i=1:251,
    a=0;
    for j=1:250,
        a=z1(i,j+1)-z1(i,j);
        RΔqx(i)=RΔqx(i)+a^2;
    end;
end;
RΔqx=sqrt(RΔqx/139);
RΔqxmean=mean(RΔqx);

for j=1:251,
    b=0;
    for i=1:250,
        b=z1(i+1,j)-z1(i,j);
        RΔqy(j)=RΔqy(j)+b^2;
    end;
end;
RΔqy=sqrt(RΔqy/139);
RΔqymean=mean(RΔqy);
```

PROGRAM FOR EVALUATING Lo ROUGHNESS PARAMETER IN BOTH X AND Y AXES

```
function [Lox, Loxmean, Loy, Loymean]=Loresults(filename)
z=textread(filename,'%f');
z1=reshape(z,251,251);
z1 =z1';
Lox=zeros(1,251);
Loy=zeros(1,251);

for i=1:251,
   a=0;
   for j=1:250,
      a=z1(i,j+1)-z1(i,j);
      Lox(i)=Lox(i)+sqrt(0.309+a^2);
   end;
end;
Loxtotal=mean(Lox);

for j=1:251,
   b=0;
   for i=1:250,
      b=z1(i+1,j)-z1(i,j);
      Loy(j)=Loy(j)+sqrt(0.309+b^2);
   end;
end;
Loytotal=mean(Loy);
```

APPENDIX 8

3D TOPOGRAPHY AND ROUGHNESS PARAMETERS VALUES

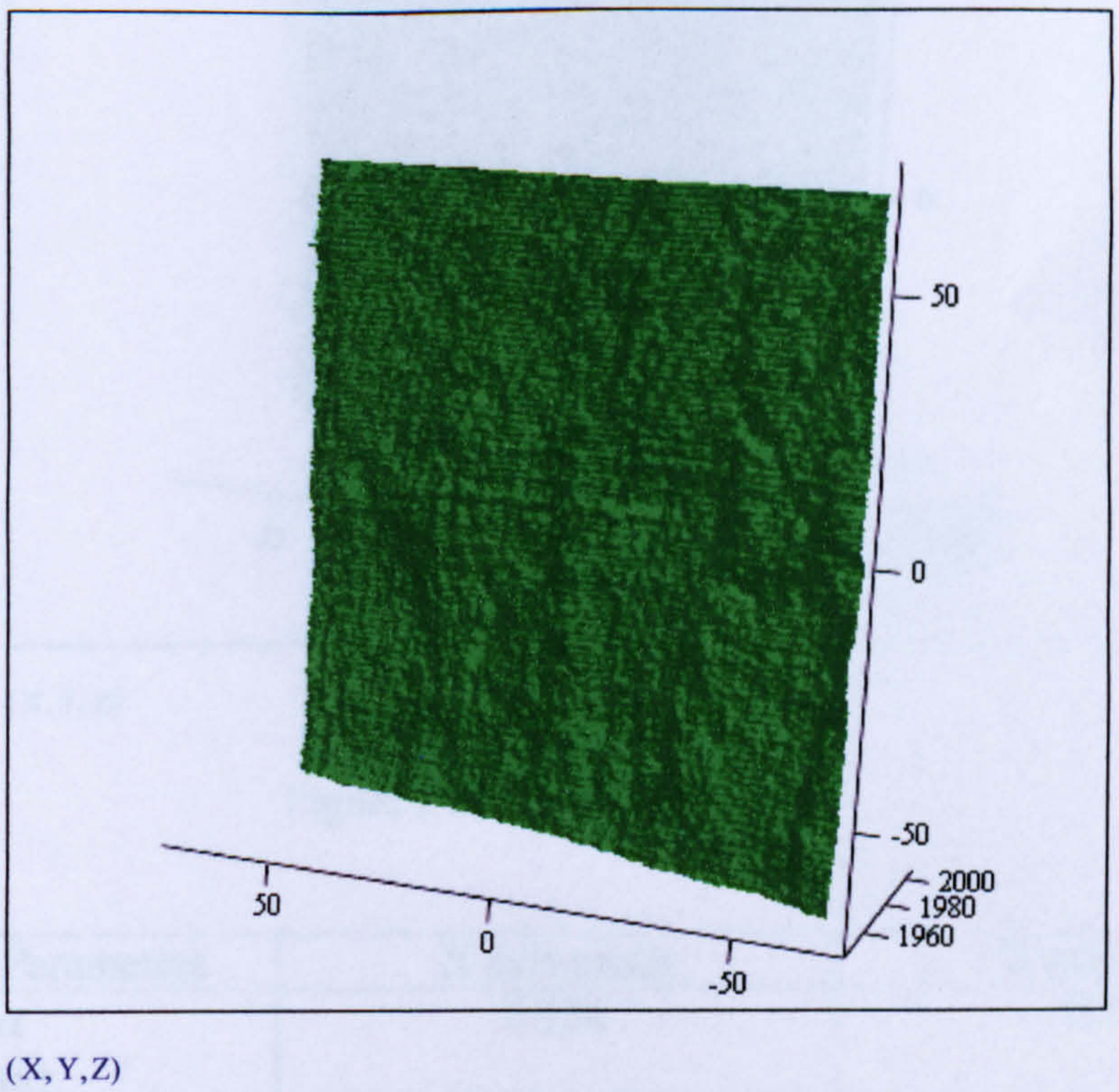

Figure 1 Slab S1 Topography

Roughness Parameters	X axis mean	Y axis mean
2α (mm)	0.522	0.641
$\frac{Da}{2W}$	0.468	0.576
$R\Delta a$	0.938	1.152
$R\Delta q$ ($mm^{1/2}$)	0.905	1.096
Lo (mm)	203.58	226.94
Lr	1.46	1.63

Table 1 Slab S1 Roughness parameters values

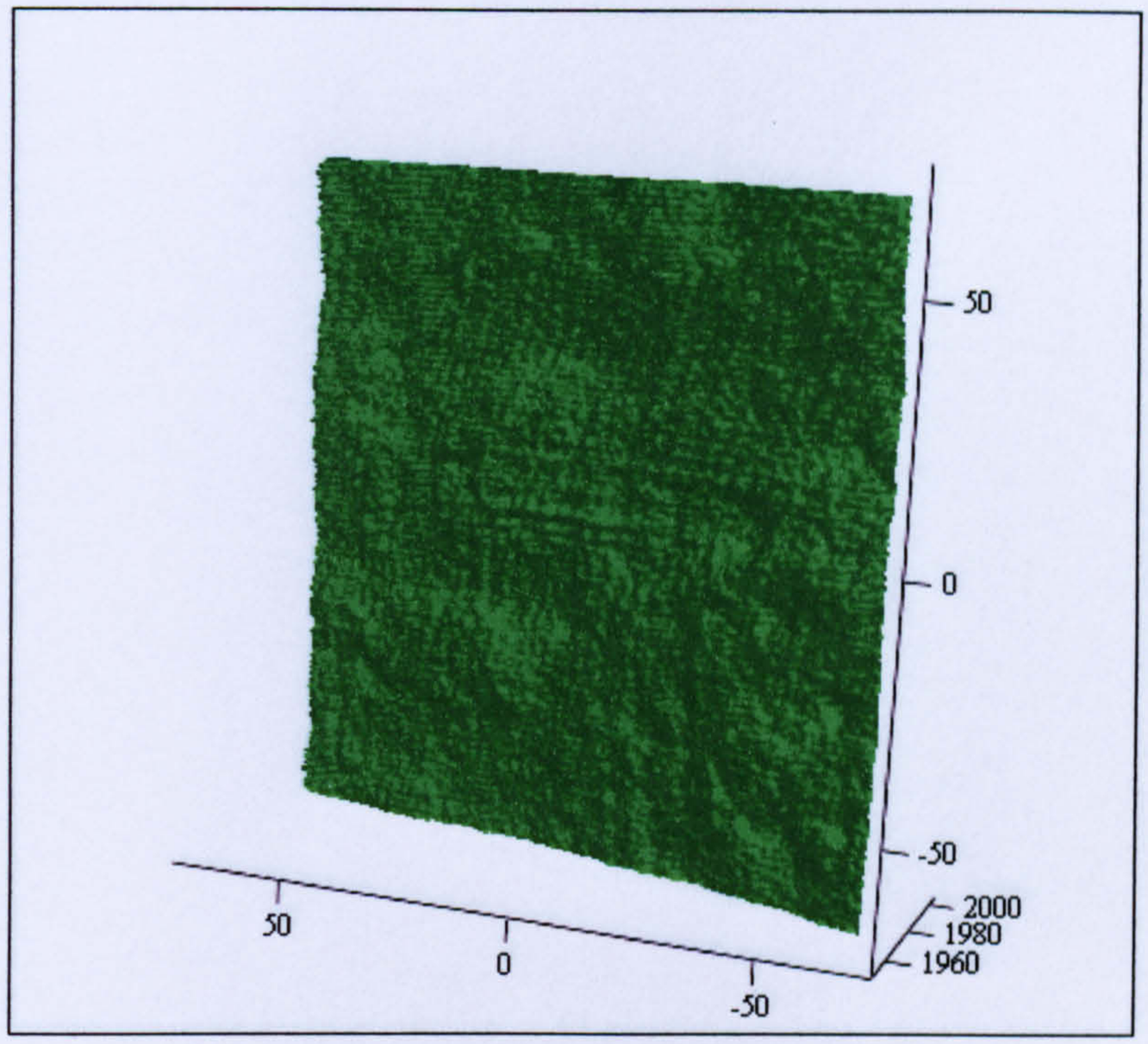

(X,Y,Z)

Figure 2 Slab S2 Topography

Roughness Parameters	X axis mean	Y axis mean
2α (mm)	0.530	0.598
$\frac{Da}{2W}$	0.476	0.538
$R\Delta a$	0.954	1.075
$R\Delta q$ ($mm^{1/2}$)	0.925	1.035
Lo (mm)	205.49	218.99
Lr	1.48	1.58

Table 2 Slab S2 Roughness parameters values

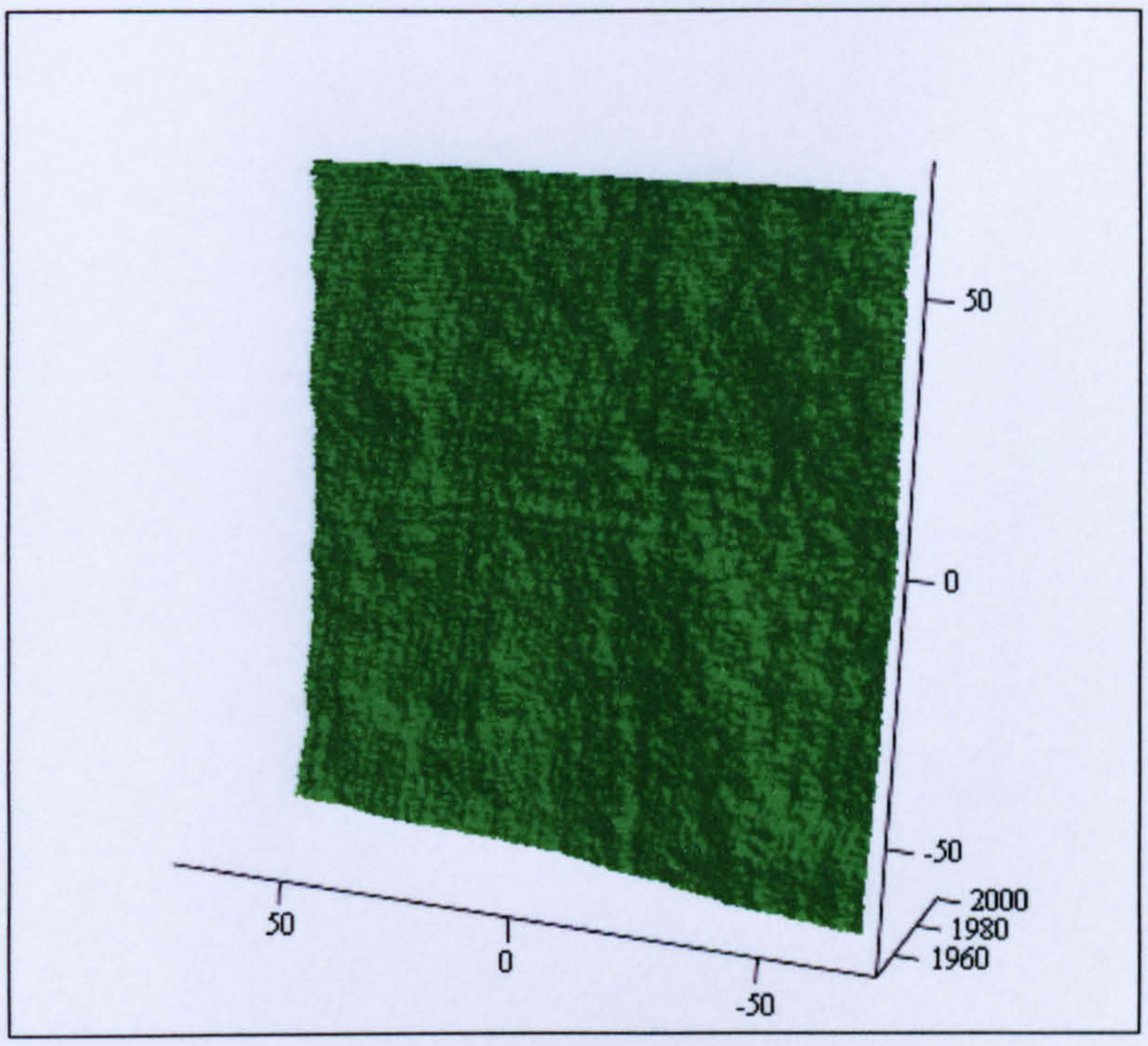

(X, Y, Z)

Figure 3 Slab S3 Topography

Roughness Parameters	X axis mean	Y axis mean
2α (mm)	0.511	0.537
$\frac{Da}{2W}$	0.459	0.484
$R\Delta a$	0.919	0.966
$R\Delta q$ ($mm^{1/2}$)	0.885	0.930
Lo (mm)	201.75	206.70
Lr	1.45	1.49

Table 3 Slab S3 Roughness parameters values

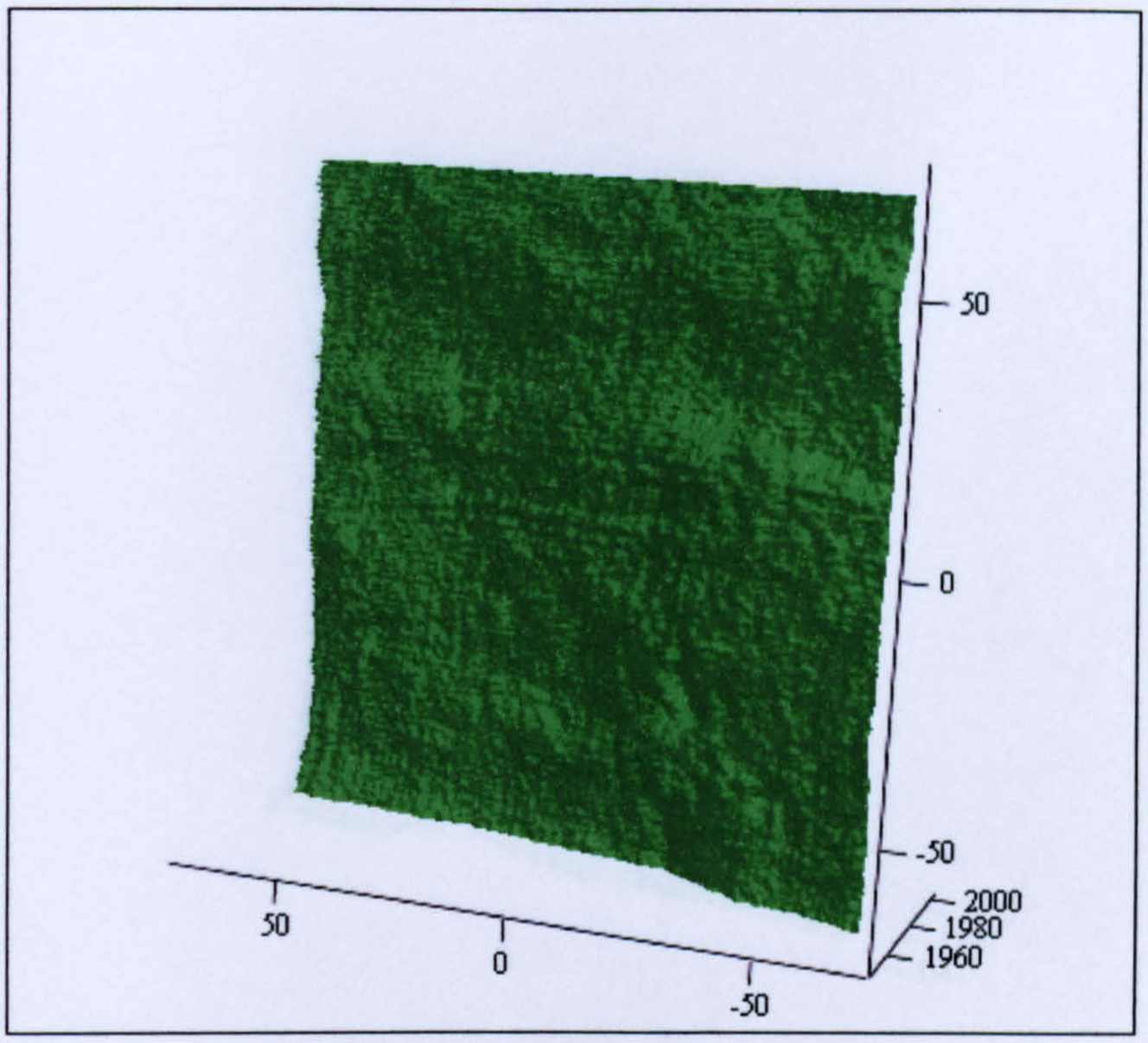

Figure 4 Slab S4 Topography

Roughness Parameters	X axis mean	Y axis mean
2α (mm)	0.499	0.535
$\frac{Da}{2W}$	0.448	0.482
$R\Delta a$	0.898	0.962
$R\Delta q$ ($mm^{1/2}$)	0.863	0.931
Lo (mm)	199.50	206.62
Lr	1.44	1.49

Table 4 Slab S4 Roughness parameters values

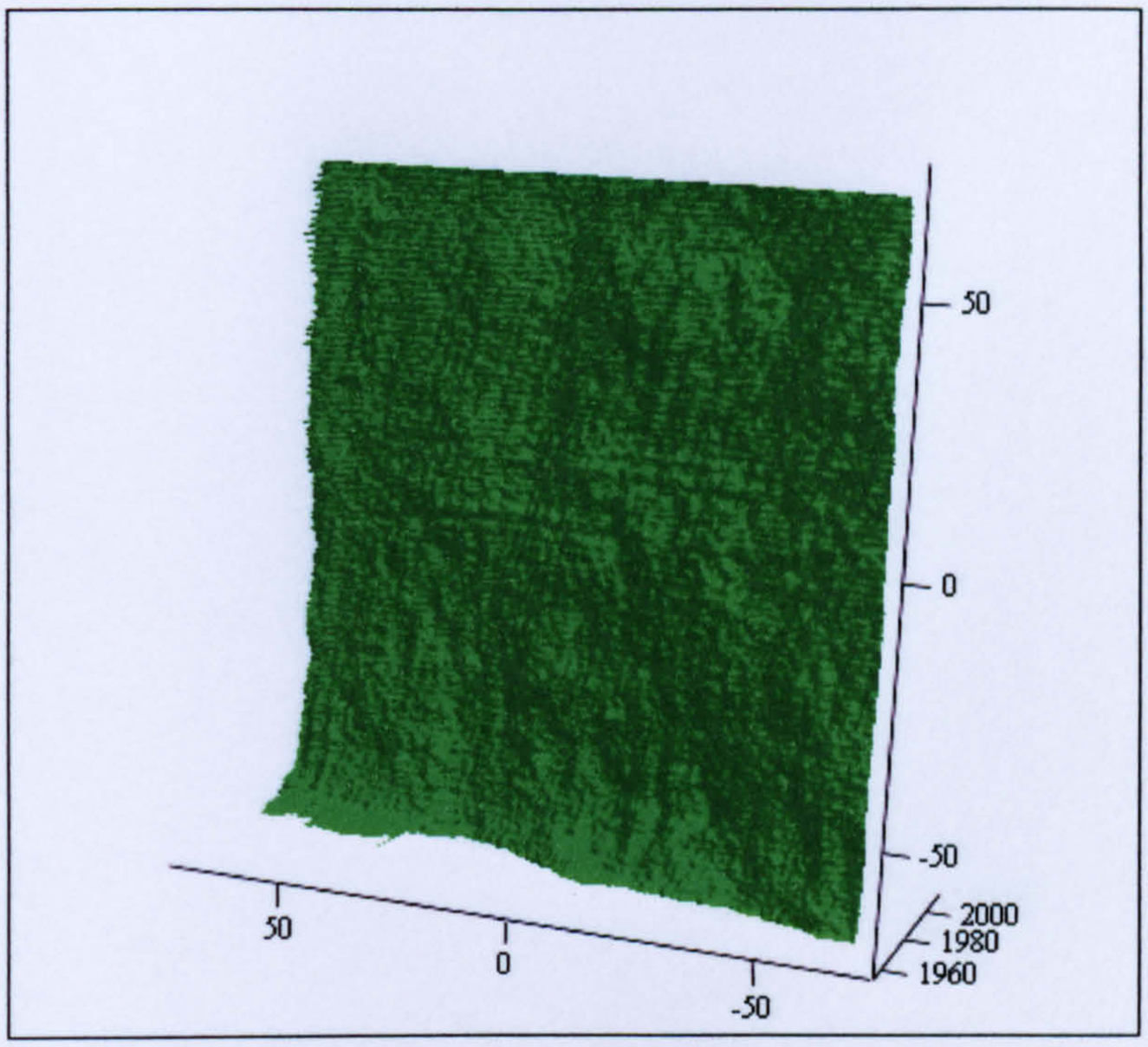

Figure 5 Slab S5 Topography

Roughness Parameters	X axis mean	Y axis mean
2α (mm)	0.540	0.659
$\frac{Da}{2W}$	0.485	0.591
$R\Delta a$	0.972	1.185
$R\Delta q$ ($mm^{1/2}$)	0.952	1.174
Lo (mm)	207.58	232.01
Lr	1.49	1.67

Table 5 Slab S5 Roughness parameters values

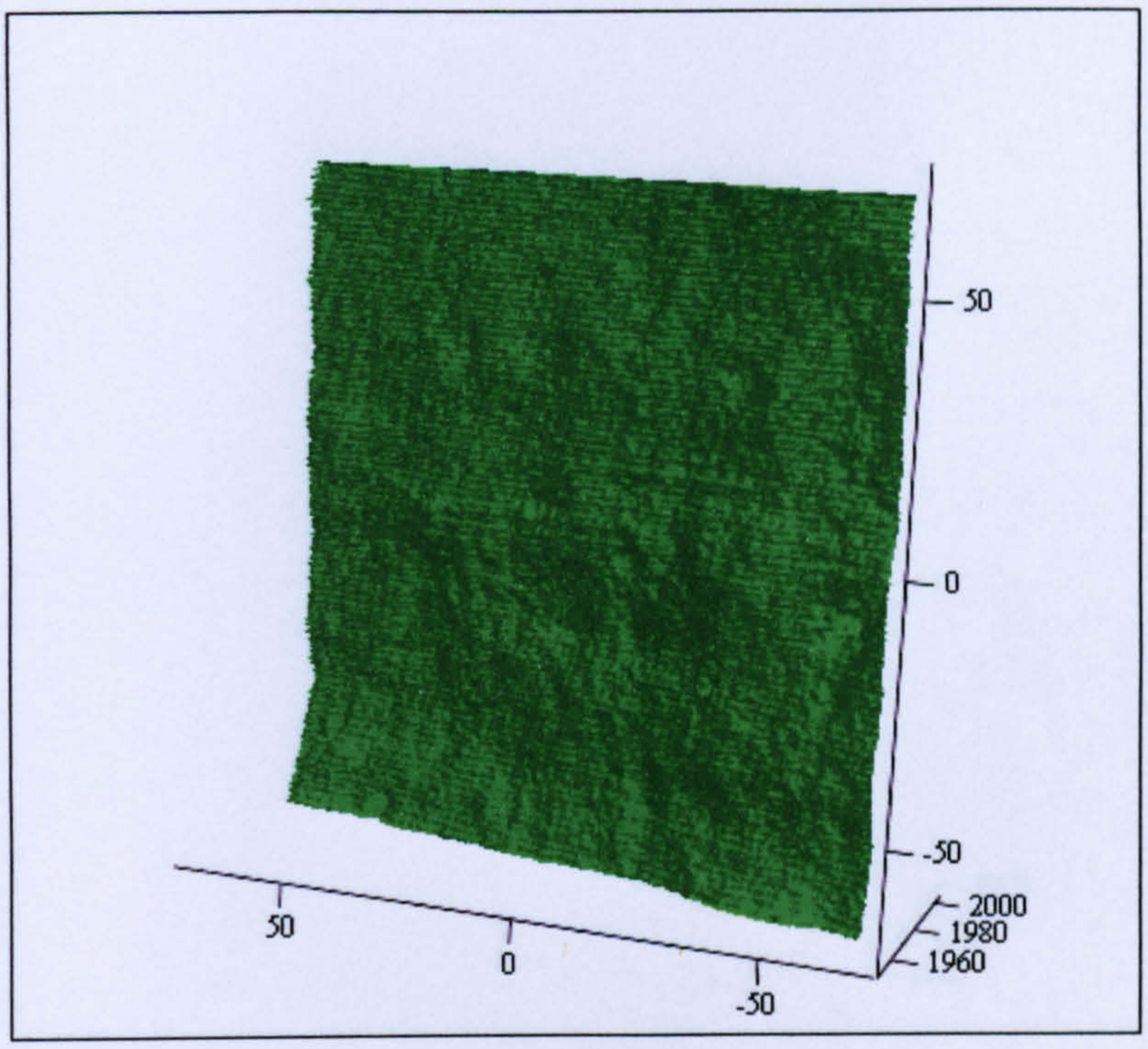

Figure 6 Slab S6 Topography

Roughness Parameters	X axis mean	Y axis mean
2α (mm)	0.504	0.812
$\frac{Da}{2W}$	0.453	0.730
$R\Delta a$	0.906	1.460
$R\Delta q$ ($mm^{1/2}$)	0.870	1.382
Lo (mm)	200.17	261.88
Lr	1.44	1.88

Table 6 Slab S6 Roughness parameters values

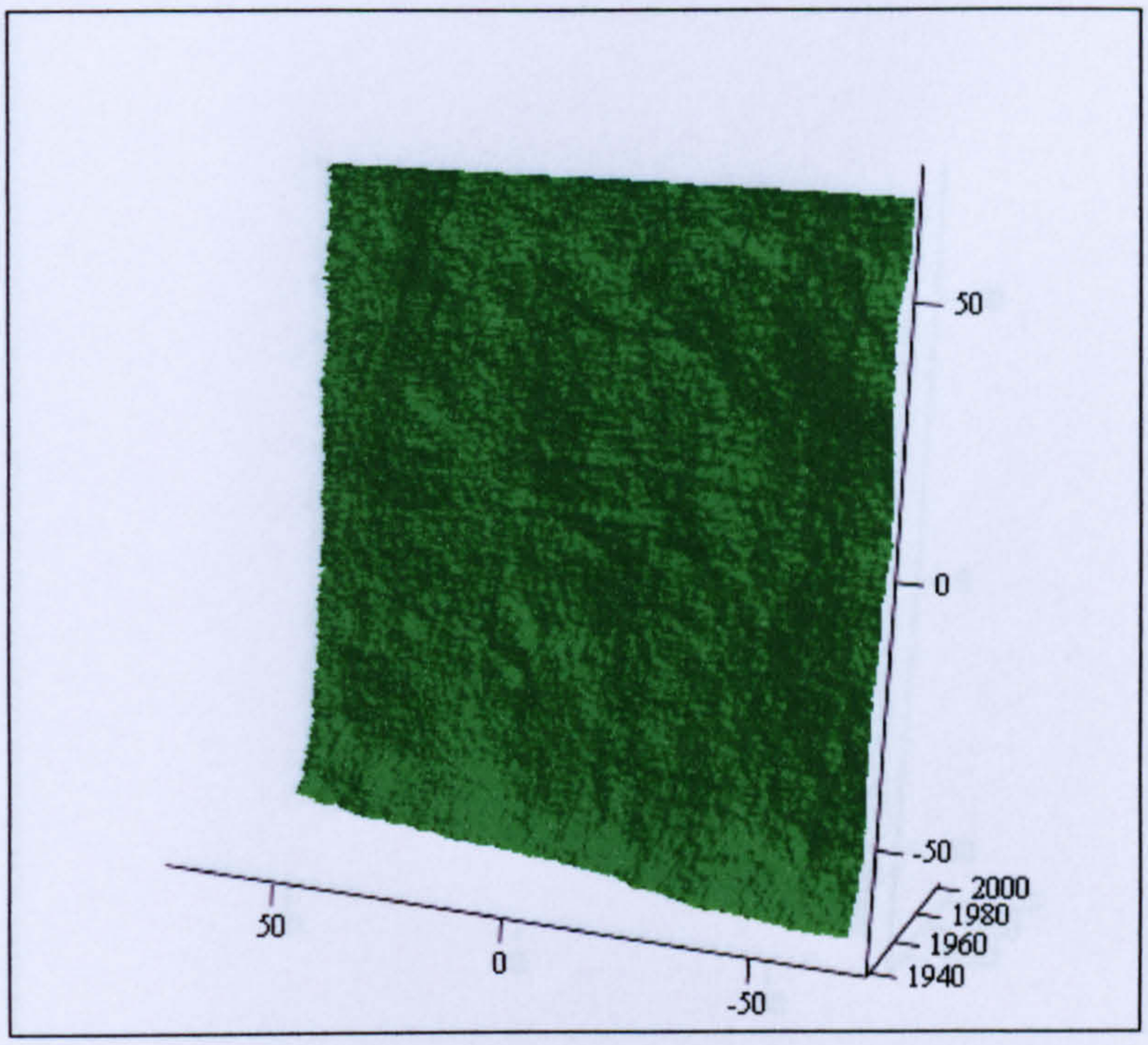

Figure 7 Slab S7 Topography

Roughness Parameters	X axis mean	Y axis mean
2α (mm)	0.540	0.568
$\frac{Da}{2W}$	0.485	0.511
$R\Delta a$	0.972	1.021
$R\Delta q$ ($mm^{1/2}$)	0.949	0.972
Lo (mm)	207.54	212.77
Lr	1.49	1.53

Table 7 Slab S7 Roughness parameters values

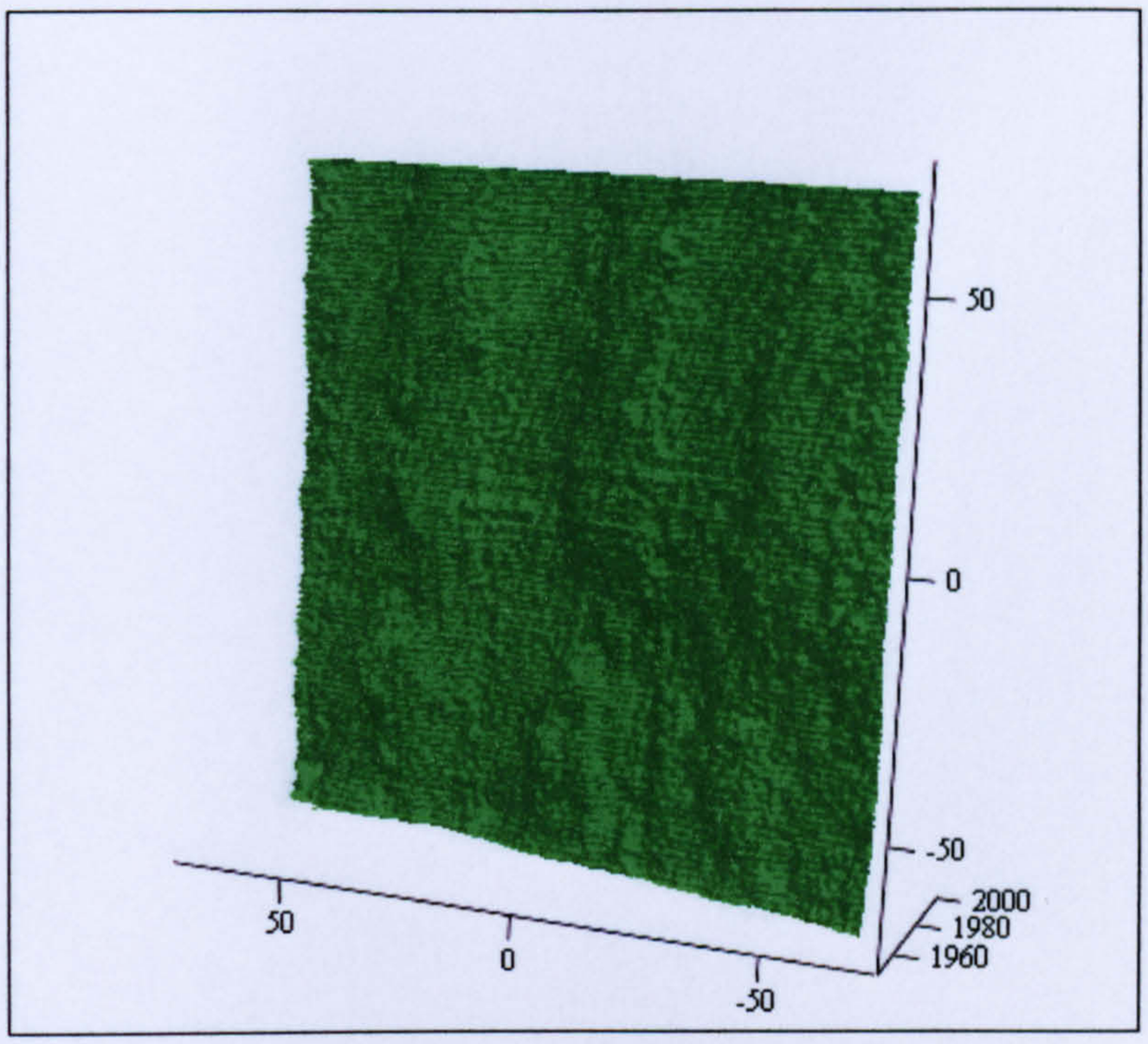

Figure 8 Slab S8 Topography

Roughness Parameters	X axis mean	Y axis mean
2α (mm)	0.554	0.849
$\frac{Da}{2W}$	0.498	0.763
$R\Delta a$	0.997	1.527
$R\Delta q$ ($mm^{1/2}$)	0.964	1.470
Lo (mm)	210.20	271.25
Lr	1.51	1.95

Table 8 Slab S8 Roughness values parameters

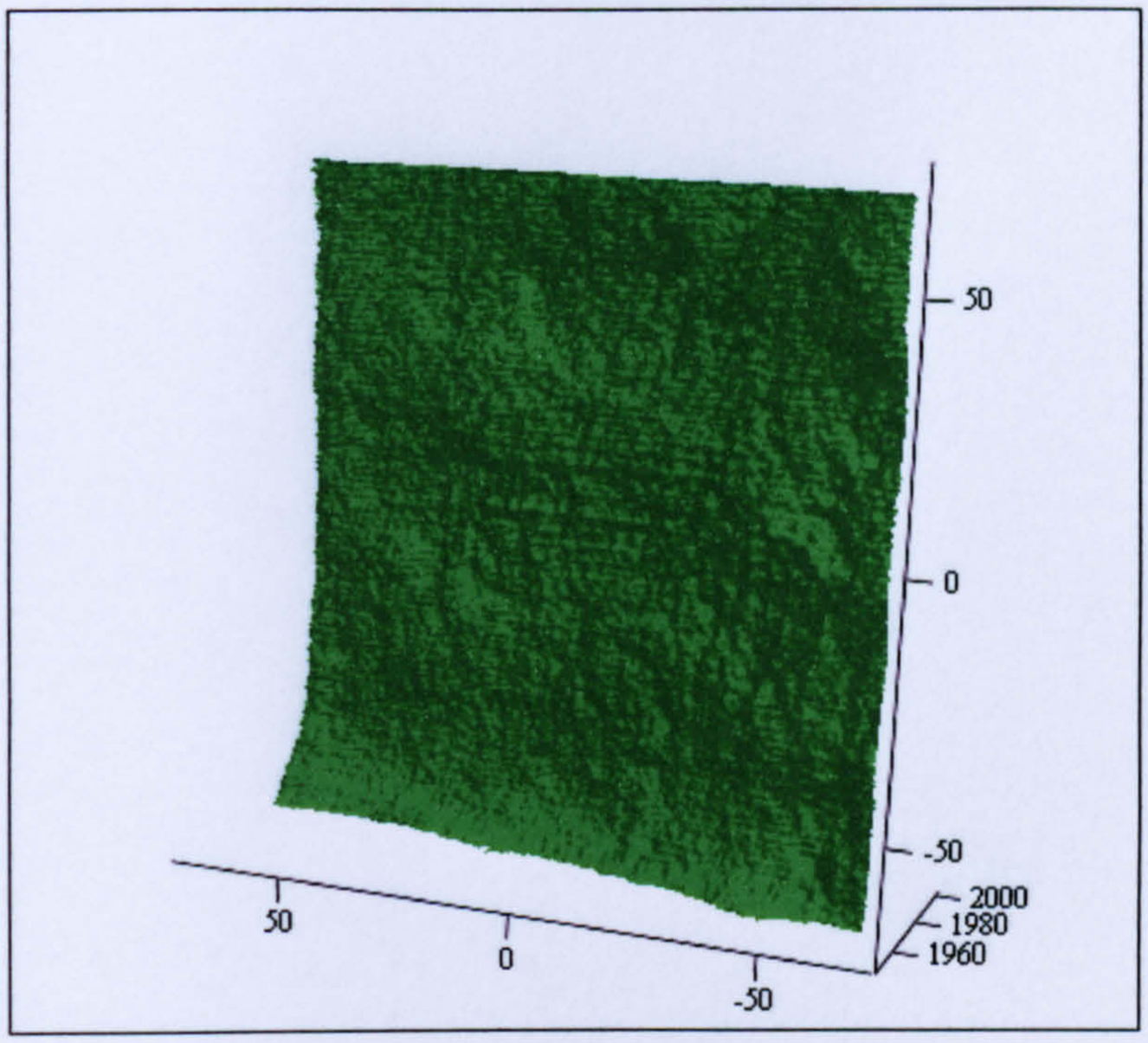

Figure 9 Slab S9 Topography

Roughness Parameters	X axis mean	Y axis mean
2α (mm)	0.549	0.636
$\frac{Da}{2W}$	0.493	0.572
$R\Delta a$	0.988	1.144
$R\Delta q$ ($mm^{1/2}$)	0.955	1.114
Lo (mm)	209.14	226.46
Lr	1.50	1.63

Table 9 Slab S9 Roughness parameters values

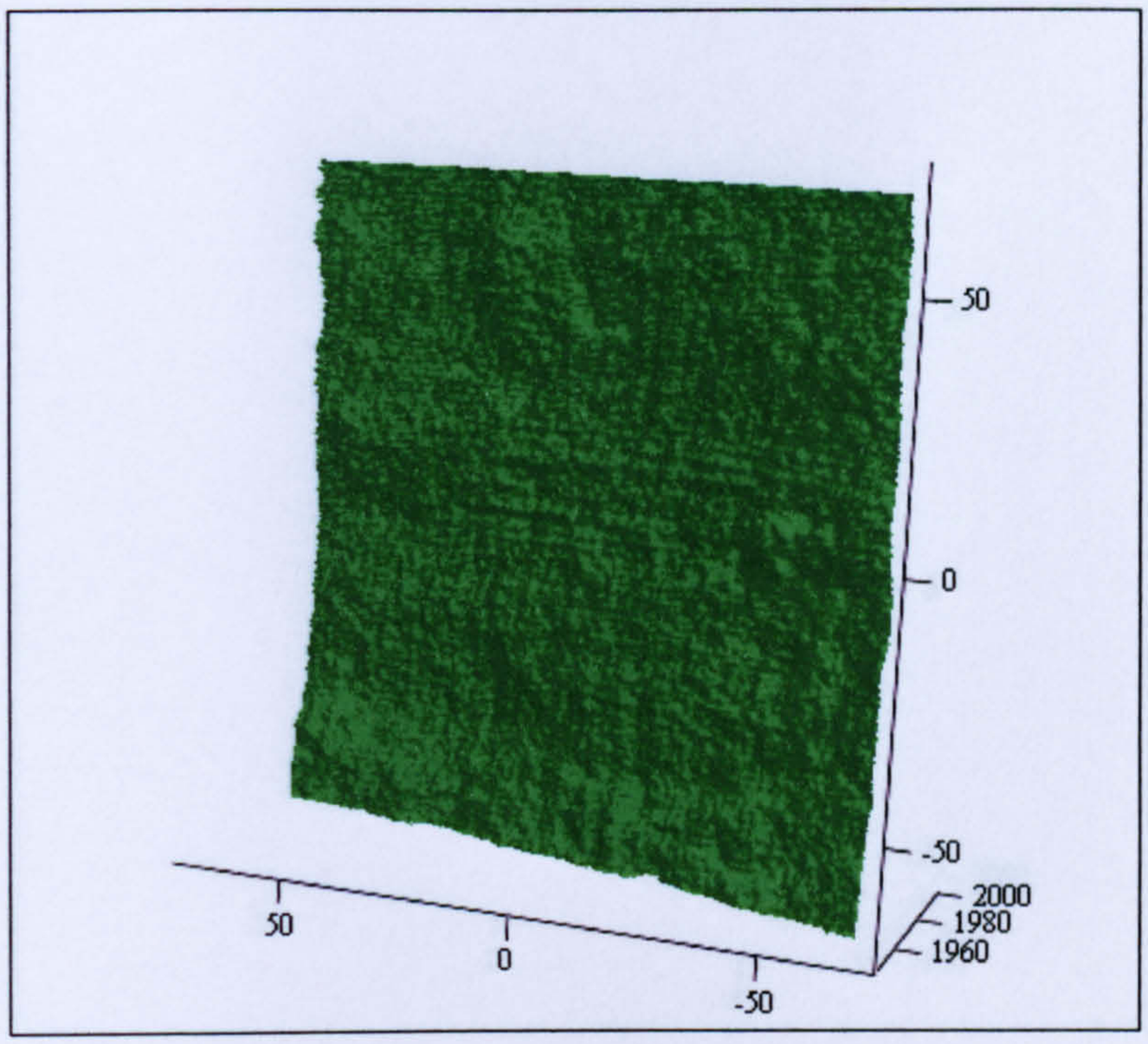

Figure 10 Slab S10 Topography

Roughness Parameters	X axis mean	Y axis mean
2α (mm)	0.536	0.571
$\frac{Da}{2W}$	0.481	0.514
$R\Delta a$	0.964	1.027
$R\Delta q$ ($mm^{1/2}$)	0.932	0.988
Lo (mm)	206.53	213.51
Lr	1.49	1.54

Table 10 Slab S10 Roughness parameters values

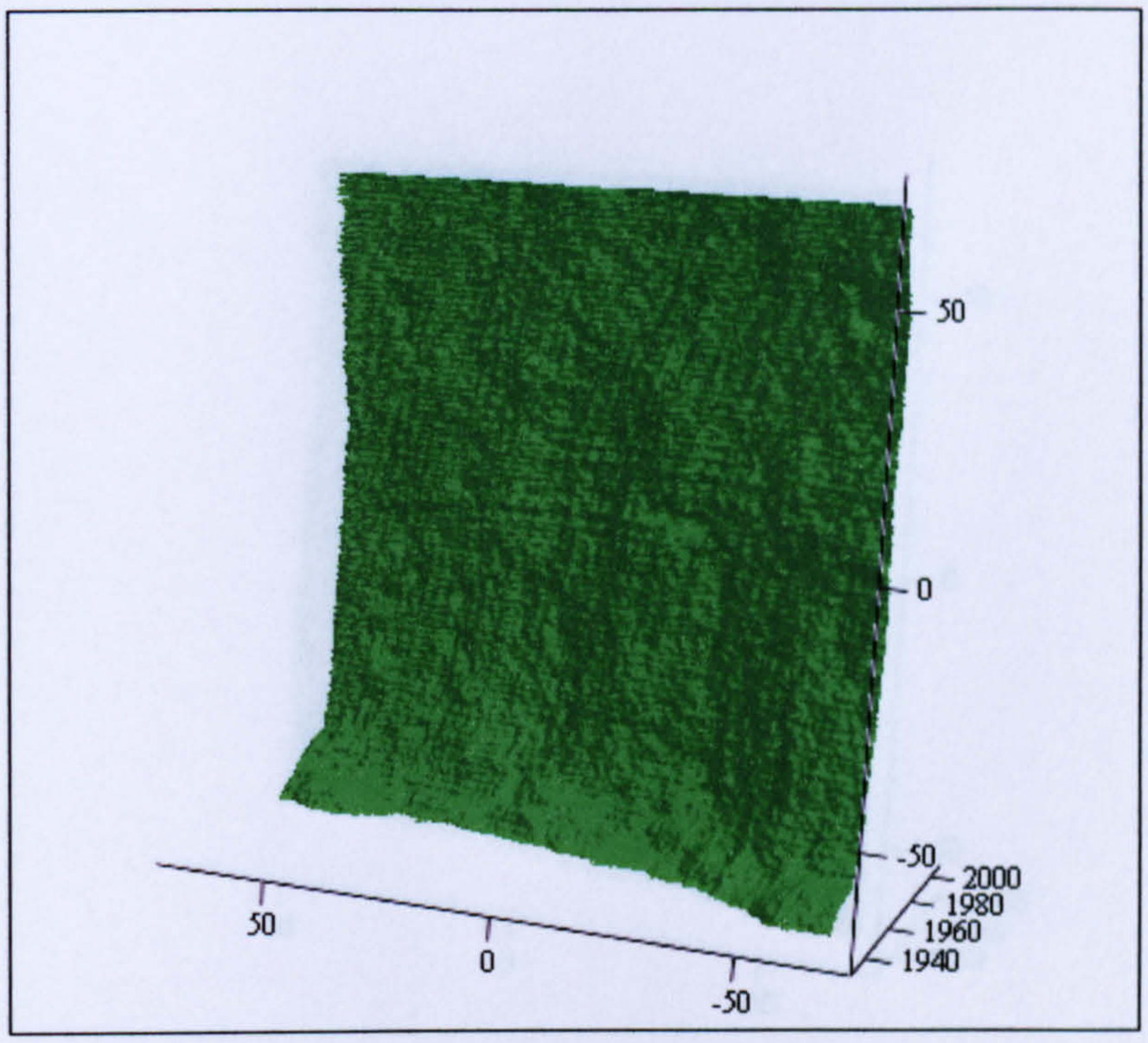

Figure 11 Slab S11 Topography

Roughness Parameters	X axis mean	Y axis mean
2α (mm)	0.546	0.721
$\frac{Da}{2W}$	0.490	0.649
$R\Delta a$	0.982	1.296
$R\Delta q$ ($mm^{1/2}$)	0.953	1.260
Lo (mm)	208.38	244.22
Lr	1.50	1.76

Table 11 Slab S11 Roughness parameters values

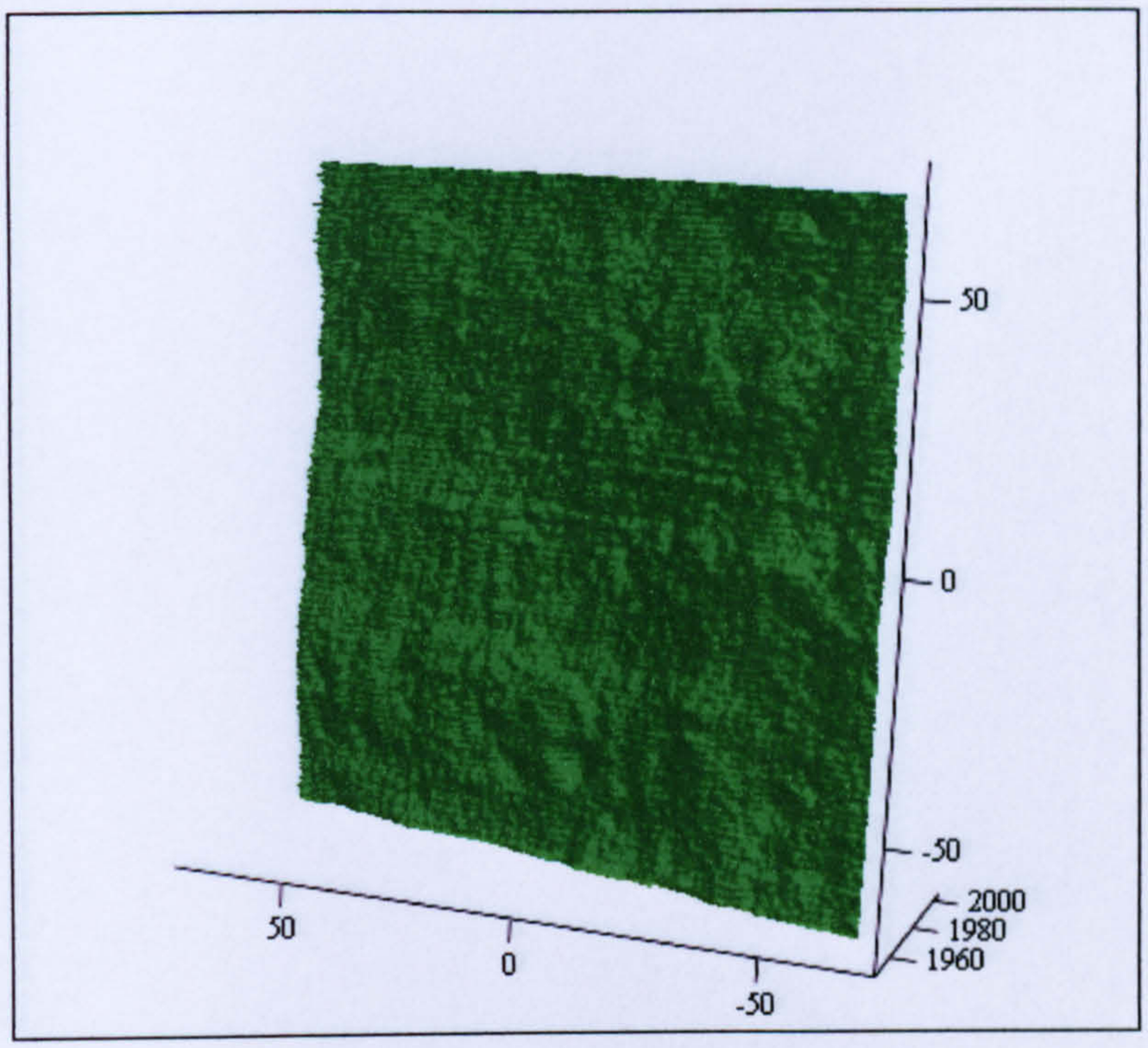

Figure 12 Slab S12 Topography

Roughness Parameters	X axis mean	Y axis mean
2α (mm)	0.451	0.546
$\frac{Da}{2W}$	0.404	0.492
$R\Delta a$	0.811	0.982
$R\Delta q$ ($mm^{1/2}$)	0.789	0.948
Lo (mm)	190.94	209.11
Lr	1.37	1.50

Table 12 Slab S12 Roughness parameters values

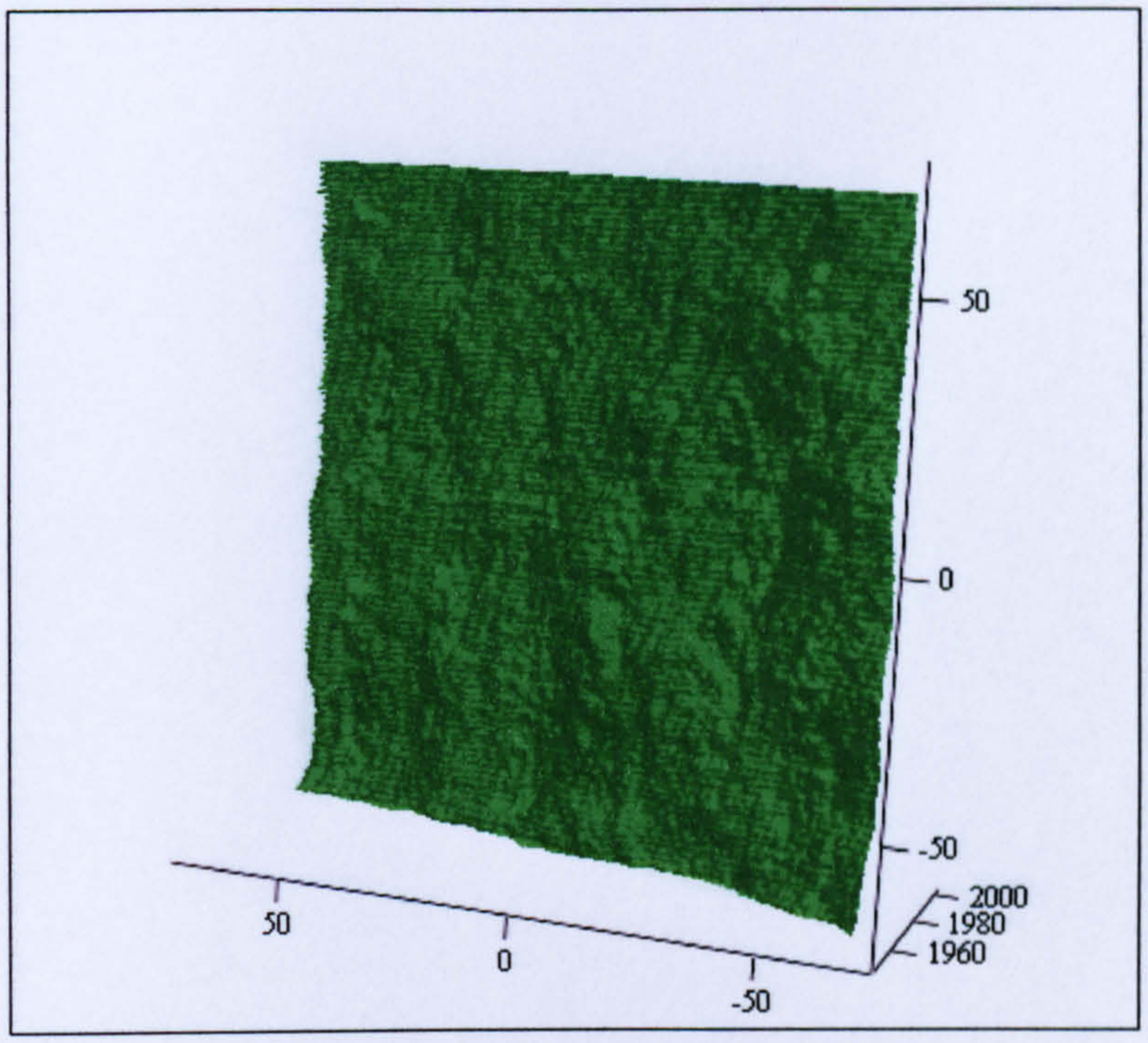

Figure 13 Slab S13 Topography

Roughness Parameters	X axis mean	Y axis mean
2α (mm)	0.512	0.818
$\frac{Da}{2W}$	0.460	0.737
$R\Delta a$	0.921	1.471
$R\Delta q$ ($mm^{1/2}$)	0.894	1.406
Lo (mm)	202.13	264.32
Lr	1.45	1.90

Table 13 Slab S13 Roughness parameters values

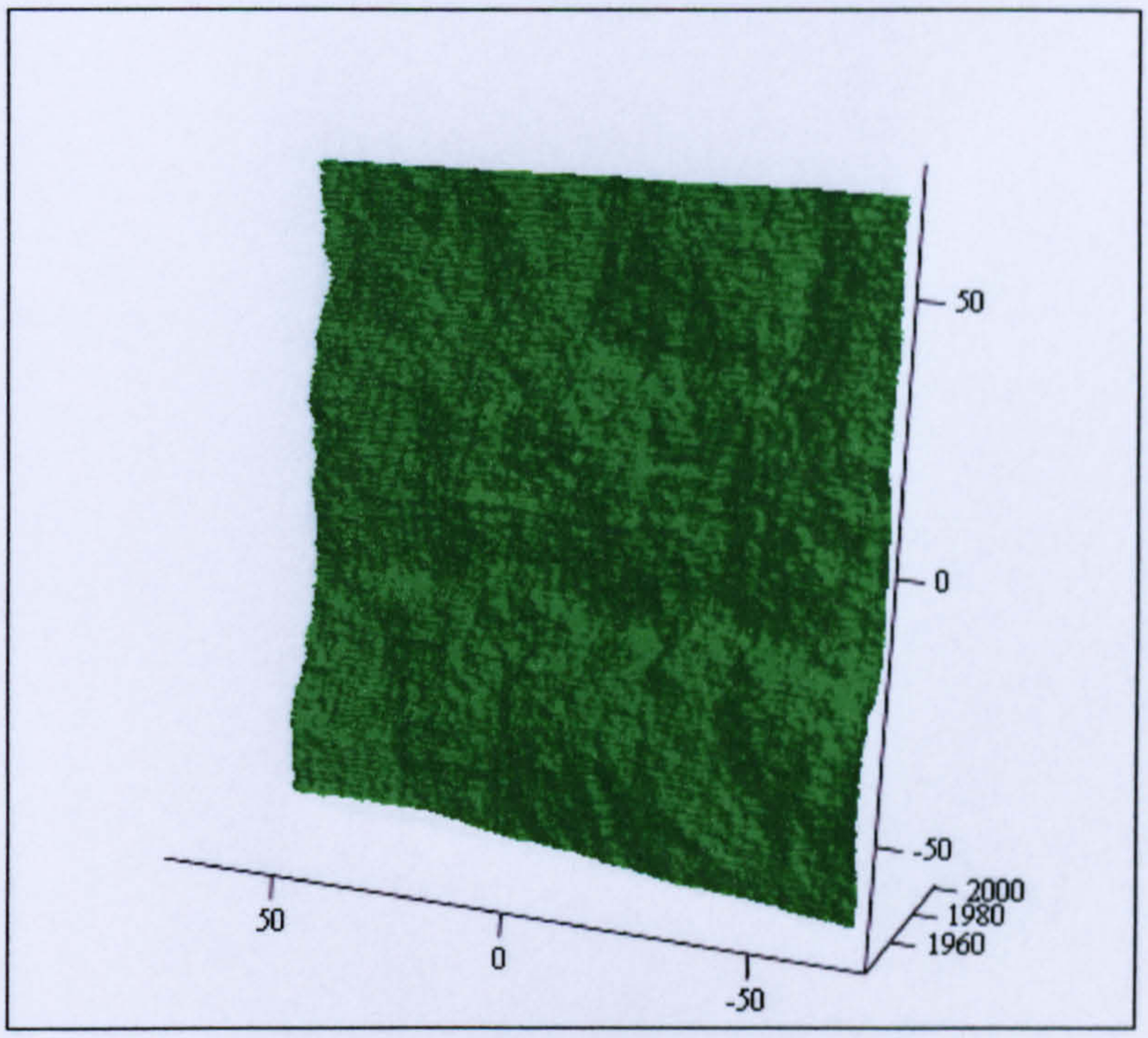

(X, Y, Z)

Table 14 Slab S14 Topography

Roughness Parameters	X axis mean	Y axis mean
2α (mm)	0.528	0.654
$\frac{Da}{2W}$	0.474	0.589
$R\Delta a$	0.950	1.177
$R\Delta q$ ($mm^{1/2}$)	0.920	1.146
Lo (mm)	205.39	230.20
Lr	1.48	1.66

Table 14 Slab S14 Roughness parameters values

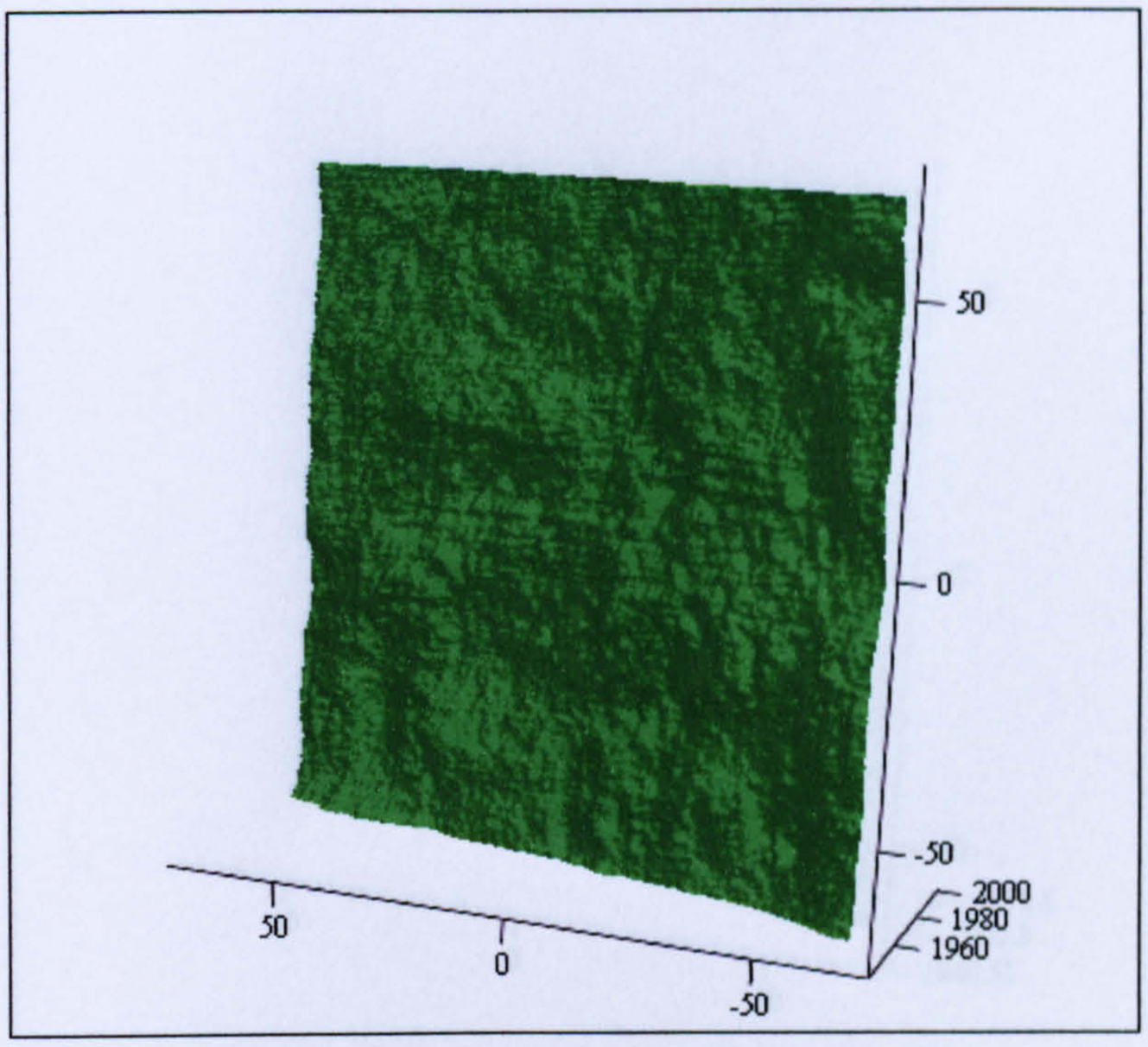

Figure15 Slab S15 Topography

Roughness Parameters	X axis mean	Y axis mean
2α (mm)	0.441	0.445
$\frac{Da}{2W}$	0.396	0.400
$R\Delta a$	0.793	0.799
$R\Delta q$ ($mm^{1/2}$)	0.766	0.766
Lo (mm)	188.83	189.81
Lr	1.36	1.37

Table 15 Slab S15 Roughness parameters values

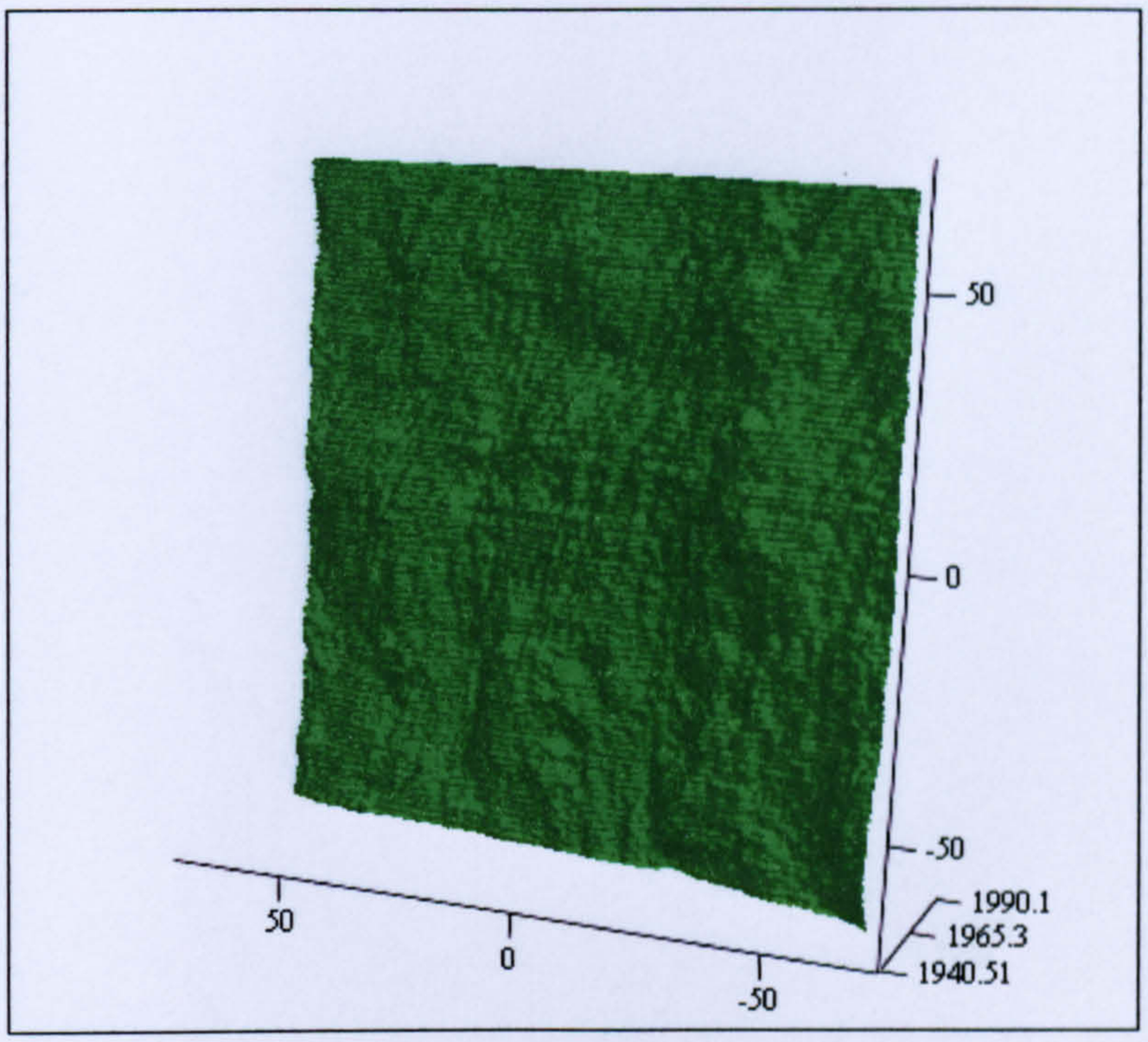

Figure16 Slab S16 Topography

Roughness Parameters	X axis mean	Y axis mean
2α (mm)	0.502	0.859
$\frac{Da}{2W}$	0.451	0.774
$R\Delta a$	0.902	1.544
$R\Delta q$ ($mm^{1/2}$)	0.870	1.507
Lo (mm)	200.12	273.65
Lr	1.44	1.97

Table 16 Slab S16 Roughness parameters values

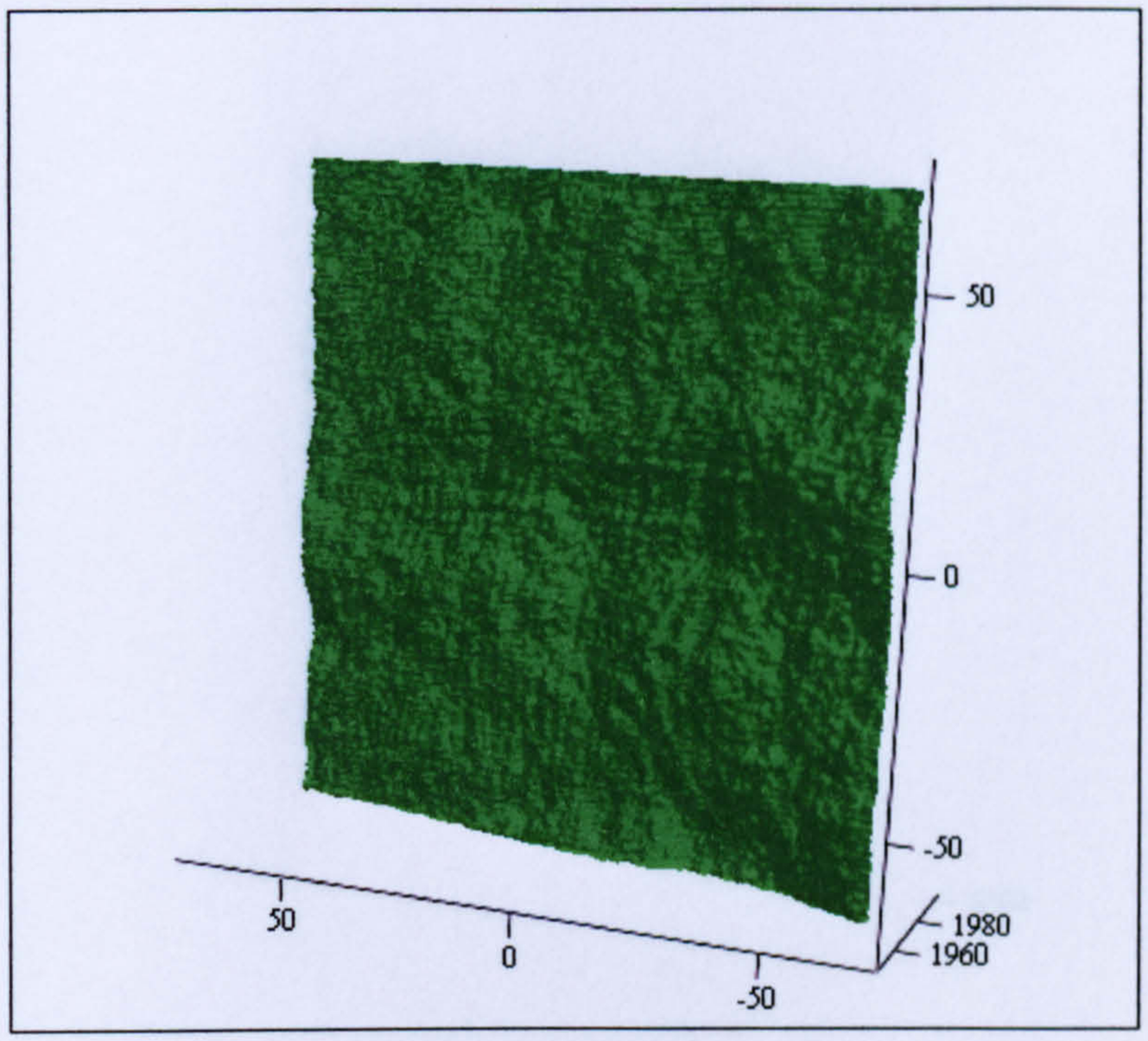

(X, Y, Z)

Figure17 Slab S17 Topography

Roughness Parameters	X axis mean	Y axis mean
2α (mm)	0.534	0.590
$\frac{Da}{2W}$	0.480	0.531
$R\Delta a$	0.960	1.060
$R\Delta q$ ($mm^{1/2}$)	0.929	1.044
Lo (mm)	206.49	217.48
Lr	1.49	1.56

Table 17 Slab S17 Roughness parameters values

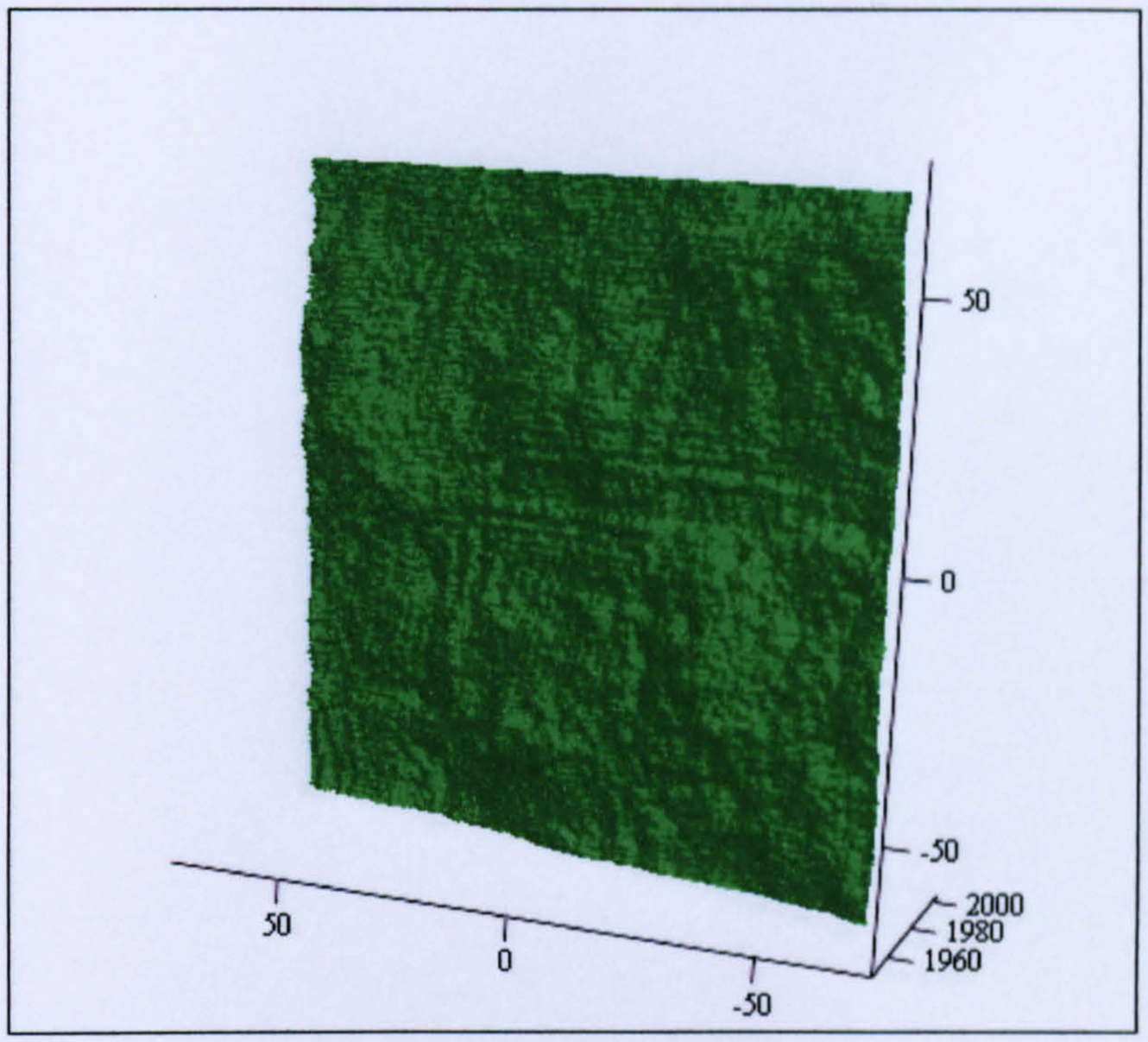

Figure18 Slab S18 Topography

Roughness Parameters	X axis mean	Y axis mean
2α (mm)	0.467	0.520
$\frac{Da}{2W}$	0.419	0.468
$R\Delta a$	0.839	0.935
$R\Delta q$ ($mm^{1/2}$)	0.827	0.927
Lo (mm)	194.45	204.60
Lr	1.40	1.47

Table 18 Slab S18 Roughness parameters values

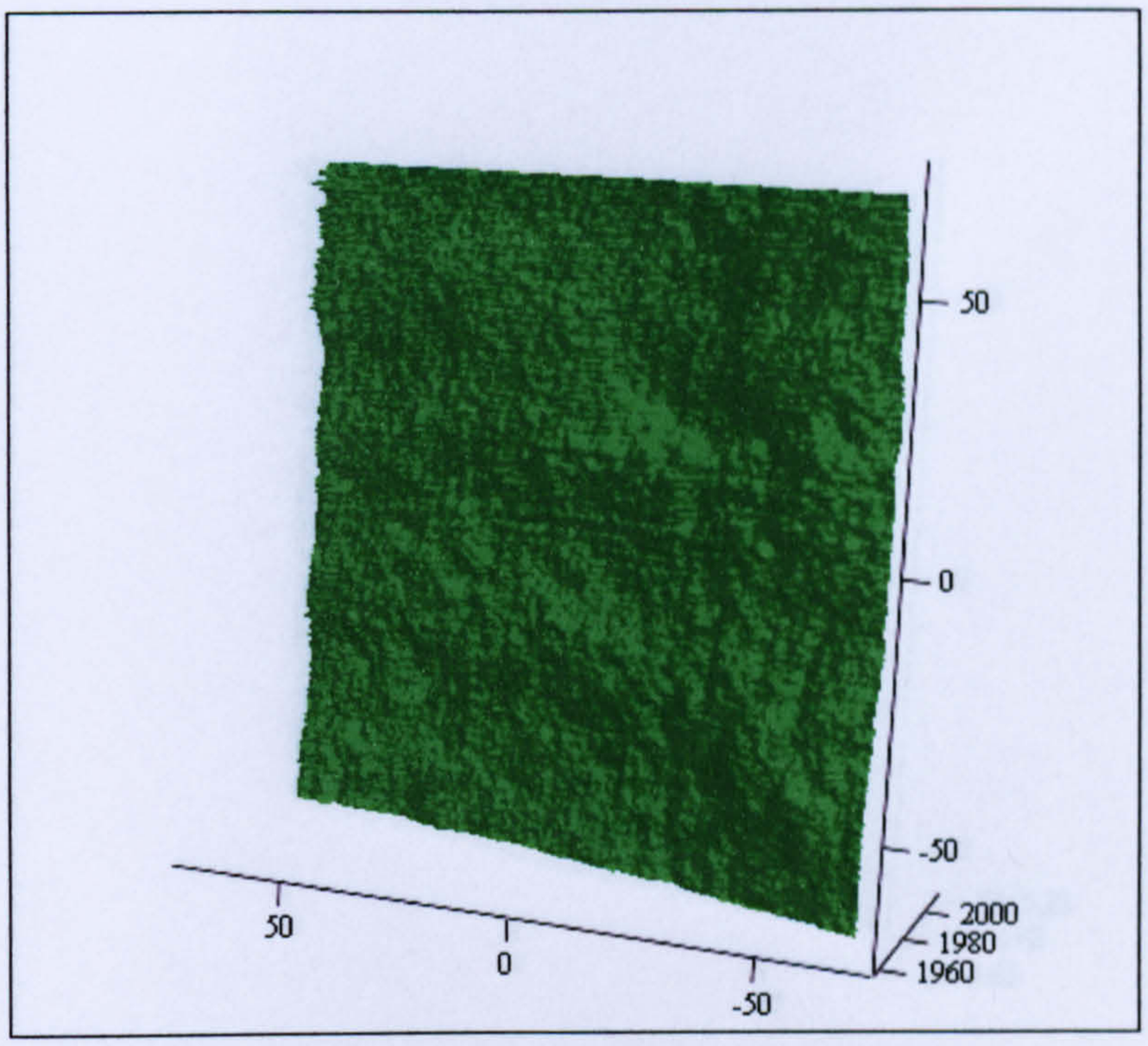

(X, Y, Z)

Figure19 Slab S19 Topography

Roughness Parameters	X axis mean	Y axis mean
2α (mm)	0.565	0.609
$\frac{Da}{2W}$	0.508	0.549
$R\Delta a$	1.017	1.096
$R\Delta q$ ($mm^{1/2}$)	0.992	1.075
Lo (mm)	212.39	221.71
Lr	1.53	1.60

Table 19 Slab S19 Roughness parameters values

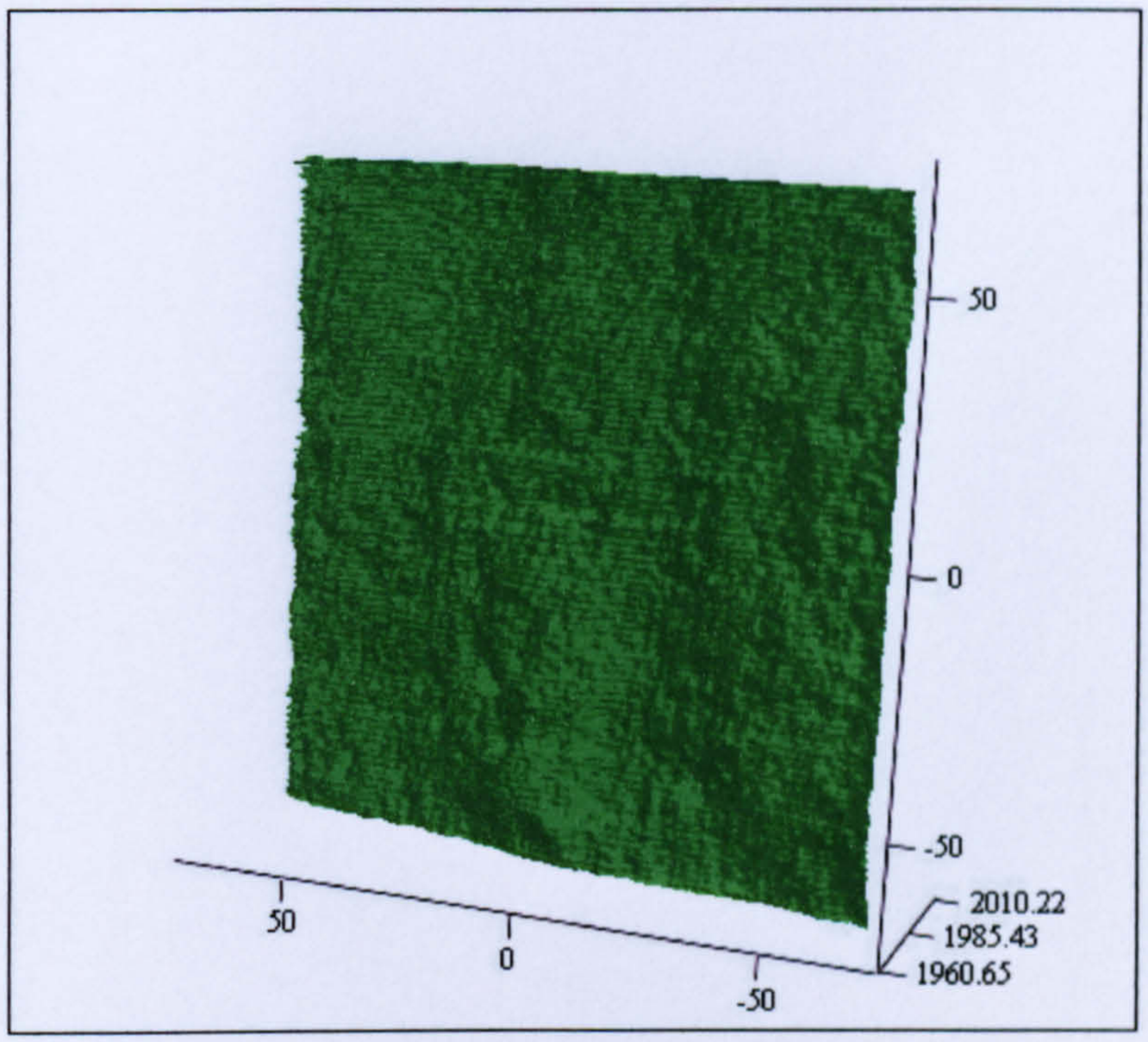

Figure 20 Slab S20 Topography

Roughness Parameters	X axis mean	Y axis mean
2α (mm)	0.546	0.791
$\frac{Da}{2W}$	0.490	0.712
$R\Delta a$	0.983	1.422
$R\Delta q$ ($mm^{1/2}$)	0.977	1.389
Lo (mm)	209.34	258.87
Lr	1.51	1.86

Table 20 Slab S20 Roughness parameters values

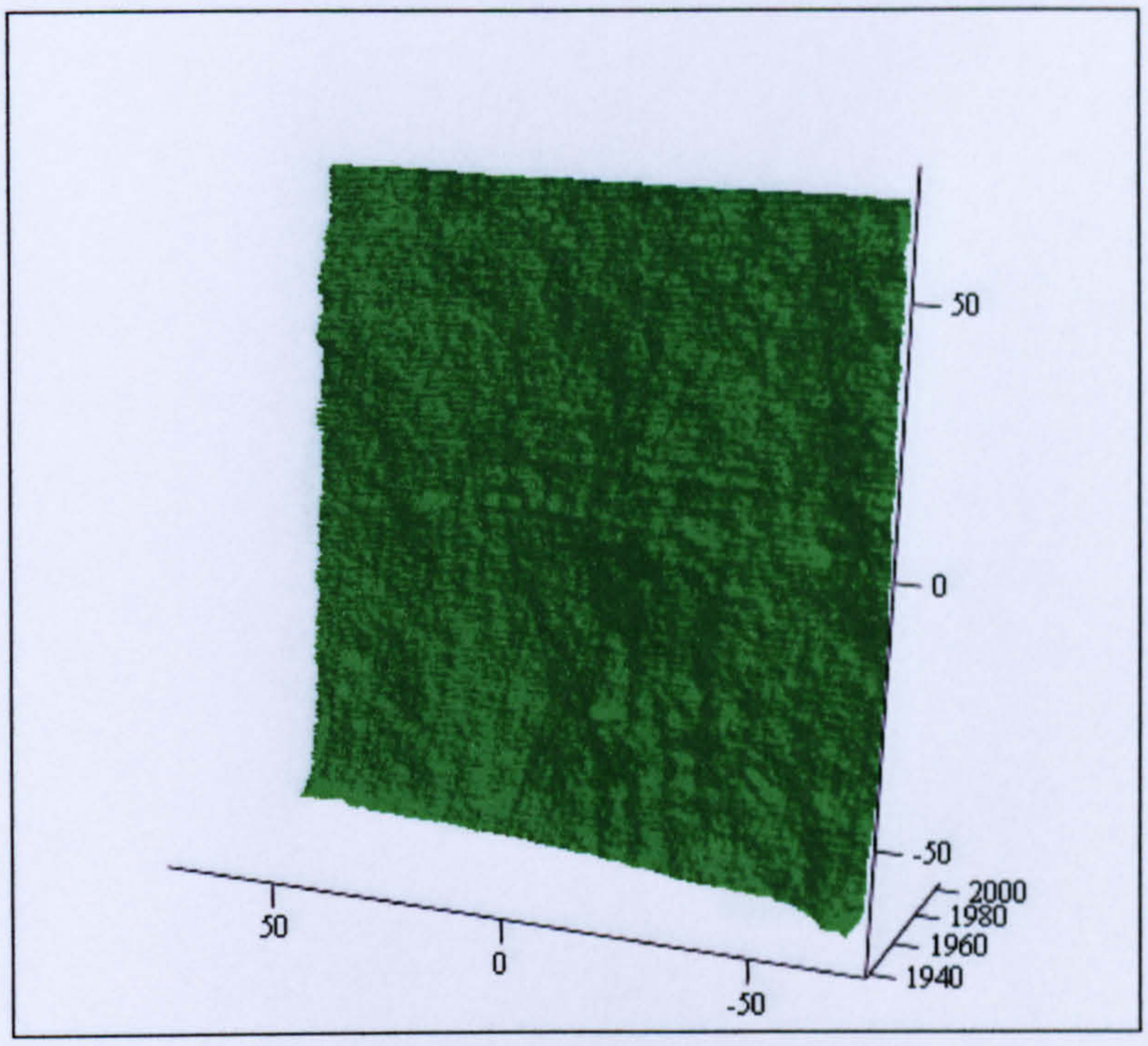

Figure 21 Slab S21 Topography

Roughness Parameters	X axis mean	Y axis mean
2α (mm)	0.510	0.602
$\frac{Da}{2W}$	0.458	0.541
$R\Delta a$	0.917	1.083
$R\Delta q$ ($mm^{1/2}$)	0.900	1.060
Lo (mm)	202.20	219.91
Lr	1.45	1.58

Table 21 Slab S21 Roughness parameters values

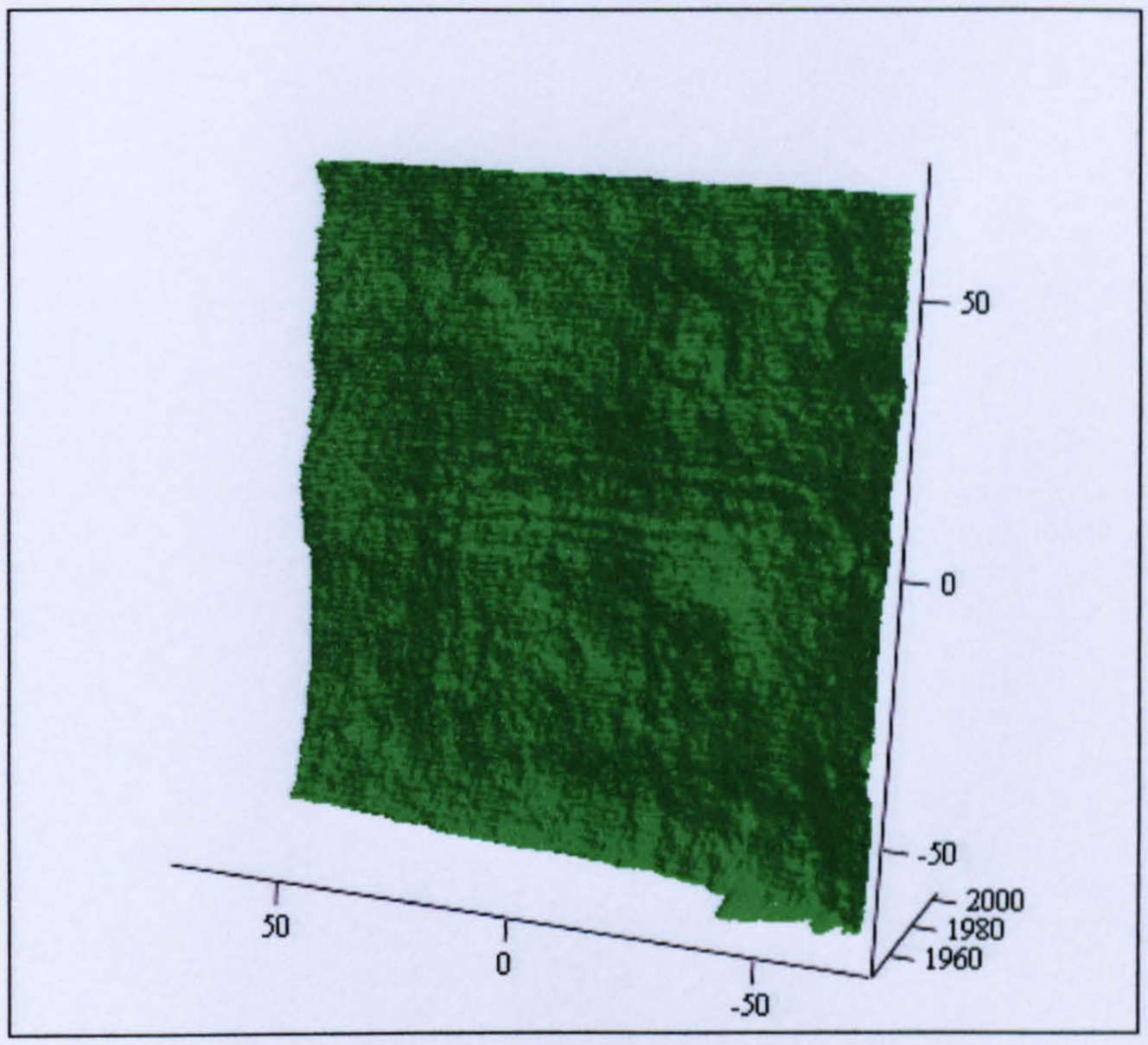

Figure 22 Slab S22 Topography

Roughness Parameters	X axis mean	Y axis mean
2α (mm)	0.489	0.551
$\frac{Da}{2W}$	0.439	0.495
$R\Delta a$	0.879	0.992
$R\Delta q$ ($mm^{1/2}$)	0.865	1.009
Lo (mm)	198.49	210.83
Lr	1.43	1.52

Table 22 Slab S22 Roughness parameters values

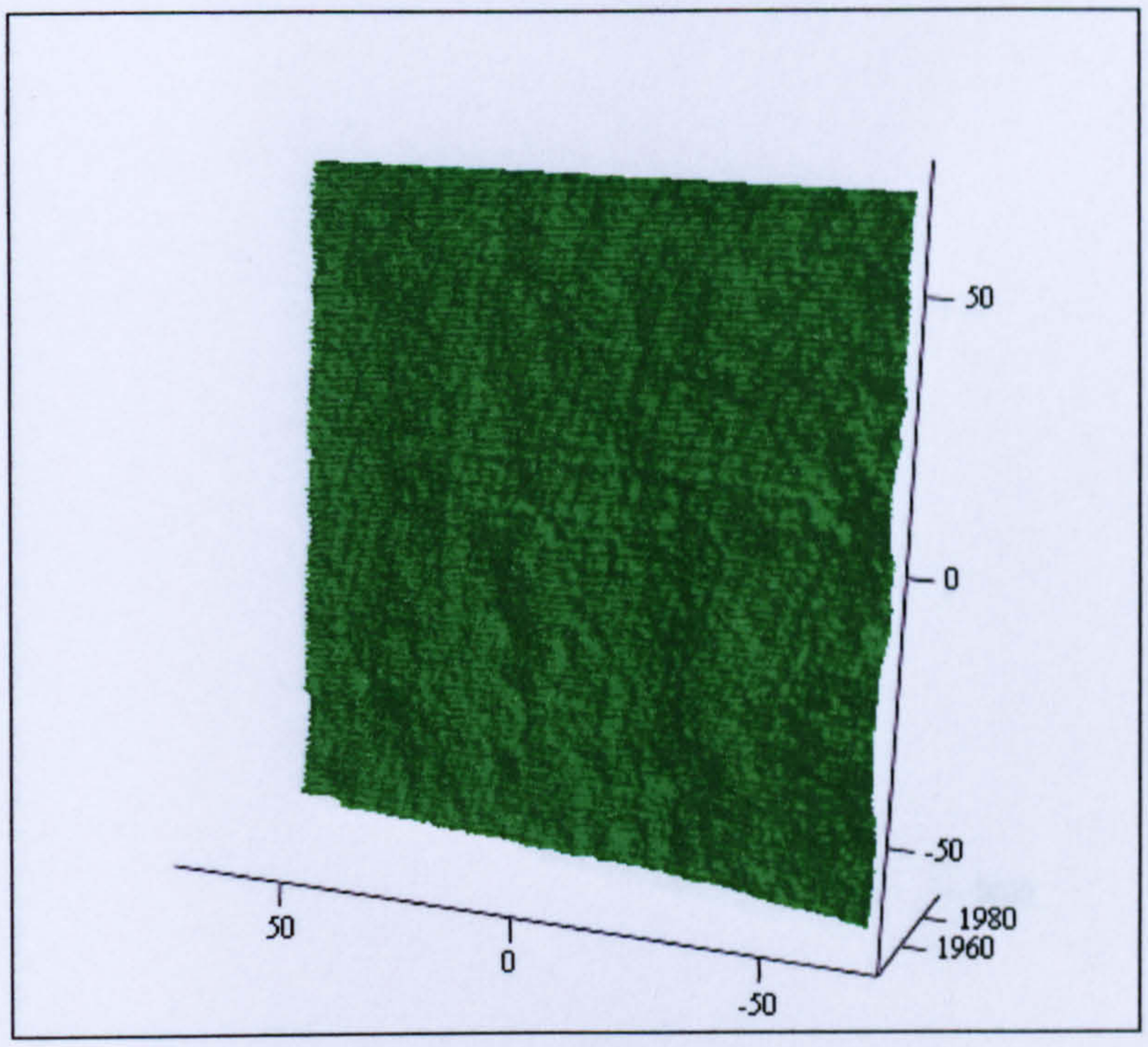

Figure 23 Slab S23 Topography

Roughness Parameters	X axis mean	Y axis mean
2α (mm)	0.541	0.811
$\frac{Da}{2W}$	0.487	0.730
$R\Delta a$	0.974	1.459
$R\Delta q$ ($mm^{1/2}$)	0.941	1.400
Lo (mm)	207.58	262.17
Lr	1.49	1.89

Table 23 Slab S23 Roughness parameters values

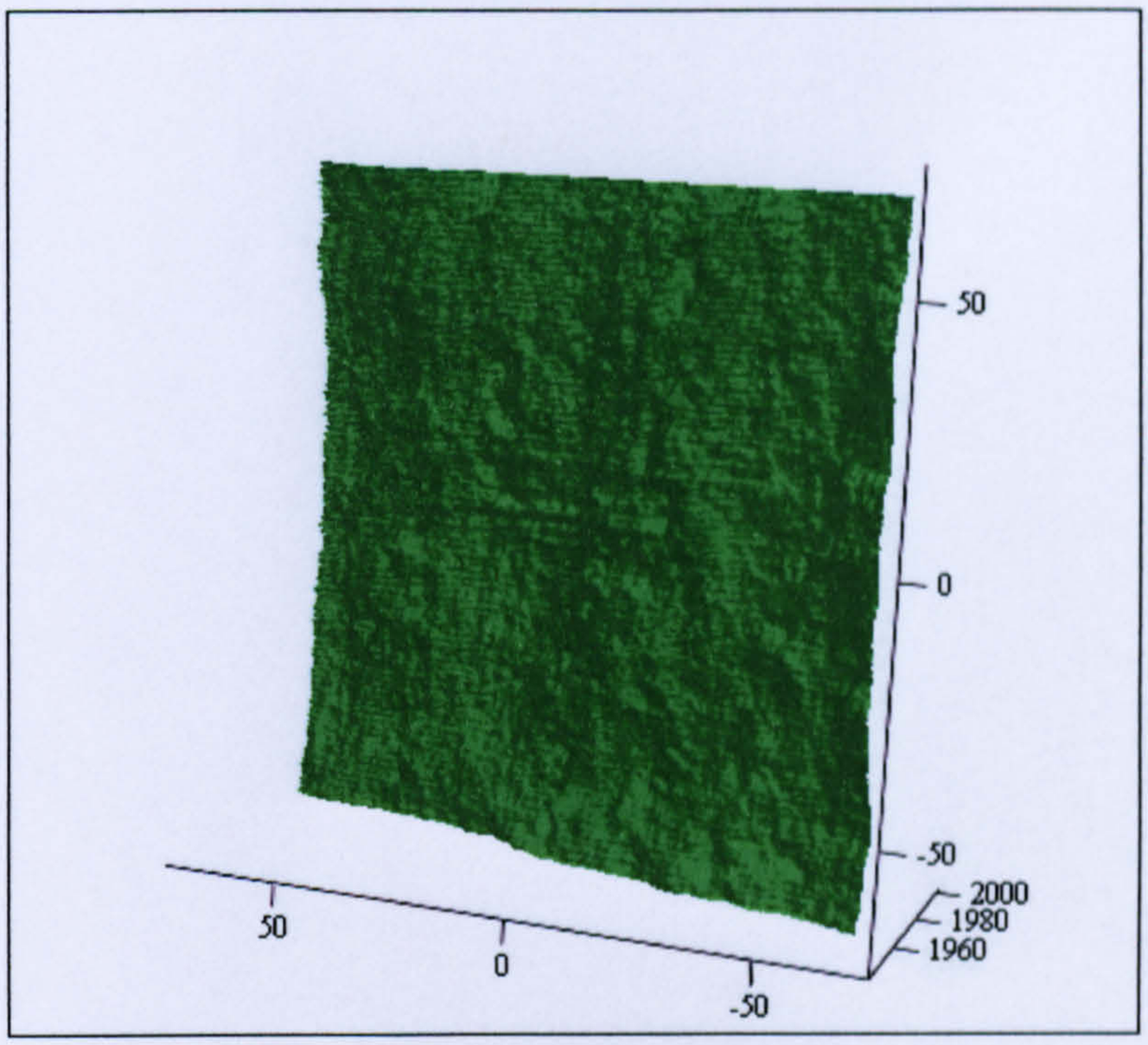

Figure 24 Slab S24 Topography

Roughness Parameters	X axis mean	Y axis mean
2α (mm)	0.487	0.598
$\frac{Da}{2W}$	0.437	0.537
$R\Delta a$	0.875	1.075
$R\Delta q$ ($mm^{1/2}$)	0.857	1.061
Lo (mm)	197.80	219.79
Lr	1.42	1.58

Table 24 Slab S24 Roughness parameters values

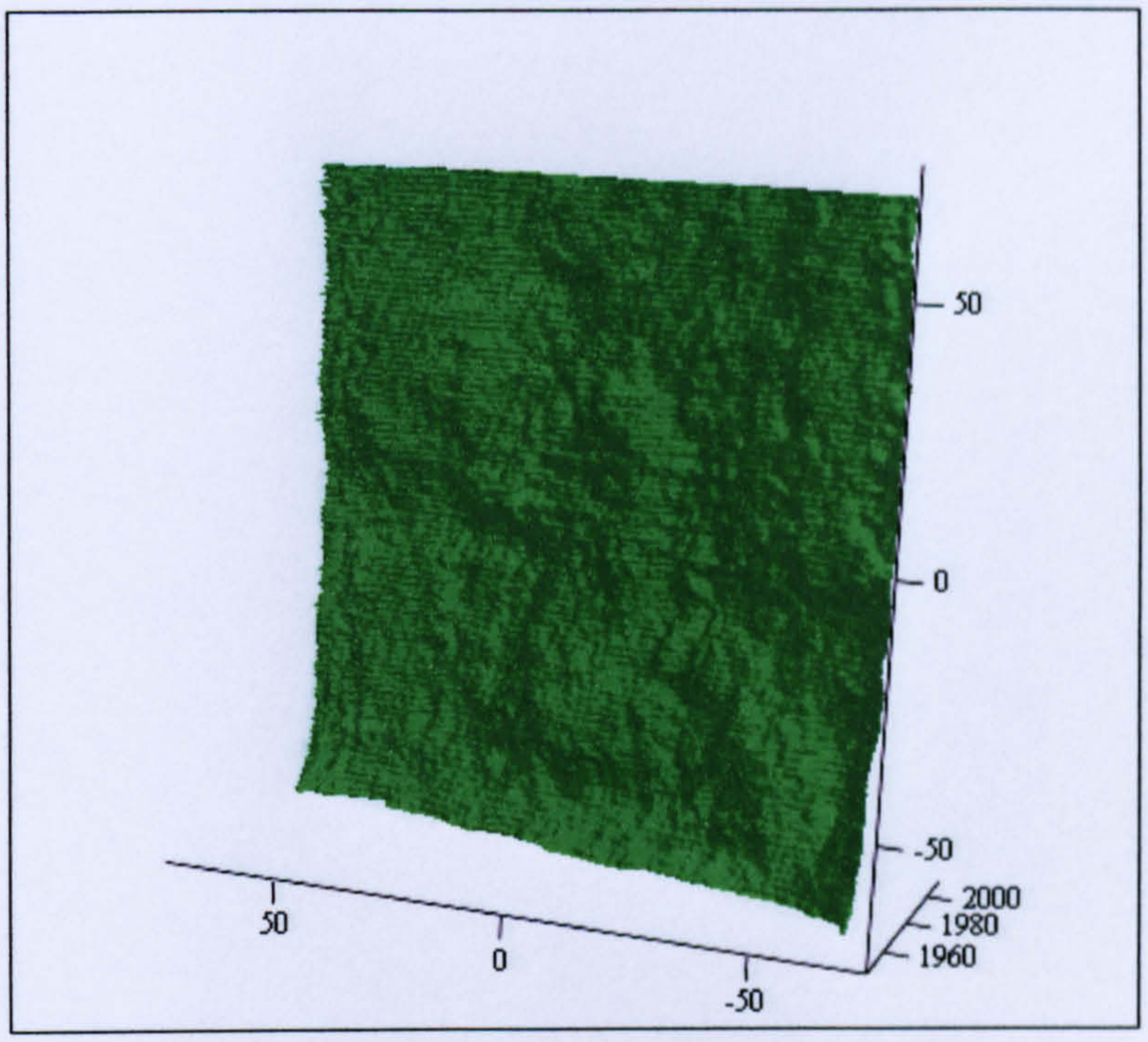

(X, Y, Z)

Figure 25 Slab S25 Topography

Roughness Parameters	X axis mean	Y axis mean
2α (mm)	0.501	0.730
$\frac{Da}{2W}$	0.451	0.656
$R\Delta a$	0.902	1.312
$R\Delta q$ ($mm^{1/2}$)	0.887	1.272
Lo (mm)	200.55	245.65
Lr	1.44	1.77

Table 25 Slab S25 Roughness parameters values

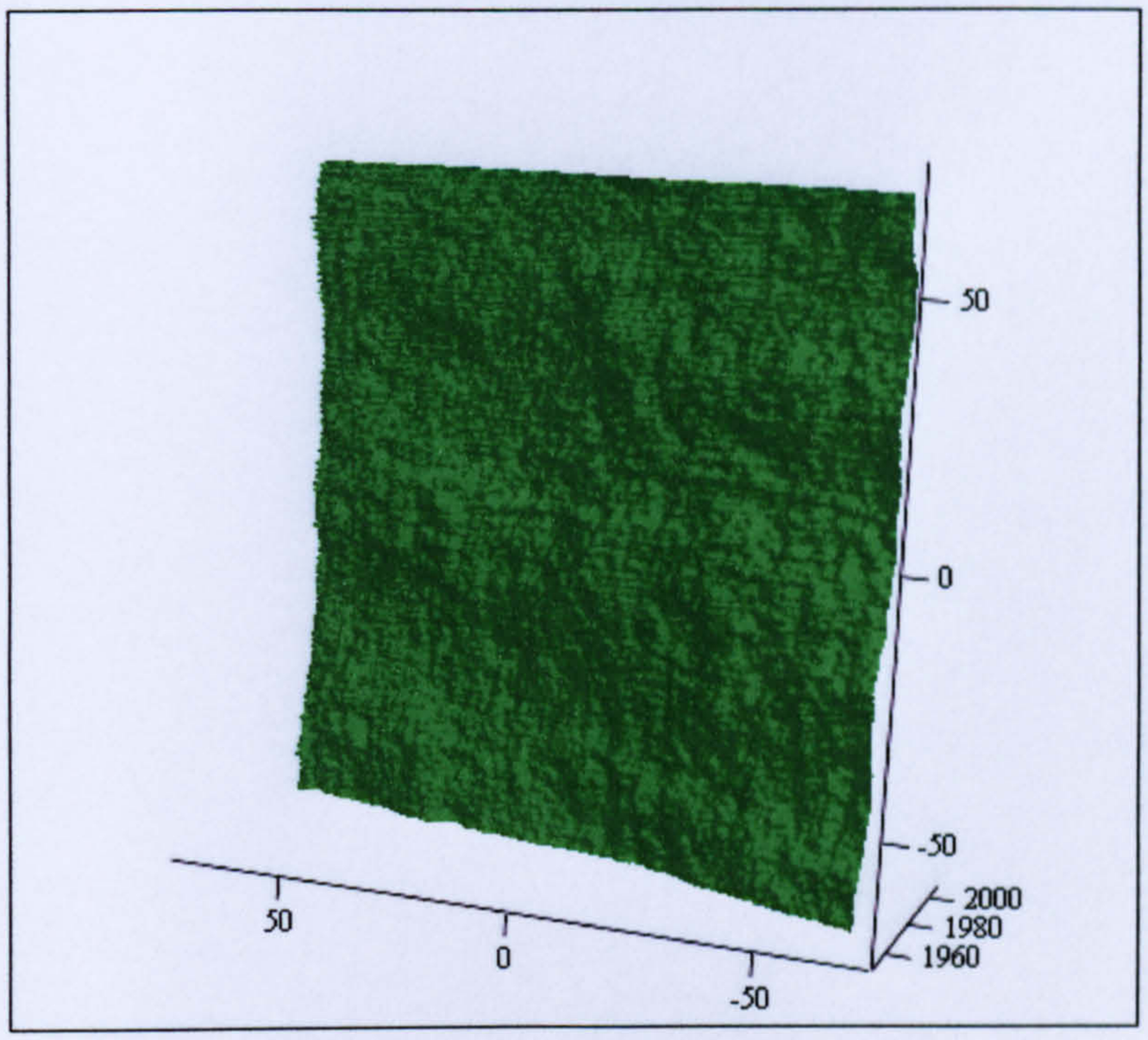

Figure 26 Slab S26 Topography

Roughness Parameters	X axis mean	Y axis mean
2α (mm)	0.548	0.615
$\frac{Da}{2W}$	0.492	0.554
$R\Delta a$	0.985	1.106
$R\Delta q$ ($mm^{1/2}$)	0.953	1.073
Lo (mm)	208.78	222.22
Lr	1.50	1.60

Table 26 Slab S26 Roughness parameters values

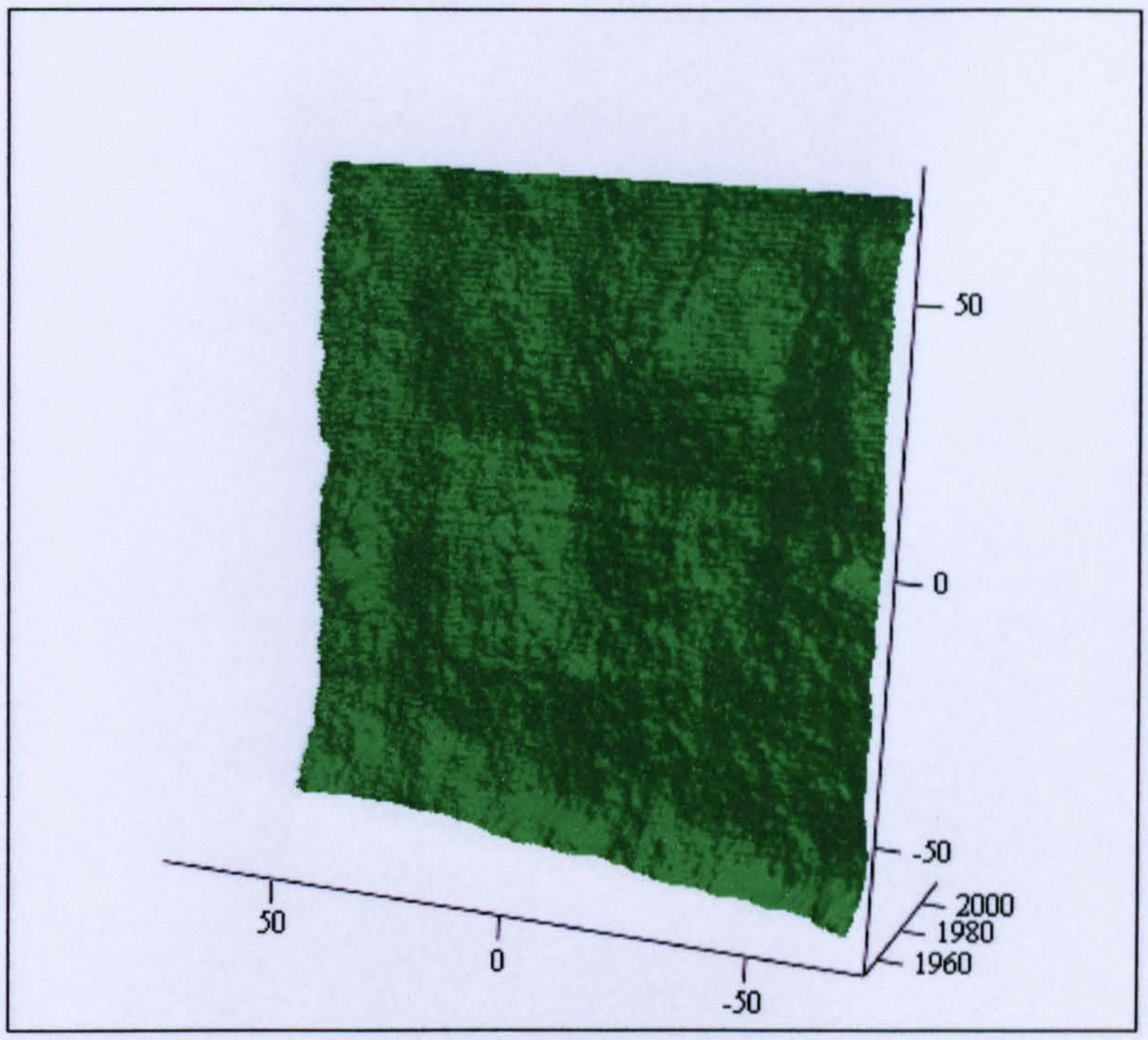

(X, Y, Z)

Figure 27 Slab S27 Topography

Roughness Parameters	X axis mean	Y axis mean
2α (mm)	0.574	0.657
$\frac{Da}{2W}$	0.515	0.591
$R\Delta a$	1.032	1.181
$R\Delta q$ ($mm^{1/2}$)	1.025	1.158
Lo (mm)	214.44	231.37
Lr	1.54	1.66

Table 27 Slab S27 Roughness parameters values

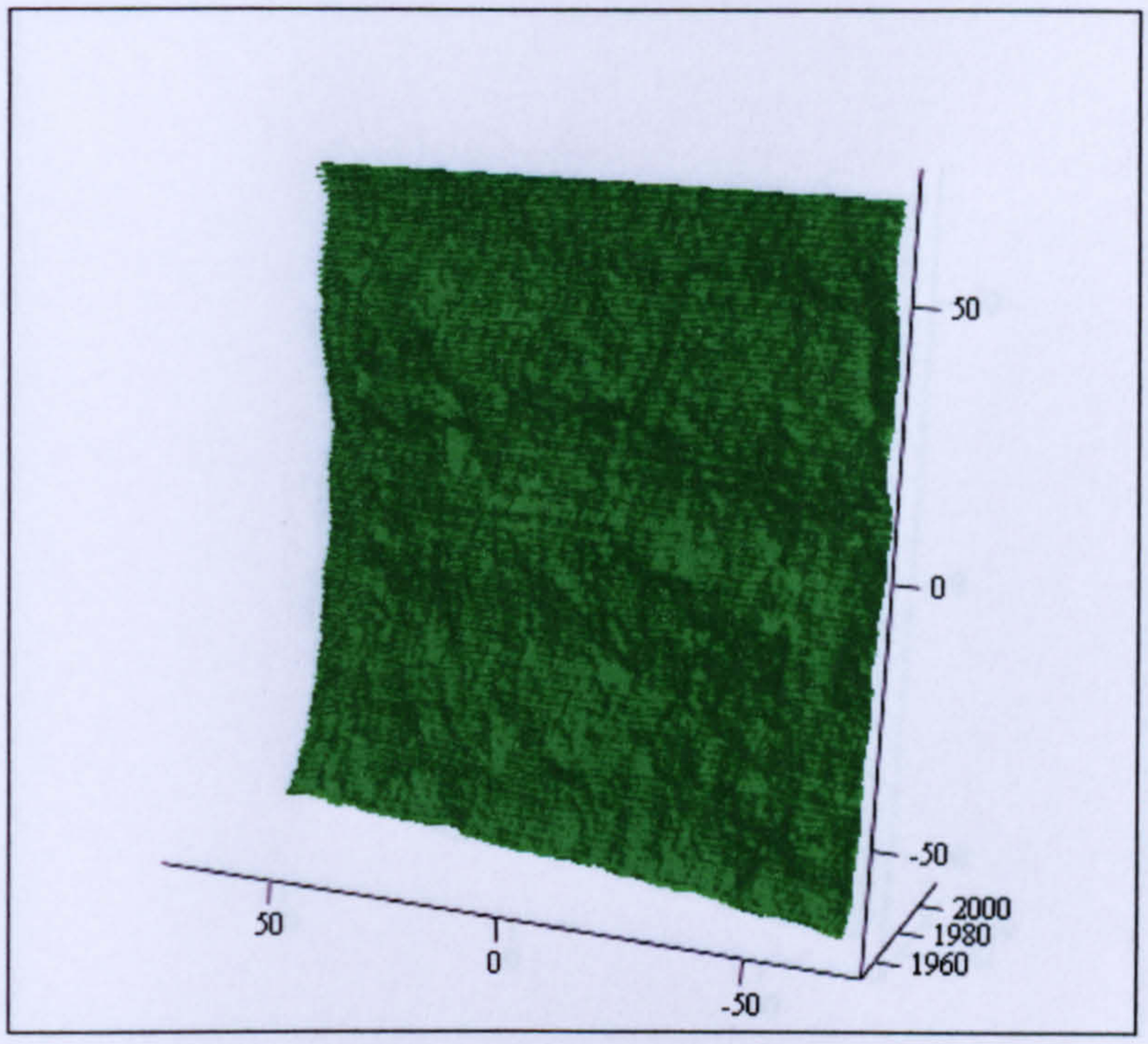

Figure 28 Slab S28 Topography

Roughness Parameters	X axis mean	Y axis mean
2α (mm)	0.527	0.880
$\frac{Da}{2W}$	0.474	0.792
$R\Delta a$	0.949	1.583
$R\Delta q$ ($mm^{1/2}$)	0.925	1.518
Lo (mm)	205.08	277.98
Lr	1.48	2.00

Table 28 Slab S28 Roughness parameters values

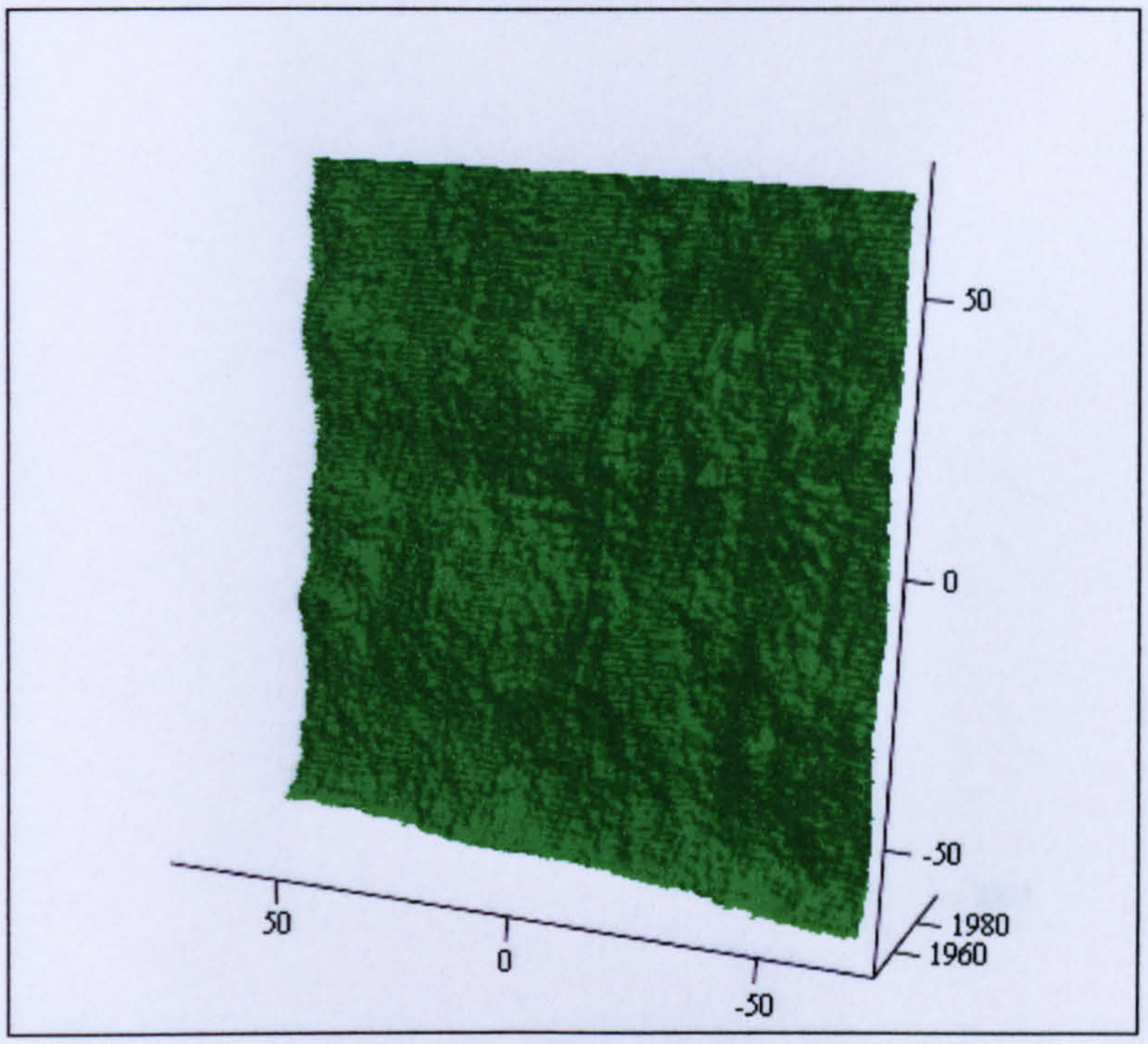

Figure 29 Slab S29 Topography

Roughness Parameters	X axis mean	Y axis mean
2α (mm)	0.540	0.746
$\frac{Da}{2W}$	0.486	0.671
$R\Delta a$	0.972	1.342
$R\Delta q$ ($mm^{1/2}$)	0.943	1.312
Lo (mm)	207.48	249.77
Lr	1.49	1.80

Table 29 Slab S29 Roughness parameters values

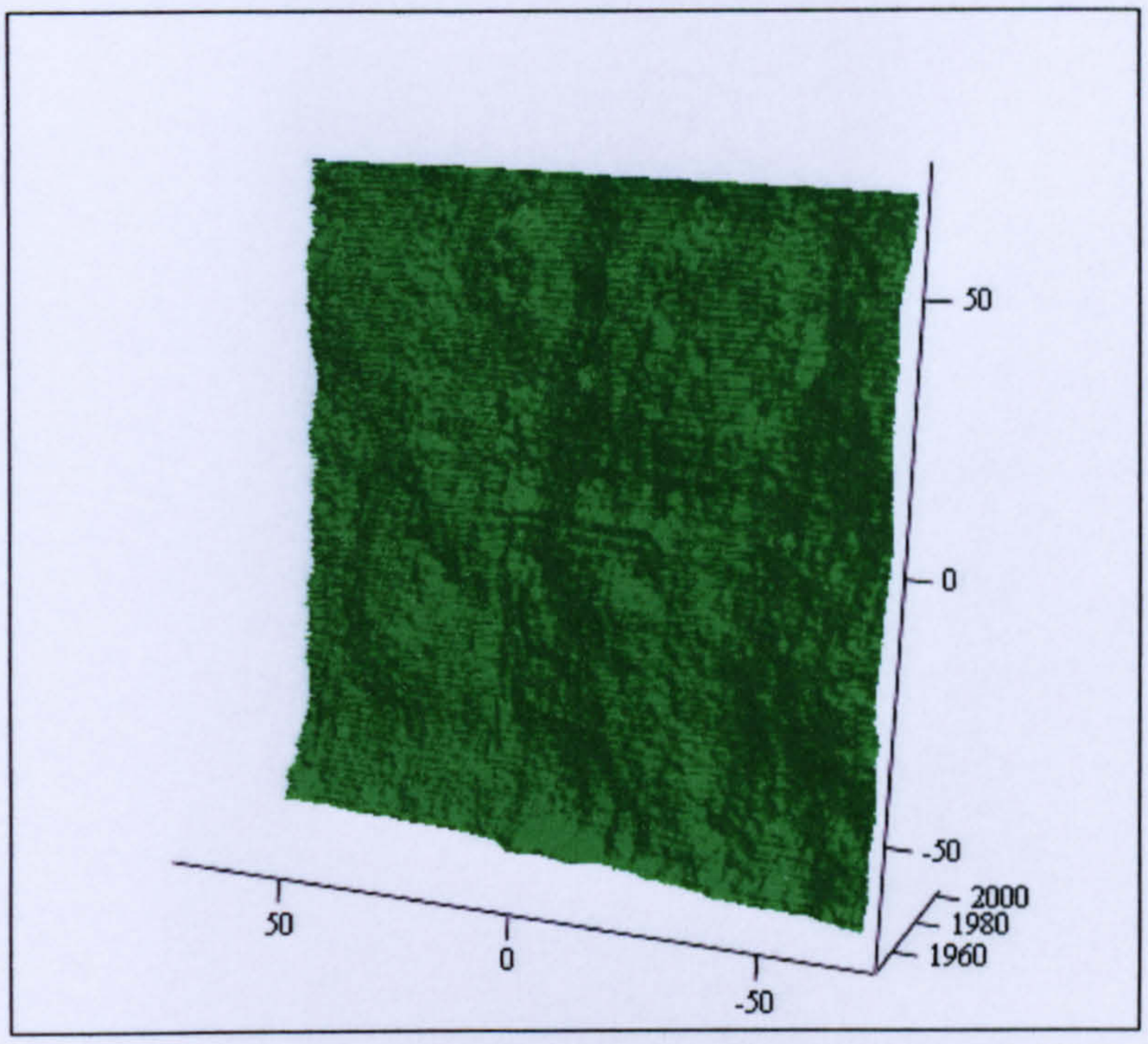

Figure 30 Slab S30 Topography

Roughness Parameters	X axis mean	Y axis mean
2α (mm)	0.536	0.705
$\frac{Da}{2W}$	0.481	0.634
$R\Delta a$	0.963	1.268
$R\Delta q$ ($mm^{1/2}$)	0.943	1.243
Lo (mm)	206.64	241.07
Lr	1.49	1.73

Table 30 Slab S30 Roughness parameters values

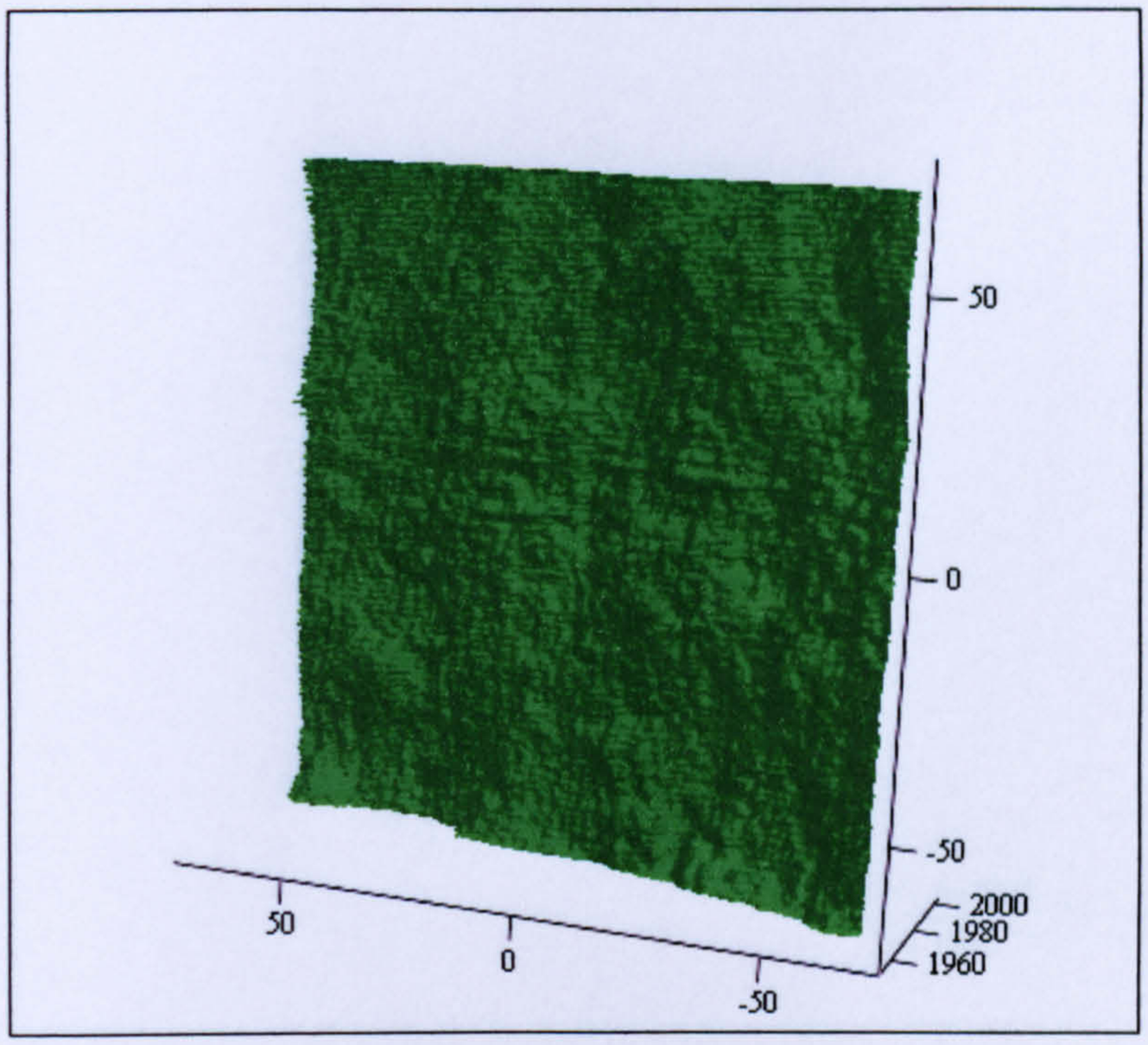

Figure 31 Slab S31 Topography

Roughness Parameters	X axis mean	Y axis mean
2α (mm)	0.501	0.586
$\frac{Da}{2W}$	0.450	0.527
$R\Delta a$	0.901	1.054
$R\Delta q$ ($mm^{1/2}$)	0.901	1.045
Lo (mm)	200.86	217.59
Lr	1.45	1.57

Table 31 Slab S31 Roughness parameters values

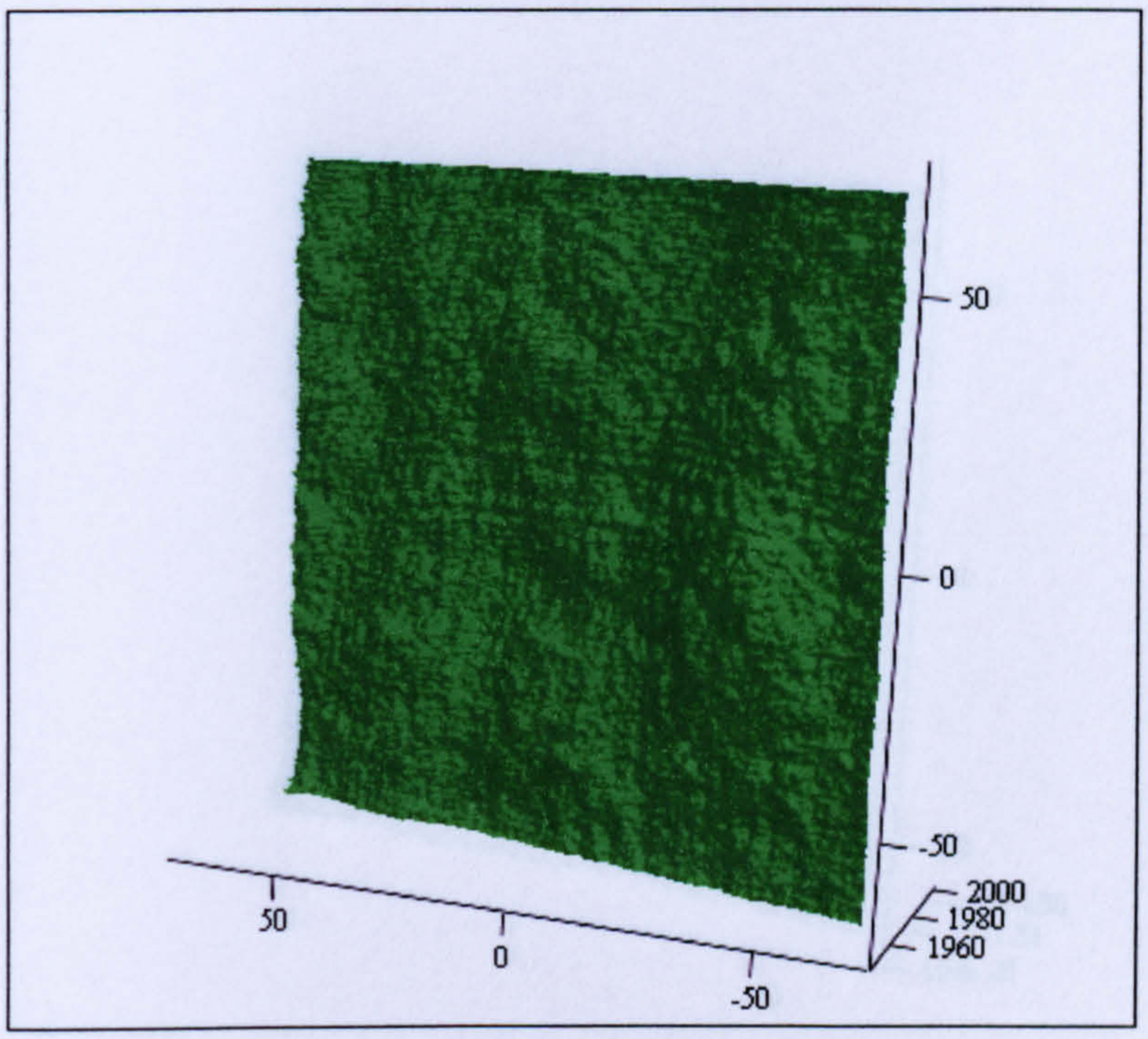

Figure 32 Slab S32 Topography

Roughness Parameters	X axis mean	Y axis mean
2α (mm)	0.528	0.550
$\frac{Da}{2W}$	0.475	0.496
$R\Delta a$	0.950	0.990
$R\Delta q$ ($mm^{1/2}$)	0.918	0.961
Lo (mm)	204.99	209.51
Lr	1.47	1.51

Table 32 Slab S32 Roughness parameters values

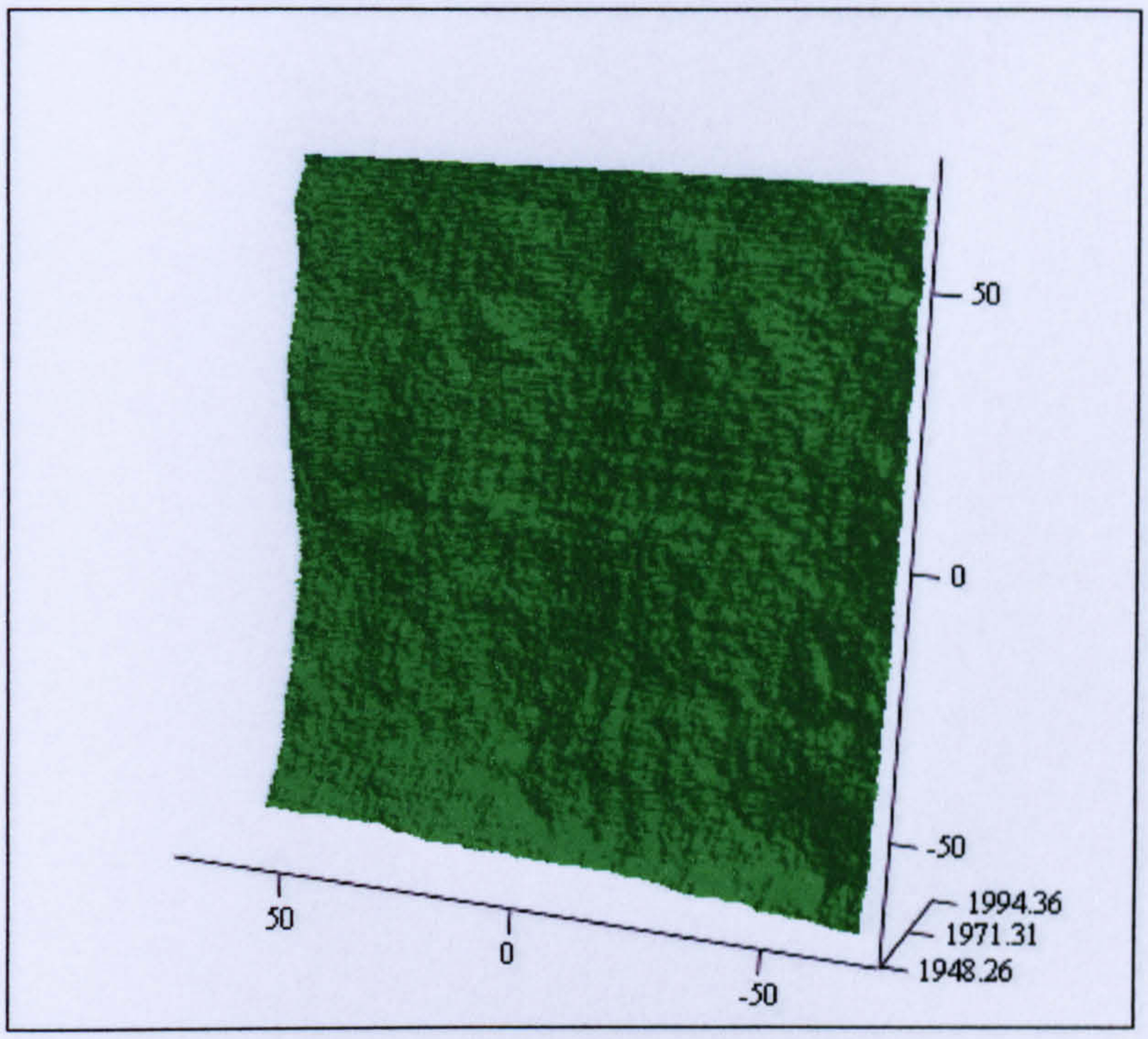

Figure 33 Slab S33 Topography

Roughness Parameters	X axis mean	Y axis mean
2α (mm)	0.547	0.646
$\frac{Da}{2W}$	0.492	0.582
$R\Delta a$	0.983	1.163
$R\Delta q$ ($mm^{1/2}$)	0.959	1.142
Lo (mm)	208.77	228.89
Lr	1.50	1.65

Table 33 Slab S33 Roughness parameters values

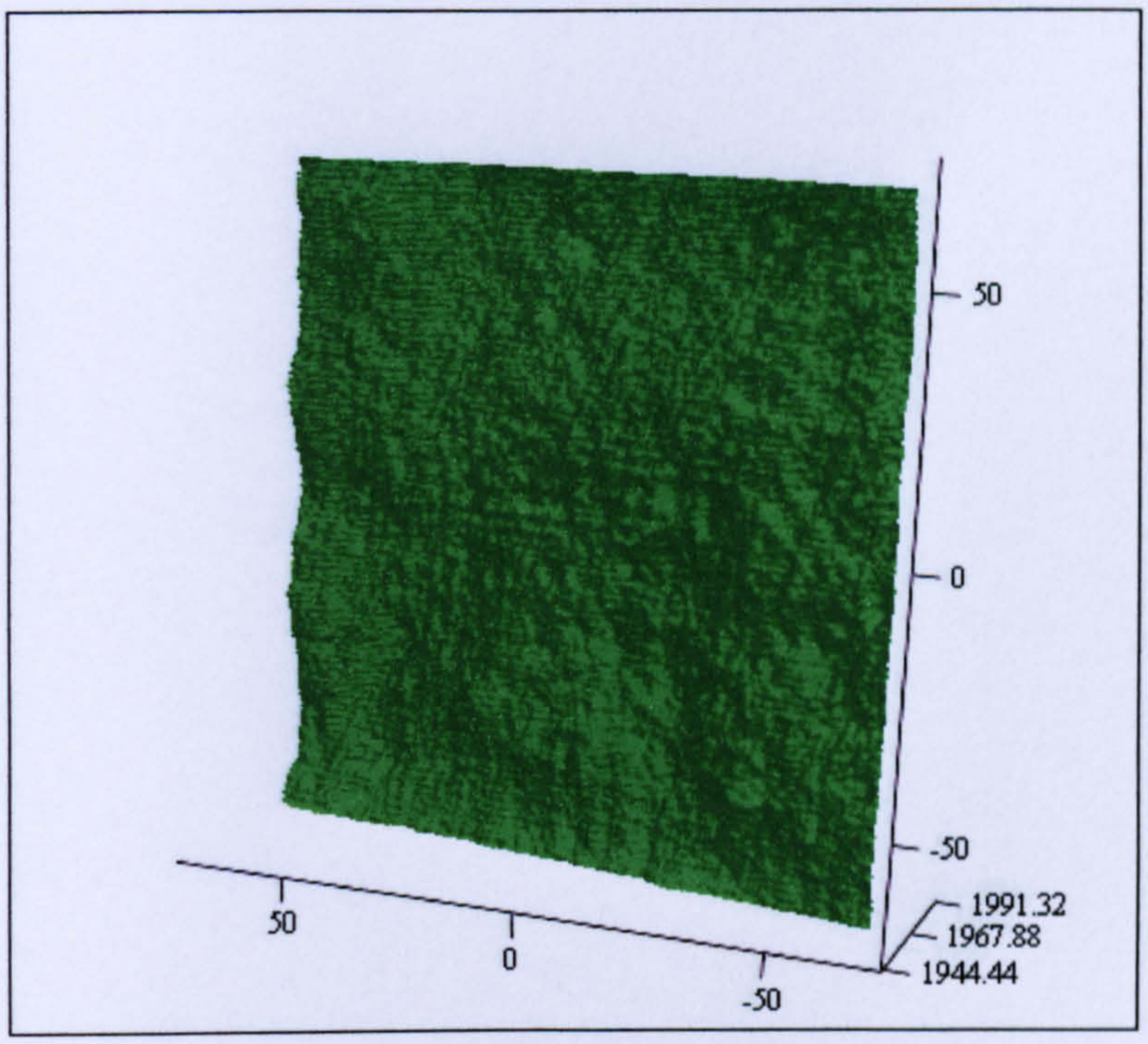

Figure 34 Slab S34 Topography

Roughness Parameters	X axis mean	Y axis mean
2α (mm)	0.546	0.673
$\frac{Da}{2W}$	0.491	0.606
$R\Delta a$	0.982	1.210
$R\Delta q$ ($mm^{1/2}$)	0.965	1.205
Lo (mm)	208.80	234.79
Lr	1.50	1.69

Table 34 Slab S34 Roughness parameters values

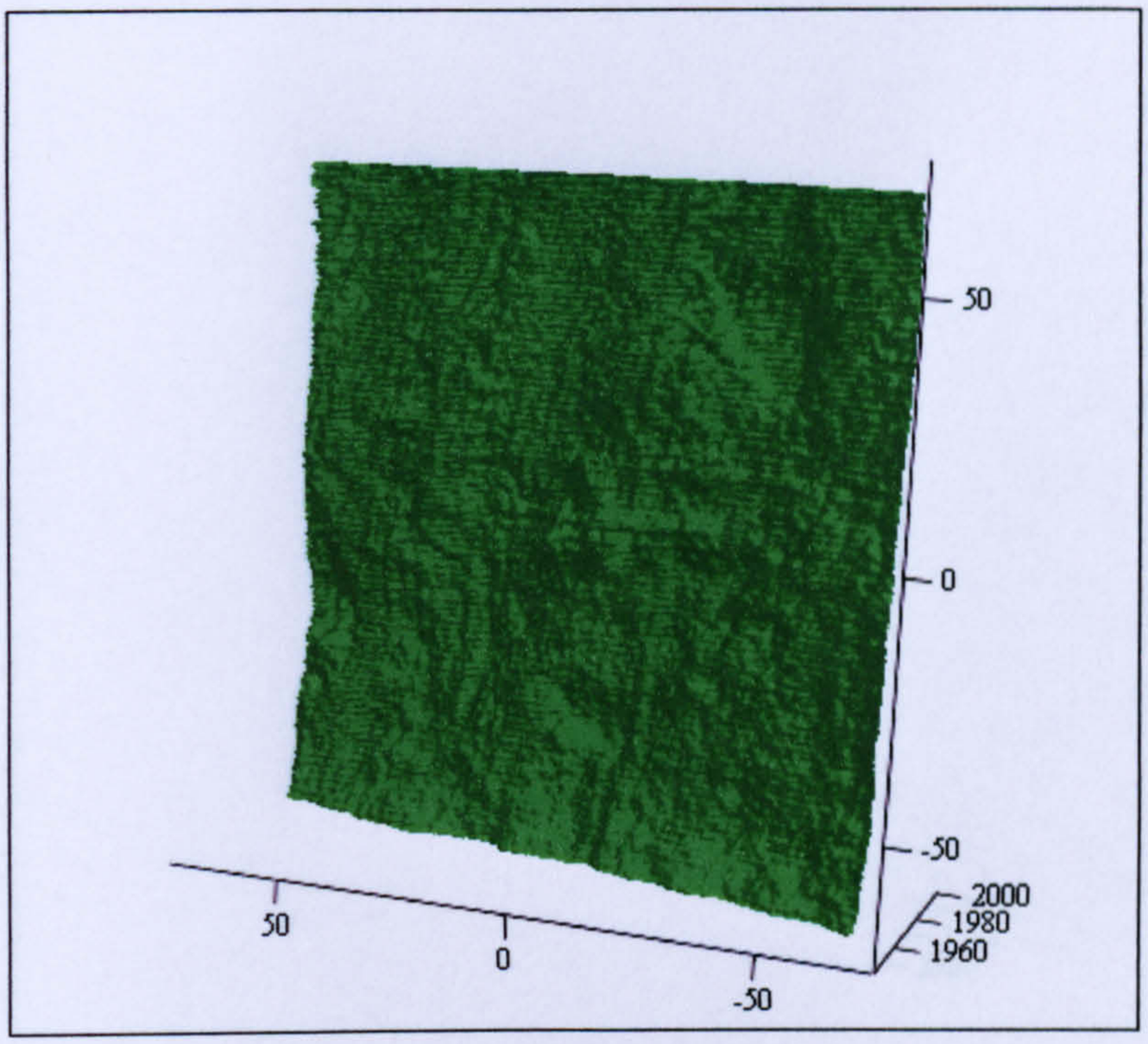

Figure 35 Slab S35 Topography

Roughness Parameters	X axis mean	Y axis mean
2α (mm)	0.504	0.703
$\frac{Da}{2W}$	0.453	0.633
$R\Delta a$	0.907	1.264
$R\Delta q$ ($mm^{1/2}$)	0.890	1.239
Lo (mm)	200.91	240.70
Lr	1.45	1.73

Table 35 Slab S35 Roughness parameters values

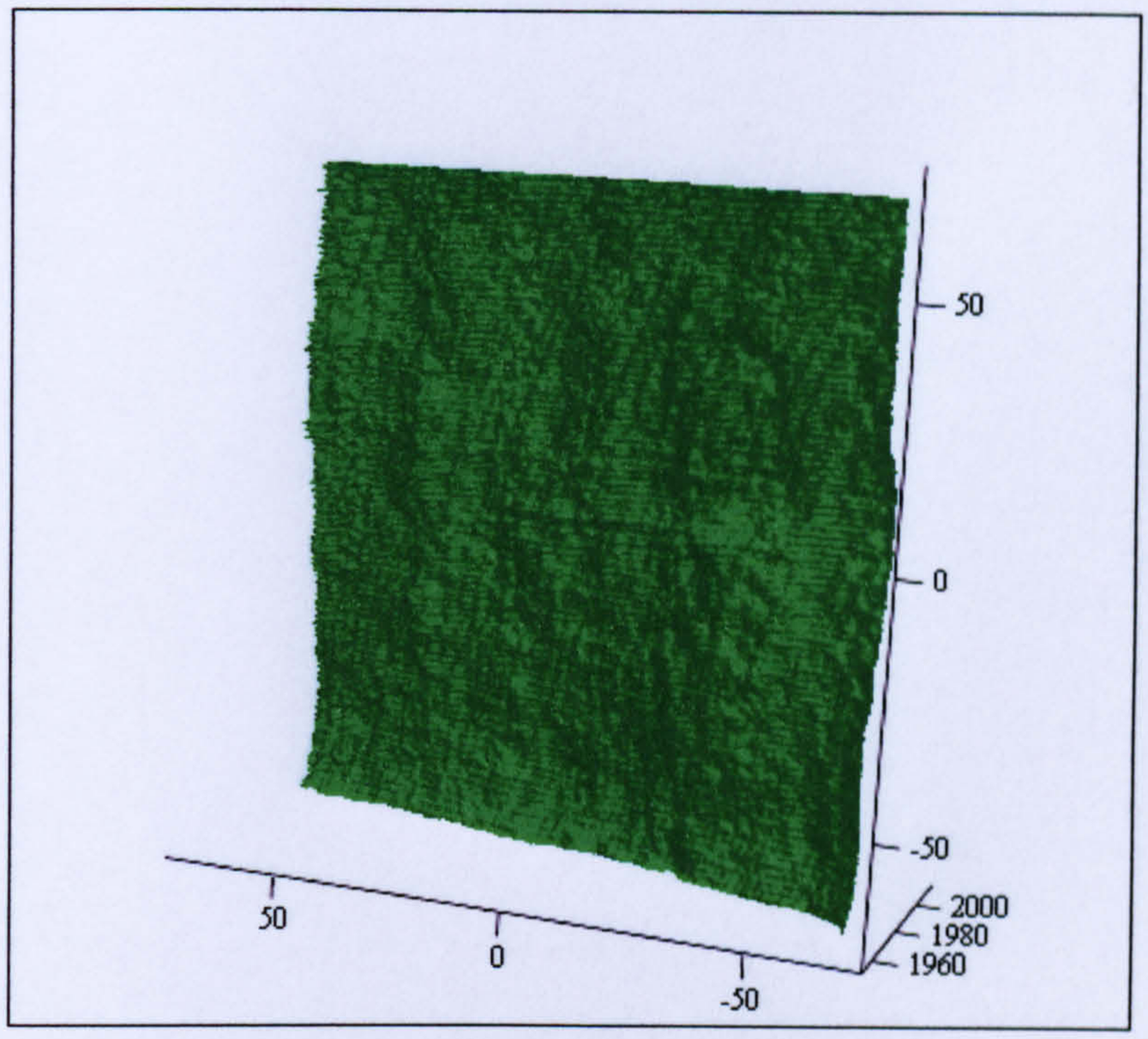

Figure 36 Slab S36 Topography

Roughness Parameters	X axis mean	Y axis mean
2α (mm)	0.545	0.746
$\frac{Da}{2W}$	0.489	0.671
$R\Delta a$	0.980	1.341
$R\Delta q$ ($mm^{1/2}$)	0.966	1.286
Lo (mm)	208.61	249.06
Lr	1.50	1.79

Table 36 Slab S36 Roughness parameters values

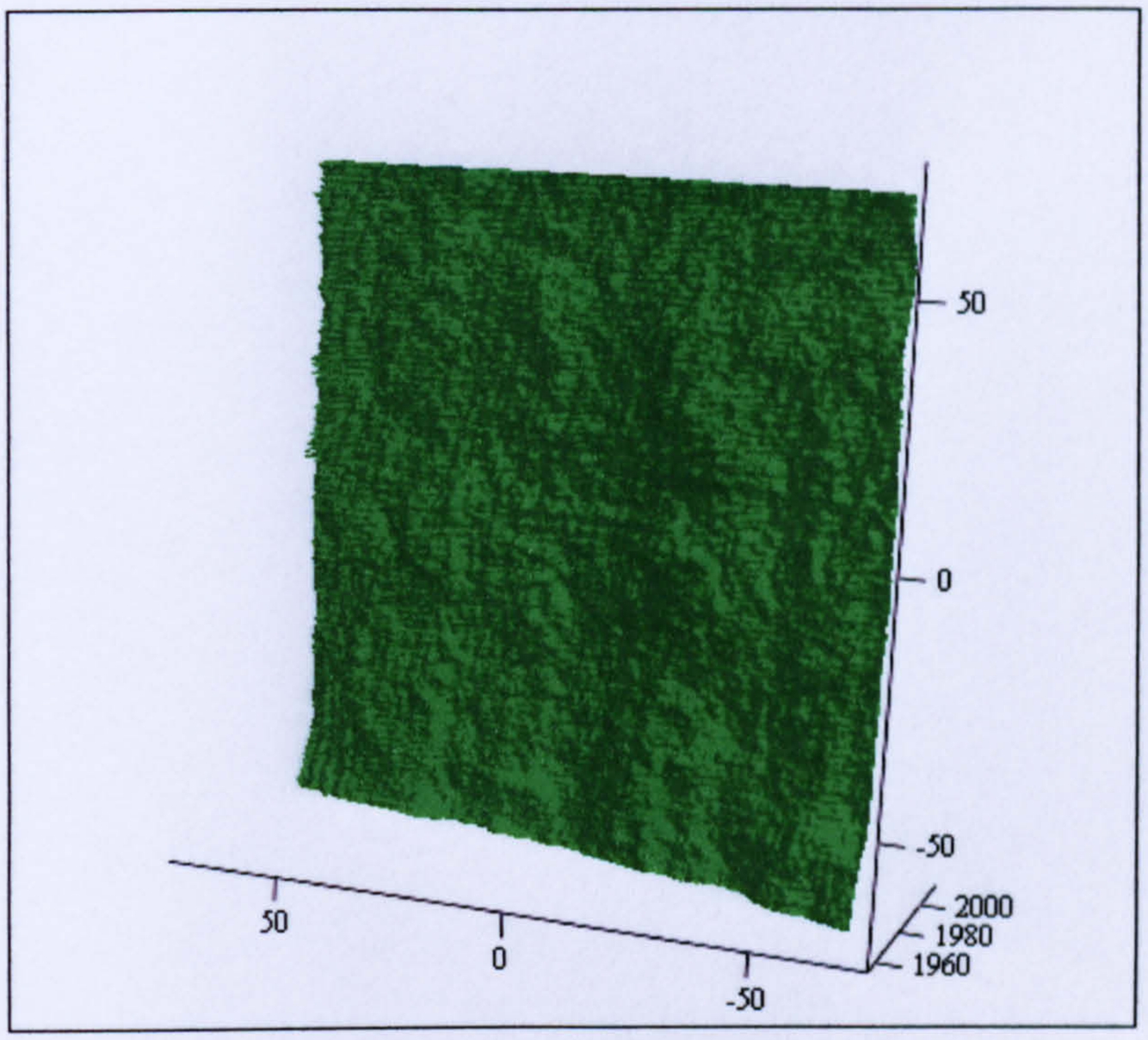

Figure 37 Slab S37 Topography

Roughness Parameters	X axis mean	Y axis mean
2α (mm)	0.542	0.626
$\frac{Da}{2W}$	0.487	0.563
$R\Delta a$	0.975	1.126
$R\Delta q$ ($mm^{1/2}$)	0.950	1.094
Lo (mm)	207.67	224.62
Lr	1.49	1.62

Table 37 Slab S37 Roughness parameters values

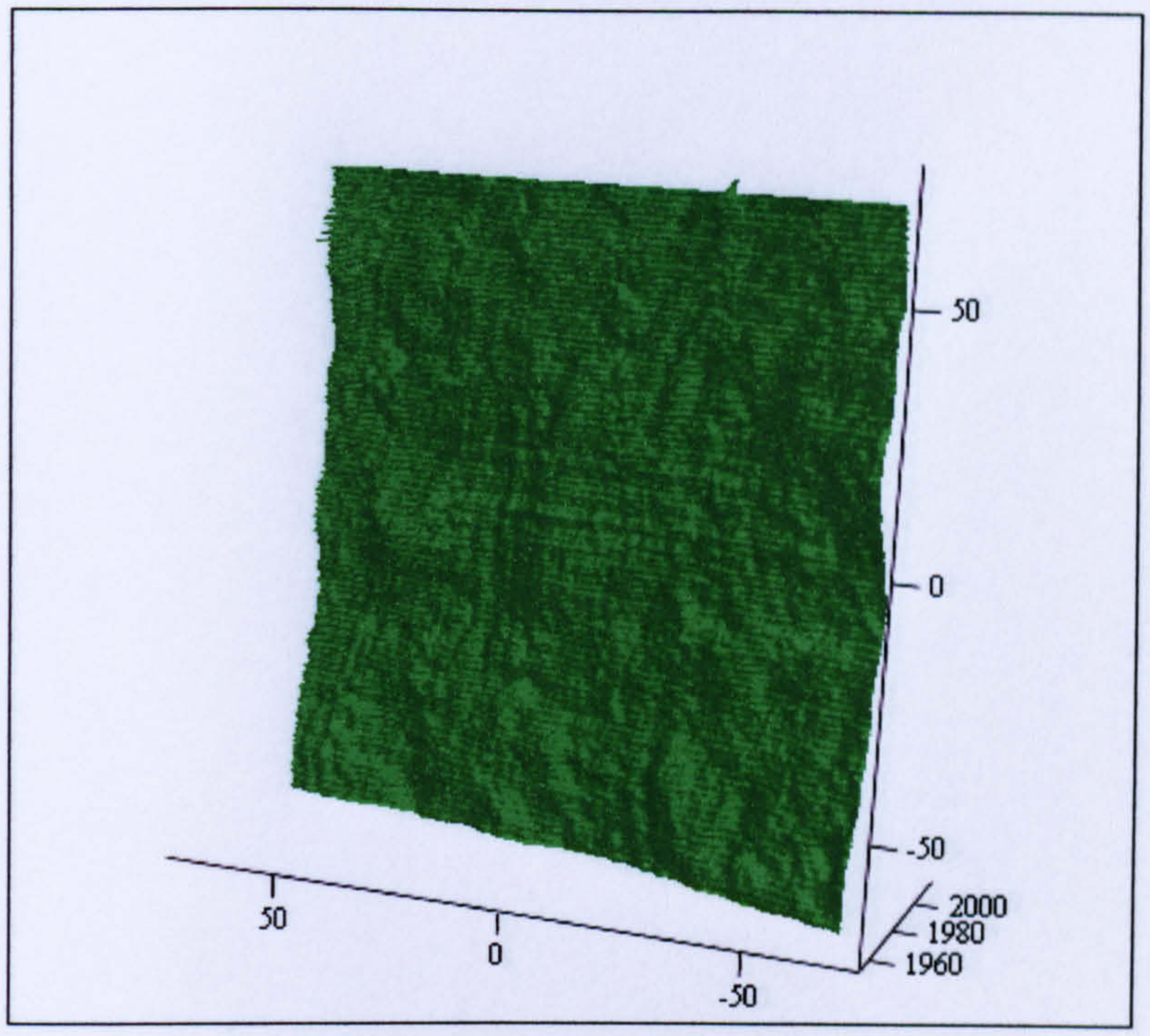

Figure 38 Slab S38 Topography

Roughness Parameters	X axis mean	Y axis mean
2α (mm)	0.455	0.821
$\frac{Da}{2W}$	0.408	0.738
$R\Delta a$	0.818	1.476
$R\Delta q$ ($mm^{1/2}$)	0.803	1.422
Lo (mm)	191.85	265.81
Lr	1.38	1.91

Table 38 Slab S38 Roughness parameters values

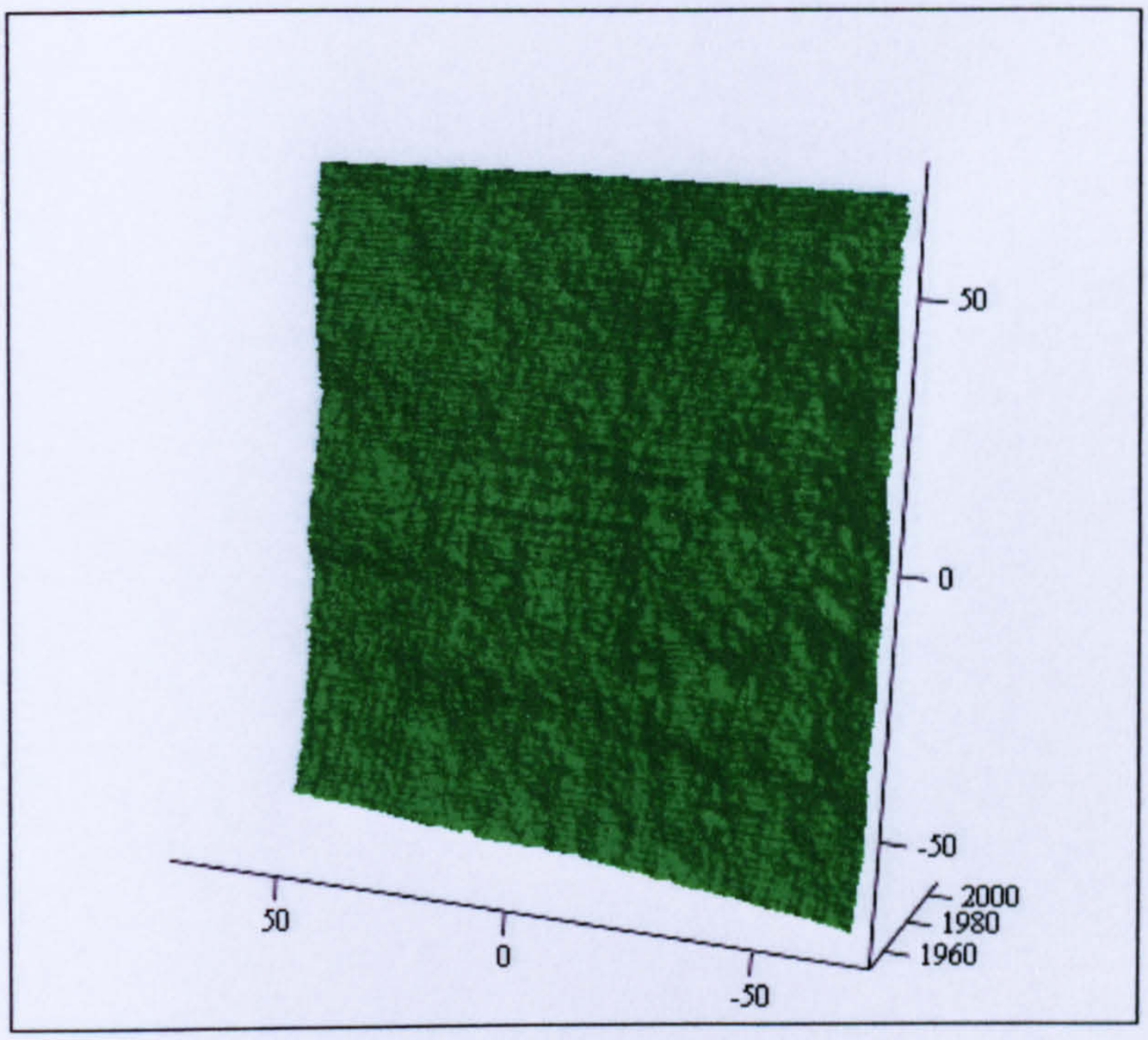

Figure 39 Slab S39 Topography

Roughness Parameters	X axis mean	Y axis mean
2α (mm)	0.514	0.645
$\frac{Da}{2W}$	0.462	0.581
$R\Delta a$	0.925	1.161
$R\Delta q$ ($mm^{1/2}$)	0.889	1.121
Lo (mm)	202.38	228.08
Lr	1.46	1.64

Table 39 Slab S39 Roughness parameters values

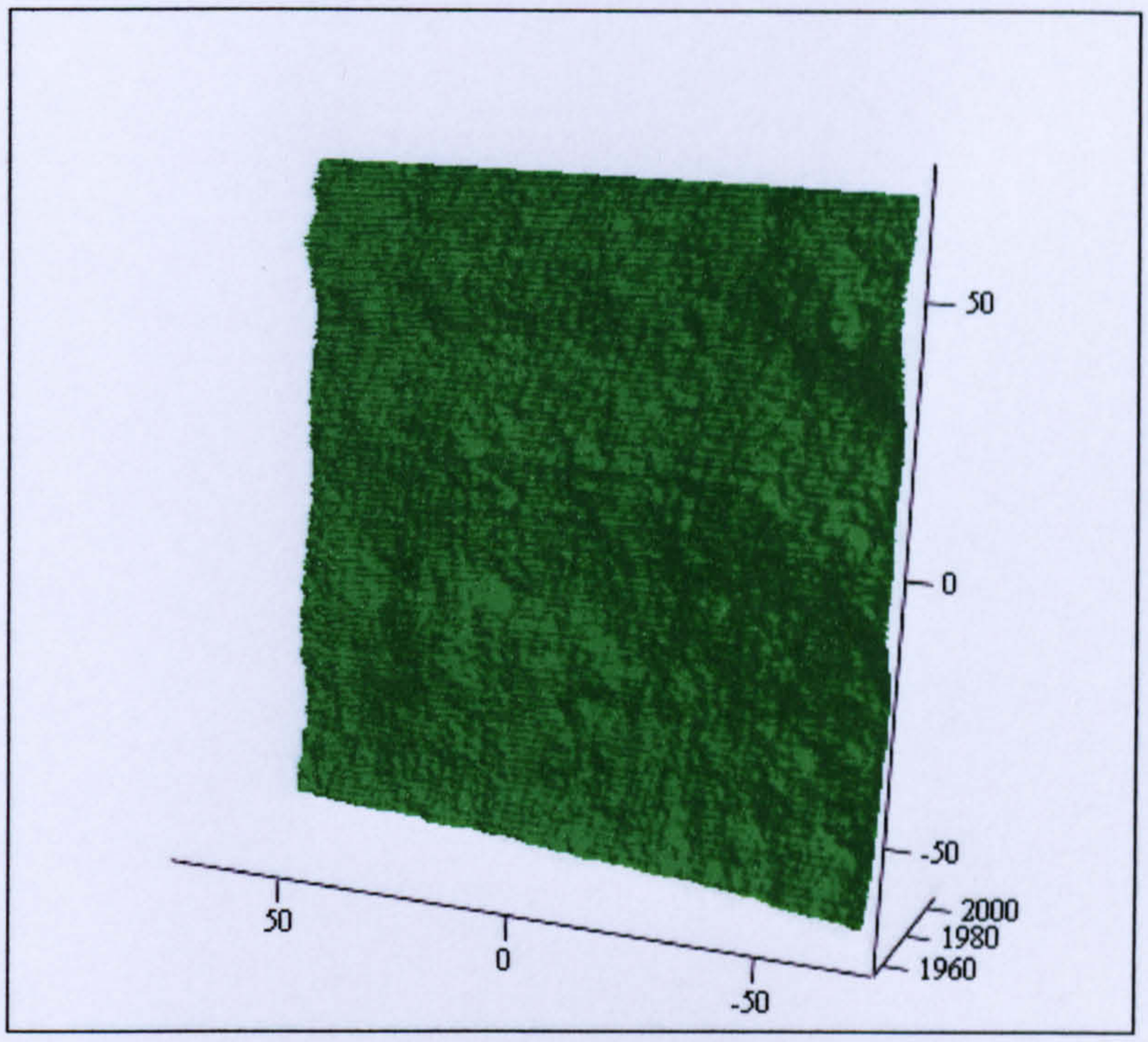

Figure 40 Slab S40 Topography

Roughness Parameters	X axis mean	Y axis mean
2α (mm)	0.503	0.711
$\frac{Da}{2W}$	0.452	0.640
$R\Delta a$	0.904	1.279
$R\Delta q$ ($mm^{1/2}$)	0.887	1.223
Lo (mm)	200.32	241.61
Lr	1.44	1.74

Table 40 Slab S40 Roughness parameters values

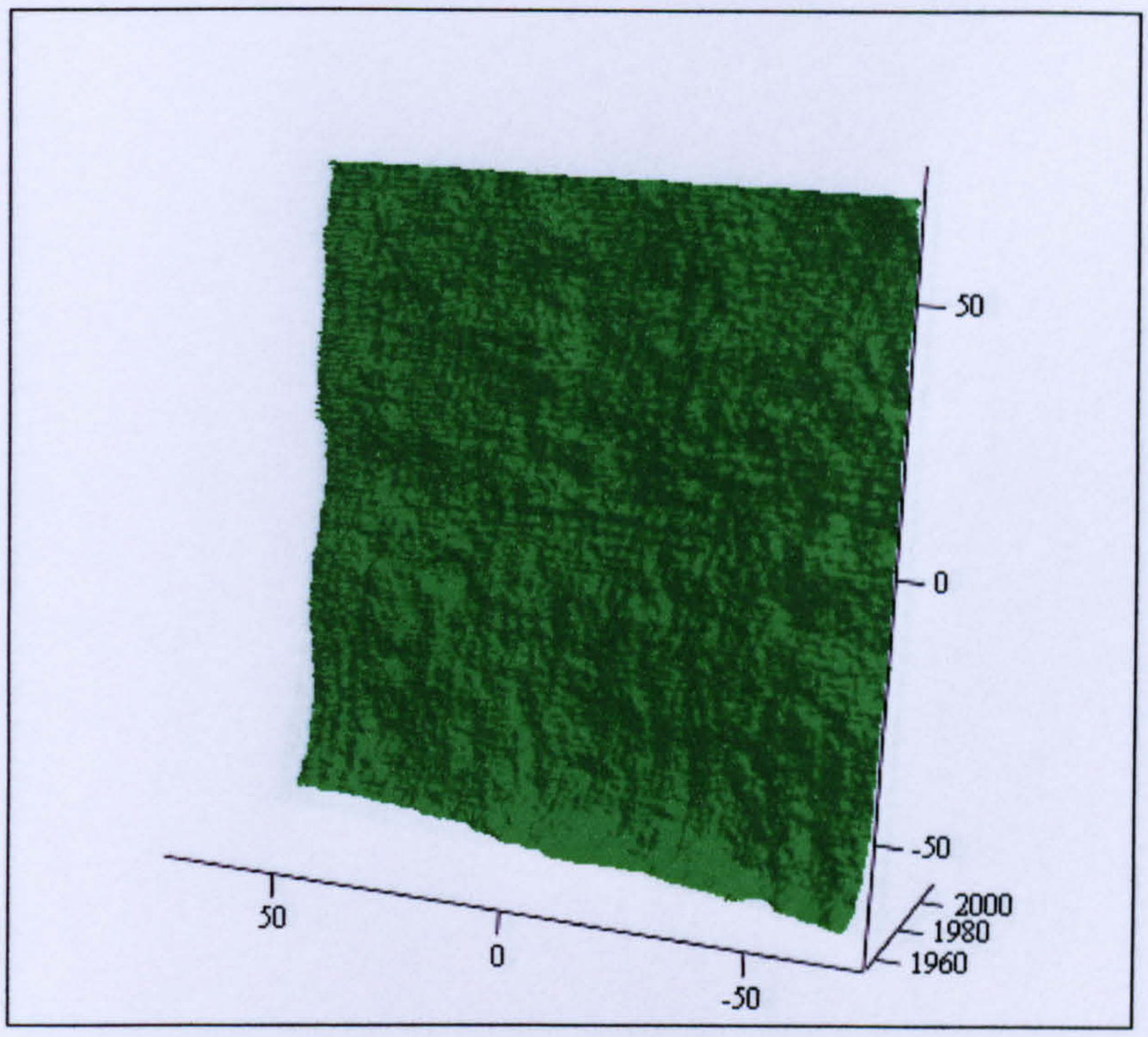

Figure 41 Slab S41 Topography

Roughness Parameters	X axis mean	Y axis mean
2α (mm)	0.487	0.553
$\frac{Da}{2W}$	0.437	0.497
$R\Delta a$	0.875	0.994
$R\Delta q$ ($mm^{1/2}$)	0.843	0.973
Lo (mm)	197.10	210.53
Lr	1.42	1.51

Table 41 Slab S41 Roughness parameters values

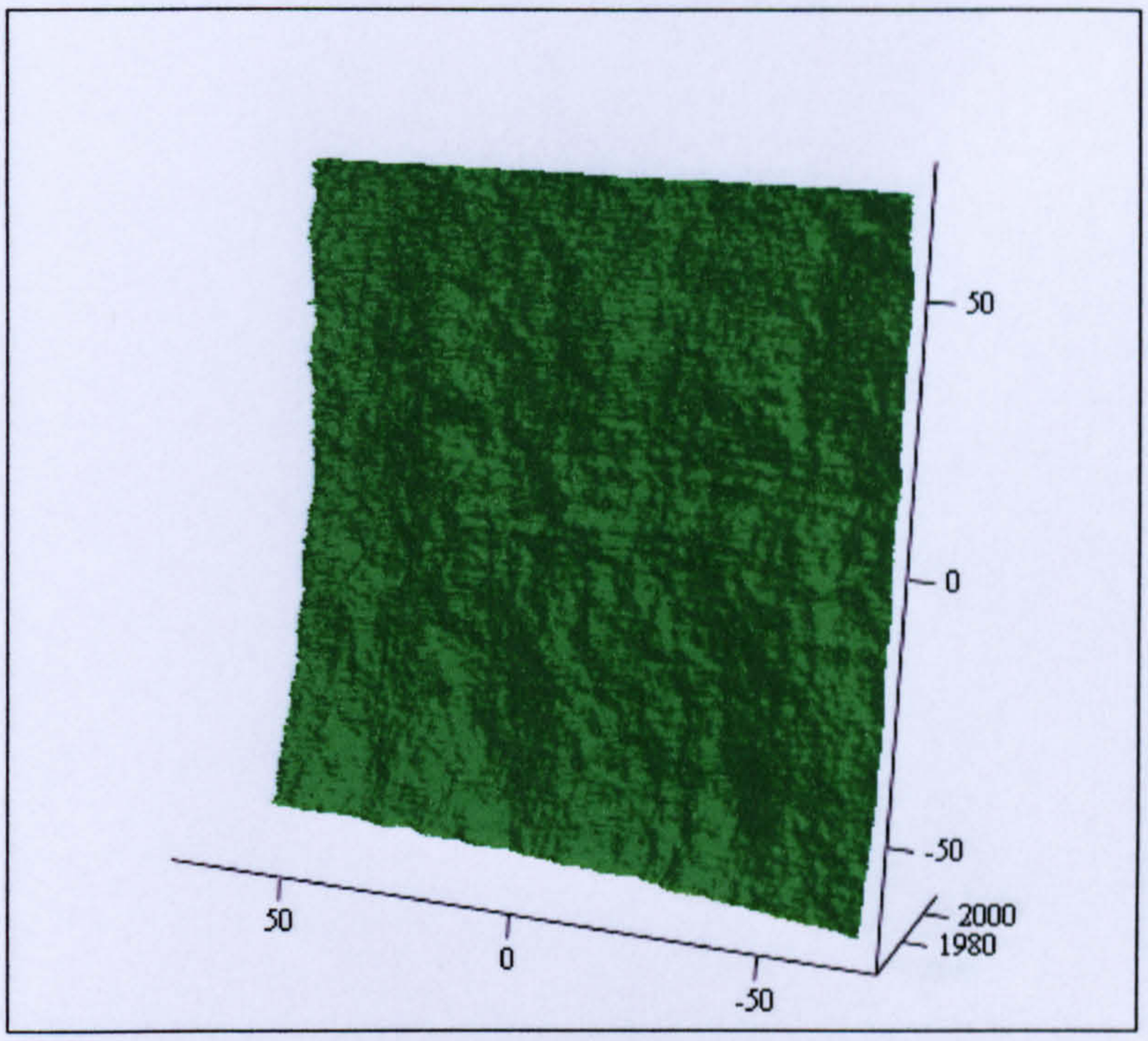

(X, Y, Z)

Figure 42 Slab S42 Topography

Roughness Parameters	X axis mean	Y axis mean
2α (mm)	0.517	0.554
$\frac{Da}{2W}$	0.465	0.499
$R\Delta a$	0.930	0.996
$R\Delta q$ ($mm^{1/2}$)	0.916	0.964
Lo (mm)	203.39	210.76
Lr	1.46	1.52

Table 42 Slab S42 Roughness parameters values

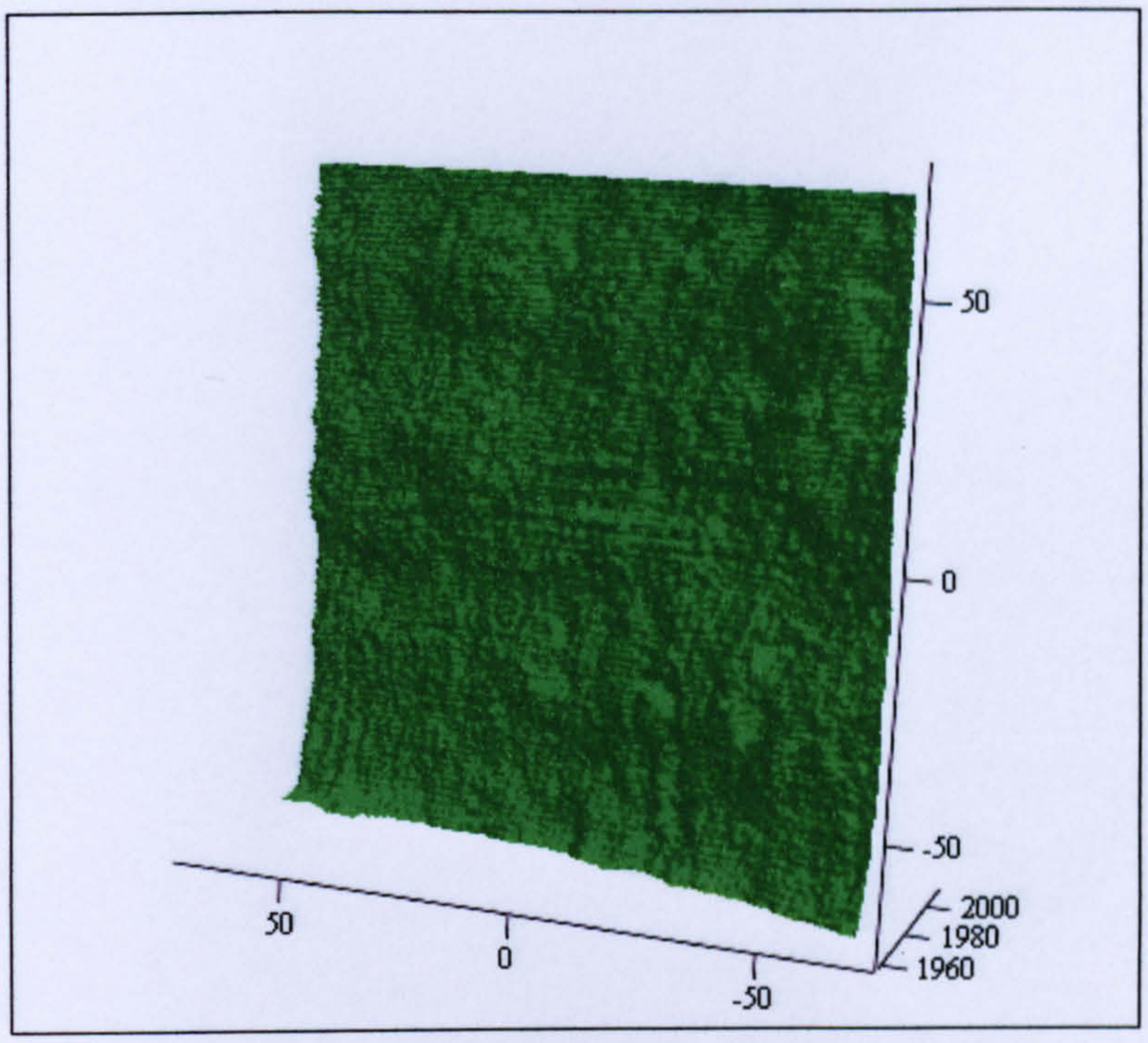

(X, Y, Z)

Figure 43 Slab S43 Topography

Roughness Parameters	X axis mean	Y axis mean
2α (mm)	0.509	0.645
$\frac{Da}{2W}$	0.458	0.581
$R\Delta a$	0.916	1.161
$R\Delta q$ ($mm^{1/2}$)	0.899	1.135
Lo (mm)	201.79	228.57
Lr	1.45	1.64

Table 43 Slab S43 Roughness parameters values

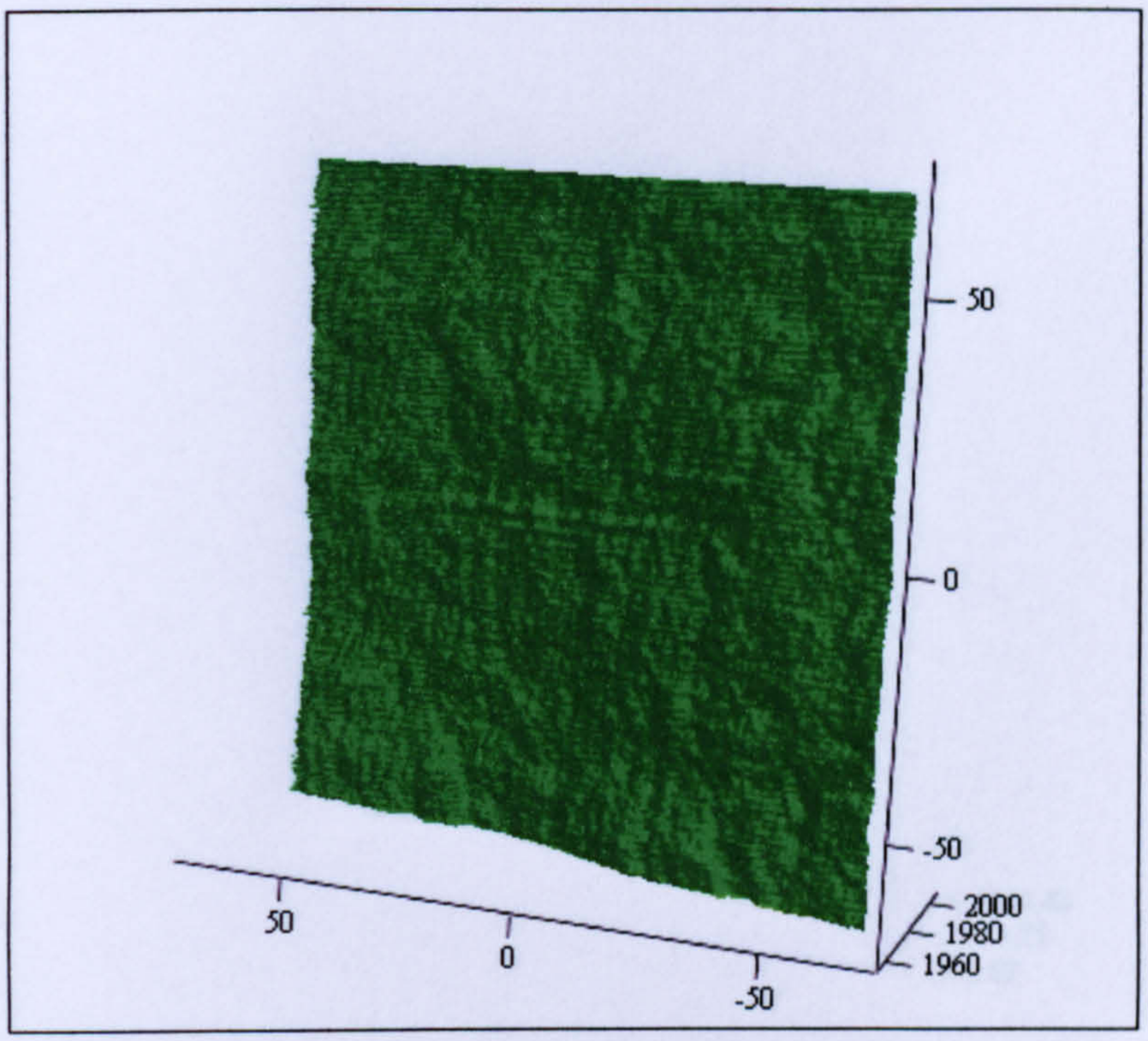

Figure 44 Slab S44 Topography

Roughness Parameters	X axis mean	Y axis mean
2α (mm)	0.485	0.635
$\frac{Da}{2W}$	0.436	0.571
$R\Delta a$	0.873	1.142
$R\Delta q$ ($mm^{1/2}$)	0.855	1.100
Lo (mm)	197.27	226.81
Lr	1.42	1.63

Table 44 Slab S44 Roughness parameters values

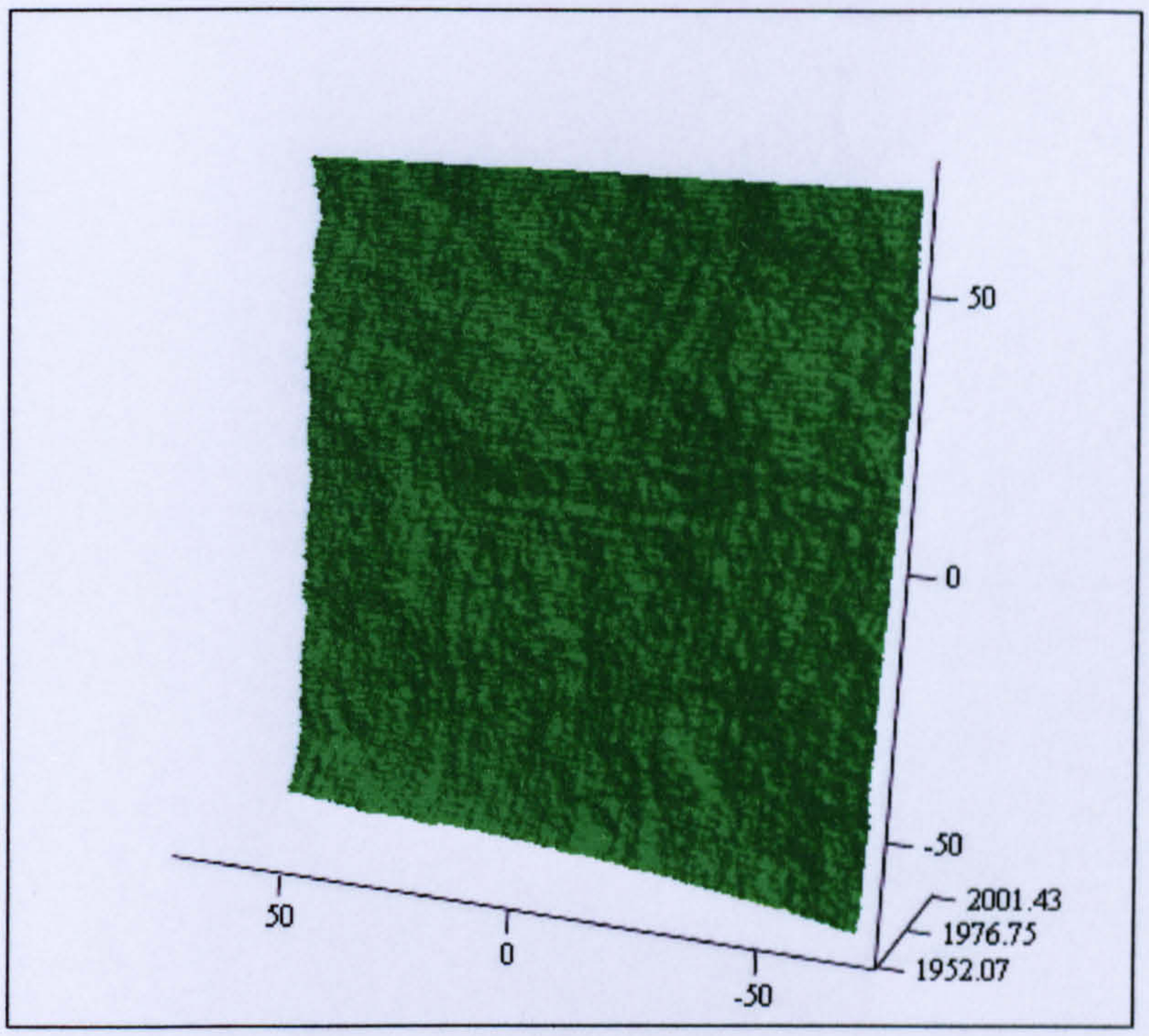

Figure 45 Slab S45 Topography

Roughness Parameters	X axis mean	Y axis mean
2α (mm)	0.484	0.563
$\frac{Da}{2W}$	0.434	0.507
$R\Delta a$	0.870	1.013
$R\Delta q$ ($mm^{1/2}$)	0.832	0.977
Lo (mm)	196.36	211.77
Lr	1.41	1.52

Table 45 Slab S45 Roughness parameters values

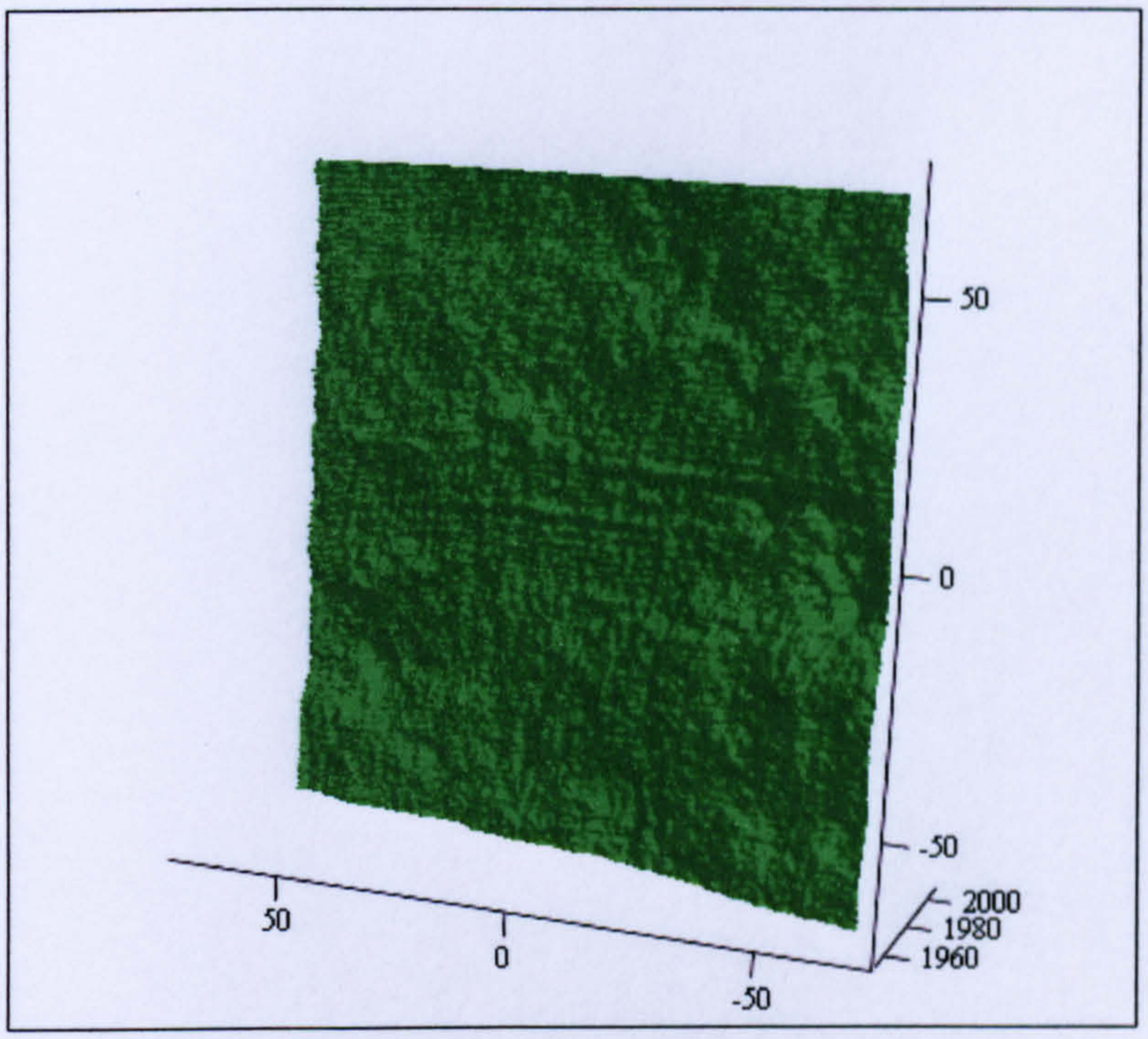

(X, Y, Z)

Figure 46 Slab S46 Topography

Roughness Parameters	X axis mean	Y axis mean
2α (mm)	0.517	0.555
$\frac{Da}{2W}$	0.464	0.500
$R\Delta a$	0.930	0.998
$R\Delta q$ ($mm^{1/2}$)	0.906	0.961
Lo (mm)	203.06	210.38
Lr	1.46	1.51

Table 46 Slab S46 Roughness parameters values

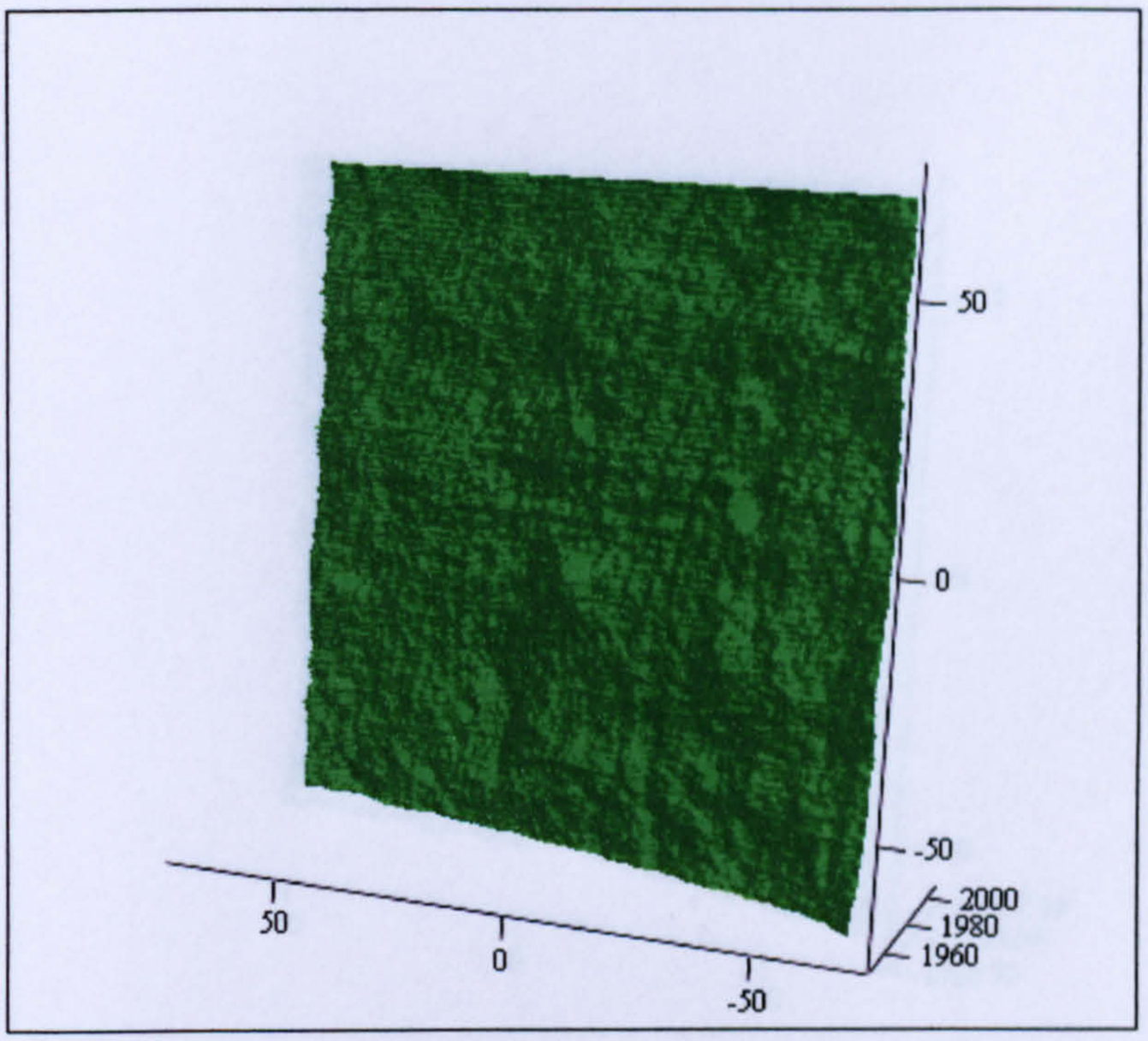

(X, Y, Z)

Figure 47 Slab S47 Topography

Roughness Parameters	X axis mean	Y axis mean
2α (mm)	0.476	0.558
$\frac{Da}{2W}$	0.428	0.502
$R\Delta a$	0.857	1.004
$R\Delta q$ ($mm^{1/2}$)	0.829	0.971
Lo (mm)	195.32	211.03
Lr	1.41	1.52

Table 47 Slab S47 Roughness parameters values

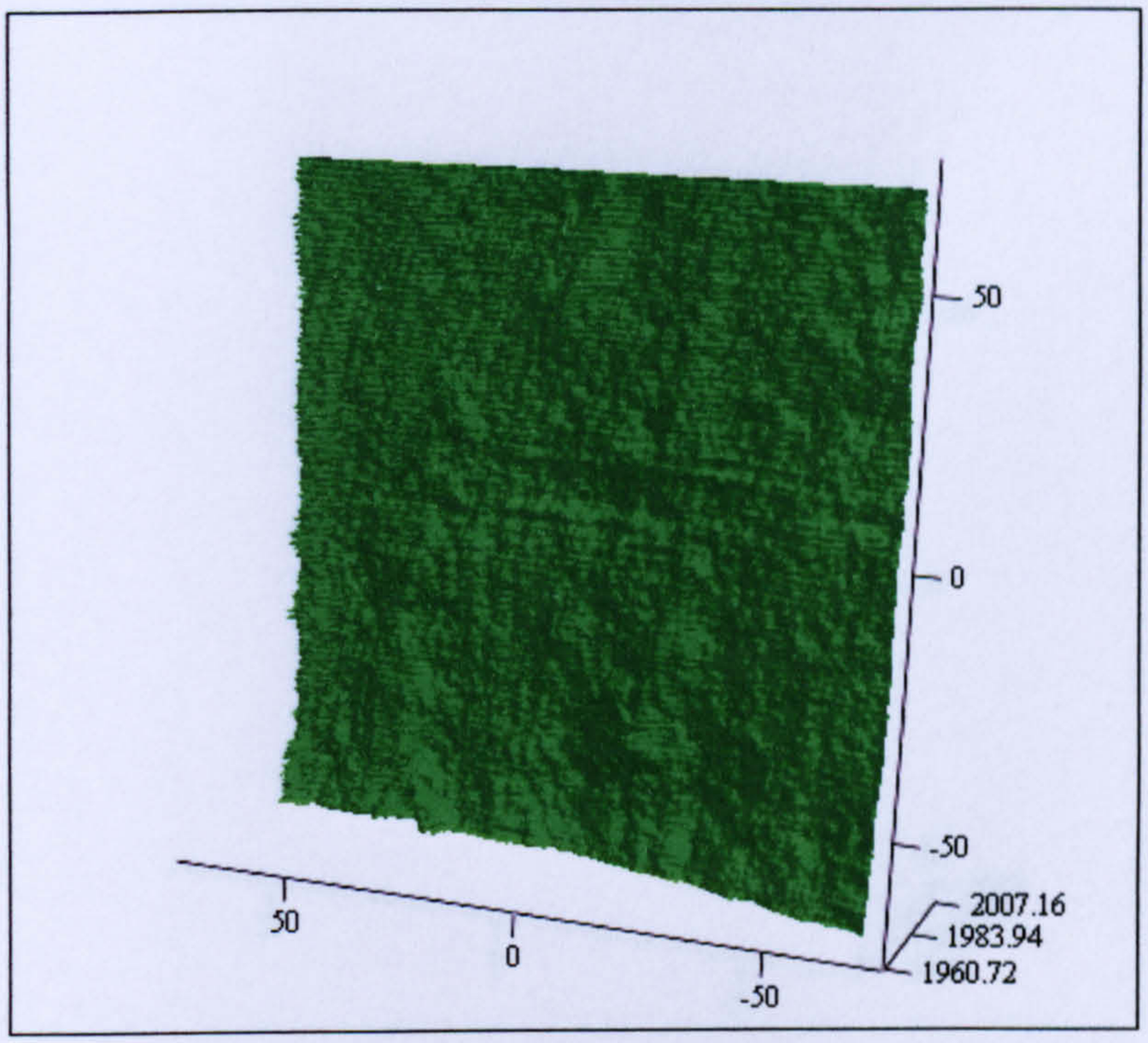

Figure 48 Slab S48 Topography

Roughness Parameters	X axis mean	Y axis mean
2α (mm)	0.510	0.668
$\frac{Da}{2W}$	0.458	0.600
$R\Delta a$	0.917	1.201
$R\Delta q$ ($mm^{1/2}$)	0.916	1.176
Lo (mm)	202.31	234.55
Lr	1.46	1.69

Table 48 Slab S48 Roughness parameters values

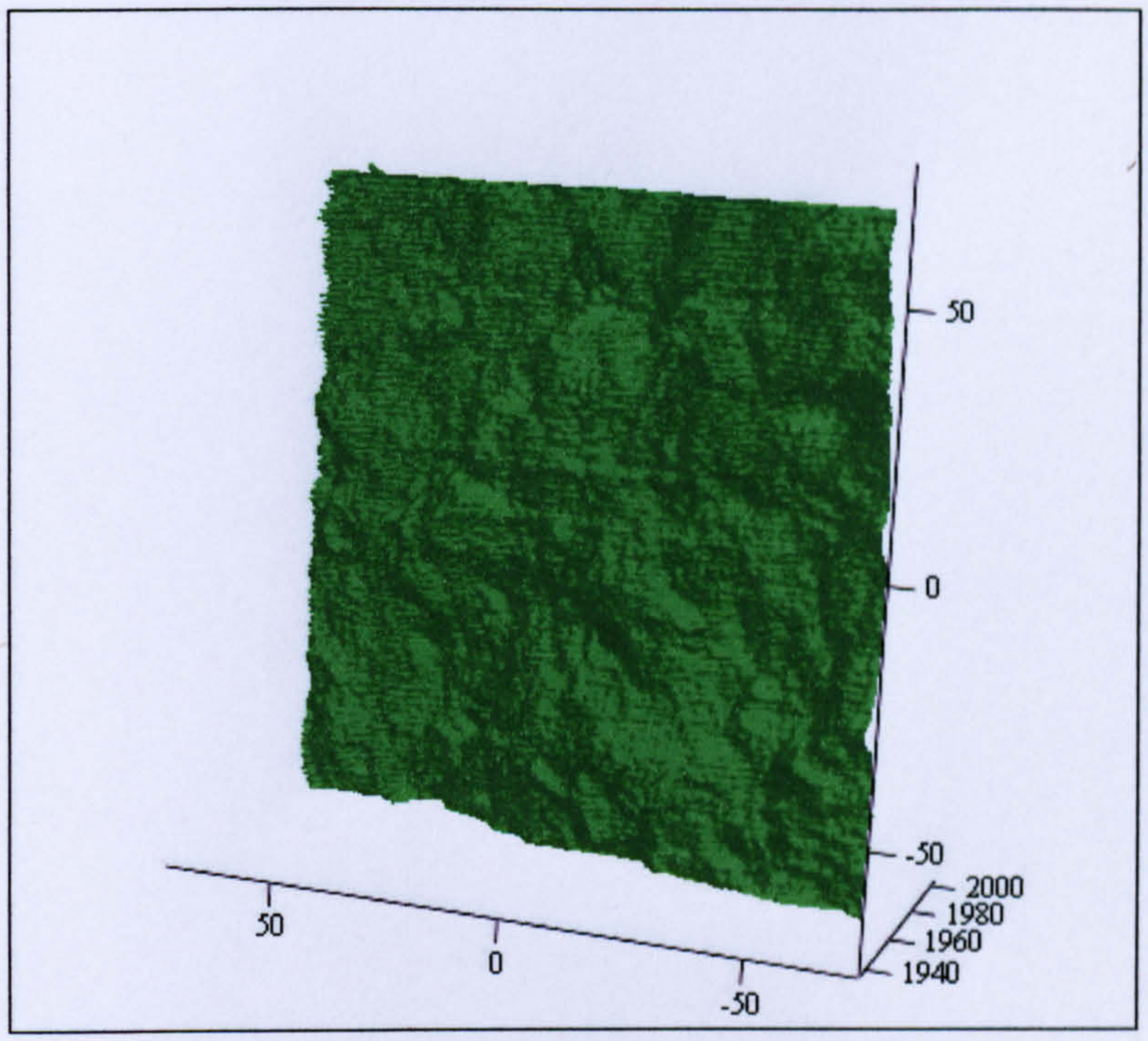

Figure 49 Slab PL2 Topography

Roughness Parameters	X axis mean	Y axis mean
2α (mm)	0.665	0.874
$\frac{Da}{2W}$	0.598	0.787
$R\Delta a$	1.197	1.572
$R\Delta q$ ($mm^{1/2}$)	1.222	1.669
Lo (mm)	233.93	279.27
Lr	1.68	2.01

Table 49 Slab PL2 Roughness parameters values

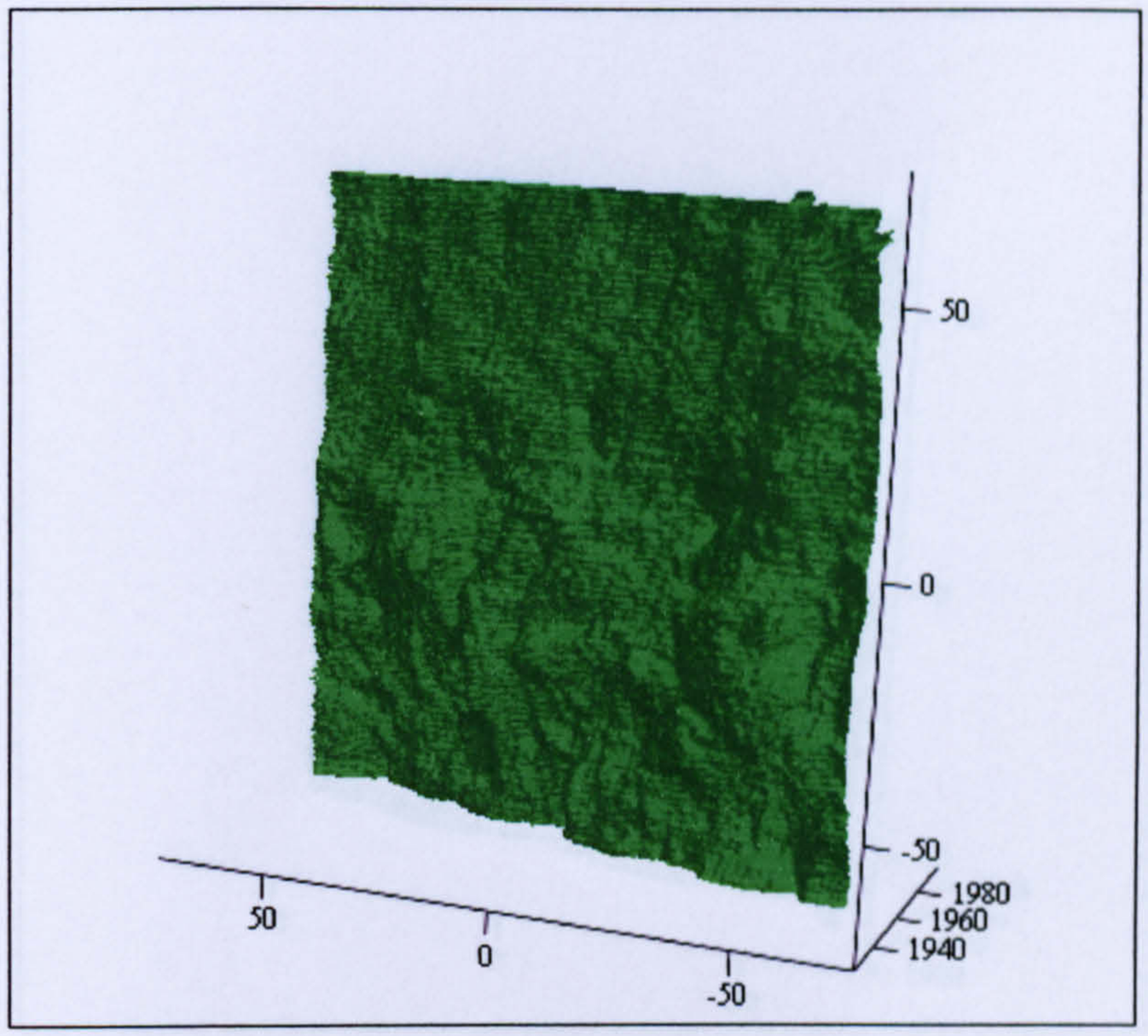

Figure 50 Slab PL5 Topography

Roughness Parameters	X axis mean	Y axis mean
2α (mm)	0.627	0.868
$\frac{Da}{2W}$	0.564	0.782
$R\Delta a$	1.280	1.561
$R\Delta q$ ($mm^{1/2}$)	1.170	1.598
Lo (mm)	225.76	276.29
Lr	1.62	1.99

Table 50 Slab PL5 Roughness parameters values

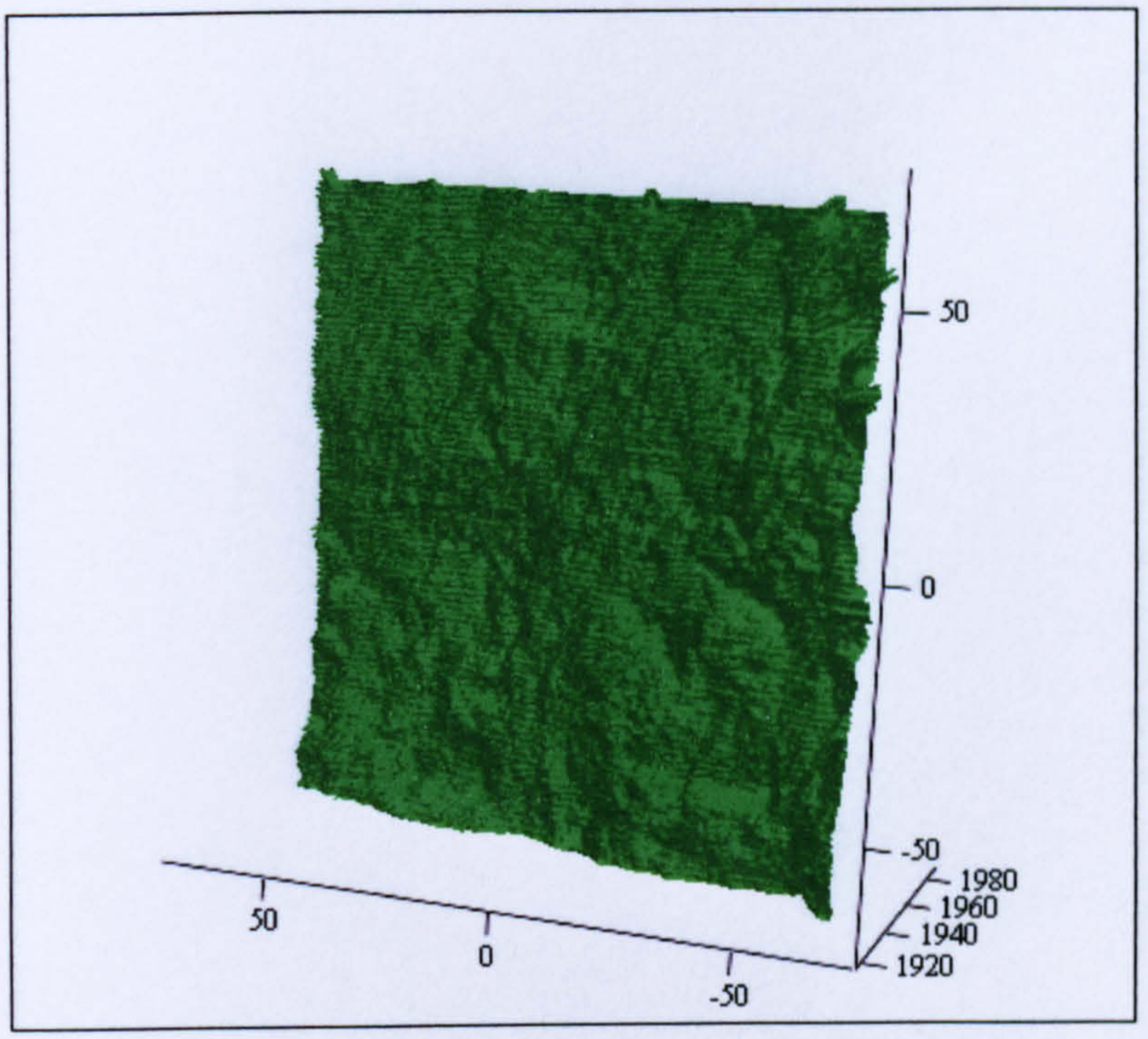

(X,Y,Z)

Figure 51 Slab PL6 Topography

Roughness Parameters	X axis mean	Y axis mean
2α (mm)	0.648	1.099
$\frac{Da}{2W}$	0.583	0.989
$R\Delta a$	1.166	1.977
$R\Delta q$ ($mm^{1/2}$)	1.191	2.071
Lo (mm)	230.67	327.37
Lr	1.66	2.36

Table 51 Slab PL6 Roughness parameters values

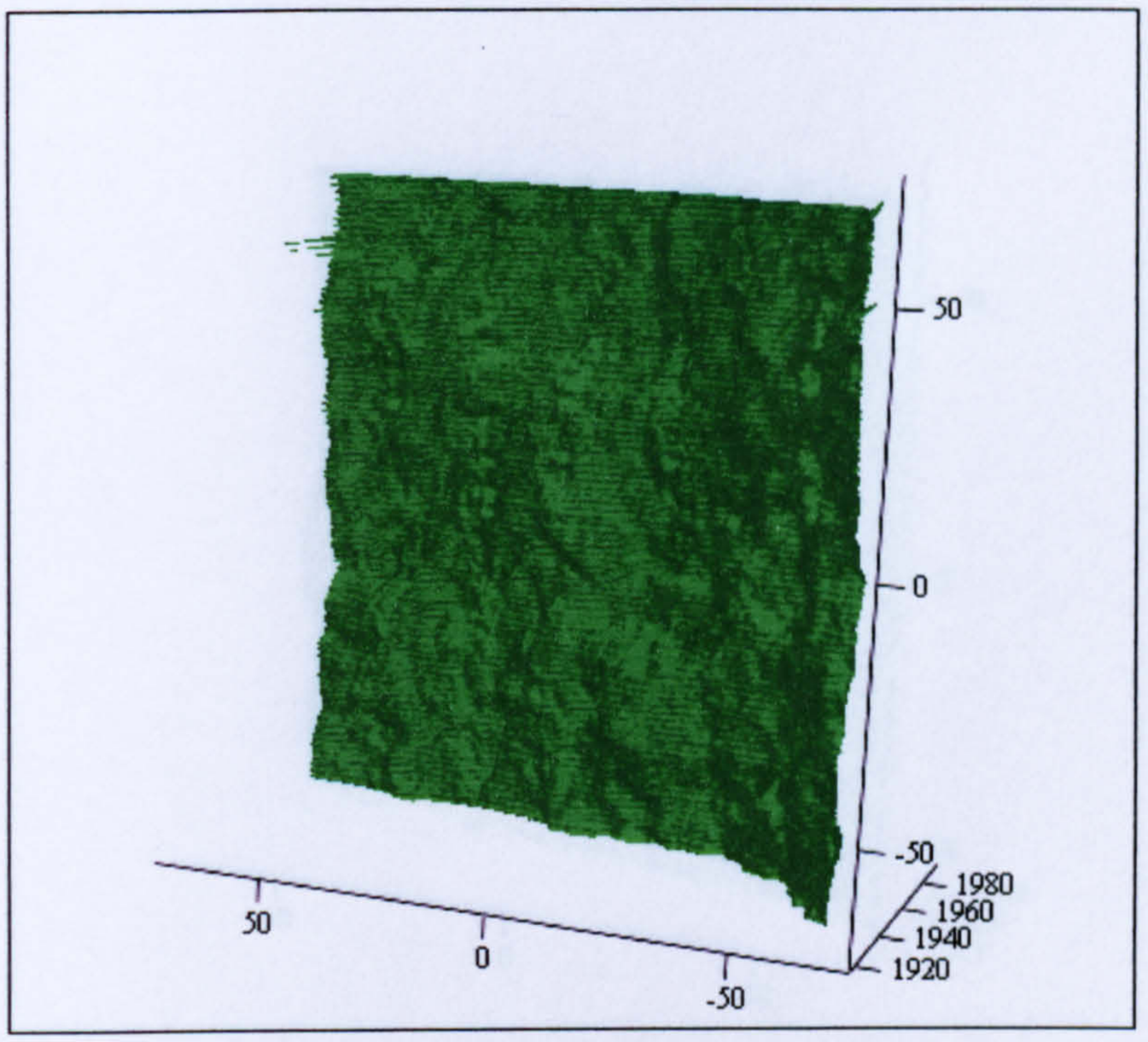

(X,Y,Z)

Figure 52 Slab PL9 Topography

Roughness Parameters	X axis mean	Y axis mean
2α (mm)	0.623	1.282
$\frac{Da}{2W}$	0.560	1.152
$R\Delta a$	1.121	2.306
$R\Delta q$ ($mm^{1/2}$)	1.213	2.388
Lo (mm)	226.20	369.58
Lr	1.63	2.66

Table 52 Slab PL9 Roughness values parameters

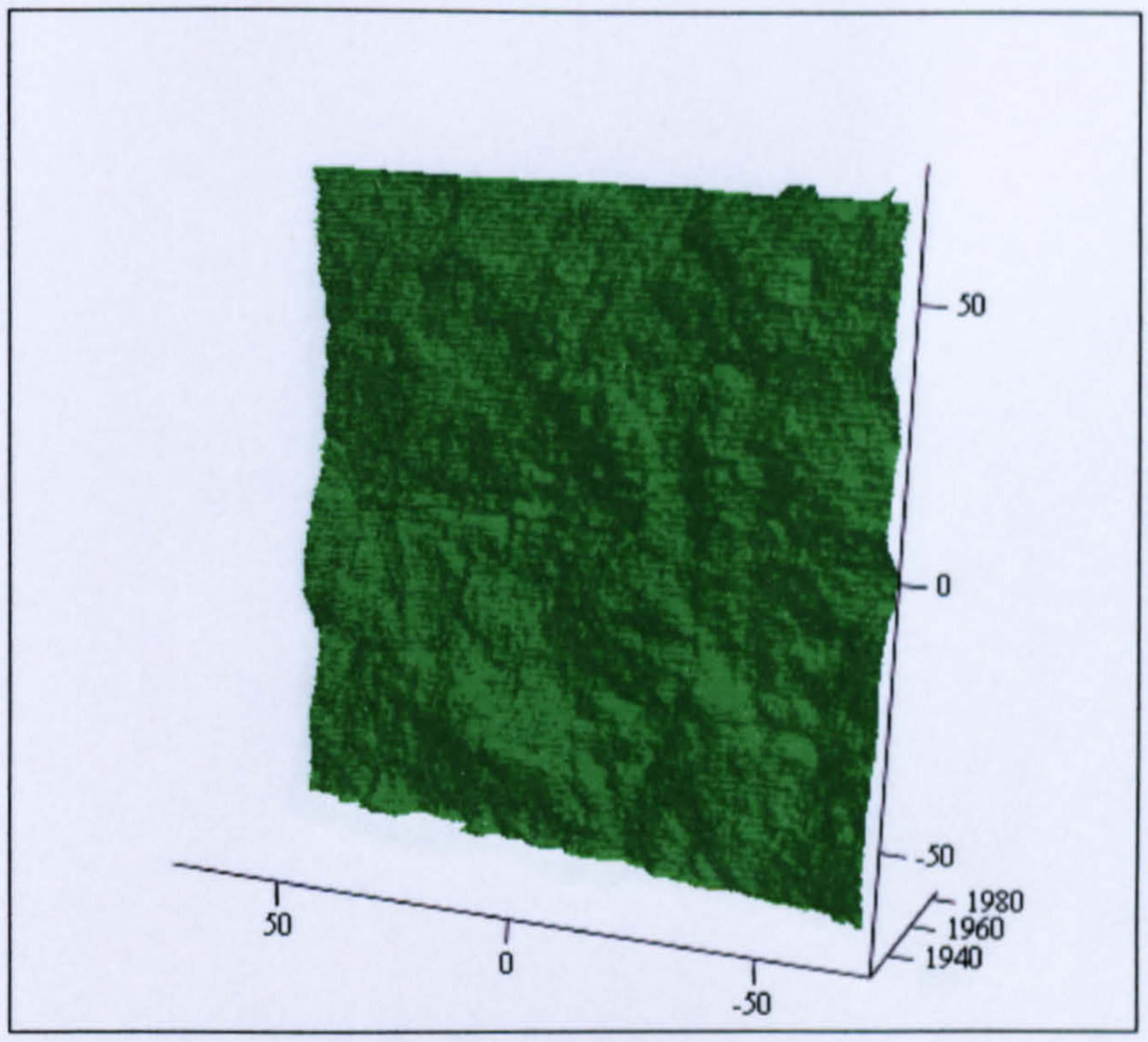

Figure 53 Slab PL10 Topography

Roughness Parameters	X axis mean	Y axis mean
2α (mm)	0.537	0.765
$\frac{Da}{2W}$	0.482	0.686
$R\Delta a$	0.965	1.377
$R\Delta q$ ($mm^{1/2}$)	0.945	1.376
Lo (mm)	207.18	253.59
Lr	1.49	1.82

Table 53 Slab PL10 Roughness parameters values

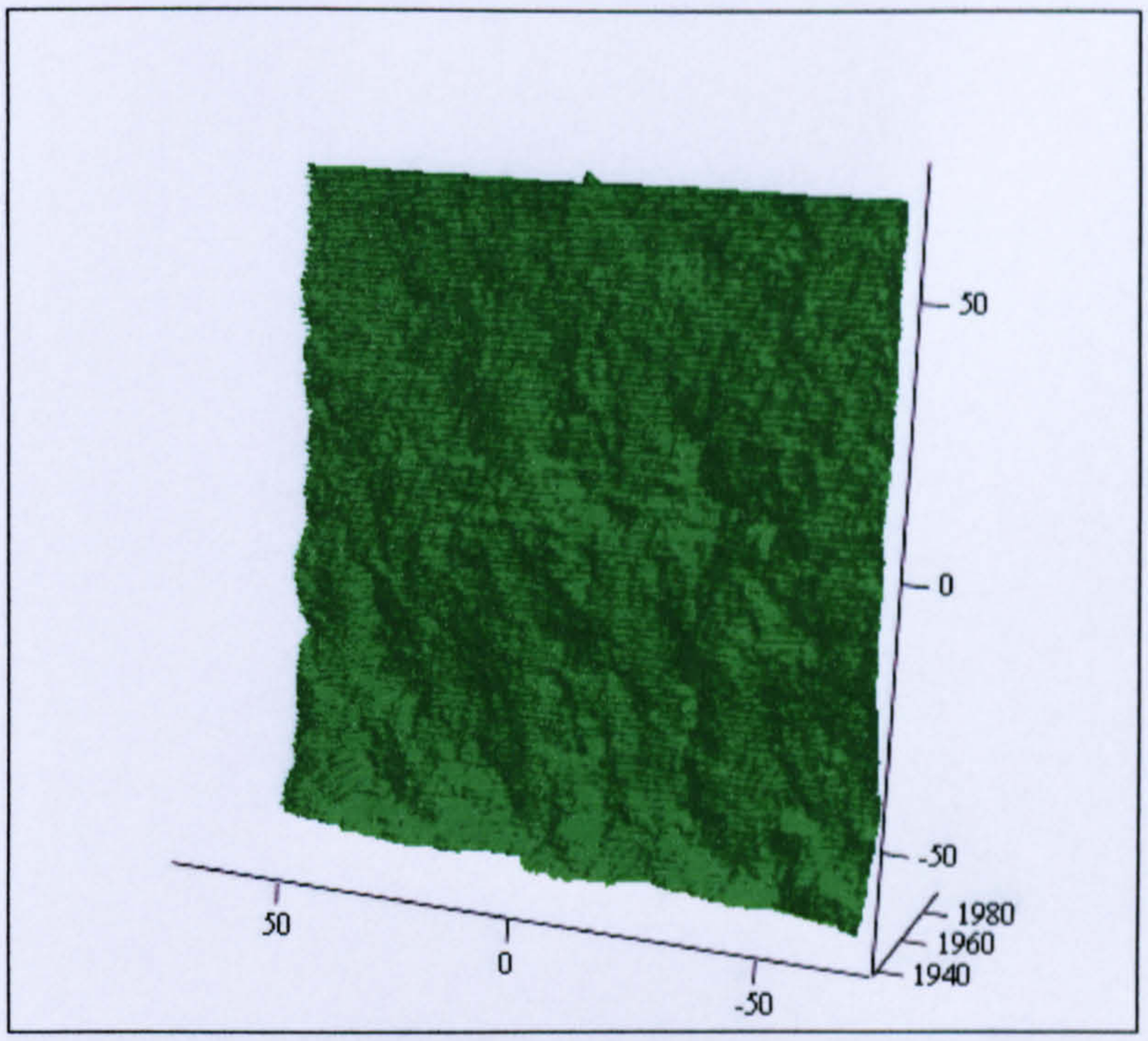

Figure 54 Slab PL11 Topography

Roughness Parameters	X axis mean	Y axis mean
2α (mm)	0.575	1.019
$\frac{Da}{2W}$	0.517	0.915
$R\Delta a$	1.034	1.832
$R\Delta q$ ($mm^{1/2}$)	1.053	1.854
Lo (mm)	215.06	309.23
Lr	1.55	2.22

Table 54 Slab PL11 Roughness parameters values

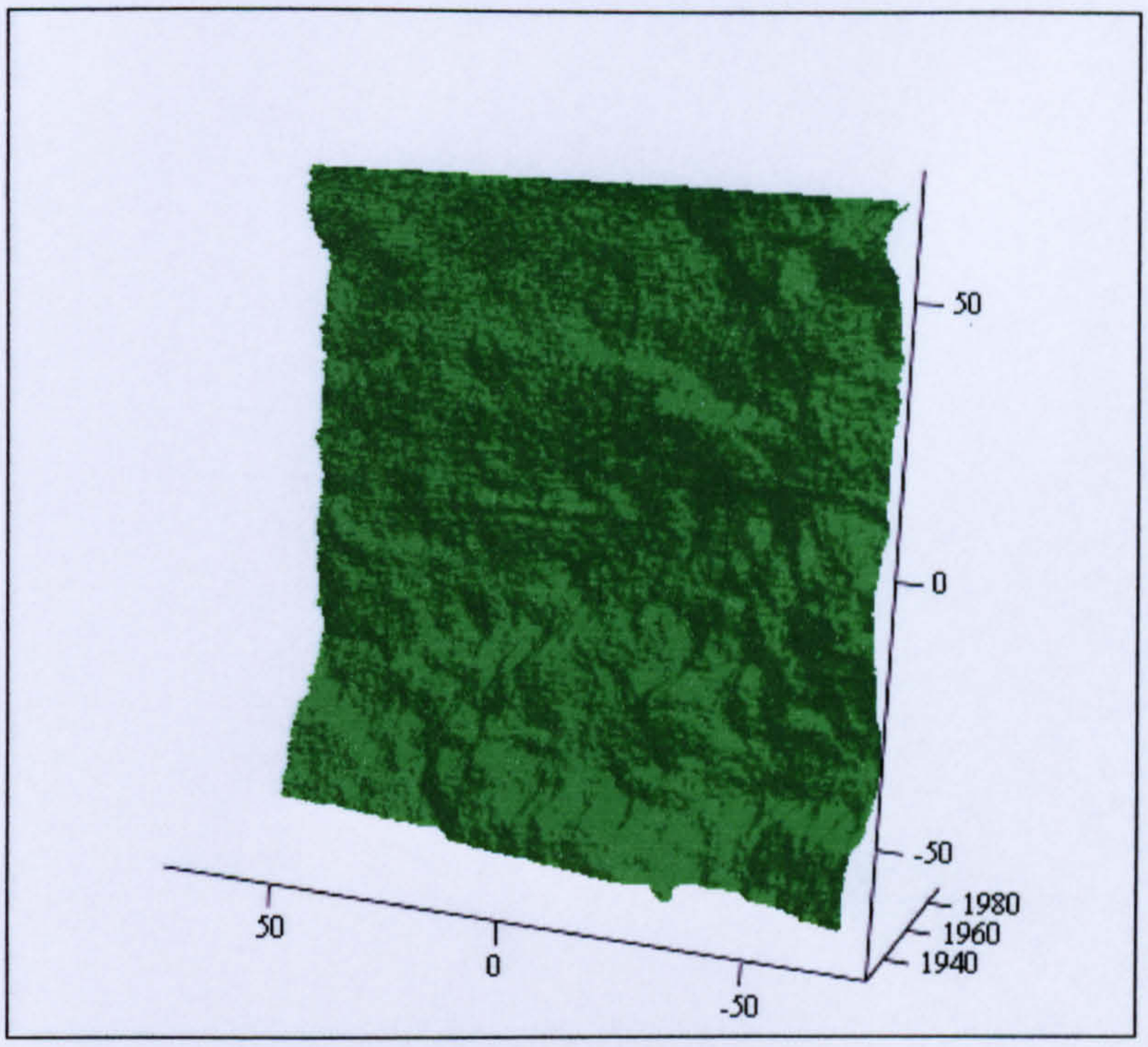

Figure 55 Slab PL13 Topography

Roughness Parameters	X axis mean	Y axis mean
2α (mm)	0.591	0.658
$\frac{Da}{2W}$	0.532	0.592
$R\Delta a$	1.063	1.183
$R\Delta q$ ($mm^{1/2}$)	1.058	1.209
Lo (mm)	218.40	232.15
Lr	1.57	1.67

Table 55 Slab PL13 Roughness parameters values

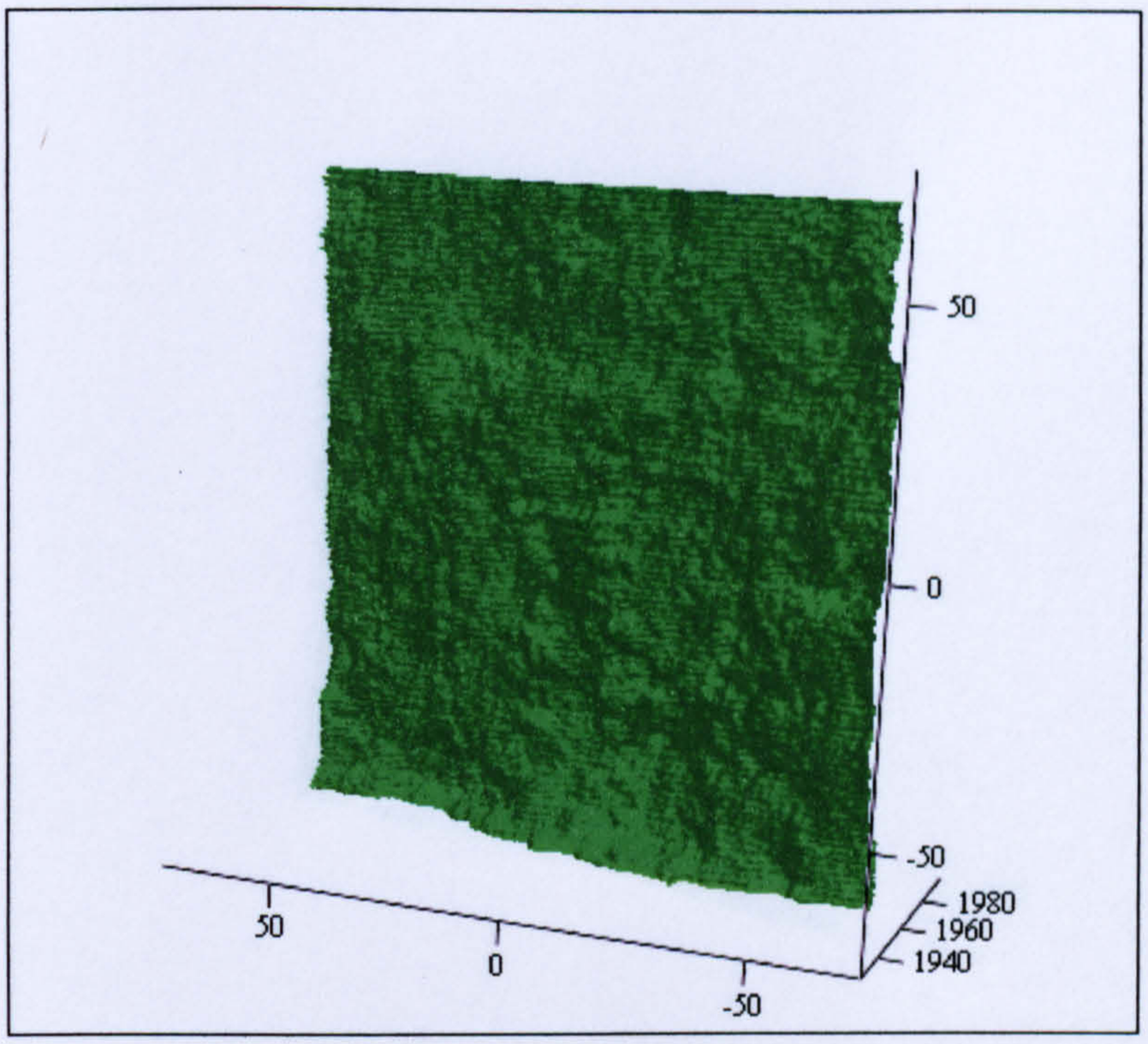

Figure 56 Slab PL14 Topography

Roughness Parameters	X axis mean	Y axis mean
2α (mm)	0.604	0.836
$\frac{Da}{2W}$	0.543	0.751
$R\Delta a$	1.087	1.503
$R\Delta q$ ($mm^{1/2}$)	1.068	1.505
Lo (mm)	220.43	268.59
Lr	1.59	1.93

Table 56 Slab PL14 Roughness parameters values

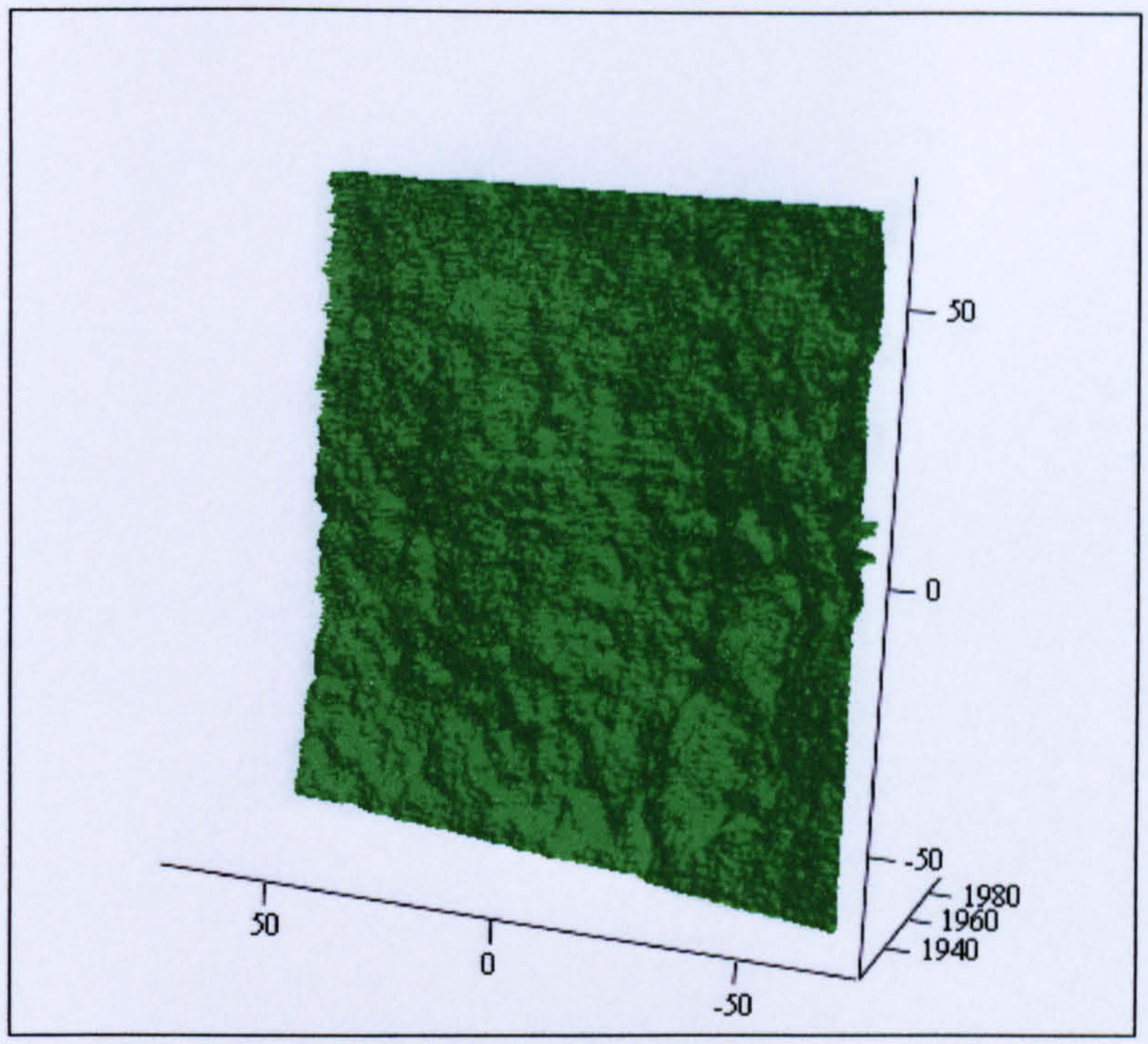

Figure 57 Slab PL15 Topography

Roughness Parameters	X axis mean	Y axis mean
2α (mm)	0.693	0.740
$\frac{Da}{2W}$	0.624	0.666
$R\Delta a$	1.247	1.330
$R\Delta q$ ($mm^{1/2}$)	1.357	1.560
Lo (mm)	239.91	250.09
Lr	1.73	1.80

Table 57 Slab PL15 Roughness parameters values

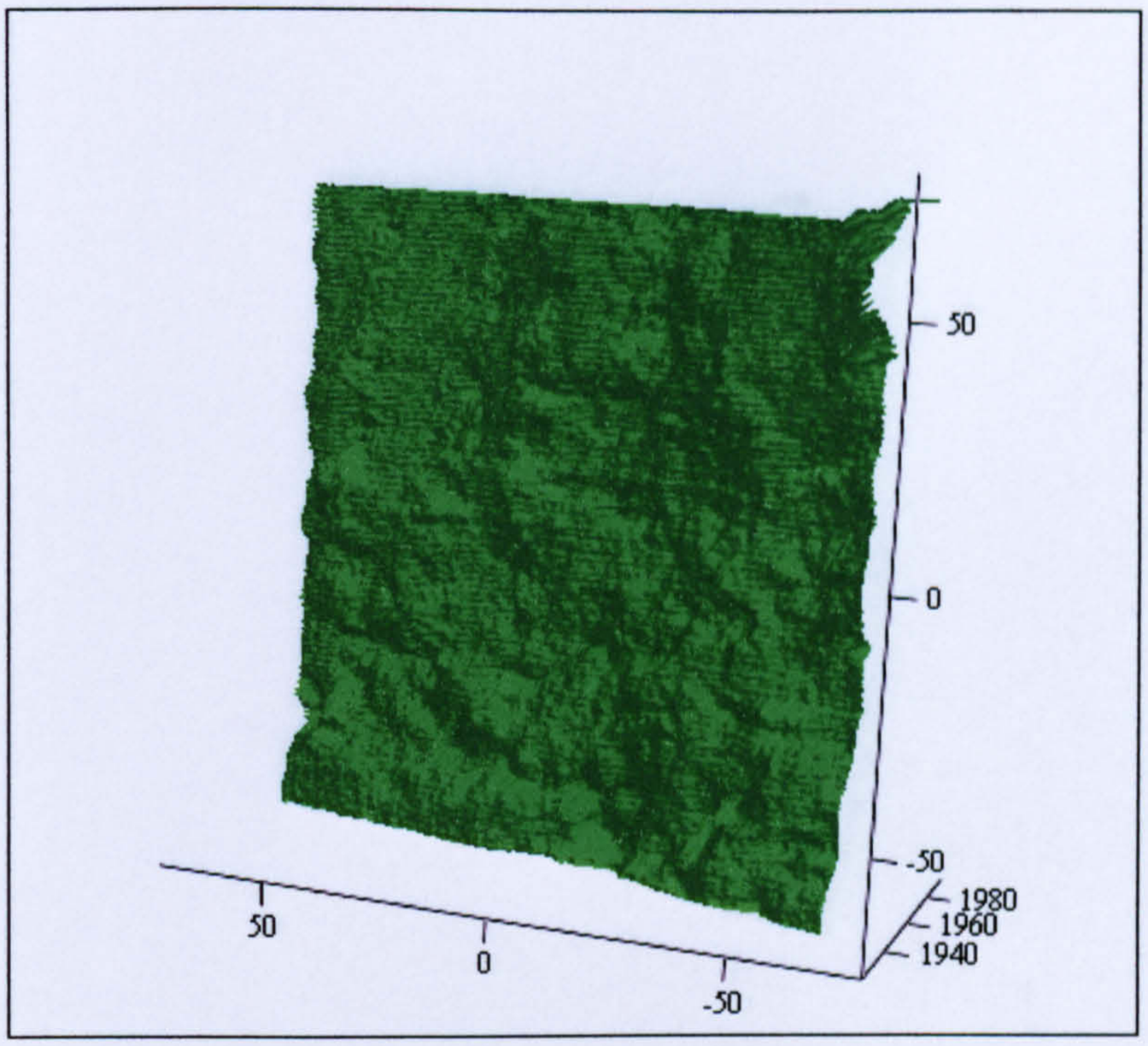

(X,Y,Z)

Figure 58 Slab PL16 Topography

Roughness Parameters	X axis mean	Y axis mean
2α (mm)	0.573	0.812
$\frac{Da}{2W}$	0.515	0.730
$R\Delta a$	1.031	1.460
$R\Delta q$ ($mm^{1/2}$)	1.030	1.496
Lo (mm)	215.09	264.66
Lr	1.55	1.90

Table 58 Slab PL16 Roughness values parameters

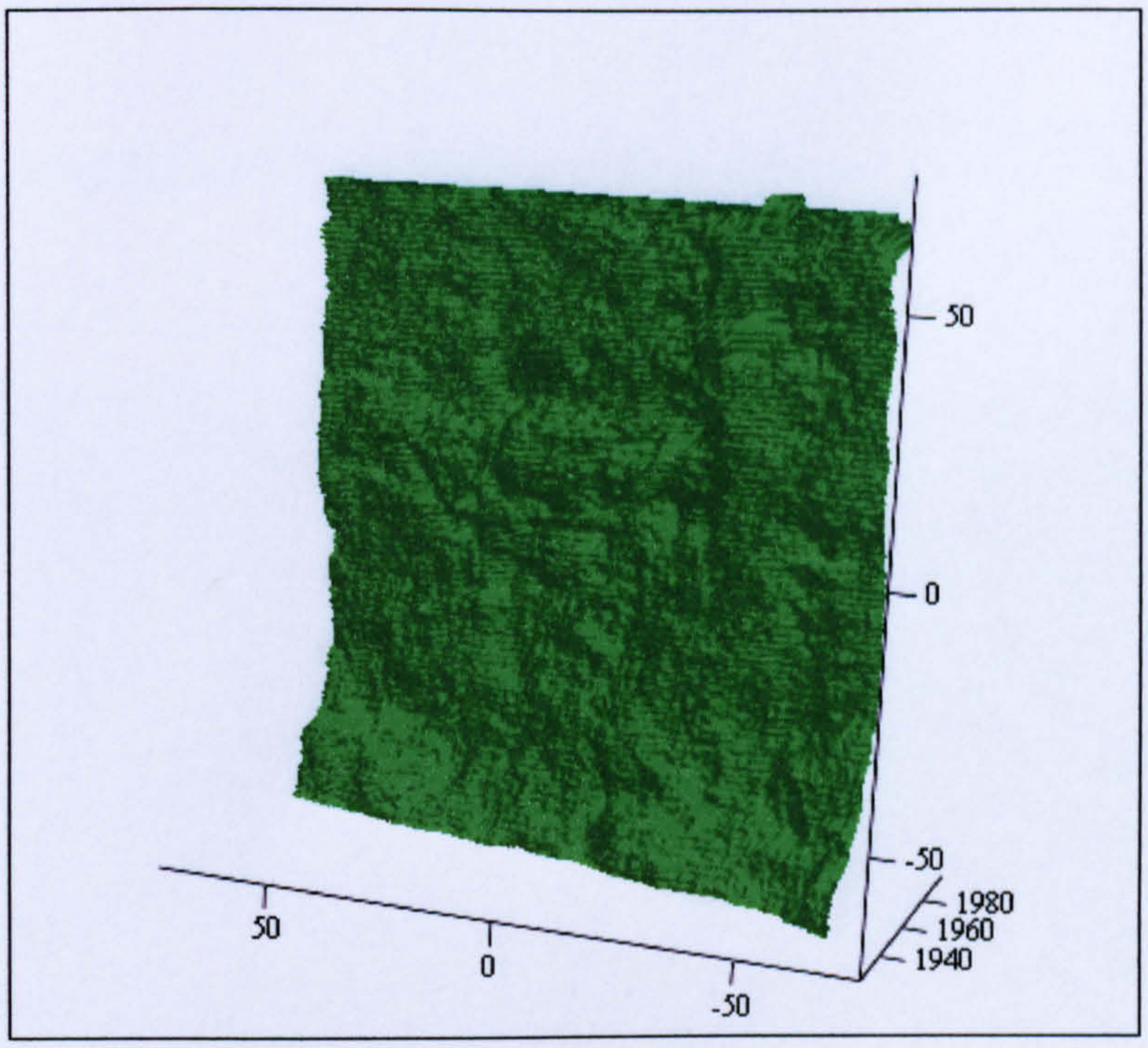

(X,Y,Z)

Figure 59 Slab P1 Topography

Roughness Parameters	X axis mean	Y axis mean
2α (mm)	0.621	0.860
$\frac{Da}{2W}$	0.558	0.775
$R\Delta a$	1.116	1.547
$R\Delta q$ ($mm^{1/2}$)	1.096	1.549
Lo (mm)	223.64	274.01
Lr	1.61	1.97

Table 59 Slab P1 Roughness parameters values

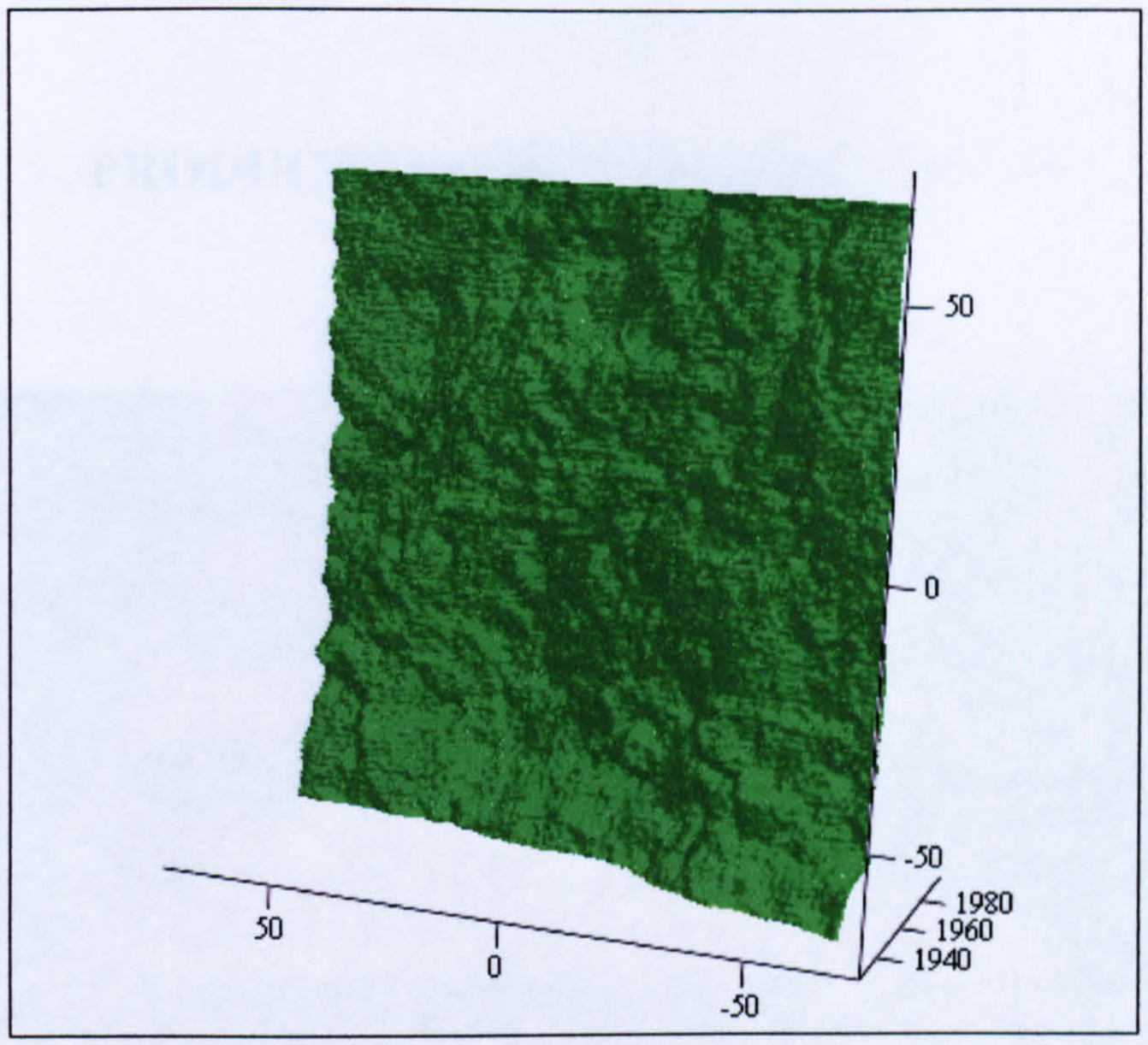

Figure 60 Slab P5 Topography

Roughness Parameters	X axis mean	Y axis mean
2α (mm)	0.631	0.733
$\frac{Da}{2W}$	0.567	0.660
$R\Delta a$	1.135	1.319
$R\Delta q$ ($mm^{1/2}$)	1.124	1.334
Lo (mm)	225.81	247.30
Lr	1.62	1.78

Table 60 Slab P5 Roughness parameters values

APPENDIX 9

PRODUCTION OF BEAM SPECIMENS

Substrate beams inside moulds ready for repair

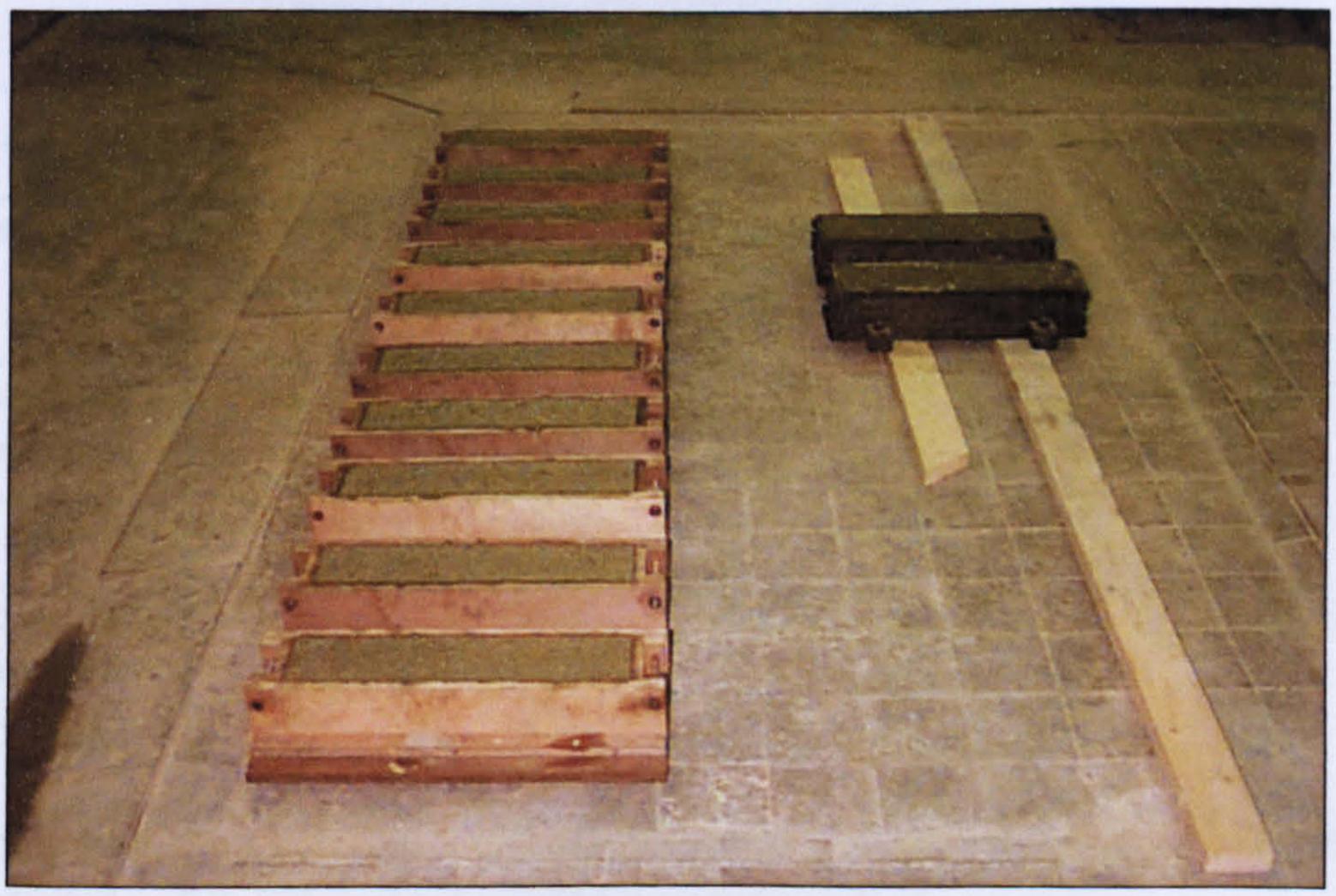

Substrate beams after filling with different types of generic repair materials

APPENDIX 10

FLEXURAL EXPERIMENTS- COMPRESSIVE STRENGTHS

Mix 1				
Material	Cube number	Compressive strength (N/mm^2)	Variation coefficient (%)	Average compressive strength (N/mm^2)
Substrate OPC Concrete (w/c = 0.45)	1	53.80	5.01	56.64
	2	57.27	1.11	
	3	59.42	4.91	
	4	56.07	1.01	
Repair material OPC Concrete (w/c = 0.4)	1	54.50	1.34	53.78
	2	51.66	3.94	
	3	54.49	1.32	
	4	54.47	1.28	
Repair material OPC Mortar (w/c = 0.4)	1	52.81	4.31	50.63
	2	49.78	1.68	
	3	49.96	1.32	
	4	49.95	1.34	
Repair material Zentrifix GM 25	1	28.48	6.39	26.77
	2	25.80	3.62	
	3	25.84	3.47	
	4	26.97	0.75	

Mix 2				
Material	Cube number	Compressive strength (N/mm^2)	Variation coefficient (%)	Average compressive strength (N/mm^2)
Substrate OPC Concrete (w/c = 0.45)	1	53.54	0.98	54.07
	2	56.08	3.72	
	3	54.96	1.65	
	4	51.68	4.42	
Repair material OPC Concrete (w/c = 0.5)	1	40.88	0.94	40.50
	2	40.67	0.42	
	3	40.50	0	
	4	39.96	1.33	
Repair material OPC Mortar (w/c = 0.5)	1	43.22	3.25	41.86
	2	42.52	1.58	
	3	41.78	0.19	
	4	39.92	4.63	
Repair material Sika MonoTop 615	1	25.71	3.71	24.79
	2	24.97	0.73	
	3	24.39	1.61	
	4	24.09	2.82	

Mix 3				
Material	Cube number	Compressive strength (N/mm^2)	Variation coefficient (%)	Average compressive strength (N/mm^2)
Substrate OPC Concrete (w/c = 0.45)	1	52.49	2.45	53.81
	2	54.38	1.06	
	3	52.46	2.51	
	4	55.92	3.92	
Repair material OPC Concrete (w/c = 0.4)	1	55.71	3.19	53.99
	2	54.92	1.72	
	3	54.59	1.11	
	4	50.73	6.04	
Repair material OPC Mortar (w/c = 0.4)	1	45.21	0.57	45.47
	2	45.47	0	
	3	44.33	2.51	
	4	46.88	3.10	
Repair material Zentrifix GM 25	1	24.60	2.96	25.35
	2	25.91	2.21	
	3	24.81	2.13	
	4	26.09	2.92	

Mix 4				
Material	Cube number	Compressive strength (N/mm^2)	Variation coefficient (%)	Average compressive strength (N/mm^2)
Substrate OPC Concrete (w/c = 0.45)	1	49.06	6.96	52.73
	2	51.71	1.93	
	3	54.71	3.75	
	4	55.43	5.12	
Repair material OPC Concrete (w/c = 0.5)	1	41.87	1.09	42.33
	2	40.39	4.58	
	3	42.40	0.17	
	4	44.65	5.48	
Repair material OPC Mortar (w/c = 0.5)	1	40.47	0.05	40.45
	2	39.63	2.03	
	3	41.01	1.38	
	4	40.70	0.62	
Repair material Sika MonoTop 615	1	26.19	3.27	25.36
	2	25.38	0.08	
	3	24.86	1.97	
	4	25.01	1.38	

Mix 5				
Material	Cube number	Compressive strength (N/mm^2)	Variation coefficient (%)	Average compressive strength (N/mm^2)
Substrate OPC Concrete (w/c = 0.45)	1	48.76	1.41	48.08
	2	47.95	0.27	
	3	46.54	3.20	
	4	49.05	2.02	
Repair material OPC Concrete (w/c = 0.4)	1	55.70	1.13	55.08
	2	55.08	0	
	3	54.69	0.71	
	4	54.85	0.42	
Repair material OPC Mortar (w/c = 0.4)	1	53.23	1.01	52.70
	2	54.12	2.69	
	3	51.72	1.86	
	4	51.74	1.82	
Repair material Zentrifix GM 25	1	25.06	2.53	25.71
	2	25.78	0.27	
	3	25.30	1.59	
	4	26.70	3.85	

Mix 6				
Material	Cube number	Compressive strength (N/mm^2)	Variation coefficient (%)	Average compressive strength (N/mm^2)
Substrate OPC Concrete (w/c = 0.45)	1	58.04	1.43	57.22
	2	59.22	3.50	
	3	56.61	1.07	
	4	55.02	3.84	
Repair material OPC Concrete (w/c = 0.5)	1	48.16	1.65	47.38
	2	47.47	0.19	
	3	46.68	1.48	
	4	47.22	0.34	
Repair material OPC Mortar (w/c = 0.5)	1	43.68	3.53	42.19
	2	41.84	0.83	
	3	41.10	2.58	
	4	42.13	0.14	
Repair material Sika MonoTop 615	1	23.99	1.36	24.32
	2	22.10	9.13	
	3	24.61	1.19	
	4	26.59	9.33	

Mix 7				
Material	Cube number	Compressive strength (N/mm^2)	Variation coefficient (%)	Average compressive strength (N/mm^2)
Substrate OPC Concrete (w/c = 0.45)	1	56.25	1.08	55.65
	2	53.73	3.45	
	3	55.96	0.56	
	4	56.65	1.80	
Repair material OPC Concrete (w/c = 0.4)	1	65.10	5.29	61.83
	2	59.94	3.06	
	3	63.02	1.92	
	4	59.24	4.19	
Repair material OPC Mortar (w/c = 0.4)	1	61.87	1.59	60.90
	2	60.55	0.57	
	3	61.38	0.79	
	4	59.80	1.81	
Repair material Zentrifix GM 25	1	28.22	0.36	28.12
	2	27.46	2.35	
	3	26.67	5.16	
	4	30.14	7.18	

Mix 8				
Material	Cube number	Compressive strength (N/mm^2)	Variation coefficient (%)	Average compressive strength (N/mm^2)
Substrate OPC Concrete (w/c = 0.45)	1	51.94	0.44	52.17
	2	53.42	2.40	
	3	51.78	0.75	
	4	51.52	1.25	
Repair material OPC Concrete (w/c = 0.5)	1	49.04	3.90	47.20
	2	45.72	3.14	
	3	46.86	0.72	
	4	47.17	0.06	
Repair material OPC Mortar (w/c = 0.5)	1	44.92	5.57	42.55
	2	41.97	1.36	
	3	46.45	9.17	
	4	36.87	13.35	
Repair material Sika MonoTop 615	1	27.39	1.40	27.01
	2	25.85	4.29	
	3	27.04	0.11	
	4	27.76	2.78	

APPENDIX 11

PRODUCTION OF CYLINDER AND CUBE SPECIMENS

Cylinders and cubes ready for performing strength and water absorption tests

APPENDIX 12

WATER ABSORPTION EXPERIMENTS

COMPRESSIVE STRENGTHS

Repair Material	Cube number	Compressive strength (N/mm^2)	Variation Coefficient (%)	Average compressive strength (N/mm^2)
OPCC w/c = 0.4	1	64.24	0	64.24
	2	66.24	3.11	
	3	63.66	0.90	
	4	62.81	2.23	
OPCC w/c = 0.5	1	45.36	0.96	44.93
	2	45.25	0.71	
	3	45.26	0.73	
	4	43.85	2.40	
OPCM w/c = 0.4	1	50.46	0.84	50.89
	2	47.13	7.39	
	3	51.50	1.20	
	4	54.46	7.02	
OPCM w/c = 0.5	1	34.51	0.66	34.74
	2	36.39	4.75	
	3	35.04	0.86	
	4	33.03	4.92	
Zentrifix GM 25	1	25.80	2.38	26.43
	2	25.37	4.01	
	3	27.06	2.38	
	4	27.50	4.05	
MonoTop 615	1	24.50	3.28	25.33
	2	25.94	2.41	
	3	25.49	0.63	
	4	25.37	0.16	

TENSILE STRENGTHS

Repair Material	Cylinder number	Tensile strength (N/mm^2)	Variation Coefficient (%)	Average tensile strength (N/mm^2)
OPCC w/c = 0.4	1	5.32	3.10	5.16
	2	4.89	5.23	
	3	5.04	2.33	
	4	5.38	4.26	
OPCC w/c = 0.5	1	4.64	2.88	4.51
	2	4.28	5.10	
	3	4.40	2.44	
	4	4.71	4.43	
OPCM w/c = 0.4	1	5.11	0.97	5.16
	2	5.20	0.78	
	3	5.13	0.58	
	4	5.18	0.39	
OPCM w/c = 0.5	1	4.12	3.26	3.99
	2	3.39	15.04	
	3	3.97	0.50	
	4	4.46	11.78	
Zentrifix GM 25	1	2.37	7.42	2.56
	2	2.85	11.33	
	3	2.58	0.78	
	4	2.43	5.08	
MonoTop 615	1	2.84	1.07	2.81
	2	2.78	1.07	
	3	3.09	9.96	
	4	2.53	9.96	

APPENDIX 13

REPAIR OF SLAB SUBSTRATES

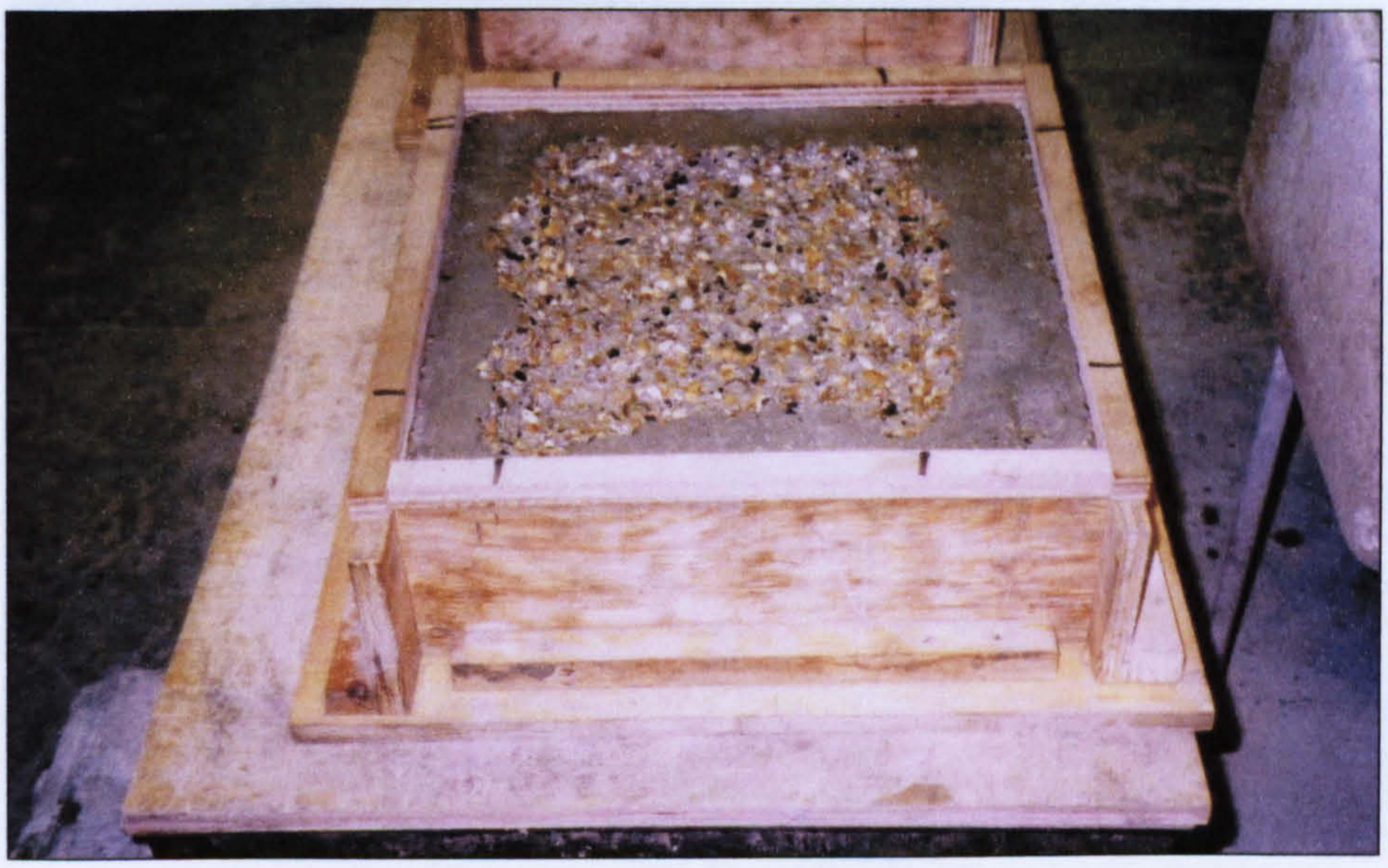

Slab substrate specimens placed inside timber moulds prior to repair

Application of bonding agent/primer Zentrifix KMH

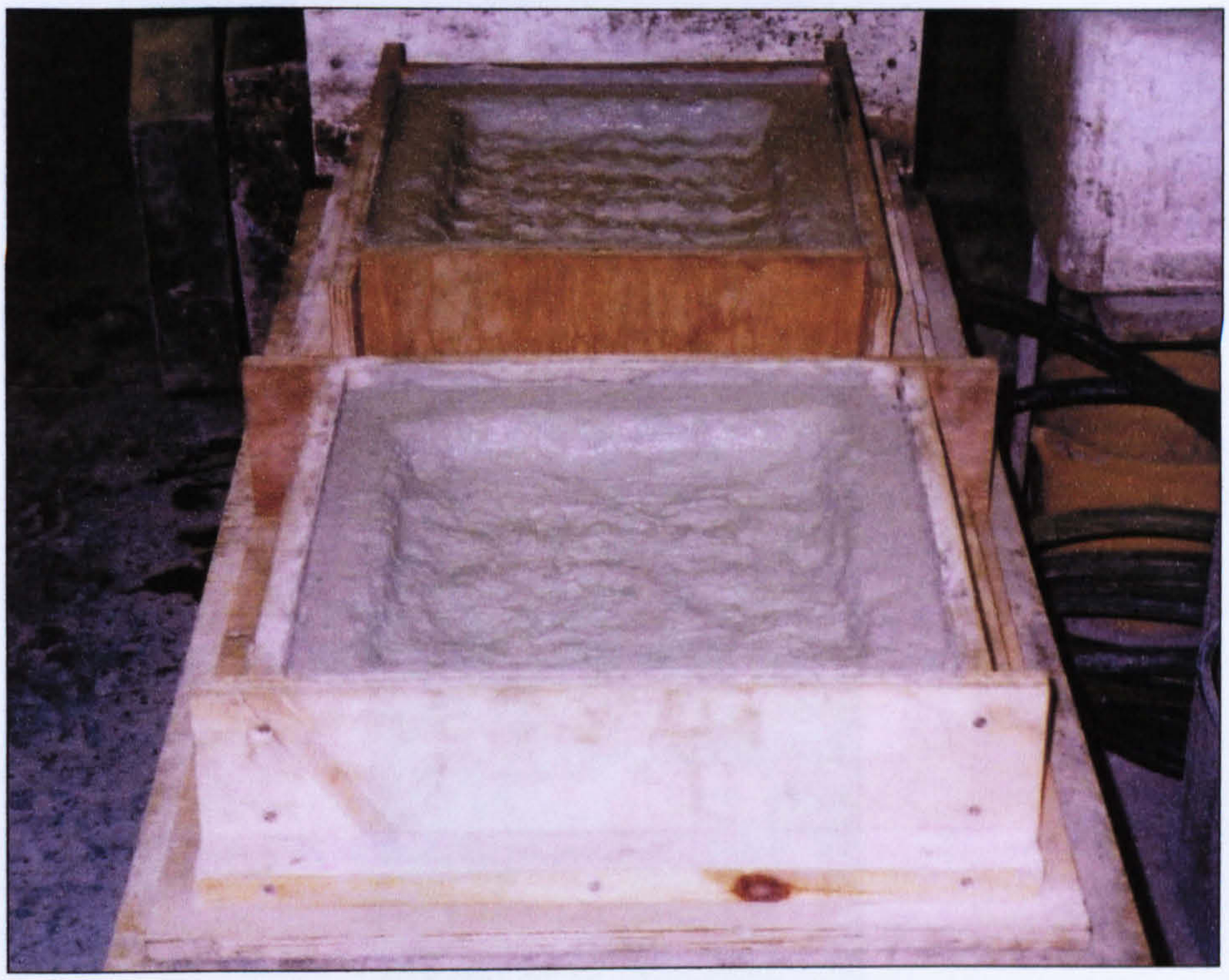

Slab substrates immediately after the application of bonding agent/primer Zentrifix KMH and ready to receive the repair material

Slab substrates immediately after the installation of the repair materials

APPENDIX 14

PULL-OFF TESTING

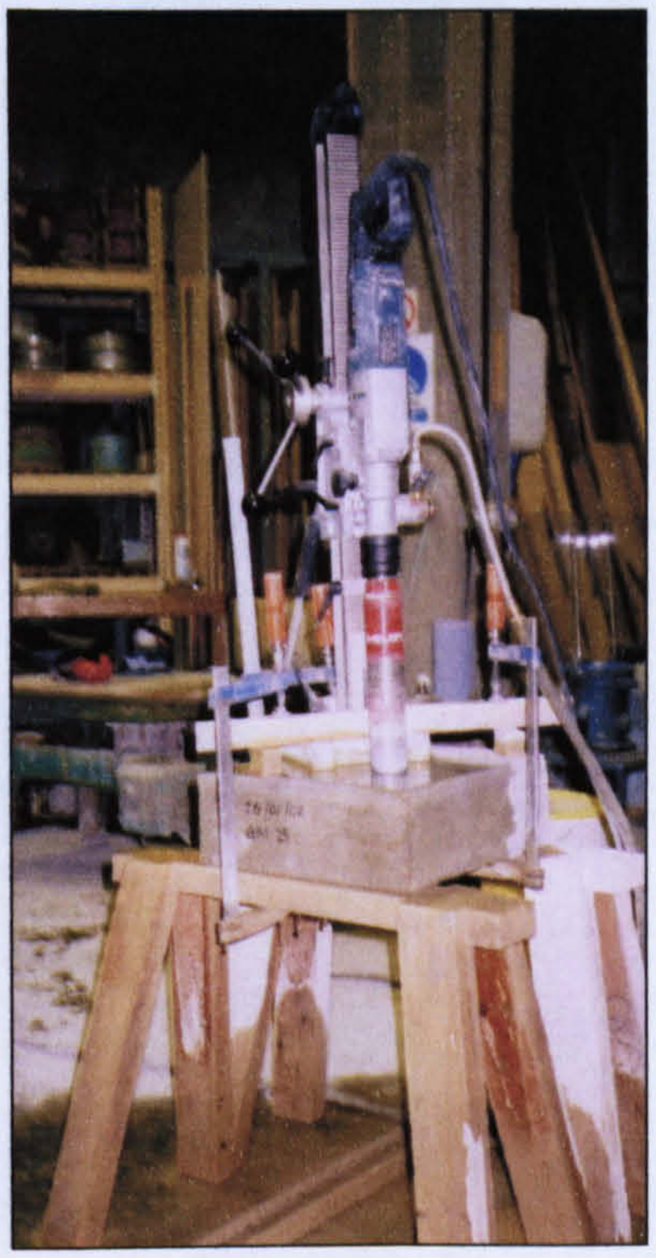

Drilling of partial cores

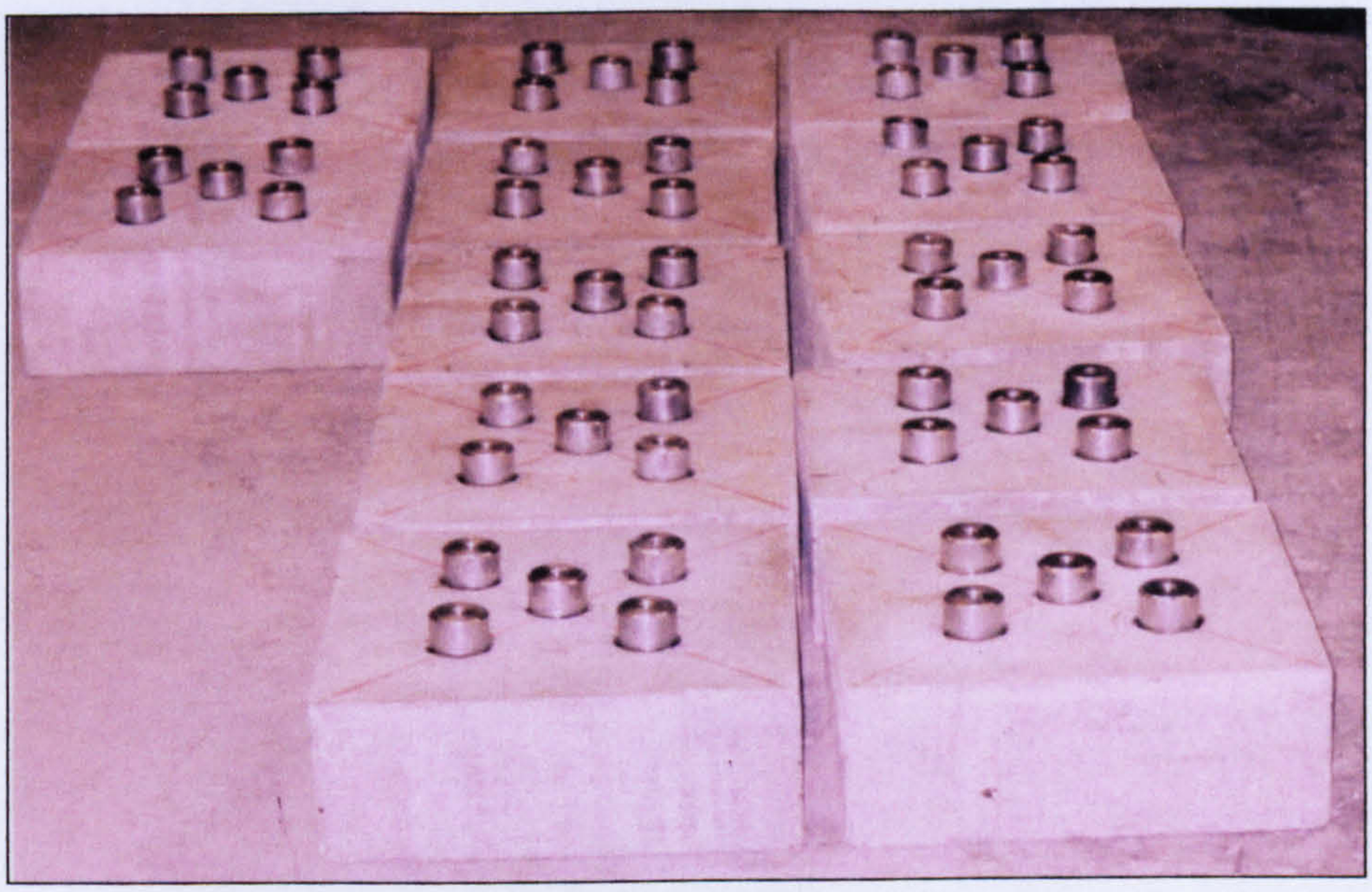

Aluminium dollies attached to the repaired slab specimens

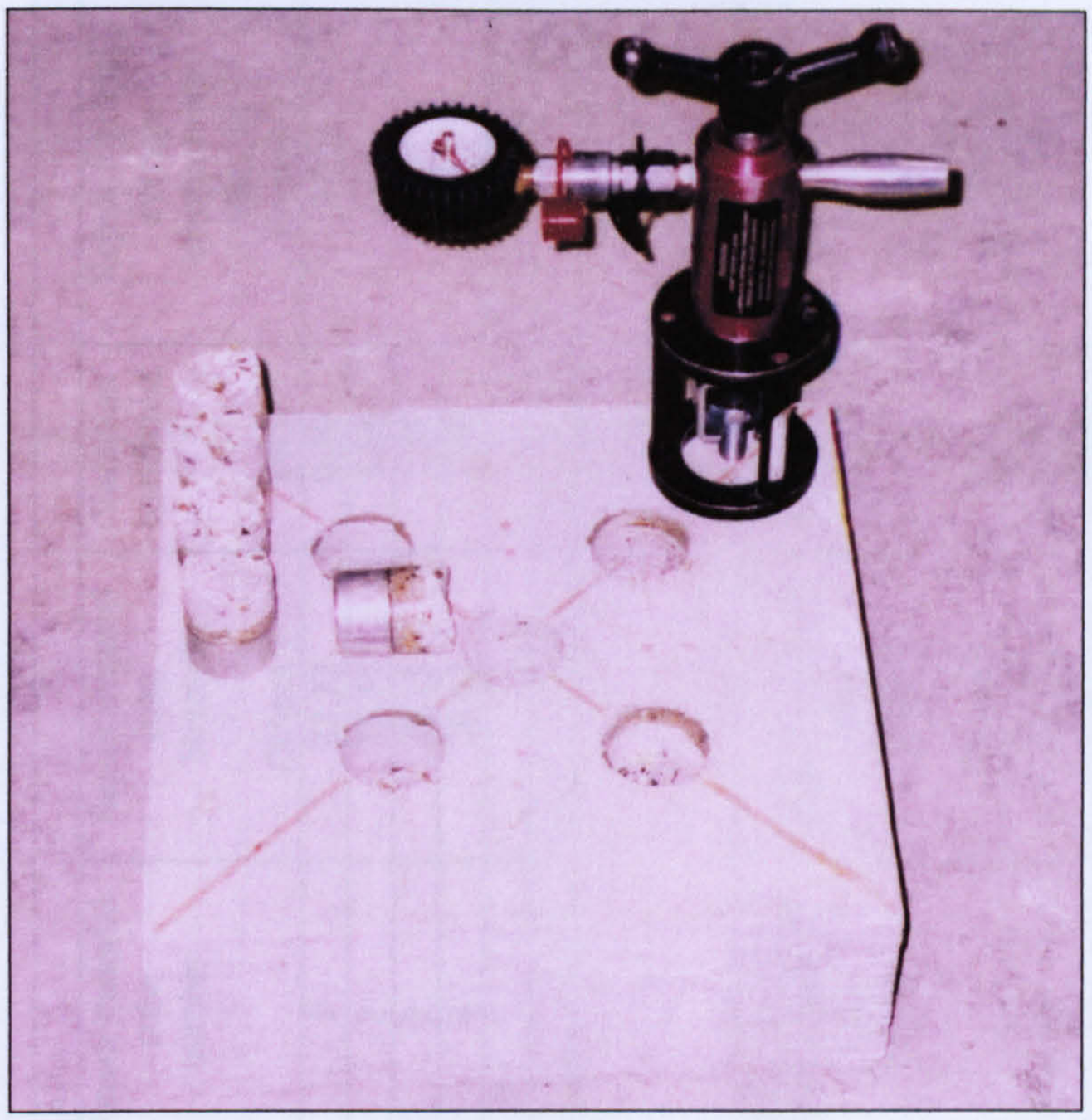

Pull-off testing

APPENDIX 15

PULL OFF EXPERIMENTS-COMPRESSIVE STRENGTHS

Mix 1 Slabs S1 and S2 (w/c = 0.4)									
Substrate cube number	Substrate cube strength (N/mm^2)	Variation coefficient (%)	Substrate average compressive strength (N/mm^2)	Repair material	Bonding agent	Repair material cube number	Repair material cube Strength (N/mm^2)	Variation coefficient (%)	Repair material average compressive strength (N/mm^2)
1	56.86	1.57	57.77	Zentrifix GM 25	N/A	1	27.32	0.59	27.16
2	55.22	4.41				2	25.57	5.85	
3	57.36	0.71				3	29.13	7.25	
4	58.94	2.03				4	26.62	1.98	
5	59.96	3.79							
6	58.26	0.85							

Mix 2 Slabs S3 and S4 (w/c = 0.4)									
Substrate cube number	Substrate cube strength (N/mm^2)	Variation coefficient (%)	Substrate average compressive strength (N/mm^2)	Repair material	Bonding agent	Repair material cube number	Repair material cube Strength (N/mm^2)	Variation coefficient (%)	Repair material average compressive strength (N/mm^2)
1	51.37	4.76	53.94	Zentrifix GM 25	Zentrifix KMH	1	27.32	0.59	27.16
2	53.66	0.52				2	25.57	5.85	
3	52.32	3.01				3	29.13	7.25	
4	53.42	0.96				4	26.62	1.98	
5	56.47	4.69							
6	56.37	4.51							

Mix 3 Slabs S5 and S6 (w/c = 0.4)									
Substrate cube number	Substrate cube strength (N/mm^2)	Variation coefficient (%)	Substrate average compressive strength (N/mm^2)	Repair material	Bonding agent	Repair material cube number	Repair material cube Strength (N/mm^2)	Variation coefficient (%)	Repair material average compressive strength (N/mm^2)
1	59.69	4.65	57.04	OPC Mortar (w/c = 0.4)	Zentrifix KMH	1	52.24	1.24	51.60
2	58.25	2.12				2	50.88	1.40	
3	58.24	2.10				3	53.38	3.45	
4	56.45	1.03				4	49.89	3.31	
5	55.41	2.86							
6	54.21	4.96							

Mix 4 Slabs S7 and S8 (w/c = 0.4)									
Substrate cube number	Substrate cube strength (N/mm^2)	Variation coefficient (%)	Substrate average compressive strength (N/mm^2)	Repair material	Bonding agent	Repair material cube number	Repair material cube Strength (N/mm^2)	Variation coefficient (%)	Repair material average compressive strength (N/mm^2)
1	55.63	4.30	58.13	OPC Mortar (w/c = 0.4)	N/A	1	52.24	1.24	51.60
2	58.71	0.99				2	50.88	1.40	
3	57.77	0.62				3	53.38	3.45	
4	58.64	0.88				4	49.89	3.31	
5	58.69	0.96							
6	59.35	2.10							

Mix 5 Slabs S9 and S10 (w/c = 0.4)									
Substrate cube number	Substrate cube strength (N/mm^2)	Variation coefficient (%)	Substrate average compressive strength (N/mm^2)	Repair material	Bonding agent	Repair material cube number	Repair material cube Strength (N/mm^2)	Variation coefficient (%)	Repair material average compressive strength (N/mm^2)
1	56.40	0.20	56.29	OPC Concrete (w/c = 0.4)	Zentrifix KMH	1	58.02	0.16	57.93
2	53.04	5.77				2	56.75	2.04	
3	58.22	3.43				3	59.81	3.25	
4	56.58	0.52				4	57.14	1.36	
5	56.56	0.48							
6	56.92	1.12							

Mix 6 Slabs S11 and S12 (w/c = 0.4)									
Substrate cube number	Substrate cube strength (N/mm^2)	Variation coefficient (%)	Substrate average compressive strength (N/mm^2)	Repair material	Bonding agent	Repair material cube number	Repair material cube Strength (N/mm^2)	Variation coefficient (%)	Repair material average compressive strength (N/mm^2)
1	55.56	0.75	55.98	OPC Concrete (w/c = 0.4)	N/A	1	58.02	0.16	57.93
2	54.67	2.34				2	56.75	2.04	
3	56.38	0.71				3	59.81	3.25	
4	56.44	0.82				4	57.14	1.36	
5	55.63	0.63							
6	57.18	2.14							

Mix 7 Slabs S13 and S14 (w/c = 0.45)									
Substrate cube number	Substrate cube strength (N/mm^2)	Variation coefficient (%)	Substrate average compressive strength (N/mm^2)	Repair material	Bonding agent	Repair material cube number	Repair material cube Strength (N/mm^2)	Variation coefficient (%)	Repair material average compressive strength (N/mm^2)
1	54.65	1.98	53.59	OPC Concrete (w/c = 0.4)	N/A	1	50.66	4.89	48.30
2	52.02	2.93				2	46.87	2.96	
3	53.87	0.52				3	46.42	3.89	
4	53.45	0.26				4	49.23	1.93	
5	52.58	1.88							
6	54.97	2.58							

Mix 8 Slabs S15 and S16 (w/c = 0.45)									
Substrate cube number	Substrate cube strength (N/mm^2)	Variation coefficient (%)	Substrate average compressive strength (N/mm^2)	Repair material	Bonding agent	Repair material cube number	Repair material cube Strength (N/mm^2)	Variation coefficient (%)	Repair material average compressive strength (N/mm^2)
1	50.29	0.30	50.44	OPC Concrete (w/c = 0.4)	Zentrifix KMH	1	50.66	4.89	48.30
2	50.97	1.05				2	46.87	2.96	
3	49.53	1.80				3	46.42	3.89	
4	50.44	0				4	49.23	1.93	
5	48.96	2.93							
6	52.47	4.02							

Mix 9 Slabs S17 and S18 (w/c = 0.45)									
Substrate cube number	Substrate cube strength (N/mm^2)	Variation coefficient (%)	Substrate average compressive strength (N/mm^2)	Repair material	Bonding agent	Repair material cube number	Repair material cube Strength (N/mm^2)	Variation coefficient (%)	Repair material average compressive strength (N/mm^2)
1	45.56	3.90	47.41	OPC Mortar (w/c = 0.4)	N/A	1	46.35	2.75	47.66
2	50.08	5.63				2	49.15	3.13	
3	46.44	2.05				3	48.19	1.11	
4	44.54	6.05				4	46.96	1.47	
5	52.06	9.80							
6	45.75	3.50							

Mix 10 Slabs S19 and S20 (w/c = 0.45)									
Substrate cube number	Substrate cube strength (N/mm^2)	Variation coefficient (%)	Substrate average compressive strength (N/mm^2)	Repair material	Bonding agent	Repair material cube number	Repair material cube Strength (N/mm^2)	Variation coefficient (%)	Repair material average compressive strength (N/mm^2)
1	50.19	0	50.19	OPC Mortar (w/c = 0.4)	Zentrifix KMH	1	46.35	2.75	47.66
2	50.84	1.30				2	49.15	3.13	
3	50.08	0.22				3	48.19	1.11	
4	49.61	1.16				4	46.96	1.47	
5	50.08	0.22							
6	50.35	0.32							

Mix 11 Slabs S21 and S22 (w/c = 0.45)									
Substrate cube number	Substrate cube strength (N/mm^2)	Variation coefficient (%)	Substrate average compressive strength (N/mm^2)	Repair material	Bonding agent	Repair material cube number	Repair material cube Strength (N/mm^2)	Variation coefficient (%)	Repair material average compressive strength (N/mm^2)
1	54.34	1.49	53.54	Zentrifix GM 25	Zentrifix KMH	1	29.90	1.29	29.52
2	54.92	2.58				2	30.82	4.40	
3	52.05	2.78				3	28.63	3.01	
4	54.09	1.03				4	28.74	2.64	
5	54.52	1.83							
6	51.32	4.15							

Mix 12 Slabs S23 and S24 (w/c = 0.45)									
Substrate cube number	Substrate cube strength (N/mm^2)	Variation coefficient (%)	Substrate average compressive strength (N/mm^2)	Repair material	Bonding agent	Repair material cube number	Repair material cube Strength (N/mm^2)	Variation coefficient (%)	Repair material average compressive strength (N/mm^2)
1	52.06	0.95	52.56	Zentrifix GM 25	N/A	1	29.90	1.29	29.52
2	54.40	3.50				2	30.82	4.40	
3	51.68	1.67				3	28.63	3.01	
4	51.10	2.78				4	28.74	2.64	
5	51.31	2.38							
6	54.80	4.26							

Mix 13 Slabs S25 and S26 (w/c = 0.5)									
Substrate cube number	Substrate cube strength (N/mm^2)	Variation coefficient (%)	Substrate average compressive strength (N/mm^2)	Repair material	Bonding agent	Repair material cube number	Repair material cube Strength (N/mm^2)	Variation coefficient (%)	Repair material average compressive strength (N/mm^2)
1	42.33	0.21	42.42	OPC Concrete (w/c=0.4)	N/A	1	51.95	0.17	52.04
2	41.46	2.26				2	52.20	0.31	
3	42.71	0.68				3	51.79	0.48	
4	44.07	3.89				4	52.20	0.31	
5	41.71	1.67							
6	42.25	0.40							

Mix 14 Slabs S27 and S28 (w/c = 0.5)									
Substrate cube number	Substrate cube strength (N/mm^2)	Variation coefficient (%)	Substrate average compressive strength (N/mm^2)	Repair material	Bonding agent	Repair material cube number	Repair material cube Strength (N/mm^2)	Variation coefficient (%)	Repair material average compressive strength (N/mm^2)
1	42.94	1.78	43.72	OPC Concrete (w/c=0.4)	Zentrifix KMH	1	51.95	0.17	52.04
2	43.72	0				2	52.20	0.31	
3	43.03	1.58				3	51.79	0.48	
4	44.01	0.66				4	52.20	0.31	
5	45.08	3.11							
6	43.55	0.39							

Mix 15 Slabs S29 and S30 (w/c = 0.5)									
Substrate cube number	Substrate cube strength (N/mm^2)	Variation coefficient (%)	Substrate average compressive strength (N/mm^2)	Repair material	Bonding agent	Repair material cube number	Repair material cube Strength (N/mm^2)	Variation coefficient (%)	Repair material average compressive strength (N/mm^2)
1	46.23	0	46.23	OPC Mortar (w/c=0.4)	N/A	1	49.24	0.96	48.77
2	44.65	3.42				2	48.91	0.29	
3	45.14	2.36				3	48.61	0.33	
4	47.16	2.01				4	48.33	0.90	
5	45.59	1.38							
6	48.59	5.10							

Mix 16 Slabs S31 and S32 (w/c = 0.5)									
Substrate cube number	Substrate cube strength (N/mm^2)	Variation coefficient (%)	Substrate average compressive strength (N/mm^2)	Repair material	Bonding agent	Repair material cube number	Repair material cube Strength (N/mm^2)	Variation coefficient (%)	Repair material average compressive strength (N/mm^2)
1	41.16	4.15	42.94	OPC Mortar (w/c=0.4)	Zentrifix KMH	1	49.24	0.96	48.77
2	42.29	1.51				2	48.91	0.29	
3	42.75	0.44				3	48.61	0.33	
4	42.80	0.33				4	48.33	0.90	
5	44.50	3.63							
6	44.16	2.84							

Mix 17 Slabs S33 and S34 (w/c = 0.5)									
Substrate cube number	Substrate cube strength (N/mm^2)	Variation coefficient (%)	Substrate average compressive strength (N/mm^2)	Repair material	Bonding agent	Repair material cube number	Repair material cube Strength (N/mm^2)	Variation coefficient (%)	Repair material average compressive strength (N/mm^2)
1	43.50	0	43.50	Zentrifix GM 25	Zentrifix KMH	1	24.42	2.56	23.81
2	43.55	0.11				2	17.98	24.49	
3	42.49	2.32				3	26.09	9.58	
4	44.09	1.36				4	26.75	12.34	
5	43.98	1.10							
6	43.39	0.25							

Mix 18 Slabs S35 and S36 (w/c = 0.5)									
Substrate cube number	Substrate cube strength (N/mm^2)	Variation coefficient (%)	Substrate average compressive strength (N/mm^2)	Repair material	Bonding agent	Repair material cube number	Repair material cube Strength (N/mm^2)	Variation coefficient (%)	Repair material average compressive strength (N/mm^2)
1	41.37	0.66	41.10	Zentrifix GM 25	N/A	1	24.42	2.56	23.81
2	41.44	0.83				2	17.98	24.49	
3	41.74	1.56				3	26.09	9.58	
4	38.92	5.30				4	26.75	12.34	
5	41.34	0.58							
6	41.78	1.65							

Mix 19 Slabs S37 and S38 (w/c = 0.55)									
Substrate cube number	Substrate cube strength (N/mm^2)	Variation coefficient (%)	Substrate average compressive strength (N/mm^2)	Repair material	Bonding agent	Repair material cube number	Repair material cube Strength (N/mm^2)	Variation coefficient (%)	Repair material average compressive strength (N/mm^2)
1	40.40	0.02	40.39	OPC Concrete (w/c = 0.4)	N/A	1	54.61	0.67	54.98
2	41.66	3.14				2	56.39	2.56	
3	40.21	0.45				3	55.59	1.11	
4	40.74	0.87				4	53.34	2.98	
5	39.80	1.46							
6	39.50	2.20							

Mix 20 Slabs S39 and S40 (w/c = 0.55)									
Substrate cube number	Substrate cube strength (N/mm^2)	Variation coefficient (%)	Substrate average compressive strength (N/mm^2)	Repair material	Bonding agent	Repair material cube number	Repair material cube Strength (N/mm^2)	Variation coefficient (%)	Repair material average compressive strength (N/mm^2)
1	39.23	2.58	40.27	OPC Concrete (w/c = 0.4)	Zentrifix KMH	1	54.61	0.67	54.98
2	40.22	0.12				2	56.39	2.56	
3	41.62	3.35				3	55.59	1.11	
4	40.27	0				4	53.34	2.98	
5	39.23	2.58							
6	41.03	1.89							

Mix 21 Slabs S41 and S42 (w/c = 0.55)									
Substrate cube number	Substrate cube strength (N/mm^2)	Variation coefficient (%)	Substrate average compressive strength (N/mm^2)	Repair material	Bonding agent	Repair material cube number	Repair material cube Strength (N/mm^2)	Variation coefficient (%)	Repair material average compressive strength (N/mm^2)
1	38.75	1.87	39.49	OPC Mortar (w/c = 0.4)	Zentrifix KMH	1	51.84	5.22	49.27
2	38.83	1.67				2	46.18	6.27	
3	41.46	4.99				3	48.32	1.93	
4	40.09	1.52				4	50.72	2.94	
5	39.44	0.13							
6	38.34	2.91							

Mix 22 Slabs S43 and S44 (w/c = 0.55)									
Substrate cube number	Substrate cube strength (N/mm^2)	Variation coefficient (%)	Substrate average compressive strength (N/mm^2)	Repair material	Bonding agent	Repair material cube number	Repair material cube Strength (N/mm^2)	Variation coefficient (%)	Repair material average compressive strength (N/mm^2)
1	38.86	4.63	37.14	OPC Mortar (w/c = 0.4)	N/A	1	51.84	5.22	49.27
2	37.12	0.05				2	46.18	6.27	
3	37.59	1.21				3	48.32	1.93	
4	36.20	2.53				4	50.72	2.94	
5	36.36	2.10							
6	36.73	1.10							

Mix 23 Slabs S45 and S46 (w/c = 0.55)									
Substrate cube number	Substrate cube strength (N/mm^2)	Variation coefficient (%)	Substrate average compressive strength (N/mm^2)	Repair material	Bonding agent	Repair material cube number	Repair material cube Strength (N/mm^2)	Variation coefficient (%)	Repair material average compressive strength (N/mm^2)
1	42.38	2.99	41.15	Zentrifix GM 25	Zentrifix KMH	1	27.59	2.89	28.41
2	41.38	0.56				2	28.27	0.49	
3	40.10	2.55				3	29.14	2.57	
4	42.39	3.01				4	28.65	0.84	
5	41.72	1.39							
6	38.90	5.47							

Mix 24 Slabs S47 and S48 (w/c = 0.55)									
Substrate cube number	Substrate cube strength (N/mm^2)	Variation coefficient (%)	Substrate average compressive strength (N/mm^2)	Repair material	Bonding agent	Repair material cube number	Repair material cube Strength (N/mm^2)	Variation coefficient (%)	Repair material average compressive strength (N/mm^2)
1	37.89	3.19	39.14	Zentrifix GM 25	N/A	1	27.59	2.89	28.41
2	39.53	0.99				2	28.27	0.49	
3	40.69	3.96				3	29.14	2.57	
4	36.59	6.52				4	28.65	0.84	
5	40.60	3.73							
6	39.55	1.05							

Slabs PL15 PL16									
Substrate cube number	Substrate cube strength (N/mm^2)	Variation coefficient (%)	Substrate average compressive strength (N/mm^2)	Repair material	Bonding agent	Repair material cube number	Repair material cube Strength (N/mm^2)	Variation coefficient (%)	Repair material average compressive strength (N/mm^2)
1	46.06	3.66	47.81	OPC Concrete (w/c = 0.4)	Zentrifix KMH	1	52.93	0.09	52.98
2	49.50	3.53				2	53.45	0.89	
3	46.35	3.05				3	52.91	0.13	
4	47.13	1.42				4	52.62	0.68	
5	49.76	4.08							
6	48.07	0.54							

Slab PL 14									
Substrate cube number	Substrate cube strength (N/mm^2)	Variation coefficient (%)	Substrate average compressive strength (N/mm^2)	Repair material	Bonding agent	Repair material cube number	Repair material cube Strength (N/mm^2)	Variation coefficient (%)	Repair material average compressive strength (N/mm^2)
1	65.30	1.71	64.20	OPC Concrete (w/c = 0.4)	N/A	1	52.93	0.09	52.98
2	65.30	1.71				2	53.45	0.89	
3	62.01	3.41				3	52.91	0.13	
						4	52.62	0.68	

Slab P5									
Substrate cube number	Substrate cube strength (N/mm^2)	Variation coefficient (%)	Substrate average compressive strength (N/mm^2)	Repair material	Bonding agent	Repair material cube number	Repair material cube Strength (N/mm^2)	Variation coefficient (%)	Repair material average compressive strength (N/mm^2)
	Strong		Strong	OPC Concrete (w/c = 0.4)	N/A	1	52.93	0.09	52.98
1	58.82	13.66	51.75			2	53.45	0.89	
2	50.89	1.66				3	52.91	0.13	
3	53.74	3.85				4	52.62	0.68	
4	49.32	4.70							
5	50.50	2.42							
6	47.24	8.71							
	Weak		Weak						
1	23.81	1.65	24.21						
2	24.58	1.53							
3	26.25	8.43							
4	23.58	2.60							
5	24.30	0.37							
6	22.71	6.20							

Slab PL11 and PL13									
Substrate cube number	Substrate cube strength (N/mm^2)	Variation coefficient (%)	Substrate average compressive strength (N/mm^2)	Repair material	Bonding agent	Repair material cube number	Repair material cube Strength (N/mm^2)	Variation coefficient (%)	Repair material average compressive strength (N/mm^2)
1	52.94	3.24	51.28	OPC Mortar (w/c = 0.4)	N/A	1	44.83	4.66	47.02
2	49.97	2.55				2	47.05	0.06	
3	48.59	5.24				3	47.25	0.49	
4	54.15	5.60				4	48.95	4.10	
5	50.61	1.31							
6	51.40	0.23							

Slab PL2									
Substrate cube number	Substrate cube strength (N/mm^2)	Variation coefficient (%)	Substrate average compressive strength (N/mm^2)	Repair material	Bonding agent	Repair material cube number	Repair material cube Strength (N/mm^2)	Variation coefficient (%)	Repair material average compressive strength (N/mm^2)
1	57.80	0.78	57.35	OPC Mortar (w/c = 0.4)	Zentrifix KMH	1	44.83	4.66	47.02
2	56.90	0.78				2	47.05	0.06	
3	57.35	0				3	47.25	0.49	
						4	48.95	4.10	

Slab P2									
Substrate cube number	Substrate cube strength (N/mm^2)	Variation coefficient (%)	Substrate average compressive strength (N/mm^2)	Repair material	Bonding agent	Repair material cube number	Repair material cube Strength (N/mm^2)	Variation coefficient (%)	Repair material average compressive strength (N/mm^2)
	Strong		Strong	OPC Mortar (w/c = 0.4)	Zentrix KMH	1	44.83	4.66	47.02
1	55.36	2.99	53.75			2	47.05	0.06	
2	52.25	2.79				3	47.25	0.49	
3	54.21	0.86				4	48.95	4.10	
4	54.59	1.56							
5	53.64	0.20							
6	52.44	2.44							
	Weak		Weak						
1	29.17	1.92	28.62						
2	29.62	3.49							
3	29.61	3.46							
4	28.62	0							
5	25.24	11.81							
6	29.43	2.83							

Slabs PL5 and PL6									
Substrate cube number	Substrate cube strength (N/mm^2)	Variation coefficient (%)	Substrate average compressive strength (N/mm^2)	Repair material	Bonding agent	Repair material cube number	Repair material cube Strength (N/mm^2)	Variation coefficient (%)	Repair material average compressive strength (N/mm^2)
1	52.71	0.45	52.95	Zentrifix GM 25	Zentrifix KMH	1	28.29	5.68	26.77
2	52.72	0.43				2	27.27	1.87	
3	53.41	0.87				3	25.09	6.28	
						4	26.41	1.34	

Slabs PL9 and PL10									
Substrate cube number	Substrate cube strength (N/mm^2)	Variation coefficient (%)	Substrate average compressive strength (N/mm^2)	Repair material	Bonding agent	Repair material cube number	Repair material cube Strength (N/mm^2)	Variation coefficient (%)	Repair material average compressive strength (N/mm^2)
1	50.27	0.38	50.08	Zentrifix GM 25	N/A	1	28.29	5.68	26.77
2	50.60	1.04				2	27.27	1.87	
3	51.59	3.02				3	25.09	6.28	
4	50.14	0.12				4	26.41	1.34	
5	51.14	2.12							
6	46.76	6.63							